EMOTIONAL DISTURBANCE AND BRAIN IMAGING IN NEUROPSYCHIATRIC DISORDERS

EDITED BY: Wenbin Guo, Fengyu Zhang, Maorong Hu, Roberto Esposito and Ping Li

PUBLISHED IN: Frontiers in Psychiatry

frontiers Research Topics

frontiers

ISSN 1664-8714
ISBN 978-2-88966-743-7
DOI 10.3389/978-2-88966-743-7

About Frontiers

Frontiers is more than just an open-access publisher of scholarly articles: it is a pioneering approach to the world of academia, radically improving the way scholarly research is managed. The grand vision of Frontiers is a world where all people have an equal opportunity to seek, share and generate knowledge. Frontiers provides immediate and permanent online open access to all its publications, but this alone is not enough to realize our grand goals.

Frontiers Journal Series

The Frontiers Journal Series is a multi-tier and interdisciplinary set of open-access, online journals, promising a paradigm shift from the current review, selection and dissemination processes in academic publishing. All Frontiers journals are driven by researchers for researchers; therefore, they constitute a service to the scholarly community. At the same time, the Frontiers Journal Series operates on a revolutionary invention, the tiered publishing system, initially addressing specific communities of scholars, and gradually climbing up to broader public understanding, thus serving the interests of the lay society, too.

Dedication to Quality

Each Frontiers article is a landmark of the highest quality, thanks to genuinely collaborative interactions between authors and review editors, who include some of the world's best academicians. Research must be certified by peers before entering a stream of knowledge that may eventually reach the public - and shape society; therefore, Frontiers only applies the most rigorous and unbiased reviews.
Frontiers revolutionizes research publishing by freely delivering the most outstanding research, evaluated with no bias from both the academic and social point of view. By applying the most advanced information technologies, Frontiers is catapulting scholarly publishing into a new generation.

What are Frontiers Research Topics?

Frontiers Research Topics are very popular trademarks of the Frontiers Journals Series: they are collections of at least ten articles, all centered on a particular subject. With their unique mix of varied contributions from Original Research to Review Articles, Frontiers Research Topics unify the most influential researchers, the latest key findings and historical advances in a hot research area! Find out more on how to host your own Frontiers Research Topic or contribute to one as an author by contacting the Frontiers Editorial Office: frontiersin.org/about/contact

EMOTIONAL DISTURBANCE AND BRAIN IMAGING IN NEUROPSYCHIATRIC DISORDERS

Topic Editors:
Wenbin Guo, Central South University, China
Fengyu Zhang, Global Clinical and Translational Research Institute, United States
Maorong Hu, Nanchang University, China
Roberto Esposito, Asur Marche, Italy
Ping Li, Qiqihar Medical University, China

Citation: Guo, W., Zhang, F., Hu, M., Esposito, R., Li, P., eds. (2021). Emotional Disturbance and Brain Imaging in Neuropsychiatric Disorders.
Lausanne: Frontiers Media SA. doi: 10.3389/978-2-88966-743-7

Table of Contents

frontiers in Psychiatry

EDITORIAL
published: 17 March 2021
doi: 10.3389/fpsyt.2021.632244

Editorial: Emotional Disturbance and Brain Imaging in Neuropsychiatric Disorders

Roberto Esposito[1,2], *Fengyu Zhang*[3,4]*, *Maorong Hu*[5], *Ping Li*[6] and *Wenbin Guo*[7,8]*

[1] Titano Diagnostic Clinic, Falciano, San Marino, [2] Area Vasta 1, Azienda Sanitaria Unica Regionale (ASUR) Marche, Pesaro, Italy, [3] Global Clinical and Translational Research Institute, Bethesda, MD, United States, [4] Beijing Huilongguan Hospital and Peking University Huilongguan Clinical Medical Institute, Beijing, China, [5] Department of Psychiatry, The First Affiliated Hospital of Nanchang University, Nanchang, China, [6] Department of Psychiatry, Qiqihar Medical University, Qiqihar, China, [7] Department of Psychiatry, National Clinical Research Center for Mental Disorders, The Second Xiangya Hospital of Central South University, Changsha, China, [8] Department of Psychiatry, The Third People's Hospital of Foshan, Foshan, China

Keywords: structural MRI, functional MRI, depression, anxiety, phobia

Editorial on the Research Topic

Editorial: Emotional Disturbance and Brain Imaging in Neuropsychiatric Disorders

INTRODUCTION

Emotional disturbances, such as depression, anxiety, and phobias, are prevalent in patients with neuropsychiatric disorders, including somatization disorder (SD), major depressive disorder (MDD), general anxiety disorder (GAD), panic disorder (PD), schizophrenia, blepharospasm, and cervical dystonia (1–5). However, the neuropathology underlying the emotional symptoms in neuropsychiatric disorders remains unclear. Brain imaging techniques provide some unprecedented opportunities to study the neural mechanisms of emotional problems and neuropsychiatric disorders (6–10). This Research Topic convened 16 research articles based on the current understanding of emotional symptoms to explore the underlying neuropathological mechanisms and address important conceptual and methodological questions.

MAJOR DEPRESSIVE DISORDER

Adolescent

Wu F. et al. explored functional and structural connectivity abnormalities within the amygdala-prefrontal circuit in first-episode medication-naive adolescents with MDD through resting-state functional magnetic resonance imaging (rs-fMRI) and diffusion tensor imaging (DTI). Rs-fMRI and DTI imaging data were acquired from 36 patients and 37 age-and sex-matched healthy controls (HCs). The patients showed decreased connectivity between the left amygdala and ventral prefrontal cortex (PFC) and lower fractional anisotropy (FA) in the left uncinate fasciculus. These findings suggest that both functional and structural abnormalities of the amygdala-prefrontal circuit may be involved in the neuropathophysiology of adolescent MDD.

Zhang et al. investigated how emotional context modulates the temporal dynamics of reward anticipation and feedback in adolescents. Electroencephalography (EEG) data from 35 patients with MDD and 37 healthy adolescents were recorded when performing a gambling task after being presented with emotional pictures. The study suggests that adolescents with MDD exhibited dissociable deficits in reward anticipation and gain or loss feedback that were distinctly modulated by emotional

OPEN ACCESS

Edited and reviewed by:
André Schmidt,
University of Basel, Switzerland

***Correspondence:**
Wenbin Guo
guowenbin76@csu.edu.cn
Fengyu Zhang
zhangfy@gcatresearch.org

Specialty section:
This article was submitted to Neuroimaging and Stimulation, a section of the journal Frontiers in Psychiatry

Received: *22 November 2020*
Accepted: *17 February 2021*
Published: *17 March 2021*

Citation:
Esposito R, Zhang F, Hu M, Li P and Guo W (2021) Editorial: Emotional Disturbance and Brain Imaging in Neuropsychiatric Disorders. Front. Psychiatry 12:632244. doi: 10.3389/fpsyt.2021.632244

contexts, which might deepen our understanding of the modulation of emotional contexts on the dynamic temporal reorganization of the reward circuit in adolescents with MDD.

Adult

Tao et al. investigated the subgenual anterior cingulate cortex (sACC) in patients with depression. Indeed, abnormal activity of the sACC is implicated as a potentially effective target for therapeutic modulation in treatment-resistant depression (TRD). The authors hypothesized that PFC areas with direct fiber connections to the sACC might be sites for effective treatment using transcranial magnetic stimulation (TMS). Two neuroimaging data sets were used to construct anatomic and functional connectivity maps using sACC as the seed region. One data set included magnetic resonance images from 20 HCs, and the other included MR images from 15 TRD patients and 15 additional HCs. Both left and right prefrontal cortex (PFC) is functionally connected to two regions relevant to depression, the sACC and the posterior cingulate cortex (PCC). These bilateral PFC sites may be targets for effective TMS treatment in TRD.

Chen et al. examined the changes in characteristics of affective network connectivity in patients with MDD before and after repetitive TMS treatment over the left dorsolateral PFC to assess how these connectivity changes are linked to the patient's clinical characteristics. rTMS can enhance affective network connectivity in patients with MDD, which is linked to emotional improvement. This study further suggests that the insula might be a potential target region for evaluating clinical efficacy for MDD in designing rational strategies for therapeutic trials.

Liu et al. examined whether the CACNA1C gene rs11832738 polymorphism and MDD had a potential interaction on untreated regional ALFF, and further determined whether the regional ALFF mediated the genetic association with MDD. With 116 patients and 66 HCs, they provided initial evidence for CACNA1C genotype-related alterations in brain function among patients with MDD, which could help better understand the neurobiological mechanisms underlying MDD. The study confirmed that the association of calcium channel dysfunction with MDD might be altered in functional brain activity.

Late-Life Depression

Li et al. aimed to identify the voxel-based whole-brain functional connectivity changes in patients with late-life depression (LLD). With 50 patients and 33 HCs, the study indicated that the intrinsic abnormality of network centrality exists in a wide range of brain areas in patients with LLD. Late-onset depression patients differ from early-onset depression in cortical network centrality.

Krause-Sorio et al. conducted a pilot study of 22 older adults with depression who randomly received escitalopram/memantine or escitalopram/placebo treatment and tested with diffusion-weighted imaging (DWI) to investigate brain white matter integrity in the fronto-limbic-striatal tracts based on fractional anisotropy and treatment response. In bilateral anterior and posterior internal capsule tracts and bilateral inferior and right superior fronto-occipital fasciculus, higher fractional anisotropy was associated with more considerable improvements in depressive symptoms for escitalopram/memantine but not escitalopram/placebo. While the findings seemed promising, it has to be noted that the study was based on a small sample with some significant losses to follow-up. Therefore, further studies with adequate statistical power are needed in the future.

Wu Y. et al. aimed to examine altruism in patients with LLD and its neurobiological mechanism. Depressive patients seemed to show less altruistic behavior, while depression and age are two primary influencing factors of altruism. Kynurenine and its metabolites can cross the brain-blood barriers, impact the central nervous system, and play a significant role in psychiatric disorders, including depression. They investigated whether metabolites in the kynurenine pathway and white matter network topological features would influence altruistic behavior in patients with LLD. With 34 patients and 36 HCs, the study showed that patients exhibited a higher level of altruism and white matter global network properties than the HC. Kynurenic acid to kynurenine ratio was associated with the Dictator Game paradigm performance and network density in the patients. Kynurenine metabolism might play an important role in altruistic behavior in LLD.

BIPOLAR DEPRESSION

Lu et al. performed a study of 27 HCs, and 36 patients with bipolar depression (BPD) treated with quetiapine. At baseline, the altered composition of gut microbiota and low B/E ratio was founded in patients with BPD, and Enterobacter spp count was significantly correlated to $CD3^+$ T cells. Antipsychotic treatment significantly improved depressive symptoms and the balance of B/E. This finding suggests that the treatment effect on depressive symptoms might be partly through the improved gut microbiota balance.

Ren et al. investigated possible age-associated alterations of white matter integrity in adolescents and young adults with BPD aged 13–30. The findings provide neuroimaging evidence supporting a back-to-front spatiotemporal directionality of the altered development of white matter integrity associated with age in patients with BPD during adolescence/young adulthood.

COMPARISON BETWEEN MDD AND BD

Takahashi et al. explored abnormal melatonin secretion in patients with MDD and BPD. They employed MRI to examine pineal gland volumes and pineal cyst prevalence in 56 patients with MDD (29 currently depressed and 27 remitted patients), 26 patients with BPD, and matched HCs (33 for MDD and 24 for BD). The pineal gland was significantly smaller in the current MDD of non-melancholic depression than in the melancholic MDD. Pineal volumes negatively correlated to the severity of loss of interest in the current MDD. The medication used and the number of affective episodes were not associated with pineal volumes in the MDD or BPD. While the findings do not suggest that pineal volumes reflect abnormal melatonin secretion in affective disorders, they point to the possibility that pineal

abnormalities are associated with clinical subtypes of MDD and its symptomatology.

SCHIZOPHRENIA

Luo et al. performed a study of dynamic functional connectivity strength (dFCS) at a different frequency with rs-fMRI data from 96 patients with schizophrenia (SZ) and 121 HCs. They found that relative to HCs, patients with SZ tend to have decreased dFCS in the salience, auditory, sensorimotor, and visual networks but increased dFCS in the cerebellum, basal ganglia, and prefrontal network consistently at low-frequency bands, which significantly interacted with disease status. However, no significant difference in dFCS was found in higher frequency. The study may provide potential implications for examining the neuropathological mechanism of SZ.

Duan and Zhu aimed to examine SZ research utilizing MRI through a bibliometric analysis of literature searched in PubMed from 2004 to 2018, divided into three 5-year periods. It showed that the utilization of MRI in SZ research was relatively diverse, but the theme clusters derived from each period reflect the evolvement from (1) the brain structure and its link to functional abnormality, metabolism, and antipsychotic efficacy and pathology; (2) the physiopathology mechanism and etiology of cognitive disorders including brain structure and function, default network, and psychology; and to (3) the neurobiology between SZ and other mental disorders, including the genetic and antipsychotic effect on brain structure and function. These findings provide useful information for developing future SZ research using MRI techniques.

SUBSTANCE ABUSE

Yang et al. examined regional Cerebral Blood Flow (rCBF) alterations and their cognitive performance in unmedicated heroin-dependent individuals (HDIs). Voxel-wise whole-brain analysis of rCBF measured arterial spin labeling (ASL) perfusion MRI showed that relative to HCs. HDIs tend to have decreased rCBF in the bilateral cortical and subcortical inferior temporal gyrus, medial frontal gyrus (MFG), orbital medial frontal cortex, precuneus, posterior cerebellar lobe/declive, and right thalamus and posterior cerebella cortex, all of which were significant between HDIs and HCs in the ROIs analysis. The rCBF at MFG was significantly associated with cognitive performance measured by Trail Making Test. These findings suggest the MFG as a critical region in HDIs and suggest ASL-derived CBF as a potential marker for use in heroin addiction studies.

Sariah et al. performed an interesting study of whether chewing betel quid had acute and longer-term addictive effects in naive and dependent users. The rs-fMRI was performed in 24 male betel quid-dependent chewers and 28 male HCs before and promptly after betel quid chewing. They found that individuals who chronically used betel quid have higher functional connectivity in the frontal, parietal, and temporal brain regions relative to HCs. However, the acute effect was observed in naive Betel-quid chewers with increased functional connectivity in some visual cortical areas of the superior and right middle occipital gyrus and subcortical caudate, putamen, pallidum, and thalamus.

OTHER PSYCHIATRIC DISORDERS

Seok and Cheong aimed to identify gray matter deficits and functional alterations using voxel-based morphometry and fMRI analyses of 15 men with intermittent explosive disorder (IED) and 15 age sex-matched HCs. Gray matter volume and brain activation while viewing the anger-inducing films were measured using 7T MRI. Men with IED had significantly reduced gray matter volume in the insula, amygdala, and orbitofrontal area relative to HC; gray matter volume in the left insula was negatively correlated with composite aggression scores. fMRI showed that men with IED showed greater activation in the insula, putamen, anterior cingulate cortex, and amygdala during anger processing. Left insula activity was positively correlated with composite aggression scores. These findings collectively suggest that structural and functional alterations in the left insula are linked to IED, thereby providing insight into IED's neural mechanisms.

CONCLUSIONS AND FUTURE PERSPECTIVES

Emotional disturbance is mostly related to mood and anxiety disorders that are highly prevalent neuropsychiatric disorders and common in older adults of general populations (11). Neuroimaging is a critical tool for understanding the neural mechanisms and defining brain circuits underlying neuropsychiatric disorders. While most articles published in this specific theme employed observations of cases and healthy controls, two studies by Chen et al. and Krause-Sorio et al. examined neuroimaging in response to antidepressant treatment, which may provide a proof of concept that neuroimaging can predict pharmacological treatment response.

The advances in neuroimaging techniques and biotechnology have provided an unprecedented opportunity to study precision neuropsychiatric disorders in past years. Advanced neuroimaging techniques have helped to investigate brain structural and functional changes in neuropsychiatric diseases through MRI [fMRI, DTI, Perfusion Weighted Imaging (PWI), Cortical Thickness, Voxel-Based Morphometry], [Positron Emission Tomography (PET), and Magnetoencephalography (MEG)]; fMRI has in particular provided information about neural connectivity at rest (rs-fMRI) and during a task. Rs-fMRI represents a promising method for investigating brain *in-vivo* in physiological and pathological conditions due to both its spatial resolution compared to other methods, such as MEG and EEG, as well as the possibility of using it with poorly compliant patients due to their clinical condition. This allows us to highlight abnormalities at multiple levels across neural systems. Rs-fMRI studies have underlined that neuropsychiatric diseases show altered interactions between different RSNs, and disease progression and treatments may modify these interactions.

Even if neuroimaging techniques (especially rs-fMRI) represent valid tools to investigate neuropsychiatric diseases, results are often inconsistent, showing significant variability, which may present problems for identifying specific biomarkers of pathology. The lack of confirmed biomarkers might be due to different variables. These may include the heterogenicity of the neuropsychiatric disease, the diversities of data analysis technique used, and the limits intrinsic to rs-fMRI, such as the scarce possibility of monitoring patients' real mental content during the acquisition phase. Future studies should include standardized protocols for enrollment of sample size, reducing the heterogeneity observed. Integration of temporal and spatial imaging as well as clinical and molecular data may improve the identification of brain circuits related to neuropsychiatric disorders and treatment response.

Moreover, a combination of multimodal imaging tools, such as PET, structural MRI, and fMRI, can help understand brain circuits' structure and function. A PET scan can reveal metabolic and functional problems at a cellular level that MRI and fMRI cannot provide, which may be critical for some neuropsychiatric diseases. These precautions could provide more power in identifying disorder-specific neural alteration and help develop specific therapeutic interventions in future precision psychiatry.

AUTHOR CONTRIBUTIONS

All authors listed have made substantial and intellectual contributions to the topic and approved this editorial for publication.

FUNDING

This study was supported by grants from the National Key R&D Program of China (Grant no. 2016YFC1307100), the National Natural Science Foundation of China (Grant no. 81771447), and the Natural Science Foundation of Hunan (Grant no. 2020JJ4784).

REFERENCES

1. Anand A, Shekhar A. Brain imaging studies in mood and anxiety disorders: special emphasis on the amygdala. *Ann N Y Acad Sci.* (2003) 985:370–88. doi: 10.1111/j.1749-6632.2003.tb07095.x
2. Worbe Y. Neuroimaging signature of neuropsychiatric disorders. *Curr Opin Neurol.* (2015) 28:358–64. doi: 10.1097/WCO.0000000000000220
3. Peedicayil J. Identification of biomarkers in neuropsychiatric disorders based on systems biology and epigenetics. *Front Genet.* (2019) 10:985. doi: 10.3389/fgene.2019.00985
4. Pan P, Wei S, Ou Y, Jiang W, Li W, Lei Y, et al. Reduced global-brain functional connectivity and its relationship with symptomatic severity in cervical dystonia. *Front Neurol.* (2020) 10:1358. doi: 10.3389/fneur.2019.01358
5. Jiang W, Lan Y, Cen C, Liu Y, Feng C, Lei Y, et al. Abnormal spontaneous neural activity of brain regions in patients with primary blepharospasm at rest. *J Neurol Sci.* (2019) 403:44–9. doi: 10.1016/j.jns.2019.06.002
6. Burhan AM, Marlatt NM, Palaniyappan L, Anazodo UC, Prato FS. Role of hybrid brain imaging in neuropsychiatric disorders. *Diagnostics.* (2015) 5:577–614. doi: 10.3390/diagnostics5040577
7. Hellwig S, Domschke K. Update on PET imaging biomarkers in the diagnosis of neuropsychiatric disorders. *Curr Opin Neurol.* (2019) 32:539–47. doi: 10.1097/WCO.0000000000000705
8. Whitfield-Gabrieli S, Ford JM. Default mode network activity and connectivity in psychopathology. *Annu Rev Clin Psychol.* (2012) 8:49–76. doi: 10.1146/annurev-clinpsy-032511-143049
9. Ott CV, Johnson CB, Macoveanu J, Miskowiak K. Structural changes in the hippocampus as a biomarker for cognitive improvements in neuropsychiatric disorders: a systematic review. *Eur Neuropsychopharmacol.* (2019) 29:319–29. doi: 10.1016/j.euroneuro.2019.01.105
10. Mohan A, Roberto AJ, Mohan A, Lorenzo A, Jones K, Carney MJ, et al. The significance of the default mode network (DMN) in neurological and neuropsychiatric disorders: a review. *Yale J Biol Med.* (2016) 89:49–57.
11. Li Y, Lu J. Childhood adversity and depression among older adults: results from a longitudinal survey in China. *Glob Clin Transl Res.* (2019) 1:53–7. doi: 10.36316/gcatr.01.0007

Conflict of Interest: The authors declare that the research was conducted in the absence of any commercial or financial relationships that could be construed as a potential conflict of interest.

frontiers in Psychiatry

ORIGINAL RESEARCH
published: 29 October 2019
doi: 10.3389/fpsyt.2019.00784

Gut Microbiota in Bipolar Depression and Its Relationship to Brain Function: An Advanced Exploration

Qiaoqiao Lu[1,2], Jianbo Lai[1,3,4], Haifeng Lu[5], Chee Ng[6], Tingting Huang[1], Hua Zhang[5], Kaijing Ding[7], Zheng Wang[1,3,4], Jiajun Jiang[1], Jianbo Hu[1,3,4], Jing Lu[1,3,4], Shaojia Lu[1,3,4], Tingting Mou[1,3,4], Dandan Wang[1,3,4], Yanli Du[1], Caixi Xi[1], Hailong Lyu[1,3,4], Jingkai Chen[1,3,4], Yi Xu[1,3,4], Zhuhua Liu[8†] and Shaohua Hu[1,3,4†]*

[1] Department of Psychiatry, the First Affiliated Hospital, College of Medicine, Zhejiang University, Hangzhou, China, [2] Department of Psychiatry, Hangzhou Seventh People's Hospital, Hangzhou, China, [3] The Key Laboratory of Mental Disorder Management of Zhejiang Province, Hangzhou, China, [4] Brain Research Institute, Zhejiang University, Hangzhou, China, [5] State Key Laboratory for Diagnosis and Treatment of Infectious Diseases, First Affiliated Hospital, Zhejiang University School of Medicine, Hangzhou, China, [6] The Melbourne Clinic, Department of Psychiatry, University of Melbourne, Melbourne, VIC, Australia, [7] Department of Children and Adolescents' Psychology, Hangzhou Seventh People's Hospital, Hangzhou, China, [8] Center of Mental Health, General Hospital of Ningxia Medical University, Yinchuan, China

OPEN ACCESS

Edited by:
Wenbin Guo,
Central South University, China

Reviewed by:
Xiancang Ma,
First Affiliated Hospital of Xi'an Jiaotong University, China
Yu-Tao Xiang,
University of Macau, China

***Correspondence:**
Shaohua Hu
dorhushaohua@zju.edu.cn

†These authors have contributed equally to this work

Specialty section:
This article was submitted to Neuroimaging and Stimulation, a section of the journal Frontiers in Psychiatry

Received: *28 August 2019*
Accepted: *02 October 2019*
Published: *29 October 2019*

Citation:
Lu Q, Lai J, Lu H, Ng C, Huang T, Zhang H, Ding K, Wang Z, Jiang J, Hu J, Lu J, Lu S, Mou T, Wang D, Du Y, Xi C, Lyu H, Chen J, Xu Y, Liu Z and Hu S (2019) Gut Microbiota in Bipolar Depression and Its Relationship to Brain Function: An Advanced Exploration. Front. Psychiatry 10:784. doi: 10.3389/fpsyt.2019.00784

The mechanism of bipolar disorder is unclear. Growing evidence indicates that gut microbiota plays a pivotal role in mental disorders. This study aimed to find out changes in the gut microbiota in bipolar depression (BD) subjects following treatment with quetiapine and evaluate their correlations with the brain and immune function. Totally 36 subjects with BD and 27 healthy controls (HCs) were recruited. The severity of depression was evaluated with the Montgomery-Asberg depression rating scale (MADRS). At baseline, fecal samples were collected and analyzed by quantitative polymerase chain reaction (qPCR). T lymphocyte subsets were measured to examine immune function. Near-infrared spectroscopy (NIRS) was used to assess brain function. All BD subjects received quetiapine treatment (300 mg/d) for four weeks, following which the fecal microbiota and immune profiles were reexamined. Here, we first put forward the new concept of brain-gut coefficient of balance (B-G_{CB}), which referred to the ratio of [oxygenated hemoglobin]/(*Bifidobacteria* to *Enterobacteriaceae* ratio), to analyze the linkage between the gut microbiota and brain function. At baseline, the $CD3^+$ T cell proportion was positively correlated with $\log_{10}$ Enterobacter spp count, whereas the correlativity between the other bacteria and immune profiles were negative. Log_{10} B-G_{CB} was positively correlated with $CD3^+$ T cell proportion. In subjects with BD, counts of *Faecalibacterium prausnitzii*, *Bacteroides–Prevotella group*, *Atopobium Cluster*, *Enterobacter spp*, and *Clostridium Cluster IV* were higher, whereas the $\log_{10}$ (B/E) were lower than HCs (B/E refers to *Bifidobacteria* to *Enterobacteriaceae* ratio and represents microbial colonization resistance). After treatment, MADRS scores were reduced, whereas the levels of *Eubacterium rectale*, *Bifidobacteria*, and B/E increased. The composition of the gut microbiota and its relationship to brain function were altered in BD subjects. Quetiapine treatment was effective for depression and influenced the composition of gut microbiota in patients.

Clinical Trial Registration: http://www.chictr.org.cn/index.aspx, identifier ChiCTR-COC-17011401, URL: http://www.chictr.org.cn/listbycreater.aspx.

Keywords: bipolar depression, gut microbiota, brain function, immune function, quetiapine treatment

INTRODUCTION

Bipolar disorder caused a high global disease burden (1) with a lifetime prevalence of 1.0% for bipolar-I disorder, 1.1% for bipolar-II disorder, and 2.4% for subthreshold bipolar disorder. The pathogenesis of bipolar disorder is unclear. Its diagnosis is based on clinical symptoms. Hence, it is frequently misdiagnosed as major depressive disorder (2, 3). The misdiagnosis results in poor therapeutic outcomes (2). Therefore, it makes great sense to study the mechanism of bipolar disorder, search for biomarkers, and find novel therapies.

Gut microbiota plays an increasingly important role in the onset and progress of psychiatric disorders. Brain-gut axis is the highway on which biochemical molecules travel between the brain and the gut. These biochemical molecules are involved in immune system, endocrine system, and the vagus nerve (4, 5). Many of these molecules can be produced by gut microbiota directly or indirectly. Therefore, we suspect that gut microbiota triggers bipolar disorder through brain-gut axis is one of the potential mechanisms of bipolar pathogenesis. This includes immune, neural, and endocrine pathways. These pathways work in tandem and is also a complex whole that communicates with each other on the way to bipolar disorder. Gut microbiota is associated with activation of pro- or anti-inflammatory responses in central nervous system (CNS) (6). Short-chain fatty acids (SCFAs) are products of carbohydrates fermented by gut bacteria. SCFAs are protective factors for inflammatory status in both peripheral and CNS (7, 8). Other gut metabolites and microbial components also contribute to inflammatory modulation, such as polyamines, polysaccharide A, formyl peptides, and D-glycero-β-D-mannoheptose-1,7-bisphosphate (8). Some bacteria, such as *Lactobacillus* strain, regulate emotion *via* vagus nerve (9). Enteroendocrine cells release mediators, such as 5-hydroxytryptamine (5-HT), cholecystokinin, glucagon-like peptide 1, peptide YY, and ghrelin. These mediators are regulated by intestinal nutrient status. They stimulate vagal afferent neurons signaling to CNS to regulate food intake behaviors in mood disorder patients (10). In particular, 5-HT plays an important role in the regulation of emotion (11). Hypothalamic-pituitary-adrenal axis is also influenced by gut microbiota (12), communicates with immune system (13), and is involved in emotion regulation (12).

A growing body of research finds that gut microbiota in bipolar patients is different from that in normal persons. In bipolar disorder patients, *Clostridiaceae* is found more abundant than that in HCs (14). Two studies observed the decline of *Faecalibacterium* in bipolar disorder subjects (15, 16), which is related to better self-reported health states (16). The presence of genus *Flavonifractor* is a risk factor for bipolar disorder and is confounded by female sex and smoking (17). As a dangerous factor, genus *Flavonifractor* may induce inflammation and oxidative stress to harm its host (17). In patients with bipolar disorder, negative correlations are found between *Lactobacillus* counts and sleep, and between *Bifidobacterium* counts and serum cortisol levels, indicating these two bacteria impact exact depressive symptoms (18). Special bacteria changes in bipolar patients in different researches are not completely coincident. Compared with HCs, phylum *Actinobacteria* and class *Coriobacteria* are more abundant in bipolar patients, whereas class *Ruminococcaceae* is more abundant in HCs (15). Two studies have analyzed gut microbiota in bipolar patients who received psychotropic medications therapy. One study shows that atypical antipsychotics treated females have lower species richness when compared with nonatypical antipsychotics treated females (19). However, this is not significant in male patients (19). In this study, the atypical antipsychotics include clozapine, olanzapine, risperidone, quetiapine, asenipine, ziprasodone, lurasidone, aripiprazole, paliperidone, and iloperidone (19). The other study identifies 30 microbial markers in bipolar depression patients, which are different from HCs, and finds the alteration of gut microbiota composition following quetiapine monotherapy (20). Moreover, 10 microbial markers are identified from the responders of patients (20).

As yet, no study has explored the connection among the brain function, gut microbiota, and immune function in BD population. This study not only attempts to compare the gut microbiota between BD and HCs but also to find this potential connection. The results will be a supplement to the brain-gut axis in the psychiatric field. Besides that, this study also tries to repeat the effects of quetiapine treatment on gut microbiota in BD patients.

MATERIALS AND METHODS

Study Design and Subjects

This study was approved by the Ethics Committee of the First Affiliated Hospital, Zhejiang University School of Medicine (a quick review of scientific research, No.397, 2017, see Supplement for the original document) and was performed in accordance with the Helsinki Declaration of 1975. The clinical trial registry number was ChiCTR-COC-17011401. All participants were provided informed consents before being recruited into the study (for adolescents, consents were provided by their guardians). The privacy rights of the recruited subjects were taken seriously.

Altogether, 36 subjects with BD were recruited from the inpatient and outpatient departments of the First Affiliated Hospital, Zhejiang University School of Medicine from May to October 2017. Twenty

Abbreviations: ANCOVA, analysis of covariance; ANOVA, analysis of variance; BD, bipolar depression; BDNF, brain-derived neurotrophic factor; B/E, Bifidobacteria to Enterobacteriaceae ratio; B-GCB, brain-gut coefficient of balance; CNS, central nervous system; deoxy-Hb, concentration of deoxygenated hemoglobin; HCs, healthy controls; MADRS, Montgomery-Asberg depression rating scale; M.I.N.I., the mini-international neuropsychiatric interview; NIRS, near-infrared spectroscopy; oxy-Hb, concentration of oxygenated hemoglobin; qPCR, quantitative polymerase chain reaction; SCFAs, short-chain fatty acids; SCID, structured clinical interview for DSM-IV-TR disorders; YMRS, young mania rating scale; 5-HT, 5-hydroxytryptamine.

six patients suffered from bipolar II, and 10 patients had bipolar I. The age of the subjects ranged from 14 to 57 years old. All subjects met the following criteria: (a) BD was diagnosed by two psychiatrists according to the Structured Clinical Interview for DSM-IV-TR disorders (SCID); there was no severity requirement for depression; (b) BD subjects who had not received any treatment (17 patients) or medications had been stopped for more than 3 months (19 patients stopped medications because of the recovery from the disease or the intolerance of side effects). The exclusion criteria included (I) comorbidity of gastrointestinal disease, infectious disease, fever, and other physical diseases; (II) suffering from autoimmune disease, endocrine disease, and other mental disorders; (III) a history of using antibiotics, probiotics, prebiotics, synbiotics, or yoghurt within a month; (IV) taking lactulose, prokinetic drugs, or antibiotics treatment in the last month; and (V) any history of substance abuse, including nicotine dependence, caffeine use, and others.

In total, 27 age-, gender-, marriage-, and BMI-matched HCs were recruited from five communities in Hangzhou, China. All HCs were excluded if they met any of the exclusion criteria of the BD group or the following criteria: irregular bowel frequency (regular frequency refers to daily or every other day); history of suicide attempts; Montgomery-Asberg depression rating scale (MADRS) (21) score greater than 8 points (22); young mania rating scale (YMRS) (23) score greater than 5 points; and any positive diagnosis on the mini-international neuropsychiatric interview (M.I.N.I.).

All BD subjects completed the rating scales and provided a 3-ml venous blood sample, which was immediately sent to the laboratory for the T lymphocyte subsets measurements. They also provided fecal samples to the State Key Laboratory for Diagnosis and Treatment of Infectious Diseases in the hospital. Sixteen patients completed the baseline test of the NIRS. As a first-line therapy for BD recommended by the Canadian Network for Mood and Anxiety Treatments and International Society for Bipolar Disorders 2018 guidelines (24), quetiapine was selected to treat BD patients in this study. All patients received a four-week treatment with quetiapine (from 50 mg/day gradually increase to 300 mg/day per person in 12 days) (25). During the treatment, no other psychotropic medications were used. Several nonpsychiatric drugs were used to ease side effects. Propranolol (10 mg–20 mg/day) was used to treat sinus tachycardia, and glycerine enema was used to treat constipation. No other medications were used. After 4 weeks, the rating scales were reassessed, and T lymphocyte subsets and fecal bacteria populations were retested. Seventeen patients completed the one-month follow up.

The HCs group also completed the rating scales for screening and provided fecal samples.

Rating Scale Assessment for Mood Symptoms

In the BD group, depression severity was assessed using MADRS (21, 22). Mania severity was measured using YMRS (23). MADRS and YMRS were measured by two independent and experienced psychiatrists who were trained simultaneously in using the MADRS and YMRS before this study began. After training, a correlation coefficient greater than 0.8 was maintained for both the MADRS and the YMRS total score by repeated assessments. Both of the scales were evaluated twice, before and after treatment.

In the HCs group, MADRS, YMRS, and M.I.N.I. were used as screening tools. All the scores were below the lowest intervention thresholds that were aforementioned.

Measurements of T Lymphocyte Subsets

Venous blood samples were collected from all patients (except one male patient who did not offer a blood sample). The proportions of T lymphocyte subsets (e.g., $CD3^+$, $CD4^+$, $CD8^+$ T cells, and NK cells) were examined by a BD FACS CantoTM II flow cytometer (BD Bioscience, CA, United States; previously described in PMID: 8404602). The blood samples were stained with antibodies as follows: Pcy5-conjugated anti-CD3, FITC-conjugated anti-CD4, P-phycoerythrin-conjugated anti-CD8 (BD Biosciences, CA, United States), and PE-conjugated anti-CD16/CD56 (Beckman Coulter, CA, United States). These tests were all carried out in triplicate using the same batch of kits.

Fecal Bacterial Population Determination

This study examined 10 common bacteria. *Faecalibacterium prausnitzii, Clostridium Cluster IV*, and *Eubacterium rectale* are butyrate producers (26–28). Sodium butyrate upregulates the level of brain-derived neurotrophic factor (BDNF) in the damaged brain (29). Levels of BDNF in the brain and serum are decreased in depressed patients (30). Thus, the fluctuation of gut *Faecalibacterium prausnitzii, Clostridium Cluster IV*, and *Eubacterium rectale* populations is responsible for the mood swing. *Enterococcus faecalis* is conditioned pathogen, and its metabolite, metalloprotease, is associated with the chronic intestinal inflammation (31). *Lactic acid bacteria* produces lactic acid. A peripheral intervention of lactate contributed to antidepressant-like effects with changes of epigenetics in hippocampus (32). Bifidobacteria is beneficial for the gut barrier, colonic immune system, and intestinal cell proliferation (33). *Enterobacter spp* have emerged as an important cause of nosocomial infections in clinic (34). Hence, we analyzed *Faecalibacterium prausnitzii, Clostridium Cluster IV, Eubacterium rectale, Enterococcus faecalis, Lactic acid bacteria,* and *Bifidobacteria* populations in feces of BD subjects. We also included *Bacteroides-Prevotella group, Clostridium Clusters I*, and *Atopobium Cluster* for population analysis. All of these bacteria were compared with those of HCs.

B/E, the gut *Bifidobacteria* to *Enterobacteriaceae* ratio, used to describe the microbial colonization resistance against pathogenic bacteria of the bowel (35–37). Its validity is widely accepted by researchers (36, 38, 39). The concept of colonization resistance (CR) was first put forward in 1971 by van der Waaij D et al. to describe the resistance that small amount of ingested Enterobacteriaceae was hard to colonize in animal intestinal tract (37). They describe CR as the endogenous anaerobic fraction of the intestinal microflora (37). Then, it was discussed again in 1992 by van der Waaij D (35). Based on this, researchers in State Key Laboratory for Diagnosis and Treatment of Infectious Diseases, First Affiliated Hospital, Zhejiang University School of Medicine, Zhongwen Wu et al. put forward a new index called B/E ratio to quantify microbial colonization resistance of the bowel (40). They also use it to evaluate the liver disease progression in a study reported in 2011 by Haifeng Lu, who is also a researcher in this laboratory (38). In 2004, B/E was used

in an intestinal microecology study in irritable bowel syndrome patients (36). In 2018, B/E was used in a research studying how green tea polyphenols modulate gut microbiota (39). Therefore, in our study, the use of B/E is a new and rational attempt.

The fecal samples were divided into small samples in smaller tubes and were freshly preserved at -80°C within 30 min of defecation. DNA was extracted from the feces and precipitates with the Qiagen Stool Kit (Qiagen, Hilden, Germany), according to a modified protocol for cell lysis (41). DNA integrity was checked by agarose gel electrophoresis and UV-light imaging with ethidium bromide staining (38).

Though the sequencing of ribosomal targets using a single or limited set of primers is a more standard way to characterize the microbiota, qPCR and immunological techniques would be more suitable for clinical use. Therefore, we chose qPCR and immunological techniques to investigate 10 bacterial populations in the feces.

The process of qPCR was the same as the previous manipulations [see Lu et al. (38)]. The primers for qPCR were referenced from earlier studies (**Table 1**). All oligonucleotide primers were synthesized by TAKARA (Dalian, China).

NIRS Measurement

The activation task in this study was the verbal fluency task, which was similar to that used by Suto et al. in 2004 (45). Patients experienced a 30-s pretask baseline, 60-s activation task, and 70-s posttask baseline. For the pre and postbaseline periods, the individuals were instructed to consecutively repeat a train of numbers as follows: 1, 2, 3, 4, and 5. During the activation period, the individuals were instructed to generate as many Chinese terms as possible with specific initial Chinese characters. There were three sets of initial Chinese characters ("tian," "da," and "bai"), and every character changed every 20 s. The performance was determined by the number of correct terms generated by participants during the activation period.

The NIRS system was a 52-channel one (ETG-4000; Hitachi Medical Co., Tokyo, Japan). A total of 33 probes consisted of 52 channels and covered the bilateral prefrontal and temporal regions (**Figure 1**). Among the 33 probes, there were 16 light emitters and 17 detectors with interoptrodes. Relative changes in oxy-Hb and deoxy-Hb were measured using two wavelengths (695 nm and 830 nm) of infrared light, based on the modified Beer-Lambert law (46–48). The temporal resolution was 0.1 sec. The distance between pairs of source-detector probes was set at 3.0 cm and the measured area involved by a pair of source-detector probes was defined as one "channel." This machine is assumed to measure a "channel" at a depth of 2-3 cm from the scalp (i.e., the surface of the cerebral cortex).

The data was analyzed using the "integral mode" to examine the task-related activation. The pretask baseline was determined by the mean over a 10-s period instantly prior to the task period, and the posttask baseline was determined by the mean over the last 10 s of the posttask period. Linear fitting was performed between the two baseline datasets.

Both increased concentrations of oxygenated (oxy-Hb) and deoxygenated hemoglobin (deoxy-Hb) in micro-blood vessels reflected the cortical activation, and this was confirmed by comparing to other methods such as PET, SPECT, and functional MRI (45). The prefrontal function of bipolar patients is off-normal (49–52). Therefore, we took the changed absolute value of mean prefrontal oxy-Hb (deoxy-Hb) concentration, [oxy-Hb], to represent the prefrontal function. [oxy-Hb] was recorded during the 60-s task period. B/E, as a representative of the microbial colonization resistance, indicates the ability against pathogenic bacteria of the bowel. It is a character of gut microecological balance. As a growing body of evidences suggest the effects of gut microbiota on bipolar pathogenesis and refer to the brain-gut axis disturbance, we tried to connect gut microbiota to prefrontal function. We creatively postulated a parameter called brain-gut coefficient of balance (B-G_{CB}) to assess the brain-gut correlations integrally. B-G_{CB} referred to the ratio of [oxy-Hb]/(B/E).

TABLE 1 | Primers used in the study.

Target group	Sequence (5′–3′)	Annealing temperature (°C)	References
Faecalibacterium prausnitzii	GATGGCCTCGCGTCCGATTAG CCGAAGACCTTCTTCCTCC	58	(41)
Enterococcus faecalis	AACCTACCCATCAGAGGG GACGTTCAGTTACTAACG	57	(41)
Bacteroides–Prevotella group	GAAGGTCCCCCACATTG CAATCGGAGTTCTTCGTG	56	(41)
Lactic acid bacteria	AGCAGTAGGGAATCTTCCA ATTYCACCGCTACACATG	58	(41)
Bifidobacterium genus	GGGTGGTAATGCCGGATG TAAGCCATGGACTTTCACACC	59	(41)
Clostridium cluster IV	GCACAAGCAGTGGAGT CTTCCTCCGTTTTGTCAA	50	(42)
Clostridium clusters I	TACCHRAGGAGGAAGCCAC GTTCTTCCTAATCTCTACGCAT	63	(43)
Eubacterium rectale	CGGTACCTGACTAAGAAGC AGTTT(C/T) ATTCTTGCGAACG	55	(44)
Atopobium cluster	GGGTTGAGAGACCGACC CGGRGCTTCTTCTGCAGG	55	(42)
Enterobacteriaceae	CATTGACGTTACCCGCAGAAGAAGC CTCTACGAGACTCAAGCTTGC	63	(41)

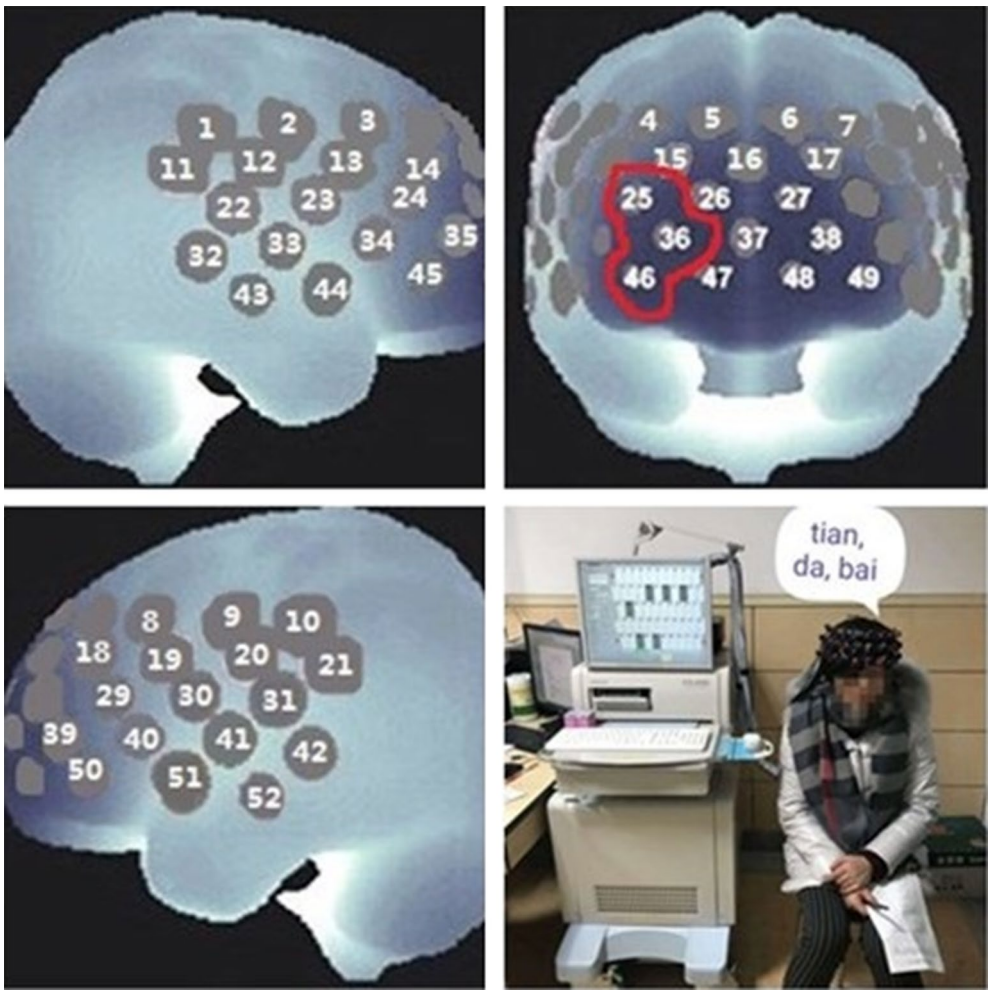

FIGURE 1 | Near-infrared spectroscopy (NIRS) measurement. In this study, the [oxy-Hb] of the prefrontal cortex was examined by channel 25, channel 36, and channel 46, and the average was used as representative.

Statistical Analysis

Statistical analysis was conducted using the SPSS 19.0 statistical software (IBM, IL, United States). All significance levels were two-tailed.

To compare the socio-demographic and clinical profiles, the χ^2 test was applied to categorical variables, and analysis of variance (ANOVA) was used for the continuous variables.

To compare the gut bacterial populations between patients and HCs, ANOVA was used to test the gut microbiota differences. Once the ANOVA was significant, the effects of gender, BMI, age, education, and smoking were tested by adding these variables to the one-way analysis of covariance (ANCOVA). The same method was used for [oxy-Hb] comparison between groups.

For the baseline data of the BD group, correlation analysis among the T lymphocyte subsets, bacterial populations, and the MADRS score was performed. Before correlation analysis, each parameter was tested normality using Kolmogorov-Smirnov test with the correction of Lilliefors. Those abnormal distributed results were logarithmically transformed and then tested for normality again. The outliers were detected by box plots (95% confidence interval) and excluded. Pearson correlations were calculated for normally distributed data, and Spearman correlations were used for data that were not normally distributed. Bonferroni correction was used during the multiple comparisons.

The relationships between the $\log_{10}$ (B-G_{CB}) and the severity of depression (MADRS score), the T lymphocyte subsets were explored using Pearson correlation analysis.

To analyze the therapeutic effect of four weeks' treatment of quetiapine, the Mann-Whitney U test was used to compare the baseline and the posttreatment data. Every gut bacterial population was analyzed. Correlation analyses were performed between the declination rate of the MADRS score (the percentage of change from baseline to the end of the study) and the difference value of each bacterial population (or the difference values between the logarithmically transformed data) in order to determine the clinical predictive value of the gut flora to BD.

Gender differences in the gut microbiota in either of the groups were examined using the Mann-Whitney U test.

RESULTS

Socio-Demographic and Clinical Characteristics

Comparing patients and HCs, no significant difference was found in age, gender, marital status, BMI, and handedness ($p > 0.1$), but the education level in the BD group was significantly different from that in HCs ($p = 0.002$). The other clinical information of the BD group was shown in **Table 2**. Socio-demographic information of patients who finished the follow up was shown in **Table 3**.

TABLE 2 | The socio-demographic and clinical profiles of participants (mean ± SD).

	BD (n = 36, BD-I: n = 10, BD-II: n = 26)	HCs (n = 27)	χ^2 or F	df	p
Age	32.64 ± 10.643	28.89 ± 11.095	1.847	1	0.179$^{\Delta}$
Gender, Male. %	58.33	55.56	0.049	1	0.825$^{\Delta}$
Marriage, Married. %	61.11	44.44	1.725	1	0.189$^{\Delta}$
Education (>12years) %	44.44	81.48	10.364	1	0.002 *$^{\Delta}$
Right-handed. %	97.22	100	0.043	1	0.836$^{\Delta}$
BMI	22.16 ± 3.631	21.84 ± 3.092	0.135	1	0.714$^{\Delta}$
BMI > 25 (overweight)	25.00%	18.52%			
Onset age	26.06 ± 12.488	–			
Duration of illness (year)	7.40 ± 7.659	–			
Number of episodes	5.83 ± 4.583	–			
N1	17				
N2	17				
N3	19				
N4	16				

$p < 0.05$ (two-tailed). $^{\Delta}$Independent-samples t test. N1, number of patients who finished one-month follow up; N2, number of BD patients who was drug naive; N3, number of patients whose medications had been stopped for more than 3 months. N4, number of patients who finished the baseline NIRS measurement; BD, bipolar depression. BD¬I: type I bipolar depression. BD-II: type II bipolar depression; BMI, body mass index; HCs, healthy controls. SD, standard deviation.

TABLE 3 | Socio-demographic information of patients who finished the follow up.

Items	Mean ± SD	Items	Percentage (%)
Age	33.59 ± 8.860	**Gender, Male.**	52.94
BMI	23.03 ± 3.757	**Marriage, Married.**	70.59
Onset age	26.24 ± 9.045	**BMI > 25 (overweight)**	29.41%
Duration of illness (year)	7.32 ± 6.915	**Education (>12years)**	47.06
Number of episodes	4.47 ± 2.294	**Right-handed.**	100
Total number	17		

BMI, body mass index; SD, standard deviation.

Comparing Gut Microbiota Between the BD Patients and HCs

The counts of *Faecalibacterium prausnitzii*, *Bacteroides–Prevotella* group, *Atopobium Cluster*, *Enterobacter spp*, and *Clostridium Cluster IV* were significantly higher in the BD group compared with HCs ($p = 0.030$, $p < 0.001$, $p < 0.001$, $p < 0.001$, and $p < 0.001$, respectively, **Table 4**). Besides, the B/E ratio of the BD group was significantly lower than HCs ($p = 0.001$, **Table 4**).

The New Conception of the Brain-Gut Coefficient of Balance and Related Results

The $\log_{10}$ B-G_{CB} was positively correlated with the $CD3^+$ T cell proportion ($r = 0.540$, $p = 0.038$, **Figure 2**).

Correlations Among Baseline Parameters Within the BD Group

We found that the $CD3^+$ T cell proportion was positively correlated with $\log_{10}$ *Enterobacter spp* count (Bonferroni corrected p = 0.048, **Table 5**).

TABLE 4 | Bacterial populations in bipolar depression patients and healthy controls.

Bacteria	BD	HCs	F	df	p	p*
$\log_{10}$ Faecalibacterium prausnitzii	7.01 ± 1.036	6.11 ± 0.892	2.545	6	0.001	0.030
$\log_{10}$ Enterococcus faecalis	4.17 ± 1.265	4.55 ± 1.377	.653	6	0.262	0.688
$\log_{10}$ Bacteroides–Prevotella group	8.70 ± 0.768	6.65 ± 1.139	14.372	6	<0.001	<0.001
$\log_{10}$ Lactic acid bacteria	4.12 ± 1.029	4.18 ± 1.239	.414	6	0.850	0.867
$\log_{10}$ Bifidobacteria	4.71 ± 1.187	4.95 ± 1.182	2.080	6	0.437	0.070
$\log_{10}$ Clostridium Clusters I	5.18 ± 1.048	4.89 ± 0.921	1.373	6	0.265	0.241
$\log_{10}$ Eubacterium rectale	6.07 ± 1.196	5.52 ± 0.804	1.374	6	0.045	0.241
$\log_{10}$ Atopobium Cluster	5.74 ± 0.758	4.96 ± 0.907	5.655	6	<0.001	< 0.001
$\log_{10}$ Enterobacter spp	6.07 ± 0.943	5.03 ± 0.746	6.137	6	<0.001	< 0.001
$\log_{10}$ (B/E)	–1.39 ± 1.157	–0.08 ± 1.005	4.381	6	<0.001	0.001
Clostridium Cluster IV count	8.54*10^7 ± 1.142*10^8	1.62*10^5 ± 1.249*10^5			<0.001△	

Indicates adjusted p using analysis of covariance (ANCOVA), with adjustments made for age, gender, education, smoking, and body mass index (BMI). △Indicates Mann-Whitney U test for data that were not normally distributed. BD, bipolar depression; HCs, healthy controls; B/E, Bifidobacteria to Enterobacteriaceae ratio.

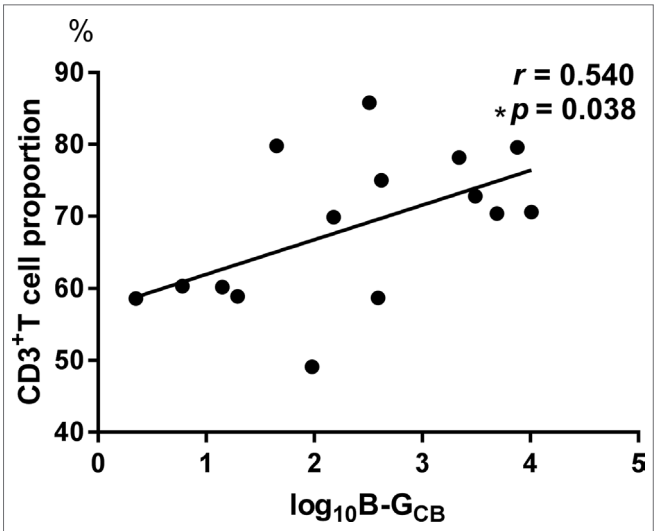

FIGURE 2 | The log10 B-G_{CB} was positively correlated with the CD3+ T cell proportion (r = 0.540, p = 0.038).

Therapeutic Effect of Quetiapine

Posttreatment results were different from the baseline data (see **Figure 3**). However, no significant correlations were found between the declination rate of the MADRS scores and the bacteria quantity variations.

Gender Difference in the Gut Microbiota

Bacteroides-Prevotella group count showed a gender difference in the BD group (see **Figure 4**) according to the baseline data. However, in the HCs, none of the bacterial populations showed any gender difference (**Table 6**).

DISCUSSION

We found that among patients with BD: (1) counts of *Faecalibacterium prausnitzii*, *Bacteroides-Prevotella group*, *Atopobium Cluster*, *Enterobacter spp*, and *Clostridium Cluster IV* were significantly increased relative to HCs, whereas microbial colonization resistance was significantly decreased; (2) after treatment, populations of *Bifidobacteria* and *Eubacterium rectale* rebounded, and microbial colonization resistance recovered along with the decline of MADRS score; (3) B-G_{CB} was positively correlated with $CD3^+$ T cell proportion; and (4) $\log_{10}$ (*Enterobacter spp* count) was positively correlated with $CD3^+$ T cell proportion.

The gut microbiota composition in BD patients was different from that in HCs and was associated with illness severity and immune alterations. The expansion of *Bacteroides-Prevotella* group and Enterobacter spp indicates the dysbiosis of gut microbiota (53). The decrease of B/E indicated a weakened microbial colonization resistance. These results suggested that gut microecology was unbalanced in BD patients. The expansion of conditioned pathogen (e.g., *Enterobacter* spp) and pathogen (e.g., *Bacteroides-Prevotella* group) reduced the ability of intestine to resist exogenous pathogen. Former research finds a decreased cytotoxic cell level and an increased plasma IL-6 level (54) in bipolar patients. The immune activation in bipolar disorder patients is probably part of the results of the gut dysbiosis. This study found that Log_{10} (*Enterobacter spp* count) was positively correlated with $CD3^+$ T cell proportion, indicating that *Enterobacter spp* expansion caused immune activation. A previous study shows a decrease in *Faecalibacterium* fractional representation in bipolar patients (16). However, our result found an elevated *Faecalibacterium prausnitzii* count. It seemed conflictive. The study design of Evans et al. was different from this study. Evans et al. recruited bipolar patients who were taking more than one psychotropic medication, whereas in this study, our patients had never received any psychotropic medcation or had stopped medication for more than 3 months. *Faecalibacterium prausnitzii* is a butyrate producer and has anti-inflammatory actions in colitis (55, 56). It helps to maintain the gut microbial balance. The discrepant results are probably associated with the different disease course and medication use. In this study, *Faecalibacterium prausnitzii* was

TABLE 5 | Correlations among baseline parameters within the BD group.

	$CD3^+$ T cell *p (r)*	$CD4^+$ T cell	$CD8^+$ T cell	NK cell	MADRS
Log_{10} Faecalibacterium prausnitzii	0.364(-0.158)	0.848 (0.034)	0.164 (-0.241)	0.551 (-0.104)	0.41 (0.141)
Log_{10} Enterococcus faecalis	0.518(0.113)	0.651 (-0.079)	0.127 (0.263)	0.408 (-0.144)	0.67 (-0.074)
Log_{10} Bacteroides–Prevotella group	0.488(-0.121)	0.538 (0.108)	0.091 (-0.29)	0.535 (-0.109)	0.343 (-0.163)
Log_{10} Lactic acid bacteria	0.665(0.076)	0.478 (0.124)	0.516 (-0.113)	0.77 (-0.051)	0.724 (0.061)
Log_{10} Bifidobacteria	0.743(-0.057)	0.57 (-0.1)	0.798 (0.045)	0.253 (0.198)	0.089 (0.288)
Log_{10} Clostridium Clusters I	0.126(-0.264)	0.536 (-0.108)	0.369 (-0.157)	0.975 (0.006)	0.754 (-0.054)
Log_{10} Eubacterium rectale	0.32(-0.173)	0.458 (0.13)	0.033 (-.362*)	0.576 (-0.098)	0.652 (-0.078)
Log_{10} Atopobium Cluster	0.619(0.087)	0.221 (0.212)	0.32 (-0.173)	0.077 (-0.303)	0.683 (0.071)
Log_{10} Enterobacter spp	0.004(.477**) 0.048△ *	0.364 (0.158)	0.027 (.374*) 0.324△	0.356 (-0.161)	0.493 (0.118)
Log_{10} Clostridium Cluster IV count	0.185(-0.229)	0.399(0.147)	0.045(-.341*) 0.54△	0.667(-0.075)	0.819(0.039)
MADRS	0.501(0.118)	0.849(-0.033)	0.658(0.077)	0.156(-0.245)	/

*The unit of measure is p (r). We used Spearman correlations for LgClostridium Cluster IV count, and the others used Pearson correlations. p values < 0.05 are in bold. *p < 0.05. **p < 0.01. △ Corrected p, refers to Bonferroni corrected p. BD, bipolar depression; MADRS, the Montgomery-Asberg depression rating scale; NK cell, natural killer cell.*

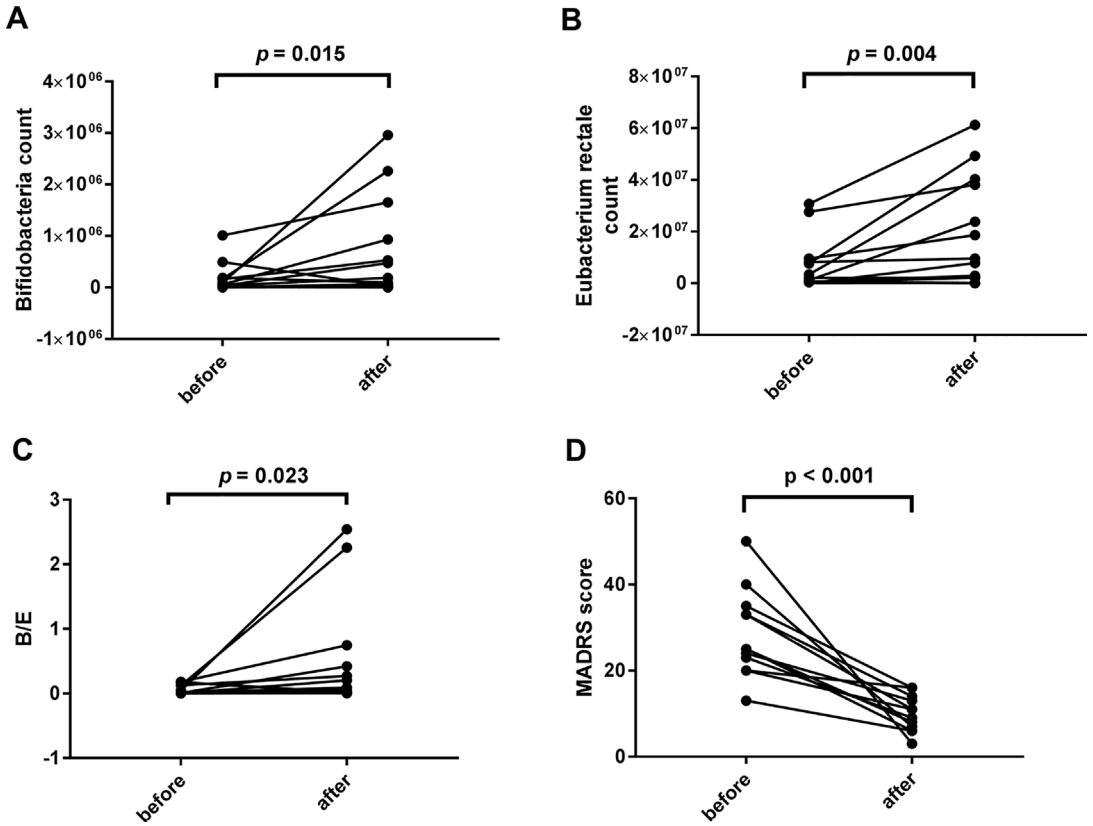

FIGURE 3 | Comparisons between the baseline and the posttreatment data of bacterial populations and the Montgomery-Asberg depression rating scale (MADRS) score. Significant increases were found in the levels of *Bifidobacteria* count (1.33*10^5 ± 2.578*10^5 vs. 5.50*10^5 ± 8.968*10^5, $p = 0.015$), *Eubacterium rectale* count (5.58*10^6 ± 9.398*10^6 vs. 3.49*10^7 ± 7.955*10^7, $p = 0.004$), and B/E (0.0594 ± 0.07385 vs. 0.446 ± 0.8213, $p = 0.023$) **(A–C)**. The decrease of the MADRS score indicates a significant improvement in depressive symptoms (28.42 ± 10.166 vs. 10.00 ± 4.200, $p < 0.001$, **D**).

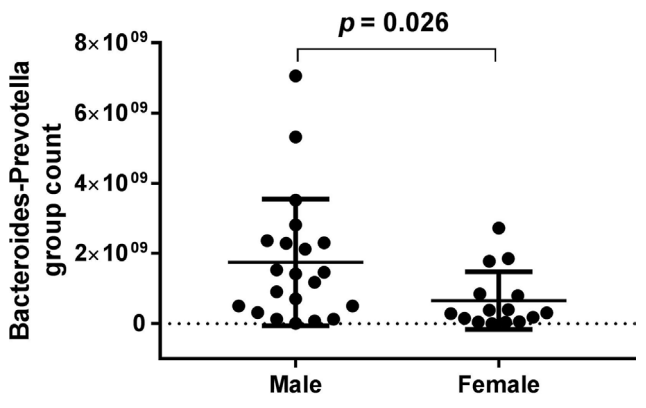

FIGURE 4 | *Bacteroides-Prevotella* group count showed a gender difference in the bipolar depression (BD) group (male: 1.75*10^9 ± 1.801*10^9, female: 6.56*10^8 ± 8.213*10^8, $p = 0.026$) according to the baseline data.

supposed to be in a compensatory state without medication influence. *Clostridium Cluster IV* is another butyrate-producing bacteria (27) and belongs to beneficial bacteria. Therefore, in this study, beneficial bacteria populations expanded parallelly with pathogenic bacteria populations. This indicated that, in the early stage of the disease, gut bacteria changed follow a compensatory mechanism. They multiplied to protect gut resistance against the pathogen proliferation. The multiplied proportion was closely related to depressive severity.

The one-month quetiapine treatment was effective. The anaerobic *Bifidobacteria* and *Eubacterium rectale* proliferated during the one-month treatment. Microbial colonization resistance was determined by endogenous anaerobic bacteria fraction in the intestine (37). Anaerobic *Bifidobacteria* and *Eubacterium rectale* populations rebounded, suggesting the recovery of the microbial colonization resistance. This conclusion was supported by the posttreatment elevation of B/E.

$B\text{-}G_{CB}$ is associated with immune disturbance when the brain-gut balance is broken. This study found that $B\text{-}G_{CB}$ was positively associated with $CD3^+$ T cell proportion. This suggested that BD subjects experienced an immune activation mediated by $CD3^+$ T cell. As a T-cell co-receptor, CD3 helps to activate both the cytotoxic T-cells and T helper cells and is involved in signaling transduction between the inner and outside cytomembrane.

Similar to previous research findings, our study found that alterations in the composition of the gut microbiota may be

TABLE 6 | Gender difference in the gut microbiota.

Bacteria	Group	Male (mean ± SD)	Female (mean ± SD)	*p*
Faecalibacterium prausnitzii	BD	3.29*10^7 ± 3.213*10^7	2.99*10^7 ± 3.380*10^7	0.619
	HCs	6.26*10^6 ± 1.134*10^7	9.47*10^6 ± 2.687*10^7	0.961
Enterococcus faecalis	BD	7.13*10^5 ± 1.976*10^6	4.14*10^4 ± 9.049*10^4	0.098
	HCs	1.32*10^6 ± 4.546*10^6	1.76*10^7 ± 6.059*10^7	0.329
Bacteroides–Prevotella group	BD	1.75*10^9 ± 1.801*10^9	6.56*10^8 ± 8.213*10^8	0.026*
	HCs	5.33*10^7 ± 9.105*10^7	2.35*10^7 ± 5.649*10^7	0.306
Lactic acid bacteria	BD	2.20*10^5 ± 5.211*10^5	5.31*10^4 ± 1.139*10^5	0.328
	HCs	2.02*10^6 ± 7.631*10^6	5.39*10^6 ± 1.864*10^7	0.922
Bifidobacteria	BD	5.43*10^5 ± 1.118*10^6	1.86*10^5 ± 2.596*10^5	0.531
	HCs	1.92*10^6 ± 3.356*10^6	1.51*10^5 ± 1.760*10^5	0.435
Clostridium Cluster IV	BD	1.11*10^8 ± 1.351*10^8	4.90*10^7 ± 6.410*10^7	0.061
	HCs	1.79*10^5 ± 1.354*10^5	1.42*10^5 ± 1.128*10^5	0.661
Clostridium Clusters I	BD	1.33*10^6 ± 2.465*10^6	5.87*10^5 ± 1.387*10^6	0.132
	HCs	9.59*10^5 ± 1.742*10^6	6.78*10^4 ± 7.702*10^4	0.157
Eubacterium rectale	BD	1.24*10^7 ± 2.782*10^7	6.93*10^6 ± 1.729*10^7	0.136
	HCs	2.41*10^6 ± 6.161*10^6	1.31*10^6 ± 2.904*10^6	0.770
Atopobium Cluster	BD	1.48*10^6 ± 1.686*10^6	1.61*10^6 ± 2.358*10^6	0.553
	HCs	8.41*10^5 ± 1.163*10^6	1.05*10^5 ± 1.389*10^5	0.088
Enterobacter spp	BD	5.54*10^6 ± 1.035*10^7	6.68*10^6 ± 1.179*10^7	0.748
	HCs	3.98*10^5 ± 5.201*10^5	2.23*10^5 ± 3.369*10^5	0.770
B/E	BD	0.563 ± .9231	0.096 ± 0.1467	0.344
	HCs	6.623 ± 10.8462	2.005 ± 3.0012	0.329

$p < 0.05$ (two-tailed). B/E, Bifidobacteria to Enterobacteriaceae ratio. SD, standard deviation.

associated with bipolar disorder and its severity (16). These BD specific bacteria can be used as screening biomarkers in clinic. *Bifidobacteria, Eubacterium rectale*, and B/E can be used as biomarkers to assess therapeutic effects. Our results found that $CD3^+$ T cell mediated immune activation in BD patients. This points to future treatment with anti-inflammatory agents and probiotics in this population. Future studies are needed to confirm the utility of the $B\text{-}G_{CB}$ in evaluating the course and treatment response in BD.

Several limitations to this study should be noted. First, the sample size is relatively small. This is not only a major limitation for the validity assessment of our findings but also for the subgroup analysis among different age groups. In this study, the wide age range of patients was downwards of 14 years old and upwards of 57 years old. It is clear that the gut microbiota of older adults differs from that of young people (57). Therefore, a larger sample size is required in future studies. Similarly, diet is an important factor that shapes the composition of gut microbiota (58). However, this report did not include any information regarding to diet. It is too difficult to analyze the impact of diet base on the small sample size and the single institution of patient source. Diet analysis is more feasible for multiregional cooperation studies. Second, 16S and metagenome sequencing are more suitable to explore the whole diversity of gut microbiota. The use of qPCR is another major limitation in this study. This should be improved in the following studies. Third, the patient group did not receive placebo treatment as a control. *Eubacterium rectale* count, *Bifidobacteria* count, and B/E (*Bifidobacteria* to *Enterobacteriaceae* ratio, microbial colonization resistance) elevated. It is hard to distinguish whether the elevation is due to the quetiapine treatment or the natural disease course. Fourth, we did not collect blood and fecal samples of HCs at four-week treatment. This study did not compare fecal microbiota of BD group and HCs at four-week treatment. Therefore, this research could not explain whether the four-week treatment makes the gut microbiota of patients approaching that of HCs. Fifth, BMI of BD group was lacking at four-week treatment. Therefore, this study failed to help patients' BMI management during quetiapine treatment. Exogenous bacteria intake may benefit the patients' BMI. Further study is needed to find the exact bacteria associated with drug-induced obesity. Atypical antipsychotics treatment causes weight gain and decreases the richness of gut microbiota (19, 59, 60). This is more remarkable in females and is closely related to drug dose (19, 59). High dose impacts more bacteria species. Olanzapine treatment using 2 mg/kg increases *Firmicutes* level, decreases *Actinobacteria* level in female rats, and reduces *Proteobacteria* level in both sexes (59). Olanzapine treatment using 4 mg/kg reduces both *Actinobacteria* and *Proteobacteria* levels in female rats, increases *Firmicutes* level, and decreases *Bacteriodetes* level in both sexes (59). In a human study, atypical antipsychotics reduces species diversity of gut bacteria in female patients. The involved genera includes *Lachnospiraceae*, *Akkermansia*, and *Sutterella* (19). Therefore, this study could not clarify the reason why *Eubacterium rectale* count, *Bifidobacteria* count, and B/E elevated. It is probably because of the recovery of the disease or just the influence of quetiapine. The fecal re-examination is needed for the follow-up BD patients with placebo treatment or who reject treatments.

In summary, this study found that the composition of the gut microbiota in BD subjects was altered. The alteration of gut microbiota was associated with immune activation and linked to brain function. Quetiapine treatment was effective for the remission of depression and influenced the gut microbiota in patients. Further studies are required to confirm our findings and achieve more clinically useful results.

DATA AVAILABILITY STATEMENT

All datasets generated for this study are included in the article/supplementary material.

ETHICS STATEMENT

The studies involving human participants were reviewed and approved by Ethics Committee of the First Affiliated Hospital, Zhejiang University School of Medicine. Written informed consent to participate in this study was provided by the participants' legal guardian/next of kin.

AUTHOR CONTRIBUTIONS

SH designed the trail and directed the entire study. YX, ZL directed the study togethor with SH. QL performed the study, analyzed the results, and wrote the manuscript. HL and HZ tested the gut microbiome. CN modified the manuscript. ZW helped with the manuscript revision and the data analysis. All authors made substantive contribution to this paper and approved the final manuscript.

FUNDING

This study was supported by the grants of the National Natural Science Foundation of China (81671357, 81971271 to SH), the National Natural Science Foundation of China (81771474 to YX), the National Key Research and Development Program of China (No. 2016YFC1307104 to SH), the general project supported by Hangzhou Health Commission (2015A32 to KD) and Science and Technology Department of Zhejiang Province (2017C37037 to NW).

REFERENCES

1. Sajatovic M. Bipolar disorder: disease burden. *Am J Manage Care* (2005) 11:S80–84.
2. Ghaemi S, Sachs G, Chiou A, Pandurangi A, Goodwin K. Is bipolar disorder still underdiagnosed? Are antidepressants overutilized? *J Affect Disord* (1999) 52:135–44. doi: 10.1016/S0165-0327(98)00076-7
3. Phillips ML, Kupfer DJ. Bipolar disorder diagnosis: challenges and future directions. *Lancet (London, England)* (2013) 381:1663–71. doi: 10.1016/S0140-6736(13)60989-7
4. Rhee SH, Pothoulakis C, Mayer EA. Principles and clinical implications of the brain-gut-enteric microbiota axis. *Nat Rev Gastroenterol Hepatol* (2009) 6:306–14. doi: 10.1038/nrgastro.2009.35
5. El Aidy S, Dinan TG, Cryan JF. Gut Microbiota: The conductor in the orchestra of immune-neuroendocrine communication. *Clin Ther* (2015) 37:954–67. doi: 10.1016/j.clinthera.2015.03.002
6. Fung TC, Olson CA, Hsiao EY. Interactions between the microbiota, immune and nervous systems in health and disease. *Nat Neurosci* (2017) 20:145–55. doi: 10.1038/nn.4476
7. Vinolo MA, Rodrigues HG, Hatanaka E, Sato FT, Sampaio SC, Curi R. Suppressive effect of short-chain fatty acids on production of proinflammatory mediators by neutrophils. *J Nutr Biochem* (2011) 22:849–55. doi: 10.1016/j.jnutbio.2010.07.009
8. Rooks MG, Garrett WS. Gut microbiota, metabolites and host immunity. *Nature reviews. Immunology* (2016) 16:341–52. doi: 10.1038/nri.2016.42
9. Bravo JA, Forsythe P, Chew MV, Escaravage E, Savignac HM, Dinan TG, et al. Ingestion of Lactobacillus strain regulates emotional behavior and central GABA receptor expression in a mouse *via the* vagus nerve. *Proc Natl Acad Sci U S A* (2011) 108:16050–5. doi: 10.1073/pnas.1102999108
10. Dockray GJ. Enteroendocrine cell signalling *via the* vagus nerve. *Curr Opin Pharmacol* (2013) 13:954–8. doi: 10.1016/j.coph.2013.09.007
11. Jenkins TA, Nguyen JC, Polglaze KE, Bertrand PP. Influence of tryptophan and serotonin on mood and cognition with a possible role of the gut-brain axis. *Nutrients* (2016) 8. doi: 10.3390/nu8010056
12. Schmidt K, Cowen PJ, Harmer CJ, Tzortzis G, Errington S, Burnet PW. Prebiotic intake reduces the waking cortisol response and alters emotional bias in healthy volunteers. *Psychopharmacology* (2015) 232:1793–801. doi: 10.1007/s00213-014-3810-0
13. Bellavance MA, Rivest S. The HPA - immune axis and the immunomodulatory actions of glucocorticoids in the brain. *Front Immunol* (2014) 5:136. doi: 10.3389/fimmu.2014.00136
14. McIntyre RS, Subramaniapillai M, Shekotikhina M, Carmona NE, Lee Y, Mansur RB, et al. Characterizing the gut microbiota in adults with bipolar disorder: a pilot study. (2019) 1–8. doi: 10.1080/1028415X.2019.1612555
15. Painold A, Morkl S. A step ahead: Exploring the gut microbiota in inpatients with bipolar disorder during a depressive episode. *Bipolar Disord* (2019) 21:40–9. doi: 10.1111/bdi.12682
16. Evans SJ, Bassis CM, Hein R, Assari S, Flowers SA, Kelly MB, et al. The gut microbiome composition associates with bipolar disorder and illness severity. *J Psychiatr Res* (2017) 87:23–9. doi: 10.1016/j.jpsychires.2016.12.007
17. Coello K, Hansen TH, Sorensen N, Munkholm K, Kessing LV, Pedersen O, et al. Gut microbiota composition in patients with newly diagnosed bipolar disorder and their unaffected first-degree relatives. *Brain Behav Immun* (2019) 75:112–8. doi: 10.1016/j.bbi.2018.09.026
18. Aizawa E, Tsuji H, Asahara T, Takahashi T, Teraishi T, Yoshida S, et al. Bifidobacterium and lactobacillus counts in the gut microbiota of patients with bipolar disorder and healthy controls. *Front Psychiatry* (2018) 9:730. doi: 10.3389/fpsyt.2018.00730
19. Flowers SA, Evans SJ, Ward KM, McInnis MG, Ellingrod VL. Interaction between atypical antipsychotics and the gut microbiome in a bipolar disease cohort. *Pharmacotherapy* (2017) 37:261–7. doi: 10.1002/phar.1890
20. Hu S, Li A, Huang T, Lai J, Li J, Sublette ME, et al. Gut microbiota changes in patients with bipolar depression. *Adv Sci (Weinh)* (2019) 6:1900752. doi: 10.1002/advs.201900752
21. Montgomery SA, Asberg M. A new depression scale designed to be sensitive to change. *Br J Psychiatry J Ment Sci* (1979) 134:382–9. doi: 10.1192/bjp.134.4.382
22. Liu J, Xiang YT, Lei H, Wang Q, Wang G, Ungvari GS, et al. Guidance on the conversion of the Chinese versions of the Quick Inventory of Depressive Symptomatology-Self-Report (C-QIDS-SR) and the Montgomery-Asberg Scale (C-MADRS) in Chinese patients with major depression. *J Affect Disord* (2014) 152-154:530–3. doi: 10.1016/j.jad.2013.09.023
23. Young RC, Biggs JT, Ziegler VE, Meyer DA. A rating scale for mania: reliability, validity and sensitivity. *Br J Psychiatry J Ment Sci* (1978) 133:429–35. doi: 10.1192/bjp.133.5.429
24. Yatham LN, Kennedy SH. Canadian Network for Mood and Anxiety Treatments (CANMAT) and International Society for Bipolar Disorders (ISBD) 2018 guidelines for the management of patients with bipolar disorder. *Bipolar Disord* (2018) 20:97–170. doi: 10.1111/bdi.12609
25. Suttajit S, Srisurapanont M, Maneeton N, Maneeton B. Quetiapine for acute bipolar depression: a systematic review and meta-analysis. *Drug Design Dev Ther* (2014) 8:827–38. doi: 10.2147/DDDT.S63779
26. Duncan SH, Hold GL, Harmsen HJ, Stewart CS, Flint HJ. Growth requirements and fermentation products of Fusobacterium prausnitzii, and a proposal to reclassify it as Faecalibacterium prausnitzii gen. nov., comb. nov. *Int J Syst Evol Microbiol* (2002) 52:2141–6. doi: 10.1099/00207713-52-6-2141
27. Moens F, De Vuyst L. Inulin-type fructan degradation capacity of Clostridium cluster IV and XIVa butyrate-producing colon bacteria and

their associated metabolic outcomes. *Benef Microbes* (2017) 8:473–90. doi: 10.3920/BM2016.0142
28. Barcenilla A, Pryde SE, Martin JC, Duncan SH, Stewart CS, Henderson C, et al. Phylogenetic relationships of butyrate-producing bacteria from the human gut. *Appl Environ Microbiol* (2000) 66:1654–61. doi: 10.1128/AEM.66.4.1654-1661.2000
29. Kim HJ, Leeds P, Chuang DM. The HDAC inhibitor, sodium butyrate, stimulates neurogenesis in the ischemic brain. *J Neurochem* (2009) 110:1226–40. doi: 10.1111/j.1471-4159.2009.06212.x
30. Castrén E, Kojima M. Brain-derived neurotrophic factor in mood disorders and antidepressant treatments. *Neurobiol Dis* (2017) 97:119–26. doi: 10.1016/j.nbd.2016.07.010
31. Steck N, Hoffmann M, Sava IG, Kim SC, Hahne H, Tonkonogy SL, et al. Enterococcus faecalis metalloprotease compromises epithelial barrier and contributes to intestinal inflammation. *Gastroenterology* (2011) 141:959–71. doi: 10.1053/j.gastro.2011.05.035
32. Carrard A, Elsayed M, Margineanu M, Boury-Jamot B, Fragniere L, Meylan EM, et al. Peripheral administration of lactate produces antidepressant-like effects. *Mol Psychiatry* (2018) 23:392–9. doi: 10.1038/mp.2016.179
33. Picard C, Fioramonti J, Francois A, Robinson T, Neant F, Matuchansky C. Review article: bifidobacteria as probiotic agents – physiological effects and clinical benefits. *Alimentary Pharmacol Ther* (2005) 22:495–512. doi: 10.1111/j.1365-2036.2005.02615.x
34. Chavda KD, Chen L, Fouts DE, Sutton G, Brinkac L, Jenkins SG, et al. Comprehensive genome analysis of carbapenemase-producing enterobacter spp.: New Insights into Phylogeny, Population Structure, and Resistance Mechanisms. *mBio* (2016) 7 (6):e02093–16. doi: 10.1128/mBio.02093-16
35. van der Waaij D. History of recognition and measurement of colonization resistance of the digestive tract as an introduction to selective gastrointestinal decontamination. *Epidemiol Infect* (1992) 109:315–26. doi: 10.1017/S0950268800050317
36. Si JM, Yu YC, Fan YJ, Chen SJ. Intestinal microecology and quality of life in irritable bowel syndrome patients. *World J Gastroenterol* (2004) 10:1802–5. doi: 10.3748/wjg.v10.i12.1802
37. van der Waaij D, Berghuis-de Vries JM, Lekkerkerk L.-v. Colonization resistance of the digestive tract in conventional and antibiotic-treated mice. *J Hygiene* (1971) 69:405–11. doi: 10.1017/S0022172400021653
38. Lu H, Wu Z, Xu W, Yang J, Chen Y, Li L. Intestinal microbiota was assessed in cirrhotic patients with hepatitis B virus infection. Intestinal microbiota of HBV cirrhotic patients. *Microb Ecol* (2011) 61:693–703. doi: 10.1007/s00248-010-9801-8
39. Yuan X, Long Y, Ji Z, Gao J, Fu T, Yan M, et al. Green tea liquid consumption alters the human intestinal and oral microbiome. *Mol Nutr Food Res* (2018) 62:e1800178. doi: 10.1002/mnfr.201800178
40. Wu Z, Li L, Ma W, Yu Y, Chen Y. The new index of intestinal microbial colonization resistance-B/E value. *Zhejiang Prev Med* (2000) 12:4–5. doi: 10.19485/j.cnki.issn1007-0931.2000.07.002
41. Bartosch S, Fite A, Macfarlane GT, McMurdo ME. Characterization of bacterial communities in feces from healthy elderly volunteers and hospitalized elderly patients by using real-time PCR and effects of antibiotic treatment on the fecal microbiota. *Appl Environ Microbiol* (2004) 70:3575–81. doi: 10.1128/AEM.70.6.3575-3581.2004
42. Matsuki T, Watanabe K, Fujimoto J, Takada T, Tanaka R. Use of 16S rRNA gene-targeted group-specific primers for real-time PCR analysis of predominant bacteria in human feces. *Appl Environ Microbiol* (2004) 70:7220–8. doi: 10.1128/AEM.70.12.7220-7228.2004
43. Song Y, Liu C, Finegold SM. Real-Time PCR Quantitation of Clostridia in Feces of Autistic Children. *Appl Environ Microbiol* (2004) 70:6459–65. doi: 10.1128/AEM.70.11.6459-6465.200460
44. Rinttila T, Kassinen A, Malinen E, Krogius L, Palva A. Development of an extensive set of 16S rDNA-targeted primers for quantification of pathogenic and indigenous bacteria in faecal samples by real-time PCR. *J Appl Microbiol* (2004), 97:1166–77. doi: 10.1111/j.1365-2672.2004.02409.x
45. Suto T, Fukuda M, Ito M, Uehara T, Mikuni M. Multichannel near-infrared spectroscopy in depression and schizophrenia: cognitive brain activation study. *Biol Psychiatry* (2004) 55:501–11. doi: 10.1016/j.biopsych.2003.09.008
46. Obrig H, Villringer A. Beyond the visible–imaging the human brain with light. *J Cereb Blood Flow Metab* (2003) 23:1–18. doi: 10.1097/01.WCB.0000043472.45775.29
47. Takamiya A, Hirano J, Ebuchi Y, Ogino S, Shimegi K, Emura H, et al. High-dose antidepressants affect near-infrared spectroscopy signals: A retrospective study. *NeuroImage. Clin* (2017) 14:648–55. doi: 10.1016/j.nicl.2017.02.008
48. Maki A, Yamashita Y, Ito Y, Watanabe E, Mayanagi Y, Koizumi H. Spatial and temporal analysis of human motor activity using noninvasive NIR topography. *Med Phys* (1995) 22:1997–2005. doi: 10.1118/1.597496
49. Chang K, Garrett A, Kelley R, Howe M, Sanders EM, Acquaye T, et al. Anomalous prefrontal-limbic activation and connectivity in youth at high-risk for bipolar disorder. *J Affect Disord* (2017) 222:7–13. doi: 10.1016/j.jad.2017.05.051
50. Miskowiak KW, Kjaerstad HL. The catechol-O-methyltransferase (COMT) Val158Met genotype modulates working memory-related dorsolateral prefrontal response and performance in bipolar disorder. *Bipolar Disord* (2017) 19:214–24. doi: 10.1111/bdi.12497
51. Prisciandaro JJ, Tolliver BK, Prescot AP, Brenner HM, Renshaw PF, Brown TR, et al. Unique prefrontal GABA and glutamate disturbances in co-occurring bipolar disorder and alcohol dependence. *Transl Psychiatry* (2017) 7:e1163. doi: 10.1038/tp.2017.141
52. Siebner HR, Macoveanu J, Ono Y, Kikuchi M, Nakatani H, Murakami M, et al. Prefrontal oxygenation during verbal fluency and cognitive function in adolescents with bipolar disorder type II. *Bipolar Disord* (2017) 25:147–53. doi: 10.1016/j.ajp.2016.11.001
53. Winter SE, Lopez CA, Baumler AJ. The dynamics of gut-associated microbial communities during inflammation. *EMBO Rep* (2013) 14:319–27. doi: 10.1038/embor.2013.27
54. Wu W, Zheng YL, Tian LP, Lai JB, Hu CC, Zhang P, et al. Circulating T lymphocyte subsets, cytokines, and immune checkpoint inhibitors in patients with bipolar II or major depression: a preliminary study. *Sci Rep* (2017) 7:40530. doi: 10.1038/srep40530
55. Miquel S, Martin R, Rossi O, Bermudez-Humaran LG, Chatel JM, Sokol H, et al. Faecalibacterium prausnitzii and human intestinal health. *Curr Opin Microbiol* (2013) 16:255–61. doi: 10.1016/j.mib.2013.06.003
56. Sokol H, Pigneur B, Watterlot L, Lakhdari O, Bermudez-Humaran LG, Gratadoux JJ, et al. Faecalibacterium prausnitzii is an anti-inflammatory commensal bacterium identified by gut microbiota analysis of Crohn disease patients. *Proc Natl Acad Sci U S A* (2008) 105:16731–6. doi: 10.1073/pnas.0804812105
57. O'Toole PW, Jeffery IB. Gut microbiota and aging. *Science (New York, N.Y.)* (2015) 350:1214–5. doi: 10.1126/science.aac8469
58. Conlon MA, Bird AR. The impact of diet and lifestyle on gut microbiota and human health. *Nutrients* (2014) 7:17–44. doi: 10.3390/nu7010017
59. Davey KJ, O'Mahony SM, Schellekens H, O'Sullivan O, Bienenstock J, Cotter PD, et al. Gender-dependent consequences of chronic olanzapine in the rat: effects on body weight, inflammatory, metabolic and microbiota parameters. *Psychopharmacology* (2012) 221:155–69. doi: 10.1007/s00213-011-2555-2
60. Davey KJ, Cotter PD, O'Sullivan O, Crispie F, Dinan TG, Cryan JF, et al. Antipsychotics and the gut microbiome: olanzapine-induced metabolic dysfunction is attenuated by antibiotic administration in the rat. *Transl Psychiatry* (2013) 3:e309. doi: 10.1038/tp.2013.83

Conflict of Interest: The authors declare that the research was conducted in the absence of any commercial or financial relationships that could be construed as a potential conflict of interest.

frontiers in Psychiatry

ORIGINAL RESEARCH
published: 28 January 2020
doi: 10.3389/fpsyt.2019.01010

Age-Related Alterations of White Matter Integrity in Adolescents and Young Adults With Bipolar Disorder

Sihua Ren[1,2], Miao Chang[1,2], Zhiyang Yin[2,3], Ruiqi Feng[1,2], Yange Wei[2,3], Jia Duan[2,3], Xiaowei Jiang[1,2], Shengnan Wei[1,2], Yanqing Tang[2,3], Fei Wang[1,2,3]* and Songbai Li[1]**

[1] Department of Radiology, The First Affiliated Hospital of China Medical University, Shenyang, China, [2] Brain Function Research Section, The First Affiliated Hospital of China Medical University, Shenyang, China, [3] Department of Psychiatry, The First Affiliated Hospital of China Medical University, Shenyang, China

OPEN ACCESS

Edited by:
Wenbin Guo,
Central South University, China

Reviewed by:
Sheng Zhang,
Yale University,
United States
Hao Yan,
Peking University, China

***Correspondence:**
Yanqing Tang
yanqingtang@163.com
Fei Wang
fei.wang@cmu.edu.cn
Songbai Li
songbaili001@163.com

Specialty section:
This article was submitted to Neuroimaging and Stimulation, a section of the journal Frontiers in Psychiatry

Received: 04 September 2019
Accepted: 20 December 2019
Published: 28 January 2020

Citation:
Ren S, Chang M, Yin Z, Feng R, Wei Y, Duan J, Jiang X, Wei S, Tang Y, Wang F and Li S (2020) Age-Related Alterations of White Matter Integrity in Adolescents and Young Adults With Bipolar Disorder. Front. Psychiatry 10:1010. doi: 10.3389/fpsyt.2019.01010

Background: Alterations of white matter integrity during adolescence/young adulthood may contribute to the neurodevelopmental pathophysiology of bipolar disorder (BD), but it remains unknown how white matter integrity changes in BD patients during this critical period of brain development. In the present study, we aimed to identify possible age-associated alterations of white matter integrity in adolescents and young adults with BD across the age range of 13–30 years.

Methods: We divided the participants into two groups by age as follows: adolescent group involving individuals of 13–21 years old (39 patients with BD and 39 healthy controls) and young adult group involving individuals of 22–30 years old (47 patients with BD and 47 healthy controls). Diffusion tensor imaging (DTI) was performed in all participants to assess white matter integrity.

Results: In the adolescent group, compared to those of healthy controls, fractional anisotropy (FA) values were significantly lower in BD patients in the left inferior longitudinal fasciculus, splenium of the corpus callosum and posterior thalamic radiation. In the young adult group, BD patients showed significantly decreased FA values in the bilateral uncinate fasciculus, genu of the corpus callosum, right anterior limb of internal capsule and fornix compared to healthy controls. White matter impairments changed from the posterior brain to the anterior brain representing a back-to-front spatiotemporal directionality in an age-related pattern.

Conclusions: Our findings provide neuroimaging evidence supporting a back-to-front spatiotemporal directionality of the altered development of white matter integrity associated with age in BD patients during adolescence/young adulthood.

Keywords: bipolar disorder, diffusion tensor imaging, fractional anisotropy, white matter, neurodevelopment

INTRODUCTION

An increasing number of studies using magnetic resonance imaging (MRI) have strongly suggested that changes in white matter (WM) may underline the disruption of the normal interactions between brain regions seen in bipolar disorder (BD) patients, thus making it possible to use neuroimaging evidence to delineate pathophysiological mechanism of BD (1–4). To measure the alterations of WM in BD patients, diffusion tensor imaging (DTI) has been widely used to assess WM integrity as fractional anisotropy (FA) obtained by DTI is generally considered a reliable index of axonal integrity and low FA values are generally related to structural damage of WM or demyelination (5, 6). Although WM impairments have been demonstrated in BD patients using DTI, the findings appeared to be inconsistent (7–12). Adolescence/young adulthood is an important period for the development of WM during which FA values tend to increase and such an increase in FA value may represent the continued myelination and thickening of the diameters of fiber tracts (13–16). During brain maturation, myelination follows a back-to-front spatiotemporal directionality and lower-order brain areas, such as sensorimotor regions, mature earlier than higher-order brain areas that are associated with emotional and cognitive functions, such as the frontal lobes (17). Deviations in the typical pattern of normal WM development may lead to the disruption of normal neural connectivity, resulting in the onset and clinical symptoms frequently manifested in BD patients (18–21).

A number of DTI studies have already found alterations of WM integrity in BD patients during adolescence/young adulthood, however, it remains unknown how WM integrity changes in BD patients during this period. A previous study showed that age-associated changes in WM integrity followed a nonlinear trajectory in the corpus callosum (CC) in BD patients across the age range of 9–62 years (21). While greater age-related alterations of WM integrity were demonstrated in BD patients beginning in the second decade of life in the splenium of corpus callosum (SCC), this effect was more evident among BD patients beginning in the third decade of life in the genu of corpus callosum (GCC). The abnormal development of WM in the CC may lead to alterations of inter-hemispheric communication. Another longitudinal study suggested that there was an absence in the expected increase of FA values in the uncinate fasciculus (UF) in adolescents and adults with BD (4), suggesting that the changes in structural development of WM in the UF could link to the abnormal neurodevelopment of BD, causing the emotional instability. Taken together, these findings suggested that the abnormal development of WM may contribute to the pathophysiology of BD.

Abbreviations: ALIC, anterior limb of internal capsule; ANOVA, analysis of variance; BD, bipolar disorder; CC, corpus callosum; DSM-IV, diagnostic and statistical manual of mental disorders, fourth edition; DTI, diffusion tensor imaging; FA, fractional anisotropy; fMRI, functional magnetic resonance imaging; GCC, genu of the corpus callosum; GRF, gaussian random field; HAMA, hamilton anxiety scale; HAMD-17, 17-item hamilton depression rating scale; HC, healthy controls; ILF, inferior longitudinal fasciculus; MNI, montreal neurological institute; MRI, magnetic resonance imaging; SCC, splenium of the corpus callosum; UF, uncinate fasciculus; WM, white matter; YMRS, young mania rating scale.

In this study, we used a voxel-based analysis of DTI to examine the WM integrity of all participants across the age range of 13–30 years by measuring FA values. fMRI findings suggested that the mean brain age achieving a maximum level of maturity is 22.3 years old and it may represent a vital period of time with a great venerability in the development of brain prior to the maturity (22, 23). Additionally, Nurnberger et al. found that clinical assessments performing on offspring aged 12–21 years from families with a proband with BD may identify those prone to the onset of major affective disorders during adolescence (24). The findings indicated that BD patients of 12–21 years old present some clinical symptoms that differ from those of BD patients older than 21 years. Furthermore, a previous study examining the contributions of age at onset and childhood psychopathology in psychotic BD patients demonstrated that onset of BD at an early age prior to twenty was generally associated with poorer functional and clinical outcomes, suggesting that differences in brain development underline the mechanisms in BD during adolescence and adulthood (25). Therefore, we divided the participants into two groups by age 21 as follows: adolescent group involving individuals of 13–21 years old and young adult group involving individuals of 22-30 years old. By comparing differences in the WM between BD patients and health controls (HC), we aimed to investigate the age-associated alterations of the brain during adolescent/young adulthood in BD patients and to delineate the neurodevelopmental pathophysiology of BD.

MATERIALS AND METHODS

Participants

There were 86 individuals with BD and 86 HC involved in the present study. All participants were divided into two groups by age as follows: adolescent group with the age range of 13–21 years and young adult group with the age range of 22–30 years. The numbers of both BD patients and HC in each group were 39 and 47, respectively. The age distribution showed as following: there were 10 individuals of 13–15 years old (5 BD patients, 5 HC), 38 individuals of 16–18 years old (17 BD patients, 21 HC), 30 individuals of 19–21 years old (17 BD patients, 13 HC), 30 individuals of 22–24 years old (15 BD patients, 15 HC), 36 individuals of 25–27 years old (18 BD patients, 18 HC), and 28 individuals of 28–30 years old (14 BD patients, 14 HC), respectively. BD patients were recruited from the outpatient services at the Department of Psychiatry, First Affiliated Hospital of China Medical University and Mental Health Center of Shenyang, while HC were recruited from the local community by advertisements matched for gender and age. After receiving a detailed description of the study, all participants (or parents or guardian for those under 18 years old) provided written informed consent. The study was approved by the Medical Research Ethics Committee of the China Medical University in accordance with the Declaration of Helsinki. Consensus was made between two trained psychiatrists to confirm the presence or absence of Axis I diagnoses using the following criteria: the Structured Clinical Interview for

Diagnostic and Statistical Manual of Mental Disorders, Fourth Edition (DSM-IV) Axis I Disorders for participants of 18 years old or older and the Schedule for Affective Disorders and Schizophrenia for School-Age Children-present and Lifetime Version for participants younger than 18 years old. BD participants met DSM-IV diagnostic criteria for BD without any other Axis I disorders. No presence of any other DSM-IV Axis I disorders was confirmed in BD patients or their first-degree family members. Individuals were excluded from participation based on the following criteria: 1) general contraindications for MRI, 2) history of substance/alcohol abuse or dependence, 3) history of head trauma with loss of consciousness for ≥ 5 min or any neurological disorder, and 4) concomitant major medical disorder. For all participants, mania scores were assessed using the Young Mania Rating Scale (YMRS), depression scores were assessed using the 17-item Hamilton Depression Rating Scale (HAMD-17), and anxiety scores were assessed using the Hamilton Anxiety Scale (HAMA). Details of age of onset, first episode, and duration of illness in BD patients were obtained. Considering mood states, in the adolescent group, there were 11 BD patients in a stable state, 16 BD patients in a depressed state and 9 BD patients in a manic state. In the young adult group, there were 13 BD patients in a stable state, 19 BD patients in a depressed state and 10 BD patients in a manic state. Considering medication status, in the adolescent group, there were 14 BD patients on mood stabilizers, 14 BD patients on antipsychotics, 9 BD patients on antidepressants, and 16 BD patients without medication. In the young adult group, there were 25 BD patients on mood stabilizers, 21 BD patients on antipsychotics, 21 BD patients on antidepressants, and 16 BD patients without medication.

DTI Acquisition and Processing

To obtain MRI data, a GE Signa HDX 3.0T MRI scanner was used with a standard head coil at this hospital. Head motion was minimized with restraining foam pads. To acquire DTI, spin-echo planar imaging sequences were used with the following parameters: TR = 17000 ms, TE = 85.4 ms, FOV = 24 cm × 24 cm, imaging matrix = 120 × 120, 65 contiguous axial slices of 2 mm without gap, 25 non-collinear directions (b = 1000 s/mm^2), axial acquisition without diffusion weighting (b = 0), and voxel size = 2.0 mm^3.

The acquired images were processed with PANDA software (http://www.nitrc.org/projects/panda). To transform individual FA images of native space to a standard Montreal Neurological Institute (MNI) space, spatial normalization (voxel size = 1 mm × 1 mm × 1 mm) was used after motion and eddy-current correction were applied. Finally, to reduce misalignment and noise, the FA images were smoothed by a 6-mm Gaussian kernel.

Statistical Analysis

We used student *t* test and χ^2 test to compare demographic data and the YMRS, HAMD-17, HAMA scores between BD patients and HC in the adolescent and young adult groups. We also used χ^2 test to compare the composition of different mood states between adolescents with BD and young adults with BD. The *t* test was also employed to determine if there was a significant difference in FA values between BD patients and controls separately in the adolescent and young adult groups. The voxel-level inference of $p < 0.005$ with Gaussian random field (GRF) correction for cluster-level inference of $p < 0.05$ was used for statistical inference in DTI images. Moreover, FA values that were extracted from the regions showing significant differences between BD patients and HC were used for partial correlation analyses to explore the clinical factors including the YMRS, HAMD-17, and HAMA scores. To rule out the possible interference on the dynamics of FA performance in the medicated patients, the difference in FA values was further determined by t test in the specified brain regions between medication-free BD patients and HC. For multiple comparisons, statistical significance was set at $p < 0.05$ corrected by Bonferroni. We also performed analysis of variance (ANOVA) by using group (BD patients vs HC) and age (adolescents versus young adults) as between subject factors to investigate the group × age interaction in the brain regions where the significant differences in FA values between BD patients and HC in the adolescent and young adult groups were observed in the above *t* tests. Post hoc analyses were used to determine the extent of alterations in FA values among adolescents with BD, healthy adolescents, young adults with BD and healthy young adults.

RESULTS

Overall, there were no significant differences in age, gender and handedness between BD patients and HC in adolescent and young adult groups. Additionally, there was no significant difference in the composition of different mood states between adolescents with BD and young adults with BD. However, BD patients had significantly greater levels of manic depression and anxiety as measured by the YMRS, HAMD-17, and HAMA compared to those of controls (**Table 1**).

In our present study, adolescents with BD showed significantly decreased FA values compared to those of healthy adolescents in the distinct brain regions as follows:1) left inferior longitudinal fasciculus (ILF), and 2) SCC and posterior thalamic radiation (MNI coordinates, respectively: x = -28 mm, y = -22 mm, z = -10 mm, 124 voxels, T = 4.11; x = -26 mm, y = -62 mm, z = 18 mm, 122 voxels, T = 4.25; $p < 0.005$ corrected by GRF) (**Figure 1**). Compared to those of HC, FA values were significant lower in BD patients in the young adult group in the following brain areas: 1) left UF, 2) right anterior limb of internal capsule (ALIC) and fornix, and 3) right UF and GCC (MNI coordinates, respectively: x = -24 mm, y = 28 mm, z = -8 mm, 138 voxels, T = 4.54; x = 16 mm, y = 6 mm, z = 0 mm, 84 voxels, T = 4.31; x = 20 mm, y = 34 mm, z = 10 mm, 181 voxels, T = 4.11; $p < 0.005$ corrected by GRF (**Figure 2**). There were no significant correlations between mean FA values and the YMRS, HAMD-17, and HAMA scores ($p > 0.05$, Bonferroni corrected for six times) in the adolescent group. In the young adult group, there were no significant correlations between mean FA values and the YMRS, HAMD-17, and HAMA scores ($p > 0.05$, Bonferroni corrected for nine times). Regardless of age, the medication-free patients showed significant differences in FA values compared to HC (adolescents

TABLE 1 | Demographic and clinical characteristics of study participants.

Characteristics	Age of 13–21 years old		t/χ^2 P	Age of 22–30 years old		t/χ^2 P
	BD (n = 39) Mean (SD)	HC(n = 39) Mean (SD)		BD (n = 47) Mean (SD)	HC (n = 47) Mean (SD)	
Age at scan (years)	17.90 (2.19)	17.85 (2.22)	0.103 0.918	25.87 (2.75)	25.72 (2.56)	0.272 0.786
Gender (male/female)	14/25	16/23	0.217 0.642	24/23	21/26	0.384 0.536
Handedness (R/L/MIX)	36/1/2	37/0/0	2.963 0.227	46/0/0	44/0/2	2.044 0.153
First episode (yes/no)	25/14	—	—	24/21	—	—
Age of onset (years)	15.6 (2.08)	—	—	22.3 (4.88)	—	—
State (stable/depressed/manic)	11/16/9	—	—	13/19/10	—	—
Medication (yes/no)	23/16	—	—	31/16	—	—
Duration (months)	22.42 (20.17)	—	—	33.52 (36.27)	—	—
YMRS	n = 39	n = 31		n = 45	n = 42	
	7.87 (10.29)	0.07 (0.25)	4.737< 0.001	8.73 (10.92)	0.12 (0.33)	5.289< 0.001
HAMD-17	n = 38	n = 31		n = 47	n = 43	
	11.7 (9.21)	1.65 (1.78)	6.584< 0.001	12.85 (11.03)	0.81 (1.20)	7.433< 0.001
HAMA	n = 36	n = 30		n = 45	n = 30	
	8.42 (7.30)	0.57 (1.07)	6.371< 0.001	9.78 (10.75)	0.47 (1.10)	5.779 < 0.001

SD, standard deviation; BD, bipolar disorder; HC, healthy controls; YMRS, Young Mania Rating Scale; HAMD, Hamilton Depression Rating Scale; HAMA, Hamilton Anxiety Scale.

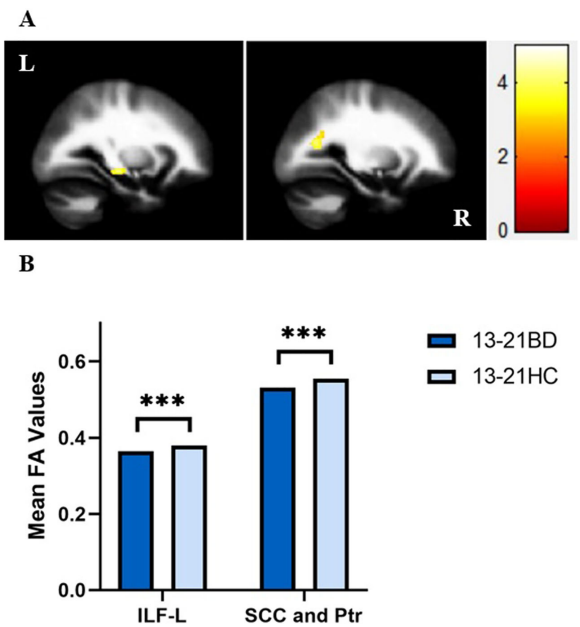

FIGURE 1 | (A) Sagittal views showing significant differences in fractional anisotropy (FA) values in the left inferior longitudinal fasciculus (ILF), splenium of corpus callosum (SCC) and posterior thalamic radiation (Ptr) between bipolar disorder (BD) patients and healthy controls (HC) in the adolescent group from left to right as follows: (1) left ILF, and (2) SCC and Ptr [Montreal Neurological Institute (MNI) coordinates, respectively: x = -28 mm, y = -22 mm, z = -10 mm, 124 voxels, T = 4.11; x = -26 mm, y = -62 mm, z = 18 mm, 122 voxels, T = 4.25, $p < 0.005$ with Gaussian random field (GRF) correction]. **(B)** FA values in white matter fibers extracted from the left ILF, SCC and Ptr in BD patients and HC in the adolescent group. ***$p < 0.001$. ILF-L, left inferior longitudinal fasciculus; L, left brain; R, right brain. Color bars represent T values.

with BD vs healthy adolescents: $p < 0.05$, Bonferroni corrected for two times; young adults with BD versus healthy young adults: $p < 0.05$, Bonferroni corrected for three times, respectively).

We further determined if there was a group × age interaction in the brain regions where the significant differences in FA values between BD patients and HC in the adolescent and young adult groups were observed in the above *t* tests. There was a significant group × age interaction in the left ILF, SCC, posterior thalamic radiation, left UF, right ALIC, and fornix (all $p < 0.05$). The *post hoc* analyses demonstrated that the larger contribution to the group × age interaction was derived mainly from the decreased FA values in the left ILF, SCC and posterior thalamic radiation in adolescents with BD compared to healthy adolescents (all $p < 0.001$). Compared to those of HC, FA values in the left ILF showed no significant differences in young adults with BD ($p > 0.05$) and greater extent of changes in the mean FA values was found in the SCC and posterior thalamic radiation in adolescents with BD ($p < 0.001$) compared to young adults with BD ($p < 0.05$). Additionally, there were significant lower FA values in the left UF, right ALIC, and fornix indicating the larger contribution to the interaction between group and age in young adults with BD compared to HC (all $p < 0.001$), and FA values in the above brain regions showed no significant differences between adolescents with BD and healthy adolescents, although the group × age interaction in the right UF and GCC was not significant (**Figure 3**).

DISCUSSION

To our knowledge, this is the first report to demonstrate the age-associated alterations of WM integrity following a back-to-front spatiotemporal directionality in BD patients during adolescence/young adulthood. Our findings yielded from DTI analysis indicated that the adolescent BD patients showed significantly lower FA values in the left ILF, SCC, and posterior thalamic radiation compared to those of HC. While in the young adult group, FA values were significantly decreased in the bilateral uncinate fasciculus, genu of the corpus callosum, right anterior limb of internal capsule, and fornix compared to those of HC.

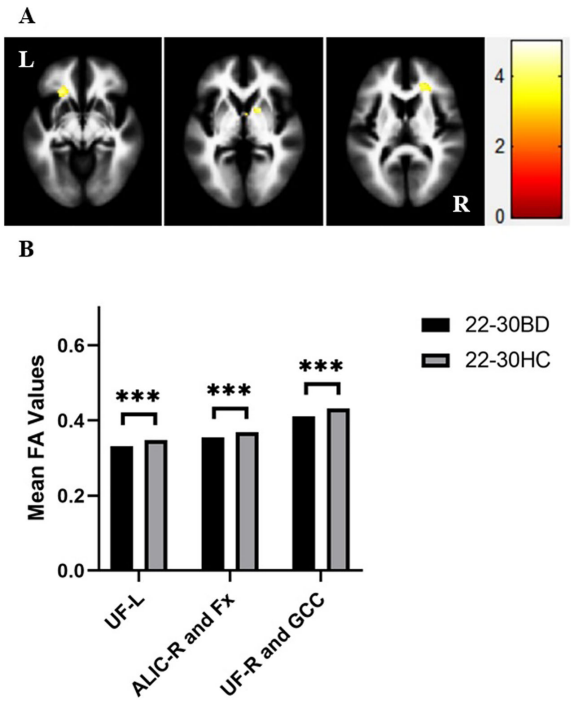

FIGURE 2 | (A) Axial views showing significant differences in fractional anisotropy (FA) values in the bilateral uncinate fasciculus (UF), genu of corpus callosum (GCC), right anterior limb of internal capsule (ALIC) and fornix (Fx) between bipolar disorder (BD) patients and healthy controls (HC) in the young adult group from left to right as follows: (1) left UF, (2) right ALIC and Fx, and (3) right UF and GCC [Montreal Neurological Institute (MNI) coordinates, respectively: x = -24 mm, y = 28 mm, z = -8 mm, 138 voxels, T = 4.54; x = 16 mm, y = 6 mm, z = 0 mm, 84 voxels, T = 4.31; x = 20 mm, y = 34 mm, z = 10 mm, 181 voxels, T = 4.11, $p < 0.005$ with Gaussian random field (GRF) correction]. **(B)** FA values in white matter fibers extracted from the bilateral UF, GCC, right ALIC and Fx in BD patients and HC in the young adult group. ***$p < 0.001$. UF-L, left uncinate fasciculus; ALIC-R, right anterior limb of the internal capsule; UF-R, right uncinate fasciculus; L, left brain; R, right brain. Color bars represent T values.

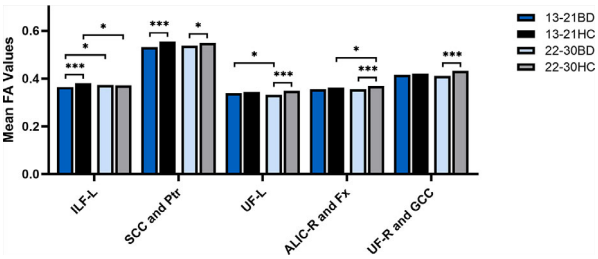

FIGURE 3 | FA values in white matter fibers focusing on the group × age interaction extracted from the left inferior longitudinal fasciculus (ILF), splenium of corpus callosum (SCC), posterior thalamic radiation (Ptr), bilateral uncinate fasciculus (UF), genu of corpus callosum (GCC), right anterior limb of internal capsule (ALIC) and fornix (Fx) in adolescents with bipolar disorder (BD), healthy adolescents, young adults with BD and healthy young adults. *$p <$ 0.05, ***$p < 0.001$. ILF-L, left inferior longitudinal fasciculus; UF-L, left uncinate fasciculus; ALIC-R, right anterior limb of the internal capsule; UF-R, right uncinate fasciculus; L, left brain; R, right brain. Color bars represent T values.

The disruptions of neural connectivity within WM apparently changed from the posterior brain to the anterior brain in an age-dependent manner. Our DTI findings further revealed that there were alternations in anatomical connectivity in neural microstructures of WM in BD patients in all age groups and highlighted the importance of considering WM integrity in the neurodevelopmental pathophysiology of BD.

One of critical findings of our study was that development of abnormal WM integrity in BD patients follows an apparent back-to-front spatiotemporal directionality of WM and it was also the age-dependent. Interestingly a similar directionality of the normal development of the brain has been reported in the previous findings (14, 17, 26). Studies using structural MRI to investigate gray matter density showed that the decline in gray matter density and increased myelination have been companied with continued normal brain growth until the age of 30 years old. The trajectory of maturational and aging changed heterogeneously over the cortex as follows: cortices such as the visual and auditory cortex myelinated earlier and showed a more linear pattern of aging compared to the frontal cortex. Another study investigating cortical development using MRI demonstrated that lower-order brain areas such as sensorimotor regions matured earlier than higher-order brain areas such as the frontal cortex. Furthermore, a previous study using DTI to investigate WM integrity also suggested a back-to-front spatiotemporal development of the normal brain (27). The findings indicated that the more rostral portions of the CC and internal capsule began the maturation process latter than the caudal regions. Interestingly, the back-to-front changes of brain were also found in BD patients demonstrated in previous studies in which either fMRI or DTI was used as a research tool (28, 29). fMRI studies investigating connectivity and network of brain showed that the abnormal input from lower-order brain regions may affect higher-order brain regions and cause dysfunction within neural circuits, which may act on sensory processing circuits later and finally lead to the clinical symptoms of BD. While a DTI study demonstrated that greater age-associated changes in WM integrity in BD patients began in the second decade of life within the SCC and began in the third decade of life within the GCC (21), which were consistent with our findings. However, a recent study showed that there was a strong correlational relationship between the extent of quadratic measurement difference and peak maturational timing (30). The findings of the study supported the last-in-first-out petrogenesis hypothesis of aging (31). To this regard, more longitudinal studies are needed to explore the neurodevelopmental pathophysiology of BD.

As suggested in our findings, WM disruptions changed from the posterior brain involving primary cortex to the anterior brain involving high-order cortex in BD patients during adolescence/young adulthood. Alterations of WM in the back of the brain have been demonstrated to be related to the impairments of

primary sensory processing by previous studies. For example, the ILF connects occipital and temporal lobes and relays information to the orbitofrontal region of the brain (32). Decrease in FA values in ILF and the changes of WM integrity were associated with the impairments of object recognition in children (33). Additionally, the decreased FA values in the posterior thalamic radiation in BD patients in the present study were almost identical to a previous study in which, using a visual backward masking task, the impairments of visual processing were associated with deficits in neural pathways involving posterior brain areas in BD patients (6, 34). As the alterations of WM were mainly confined in the front of the brain in young adults with BD as suggested by our findings, the disruptions of WM may lead to abnormal higher-order functions such as cognitive and emotional regulation. For example, the UF is crucial for communication between the amygdala and ventral prefrontal cortex and plays an important role in maintain emotional stability (4, 35–37). Decreased FA values found in the UF in BD patients could suggest there could be an abnormality in the perigenual anterior cingulate cortex-amygdala functional connection and the impairments of WM microneural connectivity may lead to the abnormality of emotional processing in BD (38). Additionally, the GCC, an area connecting the frontal cortices, participates in higher-order cognitive and emotional regulation (8, 39–44) and any deficits of prefrontal connectivity may cause clinical symptoms of BD such as altered responses to emotional stimuli (45, 46). Moreover, the ALIC may interconnects with higher-order brain regions such as prefrontal cortex and amygdala through thalamic nuclei and structural abnormalities in the ALIC and UF could cause psychotic symptoms and mood dysregulation including increased risk taking behaviors (47). Furthermore, the damage of the fornix was related to impaired amnesic function involved in the clinical manifestations of BD as the fornix serve as a major efferent fiber bundle from the hippocampus (48–50).

Moreover, there were several limitations in the present study. First, the study was cross-sectional and the potential alterations of WM integrity which may occur in the development of BD remain unknown. Further longitudinal studies may produce the validity of our findings supporting developmental changes are associated with the spectrum of BD. Second, the relative smaller sample size of this study prevents us to provide additional data critical for further delineating the neurodevelopmental pathophysiology of BD. Third, the results obtained from BD patients who received medications could complicate interpretations of the findings. However, regardless of their age, BD patients without medications showed significant differences in FA values when compared to HC and this finding was consistent with our previous findings. Further studies comprising of unmedicated patients could unambiguously exclude the effect of medication on FA values in the BD patients. Fourth, as the youngest patient in our study is only 13 years old and an age-appropriate standard template should be used in future study. Fifth, there was a partially overlapped age of onset in adolescents with BD and young adults with BD in our study. Patients in distinctive ages should be included in the further analysis in order to reduce the effect of the overlapped age. Finally, a paucity of evidence provided by DTI studies indicates that age around 21 could arguably be a pivotal timing for the development of BD, clearly, more longitudinal DTI studies are needed to confirm the hypothesis.

In summary, our study suggests that there are age-related alterations of WM integrity in adolescents and young adults with BD. A back-to-front spatiotemporal directionality of WM impairments share a similar directionality of the normal brain development. The findings highlight the importance of considering the neurodevelopmental pathophysiology of BD.

DATA AVAILABILITY STATEMENT

The datasets generated for this study are available on request to the corresponding authors.

ETHICS STATEMENT

The studies involving human participants were reviewed and approved by the Ethics Committee of the First Affiliated Hospital of China Medical University. Written informed consent to participate in this study was provided by the participants' legal guardian/next of kin or the participants themselves.

AUTHOR CONTRIBUTIONS

SR, YT, FW, and SL designed the study. MC, ZY, RF, YW, JD, XJ, and SW participated in data collection, preprocessing and analysis. All the authors were involved in data interpretation, writing, and manuscript preparation and approved the final manuscript.

FUNDING

The study was funded by National Natural Science Foundation of China (81571311 to YT, 81571331 to FW), National Science Fund for Distinguished Young Scholars (81725005 to FW), National Key Research and Development Program (2018YFC1311604 to YT, 2016YFC1306900 to YT, 2016YFC0904300 to FW), National High Tech Development Plan (863) (2015AA020513 to FW), Liaoning Science and Technology Project (2015225018 to YT), Innovation Team Support Plan of Higher Education of Liaoning Province (LT2017007 to FW), Major Special Construction Plan of China Medical University (3110117059 to FW).

ACKNOWLEDGMENTS

We would like to acknowledge all participants involved in this study.

REFERENCES

1. Torgerson CM, Irimia A, Leow AD, Bartzokis G, Moody TD, Jennings RG, et al. DTI tractography and white matter fiber tract characteristics in euthymic bipolar I patients and healthy control subjects. *Brain Imaging Behav.* (2013) 7:129–39. doi: 10.1007/s11682-012-9202-3
2. Sarrazin S, Poupon C, Linke J, Wessa M, Phillips M, Delavest M, et al. A multicenter tractography study of deep white matter tracts in bipolar I disorder: psychotic features and interhemispheric disconnectivity. *JAMA Psychiatry* (2014) 71:388–96. doi: 10.1001/jamapsychiatry.2013.4513
3. Bellani M, Boschello F, Delvecchio G, Dusi N, Altamura CA, Ruggeri M, et al. DTI and myelin plasticity in bipolar disorder: integrating neuroimaging and neuropathological findings. *Front. Psychiatry* (2016) 7:21. doi: 10.3389/fpsyt.2016.00021
4. Weathers J, Lippard ETC, Spencer L, Pittman B, Wang F, Blumberg HP. Longitudinal diffusion tensor imaging study of adolescents and young adults with bipolar disorder. *J. Am. Acad. Child. Adolesc. Psychiatry* (2018) 57:111–7. doi: 10.1016/j.jaac.2017.11.014
5. Kubicki M, Westin CF, Maier SE, Mamata H, Frumin M, Ersner-Hershfield H, et al. Diffusion tensor imaging and its application to neuropsychiatric disorders. *Harv. Rev. Psychiatry* (2002) 10:324–36. doi: 10.1093/hrp/10.6.324
6. Sarıçiçek A, Zorlu N, Yalin N, Hıdıroğlu C, Çavuşoğlu B, Ceylan D, et al. Abnormal white matter integrity as a structural endophenotype for bipolar disorder. *Psychol. Med.* (2016) 46:1547–58. doi: 10.1017/s0033291716000180
7. Bauer IE, Ouyang A, Mwangi B, Sanches M, Zunta-Soares GB, Keefe RSE, et al. Reduced white matter integrity and verbal fluency impairment in young adults with bipolar disorder: a diffusion tensor imaging study. *J. Psychiatr. Res.* (2015) 62:115–22. doi: 10.1016/j.jpsychires.2015.01.008
8. Roberts G, Wen W, Frankland A, Perich T, Holmes-Preston E, Levy F, et al. Interhemispheric white matter integrity in young people with bipolar disorder and at high genetic risk. *Psychol. Med.* (2016) 46:2385–96. doi: 10.1017/s0033291716001161
9. Ganzola R, Nickson T, Bastin ME, Giles S, Macdonald A, Sussmann J, et al. Longitudinal differences in white matter integrity in youth at high familial risk for bipolar disorder. *Bipolar Disord.* (2017) 19:158–67. doi: 10.1111/bdi.12489
10. Repple J, Meinert S, Grotegerd D, Kugel H, Redlich R, Dohm K, et al. A voxel-based diffusion tensor imaging study in unipolar and bipolar depression. *Bipolar Disord.* (2017) 19:23–31. doi: 10.1111/bdi.12465
11. Abramovic L, Boks MPM, Vreeker A, Verkooijen S, van Bergen AH, Ophoff RA, et al. White matter disruptions in patients with bipolar disorder. *Eur. Neuropsychopharmacol* (2018) 28:743–51. doi: 10.1016/j.euroneuro.2018.01.001
12. Tønnesen S, Kaufmann T, Doan NT, Alnæs D, Córdova-Palomera A, Meer DV, et al. White matter aberrations and age-related trajectories in patients with schizophrenia and bipolar disorder revealed by diffusion tensor imaging. *Sci. Rep.* (2018) 8:14129. doi: 10.1038/s41598-018-32355-9
13. Benes FM. Myelination of cortical-hippocampal relays during late adolescence. *Schizophr. Bull* (1989) 15:585–93. doi: 10.1093/schbul/15.4.585
14. Sowell ER, Peterson BS, Thompson PM, Welcome SE, Henkenius AL, Toga AW. Mapping cortical change across the human life span. *Nat. Neurosci.* (2003) 6:309–15. doi: 10.1038/nn1008
15. Giorgio A, Watkins KE, Chadwick M, James S, Winmill L, Douaud G, et al. Longitudinal changes in grey and white matter during adolescence. *Neuroimage* (2010) 49:94–103. doi: 10.1016/j.neuroimage.2009.08.003
16. Uda S, Matsui M, Tanaka C, Uematsu A, Miura K, Kawana I, et al. Normal development of human brain white matter from infancy to early adulthood: a diffusion tensor imaging study. *Dev Neurosci.* (2015) 37:182–94. doi: 10.1159/000373885
17. Gogtay N, Giedd JN, Lusk L, Hayashi KM, Greenstein D, Vaituzis AC, et al. Dynamic mapping of human cortical development during childhood through early adulthood. *Proc. Natl. Acad. Sci. U. S. A.* (2004) 101:8174–79. doi: 10.1073/pnas.0402680101
18. Blumberg HP, Kaufman J, Martin A, Charney DS, Krystal JH, Peterson BS. Significance of adolescent neurodevelopment for the neural circuitry of bipolar disorder. *Ann. N. Y. Acad. Sci.* (2004) 1021:376–83. doi: 10.1196/annals.1308.048
19. Roybal DJ, Singh MK, Cosgrove VE, Howe M, Kelley R, Barnea-Goraly N, et al. Biological evidence for a neurodevelopmental model of pediatric bipolar disorder. *Isr. J. Psychiatry Relat. Sci.* (2012) 49:28–43. doi: 10.1016/B978-0-12-398314-5.00005-2
20. Schneider MR, DelBello MP, McNamara RK, Strakowski SM, Adler CM. Neuroprogression in bipolar disorder. *Bipolar Disord.* (2012) 14:356–74. doi: 10.1111/j.1399-5618.2012.01024.x
21. Toteja N, Guvenek-Cokol P, Ikuta T, Kafantaris V, Peters BD, Burdick KE, et al. Age-associated alterations in corpus callosum white matter integrity in bipolar disorder assessed using probabilistic tractography. *Bipolar Disord.* (2015) 17:381–91. doi: 10.1111/bdi.12278
22. Craik FIM, Bialystok E. Cognition through the lifespan: mechanisms of change. *Trends Cogn. Sci.* (2006) 10:131–8. doi: 10.1016/j.tics.2006.01.007
23. Dosenbach NUF, Nardos B, Cohen AL, Fair DA, Power JD, Church JA, et al. Prediction of individual brain maturity using fMRI. *Science* (2010) 329:1358–61. doi: 10.1126/science.1194144
24. Nurnberger JI, McInnis M, Reich W, Kastelic E, Wilcox HC, Glowinski A, et al. A high-risk study of bipolar disorder: childhood clinical phenotypes as precursors of major mood disorders. *Arch. Gen. Psychiatry* (2011) 68:1012–20. doi: 10.1001/archgenpsychiatry.2011.126
25. Carlson GA, Bromet EJ, Driessens C, Mojtabai R, Schwartz JE. Age at onset, childhood psychopathology, and 2-year outcome in psychotic bipolar disorder. *Am. J. Psychiatry* (2002) 159:307–9. doi: 10.1176/appi.ajp.159.2.307
26. Sowell ER, Thompson PM, Tessner KD, Toga AW. Mapping continued brain growth and gray matter density reduction in dorsal frontal cortex: Inverse relationships during postadolescent brain maturation. *J. Neurosci.* (2001) 21:8819–29. doi: 10.1523/jneurosci.21-22-08819.2001
27. Cancelliere A, Mangano FT, Air EL, Jones BV, Altaye M, Rajagopal A, et al. DTI values in key white matter tracts from infancy through adolescence. *Am. J. Neuroradiol.* (2013) 34:1443–9. doi: 10.3174/ajnr.a3350
28. Stephan KE, Friston KJ, Frith CD. Dysconnection in schizophrenia: from abnormal synaptic plasticity to failures of self-monitoring. *Schizophr. Bull.* (2009) 35:509–27. doi: 10.1093/schbul/sbn176
29. Xia M, Womer FY, Chang M, Zhu Y, Zhou Q, Edmiston EK, et al. Shared and distinct functional architectures of brain networks across psychiatric disorders. *Schizophr. Bull.* (2019) 45:450–63. doi: 10.1093/schbul/sby046
30. Slater DA, Melie-Garcia L, Preisig M, Kherif F, Lutti A, Draganski B. Evolution of white matter tract microstructure across the life span. *Hum. Brain Mapp.* (2019) 40:2252–68. doi: 10.1002/hbm.24522
31. Raz N. Aging of the brain and its impact on cognitive performance: Integration of structural and functional findings. In: Craik FIM, TA Salthouse, editors. *The Handbook of Aging and Cognition*. Lawrence Erlbaum Associates: Mahwah, NJ (2000). p. 1–90.
32. Ashtari M. Anatomy and functional role of the inferior longitudinal fasciculus: a search that has just begun. *Dev. Med. Child. Neurol.* (2012) 54:6–7. doi: 10.1111/j.1469-8749.2011.04122.x
33. Ortibus E, Verhoeven J, Sunaert S, Casteels I, de Cock P, Lagae L. Integrity of the inferior longitudinal fasciculus and impaired object recognition in children: a diffusion tensor imaging study. *Dev. Med. Child. Neurol.* (2012) 54:38–43. doi: 10.1111/j.1469-8749.2011.04147.x
34. Macqueen GM, Grof P, Alda M, Marriott M, Young LT, Duffy A. A pilot study of visual backward masking performance among affected versus unaffected offspring of parents with bipolar disorder. *Bipolar Disord.* (2004) 6:374–78. doi: 10.1111/j.1399-5618.2004.00133.x
35. Papagno C, Miracapillo C, Casarotti A, Romero Lauro LJ, Castellano A, Falini A, et al. What is the role of the uncinate fasciculus? Surgical removal and proper name retrieval. *Brain* (2011) 134:405–14. doi: 10.1093/brain/awq283
36. Von Der Heide RJ, Skipper LM, Klobusicky E, Olson IR. Dissecting the uncinate fasciculus: disorders, controversies and a hypothesis. *Brain* (2013) 136:1692–707. doi: 10.1093/brain/awt094
37. Oishi K, Faria AV, Hsu J, Tippett D, Mori S, Hillis AE. Critical role of the right uncinate fasciculus in emotional empathy. *Ann. Neurol.* (2015) 77:68–74. doi: 10.1002/ana.24300
38. Wang F, Kalmar JH, He Y, Jackowski M, Chepenik LG, Edmiston EE, et al. Functional and structural connectivity between the perigenual anterior cingulate and amygdala in bipolar disorder. *Biol. Psychiatry* (2009) 66:516–21. doi: 10.1016/j.biopsych.2009.03.023
39. Aboitiz F, Scheibel AB, Fisher RS, Zaidel E. Fiber composition of the human corpus callosum. *Brain Res.* (1992) 598:143–53. doi: 10.1016/0006-8993(92)90178-c

40. Davidson RJ, Irwin W. The functional neuroanatomy of emotion and affective style. *Trends Cogn. Sci* (1999) 3:11–21. doi: 10.1016/s1364-6613(98)01265-0
41. Brambilla P, Nicoletti MA, Sassi RB, Mallinger AG, Frank E, Kupfer DJ, et al. Magnetic resonance imaging study of corpus callosum abnormalities in patients with bipolar disorder. *Biol. Psychiatry* (2003) 54:1294–97. doi: 10.1016/s0006-3223(03)00070-2
42. Wang F, Kalmar JH, Edmiston E, Chepenik LG, Bhagwagar Z, Spencer L, et al. Abnormal corpus callosum integrity in bipolar disorder: a diffusion tensor imaging study. *Biol. Psychiatry* (2008) 64:730–33. doi: 10.1016/j.biopsych.2008.06.001
43. Chaddock CA, Barker GJ, Marshall N, Schulze K, Hall MH, Fern A, et al. White matter microstructural impairments and genetic liability to familial bipolar I disorder. *Br. J. Psychiatry* (2009) 194:527–34. doi: 10.1192/bjp.bp.107.047498
44. Galinowski A, Miranda R, Lemaitre H, Paillere Martinot ML, Artiges E, Vulser H, et al. Resilience and corpus callosum microstructure in adolescence. *Psychol. Med.* (2015) 45:2285–94. doi: 10.1017/S0033291715000239
45. Blond BN, Fredericks CA, Blumberg HP. Functional neuroanatomy of bipolar disorder: structure, function, and connectivity in an amygdala-anterior paralimbic neural system. *Bipolar Disord.* (2012) 14:340–55. doi: 10.1111/j.1399-5618.2012.01015.x
46. Emsell L, Leemans A, Langan C, Van Hecke W, Barker GJ, McCarthy P, et al. Limbic and callosal white matter changes in euthymic bipolar I disorder: an advanced diffusion magnetic resonance imaging tractography study. *Biol. Psychiatry* (2013) 73:194–201. doi: 10.1016/j.biopsych.2012.09.023
47. Linke J, King AV, Poupon C, Hennerici MG, Gass A, Wessa M. Impaired anatomical connectivity and related executive functions: differentiating vulnerability and disease marker in bipolar disorder. *Biol. Psychiatry* (2013) 74:908–16. doi: 10.1016/j.biopsych.2013.04.010
48. Frey BN, Andreazza AC, Nery FG, Martins MR, Quevedo J, Soares JC, et al. The role of hippocampus in the pathophysiology of bipolar disorder. *Behav. Pharmacol.* (2007) 18:419–30. doi: 10.1097/fbp.0b013e3282df3cde
49. Malhi GS, Ivanovski B, Hadzi-Pavlovic D, Mitchell PB, Vieta E, Sachdev P. Neuropsychological deficits and functional impairment in bipolar depression, hypomania and euthymia. *Bipolar Disord.* (2007) 9:114–25. doi: 10.1111/j.1399-5618.2007.00324.x
50. Monks PJ, Thompson JM, Bullmore ET, Suckling J, Brammer MJ, Williams SCR, et al. A functional MRI study of working memory task in euthymic bipolar disorder: evidence for task-specific dysfunction. *Bipolar Disord.* (2004) 6:550–64. doi: 10.1111/j.1399-5618.2004.00147.x

Conflict of Interest: The authors declare that the research was conducted in the absence of any commercial or financial relationships that could be construed as a potential conflict of interest.

frontiers in Psychiatry

ORIGINAL RESEARCH
published: 31 January 2020
doi: 10.3389/fpsyt.2019.01024

Abnormal Voxel-Wise Degree Centrality in Patients With Late-Life Depression: A Resting-State Functional Magnetic Resonance Imaging Study

Jun Li[1†], Hengfen Gong[2†], Hongmin Xu[3†], Qiong Ding[4], Naying He[3], Ying Huang[2], Ying Jin[2], Chencheng Zhang[1], Valerie Voon[5], Bomin Sun[1], Fuhua Yan[3] and Shikun Zhan[1*]*

[1] Department of Functional Neurosurgery, Ruijin Hospital, Shanghai Jiao Tong University School of Medicine, Shanghai, China, [2] Department of Psychiatry, Shanghai Pudong New Area Mental Health Center, Tongji University School of Medicine, Shanghai, China, [3] Department of Radiology, Ruijin Hospital, Shanghai Jiao Tong University School of Medicine, Shanghai, China, [4] Neural and Intelligence Engineering Center, Institute of Science and Technology for Brain-Inspired Intelligence, Fudan University, Shanghai, China, [5] Department of Psychiatry, University of Cambridge, Cambridge, United Kingdom

OPEN ACCESS

Edited by:
Roberto Esposito,
A.O. Ospedali Riuniti Marche Nord, Italy

Reviewed by:
Feng Liu,
Tianjin Medical University General Hospital, China
Jiuquan Zhang,
Chongqing University, China

***Correspondence:**
Fuhua Yan
yfh11655@rjh.com
Shikun Zhan
zsk10715@rjh.com

[†]These authors have contributed equally to this work

Specialty section:
This article was submitted to Neuroimaging and Stimulation, a section of the journal Frontiers in Psychiatry

Received: 18 October 2019
Accepted: 24 December 2019
Published: 31 January 2020

Citation:
Li J, Gong H, Xu H, Ding Q, He N, Huang Y, Jin Y, Zhang C, Voon V, Sun B, Yan F and Zhan S (2020) Abnormal Voxel-Wise Degree Centrality in Patients With Late-Life Depression: A Resting-State Functional Magnetic Resonance Imaging Study. Front. Psychiatry 10:1024. doi: 10.3389/fpsyt.2019.01024

Objectives: Late-life depression (LLD) has negative impacts on somatic, emotional and cognitive domains of the lives of patients. Elucidating the abnormality in the brain networks of LLD patients could help to strengthen the understanding of LLD pathophysiology, however, the studies exploring the spontaneous brain activity in LLD during the resting state remain limited. This study aimed at identifying the voxel-level whole-brain functional connectivity changes in LLD patients.

Methods: Fifty patients with late-life depression (LLD) and 33 healthy controls were recruited. All participants underwent a resting-state functional magnetic resonance imaging scan to assess the voxel-wise degree centrality (DC) changes in the patients. Furthermore, DC was compared between two patient subgroups, the late-onset depression (LOD) and the early-onset depression (EOD).

Results: Compared with the healthy controls, LLD patients showed increased DC in the inferior parietal lobule, parahippocampal gyrus, brainstem and cerebellum ($p < 0.05$, AlphaSim-corrected). LLD patients also showed decreased DC in the somatosensory and motor cortices and cerebellum ($p < 0.05$, AlphaSim-corrected). Compared with EOD patients, LOD patients showed increased centrality in the superior and middle temporal gyrus and decreased centrality in the occipital region ($p < 0.05$, AlphaSim-corrected). No significant correlation was found between the DC value and the symptom severity or disease duration in the patients after the correction for multiple comparisons.

Conclusions: These findings indicate that the intrinsic abnormality of network centrality exists in a wide range of brain areas in LLD patients. LOD patients differ with EOD patients

in cortical network centrality. Our study might help to strengthen the understanding of the pathophysiology of LLD and the potential neural substrates underlie related emotional and cognitive impairments observed in the patients.

Keywords: late-life depression, resting state, functional magnetic resonance imaging, degree centrality, onset age

INTRODUCTION

Depression refers to a mental disorder characterized by low mood present across most situations for at least two weeks. Late-life depression (LLD) can be defined as a major depressive episode occurring in old age, usually over 60 years of age. Aside from the emotional and somatic burdens associated with depression, such as insomnia, anorexia and fatigue (1), elderly depressive patients may also show impairment in various cognitive domains including attention (2), memory (3, 4), information processing speed (5, 6), and executive functions (4, 7). All these somatic, emotional, and cognitive abnormalities may severely affect the life quality of the patients.

Elucidating the brain abnormality of LLD patients could help to strengthen the understanding of LLD pathophysiology, and develop effective interventions. Grey matter alterations have been reported in multiple brain areas including the frontal, parietal regions and limbic system in LLD patients (8, 9). Several task-based functional magnetic resonance imaging (fMRI) studies have also indicated abnormal functional activities in the areas of frontal lobes and limbic system (10, 11). While structural alterations reflect the long-term influence of depression, and task-based imaging profiles the altered brain reaction to external stimuli or under specific situations, resting-state fMRI explores the intrinsic changes of brain activity in the state without any influence of external stimuli. Resting-state fMRI studies using the method of independent component analysis has revealed that the default mode network, the frontoparietal network and the sensorimotor network showed abnormal connectivity in LLD patients (12, 13). LLD patients also exhibited abnormal local synchronization in various brain areas, as revealed by the measure of regional homogeneity (14). These observations suggest that the brain activities in the resting state have extensive cortical and subcortical abnormalities in LLD patients, which might be associated with clinical manifestations such as emotional disturbance and cognitive deficits observed in the patients.

Degree centrality (DC), an index of the total weights of connections for a given node, has recently been applied to reveal the core hub architecture of brain networks (15). Increased voxel-wise DC in a brain region indicates an elevated degree of its global connectivity, and decreased voxel-wise DC in a brain region suggests a reduced degree of its global connectivity. Voxel-wise DC has been applied to reveal the abnormal brain networks in various types of neurological or psychiatric diseases (16–22). This method has also been used to compare the brain network features of different psychiatric diseases with potentially similar neural pathology, such as autism and attention-deficit hyperactivity disorder (23), or to examine the brain-network difference between the subtypes of a disease such as the Parkinson's disease patients with depression and those without depression (24). The alterations of the whole-brain degree centrality in young patients with major depression have been illustrated in two recent studies revealing that the frontoparietal network, the limbic system, and the striatal areas show DC abnormality in the patients (25). However, depression-specific alterations of network centrality among LLD patients yet remain to be identified.

LLD can be divided into the early-onset depression (EOD, depression occurred for the first time under the age of 60) and late-onset depression (LOD, depression occurred for the first time over the age of 60) according to the onset age of depression (most studies use 60 years as the onset age to distinguish EOD and LOD). While some studies indicate that the LOD patients are not different from the EOD patients in most aspects such as etiological factors, phenomenology or clinical outcomes (26), other studies suggest that the LOD patients show a more severe emotional burden and more extensive cognitive impairments than EOD patients (27–29). Several imaging studies have indicated differences in structure or task-based functional activity between EOD and LOD patients in a wide range of brain areas, including the medial and lateral frontal areas, hippocampus and amygdala (30–35). However, only a few studies have examined the difference in resting-state functional network between EOD and LOD patients. One study using regional homogeneity and the other study using amplitude of low-frequency fluctuation as the indices suggest the local synchronization and low-frequency fluctuation differ in multiple cortical areas and brainstem between LOD and EOD patients (36, 37). The centrality profile of the resting-state brain networks has not been elucidated between LOD and EOD patients.

In the present study, we hypothesized that the architecture of brain networks reflected by degree centrality may show abnormality in cortical and subcortical areas in the LLD patients.

To explore the alterations of functional centrality in LLD patients, we examined the difference in voxel-wise DC between the LLD patients and healthy controls (HCs). To further examine the hypothesis that a difference of the architecture of brain networks may exist between EOD and LOD patients, we compared the DC between the two subgroups of patients. The relationship between the centrality indices of the brain areas being identified abnormal and the clinical assessment was also examined.

Abbreviations: DC, degree centrality; EOD, early-onset depression; fMRI, functional magnetic resonance imaging; HAMD, Hamilton Depression Scale; HC, healthy control; LLD, late-life depression; LOD, late-onset depression; MMSE, Mini-Mental State Examination.

METHODS

All procedures used in the present study were approved by the Ethics Committee of Shanghai Pudong New Area Mental Health Center (approval letter: PDJWLL2014001). Patients with LLD and HCs were recruited *via* advertisements and were fully instructed regarding experimental procedures. All participants gave their written informed consent in accordance with the Declaration of Helsinki.

Participants

Patients diagnosed with major depression according to the criteria in the International Classification of Diseases (ICD-10) by a physician were recruited at Pudong New Area Mental Health Center in Shanghai, China. Healthy volunteers whose age matched to ±10 years with the patients were recruited as controls. Participants aged under 60 or over 80, with a history of severe head trauma, with alcohol abuse, with psychiatric diseases other than depression, with claustrophobia, or with metal or electronic implants were excluded. Patients were using tricyclic, selective serotonin reuptake inhibitors or serotonin and noradrenaline reuptake inhibitors when they were recruited.

Demographics and Clinical Assessment

Basic demographics (i.e. gender, age, education level, handedness) of the participants were collected. Both the patients and HCs filled out the Hamilton Depression Scale (HAMD) (38) right before the resting-state fMRI scan. Patients were asked to report the onset age and the duration of depression. In addition, Mini-Mental State Examination (MMSE) [Folstein, (39)] was carried out and potential participants scored lower than 21, who may have moderate to severe cognitive impairment, were excluded from the study. Mann–Whitney test was used for the between-group comparisons of age, disease duration, and scores of HAMD and MMSE. Chi-square test was used for the between-group comparisons of gender and education level.

Image Acquisition

Resting-state fMRI was performed on a GE Signa HDxt 3.0 T MRI scanner using an eight-channel phased-array head coil. Each participant lay supine with their head snugly fixed by foam pads. The participant was asked to keep still as long as possible and to keep his/her eyes closed but remain awake. Resting-state fMRI was obtained using an echo-planar imaging sequence with protocols of TR = 2000 ms, TE = 30 ms, flip angle = 90°, FOV 240 mm × 240 mm, matrix = 64 × 64, voxel size 3.75 mm × 3.75 mm × 4.00 mm, 35, 37 or 39 axial slices, 210 volumes acquired in 7 min.

Imaging Data Preprocessing

Preprocessing of resting-state fMRI data was conducted using Data Processing Assistant for Resting-State fMRI (DPARSF; http://rfmri.org/dparsf) software (version 4.5) embedded in Data Processing and Analysis for Brain Imaging (DPABI; http://rfmri.org/dpabi) toolbox (version 4.1) on the MATLAB platform (MathWorks, Natick, MA, USA). In brief, the first 10 volumes of each functional time series were discarded, as the participants were adjusting themselves to the fMRI environment during that period. The remaining 200 images were slice-time-corrected with the 35th, 37th or 39th slice as the reference and spatially realigned for head motion. Head motion was assessed by evaluating three translations and three rotations for each scan. Translational thresholds were set to ± 3 mm, while rotational thresholds were limited to ± 3°. After head motion correction, functional images were spatially normalized to Montreal Neurological Institute (MNI) space using echo-planar imaging sequence templates (resampled voxel size 3 mm × 3 mm × 3 mm). All images were linearly detrended and bandpass-filtered (0.01–0.1 Hz) to have the high-frequency respiratory and cardiac noises reduced. The white matter signal, cerebrospinal fluid signal, and Friston 24 head motion parameters were regressed out from the time courses of every voxel.

Voxel-Wise Degree Centrality

The value of degree centrality was calculated using DPARSF (http://rfmri.org/dparsf). For each voxel, the blood-oxygen-level-dependent (BOLD) time course was extracted and the Pearson correlation coefficients with every other voxel in the brain were calculated. A matrix of Pearson correlation coefficients between any pair of voxels was obtained to construct the whole-brain functional connectivity matrix for each participant. Finally, the resulting matrices (DC maps) were smoothed with a Gaussian kernel (full-width half maximum = 6 mm) to enable group comparisons.

To obtain the spatial distribution of DC maps for the HC group and the LLD group, the averaged DC map was calculated for each group using the image calculator module embedded in DPABI. The resulting averaged DC maps were overlaid on rendering views with BrainNet Viewer (http://www.nitrc.org/projects/bnv).

To determine the abnormality in core brain hub architecture as reflected by DC in the LLD patient group, we identified the clusters with DC difference between the LLD patients and HCs, using two-sample *t*-test with gender, age, education level, score of MMSE and framewise displacement regressed out. To determine the difference of DC between LOD patients and EOD patients, another two-sample *t*-test was performed between the LOD group and EOD group in the same manner. AlphaSim correction was used for multiple comparisons to achieve a corrected $p < 0.05$ determined by the Monte Carlo simulation by a combination of a voxel-wise threshold of $p < 0.001$ and a minimum cluster size calculated by the AlphaSim program embedded in DPABI (https://afni.nimh.nih.gov/pub/dist/doc/manual/AlphaSim.pdf), The resulting *t* maps were overlaid on rendering views with BrainNet Viewer and on axial views in slices with the viewer module embedded in DPABI (http://rfmri.org/dpabi), and the anatomy of surviving brain regions was reported using xjView software (http://www.alivelearn.net/xjview).

To further examine whether there exists a relationship between the abnormal DC values identified in the patients and the related clinical assessment (onset age of depression, duration of depression and HAMD score), Pearson's correlation was

respectively calculated in the LLD group and two subgroups. The averaged DC values of abnormal brain regions for the relationship analyses were extracted using spheres of 6-mm radius centering at the coordinates with peak statistical difference from the between-group comparisons (LLD group vs. HC group, or LOD group vs. EOD group) using the signal extractor module embedded in DPABI. To control for multiple comparisons, we used a Bonferroni correction of $p = 0.016$ as the significant statistical threshold (three correlations were examined for each spherical region of interest).

RESULTS

Demographics and Clinical Assessment of Participants

The detailed demographics and results of the clinical assessment of the participants are illustrated in **Table 1**. The 50 LLD patients (19 males, 31 females) had a mean age of 66.6 ± 0.7 (range: 60–78) years, 84.0 ± 17.2 months of disease duration, mean scores of 21.9 ± 1.5 on HAMD and 28.1 ± 0.3 on MMSE. The 33 HCs (17 males, 16 females) had a mean age of 67.2 ± 0.8 (range: 60–78) years. All participants were right-handed. The gender, age and mean score on MMSE were not significant between the patients and healthy controls (ps > 0.091). The education level ($p = 0.043$) and score on HAMD ($p < 0.001$) differed significantly between the groups.

The demographics and clinical assessment of EOD patients and LOD patients are also illustrated in **Table 1**. The two subgroups of patients did not differ in gender, education, scores on HAMD or MMSE (ps > 0.079). There was a significant between-group difference of age (LOD: 68.5 ± 1.0, EOD: 64.0 ± 0.7, $p = 0.002$). Gender, age, education level and score on MMSE were used as covariates in the between-group comparisons of DC maps, in order to exclude the potential impact from demographics.

TABLE 1 | Demographics and clinical assessment of the participants.

	LLD Patients		HC	*p* value
Numbers	50		33	
Gender (M/F)	19/31		17/16	0.224
Age (year)	66.6 ± 0.7		67.2 ± 0.8	0.499
Education (I/E/S/H/C)	1/5/32/6/6		1/4/10/8/10	0.043*
Onset age (year)	59.6 ± 1.6		NA	
Duration (month)	84.0 ± 17.2		NA	
HAMD-24	21.9 ± 1.5		2.4 ± 0.6	<0.001*
MMSE	28.1 ± 0.3		28.9 ± 0.2	0.091
	LOD patients	**EOD patients**	***p* value**	
Numbers	29	21		
Gender (M/F)	14/15	5/16	0.079	
Age (year)	68.5 ± 1.0	64.0 ± 0.7	0.002*	
Education (I/E/S/H/C)	1/2/16/5/5	0/3/16/1/1	0.249	
Onset age (year)	66.7 ± 1.0	49.9 ± 2.3	<0.001*	
Duration (month)	22.4 ± 4.8	169.1 ± 32.5	<0.001*	
HAMD-24	21.7 ± 2.1	22.3 ± 2.3	0.911	
MMSE	28.2 ± 0.4	28.0 ± 0.5	0.980	

*C, college and above; E, elementary school; EOD, early-onset depression; F, female; HAMD, H, high school; Hamilton Depression Scale; HC, healthy control; I, illiteracy; LOD, late-onset depression; M, male; MMSE, Mini-Mental State Examination; p, probability; S, secondary school. * indicates significant difference (p < 0.05) between the groups.*

DC Difference Between LLD Patients and HCs

The mean framewise displacement of the LLD group (0.20 ± 0.02 mm) was slightly larger than that of the HC group (0.14 ± 0.01 mm, $p = 0.009$), and thus was also used as a covariate in the statistical analyses of DC. DC maps for the HC group and the LLD group are presented in **Figure 1**. The estimated smoothness of the DC map is FWHMx = 6.203 mm, FWHMy = 6.402 mm, FWHMz = 6.169 mm, dLh = 0.512. AlphaSim correction is performed with a combination of voxel $p < 0.001$ and cluster size > 12. Compared with the HCs, the LLD patients showed increased DC in the right inferior parietal lobule, right parahippocampal gyrus, right cerebellum and bilateral brainstem (p <0.05, AlphaSim-corrected, **Figure 2**, **Table 2**). The LLD patients showed decreased DC in the brain areas of the left precentral and postcentral gyri, and the left cerebellum ($p < 0.05$, AlphaSim-corrected, **Figure 2**, **Table 2**).

The result with AlphaSim correction by a combination of voxel $p < 0.01$ and cluster size >29 is also presented in the supplementary material (**Figure S1**, **Table S1**) for reference only, in case some brain areas with potential differences couldn't survive the voxel p level of 0.001 due to the relatively small sample size.

DC Difference Between LOD Patients and EOD Patients

Brain areas with a statistical difference in DC between the LOD patients and EOD patients were examined using between-group comparison. The mean framewise displacement of the LOD patient group (0.14 ± 0.02 mm) was not different from that of the EOD patient group (0.15 ± 0.02 mm, $p = 0.158$). The estimated smoothness of the DC map is FWHMx = 6.123 mm, FWHMy = 6.306 mm, FWHMz = 6.065 mm, dLh = 0.539. AlphaSim correction is performed with a combination of voxel $p < 0.001$ and cluster size >12. Compared with the EOD patient group, the LOD patient group showed increased DC in the area of right superior and middle temporal gyri ($p < 0.05$, AlphaSim-corrected, **Figure 3**, **Table 3**). Decreased DC was found in the right cuneus in the LOD patients, compared with the EOD patients ($p < 0.05$, AlphaSim-corrected, **Figure 3**, **Table 3**).

The result with AlphaSim correction by a combination of voxel $p < 0.01$ and cluster size >28 is also presented in the supplementary material (**Figure S2**, **Table S2**) for reference only.

Relationship of DC With Clinical Assessment

The relationship of DC with clinical assessment was explored by the calculation of Pearson's correlation. No significant correlation was found between the DC and the clinical assessment values (onset age of depression, disease duration or HAMD score) after the Bonferroni correction for multiple comparisons in the LLD patient group (ps > 0.094), or in the two subgroups (LOD: ps > 0.056; EOD group: ps > 0.094).

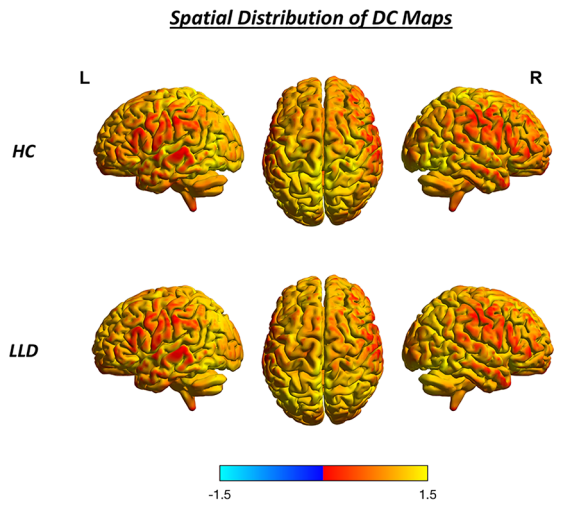

FIGURE 1 | Spatial distribution of DC maps in the HC group and the LLD patient group. Color bars indicate DC values; brighter color indicates DC values higher than the whole-brain average. HC, healthy control; L, left; LLD, late-life depression; R, right.

TABLE 2 | Brain areas showing different DC between LLD patients and HCs ($p < 0.05$, corrected).

Region (AAL name)	Peak MNI coordinate			Voxel size	Peak *T* value
	x	*y*	*z*		
LLD > HC					
Parietal_Inf_R	54	−45	54	13	4.94
Parahippocampal Gyrus_R	15	−15	−27	29	5.21
Brainstem_R/L	3	−39	−33	19	4.42
Cerebelum_Crus2_L	−3	−84	−27	19	4.71
LLD < HC					
Postcentral_L	−21	−42	57	17	−4.27
Precentral_L	−24	−30	54	13	−5.44
Cerebelum_8_L	−24	−69	−57	13	−4.22

AAL, automated anatomical labeling; HC, healthy control; L, left; LLD, late-life depression; MNI, Montreal Neurological Institute; R, right.

DISCUSSION

In the present study, the voxel-wise whole-brain functional connectivity in patients with late-life depression was explored using resting-state fMRI techniques. We found a unique pattern of alterations in the brain activity of the patients. Centrality indices, measured by voxel-wise degree centrality, were found to be abnormal in late-life depressive patients in the somatosensory-motor areas, inferior parietal lobule, parahippocampal gyrus, cerebellum, and brainstem. Furthermore, differentiated cortical areas with DC values were observed in the LOD patients compared with the EOD patients, in the posterior temporal gyrus and occipital region. No correlation was found between the abnormal centrality indices and the clinical assessment in the patients. The general function of brain areas with an abnormal degree centrality in the LLD patients, as well as the difference between EOD and LOD subgroups, may strengthen the understanding of the intrinsic neural-network profiles of LLD.

The somatosensory cortex receives all sensory inputs from the body, and it is responsible for somatosensory perception (40).

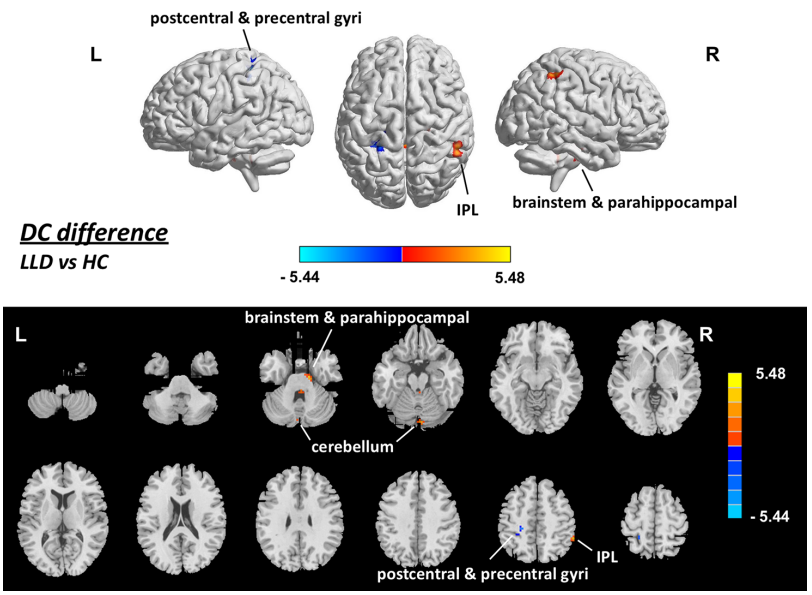

FIGURE 2 | Brain areas showing difference in DC between LLD patients and HCs ($p < 0.05$, corrected), with gender, age, education, score on MMSE and framewise displacement regressed out. Upper: rendering views. Lower: axial slice views. Color bars indicate *T*-score; a warm color indicates areas where DC value in LLD patients > DC value in HCs, a cold color indicates areas where DC value in LLD patients < DC value in HCs. DC, degree centrality; HC, healthy control; IPL, inferior parietal lobule; L, left; LLD, late-life depression; R, right.

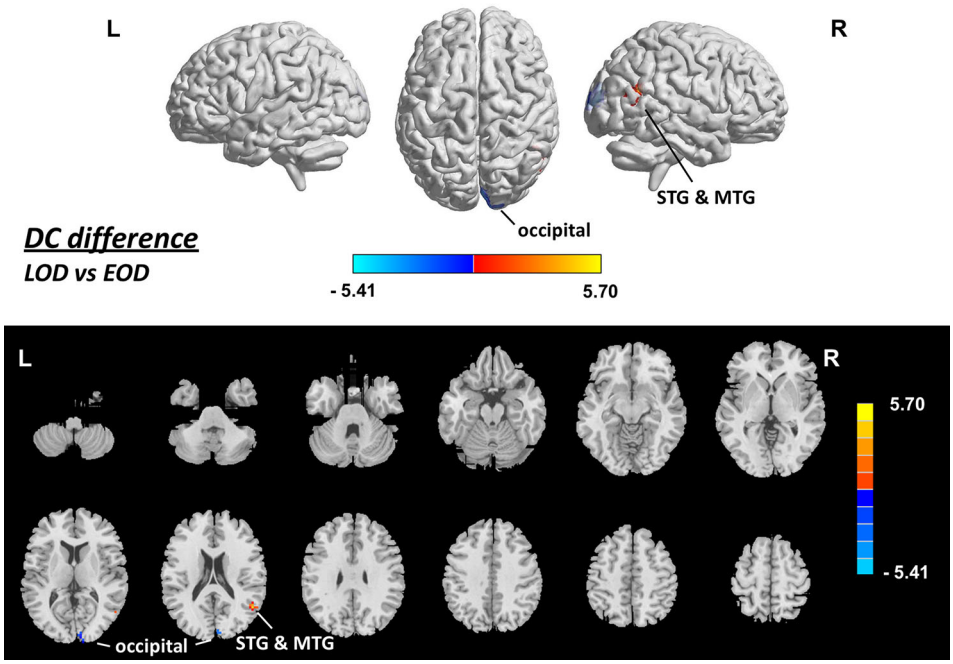

FIGURE 3 | Brain areas showing difference in DC between LOD and EOD patients ($p < 0.05$, corrected), with gender, age, education, score on MMSE and framewise displacement regressed out. Upper: rendering views. Lower: axial slice views. Color bars indicate *T*-score; warm color indicates areas whose DC value in LOD patients > DC value in EOD patients, cold color indicates areas whose DC value in LOD patients < DC value in EOD patients. EOD, early-onset depression; HC, healthy control; L, left; LOD, late-onset depression; MTG, middle temporal gyrus; R, right; STG, superior temporal gyrus.

TABLE 3 | Brain areas showing different DC between LOD and EOD patients ($p < 0.05$, corrected).

Region (AAL name)	Peak MNI coordinate			Voxel size	Peak *T* value
	x	*y*	*z*		
LOD > EOD					
Temporal_Sup_R	51	–57	21	13	5.27
Temporal_Mid_R	54	–63	12	13	5.70
LOD < EOD					
Cuneus_R	12	–93	12	36	–5.41

AAL, automated anatomical labeling; EOD, early-onset depression; L, left; LOD, late-onset depression; MNI, Montreal Neurological Institute; R, right.

Abnormal somatic symptoms such as somatization, defined as physical symptoms developed as a result of stress or emotional problems, have often been observed in depressive patients (41, 42). Alteration of activity in the somatosensory cortex has been suggested to be involved in the neural underpinnings of somatic symptom disorder (43). The motor cortex and cerebellum are regarded as important brain regions related to voluntary movement and motor control (44, 45). Deficits in motor-related functions have recently been observed in LLD patients (46). Thus, our observation of decreased DC in somatosensory-motor cortices and altered cerebellar DC in the LLD patients might be related to the somatosensory abnormalities and motor deficits associated with depression.

The inferior parietal lobule, a major network hub of the human brain, is involved in a broad range of behaviors and functions from bottom-up perception to social cognition and plays as important nodes in multiple network, including the frontoparietal control network, default mode network, cingulo-opercular network and ventral attention network (47). A resting-state fMRI study indicated that the connectivity between the dorsomedial prefrontal cortex and the inferior parietal lobule is related with negative self-focused thought associated with depressive symptoms in the patients with major depression (48). Our observation of increased DC at inferior parietal lobule indicates an intrinsic functional alteration in this parietal hub area in the LLD patients.

The parahippocampal gyrus is a limbic structure mainly associated with visuospatial processing and episodic memory (49). Previous studies have revealed that LLD is associated with impaired visuospatial memory and episodic memory (50, 51). The white matter integrity of parahippocampal gyrus was found disrupted in the LLD patients (52). An fMRI study indicated abnormal activation of parahippocampal gyrus while performing a memory task in LLD patients (53). Another study including 1,017 participants from the Human Connectome Project revealed that increased functional connectivity of the parahippocampal gyrus is associated with poor sleep quality and depressive problems scores (54). Thus, the increased centrality in parahippocampal gyrus observed in the present study may be related with impaired memory and depressive symptoms and poor sleep quality in the LLD patients.

The brainstem is an important structure that regulates autonomic functions, relays sensory and motor information, and

modulates cognition, mood, and emotions. The brainstem is particularly critical in the modulation of emotion, as it is the home to a group of modulatory neurotransmitters such as serotonin, dopamine, and norepinephrine (55). Imaging studies have reported structural and functional abnormalities in the brainstem of patients with major depression (56, 57). Some studies also indicate that the brainstem aminergic nuclei is closely associated with late-life depressive symptoms (58, 59). Our observation of decreased network centrality of brainstem confirms an intrinsic functional abnormality of brainstem nuclei in the late-life depressive individuals.

Besides the brain areas with abnormal DC between LLD patients and HCs, we also observed DC differences between LOD patients and EOD patients, which supports the perspective that the LOD patients and EOD patients have differentiated intrinsic brain networks. The posterior middle temporal gyrus has been suggested to play critical roles in the integration of automatic information retrieval and executively-demanding goal-oriented cognition (60). The occipital cortex is mainly responsible for visual stimulus processing (61). Some studies have revealed that LOD patients have more extensive deficits than EOD patients in some cognitive domains, including the realm of memory and visual-spatial processing (27–29). In the present study, brain areas of posterior temporal gyrus and occipital areas were found with different DC values in the LOD patients and the EOD patients. It is tempting to assume that the differentiated levels of DC may be associated with the neural basis for different degrees of impairment in high cognition between LOD and EOD patients.

The study had several limitations. First, the negative result of the relationship of DC with clinical assessment (depression severity, duration of depression, and onset age) indicates that the abnormality in DC might not directly contributed to depression-related manifestations, and suggests that the abnormality might be associated with the somatic and emotional burden, and cognitive deficits other than depression itself. However, the resting-state fMRI was performed without tasks measuring emotional and cognitive processing in the patients. In future studies, the relationship of abnormal centrality indices and the emotional processing/cognitive functions needs to be examined by introducing tasks being tested in the patients. Second, although the abnormality of DC in LLD patients has been identified, the sample size of the present study is relatively small. The negative effects of DC difference in the prefrontal regions and the negative result of the relationship between DC and clinical assessment indicates may be attributed to the relatively small sample size. The findings need to be confirmed in future studies using large sample sizes. Third, the antidepressants the patients took may affect the resting-state brain activity. Our findings also did not assess the role of medicine elution which may contribute to the abnormality of the brain-network profile of the patients.

CONCLUSION

Our findings in the present study indicate that the voxel-wise DC displays abnormality in LLD patients in a wide range of brain areas, which might be associated with the sensorimotor- and emotion-related alterations, and cognitive impairments observed in the patients. Also, there exists a difference in DC patterns between EOD and LOD patients. Our study might help to strengthen the understanding of the pathophysiology of LLD.

DATA AVAILABILITY STATEMENT

The datasets generated for this study are available on request to the corresponding authors.

ETHICS STATEMENT

The studies involving human participants were reviewed and approved by Ethics Committee of Shanghai Pudong New Area Mental Health Center. The patients/participants provided their written informed consent to participate in this study.

AUTHOR CONTRIBUTIONS

HG, YH, YJ, CZ, VV, BS, FY and SZ conceived and designed the study. HG, YH and YJ recruited the participants. QD and NH collected the data. QD, NH, JL and HX analyzed the data. JL, HG, HX, CZ, VV, BS, FY and SZ interpreted the data and wrote the paper.

FUNDING

This work was supported by the National Natural Science Foundation of China (81771482 to BS); Shanghai Science and Technology Committee (18410710400 to BS); Shanghai Pudong New District Health and Family Planning Commission Key Discipline Construction Fund Project (PWZxk2017-29); Outstanding Clinical Discipline Project of Shanghai Pudong (PWYgy2018-10). Dr. VV is supported by a Medical Research Council Senior Clinical Fellowship (MR/P008747/1). The funding organizations played no further role in study design, data collection, analysis and interpretation and paper writing.

ACKNOWLEDGMENTS

The authors thank all the individuals who served as the research participants.

SUPPLEMENTARY MATERIAL

The Supplementary Material for this article can be found online at: https://www.frontiersin.org/articles/10.3389/fpsyt.2019.01024/full#supplementary-material

REFERENCES

1. BirrerRB, VemuriSP. Depression in later life: a diagnostic and therapeutic challenge. *Am Fam Physician* (2004) 69(10):2375–82.
2. RiddleM, Potter GG, McQuoid DR, Steffens DC, Beyer JL, Taylor WD. Longitudinal cognitive outcomes of clinical phenotypes of late-life depression. *Am J Geriatr Psychiatry* (2017) 25(10):1123–34. doi: 10.1016/j.jagp.2017.03.016
3. Maeshima H, Baba H, Nakano Y, Satomura E, Namekawa Y, Takebayashi N, et al. Time course for memory dysfunction in early-life and late-life major depression: a longitudinal study from the juntendo university mood disorder project. *J Affect Disord* (2013) 151(1):66–70. doi: 10.1016/j.jad.2013.05.050
4. Liao W, Zhang X, Shu H, Wang Z, Liu D, Zhang Z. The characteristic of cognitive dysfunction in remitted late life depression and amnestic mild cognitive impairment. *Psychiatry Res* (2017) 251:168–75. doi: 10.1016/j.psychres.2017.01.024
5. Dybedal GS, Tanum L, Sundet K, Gaarden TL, Bjolseth TM. Neuropsychological functioning in late-life depression. *Front Psychol* (2013) 4:381. doi: 10.3389/fpsyg.2013.00381
6. Potter GG, Madden DJ, Costello MC, Steffens DC. Reduced comparison speed during visual search in late life depression. *J Clin Exp Neuropsychol* (2013) 35 (10):1060–70. doi: 10.1080/13803395.2013.856381
7. Rajtar-Zembaty A, Salakowski A, Rajtar-Zembaty J, Starowicz-Filip A. Executive dysfunction in late-life depression. *Psychiatr Pol* (2017) 51 (4):705–18. doi: 10.12740/PP/OnlineFirst/63765
8. Schweitzer I, Tuckwell V, Ames D, O'Brien J. Structural neuroimaging studies in late-life depression: a review. *World J Biol Psychiatry* (2001) 2(2):83–8. doi: 10.3109/15622970109027497
9. Du M, Liu J, Chen Z, Huang X, Li J, Kuang W, et al. Brain grey matter volume alterations in late-life depression. *J Psychiatry Neurosci* (2014) 39(6):397–406. doi: 10.1503/jpn.130275
10. Aizenstein HJ, Butters MA, Wu M, Mazurkewicz LM, Stenger VA, Gianaros PJ, et al. Altered functioning of the executive control circuit in late-life depression: episodic and persistent phenomena. *Am J Geriatr Psychiatry* (2009) 17(1):30–42. doi: 10.1097/JGP.0b013e31817b60af
11. Leal SL, Noche JA, Murray EA, Yassa MA. Disruption of amygdala-entorhinal-hippocampal network in late-life depression. *Hippocampus* (2017) 27(4):464–76. doi: 10.1002/hipo.22705
12. Eyre HA, Yang H, Leaver AM, Van Dyk K, Siddarth P, Cyr NS, et al. Altered resting-state functional connectivity in late-life depression: a cross-sectional study. *J Affect Disord* (2016) 189:126–33. doi: 10.1016/j.jad.2015.09.011
13. Cieri F, Esposito R, Cera N, Pieramico V, Tartaro A, di Giannantonio M. Late-life depression: modifications of brain resting state activity. *J Geriatr Psychiatry Neurol* (2017) 30(3):140–50. doi: 10.1177/0891988717700509
14. Liu F, Hu M, Wang S, Guo W, Zhao J, Li J, et al. Abnormal regional spontaneous neural activity in first-episode, treatment-naive patients with late-life depression: a resting-state fMRI study. *Prog Neuropsychopharmacol Biol Psychiatry* (2012) 39(2):326–31. doi: 10.1016/j.pnpbp.2012.07.004
15. Zuo XN, Ehmke R, Mennes M, Imperati D, Castellanos FX, Sporns O, et al. Network centrality in the human functional connectome. *Cereb Cortex* (2012) 22(8):1862–75. doi: 10.1093/cercor/bhr269
16. Liu F, Zhu C, Wang Y, Guo W, Li M, Wang W, et al. Disrupted cortical hubs in functional brain networks in social anxiety disorder. *Clin Neurophysiol* (2015) 126(9):1711–6. doi: 10.1016/j.clinph.2014.11.014
17. Guo Z, Liu X, Hou H, Wei F, Liu J, Chen X. Abnormal degree centrality in Alzheimer's disease patients with depression: A resting-state functional magnetic resonance imaging study. *Exp Gerontol* (2016) 79:61–6. doi: 10.1016/j.exger.2016.03.017
18. Eijlers AJ, Meijer KA, Wassenaar TM, Steenwijk MD, Uitdehaag BM, Barkhof F, et al. Increased default-mode network centrality in cognitively impaired multiple sclerosis patients. *Neurology* (2017) 88(10):952–60. doi: 10.1212/WNL.0000000000003689
19. Zhou Q, Womer FY, Kong L, Wu F, Jiang X, Zhou Y, et al. Trait-related cortical-subcortical dissociation in bipolar disorder: analysis of network degree centrality. *J Clin Psychiatry* (2017) 78(5):584–91. doi: 10.4088/JCP.15m10091
20. Wang H, Zhang B, Zeng B, Tang Y, Zhang T, Zhao S, et al. Association between catechol-O-methyltransferase genetic variation and functional connectivity in patients with first-episode schizophrenia. *Schizophr Res* (2018b) 199:214–20. doi: 10.1016/j.schres.2018.04.023
21. Liu F, Tian H, Li J, Li S, Zhuo C. Altered voxel-wise gray matter structural brain networks in schizophrenia: Association with brain genetic expression pattern. *Brain Imaging Behav* (2019) 13(2):493–502. doi: 10.1007/s11682-018-9880-6
22. Zhou M, Yang C, Bu X, Liang Y, Lin H, Hu X, et al. Abnormal functional network centrality in drug-naive boys with attention-deficit/hyperactivity disorder. *Eur Child Adolesc Psychiatry* (2019) 28(10):1321–8. doi: 10.1007/s00787-019-01297-6
23. Di Martino A, Zuo XN, Kelly C, Grzadzinski R, Mennes M, Schvarcz A, et al. Shared and distinct intrinsic functional network centrality in autism and attention-deficit/hyperactivity disorder. *Biol Psychiatry* (2013) 74(8):623–32. doi: 10.1016/j.biopsych.2013.02.011
24. Wang H, Chen H, Wu J, Tao L, Pang Y, Gu M, et al. Altered resting-state voxel-level whole-brain functional connectivity in depressed Parkinson's disease. *Parkinsonism Relat Disord* (2018a) 50:74–80. doi: 10.1016/j.parkreldis.2018.02.019
25. Li M, Das T, Deng W, Wang Q, Li Y, Zhao L, et al. Clinical utility of a short resting-state MRI scan in differentiating bipolar from unipolar depression. *Acta Psychiatr Scand* (2017) 136(3):288–99. doi: 10.1111/acps.12752
26. Grayson L, Thomas A. A systematic review comparing clinical features in early age at onset and late age at onset late-life depression. *J Affect Disord* (2013) 150(2):161–70. doi: 10.1016/j.jad.2013.03.021
27. Sachs-Ericsson N, Corsentino E, Moxley J, Hames JL, Rushing NC, Sawyer K, et al. A longitudinal study of differences in late- and early-onset geriatric depression: depressive symptoms and psychosocial, cognitive, and neurological functioning. *Aging Ment Health* (2013) 17(1):1–11. doi: 10.1080/13607863.2012.717253
28. Mackin RS, Nelson JC, Delucchi KL, Raue PJ, Satre DD, Kiosses DN, et al. Association of age at depression onset with cognitive functioning in individuals with late-life depression and executive dysfunction. *Am J Geriatr Psychiatry* (2014) 22(12):1633–41. doi: 10.1016/j.jagp.2014.02.006
29. Hashem AH, Nasreldin M, Gomaa MA, Khalaf O. O. Late versus early onset depression in elderly patients: vascular risk and cognitive impairment. *Curr Aging Sci* (2017) 10(3)211–6. doi: 10.2174/1874609810666170404105634
30. Lloyd AJ, Ferrier IN, Barber R, Gholkar A, Young AH, O'Brien JT. Hippocampal volume change in depression: late- and early-onset illness compared. *Br J Psychiatry* (2004) 184:488–95. doi: 10.1192/bjp.184.6.488
31. Hickie I, Naismith S, Ward PB, Turner K, Scott E, Mitchell P, et al. Reduced hippocampal volumes and memory loss in patients with early- and late-onset depression. *Br J Psychiatry* (2005) 186:197–202. doi: 10.1192/bjp.186.3.197
32. Janssen J, Hulshoff Pol HE, de Leeuw FE, Schnack HG, Lampe IK, Kok RM, et al. Hippocampal volume and subcortical white matter lesions in late life depression: comparison of early and late onset depression. *J Neurol Neurosurg Psychiatry* (2007) 78(6):638–40. doi: 10.1136/jnnp.2006.098087
33. Ballmaier M, Narr KL, Toga AW, Elderkin-Thompson V, Thompson PM, Hamilton L, et al. Hippocampal morphology and distinguishing late-onset from early-onset elderly depression. *Am J Psychiatry* (2008) 165(2):229–37. doi: 10.1176/appi.ajp.2007.07030506
34. Disabato BM, Morris C, Hranilovich J, D'Angelo GM, Zhou G, Wu N, et al. Comparison of brain structural variables, neuropsychological factors, and treatment outcome in early-onset versus late-onset late-life depression. *Am J Geriatr Psychiatry* (2014) 22(10):1039–46. doi: 10.1016/j.jagp.2013.02.005
35. Lebedeva A, Borza T, Haberg AK, Idland AV, Dalaker TO, Aarsland D, et al. Neuroanatomical correlates of late-life depression and associated cognitive changes. *Neurobiol Aging* (2015) 36(11):3090–9. doi: 10.1016/j.neurobiolaging.2015.04.020
36. Chen JD, Liu F, Xun GL, Chen HF, Hu MR, Guo XF, et al. Early and late onset, first-episode, treatment-naive depression: same clinical symptoms, different regional neural activities. *J Affect Disord* (2012) 143(1-3):56–63. doi: 10.1016/j.jad.2012.05.025
37. Guo WB, Liu F, Xun GL, Hu MR, Guo XF, Xiao CQ, et al. Reversal alterations of amplitude of low-frequency fluctuations in early and late onset, first-episode, drug-naive depression. *Prog Neuropsychopharmacol Biol Psychiatry* (2013) 40:153–9. doi: 10.1016/j.pnpbp.2012.08.014
38. Hamilton M. A rating scale for depression. *J Neurol Neurosurg Psychiatry* (1960) 23:56–62. doi: 10.1136/jnnp.23.1.56

39. Folstein MF, Folstein SE, McHugh PR. "Mini-mental state". A practical method for grading the cognitive state of patients for the clinician. *J Psychiatr Res* (1975) 12(3):189–98. doi: 10.1016/0022-3956(75)90026-6
40. Harding-Forrester S, Feldman DE. Somatosensory maps. *Handb Clin Neurol* (2018) 151:73–102. doi: 10.1016/B978-0-444-63622-5.00004-8
41. Chakraborty K, Avasthi A, Grover S, Kumar S. Functional somatic complaints in depression: an overview. *Asian J Psychiatr* (2010) 3(3):99–107. doi: 10.1016/j.ajp.2010.07.003
42. Bekhuis E, Boschloo L, Rosmalen JG, de Boer MK, Schoevers RA. The impact of somatic symptoms on the course of major depressive disorder. *J Affect Disord* (2016) 205:112–8. doi: 10.1016/j.jad.2016.06.030
43. Li Q, Xiao Y, Li Y, Li L, Lu N, Xu Z, et al. Altered regional brain function in the treatment-naive patients with somatic symptom disorder: a resting-state fMRI study. *Brain Behav* (2016) 6(10):e00521. doi: 10.1002/brb3.521
44. Ebbesen CL, Brecht M. Motor cortex - to act or not to act? *Nat Rev Neurosci* (2017) 18(11):694–705. doi: 10.1038/nrn.2017.119
45. D'Angelo E. Physiology of the cerebellum. *Handb Clin Neurol* (2018) 154:85–108. doi: 10.1016/B978-0-444-63956-1.00006-0
46. O'Brien JT, Gallagher P, Stow D, Hammerla N, Ploetz T, Firbank M, et al. A study of wrist-worn activity measurement as a potential real-world biomarker for late-life depression. *Psychol Med* (2017) 47(1):93–102. doi: 10.1017/S0033291716002166
47. Igelstrom KM, Graziano MSA. The inferior parietal lobule and temporoparietal junction: a network perspective. *Neuropsychologia* (2017) 105:70–83. doi: 10.1016/j.neuropsychologia.2017.01.001
48. Philippi CL, Cornejo MD, Frost CP, Walsh EC, Hoks RM, Birn R, et al. Neural and behavioral correlates of negative self-focused thought associated with depression. *Hum Brain Mapp* (2018) 39(5):2246–57. doi: 10.1002/hbm.24003
49. Aminoff EM, Kveraga K, Bar M. The role of the parahippocampal cortex in cognition. *Trends Cognit Sci* (2013) 17(8):379–90. doi: 10.1016/j.tics.2013.06.009
50. Herrmann LL, Goodwin GM, Ebmeier KP. The cognitive neuropsychology of depression in the elderly. *Psychol Med* (2007) 37(12):1693–702. doi: 10.1017/S0033291707001134
51. Klojcnik M, Kavcic V, Bakracevic Vukman K. Relationship of depression with executive functions and visuospatial memory in elderly. *Int J Aging Hum Dev* (2017) 85(4):490–503. doi: 10.1177/0091415017712186
52. Guo W, Liu F, Xun G, Hu M, Guo X, Xiao C, et al. Disrupted white matter integrity in first-episode, drug-naive, late-onset depression. *J Affect Disord* (2014) 163:70–5. doi: 10.1016/j.jad.2014.03.044
53. Weisenbach SL, Kassel MT, Rao J, Weldon AL, Avery ET, Briceno EM, et al. Differential prefrontal and subcortical circuitry engagement during encoding of semantically related words in patients with late-life depression. *Int J Geriatr Psychiatry* (2014) 29(11):1104–15. doi: 10.1002/gps.4165
54. Cheng W, Rolls ET, Ruan H, Feng J. Functional connectivities in the brain that mediate the association between depressive problems and sleep quality. *JAMA Psychiatry* (2018) 75(10):1052–61. doi: 10.1001/jamapsychiatry.2018.1941
55. Venkatraman A, Edlow BL, Immordino-Yang MH. The brainstem in emotion: a review. *Front Neuroanat* (2017) 11:15. doi: 10.3389/fnana.2017.00015
56. Supprian T, Reiche W, Schmitz B, Grunwald I, Backens M, Hofmann E, et al. MRI of the brainstem in patients with major depression, bipolar affective disorder and normal controls. *Psychiatry Res* (2004) 131(3):269–76. doi: 10.1016/j.pscychresns.2004.02.005
57. Song YJ, Korgaonkar MS, Armstrong LV, Eagles S, Williams LM, Grieve SM. Tractography of the brainstem in major depressive disorder using diffusion tensor imaging. *PloS One* (2014) 9(1):e84825. doi: 10.1371/journal.pone.0084825
58. Manji HK, Drevets WC, Charney DS. The cellular neurobiology of depression. *Nat Med* (2001) 7(5):541–7. doi: 10.1038/87865
59. Wilson RS, Nag S, Boyle PA, Hizel LP, Yu L, Buchman AS, et al. Brainstem aminergic nuclei and late-life depressive symptoms. *JAMA Psychiatry* (2013) 70(12):1320–8. doi: 10.1001/jamapsychiatry.2013.2224
60. Davey J, Thompson HE, Hallam G, Karapanagiotidis T, Murphy C, De Caso I, et al. Exploring the role of the posterior middle temporal gyrus in semantic cognition: integration of anterior temporal lobe with executive processes. *Neuroimage* (2016) 137:165–77. doi: 10.1016/j.neuroimage.2016.05.051
61. Wandell BA, Dumoulin SO, Brewer AA. Visual field maps in human cortex. *Neuron* (2007) 56(2):366–83. doi: 10.1016/j.neuron.2007.10.012

Conflict of Interest: The authors declare that the research was conducted in the absence of any commercial or financial relationships that could be construed as a potential conflict of interest.

frontiers in Psychiatry

ORIGINAL RESEARCH
published: 05 February 2020
doi: 10.3389/fpsyt.2019.00983

Abnormal Functional and Structural Connectivity of Amygdala-Prefrontal Circuit in First-Episode Adolescent Depression: A Combined fMRI and DTI Study

Feng Wu[1†], Zhaoyuan Tu[1†], Jiaze Sun[1], Haiyang Geng[2], Yifang Zhou[3], Xiaowei Jiang[2,4], Huizi Li[1] and Lingtao Kong[1]*

[1] Department of Psychiatry, The First Affiliated Hospital of China Medical University, Shenyang, China, [2] Department of Radiology, The First Affiliated Hospital of China Medical University, Shenyang, China, [3] Department of Gerontology, The First Affiliated Hospital of China Medical University, Shenyang, China, [4] Brain Function Research Section, The First Affiliated Hospital of China Medical University, Shenyang, China

OPEN ACCESS

Edited by:
Wenbin Guo,
Central South University, China

Reviewed by:
Sheng Zhang,
Yale University, United States
Qiu Chang Jian,
Sichuan University, China

****Correspondence:***
Lingtao Kong
ltkong@cmu.edu.cn

[†]These authors have contributed equally to this work

Specialty section:
This article was submitted to Neuroimaging and Stimulation, a section of the journal Frontiers in Psychiatry

Received: *18 September 2019*
Accepted: *11 December 2019*
Published: *05 February 2020*

Citation:
Wu F, Tu Z, Sun J, Geng H, Zhou Y, Jiang X, Li H and Kong L (2020) Abnormal Functional and Structural Connectivity of Amygdala-Prefrontal Circuit in First-Episode Adolescent Depression: A Combined Fmri and DTI Study. Front. Psychiatry 10:983. doi: 10.3389/fpsyt.2019.00983

Background: Abnormalities of functional and structural connectivity in the amygdala-prefrontal circuit which involved with emotion processing have been implicated in adults with major depressive disorder (MDD). Adolescent MDD may have severer dysfunction of emotion processing than adult MDD. In this study, we used resting-state functional magnetic resonance imaging (rs-fMRI) and diffusion tensor imaging (DTI) to examine the potential functional and structural connectivity abnormalities within amygdala-prefrontal circuit in first-episode medication-naïve adolescents with MDD.

Methods: Rs-fMRI and DTI data were acquired from 36 first-episode medication-naïve MDD adolescents and 37 healthy controls (HC). Functional connectivity between amygdala and the prefrontal cortex (PFC) and fractional anisotropy (FA) values of the uncinate fasciculus (UF) which connecting amygdala and PFC were compared between the MDD and HC groups. The correlation between the FA value of UF and the strength of the functional connectivity in the PFC showing significant differences between the two groups was identified.

Results: Compared with the HC group, decreased functional connectivity between left amygdala and left ventral PFC was detected in the adolescent MDD group. FA values were significant lower in the left UF within the adolescent MDD group compared to the HC group. There was no significant correlation between the UF and FA, and the strength of functional connectivity within the adolescent MDD group.

Conclusions: First-episode medication-naïve adolescent MDD showed decreased functional and structural connectivity in the amygdala-prefrontal circuit. These findings suggest that both functional and structural abnormalities of the amygdala-prefrontal circuit

may present in the early onset of adolescent MDD and play an important role in the neuropathophysiology of adolescent MDD.

Keywords: adolescent major depressive disorder, functional connectivity, magnetic resonance imaging, diffusion tensor imaging, amygdala, ventral prefrontal cortex

INTRODUCTION

Major depressive disorder (MDD) is characterized by emotional dysregulation, implicating abnormalities of frontal-limbic neural circuits involved in emotional processing as the core feature. Convergent studies provide consistent evidence for functional and structural abnormalities in the prefrontal cortex (PFC) and amygdala, the key components of frontal-limbic neural circuits in adult MDD. Adolescent MDD is associated with the prominence of irritability, mood reactivity, and fluctuating symptoms (1), reflecting possible severer emotional processing dysfunction than adult MDD. Furthermore, as its strong links with recurrence later in life (2), investigation of depression in adolescence may help us to further understand the role of abnormal developmental process leading to adult MDD.

Dysfunction of amygdala-prefrontal circuits has been implicated in MDD through functional magnetic resonance imaging (fMRI). Hyperactivation of amygdala and hypoactivation of PFC were shown in task-related fMRI studies within adult MDD, as well as adolescent MDD. Recently, resting-state fMRI (rs-fMRI) was used to investigate resting state functional connectivity (rsFC), the correlation of low frequency blood oxygen level-dependent signal fluctuations between brain regions in MDD (3). Our previous study demonstrated decreased amygdala-PFC functional connectivity in adult MDD (4). Other researchers also reported similar findings (5, 6), suggesting that dysfunction of these circuits may play an important role in the neuropathophysiology of MDD. Correspondingly, few studies detected functional connectivity between amygdala and other brain regions in adolescent MDD. Connolly et al's study reported decreased amygdala-dorsolateral prefrontal cortex (DLPFC) functional connectivity and amygdala-ventromedial prefrontal cortex (VMPFC) functional connectivity in adolescent MDD patients (7). Cullen et al's two studies failed to find amygdala-PFC functional connectivity abnormalities, but find decreased functional connectivity in amygdala-limbic networks and anterior cingulate cortex (ACC)-based networks (8, 9). Luking et al.'s another study reported reduced amygdala functional connectivity with dorsal frontal/parietal and limbic regions in children with MDD history (10). Taken together, inconsistent findings suggest that functional connectivity of amygdala-related circuits need to be further investigated in adolescent MDD.

As white matter fibers structural connecting brain regions into neural circuits, disconnection of white matter fibers may provide the structural basis of functional connectivity abnormalities in the brain (11). Diffusion tensor imaging (DTI) is a MRI technique for detecting white matter microstructure integrity *in vivo*. Fractional anisotropy (FA) which measures the principal directionality of water diffusion is the commonly used parameter to assess whiter matter integrity in DTI studies. Decreased FA values were detected in the uncinate fasciculus, the superior longitudinal fasciculus, the cingulum, the corpus callosum (12), the genu and UF (13) in adult MDD, indicating abnormalities of white matter fiber integrity. In the recent studies of adolescent MDD, Cullen et al. reported lower FA in the tract connecting subgenual ACC to amygdala (14), Bessette et al. reported lower FA in corpus callosum, midbrain white matter tracts, and corticospinal tracts (15), while Aghajani et al. reported lower FA in the body of the corpus callosum, as well as higher FA in the uncinate fasciculus (16), Taken together, these findings support the hypothesis that white matter deficits of frontal-limbic neural circuits may present in the early stage of depression.

The relationship between structural and functional connectivity has been noticed. Kim et al. reported a positive relationship between amygdala reactivity and white matter integrity of the uncinate fasciculus in healthy controls, suggesting the relationship between functional and structural connectivity in amygdala-prefrontal circuits (17). Furthermore, negative relationship between amygdala volume and activity during emotional processing tasks in MDD (18). The positive correlations between FA values of left UF and resting state functional connectivity of the left vlPFC-amygdala and the left vlPFC-hippocampus in late life depression (19). One previous study reported that amygdala volume changes is negative to the age of on set, and younger MDD adults (< 30 years old) show more abnormal FC changes in left amygdala, while older MDD adults (≥30 years old) are in right amygdala (20). However, the relationship between functional and structural connectivity in adolescent MDD is not fully explored. Hence, we combined rs-fMRI and DTI in the current study to examine the functional and structural connectivity and their relationship within amygdala-prefrontal circuits in first-episode medication-naïve MDD adolescents. In our hypothesis, functional and structural connectivity abnormalities would be detected between amygdala and PFC within adolescent MDD, as well as an association between the functional and structural connectivity in this circuitry.

Abbreviations: ACC, anterior cingulate cortex; AC–PC, anterior–posterior commissure; BA, Brodmann areas; DTI, diffusion tensor imaging; FA, fractional anisotropy; fMRI, functional magnetic resonance imaging; HAMD-17, The 17-item Hamilton Depression Rating Scale; HC, healthy control subjects; KSADS-PL, the Schedule for Affective Disorders and Schizophrenia for School-Age Children; MDD, major depressive disorder; MNI, Montreal Neurological Institute; PFC, prefrontal cortex; rs-fMRI, resting-state fMRI; rsFC, resting state functional connectivity; ROI, regions of interest; VPFC,ventral prefrontal cortex.

MATERIALS AND METHODS

Participants

We recruited 36 medication-naïve adolescent outpatients with MDD from the outpatient clinic of the Department of Psychiatry and 37 healthy control subjects (HC) matched for sex, age and education by advertisements in the Frist Affiliated Hospital of China Medical University. A trained psychiatrist individually diagnosed all participants using the Schedule for Affective Disorders and Schizophrenia for School-Age Children (KSADS-PL). All MDD patients met the following inclusion criteria: fulfilling KSADS-PL criteria for MDD; first depressive episode; onset age between 13 and 17; no comorbid diagnosis of other affective and psychotic disorders; We used the 17-item Hamilton Depression Rating Scale (HAMD-17) (21) to score the severity of depression. All HC adolescents were confirmed the absence of psychiatric disorders. Any HC was excluded if he/she had any family history of psychiatric disorders in their first- or second-degree relatives. Any participant with the following additional criteria was excluded: history of head injury or neurological disorder; history of drug abuse or dependence; contraindications for MRI. All participants were scanned within 24 h of initial contact, and rated on the HAMD-17 at the time of scanning.

The study was approved by the Institutional Review Board of the China Medical University. All participants and their parent/legal guardian received a detailed description of the study, after that, they provided written informed consent to make sure they fully understand and agree their involvement of the study.

Mri Data Acquisition

A GE Signa HDX 3.0T MRI scanner (General Electric, Milwaukee, USA) with a standard head coil at the First Affiliated Hospital of China Medical University was used to perform the magnetic resonance imaging scan. Restraining foam pads and ear plugs were used for each participant to minimize the head motion and reduce the noise interference during the scan. Participants were asked to remain awake throughout the scan and keep their eyes closed. We used a gradient-echo planar imaging sequence to collect the rs-fMRI data with the following scan parameters: TR 2,000 ms, TE 30ms, 35 contiguous axial slices, 3 mm thickness, without gap, matrix 64 × 64, FOV 240 × 240mm^2, flip angle 90°. We used a spin-echo planar imaging sequence to collect the DTI data with the following scan parameters: 25 non-collinear directions, b = 1,000 s/mm^2, TR 17,000 ms, TE 85.4 ms, 65 contiguous axial slices, 2 mm thickness, without gap, imaging matrix 120 × 120, FOV = 240 × 240 mm^2.

Rs-fMRI Data Processing

We used Resting-State fMRI Data Analysis Toolkit (REST) with Statistical Parametric Mapping 8 (SPM8) to processed the rs-fMRI data. The first 10 volumes of scanned data of each participant were deleted due to magnetic saturation effects. The remaining images were preprocessed with the following steps: First, slice timing and head motion correction: head motion parameters were computed by estimating translation in each direction and the angular rotation about each axis for each volume. The rs-fMRI data was excluded if their head motion was >2 mm maximum displacement in any of the x, y, or z directions or 2° of any angular motion throughout the course of the scan (no participants were excluded). Second, spatial normalization image to the standard Montreal Neurological Institute (MNI) space and resampled voxel size into 3 × 3 × 3 mm^3 voxels then smoothing with a Gaussian filter of 6 mm full-width at half-maximum (FWHM). Then REST software was used to remove linear drift through linear regression and temporal band-pass filtering (0.01–0.08 Hz) to reduce the effects of low-frequency drifts and physiological high-frequency noise. Linear regression of head motion parameters, global mean signal, white matter signal and cerebrospinal fluid signal was performed to remove the effects of the nuisance covariates.

The left and right amygdala ROIs were defined separately according to the automated anatomical labeling (AAL) template contained in REST (22). The time course for all voxels of each ROI were averaged to calculate the mean time course for each amygdala ROI. The time course of each amygdala ROI was then correlated with the time course of each pixel in the brain, resulted with a correlation map for each subject that contained the correlation coefficient for each voxel with that of the amygdala ROI. The resulting correlation coefficients were transformed into z-scores. Subject-specific maps of resting state correlations to each amygdala ROI were created.

DTI Data Processing

We processed DTI data using the PANDA toolbox (23) in FSL diffusion toolkit and MRIcron. DICOM files were first converted into NIfTI images, then estimate the brain mask, crop images, correct for the eddy-current effect, average acquisitions, and calculate DTI metrics. Finally, diffusion metrics were produced ready for statistical analysis. The individual diffusion metric images were transformed from native space into a standard Montreal Neurological Institute (MNI) space (voxel size 1mm×1mm×1mm^3) *via* spatial normalization. The ICBM-DTI-81 WM labels atlas in the standard space allow for parcellation of the entire white matter into multiple regions of interest (ROI) (24). PANDA toolbox was used to calculate the regional diffusion metrics by averaging the values within each region of the WM atlases. These resultant ROI-based data was statistically analyzed with SPSS and other statistical packages. In our study, we selected left and right uncinate fasciculus (UF) as the ROIs.

Statistical Analysis

We used the independent two-sample t tests and χ^2 tests compare demographic data and HAMD scores between the MDD and HC groups with SPSS 22.0. Two-tailed values of $P < 0.05$ were considered statistically significant.

The subject-specific maps of resting state correlations from the amygdala to all brain voxels of rs-fMRI data were combined across subjects within the MDD group and within the HC group. With age as covariate, Voxel-based 1-sample t-tests were used to produce group whole-brain composite maps. Then we created the contrast maps to assess between-group differences using

voxel-based 2-sample (MDD vs. HC) t-tests. The contrast maps were corrected for multiple comparisons using Monte Carlo simulation within the PFC which was our hypothesized region. We defined the PFC ROI including 20 labels of AAL template, corresponding to Brodmann areas (BA) 9, 10, 11, 12, 24, 25, 32, 44, 45, 46, 47. The contrast map threshold was set at $p < 0.05$ for each voxel, with cluster size of at least 32 voxels ($864mm^3$), corresponding to the $p < 0.05$ corrected by AlphaSim.

We used two sample t-tests to compare group differences in the FA values separately for the atlas-based ROIs in SPSS. Two-tailed values of $p < 0.05$ were considered statistically significant.

To further evaluate the relationship between functional and structural connectivity, we investigated the correlations in MDD and HC participants separately between the FA values of UF and the strength of the functional connectivity in the regions showing significant differences between the two groups. Pearson's correlation analysis was used, and statistical significance was set at 0.05 (two-tailed).

TABLE 1 | Demographic and clinical data of participants.

Characteristic	MDD	HC	Statistic	p-value
Number	36	37		
Age (year, mean ± SD)	15.6 ± 1.27	15.6 ± 1.30	t = 0.03	0.972
Gender (male/female)	12/24	18/19	$\chi^{2} = 1.768$	0.236
Education (year, mean ± SD)	9.86 ± 1.46	10.03 ± 1.63	t = 1.217	0.228
HAMD-17 score (mean ± SD)	23.19 ± 7.54	1.41 ± 1.64	t = 17.161	0.000*
Illness duration (month, mean ± SD)	10.11 ± 10.61	NA	NA	NA

*p < 0.05 SD, standard deviation.
MDD, major depression disorder.
HC, healthy controls.
HAMD, Hamilton Depression Rating Scale.
NA, not applicable.

RESULTS

Demographic and Clinical Scales

There were no significant differences in age ($p = 0.972$), gender ($p = 0.236$),or education ($p = 0.228$) between the adolescent MDD and the HC groups. MDD adolescents had significantly higher HAMD scores than the HC ($p < 0.001$, **Table 1**).

Between-Group Differences in rsFC and DTI

With age as covariant We found significantly decreased left ventral PFC (VPFC, BA 47) rsFC from the left amygdala in the adolescent MDD group, compared with the HC group [peak MNI coordinates of the left VPFC region: x = -35, y = 21, z = -11, 45 voxels ($1215mm^3$), T = 3.53] (**Figure 1**, **Table 2**). This finding correspond to a corrected $P < 0.05$ by AlphaSim correction. Compared with the HC group, the MDD group showed no significant region in rsFC between the right amygdala and PFC regions.

Compared with healthy controls, MDD group had significant decreased FA values in the left UF. There were no significant findings of right UF in MDD relative to controls (**Table 3**).

Correlation Between FA and the Strength of Functional Connectivity

In post-hoc correlation analyses, no significant association was detected between FA value of the left UF and the strength of rsFC of VPFC from the left amygdala in the MDD group ($r = -0.377$, $P = 0.058$). There was also no significant correlation in the HC group ($r = -0.118$, $P = 0.574$).

DISCUSSION

In this study, we reported decreased rsFC between left amygdala and left VPFC in adolescent MDD compared to HC. Furthermore, deficits of white matter integrity in the left uncinate fasciculus, fiber tracts connecting VPFC to temporal regions (including amygdala and hippocampus) were detected in adolescent MDD compared to HC. To our knowledge, this is the first study using differential MRI methods to explore functional and structural connectivity abnormalities in the amygdala-prefrontal circuits within adolescent MDD. Our findings provide primary evidence implicating abnormalities of amygdala-prefrontal circuits as the key components in the pathophysiology of adolescent MDD.

Our results of decreased rsFC between left amygdala and left VPFC in adolescent MDD (age 13–17) compared to HC are consistent with our previous findings of both rs-fMRI and task-fMRI in adult MDD (age 18–45) (4, 25). Amygdala-VPFC circuits play an important role in emotion processing (26). Dysfunction of amygdala and ventral frontal regions including VPFC and subgenual ACC were widely reported in adult MDD. Recently, several fMRI studies with adolescent MDD also focused on the function of amygdala and related circuits mediating emotion processing. Hyperactivation of amygdala and ACC were shown during facial-emotion matching task within adolescent MDD (27). In rs-fMRI studies, Cullen et al. reported decreased functional connectivity in the subgenual ACC-based network (8) and amygdala-hippocampus/brainstem circuits (9), but failed to find amygdala-frontal functional connectivity abnormalities. Taken together, our findings suggest that deficits of amygdala-prefrontal functional connectivity may emerge in the early onset of MDD and reflect the emotional dysfunction of adolescent MDD as well as adult MDD.

In this study, adolescents with MDD showed decreased FA values in the left UF compared to HC. The UF connects the amygdala with inferior frontal regions including VPFC and ACC, which are key components of the frontal-limbic neural circuits involved in emotional processing (26, 28). Dysfunction of the amygdala-VPFC circuit have proved to play an important role in the pathophysiology of adolescent MDD (8, 27, 29, 30). The prior study with adult MDD have demonstrated decreased FA values in the dorsal part of the UF (31). In the recent DTI studies with adolescent MDD, Cullen et al. reported reduced FA

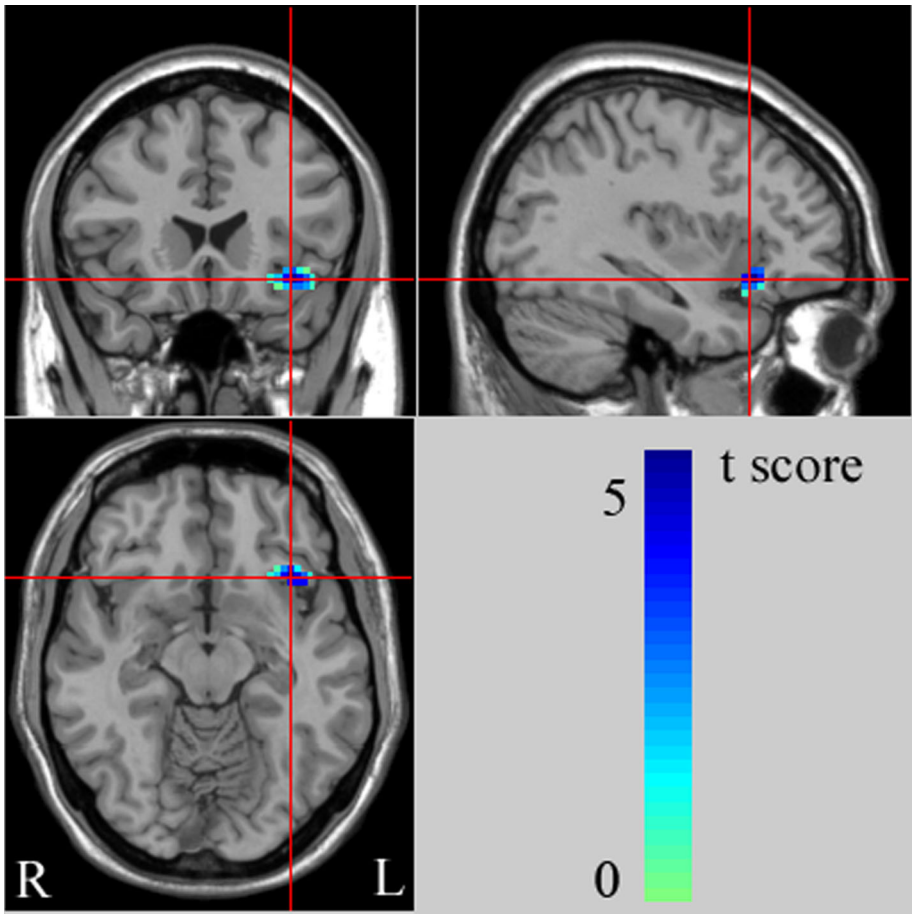

FIGURE 1 | The images (MNI coordinate x = -35mm, y = 21mm, z = -11mm) display the regions in left ventral prefrontal cortex (VPFC) that show decreased functional connectivity from the left amygdala in adolescents with major depressive disorder (MDD), compared to healthy controls (HC) at rest. The color bar represents the range of T values. L, left brain; R, right brain.

values in the right UF (14), while LeWinn et al. reported lower FA and higher RD in bilateral UF (32). As in the medication-naïve adolescent MDD sample of our study, the current findings of decreased FA values in the left UF provide preliminary evidence that abnormal white matter structural integrity in amygdala-VPFC circuit may be present early in the unmedicated adolescent MDD and play an important role in the pathophysiology of adolescent MDD.

The major strength of our study is that multiple MRI methods (rs-fMRI and DTI) were used to detect functional connectivity, structural connectivity and their relationship in the same adolescent MDD sample. Our present results of decreased functional connectivity within amygdala-VPFC circuits as well as reduced structural connectivity between amygdala and VPFC in adolescent MDD suggest the potential association between functional and structural connectivity. Our explanation is that

TABLE 2 | Regions with decreased rsFC from the amygdala in subjects with major depressive disorder compared to health control subjects.

Regions	BA	Peak MNI coordinate			Voxel size	t value	P value
		X	Y	Z			
Left VPFC	47	-35	21	-11	45	3.53	<0.05

rsFC, Resting state functional connectivity.
VPFC, ventral prefrontal cortex.
BA, Brodmann areas.
MNI, Montreal Neurological Institute.

TABLE 3 | Two sample t test results for FA values of left and right UF.

Regions	FA (mean ± SD)			t value	P value
	MDD (n = 36)	HC(n = 37)			
Left UF	0.382 ± 0.02	0.392 ± 0.02	2.059	0.043*	
Right UF	0.388 ± 0.03	0.392 ± 0.02	0.678	0.500	

**t < 0.05UF, uncinate fasciculus.*
SD, standard deviation.
MDD, major depression disorder.
HC, healthy controls.

deficits of white matter integrity in the UF might contribute to the decrease of functional connectivity between amygdala and VPFC. We speculate that early abnormalities of brain development may be present in some adolescent MDD patients early in life, even before illness episodes. The unmaturation of brain development in adolescent may cause the inadequate compensatory mechanism, hence lead to the decrease of both functional and structural connectivity in adolescent MDD. The association between functional and structural disconnectivity in the amygdala-VPFC circuit may reflect the early onset mechanism of adolescent MDD, which need to be further investigated in future longitudinal studies including adolescents with high-risk of depression.

The limitation of our findings is that as no significant correlation between strength of functional connectivity and white matter integrity detected, the direct relationship between functional and structural connectivity in the amygdala-VPFC circuit within adolescent is still unclear. Since a borderline significant correlation was detected in the MDD group, our speculation is that the relative small sample size may limit our ability to detect the statistical significance in current study. Future studies with large sample size is important to further understand the relationship between functional and structural connectivity and the neurodevelopmental mechanism of adolescent MDD.

CONCLUSIONS

Our study present the primary evidence of both functional and structural connectivity abnormalities of amygdala-VPFC circuit in the sample of first-episode medication-naïve adolescent MDD. The abnormal white matter structural integrity in adolescent MDD may reflect the unmaturation of early brain development in adolescent, which may cause the functional dis connectivity in the same circuit. Both functional and structural abnormalities of amygdala-VPFC circuit may present in the early onset of adolescent MDD and play an important role in the neuropathophysiology of adolescent MDD.

DATA AVAILABILITY STATEMENT

The datasets used and/or analyzed during the current study are available from the corresponding author on reasonable request.

ETHICS STATEMENT

The studies involving human participants were reviewed and approved by the Medical Science Research Ethics Committee of the First Affiliated Hospital of China Medical University (approval reference number [2012]25-1). Written informed consent to participate in this study was provided by the participants' legal guardian/next of kin.

AUTHOR CONTRIBUTIONS

FW, LK, and JS designed the study. JS, YZ, XJ, ZT, and HL acquired the data. LK, JS, and HG analyzed the data. FW, LK, JS, and ZT wrote the article.

FUNDING

This study was supported by the National Natural Science Foundation of China (U1808204 and 81101012 to FW, 81301166 to LK), the Liaoning Scientific Foundation (2015020532 to FW and 201602833 to LK).

ACKNOWLEDGMENTS

The authors are grateful to all study participants in this study. We would also like to thank Qian Zhou, Jia Duan, Pengshuo Wang, Ran Zhang, Huizi Li, Jiahui Kang, Yixiao Xu, Luyu Liu and Xuemei Chen for their assistant in subject recruiting.

REFERENCES

1. Thapar A, Collishaw S, Pine DS, Thapar AK. Depression in adolescence. *Lancet* (2012) 379(9820):1056–67. doi: 10.1016/S0140-6736(11)60871-4
2. Birmaher B, Williamson DE, Dahl RE, Axelson DA, Kaufman J, Dorn LD, et al. Clinical presentation and course of depression in youth: does onset in childhood differ from onset in adolescence? *J Am Acad Child Adolesc Psychiatry* (2004) 43(1):63–70. doi: 10.1097/00004583-200401000-00015
3. Lowe MJ, Dzemidzic M, Lurito JT, Mathews VP, Phillips MD. Correlations in low-frequency BOLD fluctuations reflect cortico-cortical connections. *Neuroimage* (2000) 12(5):582–7. doi: 10.1006/nimg.2000.0654S1053-8119(00)90654-2
4. TangY, Kong L, Wu F, Womer F, Jiang W, Cao Y, et al. Decreased functional connectivity between the amygdala and the left ventral prefrontal cortex in treatment-naive patients with major depressive disorder: a resting-state functional magnetic resonance imaging study. *Psychol Med* (2013) 43(9):1921–7. doi: 10.1017/S0033291712002759
5. Dannlowski U, Ohrmann P, Konrad C, Domschke K, Bauer J, Kugel H, et al. Reduced amygdala-prefrontal coupling in major depression: association with MAOA genotype and illness severity. *Int J neuropsychopharmacol/off Sci J Collegium Int Neuropsychopharmacologicum* (2009) 12(1):11–22. doi: 10.1017/S1461145708008973
6. Matthews SC, Strigo IA, Simmons AN, Yang TT, Paulus MP. Decreased functional coupling of the amygdala and supragenual cingulate is related to increased depression in unmedicated individuals with current major depressive disorder. *J Affect Disord* (2008) 111(1):13–20. doi: 10.1016/j.jad.2008.05.022
7. Connolly CG, Ho TC, Blom EH, LeWinn KZ, Sacchet MD, Tymofiyeva O. Resting-state functional connectivity of the amygdala and longitudinal changes in depression severity in adolescent depression. *J Affect Disord* (2017) 207:86–94. doi: 10.1016/j.jad.2016.09.026
8. Cullen KR, Gee DG, Klimes-Dougan B, Gabbay V, Hulvershorn L, Mueller BA, et al. A preliminary study of functional connectivity in comorbid adolescent depression. *Neurosci Lett* (2009) 460(3):227–31. doi: 10.1016/j.neulet.2009.05.022

9. Cullen KR, Westlund MK, Klimes-Dougan B, Mueller BA, Houri A, Eberly LE, et al. Abnormal amygdala resting-state functional connectivity in adolescent depression. *JAMA Psychiatry* (2014) 71(10):1138–47. doi: 10.1001/jamapsychiatry.2014.1087
10. Luking KR, Repovs G, Belden AC, Gaffrey MS, Botteron KN, Luby JL, et al. Functional connectivity of the amygdala in early-childhood-onset depression. *J Am Acad Child Adolesc Psychiatry* (2011) 50(10):1027–41 e3. doi: 10.1016/j.jaac.2011.07.019
11. Honey CJ, Sporns O, Cammoun L, Gigandet X, Thiran JP, Meuli R, et al. Predicting human resting-state functional connectivity from structural connectivity. *Proc Natl Acad Sci United States America* (2009) 106(6):2035–40. doi: 10.1073/pnas.0811168106
12. Xu K, Jiang W, Ren L, Ouyang X, Jiang Y, Wu F, et al. Impaired interhemispheric connectivity in medication-naive patients with major depressive disorder. *J Psychiatry neurosci: JPN* (2013) 38(1):43–8. doi: 10.1503/jpn.110132
13. Dillon DG, Gonenc A, Belleau E, Pizzagalli DA. Depression is associated with dimensional and categorical effects on white matter pathways. *Depress Anxiety* (2018) 35(5):440–7:2018. doi: 10.1002/da.22734
14. Cullen KR, Klimes-Dougan B, Muetzel R, Mueller BA, Camchong J, Houri A, et al. Altered white matter microstructure in adolescents with major depression: a preliminary study. *J Am Acad Child Adolesc Psychiatry* (2010) 49(2):173–83 e1. doi: 10.1097/00004583-201002000-00011
15. Bessette KL, Nave AM, Caprihan A, Stevens MC. White matter abnormalities in adolescents with major depressive disorder. *Brain Imaging Behav* (2014) 8 (4):531–41. doi: 10.1007/s11682-013-9274-8
16. Aghajani M, Veer IM, van Lang ND, Meens PH, van den Bulk BG, Rombouts SA, et al. Altered white-matter architecture in treatment-naive adolescents with clinical depression. *Psychol Med* (2014) 44(11):1–12. doi: 10.1017/S0033291713003000
17. Kim MJ, Whalen PJ. The structural integrity of an amygdala-prefrontal pathway predicts trait anxiety. *J neurosci: Off J Soc Neurosci* (2009) 29 (37):11614–8. doi: 10.1523/JNEUROSCI.2335-09.2009
18. Siegle GJ, Konecky RO, Thase ME, Carter CS. Relationships between amygdala volume and activity during emotional information processing tasks in depressed and never-depressed individuals: an fMRI investigation. *Ann New Y Acad Sci* (2003) 985:481–4. doi: 10.1111/j.1749-6632.2003.tb07105.x
19. Steffens DC, Taylor WD, Denny KL, Bergman SR, Wang L. Structural integrity of the uncinate fasciculus and resting state functional connectivity of the ventral prefrontal cortex in late life depression. *PloS One* (2011) 6(7): e22697. doi: 10.1371/journal.pone.0022697
20. Ye J, Shen Z, Xu X, Yang S, Chen W, Liu X, et al. Abnormal functional connectivity of the amygdala in first-episode and untreated adult major depressive disorder patients with different ages of onset. *Neuroreport* (2017) 28(4):214–21. doi: 10.1097/WNR.0000000000000733
21. Hamilton M. A rating scale for depression. *J Neurol Neurosurg Psychiatry* (1960) 23:56–62. doi: 10.1136/jnnp.23.1.56
22. Tzourio-Mazoyer N, Landeau B, Papathanassiou D, Crivello F, Etard O, Delcroix N, et al. Automated anatomical labeling of activations in SPM using a macroscopic anatomical parcellation of the MNI MRI single-subject brain. *Neuroimage* (2002) 15(1):273–89. doi: 10.1006/nimg.2001.0978S1053811901909784
23. Cui Z, Zhong S, Xu P, He Y, Gong G. PANDA: a pipeline toolbox for analyzing brain diffusion images. *Front Hum Neurosci* (2013) 7:42. doi: 10.3389/fnhum.2013.00042
24. Mori S, Oishi K, Jiang H, Jiang L, Li X, Akhter K, et al. Stereotaxic white matter atlas based on diffusion tensor imaging in an ICBM template. *Neuroimage* (2008) 40(2):570–82. doi: 10.1016/j.neuroimage.2007.12.035
25. Kong L, Chen K, Tang Y, Wu F, Driesen N, Womer F, et al. Functional connectivity between the amygdala and prefrontal cortex in medication-naive individuals with major depressive disorder. *J Psychiatry Neurosci: JPN* (2013) 38(6):417–22. doi: 10.1503/jpn.120117
26. Pessoa L. Beyond brain regions: network perspective of cognition-emotion interactions. *Behav Brain Sci* (2012) 35(3):158–9. doi: 10.1017/S0140525X11001567
27. Yang TT, Simmons AN, Matthews SC, Tapert SF, Frank GK, Max JE, et al. Adolescents with major depression demonstrate increased amygdala activation. *J Am Acad Child Adolesc Psychiatry* (2010) 49(1):42–51. doi: 10.1097/00004583-201001000-00008
28. Ochsner KN, Gross JJ. The neural architecture of emotion regulation. *Handb Emotion Regul* (2007) 1:87–109.
29. Ho TC, Yang G, Wu J, Cassey P, Brown SD, Hoang N, et al. Functional connectivity of negative emotional processing in adolescent depression. *J Affect Disord* (2014) 155:65–74. doi: 10.1016/j.jad.2013.10.025
30. Perlman G, Simmons AN, Wu J, Hahn KS, Tapert SF, Max JE, et al. Amygdala response and functional connectivity during emotion regulation: a study of 14 depressed adolescents. *J Affect Disord* (2012) 139(1):75–84. doi: 10.1016/j.jad.2012.01.044
31. de Kwaasteniet B, Ruhe E, Caan M, Rive M, Olabarriaga S, Groefsema M, et al. Relation between structural and functional connectivity in major depressive disorder. *Biol Psychiatry* (2013) 74(1):40–7. doi: 10.1016/j.biopsych.2012.12.024
32. LeWinn KZ, Connolly CG, Wu J, Drahos M, Hoeft F, Ho TC, et al. White matter correlates of adolescent depression: structural evidence for frontolimbic disconnectivity. *J Am Acad Child Adolesc Psychiatry* (2014) 53 (8):899–909e1–7. doi: 10.1016/j.jaac.2014.04.021

Conflict of Interest: The authors declare that the research was conducted in the absence of any commercial or financial relationships that could be construed as a potential conflict of interest.

frontiers in Psychiatry

ORIGINAL RESEARCH
published: 07 February 2020
doi: 10.3389/fpsyt.2020.00027

Mapping Theme Trends and Knowledge Structure of Magnetic Resonance Imaging Studies of Schizophrenia: A Bibliometric Analysis From 2004 to 2018

Li Duan[1] *and Gang Zhu*[1,2]*

[1] Department of Psychiatry, the First Affiliated Hospital of China Medical University, Shenyang, China, [2] Central Laboratory, the First Affiliated Hospital of China Medical University, Shenyang, China

OPEN ACCESS

Edited by:
Wenbin Guo,
Central South University, China

Reviewed by:
Jun Chen,
Shanghai Mental Health Center (SMHC), China
Mingrui Xia,
Beijing Normal University, China

***Correspondence:**
Gang Zhu
gzhu@cmu.edu.cn

Specialty section:
This article was submitted to Neuroimaging and Stimulation, a section of the journal Frontiers in Psychiatry

Received: 24 October 2019
Accepted: 10 January 2020
Published: 07 February 2020

Citation:
Duan L and Zhu G (2020) Mapping Theme Trends and Knowledge Structure of Magnetic Resonance Imaging Studies of Schizophrenia: A Bibliometric Analysis From 2004 to 2018. Front. Psychiatry 11:27. doi: 10.3389/fpsyt.2020.00027

Background: Recently, magnetic resonance imaging (MRI) technology has been widely used to quantitatively analyze brain structure, morphology, and functional activities, as well as to clarify the neuropathological and neurobiological mechanisms of schizophrenia. However, although there have been many relevant results and conclusions, there has been no systematic assessment of this field.

Aim: To analyze important areas of research utilizing MRI in studies of schizophrenia and explore major trends and the knowledge structure using bibliometric analysis.

Methods: Literature related to MRI studies of schizophrenia published in PubMed between January 1, 2004 and December 31, 2018 were retrieved in 5-year increments. The extracted major Medical Subject Headings (MeSH) terms/MeSH subheadings were analyzed quantitatively. Bi-clu-stering analysis, social network analysis (SNA), and strategic diagrams were employed to analyze the word matrix and co-occurrence matrix of high-frequency MeSH terms.

Results: For the periods of 2004 to 2008, 2009 to 2013, and 2014 to 2018, the number of relevant retrieved publications were 916, 1,344, and 1,512 respectively, showing an overall growth trend. 26, 34, and 36 high-frequency major MeSH terms/MeSH subheadings were extracted in each period, respectively. In line with strategic diagrams, the main undeveloped theme clusters in 2004–2008 were effects of antipsychotics on brain structure and their curative efficacy. These themes were replaced in 2009–2013 by physiopathology mechanisms of schizophrenia, etiology of cognitive disorder, research on default mode network and schizophrenic psychology, and were partially replaced in 2014–2018 by studies of differences in the neurobiological basis for schizophrenia and other mental disorders. Based on SNA, nerve net/physiopathology and psychotic disorder/pathology were considered the emerging hotspots of research in 2009–2013 and 2014–2018.

Conclusions: MRI studies on schizophrenia were relatively diverse, but the theme clusters derived from each period may reflect the publication trends to some extent. Bibliometric research over a 15-year period may be helpful in depicting the overall scope of research interest and may generate novel ideas for researchers initiating new projects.

Keywords: schizophrenia, magnetic resonance imaging, bibliometric analysis, co-occurrence analysis, social network analysis, strategic diagram

INTRODUCTION

Schizophrenia, as a common and devastating mental disorder, has been characterized by abnormal social behavior and the failure to understand reality, accompanied by emotional disorder or substance abuse, and even suicide (approximately 5%) (1), which leads to high risk for physical diseases, increased disability and recurrence for patients, and places a serious burden on their families and society (2, 3). The prevalence of schizophrenia has been stable at around 1% (4), and the years lived with disability (YLD) due to schizophrenia in 2016 was estimated to be 13.4 million years [95% uncertainty interval (UI), 9.9–16.7 million years], accounting for 1.7% of all YLDs and ranking 15th among all diseases worldwide (5). Nevertheless, the underlying etiology and pathogenesis of schizophrenia have not been fully elucidated, but scholars have come to the consensus that it is a disabling encephalopathy caused by a group of genetic factors, as well as heterogeneous neurodevelopmental risk factors and adverse environmental stimuli (6–9).

At present, clinical diagnosis of schizophrenia is mainly based on patients' abnormal behavior. Clinical symptoms are described with quantitative dimensions, such as the quantitative evaluation of symptoms with the Positive and Negative Syndrome Scale (10). However, when patients exhibit typical psychotic symptoms and abnormal behaviors, they usually have advanced or relapsed into the middle and late stages of schizophrenia, which is not conducive to the implementation of rapid and effective treatment programs and the long-term recovery of patients. In recent years, neuroimaging technology has become an important way to understand normal physiological functions and pathological phenomena in the brain. Although patients with schizophrenia usually have anomalous brain structure and function, as well as neurological damage, it is possible for psychiatrists to explore early diagnosis, screen for specific biomarkers, monitor pathogenetic progression and therapeutic efficacy, and uncover pathophysiological mechanisms by employing structural and functional imaging technologies (11–15). Magnetic resonance imaging (MRI) scanning techniques focus primarily on structural magnetic resonance imaging, resting-state functional magnetic resonance imaging and diffuse tensor imaging (DTI). As early as 1927, scientists began to perform brain scans of schizophrenia patients, but the traumatic operation (injecting air into the cerebrospinal canal) meant that patients had to endure pain for months (16). It wasn't until 1976 that Johnstone used computerized tomography technology to make the first non-invasive study of the brain of schizophrenia patients with enlarged lateral ventricles (17). Later, to improve the poor discrimination of soft tissue, Smith et al. conducted the first MRI study on schizophrenia patients in 1984 (18). Depending on the characteristics of the various imaging diagnostic techniques employed, the scope of MRI applications may differ; for example, structural magnetic resonance imaging (sMRI) enables high resolution spatial imaging of the brain *in vivo* based on its unique advantages which provide noninvasive, harmless and high spatial resolution, while DTI allows observation of the direction and structural integrity of nerve fiber bundles in the white matter *in vivo*, and functional MRI (fMRI) can detect functional activity of the brain. Furthermore, with the development of magnetic resonance technology, researchers are gradually extending their exploration of the brain of patients with schizophrenia and achieving fruitful results to better carry out clinical work and provide more professional advice for patients.

Bibliometrics, as a branch of library and information science, originated in the early 20th century. It is a comprehensive application of mathematics and statistics to conduct quantitative analysis and description of various characteristics of published literatures, so as to provide an easy method to evaluate research status and predict the developmental trends (19). Therefore, bibliometric analysis, including co-citation analysis, co-word analysis, and other methods, can help researchers grasp the changing trends of a given research field (20). While these methods have enriched the research content of MRI studies on schizophrenia, at present, few studies have attempted to focus on and sort out the important issues and research context from the perspective of bibliometrics. In view of this situation, this study attempted to analyze and summarize the internal and external characteristics of related literatures and track and intuitively display the research trends and frontiers in the field of MRI studies on schizophrenia by the integrated application of co-word analysis, bi-clustering analysis, strategic diagram, and social network analysis (SNA). Our goal is to promote public knowledge and provide reference for the increasing depth and breadth of future research on schizophrenia.

METHODS

Data Collection, Data Extraction, and Bibliographic Matrix Setup

Literature involved in this study were retrieved and downloaded from the PubMed database(National Center for Biotechnology Information, U.S. National Library of Medicine, Rockville Pike, Bethesda MD, USA). Medical Subject Headings (MeSH) which are characterized by accuracy (accurately revealing the subject of the literature) and specificity can be used to index and catalog

literatures in PubMed. In this study, the retrieval model was set as ["Magnetic Resonance Imaging"(Mesh) OR "Diffusion Tensor Imaging"(Mesh) OR "Diffusion Tensor Imaging"(Title/Abstract) AND "Schizophrenia"(Mesh)] with the filter restriction of literature type as "journal article" and language as "English". In addition, in order to dynamically analyze the changes in hotspots, theme trends and knowledge structure of related studies of MRI and schizophrenia, the publication scope was divided into three periods (January 1, 2004 to December 31, 2008, January 1, 2009 to December 31, 2013, and January 1, 2014 to December 31, 2018). Finally, 916, 1,344, and 1,512 related literatures were retrieved in each period, respectively. Additionally, two researchers are required to carry out the primary retrieval and literature screening based on reviewing titles, abstracts, as well as full text in some cases independently.

Bibliographic information, including publication dates, countries, titles, authors, journal categories, major MeSH terms, MeSH subheading terms, abstracts, and other related characteristics of these literatures were accurately extracted and properly kept in XML format. The principle of h-index (21) was followed to set the threshold value of the high- and low-frequency major MeSH terms/MeSH subheadings. As a hybrid quantitative index, it was originally proposed by Hirsch to quantify the output of an individual researcher and gradually expand the index to evaluate the influence of patents (22), academic journals (23), research institutions (24), and so on. In this study, the Bibliographic Item Co-occurrence Matrix Builder (BICOMB) (25) was applied to read and analyze the bibliographic information of these retrieved literatures. Word frequency statistics in descending order were obtained with "major MeSH terms/MeSH subheadings." When the word frequency was consistent with its rank, all major MeSH terms/MeSH subheadings greater than or equal to the rank were considered high frequency. Thereafter, fundamental data from the term-source literature and the term-term co-occurrence matrix were also generated to prepare for the subsequent bibliometric analysis.

Bi-Clustering Analysis of High-Frequency Mesh Terms

Bi-clustering analysis, also known as two-way clustering, was first proposed by Hartigan in 1972 (26). It refers to the concurrent clustering of rows and columns of data, and the simultaneous application of objects and their attributes to extract their common information. In this study, bi-clustering analysis of high-frequency major MeSH terms/MeSH subheadings was conducted on the basis of the term-source literature matrix by employing gCLUTO (Graphical Clustering Toolkit) software (http://glaros.dtc.umn.edu/gkhome/cluto/gcluto/download), with the aim of assessing the knowledge structure of studies on MRI of schizophrenia. The results are presented in the form of a visual matrix and visual mountain.

The two-dimensional matrix visualization, as a colorful interactive matrix, is composed of horizontal rows of high-frequency major MeSH terms/MeSH subheadings and vertical columns of PubMed unique identifiers (PMID) of these retrieved literatures, which are showed on the left and the top of the matrix, respectively. Mountain visualization attempts to describe the relationship between clusters from a three-dimensional perspective, and we can estimate the relative similarity between peaks by estimating the distance between them. The volume and height of each mountain is proportional to the number of high-frequency MeSH terms contained in a cluster and their similarity within the cluster, respectively. The greater the similarity within a cluster, the steeper the mountain. In addition, the colors of peaks include red, yellow, light blue, and dark blue. Red represents a lower standard deviation of the internal similarity in the cluster, while blue denotes a higher standard deviation. In addition, the closer the color is to a single color, the smaller is the deviation between the internal MeSH terms of various clusters and the greater is their similarity.

Furthermore, according to calculate statistical indices, including descriptive (literatures that represents this class of characteristics) and discriminating (literatures that distinguishes it from other clusters) of each high-frequency major MeSH terms/MeSH subheadings to the clusters, trace back to the source literatures by identifying the PMID that contributes the most to the formation of each cluster as the significant representative literatures. These extracted representative literatures can be used to summarize and interpret content of the theme cluster.

Strategic Diagram Analysis

The analysis method of strategic diagram was first proposed by Law et al. in 1988 and aimed to describe the complex internal structure and developmental trend of hotspots in a research field on the basis of the co-occurrence matrix and bi-cluster analysis (27). The two-dimensional strategic diagram (28), formed by employing software of GraphPad Prism 5.0 (Graphpad, Inc., La Jolla, CA, USA), places on the horizontal axis centrality or degree of external cohesion, namely, the central position of the theme cluster with other clusters. The vertical axis specifies the density or degree of internal cohesion, namely, the conceptual development of the theme cluster.

The strategic diagram can be divided into four quadrants moving counterclockwise (**Figure 5A**). The theme cluster which is located in the first quadrant (Quadrant I, upper right), represents the development core and relatively mature hotspots in the field, implying strong centrality, and high density. Theme clusters in the second quadrant (Quadrant II, upper left) are characterized by inadequate external interactions, but high density of terms in periphery development in this research field. The third quadrant (Quadrant III, lower left) consists of theme clusters with weak centrality and low density, which are identified as emerging or vanishing. Although the density of theme clusters contained in the fourth quadrant (Quadrant IV, lower right) is low, it has high centrality, which indicates that its internal structure is loose and its development has not achieved sufficient maturity.

Social Network Analysis

SNA, as an increasingly applied and rapidly developing method in variety of fields (e.g., psychology, sociology, mathematics, statistics, and others), emphasizes the connectivity and interdependence of elements in a group (29). In this study, to analyze and interpret the theme trends and knowledge structural

characteristics of MRI studies of schizophrenia, we employed the "centrality" concept from SNA on the basis of the high-frequency major Mesh terms/MeSH subheadings co-occurrence matrix. Furthermore, to assess the importance of each node, statistical indices including degree, betweenness, and closeness centrality were selected to perform the network analysis. The connotation of each index is explained as follows: (1) Degree centrality is calculated by the number of direct links associated with or connected to one node within the network (30). This index is suitable for evaluating the co-occurrence level among nodes, indicating the importance of one given node to the network. This is evaluated by their degree centrality. (2) Betweenness centrality is calculated by the number of shortest paths between two other nodes that pass through one given node (31). This index can indicate the influence of this node to the network, that is, the higher the betweenness centrality value, the more powerful is this node in controlling other nodes within a network (32). (3) Closeness centrality also can be used as another measure for quantifying the importance of a given node (33). In contrast to betweenness centrality, this index is calculated from the reciprocal of the sum of the lengths of the shortest paths between the node and all other nodes within the network. Therefore, the larger the closeness centrality value of the given node, the closer it is to all the other nodes within the network.

Given that betweenness centrality, as a mediating role, is more applicable to describe the decisive effect within the whole network, we chose it to scale the node sizes. Calculation of the related statistical indices and drawing of the network diagrams were completed using Ucinet 6.0 software (Analytic Technologies Co., Nicholasville, Kentucky, USA), while visualization of the network structure was demonstrated using NetDraw 2.084 software (http://www.analytictech.com/downloadnd.htm).

RESULTS

Distribution Characteristics of Related Publications

In this study, 916, 1,344, and 1,512 literatures were retrieved from the three periods of 2004 to 2008, 2009 to 2013, and 2014 to 2018, respectively, which were then subjected to comparative analysis using the statistical indices of authors, source of countries, and journals. The annual total number of MRI studies on schizophrenia presented an overall growth trend (**Figure 1**). The top five countries in this research field in the first period, in descending order of production, were the United States, England, Netherlands, Ireland, and Germany, while Netherlands overtook England for the second place in other two periods (**Table 1**). Additionally, it was clear that the proportion of publications in the U.S., which was the highest in all three periods, has been trending down, while Netherlands and England's percentage of publication have continuously increased. The top two journals were *Schizophrenia Research* and *Psychiatry Research* in the first two periods, while *Biological Psychiatry* in 2004–2013 was replace by *Schizophrenia Bulletin* in 2009–2013. These three journals together contained more than 33.54% and 33.65% of the total number of searched publications in this field in the first two periods, respectively. From 2014 to 2018, the top three journals were *Schizophrenia Research*, *Schizophrenia Bulletin,* and *NeuroImage. Clinical*. Furthermore, the journal *Schizophrenia Research* ranked first in the number of articles published in all three periods, but its proportion of the total number of searched publications declined slightly. In addition, Shenton ME was the greatest contributor to MRI studies on schizophrenia research in the first period, while Calhoun VD contributed the most academic papers in the last two periods.

Research Hotspots Identified and Theme Clusters Summarized Based on MeSH Term Clusters

From the searched literature, 26, 34, and 36 high-frequency major MeSH terms/MeSH subheadings were extracted in each period, respectively, and their cumulative frequency percentages were 49.0459, 53.8805, and 52.1285% of the total, and thus could be considered as the research hotspots of MRI studies on schizophrenia in the past three 5-year time periods (**Table 2**). And, it should be pointed out that in the second period of 2009–2013, the word frequency values of 33rd and 34th major MeSH

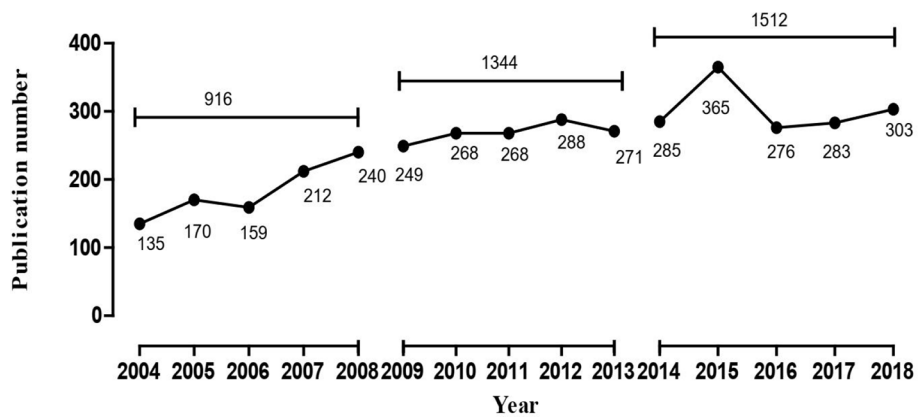

FIGURE 1 | The number of publications of MRI studies on schizophrenia in PubMed from 2004 to 2018.

TABLE 1 | Temporal distribution of publications of MRI studies on schizophrenia in PubMed from 2004 to 2018.

Period	Rank	Country		Top journal		Author	
		Name	Publications, n (%)	Title	Publication, n (%)	Name	Number of papers
2004- 2008	1	United States	427(44.11%)	*Schizophrenia research*	162(16.71%)	Shenton ME	35
	2	England	178(18.39%)	*Psychiatry research*	86(8.88%)	McCarley RW	34
	3	Netherlands	178(18.39%)	*Biological psychiatry*	77(7.95%)	Lawrie SM	30
	4	Ireland	96(9.92%)	*NeuroImage*	73(7.53%)	Johnstone EC	29
	5	Germany	42(4.34%)	*The American journal of psychiatry*	67(6.91%)	Keshavan MS	26
	Total		921(95.15%)		465(47.98%)		
2009- 2013	1	United States	574(39.70%)	*Schizophrenia research*	242(16.69%)	Calhoun VD	58
	2	Netherlands	285(19.71%)	*Psychiatry research*	132(9.10%)	Shenton ME	41
	3	England	273(18.88%)	*Schizophrenia bulletin*	114(7.86%)	Keshavan MS	40
	4	Ireland	144(9.96%)	*NeuroImage*	96(6.62%)	Kubicki M	37
	5	Germany	70(4.84%)	*Biological psychiatry*	61(4.20%)	Kahn RS	35
	Total		1346(93.09%)		645(44.47%)		
2014- 2018	1	United States	573(37.26%)	*Schizophrenia research*	222(14.37%)	Calhoun VD	77
	2	Netherlands	425(27.63%)	*Schizophrenia bulletin*	125(8.09%)	Pearlson GD	36
	3	England	311(20.22%)	*NeuroImage. Clinical*	81(5.24%)	Andreassen OA	36
	4	Ireland	74(4.81%)	*Psychiatry research. Neuroimaging*	63(4.08%)	Agartz I	35
	5	Germany	45(2.93%)	*Psychiatry research*	62(4.01%)	Guo W	34
	Total		1428(92.85%)		553(35.79%)		

terms/MeSH subheadings were the same as 33, so we extracted 34 high-frequency MeSH terms.

According to bi-clustering analysis, 26, 34, and 36 high-frequency major MeSH terms/MeSH subheadings in each period were evenly divided into three clusters (**Figures 2–4**). For the results of mountain visualization, Cluster 0 in the first period, Clusters 1 and 2 in the second period, and Clusters 0 and 1 in the third period were marked with red peaks, which represented the most significant results with centralized distribution and low internal standard deviation of the internal similarity within clusters. Furthermore, we have made explicit the relationships among high-frequency major MeSH terms/MeSH subheadings and involved literatures from matrix visualization in each period. The major MeSH terms/MeSH subheadings contained in each cluster are displayed on the right side of the matrix, and the number before them referred to the descending rank of the frequency or proportion of frequency from the included literatures in each period. Moreover, an in-depth understanding of the meaning of the MeSH terms themselves, term-source literatures, as well as the significant representative literatures selected by bi-clustering analysis would be conducive to analyze and summarize the theme of each cluster. At the same time, it would also helpful to further interpret the connotation of the relevant literatures in each cluster.

TABLE 2 | Distribution of the high-frequency major MeSH terms/MeSH subheadings of MRI studies on schizophrenia in PubMed from 2004 to 2018.

Period	Threshold value of high- and low-frequency of MeSH terms	Number of high-frequency of MeSH terms	Frequency		Cumulative frequency
			Min	Max	
2004-2008	26	26	26	327	49.0459%
2009-2013	33	34	33	663	53.8805%
2014-2018	36	36	36	605	52.1285%

*The high-frequency MeSH terms in each period can be seen in **Figures 2–4**.*

Theme Trends of MRI Studies on Schizophrenia

In this study, we plotted strategic diagrams so as to systematically compare similarities and differences of the theme clusters in the three periods and explore the developmental trends of MRI studies on schizophrenia. The number of high-frequency major MeSH terms/MeSH subheadings involved in each cluster can be reflected by the area of the nodes, that is, the greater the number, the larger the area (**Figure 5B–D**).

In the first period of 2004–2008, Cluster 0 and Cluster 1 were located in Quadrant I. Cluster 0 represents the correlation between brain structural abnormalities and brain function changes to explore physiopathology mechanism of schizophrenia, while Cluster 1 represented neurodevelopmental abnormalities in patients with schizophrenia and analysis of regional abnormal structural features and influencing factors in the brain. These two clusters were developed and in the core status with adequate centrality and high density. Cluster 2 in Quadrant III represented analysis of metabolism, therapeutic efficacy of antipsychotic agents on brain structure and schizophrenia pathology, which had not matured and were in the beginning stages of research in this field.

Compared with the results of 2004–2008, research on brain structure and function in the 2009–2013 period was still located in Quadrant I and was regarded as a mature and developed research area. However, in contrast to the similar theme cluster contents in the previous period, research in the 2009–2013 period was not only focused on the study of brain structure and function in patients with schizophrenia, but also paid more attention to the differential diagnosis of patients with bipolar disorder or other mental disorders. Furthermore, research on the physiopathology mechanisms of schizophrenia and the etiology of cognitive disorder and other complications, the structure and function

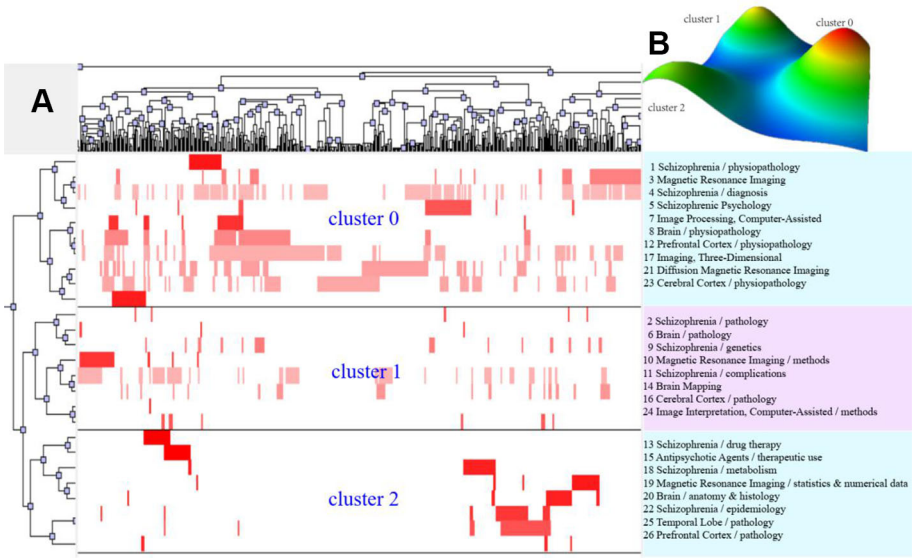

FIGURE 2 | Bi-clustering analysis of 26 high-frequency MeSH terms/MeSH subheadings and literatures of MRI studies on schizophrenia in 2004 to 2008. **(A)** Matrix visualization of bi-clustering of 26 high-frequency major MeSH terms/MeSH subheadings and PubMed unique identifiers of literatures. **(B)** Mountain visualization of bi-clustering of 26 high-frequency major MeSH terms/MeSH subheadings and literatures.

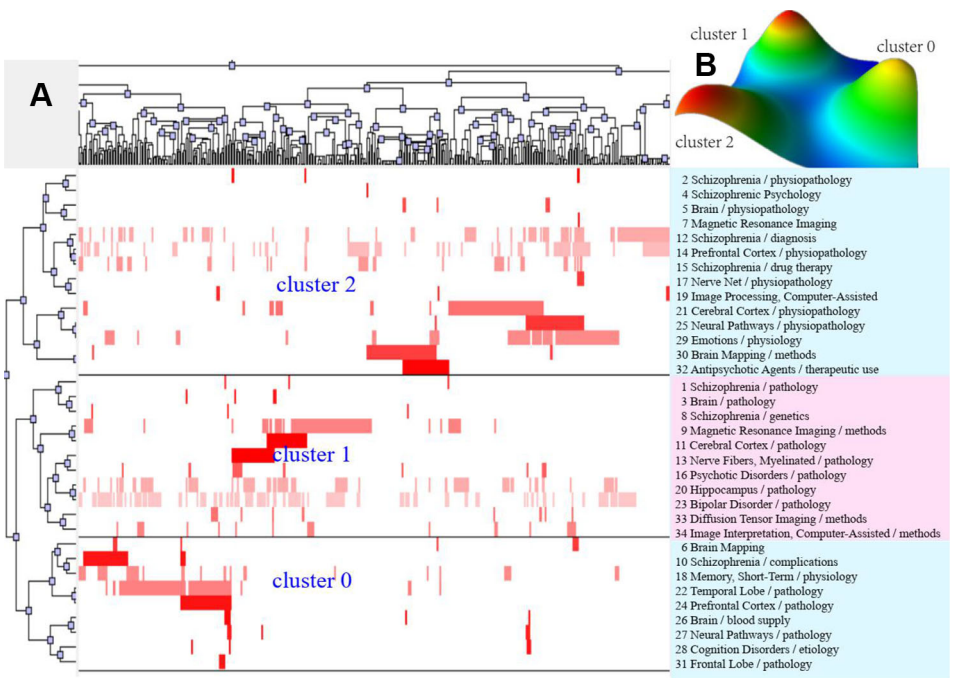

FIGURE 3 | Bi-clustering analysis of 34 high-frequency major MeSH terms/MeSH subheadings and literatures of MRI studies on schizophrenia in 2009 to 2013. **(A)** Matrix visualization of bi-clustering of 34 high-frequency major MeSH terms/MeSH subheadings and PubMed unique identifiers of literatures. **(B)** Mountain visualization of bi-clustering of 34 high-frequency major MeSH terms/MeSH subheadings and literatures.

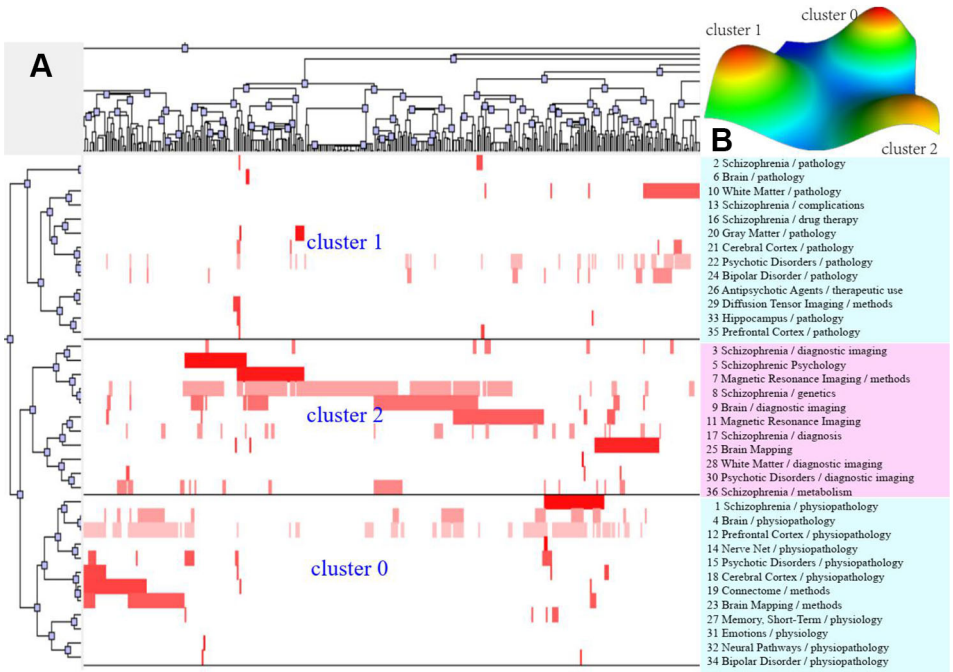

FIGURE 4 | Bi-clustering analysis of 36 high-frequency major MeSH terms/MeSH subheadings and literatures of MRI studies on schizophrenia in 2014 to 2018. **(A)** Matrix visualization of bi-clustering of 36 high-frequency major MeSH terms/MeSH subheadings and PubMed unique identifier of literatures. **(B)** Mountain visualization of bi-clustering of 36 high-frequency major MeSH terms/MeSH subheadings and literatures.

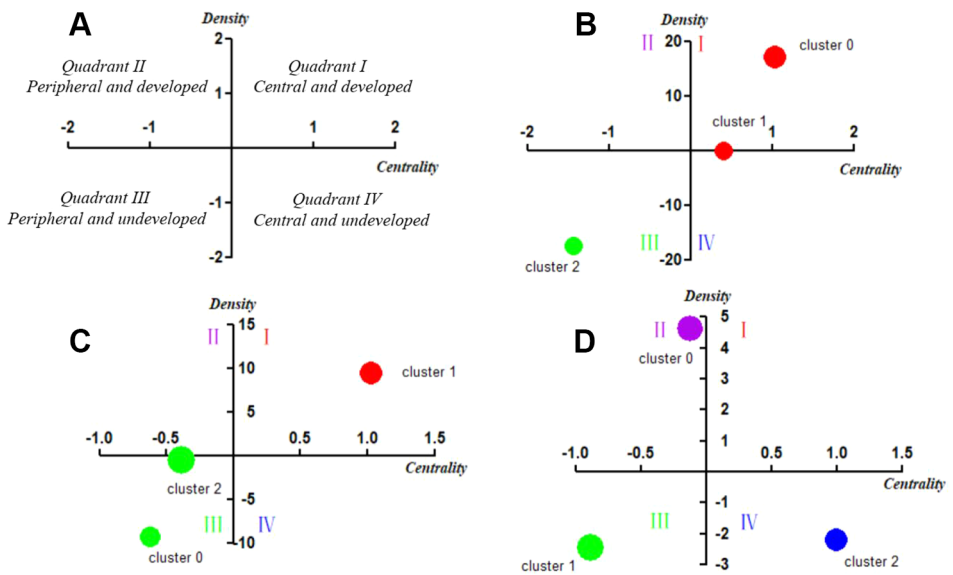

FIGURE 5 | Strategic diagrams for MRI studies on schizophrenia in three different periods. **(A)** Explanation of the strategic diagram. **(B)** Strategic diagram for MRI studies on schizophrenia in 2004–2008. The coordinate values of Cluster 1 are (0.40787, 0.07288), which locates it in Quadrant I. **(C)** Strategic diagram for MRI studies on schizophrenia in 2009–2013. **(D)** Strategic diagram for MRI studies on schizophrenia in 2014–2018. The coordinate values of Cluster 2 are (-0.39885, -0.37111), which locates it in Quadrant I. Clusters in each strategic diagram refer to the bi-clustering results presented in **Table 3**. The size of each single node is proportional to the number of high-frequency major MeSH terms/MeSH subheadings involved in each cluster (**Figures 5 A – D**).

TABLE 3 | Cluster interpretation of high-frequency major MeSH terms/MeSH subheadings of MRI studies on schizophrenia in PubMed from 2004 to 2018.

Period	Cluster	Content and interpretation of the cluster	Rank of MeSH terms	Representative literatures (PMID)
2004-2008	Cluster 0	Correlation between brain structural (e.g. cerebral cortex, prefrontal cortex) abnormalities and brain function changes to explore physiopathology mechanism of schizophrenia	1, 3, 4, 5, 7, 8, 12, 17, 21, 23	17085018, 17913465, 16797186, 19042913
	Cluster 1	1. Neurodevelopmental abnormalities in patients with schizophrenia 2. Analysis of regional abnormal structural features and influencing factors of the brain	2, 6, 9, 10, 11, 14, 16, 24	18793730, 17166743, 17689500, 16179202
	Cluster 2	1. Analysis of metabolism, therapeutic efficacy of antipsychotic agents on brain structure 2. Schizophrenia pathology (from the perspective of temporal lobe, prefrontal cortex and anatomy and histology of brain structure)	13, 15, 18, 19, 20, 22, 25, 26	15201569, 17507880, 15520356, 16005383, 15809403
2009–2013	Cluster 0	Research on the physiopathology mechanism (from the perspective of frontal lobe, temporal lobe, prefrontal cortex, neural pathways) of schizophrenia and the etiology of cognitive disorder and other complications	6, 10, 18, 22, 24, 26, 27, 28, 31	19097861, 20452574, 21868203, 19683896, 22105156
	Cluster 1	1. Research on brain structure and function (e.g. hippocampus, nerve fibers, cerebral cortex) and differentiate schizophrenia from bipolar disorder based on MRI 2. MRI (including DTI) usages, image interpretations	1, 3, 8, 9, 11, 13, 16, 20, 23, 33, 34	24004694, 22832855, 20573561, 21878411, 19042913, 22945617
	Cluster 2	1. Research on default mode network in schizophrenia patients 2. Schizophrenic psychology (association between anatomical and functional cerebral deficits with related clinical symptoms)	2, 4, 5, 7, 12, 14, 15, 17, 19, 21, 25, 29, 30, 32	21095105, 21147518, 19931396, 21277171
2014–2018	Cluster 0	Research on brain structural and functional abnormality (e.g. prefrontal cortex, nerve net) of patients with schizophrenia, as well as physiopathology mechanism of the disease	1, 4, 12, 14, 15, 18, 19, 23, 27, 31, 32, 34	24306091, 26123450, 28338738, 29527474, 26908926, 28207073
	Cluster 1	1. Research on the difference of neurobiological basis between schizophrenia and other mental diseases 2. Effects of antipsychotics on brain structural changes	2, 6, 10, 13, 16, 20, 21, 22, 24, 26, 29, 33, 35	28347393, 25904725, 25089761, 29257977, 25829144, 25968549
	Cluster 2	1. Effects of genetic load on brain function of schizophrenia patients 2. Identification of schizophrenia biomarkers	3, 5, 7, 8, 9, 11, 17, 25, 28, 30, 36	27479923, 27375133, 27829096, 29935206, 29247760

"Rank of MeSH terms" represents the number of high-frequency major MeSH terms/MeSH subheadings in each period as shown in ***Figures 2–4****.*

of the brain default mode network, as well as schizophrenic psychology were newly developed themes.

In the third period of 2014–2018, theme clusters in Quadrant III, including research on differences in the neurobiological basis between schizophrenia and other mental diseases, were similar to the developed and mature theme contents in the first and second periods, which were identified as peripheral and undeveloped themes in the most recent 5 years. In addition, new emerging theme clusters researching on brain structural and functional abnormality of patients with schizophrenia, as well as physiopathology mechanism of the disease were located in Quadrant II, indicating they were developed but still peripheral research areas. Other emerging theme clusters, including effects of genetic load on brain function of schizophrenia patients, as well as identification of schizophrenia biomarkers, were new main undeveloped themes situated in Quadrant IV, which represented central and undeveloped research topics.

To summarize, these three strategic diagrams clearly revealed the current situation and development tendency of each theme cluster of MRI studies on schizophrenia during three different periods.

Knowledge Structure of MRI Studies on Schizophrenia

In this study, statistical indices of degree, betweenness and closeness centrality were applied to describe the knowledge structure of SNA networks in three different periods (**Tables 4** and **5**). The three SNAs were plotted on the basis of betweenness centrality to gain insight into the results (**Figure 6**). As we commented in the figure legends, the size of nodes was proportional to the betweenness centrality of the major MeSH terms/MeSH subheadings, and the thickness of the lines represents the term-term co-occurrence frequency.

In the period of 2004–2008, eight major MeSH terms/MeSH subheadings were shown to have a high degree centrality (greater than the mean value of 203.69, **Table 4**) within the network of MRI studies on schizophrenia. As can be seen in **Table 5**, Magnetic Resonance Imaging (674.000) and Schizophrenia/physiopathology (663.000) had higher degree centrality among the eight high-frequency major MeSH term/MeSH subheadings and showed a larger gap between the others. Furthermore, **Table 4** also shows that the top two betweenness centrality values listed in **Table 5** are the same (8.417), which meant that the two major MeSH terms/MeSH subheadings (Schizophrenia/physiopathology, Schizophrenia/diagnosis) had the strongest mediating effect within the network of the first period. Additionally, both terms had the highest closeness values of 100.000, indicating that they had a tight connection with the other nodes. As shown in **Table 5**, another seven major MeSH terms/MeSH subheadings had high betweenness values (greater than the mean value of 3.39, **Table 4**), which suggested that these MeSH terms also played a critical mediating role within the network. In addition, according to **Figure 6A**, the total number of new emerging hotspots in this period was 12, including Magnetic Resonance Imaging/statistics & numerical data, Schizophrenia/epidemiology, Brain Mapping, Brain/anatomy &

TABLE 4 | Descriptive statistics for centrality measures of MRI studies on schizophrenia from 2004 to 2018.

Period	Density	Degree				Closeness				Betweenness			
		Max	Min	$\bar{x}$± S	Network centralization	Max	Min	$\bar{x}$± S	Network centralization	Max	Min	$\bar{x}$± S	Network centralization
2004–2008	8.145±15.599	674.00	41.00	203.69 ± 184.44	17.88%	100.00	62.50	79.90 ± 10.10	42.69%	8.42	0.48	3.39 ± 2.38	1.74%
2009–2013	8.080 ± 17.782	1311.00	73.00	266.65 ± 273.88	15.80%	100.00	66.00	80.05 ± 9.82	41.76%	10.61	0.61	4.41 ± 2.95	1.21%
2014-2018	7.062 ± 16.209	1204.00	48.00	247.17 ± 241.62	13.47%	97.22	64.82	81.18 ± 8.76	33.49%	9.38	0.89	4.31 ± 2.33	0.88%

histology, Schizophrenia/complications, Schizophrenia/metabolism, Diffusion Magnetic Resonance Imaging, Imaging, Three-Dimensional, Cerebral Cortex/pathology, Imaging Interpretation, Computer-Assisted/methods, as well as Cerebral Cortex/physiopathology, which were located on the edge of the network.

Compared with the SNA of the first period, another four new major MeSH terms/MeSH subheadings (**Table 5** and **Figure 6B**), including Brain Mapping, Schizophrenia/complications, Magnetic Resonance Imaging/methods and Schizophrenia/genetics were added to the nodes with high degree centrality in the second period of 2009–2013. Meanwhile, in addition to Brain Mapping and Schizophrenia/complications, another two MeSH terms (Nerve Net/physiopathology and Memory, Short-Term/physiology) were added to the nodes with high betweenness centrality (greater than the mean value of 4.41, **Tables 4** and **5**). Furthermore, the MeSH terms Schizophrenia/pathology and Schizophrenic Psychology had the highest betweenness centrality values (10.606) and the highest closeness centrality values (100.00) (**Table 5**). According to **Figure 6B**, another 12 new emerging nodes were located at the edge of the network, including Brain Mapping/methods, Neural Pathways/physiopathology, Emotions/physiology, Nerve Net/physiopathology, Prefrontal Cortex/physiopathology, Antipsychotic Agents/therapeutic use, Brain/blood supply, Prefrontal Cortex/pathology, Cognition Disorders/etiology, Hippocampus/pathology, Bipolar Disorder/pathology, and Diffusion Tensor Imaging/methods, identifying them as emerging hotspots of MRI studies on schizophrenia in 2009–2013.

In the SNA of 2014–2018, five new major MeSH terms/MeSH subheadings were added to the nodes (**Figure 6C**), including Schizophrenia/diagnostic imaging, White Matter/pathology, Nerve Net/physiopathology, Psychotic Disorders/physiopathology, Brain Mapping/methods, which were characterized by high betweenness values (greater than the mean value of 4.31, **Table 4**). Compared with the SNA of 2009–2013 (**Figure 6B**), a total of six new emerging nodes, including Brain/diagnostic imaging, Bipolar Disorder/physiopathology, Memory, Short-Term/physiology, Psychotic Disorder/pathology, Prefrontal Cortex/physiopathology, and White Matter/diagnostic imaging, were considered as emerging hotspots of MRI studies on schizophrenia in the third period of 2014–2018 (**Figure 6C**).

DISCUSSION

The human brain is a complex, efficient, and organic system with nearly 100 billion neurons, but during its process of development, a range of genetic, infectious, stress, family, and social environment factors can cause structural and functional abnormalities (34). Schizophrenia has been recognized as the most important brain degeneration disease treated by psychiatrists. Neuroimaging studies have shown that mental disorders can lead to structural and functional changes in brain regions (35, 36), and the structural changes of brain regions are also important risk factors affecting the prodromal stage of schizophrenia (37, 38). The present study evaluated MRI studies on schizophrenia in recent decades by exploring bibliometrics to reach the conclusion that publication of MRI studies on schizophrenia showed an increasing trend in the last

TABLE 5 | Descriptive statistics for centrality measure about MRI studies on schizophrenia from 2004 to 2018.

Period	Rank of MeSH terms	High-frequency MeSH terms/MeSH subheadings	Centrality			Rank of MeSH terms	High-frequency MeSH terms/MeSH subheadings	Centrality		
			Degree	Betweenness	Closeness			Degree	Betweenness	Closeness
2004–2008	3	Magnetic Resonance Imaging	674.000	5.320	89.286	15	Antipsychotic Agents/ therapeutic use	99.000	3.174	80.645
	1	Schizophrenia/ physiopathology	663.000	8.417	100.000	16	Cerebral Cortex/ pathology	93.000	2.587	75.758
	4	Schizophrenia/ diagnosis	461.000	8.417	100.000	14	Brain Mapping	91.000	1.650	71.429
	5	Schizophrenic Psychology	429.000	5.313	92.593	21	Diffusion Magnetic Resonance Imaging	86.000	1.927	71.429
	2	Schizophrenia/ pathology	415.000	7.593	96.154	20	Brain/anatomy & histology	81.000	1.653	73.529
	7	Image Processing, Computer-Assisted	389.000	1.736	78.125	24	Image Interpretation, Computer-Assisted/ methods	72.000	0.482	62.500
	6	Brain/pathology	299.000	3.682	80.645	25	Temporal Lobe/ pathology	69.000	2.238	73.529
	8	Brain/physiopathology	275.000	5.543	86.207	11	Schizophrenia/ complications	69.000	1.530	71.429
	9	Schizophrenia/ genetics	178.000	7.441	96.154	23	Cerebral Cortex/ physiopathology	67.000	1.454	71.429
	17	Imaging, Three-Dimensional	162.000	1.246	73.529	19	Magnetic Resonance Imaging/statistics & numerical data	65.000	1.313	71.429
	12	Prefrontal Cortex/ physiopathology	144.000	3.388	80.645	26	Prefrontal Cortex/ pathology	63.000	1.480	75.758
	10	Magnetic Resonance Imaging/methods	135.000	4.448	83.333	22	Schizophrenia/ epidemiology	55.000	2.312	73.529
	13	Schizophrenia/drug therapy	121.000	2.806	80.645	18	Schizophrenia/ metabolism	41.000	0.851	67.568
2009– 2013	1	Schizophrenia/ pathology	1322.000	10.606	100.000	16	Psychotic Disorders/ pathology	140.000	4.133	80.488
	2	Schizophrenia/ physiopathology	909.000	9.658	97.059	27	Neural Pathways/ pathology	127.000	4.210	80.488
	4	Schizophrenic Psychology	754.000	10.606	100.000	22	Temporal Lobe/ pathology	114.000	3.411	78.571
	3	Brain/pathology	700.000	7.333	91.667	25	Neural Pathways/ physiopathology	114.000	2.137	71.739
	5	Brain/physiopathology	488.000	5.934	84.615	23	Bipolar Disorder/ pathology	114.000	1.953	71.739
	7	Magnetic Resonance Imaging	447.000	8.232	91.667	28	Cognition Disorders/ etiology	113.000	2.103	71.739
	6	Brain Mapping	397.000	8.011	91.667	21	Cerebral Cortex/ physiopathology	111.000	2.063	71.739
	10	Schizophrenia/ complications	320.000	6.084	84.615	26	Brain/blood supply	111.000	0.794	67.347
	9	Magnetic Resonance Imaging/methods	302.000	6.204	84.615	20	Hippocampus/ pathology	104.000	3.953	78.571
	8	Schizophrenia/ genetics	281.000	9.526	97.059	29	Emotions/physiology	102.000	1.975	71.739
	12	Schizophrenia/ diagnosis	246.000	7.139	89.189	34	Image Interpretation, Computer-Assisted/ methods	100.000	1.012	67.347
	11	Cerebral Cortex/ pathology	244.000	4.293	82.500	30	Brain Mapping/ methods	98.000	2.873	75.000
	19	Image Processing, Computer-Assisted	204.000	3.886	78.571	24	Prefrontal Cortex/ pathology	94.000	0.607	66.000
	13	Nerve Fibers, Myelinated/pathology	200.000	5.405	84.615	15	Schizophrenia/drug therapy	91.000	2.404	75.000
	17	Nerve Net/ physiopathology	172.000	1.468	70.213	31	Frontal Lobe/pathology	86.000	3.229	76.744
	14		155.000	2.383	71.739	33		85.000	0.917	68.750

(Continued)

TABLE 5 | Continued

Period	Rank of MeSH terms	High-frequency MeSH terms/MeSH subheadings	Centrality			Rank of MeSH terms	High-frequency MeSH terms/MeSH subheadings	Centrality		
			Degree	Betweenness	Closeness			Degree	Betweenness	Closeness
		Prefrontal Cortex/ physiopathology					Diffusion Tensor Imaging/methods			
	18	Memory, Short-Term/ physiology	148.000	4.309	78.571	32	Antipsychotic Agents/ therapeutic use	73.000	1.154	70.213
2014- 2018	1	Schizophrenia/ physiopathology	1240.000	7.924	97.222	13	Schizophrenia/ complications	166.000	7.320	89.744
	2	Schizophrenia/ pathology	945.000	8.434	97.222	21	Cerebral Cortex/ pathology	155.000	4.272	79.545
	4	Brain/physiopathology	577.000	3.869	83.333	16	Schizophrenia/drug therapy	154.000	3.862	81.395
	3	Schizophrenia/ diagnostic imaging	514.000	7.642	94.595	24	Bipolar Disorder/ pathology	131.000	0.889	64.815
	5	Schizophrenic Psychology	466.000	7.722	94.595	23	Brain Mapping/ methods	129.000	4.990	83.333
	6	Brain/pathology	407.000	5.881	85.366	17	Schizophrenia/ diagnosis	126.000	5.120	83.333
	7	Magnetic Resonance Imaging/methods	360.000	9.382	97.222	34	Bipolar Disorder/ physiopathology	117.000	1.391	70.000
	9	Brain/diagnostic imaging	279.000	2.225	76.087	27	Memory, Short-Term/ physiology	113.000	1.535	71.429
	10	White Matter/ pathology	262.000	5.741	87.500	25	Brain Mapping	111.000	4.194	79.545
	14	Nerve Net/ physiopathology	240.000	4.592	83.333	30	Psychotic Disorders/ diagnostic imaging	111.000	3.946	81.395
	15	Psychotic Disorders/ physiopathology	237.000	5.823	89.744	28	White Matter/ diagnostic imaging	108.000	2.059	72.917
	8	Schizophrenia/ genetics	213.000	7.621	92.105	29	Diffusion Tensor Imaging/methods	107.000	4.112	74.468
	11	Magnetic Resonance Imaging	205.000	7.086	89.744	26	Antipsychotic Agents/ therapeutic use	101.000	2.463	72.917
	12	Prefrontal Cortex/ physiopathology	198.000	2.618	76.087	32	Neural Pathways/ physiopathology	99.000	1.663	72.917
	19	Connectome/methods	194.000	3.040	79.545	31	Emotions/physiology	93.000	2.463	76.087
	18	Cerebral Cortex/ physiopathology	182.000	2.482	77.778	35	Prefrontal Cortex/ pathology	88.000	3.268	76.087
	22	Psychotic Disorders/ pathology	176.000	2.386	72.917	33	Hippocampus/ pathology	78.000	1.446	70.000
	20	Gray Matter/pathology	168.000	4.280	79.545	36	Schizophrenia/ metabolism	48.000	1.257	68.627

"Rank of MeSH terms" represents the number of high-frequency major MeSH terms/MeSH subheadings in each period as shown in ***Figures 2–4****.*

15 years. However, after in-depth analysis, we observed that growth of the third period became slower than the second, but the number of papers published in 2015 is the largest, showing the peak in three curves. In addition, based on the results of the strategic diagram, we observed that contents of theme clusters in each quadrant have changed to some extend so that we could have a preliminary understanding of the theme trends from 2004 to 2018.

In the first period (2004–2008), theme Cluster 0 and Cluster 1 were located in Quadrant I, representing well-developed and mature topics. From the literature analysis, we found that previous research clarified the relationship between brain structural changes and functional abnormalities and analyzed the structural deficit in the corticothalamic system (39), anatomical changes in the frontal-temporal circuit and functional alterations in the prefrontal cortex (40) for the purpose of exploring the etiology and physiopathology of schizophrenia. Furthermore, the structural parts of abnormal brain regions that led to dysfunction and perceived sources of information were identified and positioned (41).

Another theme (Cluster 2) located in Quadrant I. indicated that research on the analysis of metabolism, therapeutic efficacy of antipsychotic agents on brain structure and schizophrenia pathology was immature and needed further study. Previous reports had suggested that after controlling for confounding factors such as sex and age, antipsychotics could alleviate or treat clinical symptoms by altering brain structure (42, 43), but more recent research has found that first-generation antipsychotic drugs may increase oxidative stress and damage cerebral function (44); therefore, whether antipsychotic agents have a protective or destructive effect on brain structure has not been consistently shown. Moreover, numerous studies have demonstrated that almost all cortical and subcortical structures in schizophrenia patients showed morphological abnormalities,

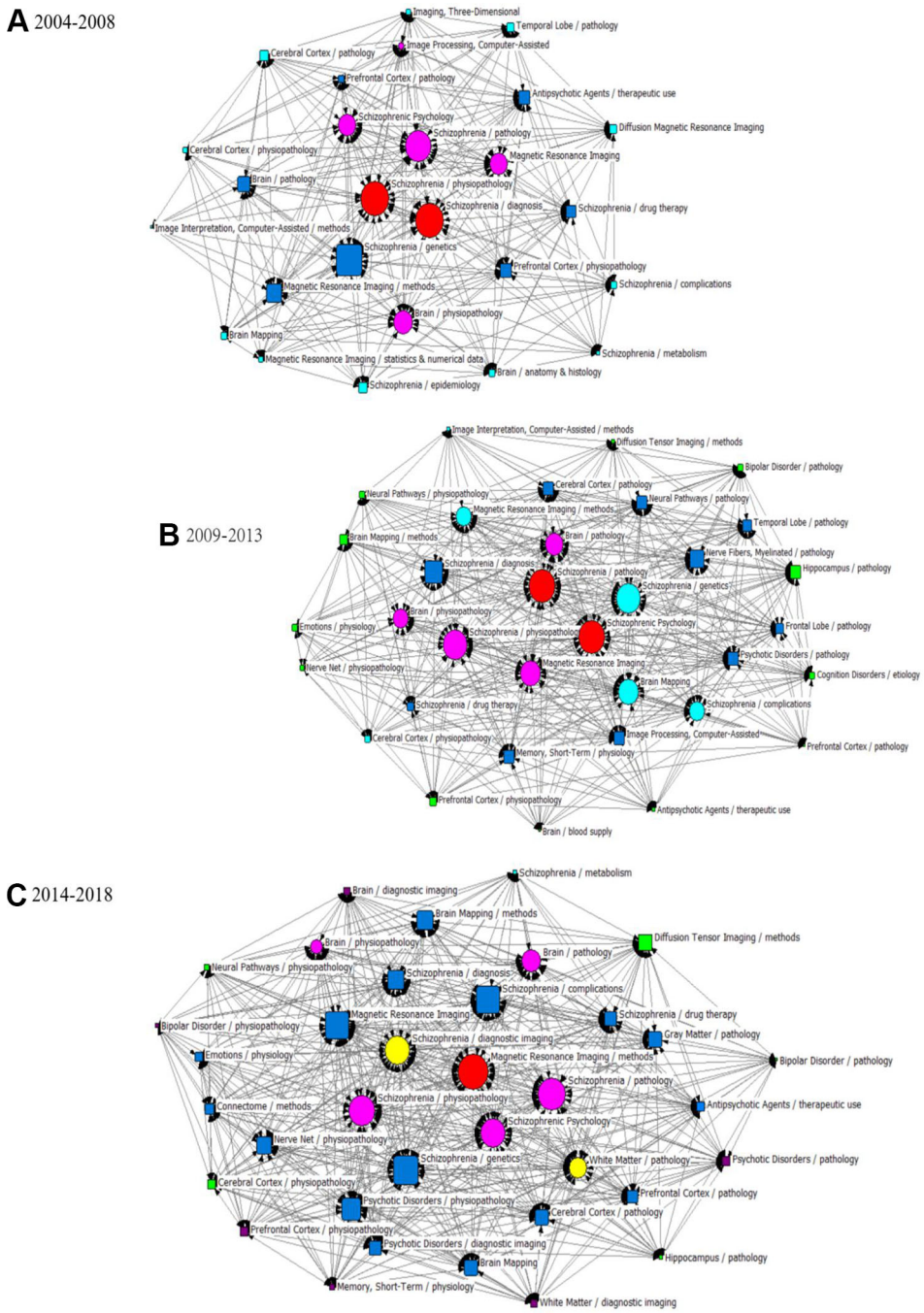

FIGURE 6 | SNA for high-frequency major MeSH terms/MeSH subheadings applied to MRI studies on schizophrenia. **(A)** SNA for 26 high-frequency major MeSH terms/MeSH subheadings in 2004–2008. **(B)** SNA for 34 high-frequency major MeSH terms/MeSH subheadings in 2009–2013. **(C)** SNA for 36 high-frequency major MeSH terms/MeSH subheadings in 2014–2018. The size of the nodes and the thickness of the lines within the networks represent centrality of MeSH terms and the co-occurrence frequency of MeSH terms pairs, respectively. *Red icons* ( ): Node with the highest betweenness centrality. *Circle icons:* Nodes highly co-occurred with other nodes since the period of 2004–2008 ( ), 2009–2013 ( ) and 2014–2018 ( ), respectively (**Figure 6A–C**). *Box icons:* Emerging nodes in 2004–2008 ( ), 2009–2013 ( ) and 2014–2018( ), respectively.

including changes in the volume of brain structures such as the whole brain, temporal lobe, amygdala and hippocampus (45–47). Meantime, Fornito, et al. also suggested that impaired brain network connectivity is the pathophysiological basis for diverse clinical symptoms and cognitive impairment of schizophrenia (48). As a result, it is difficult to identify which parts of a brain region that are structurally and functionally abnormal directly contribute to schizophrenia. Therefore, it will be a long process and difficult project to explore the pathological mechanisms of schizophrenia through MRI studies.

During the second period of 2009–2013, partial theme contents of Cluster 1 (research on brain structure and function) were still located in Quadrant I, indicating that researchers kept on paying close attention to the related research topic. With the exception of in-depth studies on nerve fibers, hippocampus, and cerebral cortex (49, 50), good progress has been made in the use of brain imaging to distinguish between schizophrenia and bipolar disorder (51, 52). Moreover, researchers have acquired better understanding of the use of various MRI techniques, their analysis, and interpretation of results (53, 54). In addition, we determined that research on the pathological mechanism of schizophrenia (partial theme contents of Cluster 0, located in Quadrant III) has not yet been fully elucidated and remains as an undeveloped theme. As for the new theme cluster schizophrenia psychology, researchers are dedicated to identifying the basis for the structural and functional activities of brains that cause abnormal psychological symptoms (e.g., emotional withdrawal) in patients with schizophrenia (55, 56). However, due to the diversity of abnormal psychological symptoms in patients and the complicated influencing factors (e.g., course of disease and medication), this field needs further development. Another new theme cluster is brain default mode network (DMN), in which brain network studies have shown changes in the default network functional connectivity in schizophrenia. While results in this area are inconsistent, most studies have shown increased DMN functional connectivity in schizophrenia, as well as weaken functional connections in the prefrontal cortex (57, 58). Nevertheless, taking antipsychotics and changes in psychiatric symptoms can influence resting brain networks, and the intrinsic relationship between genes and DMN have gradually become noteworthy academic issues in recent years (59, 60).

In the third period of 2014–2018, Cluster 1, whose theme contents involve research on differences in the neurobiological basis of schizophrenia and other mental diseases and include studies of the effects of antipsychotics on brain structural changes, was located in Quadrant III. The theme of differential diagnosis of schizophrenia and other mental disorder (e.g., bipolar disorder, schizoaffective disorder), which was originally in Quadrant Iin the second period (2009–2013), is now situated in Quadrant III during the third period (2014-2018). Based on MRI techniques, researchers have studied the similarities and differences in brain structure among patients with schizophrenia and bipolar disorder, such as the two major psychotic disorder have a shared white-matter dysconnectivity in callosal, paralimbic, and fronto-occipital regions (61), but volume reductions in several brain regions of schizophrenic patients, such as the medial frontal cortex, parts of the temporal lobe cortex, the insula and hippocampus cannot be observed in bipolar patients (62). And they also have identified the risk alleles associated with the disease to facilitate more accurate identification and diagnosis (63). Relevant research needs to be further developed and improved.

In addition, as mentioned above, reports about the use of antipsychotics to prevent the progression of brain damage are as yet inconsistent. Numerous studies have found that changes in brain imaging occurred at an early stage in schizophrenia, while structural and functional abnormalities in brain regions caused by grey and white matter volume reductions and anomalous connections, became more prominent with the progression of the condition. But Emsley et al. argued that the brain volume reductions are not directly associated with antipsychotic treatment during the first year of medication, and decrease in brain volume may have more to do with neurotoxicity of drugs than with the therapeutic effect (64). However, due to the differences in research facilities and measuring methods, conclusions are still controversial because abnormal brain regions in various studies do not completely overlap. It remains to be seen whether our next study should take steps to repair brain damage, or whether it should delay, prevent, or interfere with the continued damage to brain structure caused by antipsychotics.

Finally, we can also conclude that the MeSH terms Schizophrenia/physiopathology, Schizophrenia/pathology, and Schizophrenia Psychology have higher or the highest values of betweenness centrality, implying that they have the largest number of direct connections with other nodes, as well as being situated at the core position within the networks. In other words, research on the pathological and physio-pathological mechanisms of schizophrenia, as well as analysis of abnormal psychological and behavioral symptoms from the perspective of brain imaging, are significant and potentially important academic issues in this research field. In addition, the new emerging hotspots in these three periods should be viewed as a guide to finding new directions for research.

CONCLUSION

The main finding of this study was that MRI studies on schizophrenia have been an issue of general concern, but the progress (e.g. pathogenesis of schizophrenia) is relatively slow in recent years. Further research is necessary to investigate the undeveloped, immature, and emerging hotspots and theme clusters mentioned above so as to provide medical staff, scientific researchers, and frontline educators with new directions in the field of MRI studies on schizophrenia.

LIMITATION

There are several limitations to consider in the current study. To better present results, years were selected as the time unit to divide time periods and complete statistics. However, the complete data of 2019 has not yet been obtained, so the literature published in this year was not included. In addition, this study only included journals articles, so some research hotspots might have been omitted due to the exclusion of conference papers, reviews, and other types of literature. In addition, there are certain limitations in the scope of the PubMed database collection and in the indexing of MeSH terms, so that literature retrieval based on MeSH terms may miss some publications. Furthermore, this study selected the index of major MeSH terms/MeSH subheadings to extract high-frequency MeSH terms, and we cannot completely exclude the possibility that other low-frequency MeSH terms may become hotspots of research in the future. Finally, the data source only selects the published literatures, which may lead to publication bias.

AUTHOR CONTRIBUTIONS

GZ designed and corrected the paper. LD wrote the paper.

FUNDING

This work was supported by grants from the Major Project of the Department of Science &Technology of Liaoning Province (2019JH8/10300019).

REFERENCES

1. Hor K, Taylor M. Suicide and schizophrenia: a systematic review of rates and risk factors. *J Psychopharmacol* (2010) 24:81–90. doi: 10.1177/1359786810385490
2. Buckley PF, Miller BJ, Lehrer DS, Castle DJ. Psychiatric comorbidities and schizophrenia. *Schizophr Bull* (2009) 35:383–402. doi: 10.1093/schbul/sbn135
3. Wieronska JM, Zorn SH, Doller D, Pilc A. Metabotropic glutamate receptors as targets for new antipsychotic drugs: historical perspective and critical comparative assessment. *Pharmacol Ther* (2016) 157:10–27. doi: 10.1016/j.pharmthera.2015.10.007
4. McGrath J, Saha S, Welham J, El Saadi O, MacCauley C, Chant D. A systematic review of the incidence of schizophrenia: the distribution of rates and the influence of sex, urbanicity, migrant status and methodology. *BMC Med* (2004) 2:13. doi: 10.1186/1741-7015-2-13
5. GBD 2016 Disease and Injury Incidence and Prevalence Collaborators. Global, regional, and national incidence, prevalence, and years lived with disability for 328 diseases and injuries for 195 countries, 1990-2016: a systematic analysis for the global burden of disease study 2016. *Lancet* (2017) 390:1211–59. doi: 10.1016/S0140-6736(17)32154-2
6. Sandstrom A, Sahiti Q, Pavlova B, Uher R. Offspring of parents with schizophrenia, bipolar disorder, and depression: a review of familial high-risk and molecular genetics studies. *Psychiatr Genet* (2019) 29:160–9. doi: 10.1097/YPG.0000000000000240
7. Hameed MA, Lewis AJ. Offspring of parents with schizophrenia: a systematic review of developmental features across childhood. *Harv Rev Psychiatry* (2016) 24:104–17. doi: 10.1097/HRP.0000000000000076
8. van Os J, Kenis G, Rutten BP. The environment and schizophrenia. *Nature* (2010) 468:203–12. doi: 10.1038/nature09563
9. Weinberger DR. Future of days past: neurodevelopment and schizophrenia. *Schizophr Bull* (2017) 43:1164–8. doi: 10.1093/schbul/sbx118
10. Kay SR, Fiszbein A, Opler LA. The positive and negative syndrome scale (panss) for schizophrenia. *Schizophr Bull* (1987) 13:261–76. doi: 10.1093/schbul/13.2.261
11. Kaneko G, Sanganahalli BG, Groman SM, Wang H, Coman D, Rao J, et al. Hypofrontality and posterior hyperactivity in early schizophrenia: Imaging and behavior in a preclinical model. *Biol Pychiatry* (2017) 81:503–13. doi: 10.1016/j.biopsych.2016.05.019
12. Gilmore JH, Smith LC, Wolfe HM, Hertzberg BS, Smith JK, Chescheir NC, et al. Prenatal mild ventriculomegaly predicts abnormal development of the neonatal brain. *Biol Psychiatry* (2008) 64:1069–76. doi: 10.1016/j.biopsych.2008.07.031
13. Li G, Wang L, Shi F, Lyall AE, Ahn M, Peng Z, et al. Cortical thickness and surface area in neonates at high risk for schizophrenia. *Brain Struct Funct* (2016) 221:447–61. doi: 10.1007/s00429-014-0917-3
14. Koike S. Clinical status and outcome biomarkers in schizophrenia: a review for near-infrared spectroscopy studies. *Seishin Shinkeigaku Zasshi* (2013) 115:863–73.
15. Szulc A, Galińska B, Tarasów E, Kubas B, Dzienis W, Konarzewska B, et al. N-acetylaspartate (NAA) levels in selected areas of the brain in patients with chronic schizophrenia treated with typical and atypical neuroleptics: a proton magnetic resonance spectroscopy (1H MRS) study. *Med Sci Monit* (2007) 13:17–22.
16. Jacobi W, Winkler H. Encephalographische studien an schizophrenen. *Archiv Für Psychiatr Und Nervenkrankheiten* (1927) 81:299–332. doi: 10.1007/BF01825649
17. Johnstone EC, Crow TJ, Frith CD, Husband J, Kreel L. Cerebral ventricular size and cognitive impairment in chronic schizophrenia. *Lancet* (1976) 2:924–6. doi: 10.1016/S0140-6736(76)90890-4
18. Smith RC, Calderon M, Ravichandran GK, Largen J, Vroulis G, Shvartsburd A, et al. Nuclear magnetic resonance in schizophrenia: A preliminary study. *Psychiatry Res* (1984) 12:137–47. doi: 10.1016/0165-1781(84)90013-1
19. Johnson MH, Cohen J, Grudzinskas G. The uses and abuses of bibliometrics. *Reprod BioMed Online* (2012) 24:485–6. doi: 10.1016/j.rbmo.2012.03.007
20. Yao Q, Chen K, Yao L, Lyu PH, Yang TA, Luo F, et al. Scientometric trends and knowledge maps of global health systems research. *Health Res Policy Syst* (2014) 12:26. doi: 10.1186/1478-4505-12-26
21. Hirsch JE. An index to quantify an individual's scientific research output. *Proc Natl Acad Sci U S A.* (2005) 102:16569–72. doi: 10.1073/pnas.0507655102
22. Guan JC, Gao X. Exploring the h-index at patent level. *J Am Soc Inf Sci Technol* (2008) 60:35–40. doi: 10.1002/asi.20954
23. Braun T, Glänzel W, Schubert A. A Hirsch-type index for journals. *Scientometrics* (2006) 69:169–73. doi: 10.1007/s11192-006-0147-4
24. Raan AFJV. Comparison of the Hirsch-index with standard bibliometric indicators and with peer judgment for 147 chemistry research groups. *Scientometrics* (2006) 67:491–502. doi: 10.1556/Scient.67.2006.3.10
25. Li F, Li M, Guan P, Ma S, Cui L. Mapping publication trends and identifying hot spots of research on Internet health information seeking behavior: a quantitative and co-word biclustering analysis. *J Med Internet Res* (2015) 17:e81. doi: 10.2196/jmir.3326
26. Hartigan JA. Direct clustering of a data matrix. *Publ Am Stat Assoc* (1972) 67:7. doi: 10.1080/01621459.1972.10481214
27. Law J, Bauin S, Courtial JP, Whittaker J. Policy and the mapping of scientific change: a co-word analysis of research into environmental acidification. *Scientometrics* (1988) 14:251–64. doi: 10.1007/BF02020078
28. Viedma-Del-Jesus MI, Perakakis P, Muñoz M, López-Herrera AG, Vila J. Sketching the first 45 years of the journal psychophysiology (1964-2008): a co-word-based analysis. *Psychophysiology* (2011) 48:1029–36. doi: 10.1111/j.1469-8986.2011.01171.x
29. Parnell JM, Robinson JC. Social network analysis: presenting an underused method for nursing research. *J Adv Nurs* (2018) 74:1310–8. doi: 10.1111/jan.13541
30. Guillon Q, Afzali MH, Rogé B, Baduel S, Kruck J, Hadjikhani N. The importance of networking in autism gaze analysis. *PloS One* (2015) 10:e0141191. doi: 10.1371/journal.pone.0141191
31. APA Brede M. Networks—an introduction. mark e. j. newman. (2010, oxford university press.). *Artif Life* (2012) 18:241–:2. doi: 10.1162/artl_r_00062
32. Freeman LC. A set of measures of centrality based on betweenness. *Sociometry* (1977) 40:35–41. doi: 10.2307/3033543

33. Sadria M, Karimi S, Layton AT. Network centrality analysis of eye-gaze data in autism spectrum disorder. *Comput Biol Med* (2019) 111:103332. doi: 10.1016/j.compbiomed.2019.103332
34. Liang X. Human connectome: structural and functional brain networks. *Chin J* (2010) 55:1565. doi: 10.1360/972009-2150
35. Fusar-Poli P. Voxel-wise meta-analysis of fMRI studies in patients at clinical high risk for psychosis. *J Psychiatry Neurosci* (2012) 37:106–12. doi: 10.1503/jpn.110021
36. Smieskova R, Fusar-Poli P, Allen P, Bendfeldt K, Stieglitz RD, Drewe J, et al. Neuroimaging predictors of transition to psychosis–a systematic review and meta-analysis. *Neurosci Biobehav Rev* (2010) 34:1207–22. doi: 10.1016/j.neubiorev.2010.01.016
37. Nenadic I, Dietzek M, Schönfeld N, Lorenz C, Gussew A, Reichenbach JR, et al. Brain structure in people at ultra-high risk of psychosis, patients with first-episode schizophrenia, and healthy controls: a VBM study. *Schizophr Res* (2015) 161:169–76. doi: 10.1016/j.schres.2014.10.041
38. Lesh TA, Careaga M, Rose DR, McAllister AK, Van de Water J, Carter CS, et al. Cytokine alterations in first-episode schizophrenia and bipolar disorder: Relationships to brain structure and symptoms. *J Neuroinflamm* (2018) 15:165. doi: 10.1186/s12974-018-1197-2
39. Kim JJ, Kim DJ, Kim TG, Seok JH, Chun JW, Oh MK, et al. Volumetric abnormalities in connectivity-based subregions of the thalamus in patients with chronic schizophrenia. *Schizophr Res* (2007) 97:226–35. doi: 10.1016/j.schres.2007.09.007
40. Schlösser RG, Nenadic I, Wagner G, Güllmar D, von Consbruch K, Köhler S, et al. White matter abnormalities and brain activation in schizophrenia: a combined DTI and fMRI study. *Schizophr Res* (2007) 89:1–11. doi: 10.1016/j.schres.2006.09.007
41. Simons JS, Davis SW, Gilbert SJ, Frith CD, Burgess PW. Discriminating imagined from perceived information engages brain areas implicated in schizophrenia. *Neuroimage* (2006) 32:696–703. doi: 10.1016/j.neuroimage.2006.04.209
42. Molina V, Sanz J, Benito C, Palomo T. Direct association between orbitofrontal atrophy and the response of psychotic symptoms to olanzapine in schizophrenia. *Int Clin Psychopharmacol* (2004) 19:221–8. doi: 10.1097/01.yic.0000125753.01426.d7
43. van Haren NE, Hulshoff Pol HE, Schnack HG, Cahn W, Mandl RC, Collins DL, et al. Focal gray matter changes in schizophrenia across the course of the illness: a 5-year follow-up study. *Neuropsychopharmacology* (2007) 32:2057–66. doi: 10.1038/sj.npp.1301347
44. Bai ZL, Li XS, Chen GY, Du Y, Wei ZX, Chen X, et al. Serum oxidative stress marker levels in unmedicated and medicated patients with schizophrenia. *J Mol Neurosci* (2018) 66:428–36. doi: 10.1007/s12031-018-1165-4
45. James AC, James S, Smith DM, Javaloyes A. Cerebellar, prefrontal cortex, and thalamic volumes over two time points in adolescent-onset schizophrenia. *Am J Psychiatry* (2004) 161:1023–9. doi: 10.1176/appi.ajp.161.6.1023
46. Staal WG, Hulshoff Pol HE, Schnack HG, van Haren NE, Seifert N, Kahn RS. Structural brain abnormalities in chronic schizophrenia at the extremes of the outcome spectrum. *Am J Psychiatry* (2001) 158:1140–2. doi: 10.1176/appi.ajp.158.7.1140
47. Buchsbau MS, Friedman J, Chu KW, Newmark R, Schneiderman JS, Torosjan Y, et al. Diffusion tensor imaging in schizophrenia. *Biol Psychiatry* (2005) 58:921–9. doi: 10.1016/j.schres.2007.10.009
48. Fornito A, Yoon J, Zalesky A, Bullmore ET, Carter CS. General and specific functional connectivity disturbances in first-episode schizophrenia during cognitive control performance. *Biol Psychiatry* (2011) 70:64–72. doi: 10.1016/j.biopsych.2011.02.019
49. Gogtay N, Hua X, Stidd R, Boyle CP, Lee S, Weisinger B, et al. Delayed white matter growth trajectory in young nonpsychotic siblings of patients with childhood-onset schizophrenia. *Arch Gen Psychiatry* (2012) 69:875–84. doi: 10.1001/archgenpsychiatry.2011.2084
50. Mandl RC, Schnack HG, Luigjes J, van den Heuvel MP, Cahn W, Kahn RS, et al. Tract-based analysis of magnetization transfer ratio and diffusion tensor imaging of the frontal and frontotemporal connections in schizophrenia. *Schizophr Bull* (2010) 36:778–87. doi: 10.1093/schbul/sbn161
51. Schnack HG, Nieuwenhuis M, van Haren NE, Abramovic L, Scheewe TW, Brouwer RM, et al. Can structural MRI aid in clinical classification? A machine learning study in two independent samples of patients with schizophrenia, bipolar disorder and healthy subjects. *Neuroimage* (2014) 84:299–306. doi: 10.1016/j.neuroimage.2013.08.053
52. Morris RW, Sparks A, Mitchell PB, Weickert CS, Green MJ. Lack of cortico-limbic coupling in bipolar disorder and schizophrenia during emotion regulation. *Transl Psychiatry* (2012) 2:e90. doi: 10.1038/tp.2012.16
53. Voineskos AN, O'Donnell LJ, Lobaugh NJ, Markant D, Ameis SH, Niethammer M, et al. Quantitative examination of a novel clustering method using magnetic resonance diffusion tensor tractography. *Neuroimage* (2009) 45:370–6. doi: 10.1016/j.neuroimage.2008.12.028
54. Venkataraman A, Rathi Y, Kubicki M, Westin CF, Golland P. Joint modeling of anatomical and functional connectivity for population studies. *IEEE Trans Med Imaging* (2012) 31:164–82. doi: 10.1109/TMI.2011.2166083
55. Kumari V, Fannon D, Ffytche DH, Raveendran V, Antonova E, Premkumar P, et al. Functional MRI of verbal self-monitoring in schizophrenia: performance and illness-specific effects. *Schizophr Bull* (2010) 36:740–55. doi: 10.1093/schbul/sbn148
56. Herold R, Feldmann A, Simon M, Tényi T, Kövér F, Nagy F, et al. Regional gray matter reduction and theory of mind deficit in the early phase of schizophrenia: a voxel-based morphometric study. *Acta Psychiatr Scand* (2009) 119:199–208. doi: 10.1111/j.1600-0447.2008.01297.x
57. Greicius MD, Supekar K, Menon V, Dougherty RF. Resting-state functional connectivity reflects structural connectivity in the default mode network. *Cereb Cortex* (2009) 19:72–8. doi: 10.1093/cercor/bhn059
58. Shen H, Wang L, Liu Y, Hu D. Discriminative analysis of resting-state functional connectivity patterns of schizophrenia using low dimensional embedding of fMRI. *Neuroimage* (2010) 49:3110–21. doi: 10.1016/j.neuroimage.2009.11.011
59. Zong X, Hu M, Pantazatos SP, Mann JJ, Wang G, Liao Y, et al. A dissociation in effects of risperidone monotherapy on functional and anatomical connectivity within the default mode network. *Schizophr Bull* (2018) 45:1309-18. doi: 10.1093/schbul/sby175
60. Richiardi J, Altmann A, Milazzo AC, Chang C, Chakravarty MM, Banaschewski T, et al. BRAIN NETWORKS. Correlated gene expression supports synchronous activity in brain networks. *Science* (2015) 348:1241–4. doi: 10.1126/science.1255905
61. Kumar J, Iwabuchi S, Oowise S, Balain V, Palaniyappan L, Liddle PF. Shared white-matter dysconnectivity in schizophrenia and bipolar disorder with psychosis. *Psychol Med* (2015) 45:759–70. doi: 10.1017/S0033291714001810
62. Amann BL, Canales-Rodríguez EJ, Madre M, Radua J, Monte G, Alonso-Lana S, et al. Brain structural changes in schizoaffective disorder compared to schizophrenia and bipolar disorder. *Acta Psychiatr Scand* (2016) 133:23–33. doi: 10.1111/acps.12440
63. Tecelão D, Mendes A, Martins D, Bramon E, Toulopoulou T, Kravariti E, et al. The impact of psychosis genome-wide associated ZNF804A variation on verbal fluency connectivity. *J Psychiatr Res* (2018) 98:17–21. doi: 10.1016/j.jpsychires.2017.12.005
64. Emsley R, Asmal L, du Plessis S, Chiliza B, Phahladira L, Kilian S. Brain volume changes over the first year of treatment in schizophrenia: relationships to antipsychotic treatment. *Psycholl Med* (2017) 47:2187–96. doi: 10.1017/S0033291717000642

Conflict of Interest: The authors declare that the research was conducted in the absence of any commercial or financial relationships that could be construed as a potential conflict of interest.

frontiers in Psychiatry

ORIGINAL RESEARCH
published: 12 February 2020
doi: 10.3389/fpsyt.2019.00995

Dynamic Functional Connectivity Strength Within Different Frequency-Band in Schizophrenia

Yuling Luo†, Hui He†, Mingjun Duan, Huan Huang, Zhangfeng Hu, Hongming Wang, Gang Yao, Dezhong Yao, Jianfu Li and Cheng Luo*

The Clinical Hospital of Chengdu Brain Science Institute, MOE Key Lab for Neuroinformation, High-Field Magnetic Resonance Brain Imaging Key Laboratory of Sichuan Province, University of Electronic Science and Technology of China, Chengdu, China

OPEN ACCESS

Edited by:
Roberto Esposito, A.O. Ospedali Riuniti Marche Nord, Italy

Reviewed by:
Feng Liu, Tianjin Medical University General Hospital, China
Dahua Yu, Inner Mongolia University of Science and Technology, China

***Correspondence:**
Jianfu Li
leed1005@163.com

†*These authors have contributed equally to this work*

Specialty section:
This article was submitted to Neuroimaging and Stimulation, a section of the journal Frontiers in Psychiatry

Received: *08 October 2019*
Accepted: *17 December 2019*
Published: *12 February 2020*

Citation:
Luo Y, He H, Duan M, Huang H, Hu Z, Wang H, Yao G, Yao D, Li J and Luo C (2020) Dynamic Functional Connectivity Strength Within Different Frequency-Band in Schizophrenia. Front. Psychiatry 10:995. doi: 10.3389/fpsyt.2019.00995

As a complex psychiatric disorder, schizophrenia is interpreted as a "dysconnection" syndrome, which is linked to abnormal integrations in between distal brain regions. Recently, neuroimaging has been widely adopted to investigate how schizophrenia affects brain networks. Furthermore, some studies reported frequency dependence of the abnormalities of functional network in schizophrenia, however, dynamic functional connectivity with frequency dependence is rarely used to explore changes in the whole brain of patients with schizophrenia (SZ). Therefore, in the current study, dynamic functional connectivity strength (dFCS) was performed on resting-state functional magnetic resonance data from 96 SZ patients and 121 healthy controls (HCs) at slow-5 (0.01–0.027 Hz), slow-4 (0.027–0.073 Hz), slow-3 (0.073–0.198 Hz), and slow-2 (0.198–0.25 Hz) frequency bands and further assessed whether the altered dFCS was correlated to clinical symptoms in SZ patients. Results revealed that decreased dFCS of schizophrenia were found in salience, auditory, sensorimotor, visual networks, while increased dFCS in cerebellum, basal ganglia, and prefrontal networks were observed across different frequency bands. Specifically, the thalamus subregion of schizophrenic patients exhibited enhanced dynamic FCS in slow-5 and slow-4, while reduced in slow-3. Moreover, in slow-5 and slow-4, significant interaction effects between frequency and group were observed in the left calcarine cortex, the bilateral inferior orbitofrontal gyrus, and anterior cingulum cortex (ACC). Furthermore, the altered dFCS of insula, thalamus (THA), calcarine cortex, orbitofrontal gyrus, and paracentral lobule were partial correlated with clinical symptoms of SZ patients in slow-5 and slow-4 bands. These results demonstrate the abnormalities of dFCS in schizophrenia patients is rely on different frequency bands and may provide potential implications for exploring the neuropathological mechanism of schizophrenia.

Keywords: Schizophrenia, dynamic functional connectivity strength, rest-state functional magnetic resonance imaging, different, frequency band

INTRODUCTION

Schizophrenia (SZ) is a chronic and diverse pathological psychiatric disorder. It typically emerges during adolescence or young adulthood (15–35 years old), and clinically characterized by emotional, attentional, and cognitive dysfunction, accompanied by some symptoms such as hallucinations and delusions. Yet, neural mechanism and pathogenesis of SZ remain poorly understood. Converging studies suggest that the pathology of SZ is related to abnormal structure and functional of large- scale brain network (1–3).

The development and application of functional magnetic resonance imaging (fMRI) has shedded a new light on exploring the pathogenesis of SZ. Findings from fMRI studies have reported abnormal low-frequency (0.01–0.08 Hz) functional connectivity of SZ patients in the default mode network (DMN) (4), sensorimotor network (SMN) (5–7), salience network (SN) (8). Furthermore, based on earlier neurophysiological studies, Gohel and colleagues observed the resting-state functional connectivity of brain regions was differently across diverse frequency bands (9, 10). Moreover, previous studies had demonstrated that blood-oxygen-level-dependent imaging (BOLD) fMRI fluctuations >0.1 Hz had physiological significance (10, 11). While, most previous findings were observed within low frequency band functional networks (12). For example, Yu et al. (2014) researched frequency-specific alternation in SZ patients using the amplitude of low-frequency fluctuations (ALFF) (13). Zou et al. (2019) employed multi-frequency dynamic functional connectivity (dFC) to classify SZ patients from normal controls in low-frequency (14). Taken together, multiple frequency-dependent and higher-frequency brain network information would further provide the evidence to explore underlying etiology and mechanisms of SZ.

Prior neuroimaging researchers had found that distinct oscillator with specific properties and physiological functions could produce independent frequency bands. That was to say physiological signals of different frequency bands were generated by different functional regions of the brain (9). And physiological signals in the same brain network might be competing or cooperating with each other in different frequency bands (15). For instance, Zuo et al. (2010) found that the ALFF of basal ganglia network in slow-5 (0.01–0.027 Hz) were lower than that in slow-4 (0.027–0.073 Hz) frequency band (16).

Previous studies had focused on the analysis the static functional connectivity (sFC) of brain network in multiple-frequency of SZ. Recently, increasing evidence suggested that sFC was insufficient to explain the time-varying dynamic information interactions of brain (17–21), and dFC could offer much more nuanced characterization of dynamic brain function on a time scale (22, 23). The traditional and most widely used method for estimating dFC is the "sliding windows," which divide the scan session into different sub-interval or windows (24–26). Using a sliding-window analysis, Sakoglu et al. (2010) evaluated dynamic changes of brain network in SZ when task stimulus (26). In recent years, a growing body of research employed dFC analysis to explore changes in neural activity patterns of patients with SZ. Dynamic multiple-frequency brain network analysis may further provide more evidence to explore pathogeny of SZ.

Based on evidence from the research of patients with SZ and functional neuroimaging studies, we hypothesized that the brain network connections were frequency dependence in SZ patients, and these abnormal dynamic frequency-specific might associated with sensory motor, visual processing, auditory, salience networks. To investigate this issue, the current study will measure the frequency-specific variability of large-scale functional network in SZ subjects. Studies had shown that functional connectivity strength (FCS) metric was closely related to physiological measures such as glucose metabolism, oxygen and regional cerebral blood flow (27, 28). Therefore, FCS metric can be used as an indicator to examine hub connectivity in brain network. In our study, FCS analysis was employed to investigate altered patterns of SZ patients compared to healthy controls (HCs) at four frequency bands (slow-5: 0.01–0.027 Hz, slow-4: 0.027–0.073 Hz, slow-3: 0.073–0.198 Hz, slow-2: 0.198–0.25 Hz) (16). Altered frequency-dependent dFCS might provide more insight into the neurobiological processes of schizophrenia.

MATERIALS AND METHODS

Participants

Ninety-six patients with schizophrenia and 121 gender and age-matched healthy controls were obtained from our dataset, in which participants were recruited in the Clinical Hospital of Chengdu Brain Science Institute. All patients were diagnosed using the structured clinical interview for the DSM-IV axis I disorders-clinical version (SCID-I-CV), and they were taking the medication (e.g., antipsychotics). We excluded subjects with a history of brain damage, a history of substance-related illness, a major medical or neurological disease. The positive and negative symptom scale (PANSS) were employed to assess the severity of symptoms in patients with schizophrenia. All of data were included in our previous study (29), however, whole brain dFCS with frequency dependence were first evaluated in the dataset, differ from Dong's study. The Ethics Committee of the Clinical Hospital of Chengdu Brain Science Institute approved the study in accordance with the Helsinki Declaration. Written assents were obtained from all subjects.

Data Acquisition

All subjects underwent structural and functional MRI scan on a 3-T scanner (GE DISCOVERY MR 750, USA) with 32 channel head coil at the University of Electronic Science and Technology of China. Soft foam and earplugs were used to fix subjects head and reduce scanning noise during the scanning process. High-resolution T1-weighted images were acquired by a three-dimensional fast spoiled gradient-echo (T1-3D FSPGR) sequence [repetition time (TR) = 6.008 ms, flip angle (FA) =9, matrix = 256 × 256, field of view (FOV) = 256 × 256 mm2, slice thickness = 1 mm, no gap, 152 slices]. Resting state functional images were performed with a gradient-echo echo planar

sequence [TR =2,000 ms, echo time (TE) = 30 ms, FA =90, matrix = 64×64, FOV = 240×240 mm^2, slice thickness = 4 mm, gap = 0.4 mm, number of slice = 35, scanning time = 510 s (255 volumes)]. All subjects were instructed to relax with eyes closed and think of nothing in particular, then kept their head not move as little as possible and without falling asleep.

Data Preprocessing

Image preprocessing was conducted using NIT (http://www.neuro.uestc.edu.cn/NIT.html) software (30). Similar our previous research, normal data preprocessing steps were included in this study as following (31): 1) removing the first ten volumes; 2) slice timing; 3) realignment; 4) spatial normalization of the functional images was performed using 3D T1-based transformation. We coregistered individual 3D T1 images to functional images. The 3D T1 images were segmented and normalized to Montreal Neurologic Institute (MNI) space by a 12-parameter nonlinear transformation. 5) Filtering with a typical temporal bandpass, including slow-5 bandpass (0.001–0.027 Hz), slow-4 (0.027–0.073 Hz), slow-3 (0.073–0.198 Hz), and slow-2 (0.198–0.25 Hz) respectively. The global signal was not regressed out, as has been recently suggested in processing the schizophrenia functional data (32). In addition, we assessed framewise displacement (FD) of each subject using the following formula (33):

$$\mathrm{FD} = \frac{1}{M-1}\sum_{i=2}^{M}\sqrt{\left|\Delta t_{x_i}\right|^2+\left|\Delta t_{y_i}\right|^2+\left|\Delta t_{z_i}\right|^2+\left|\Delta d_{x_i}\right|^2+\left|\Delta d_{y_i}\right|^2+\left|\Delta d_{z_i}\right|^2},$$

where M is the length of time courses (M = 245 in this study), *xi*, *yi*, and *zi* are translations/rotations at i^{th} time point in the x, y, and z directions, $\Delta t_{x_i} = \Delta x_i - x_{i-1}$, similar for Δt_{y_i} and Δt_{z_i}; and Δt represents the FD rotations, Δd represents the FD translations. Then we also examined group-level head-motion (mean FD) difference between two group using the two-sample t-test. After the above processing, residual time-series were extracted for each voxel and used in subsequent analysis.

Dynamic Functional Connectivity Strength Analysis

Dynamic FCS of the whole brain voxels were assessed in four frequency bands respectively for each subject. The steps included following: 1) whole time series of one subject was divided into L sliding windows (24, 34), the interval of each window was 5TR (10 s). Since recent studies had shown that the minimum window length of dFC based on sliding window should not be less than $1/_{\mathrm{fmin}}$ (35), thus we selected the time window length of 100 s ($_{\mathrm{fmin}}$ =0.01 Hz). We were able to acquire 40 FCS maps for each subject. Next, within the ith time window, the FCS was calculated. 2) In order to exclude the interference of the non-gray matter signals and limit the calculation range, the gray matter template (the GM volume threshold was greater than 0.2) was extracted from the average structure gray matter map of all the subjects. 3) The time course after preprocessing of each voxel was extracted in the gray matter template, and the Pearson correlation coefficient between two voxels time signals was calculated. 4) Fisher's r-to-z transformation was performed. 5) For each voxel in the gray matter template of the brain (brain network node), calculated the sum of the weights (z values) of functional connectivity between this voxel and remaining voxels as nodal FCS. Meanwhile, to avoid the influence of weak correlation functional connections, we set the calculation range to the whole brain voxel with correlation coefficient r > 0.2 (36). 6) In order to better quantify dFCS, we defined the dynamic functional connectivity index of a voxel k as:

$$I_k = \frac{\sum_{t=1}^{n}(f_t - f_{static})^2}{n}$$

which came from the previous study (37), where *ft* was the FCS of the k at the time window *t*, t = 1,2,…n. According to Hui He et al. (37), this dynamic index was an overall metrics, which reflected an average dynamic change relative to its static FCS value. 7) We performed the calculation of this index under the 40 windows each participant and finally obtained the dFCS map. 8) Finally, dFCS maps were apatially smoothed (FWHM = 6 mm).

Firstly, two-sample t-test were used to access group difference in frequency bands respectively. In general, the resting state fMRI signal predominantly distributed in the low-frequency range (0.01–0.1 Hz). Thus, we used repeated measured ANOVA to measure the frequency main effect and interaction effect between frequency and group using SPM12 (www.fil.ion.ucl.ac.uk/spm) in slow-5 and slow-4 frequency bands. During post hoc analysis, we conducted two-sample t-test between groups, and partial t-test between frequency bands. Multiple correction was used for comparison results (false discovery rate correction, p<0.05). During statistical analysis, we controlled age, sex as covariates of no interest. Given previous studies about significant reduction in gray matter (GM) volume of SZ patients (38, 39), we also regressed GM volume during tests.

Correlation Analysis

In this study, partial correlations between the mean dFCS values of brain regions and the clinical symptoms of the schizophrenia patients were performed. During correlation analysis, to avoid compromising our result, age, gender, and gray matter volume were also considered as covariates to regress.

Validation Analysis

To keep the robustness of results, validation analysis was performed in randomly selected half of subjects in two groups respectively. Two-sample t-test were used to assess difference between groups in different frequency bands respectively, repeated measured ANOVA were employed to measure interaction effect in slow-5 and slow-4 bands. In addition, we calculated the correlation between drug equivalents of some patients and dFCS of the patients.

RESULTS

Demographic Characteristics and Clinical Symptoms

There were no overall significant differences between SZ patients and HCs in distribution of age, gender, mean head motion (two-sample t-test). Of note, only 88 patients had the duration of illness information, and 64 of them participated in the evaluation of PANSS. Detailed participant information was shown in (29).

The Difference of Dynamic Functional Connectivity Strength Across Frequency Bands in Schizophrenia

In four different frequency bands, the spatial pattern of mean dFCS was similar between SZ and HC groups. As shown in **Figure 1**, the brain network with higher dFCS in slow-5 band mainly included visual network (VN) (lingual gyrus and cuneus), basal ganglia network (BGN) (thalamus and caudate), SMN [postcentral gyrus and supplementary motor area (SMA)], SN [insula and anterior cingulate (ACC)]. Moreover, slow-4 and slow-3 frequency bands were found to be highly similar in schizophrenia patients. They also presented greater dFCS in VN, SN, SMN, the frontal and parietal lobule of frontoparietal network (FPN) (**Figure 1**).

Compared to HC, SZ patients showed increased dFCS in cerebellum, BGN (thalamus and caudate), DMN (angular gyrus), while decreased dFCS in auditory network (AN) (insula and superior temporal gyrus), SN (anterior insula and ACC), VN (lingual gyrus), SMN (SMA) in slow-5 band. In the slow-4, SZ patients relative to controls exhibited significantly higher dFCS in cerebellum, prefrontal network (PFN), BGN, and DMN. These brain networks major contained: cerebellum crus I and II, orbital middle frontal and orbital inferior frontal gyrus, thalamus and caudate, and bilateral angular gyrus. Nevertheless, in slow-4 frequency band, SZ patients presented lower dFCS in VN (lingual gyrus, cuneus, inferior occipital gyrus), SMN (postcentral gyrus and paracentral lobule), and SN (insula and right ACC). In slow-3 band, significantly increased dFCS were observed in SZ, within cerebellum crus, PFN (medial superior frontal gyrus, orbitofrontal cortex), BGN (middle temporal gyrus and left caudate), hippocampus, and fusiform gyrus. In addition, we also observed decreased dFCS in AN (rolandic operculum and superior temporal gyrus), VN (cuneus, calcarine, and middle temporal gyrus), SMN (precentral gyrus, SMA, and postcentral gyrus). Especially, we found decreased dFCS in thalamus and putamen of BGN in slow-3 (**Figure 2**, **Table 1**). However, there was no significant difference of schizophrenic subjects in slow-2 compared to healthy controls.

Main Effect of Frequency Factor in Slow-5 and Slow-4

Brain regions showed a significant main effect of frequency bands, and post hoc analysis indicated that dFCS of slow-5 band were greater than slow-4 band mainly in cerebellum VIII region, BGN, SMN, PFN, SN. The region of BGN includes hippocampus, parahippocampal gyrus, putamen, caudate, superior temporal pole. The SMN primarily contained left paracentral lobule, right precentral, SMA. FPN showed spatial patterns comprising the orbital superior frontal and orbital inferior frontal gyrus, superior frontal. The SN mainly encompassed ACC. However, the brain regions of slow-4 were higher than slow-5 band mainly distributed in VN, FPN, DMN, and cerebellum, which include calcarine, middle occipital and superior occipital gyrus, cuneus, lingual gyrus, left inferior parietal, precuneus, frontal cortex, angular gyrus, cerebellum crus I and II (**Figure 3**, **Table 2**). The main effect of group identified brain regions was similar to those reported in previous analysis using two-sample *t*-test.

Frequency and Group Interaction Effects

Remarkable interactions between group (SZ and HC) and frequency (slow-5 and slow-4) were found in left calcarine, the bilateral inferior orbitofrontal cortex, and the anterior cingulum ($p < 0.005$, uncorrected; **Figure 4**, **Table 3**). Further post-hoc tests indicated that within SZ group, the dFCS in left calcarine of

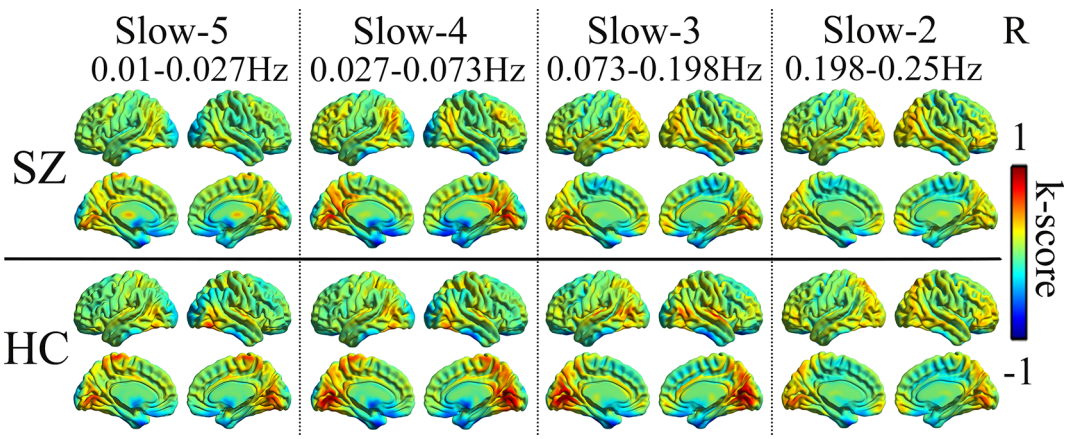

FIGURE 1 | Mean dFCS maps of the SZ and HC in frequency bands from slow-5 to slow-2. dFCS, dynamic functional connectivity strength; SZ, patients with schizophrenia; HC, healthy controls.

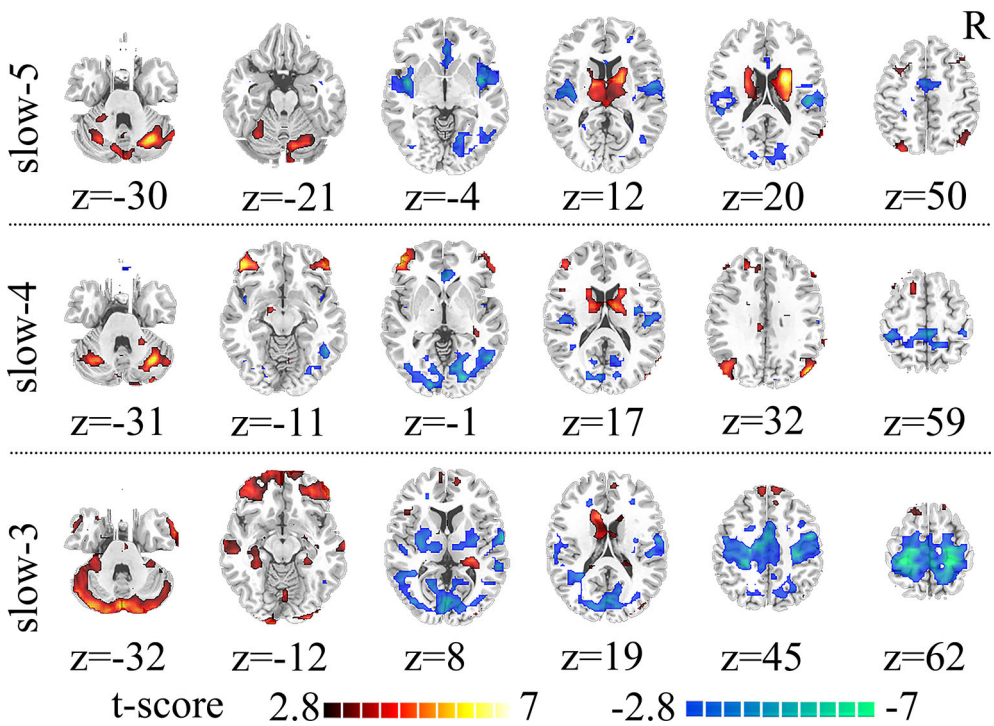

FIGURE 2 | Significant differences in dFCS across frequency bands between the SZ and HC groups. The results were obtained by two-sample t-test. Hot color represents the SZ group had increased dFCS compared with HC group; cold color represents the opposite. Statistical significance level is corrected for multiple comparisons using FDR with ($p<0.05$, voxels>23). dFCS, dynamic functional connectivity strength; SZ, patients with schizophrenia; HC, healthy controls; FDR, false discovery rate correction.

slow-4 was significantly lower than slow-5, and in slow-4, the dFCS of SZ group was marginally significantly reduced compared with HCs ($p = 0.066$, $t = -1.849$) (**Figure 4A**). Moreover, in the bilateral inferior orbitofrontal cortex, post-hoc two-sample t-test both showed that compared with slow-5, significantly increased dFCS were observed in slow-4 of the SZ group, and the dFCS of patient group was significantly higher than the HC group at slow-4 band (**Figures 4B, C**). In addition, within SZ group, we also found that significant increased dFCS of the anterior cingulum in slow-4. Also, in the slow-5 frequency band, the dFCS of SZ was marginally significantly lower than HC group ($p = 0.093$, $t = -1.687$) (**Figure 4D**).

Correlation Between the Dynamic Functional Connectivity Strength With Clinical Symptoms

Firstly, we extracted dFCS values of patients group from significantly interaction effects, their correlation analysis with clinical symptoms showed decreased dFCS of left calcarine was negatively correlated with duration of illness in slow-4 band ($p = 0.036$, $r = -0.227$) (**Figure 6**). Then in four different frequency bands, correlation between brain regions of significant group differences and clinical symptoms revealed that decreased dFCS of left insula was negatively correlated with the PANSS total score ($p = 0.022$, $r = -0.292$) in slow-5 band (**Figure 5A**). And the dFCS of right insula was negatively correlated with the PANSS negative score ($p = 0.037$, $r = -0.268$) (**Figure 5B**) and total score ($p = 0.03$, $r = -0.278$) (**Figure 5C**). Moreover, positive correlations between the increased dFCS of left thalamus and PANSS positive score ($p = 0.014$, $r = 0.315$) (**Figure 5D**) and total score ($p = 0.02$, $r = 0.296$) (**Figure 5E**) were observed in slow-5. Secondly, in slow-4 frequency band of SZ group, a positive correlation between the dFCS of the left orbital inferior frontal gyrus and PANSS negative score ($p = 0.006$, $r = 0.345$) (**Figure 5F**) was discovered, and the decreased dFCS of the left paracentral lobule was negatively correlated with PANSS total score ($p = 0.024$, $r = -0.289$) (**Figure 5G**).

We found similar results through validation analysis.

DISCUSSION

Through dFCS analysis, the current study investigated the difference of frequency-dependent whole brain dynamic functional connection in schizophrenia. Consistent with our hypothesis, significantly altered dFCS of SZ mainly distributed in cerebellum, VN, AN, SN, PFN, SMN, DMN, and BGN in different frequency bands. Interesting, compared to HC group, the thalamic subregion of SZ group exhibited enhanced dynamic FCS in slow-5 and slow-4, while reduced in slow-3. Moreover, in slow-5 and slow-4, significant frequency-by-group interaction effect were observed in the left calcarine, the bilateral inferior

TABLE 1 | Brain regions with significant differences in dynamic functional connectivity strength (dFCS) across frequency bands (slow-5 to slow-2) based on the two-sample t-test of the results between the patients with schizophrenia (SZ) and health control (HC) groups.

Brain regions (AAL)	Cluster size (voxels)[a]	Peak coordinates (MNI)			T value
		x	y	z	
Slow-5: SZ>HC					
Cerebelum_Crus1_R	1,206	30	−69	−30	7.160
Cerebelum_Crus1_L					
Cerebelum_Crus2_L/R					
Caudate_R	447	17	2	18	6.547
Thalamus_L/R					
Caudate_L					
Angular_R	138	63	−60	21	4.620
Slow-5: SZ<HC					
Insula_R	458	37	0	−5	−6.104
Temporal_Sup_R					
Temporal_Sup_L	397	−42	0	−9	−6.320
Insula_L					
Lingual_R	296	15	−69	−3	−5.070
Cuneus_L/R					
Supp_Motor_Area_R	159	4	−2	50	−4.333
Supp_Motor_Area_L					
Cingulum_Ant_R	73	3	33	−3	−4.770
Cingulum_Ant_L					
Slow-4: SZ>HC					
Cerebelum_Crus1_R	272	30	−72	−27	5.920
Cerebelum_Crus1_L	144	−32	−64	−30	4.506
Frontal_Inf_Orb_L	367	−42	42	−15	5.580
Frontal_Inf_Tri_L					
Frontal_Mid_Orb_L					
Frontal_Inf_Orb_R	171	51	42	−9	5.090
Frontal_Mid_Orb_R					
Caudate_R	244	19	−1	19	4.262
Caudate_L					
Thalamus_L/R					
Angular_R	190	51	−78	27	5.560
Angular_L					
Slow-4: SZ<HC					
Rolandic_Oper_R	217	58	−14	20	−4.380
Insula_R					
Calcarine_R	873	18	−86	6	−5.530
Calcarine_L					
Lingual_L/R					
Occipital_Inf_L/R					
Cuneus_L/R					
Rolandic_Oper_L	101	−42	3	−12	−4.440
Insula_L					
Cingulum_Ant_R	23	3	27	0	−4.490
Postcentral_R	596	9	−48	63	−4.930
Postcentral_L					
Paracentral_Lobule_L/R					
Slow-3: SZ>HC					
Cerebelum_Crus1_L	3,672	−41	−78	−28	5.260
Cerebelum_Crus1_R					
Temporal_Mid_L/R					
Cerebelum_Crus2_L/R					
Temporal_Inf_L/R					
Frontal_Inf_Orb_L/R					
Frontal_Mid_Orb_L/R					
Hippocampus_L/R					
Fusiform_L/R					
Caudate_L					
Frontal_Sup_Medial_L	299	15	18	69	4.950
Frontal_Sup_Medial_R					
Slow-3: SZ<HC					
Postrcentral_R	4,834	24	−33	60	−7.830
Postrcentral_L					
Temporal_Mid_L/R					
Precentral_L/R					
Calcarine_L/R					
Cuneus_L/R					
Supp_Motor_Area_L/R					
Temporal_Sup_L/R					
Rolandic_Oper_R					
Thalamus_R					
Putamen_R					
Putamen_L	204	−30	−12	3	−5.140
Thalamus_L					

MNI, Montreal Neurological Institute; L, left; R, right.

[a]*The cluster size represents the number of voxels within the cluster.*

orbitofrontal gyrus and ACC. Furthermore, the altered dFCS of insula, thalamus, calcarine cortex, orbitofrontal gyrus, and paracentral lobule were partial correlated with clinical symptoms of SZ patients in slow-5 and slow-4 bands respectively. Together, these results demonstrate that altered dFCS in the SZ patients distribute throughout the whole brain, and the abnormal dynamic changes is frequency dependent. These findings may offer more evidence to explore the underlying pathological mechanism of SZ.

Altered Dynamic Functional Connectivity Strength Across Four Frequency Bands in Schizophrenia

Previous studies suggested that decreased functional connectivity (FC) of somatosensory and visual network were a potential mechanism for self-disorder in SZ (40). Kraepelin and Bleuler firstly found sensorimotor processing dysfunction and integration defect of multiple sensory functions in patients with SZ, and they put these as a possible psychopathological mechanism in SZ (41). Moreover, the lower FC of visual network in multiple frequency bands had been reported in several researches (13, 42, 43). These researches indicate disturbed abnormally integration in perception-motor processing of SZ. In the current study, the reduced dFCS of the somatosensory and visual network in slow-5, slow-4, and slow-3 may make it difficult for patients to perceive their own state. The significantly negative correlation between reduced dFCS of insula, paracentral lobule, and clinical symptoms suggest that abnormal processing of perceptional information in SZ helps us to understand the pathological mechanisms involved self-disorder. Moreover, we also found increased dFCS of cerebellum and BGN in different frequency bands. Cerebellum and BGN were considered as a partially functional and strongly connected nervous system (44), a functional abnormality in one network will have the same

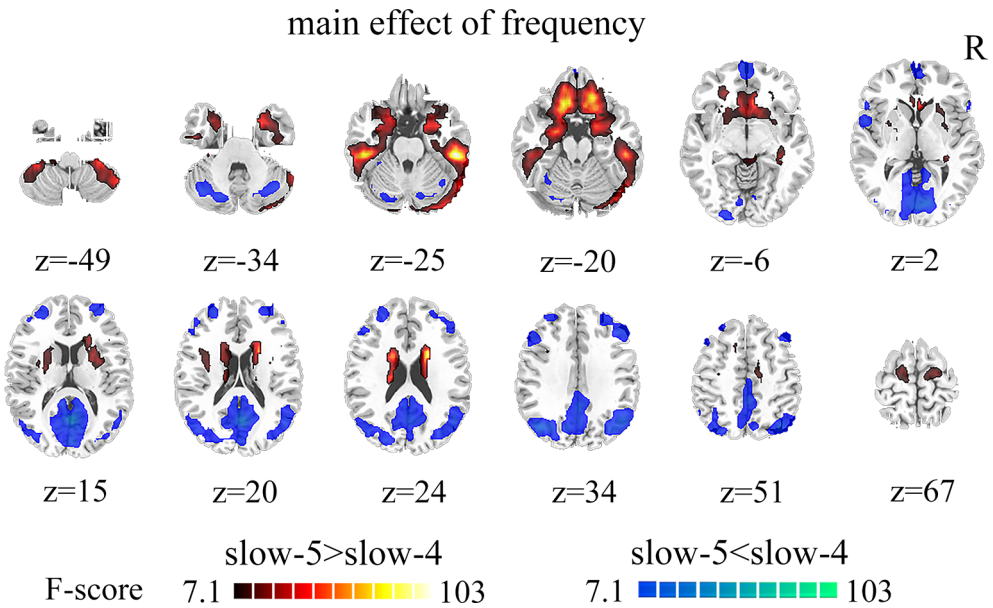

FIGURE 3 | The main effect of frequency band (slow-5, slow-4) across groups on dFCS. The results were obtained by two-way ANOVA (FDR corrected, $p < 0.05$, voxels > 23). Hot color represents the slow-5 had increased dFCS compared with slow-4; cold color represents the opposite. dFCS, dynamic functional connectivity strength; ANOVA, analysis of variance; FDR, false discovery rate correction.

impact on another neural network (45, 46). Therefore, abnormality in cerebellar function in patients with SZ may be strongly correlated with abnormality in the BGN. The current findings reveal that abnormal cerebellar and BGN functional connections may play a crucial role in cerebellar-BGN-cortical network circuits and may lead to dysfunctional interaction between the subcortical network and the cerebral cortex network in patients with SZ. Especially, the abnormal functional integration of this loop is modulated by frequency band.

Interestingly, we found the dFCS of subregion thalamus presented an imbalance in different frequency bands of SZ subjects. The thalamus is a crucial node for brain physiology implicating in processing of sensorial inputs and emotion processing (47, 48). The BGN received incoming signals from different regions of the brain and projected them back through the thalamus to the cortex. Recently, altered thalamus and cortico-thalamic dysconnection had been revealed in patients with SZ (49–51). Our study extended previous findings to higher frequency band, interestingly, the different thalamic subregion of schizophrenic patients exhibited enhanced dynamic FCS in slow-5 and slow-4, while reduced in slow-3. Besides, we also found that the dFCS of the left THA was positively correlated with PANSS positive/total score in slow-5 of SZ subjects. This imbalance suggests that the dynamic abnormality of THA in patients with SZ may be modulated by frequency band, and thalamus showed competitive signals in different frequency bands, which may be related abnormal affective perception and higher cognitive processing in patients with SZ. In the future, the function of thalamic subregion in different frequency bands should be explore.

Frequency Specific Changes in Dynamic Functional Connectivity Strength Schizophrenia (Slow-5, Slow-4)

In the main effect of the frequency band (slow-5 and slow-4), we found that the cerebellum, BGN, SMN, PFN, and SN had higher dFCS in slow-5, while VN, FPN, DMN had stronger dFCS in slow-5. The cerebellum plays an essential role in the functional interaction between the cortex and the subcortex. The dorsolateral prefrontal lobe (DLPFC) and posterior parietal lobes are the core nodes of the frontoparietal network (FPN). Some neuroimaging studies found that cerebellum and FPN are involved in advanced cognitive information processing (45, 52). Our results indicate that the process of high-frequency information processing in the cerebellum and FPN may enhance the efficiency of advanced cognitive processing. During the processing of cognitive information, the cerebellum, as an unsupervised regulatory brain region, no need the feedback of the higher network. Conversely, the striatum system, particularly the caudate nucleus and frontal cortex, conduct some supervised neuro modulation of speech, memory, mood, and behavior (53–55). Moreover, higher low frequency signals may improve the stability of supervisory regulation during the processing of information and high frequency signals. Therefore, in future researches of schizophrenia, we should consider the frequency band information.

In the visual cortex, orbitofrontal cortex (OFC) and ACC, frequency-by-group interactions between SZ patients and HC controls were observed in our study. The PFN was considered crucial for higher cognitive functions of the brain, such as working memory, control of goal-directed, integration, and coordination of complex cognitive activities (56), OFC and

TABLE 2 | Brain regions with significant main effect of frequency band (slow-5, slow-4) differences in dynamic functional connectivity strength (dFCS).

Brain regions	Cluster size (voxels)[a]	Peak coordinates (MNI)			F-value
(AAL)		x	y	z	
Slow-5<Slow-4					
Calcarine_R	3,869	3	−66	15	53.080
Calcarine_L					
Precuneus_L/R					
Angular_L/R					
Occipital_Mid_L/R					
Cuneus_L/R					
Lingual_L/R					
Cerebelum_Crus1_L/R					
Occipital_Sup_L/R					
Cerebelum_Crus2_L/R					
Parietal_Inf_L					
Frontal_Mid_R	503	42	24	42	25.040
Frontal_Sup_R					
Frontal_Inf_Tri_R					
Frontal_Mid_L	353	−45	24	39	26.180
Frontal_Inf_Tri_L					
Slow-5>Slow-4					
Temporal_Inf_R	2,448	51	−30	−27	103.670
Temporal_Inf_L					
Putamen_L/R					
Cerebelum_8_L/R					
ParaHippocampal_L/R					
Frontal_Sup_Orb_L/R					
Hippocampus_L/R					
Frontal_Inf_Orb_L/R					
Caudate_L/R					
Temporal_Pole_Sup_L/R					
Cingulum_Ant_L					
Supp_Motor_Area_L	173	−15	−12	63	29.600
Paracentral_Lobule_L					
Frontal_Sup_L					
Frontal_Sup_R	127	18	−8	67	18.460
Supp_Motor_Area_R					
Precentral_R					

MNI, Montreal Neurological Institute; L, left; R, right.

[a]*The cluster size represents the number of voxels within the cluster.*

ACC were considered the part of PFN (57). The OFC is known to be closely related to emotional expression, decision making, hedonic experience, and plays a key role in tasks requiring response inhibition (58–60). The ACC is the part of medial PFN, and is critical for executive attention, regulation of motivational and emotional behavior (61). Abnormalities of the OFC and ACC in schizophrenia patients have been reported in several studies (62–64), and these impairments appear to be with the core disease pathophysiology (65). Consistent with previous studies, we also found abnormalities of OFC and ACC in SZ in current study, interestingly, in our study, these dynamic changes were modulated by frequency band. Within SZ group, the dFCS in OFC and ACC of slow-4 was both significantly greater than slow-5 band. The two brain regions of patients have abnormal dynamic characteristics of reduced low frequency signal and increased high frequency signal in their respective frequency bands, which may affect the failure of executive attention, regulation of motivational and emotional behavior, further affect organization and control of goal-directed thought in PFN.

Moreover, compared with HC controls, in slow-5 of the current study, the dFCS of schizophrenic subjects ACC was reduced, while increased dFCS of the OFC in slow-4. A recent study suggested that in brain functional networks, physiological signals in different frequency bands could compete or interacted with each other in the same functional network (66). For the cognitive function of PFN, researchers suggested that lateral PFC was responsible for selection, monitoring and manipulation, medial PFC updated tasks, and OFC conferred social and emotional significance to tasks (61). Thus, our results suggest OFC and ACC interconnect in different frequency bands, their dysfunction may lead to the regulation disorder of cognition and emotions in SZ patients, further some abnormal behavioral.

Previous studies suggested that reduced activation region in the visual magnocellular pathway was related to the deficits in motion processing in schizophrenia (67). Converging evidence suggests that the high frequency visual information collection and transmission may help the bottom-up information integration of the brain. In this study, we observed interaction effect in visual network and the significant negative relationships

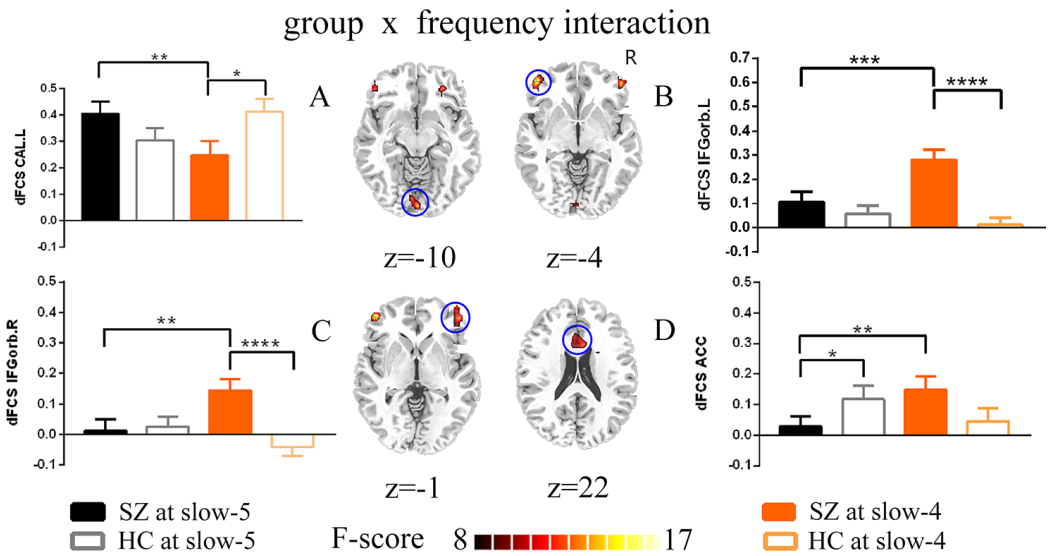

FIGURE 4 | The interaction between the group and frequency band (slow-5 and slow-4) on dFCS. The results were obtained by two-way ANOVA and post-hoc test (p<0.005, uncorrected). **(A–D)** separately represent significant group *frequency interactions and post-hoc test of the left calcarine, the left inferior orbitofrontal cortex, the right inferior orbitofrontal cortex and the anterior cingulum. The data were expressed as the mean value and standard error. *p<0.1, **p<0.05, ***p<0.005, ****p<0.0001. ANOVA, analysis of variance; dFCS, dynamic functional connectivity strength; SZ, patients with schizophrenia; HC, healthy controls; CAL.L, the left calcarine; IFGorb.L, the left inferior orbitofrontal cortex; IFGorb.R, the right inferior orbitofrontal cortex; ACC, the anterior cingulum.

TABLE 3 | Significant interaction effects between the frequency band (slow-4 and slow-5) and group by a two-way ANOVA and a post-hoc test.

Brain regions (AAL)	Cluster size (voxels)	Peak coordinates (MNI)			F value0
		x	y	z	
Calcarine_L	28	0	−91	−10	15.330
Frontal_Inf_Orb_L	31	−49	46	−4	14.200
Frontal_Inf_Orb_R	40	46	48	−1	16.180
Cingulum_Ant	31	3	29	20	14.440

MNI, Montreal Neurological Institute; L, left; R, right.

between dFCS in the left calcarine and duration disease (**Figure 6**). We also found that the dFCS of SZ visual cortex was reduced in slow-4, while the opposite in HC group. Namely, our finding suggest that the reduction of high-frequency dynamic information in primary visual cortex of SZ may affect the collection and transmission of primary information, and may further affect its advanced cognitive function.

LIMITATIONS

Some limitations should be taken into account in the current study. Firstly, of note, most of patients with schizophrenia were taking the medication (e.g., antipsychotics). Although we assessed the correlation between drug equivalents of some patients and dFCS of these patients, the results showed no significant correlation, we could not rule out whether the antipsychotic medications has an effect on the observed findings. Thus, in future study, we should validate our findings in first-episode schizophrenic patients. Secondly, although we had regressed 12 head motion parameters, it was still possible that some of the results were affected by motion-induced artifact. Finally, BOLD fMRI signal in high frequency (>0.1 Hz) usually considered physiological noises (respiration and cardiac signal) and are regressed, however, recent studies had confirmed that high-frequency information in resting-state fMRI signal may provide useful information in clinical studies (68, 69). In our study, we were lacked of collecting the physiological signals (respiration and cardiac signal) of subjects, so we couldn't use the general linear model (GLM) to remove the physiological signal noise, there might be some influence. In future research, we will collect physiological signal and conduct further analysis.

CONCLUSIONS

In this study, we found the altered dFCS within the brain of SZ patients was sensitive to specificity of frequency band. Significantly abnormal dFCS of schizophrenia mainly within cerebellum, SN, FPN, AN, SMN, VN, BGN, and PFN. Specially, the dFCS of subregion thalamus presented an imbalance in different frequency bands of SZ subjects, and the dFCS of calcarine cortex, insula, THA, OFC, PCL were associated with clinical symptoms, implying that the symptoms were related to abnormally dFCS at specific frequency bands. Moreover, in slow-5 and slow-4, significant frequency-by-group interaction effects were observed in the

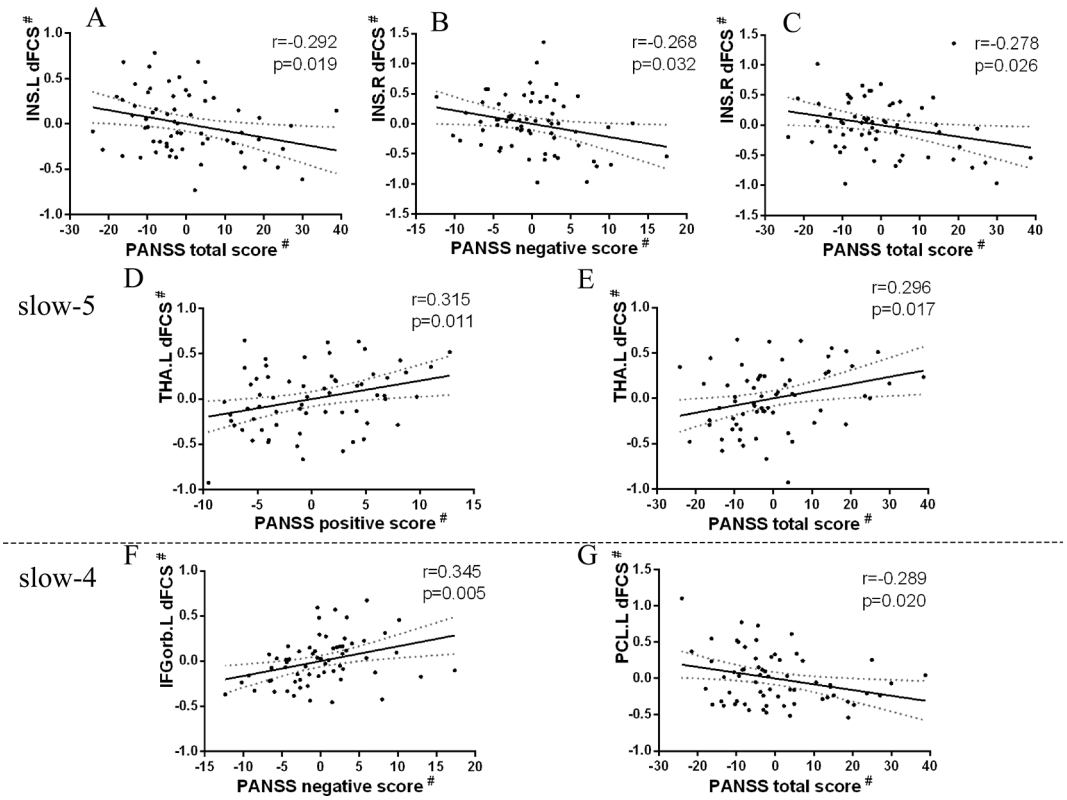

FIGURE 5 | Relationship between regions showing significant two-sample t-test results and clinical scale of symptoms in patients with SZ ($p < 0.05$). Partial correlations were calculated over the data after regressing covariate (age, sex, GM). # represents the residuals after regression of age, sex, and GM volumes using a general linear model. **(A)** Significant negative correlation between the left insula and PANSS total score in slow-5 band. **(B)** Significant negative correlation between the right insula and PANSS negative score in slow-5 band. **(C)** Significant negative correlation between the right insula and PANSS total score in slow-5 band. **(D)** Significant positive correlation between the left thalamus and PANSS positive score in slow-5 band. **(E)** Significant positive correlation between the left thalamus and PANSS total score in slow-5 band. **(F)** Significant positive correlation between the left inferior orbitofrontal cortex and PANSS negative score in slow-4 band. **(G)** Significant negative correlation between the left paracentral lobule and PANSS total score in slow-4 band. SZ, patients with schizophrenia; GM, the volume of grey matter; dFCS, dynamic functional connectivity strength; PANSS, the positive and negative symptom scale; INS.L, the left insula; INS.R, the right insula; THA.L, the left thalamus; IFGorb.L, the left inferior orbitofrontal cortex; PCL.L, the left paracentral lobule.

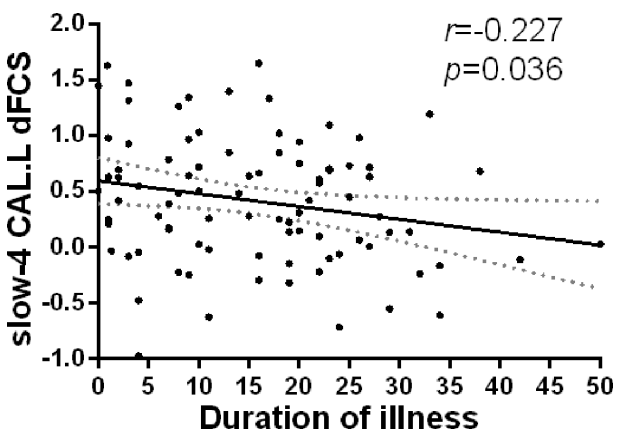

FIGURE 6 | Relationship between regions showing significant interaction effect results and duration of illness in patients with SZ ($p<0.05$). Partial correlations were calculated over the data after regressing covariate (age, sex, GM). SZ, patients with schizophrenia; GM, the volume of grey matter; dFCS, dynamic functional connectivity strength; CAL.L, the left calcarine.

left calcarine, the bilateral inferior orbitofrontal gyrus and ACC. Our results may provide potential implications for exploring the neuropathological mechanism of schizophrenia.

DATA AVAILABILITY STATEMENT

The datasets generated for this study are available on request to the corresponding author.

ETHICS STATEMENT

The studies involving human participants were reviewed and approved by the Ethics Committee of the Clinical Hospital of Chengdu Brain Science Institute. The patients/participants provided their written informed consent to participate in this study.

AUTHOR CONTRIBUTIONS

DY, JL, CL, and HHe designed and checked the study. HHu, ZH, and YL analyzed the imaging data. YL wrote the first manuscript. YL, HHe, MD, HW, GY, DY, JL, and CL participated in the conception, drafting, and revision of the article. All authors contributed to and gave final approval of the manuscript.

FUNDING

This work was partly supported by a grant from the National Key R&D Program of China (2018YFA0701400) and grants from the National Natural Science Foundation of China (grant numbers: 61933003, 61761166001, 81471638, 81571759).

REFERENCES

1. Dong D, Wang Y, Chang X, Luo C, Yao D. Dysfunction of large-scale brain networks in schizophrenia: a meta-analysis of resting-state functional connectivity. *Schizophrenia Bull* (2018) 44:168–81. doi: 10.1093/schbul/sbx034
2. Lynall ME, Bassett DS, Kerwin R, McKenna PJ, Kitzbichler M, Muller U, et al. Functional connectivity and brain networks in schizophrenia. *J Neurosci* (2010) 30:9477–87. doi: 10.1523/Jneurosci.0333-10.2010
3. Rubinov M, Bullmore E. Schizophrenia and abnormal brain network hubs. *Dialogues Clin Neurosci* (2013) 15:339–49.
4. Bluhm RL, Miller J, Lanius RA, Osuch EA, Boksman K, Neufeld RW, et al. Spontaneous low-frequency fluctuations in the BOLD signal in schizophrenic patients: anomalies in the default network. *Schizophrenia Bull* (2007) 33:1004–12. doi: 10.1093/schbul/sbm052
5. Chai XJ, Whitfield-Gabrieli S, Shinn AK, Gabrieli JD, Nieto Castanon A, McCarthy JM, et al. Abnormal medial prefrontal cortex resting-state connectivity in bipolar disorder and schizophrenia. *Neuropsychopharmacol: Official Public Am College Neuropsychopharmacol* (2011) 36:2009–17. doi: 10.1038/npp.2011.88
6. Zhou Y, Liang M, Jiang TZ, Tian LX, Liu Y, Liu ZN, et al. Functional dysconnectivity of the dorsolateral prefrontal cortex in first-episode schizophrenia using resting-state fMRI. *Neurosci Lett* (2007) 417:297–302. doi: 10.1016/j.neulet.2007.02.081
7. Javitt DC. Sensory processing in schizophrenia: neither simple nor intact. *Schizophrenia Bull* (2009) 35:1059–64. doi: 10.1093/schbul/sbp110
8. Dong D, Wang Y, Chang X, Luo C, Yao D. Dysfunction of large-scale brain networks in schizophrenia: a meta-analysis of resting-state functional connectivity. *Schizophrenia Bull* (2018) 44:168–81. doi: 10.1093/schbul/sbx034
9. Buzsaki G, Draguhn A. Neuronal oscillations in cortical networks. *Science* (2004) 304:1926–9. doi: 10.1126/science.1099745
10. Gohel SR, Biswal BB. Functional integration between brain regions at rest occurs in multiple-frequency bands. *Brain Connectivity* (2015) 5:23–34. doi: 10.1089/brain.2013.0210
11. Cordes D, Haughton VM, Arfanakis K, Carew JD, Turski PA, Moritz CH, et al. Frequencies contributing to functional connectivity in the cerebral cortex in " Resting-state " data. *AJNR Am J Neuroradiol* (2001) 22:1326–33.
12. Guo WB, Liu F, Xue ZM, Xu XJ, Wu RR, Ma CQ, et al. Alterations of the amplitude of low-frequency fluctuations in treatment-resistant and treatment-response depression: a resting-state fMRI study. *Progress Neuro-psychopharmacol Biological Psychiatry* (2012) 37:153–60. doi:10.1016/j.pnpbp.2012.01.011
13. Yu R, Chien YL, Wang HL, Liu CM, Liu CC, Hwang TJ, et al. Frequency-specific alternations in the amplitude of low-frequency fluctuations in schizophrenia. *Hum Brain Mapp* (2014) 35:627–37. doi: 10.1002/hbm.22203
14. Zou H, Yang J. Multi-frequency dynamic weighted functional connectivity networks for schizophrenia diagnosis. *Appl Magnet Resonance* (2019) 50:847–59.
15. Engel AK, Fries P, Singer W. Dynamic predictions: oscillations and synchrony in top-down processing. *Nat Rev Neurosci* (2001) 2:704–16.doi: 10.1038/35094565
16. Zuo XN, Di Martino A, Kelly C, Shehzad ZE, Gee DG, Klein DF, et al. The oscillating brain: complex and reliable. *Neuroimage* (2010) 49:1432–45. doi: 10.1016/j.neuroimage.2009.09.037
17. Betzel RF, Fukushima M, He Y, Zuo XN, Sporns O. Dynamic fluctuations coincide with periods of high and low modularity in resting-state functional brain networks. *Neuroimage* (2016) 127:287–97. doi: 10.1016/j.neuroimage.2015.12.001
18. Chang C, Glover GH. Time–frequency dynamics of resting-state brain connectivity measured with fMRI. *NeuroImage* (2010) 50:81–98. doi: 10.1016/j.neuroimage.2009.12.011
19. Hutchison RM, Womelsdorf T, Allen EA, Bandettini PA, Calhoun VD, Corbetta M, et al. Dynamic functional connectivity: promise, issues, and interpretations. *NeuroImage* (2013) 80:360–78. doi: 10.1016/j.neuroimage.2013.05.079
20. Calhoun VD, Miller R, Pearlson G, Adali T. The chronnectome: time-varying connectivity networks as the next frontier in fMRI data discovery. *Neuron* (2014) 84:262–74. doi: 10.1016/j.neuron.2014.10.015
21. Kopell NJ, Gritton HJ, Whittington MA, Kramer MA. Beyond the connectome: the dynome. *Neuron* (2014) 83:1319–28. doi: 10.1016/j.neuron.2014.08.016
22. Nomi JS, Farrant K, Damaraju E, Rachakonda S, Calhoun VD, Uddin LQ. Dynamic functional network connectivity reveals unique and overlapping profiles of insula subdivisions. *Hum Brain Mapp* (2016) 37:1770–87. doi: 10.1002/hbm.23135
23. Liu F, Wang Y, Li M, Wang W, Li R, Zhang Z, et al. Dynamic functional network connectivity in idiopathic generalized epilepsy with generalized tonic-clonic seizure. *Hum Brain Mapp* (2017) 38:957–73. doi:10.1002/hbm.23430
24. Allen EA, Damaraju E, Plis SM, Erhardt EB, Eichele T, Calhoun VD. Tracking whole-brain connectivity dynamics in the resting state. *Cerebral Cortex* (2014) 24:663–76. doi: 10.1093/cercor/bhs352
25. Damaraju E, Allen EA, Belger A, Ford JM, McEwen S, Mathalon DH, et al. Dynamic functional connectivity analysis reveals transient states of dysconnectivity in schizophrenia. *Neuroimage-Clin* (2014) 5:298–308. doi: 10.1016/j.nicl.2014.07.003
26. Sakoglu U, Pearlson GD, Kiehl KA, Wang YM, Michael AM, Calhoun VD. A method for evaluating dynamic functional network connectivity and task-

modulation: application to schizophrenia. *Magn Reson Mater Phy* (2010) 23:351–66. doi: 10.1007/s10334-010-0197-8
27. Yang M, He H, Duan MJ, Chen X, Chang X, Lai YX, et al. The effects of music intervention on functional connectivity strength of the brain in schizophrenia. *Neural Plasticity* (2018). doi: 10.1155/2018/2821832
28. Liang X, Zou Q, He Y, Yang Y. Coupling of functional connectivity and regional cerebral blood flow reveals a physiological basis for network hubs of the human brain. *Proc Natl Acad Sci U. S. A.* (2013) 110:1929–34. doi: 10.1073/pnas.1214900110
29. Dong D, Duan M, Wang Y, Zhang X, Jia X, Li Y, et al. Reconfiguration of dynamic functional connectivity in sensory and perceptual system in Schizophrenia. *Cereb Cortex* (2018) 29:3577–89. doi: 10.1093/cercor/bhy232
30. Dong L, Luo C, Liu X, Jiang S, Li F, Feng H, et al. Neuroscience information toolbox: an open source toolbox for EEG-fMRI multimodal fusion analysis. *Front Neuroinform* (2018) 12:56. doi: 10.3389/fninf.2018.00056
31. Jiang Y, Xia M, Li X, Tang Y, Li C, Huang H, et al. Insular changes induced by electroconvulsive therapy response to symptom improvements in schizophrenia. *Progress Neuro-psychopharmacol Biological Psychiatry* (2019) 89:254–62. doi: 10.1016/j.pnpbp.2018.09.009
32. Yang GJ, Murray JD, Repovs G, Cole MW, Savic A, Glasser MF, et al. Altered global brain signal in schizophrenia. *Proc Natl Acad Sci U. S. A.* (2014) 111:7438–43. doi: 10.1073/pnas.1405289111
33. Power JD, Barnes KA, Snyder AZ, Schlaggar BL, Petersen SE. Spurious but systematic correlations in functional connectivity MRI networks arise from subject motion. *Neuroimage* (2012)59(3):2142–54. doi: 10.1016/j.neuroimage.2011.10.018
34. Shirer WR, Ryali S, Rykhlevskaia E, Menon V, Greicius MD. Decoding subject-driven cognitive states with whole-brain connectivity patterns. *Cerebral Cortex* (2012) 22:158–65. doi: 10.1016/j.neuroimage.2012.01.069
35. Leonardi N, Van De Ville D. On spurious and real fluctuations of dynamic functional connectivity during rest (vol 104, pg 430, 2015). *NeuroImage* (2015) 104:464–5. doi: 10.1093/cercor/bhr099
36. Wang L, Xia M, Li K, Zeng Y, Su Y, Dai W, et al. The effects of antidepressant treatment on resting-state functional brain networks in patients with major depressive disorder. *Hum Brain Mapping* (2015) 36:768–78. doi: 10.1016/j.neuroimage.2014.10.045
37. He H, Luo C, Luo Y, Duan M, Yi Q, Biswal BB, et al. Reduction in gray matter of cerebellum in schizophrenia and its influence on static and dynamic connectivity. *Hum Brain Mapp* (2019) 40:517–28. doi: 10.1002/hbm.22663
38. Zipursky RB, Lim KO, Sullivan EV, Brown BW, Pfefferbaum A. widespread cerebral gray-matter volume deficits in schizophrenia. *Arch Gen Psychiat* (1992) 49:195–205. doi: 10.1002/hbm.24391
39. Hulshoff HE, Schnack HG, Bertens MGBC, van Haren NEM, van der Tweel I, Staal WG, et al. Volume changes in gray matter in patients with schizophrenia. *Am J Psychiat* (2002) 159:244–50.
40. Chen X, Duan M, Xie Q, Lai Y, Dong L, Cao W, et al. Functional disconnection between the visual cortex and the sensorimotor cortex suggests a potential mechanism for self-disorder in schizophrenia. *Schizophr Res* (2015) 166:151–7. doi: 10.1176/appi.ajp.159.2.244
41. Bleuler M, Bleuler R. Dementia praecox oder die Gruppe der Schizophrenien: eugen bleuler. *Br J Psychiatry : J Ment Sci* (1986) 149:661–2. doi: 10.1016/j.schres.2015.06.014
42. Hoptman MJ, Zuo XN, Butler PD, Javitt DC, D'Angelo D, Mauro CJ, et al. Amplitude of low-frequency oscillations in schizophrenia: a resting state fMRI study. *Schizophr Res* (2010) 117:13–20. doi: 10.1192/bjp.149.5.661
43. Yang M, He H, Duan M, Chen X, Chang X, Lai Y, et al. the effects of music intervention on functional connectivity strength of the brain in Schizophrenia. *Neural Plasticity* (2018) 2018:2821832. doi: 10.1016/j.schres.2009.09.030
44. Akkal D, Dum RP, Strick PL. Supplementary motor area and presupplementary motor area: targets of basal ganglia and cerebellar output. *J Neurosci* (2007) 27:10659–73. doi: 10.1155/2018/2821832
45. Bostan AC, Dum RP, Strick PL. Cerebellar networks with the cerebral cortex and basal ganglia. *Trends Cogn Sci* (2013) 17:241–54. doi: 10.1523/Jneurosci.3134-07.2007
46. O'Doherty JP, Dayan P, Friston KJ, Critchley H, Dolan RJ. Temporal difference models and reward-related learning in the human brain. *Neuron* (2003) 38:329–37. doi: 10.1016/j.tics.2013.03.003
47. Pergola G, Selvaggi P, Trizio S, Bertolino A, Blasi G. The role of the thalamus in schizophrenia from a neuroimaging perspective. *Neurosci Biobehav Rev* (2015) 54:57–75. doi: 10.1016/j.neubiorev.2015.01.013
48. Yu DH, Yuan K, Cheng JD, Guan YY, Li YD, Bi YZ, et al. Reduced thalamus volume may reflect nicotine severity in young male smokers. *Nicotine Tob Res* (2018) 20:434–9. doi: 10.1016/j.neubiorev.2015.01.013
49. Tu PC, Lee YC, Chen YS, Hsu JW, Li CT, Su TP. Network-specific cortico-thalamic dysconnection in schizophrenia revealed by intrinsic functional connectivity analyses. *Schizophr Res* (2015) 166:137–43. doi: 10.1093/ntr/ntx146
50. Hoflich A, Hahn A, Kublbock M, Kranz GS, Vanicek T, Windischberger C, et al. Ketamine-induced modulation of the thalamo-cortical network in healthy volunteers as a model for Schizophrenia. *international J Neuropsychopharmacol* (2015) 18. doi: 10.1016/j.schres.2015.05.023
51. Gong J, Luo C, Li X, Jiang S, Khundrakpam BS, Duan M, et al. Evaluation of functional connectivity in subdivisions of the thalamus in schizophrenia. *Br J Psychiatry: J Ment Sci* (2019) 214:288–96. doi: 10.1093/ijnp/pyv040
52. Schmahmann JD. From movement to thought: anatomic substrates of the cerebellar contribution to cognitive processing. *Hum Brain Mapping* (1996) 4:174–98. doi: 10.1192/bjp.2018.299
53. Knight RT, Staines WR, Swick D, Chao LL. Prefrontal cortex regulates inhibition and excitation in distributed neural networks. *Acta Psychol (Amst)* (1999) 101:159–78. doi: 10.1002/(Sici)1097-0193(1996)4:3<174::Aid-Hbm3>3.3.Co;2-W
54. Bissonette GB, Powell EM, Roesch MR. Neural structures underlying set-shifting: roles of medial prefrontal cortex and anterior cingulate cortex. *Behav Brain Res* (2013) 250:91–101.
55. Chudasama Y. Animal models of prefrontal-executive function. *Behav Neurosci* (2011) 125:327–43. doi: 10.1016/j.bbr.2013.04.037
56. Szczepanski SM, Knight RT. Insights into human behavior from lesions to the prefrontal cortex. *Neuron* (2014) 83:1002–18. doi: 10.1037/a0023766
57. Zhou Y, Fan LZ, Qiu CX, Jiang TZ. Prefrontal cortex and the dysconnectivity hypothesis of schizophrenia. *Neurosci Bull* (2015) 31:207–19. doi: 10.1007/s12264-014-1502-8
58. Kringelbach ML. The human orbitofrontal cortex: linking reward to hedonic experience. *Nat Rev Neurosci* (2005) 6:691–702. doi: 10.1007/s12264-014-1502-8
59. Nakamura M, Nestor PG, McCarley RW, Levitt JJ, Hsu L, Kawashima T, et al. Altered orbitofrontal sulcogyral pattern in schizophrenia. *Brain : J Neurol* (2007) 130:693–707. doi: 10.1038/nrn1747
60. Kringelbach ML, Rolls ET. The functional neuroanatomy of the human orbitofrontal cortex: evidence from neuroimaging and neuropsychology. *Progress Neurobiol* (2004) 72:341–72.doi: 10.1093/brain/awm007
61. Szczepanski SM, Knight RT. Insights into human behavior from lesions to the prefrontal cortex. *Neuron* (2014) 83:1002–18. doi: 10.1016/j.pneurobio.2004.03.006
62. Stip E. Memory impairment in schizophrenia: perspectives from psychopathology and pharmacotherapy. *Can J Psychiatry Revue Canadienne Psychiatrie* (1996) 41:S27–34. doi: 10.1177/070674379604100822
63. Bartels SJ, Drake RE. Depressive symptoms in schizophrenia: comprehensive differential diagnosis. *Compr Psychiatry* (1988) 29:467–83. doi: 10.1177/070674379604100822
64. Schneider F, Gur RC, Gur RE, Shtasel DL. Emotional processing in schizophrenia: neurobehavioral probes in relation to psychopathology. *Schizophrenia Res* (1995) 17:67–75.
65. Lacerda AL, Hardan AY, Yorbik O, Vemulapalli M, Prasad KM, Keshavan MS. Morphology of the orbitofrontal cortex in first-episode schizophrenia: relationship with negative symptomatology. *Progress Neuro-psychopharmacol Biological Psychiatry* (2007) 31:510–6.
66. Engel AK, Fries P, Singer W. Dynamic predictions: oscillations and synchrony in top-down processing. *Nat Rev Neurosci* (2001) 2:704–16. doi: 10.1016/j.pnpbp.2006.11.022

67. Kim D, Wylie G, Pasternak R, Butler PD, Javitt DC. Magnocellular contributions to impaired motion processing in schizophrenia. *Schizophrenia Res* (2006) 82:1–8. doi: 10.1038/35094565
68. Wu CWW, Gu H, Lu HB, Stein EA, Chen JH, Yang YH. Frequency specificity of functional connectivity in brain networks. *Neuroimage* (2008) 42:1047–55. doi: 10.1016/j.schres.2005.10.008
69. Yue YY, Jia XZ, Hou ZH, Zang YF, Yuan YG. Frequency-dependent amplitude alterations of resting-state spontaneous fluctuations in late-onset depression. *Biomed Res Int* (2015) 2015:9. doi: 10.1016/j.neuroimage.2008.05.035

Conflict of Interest: The authors declare that the research was conducted in the absence of any commercial or financial relationships that could be construed as a potential conflict of interest.

frontiers in Psychiatry

ORIGINAL RESEARCH
published: 25 February 2020
doi: 10.3389/fpsyt.2020.00073

CACNA1C Gene rs11832738 Polymorphism Influences Depression Severity by Modulating Spontaneous Activity in the Right Middle Frontal Gyrus in Patients With Major Depressive Disorder

*Xiaoyun Liu[1], Zhenghua Hou[1], Yingying Yin[1], Chunming Xie[2], Haisan Zhang[3], Hongxing Zhang[4], Zhijun Zhang[2] and Yonggui Yuan[1]**

[1] Department of Psychosomatics and Psychiatry, Zhongda Hospital, School of Medicine, Southeast University, Nanjing, China, [2] Department of Neurology, ZhongDa Hospital, School of Medicine, Southeast University, Nanjing, China, [3] Department of Clinical Magnetic Resonance Imaging, the Second Affiliated Hospital of Xinxiang Medical University, Xinxiang, China, [4] Department of Psychiatry, the Second Affiliated Hospital of Xinxiang Medical University, Xinxiang, China

OPEN ACCESS

Edited by:
Wenbin Guo,
Central South University, China

Reviewed by:
Zhifen Liu,
First Hospital of Shanxi Medical University, China
Yun-Ai Su,
Peking University Sixth Hospital, China

***Correspondence:**
Yonggui Yuan
yygylh2000@sina.com

Specialty section:
This article was submitted to Neuroimaging and Stimulation, a section of the journal Frontiers in Psychiatry

Received: 25 October 2019
Accepted: 28 January 2020
Published: 25 February 2020

Citation:
Liu X, Hou Z, Yin Y, Xie C, Zhang H, Zhang H, Zhang Z and Yuan Y (2020) CACNA1C Gene rs11832738 Polymorphism Influences Depression Severity by Modulating Spontaneous Activity in the Right Middle Frontal Gyrus in Patients With Major Depressive Disorder. Front. Psychiatry 11:73. doi: 10.3389/fpsyt.2020.00073

Objectives: This study aimed to examine whether the CACNA1C gene rs11832738 polymorphism and major depressive disorder (MDD) have an interactive effect on the untreated regional amplitude of low-frequency fluctuation (ALFF) and to determine whether regional ALFF mediates the association between CACNA1C rs11832738 and MDD.

Methods: A total of 116 patients with MDD and 66 normal controls (NCs) were recruited. The MDD and NC groups were further divided into two groups according to genotype: carriers of the G allele (G-carrier group, GG/GA genotypes; MDD, n = 61; NC, n = 26) and AA homozygous group (MDD, n = 55; NC, n = 40). MDD was diagnosed based on the *Diagnostic and Statistical Manual of Mental Disorders, Fourth Edition*. Depression severity was assessed using the Hamilton Depression Scale-24 (HAMD-24) at baseline and follow-up (after 2 and 8 weeks of treatment). All subjects underwent functional MRI (fMRI) scans at baseline, and the ALFF was calculated to reflect spontaneous brain activity. The interactions between MDD and CACNA1C single nucleotide polymorphism rs11832738 were determined using two-way factorial analysis of covariance, with age, sex, education, and head motion as covariates. We performed mediation analysis to further determine whether regional ALFF strength could mediate the associations between rs11832738 and depression severity, MDD treatment efficacy.

Results: MDD had a main effect on regional ALFF distribution in three brain areas: the right medial frontal gyrus (MFG_R), the left anterior cingulate cortex (ACC_L), and the right cerebellum posterior lobe (CPL_R); CACNA1C showed a significant interactive effect with MDD on the ALFF of MFG_R. For CACNA1C G allele carriers, the ALFF of MFG_R had a significant positive correlation with the baseline HAMD-24 score. Exploratory mediation

analysis revealed that the intrinsic ALFF in MFG_R significantly mediated the association between the CACNA1C rs11832738 polymorphism and baseline HAMD-24 score.

Conclusions: A genetic variant in CACNA1C rs11832738 may influence depression severity in MDD patients by moderating spontaneous MFG_R activity.

Keywords: major depressive disorder (MDD), amplitude of low-frequency fluctuation (ALFF), right medial frontal gyrus (MFG), mediation effect, depression severity, CACNA1C

INTRODUCTION

Major depressive disorder (MDD) is a highly prevalent psychological condition characterized by a persistent low mood and anhedonia (1). The lifetime prevalence of MDD is approximately 17% (2), affecting approximately 350 million people worldwide (3, 4). According to recent data from 2019, the lifetime prevalence of MDD in China is as high as 3.4%, and it is estimated that approximately 44 million people suffer from this disease (5). More importantly, MDD is associated with substantial disability, mortality, and a high suicide rate, which places a heavy burden on patients, families, and the society, potentially making it the world's most economically burdensome illness by 2030 (6). Unfortunately, the current diagnostic criteria for MDD are mainly based on clinical symptoms, and the diagnostic consistency is very low (only 28%) (1). Poor consistency in diagnostic criteria can seriously affect the clinical efficacy of depression treatment: approximately 20% of patients with MDD fail to respond to standard antidepressant treatment, and up to 60% of patients with MDD still have residual symptoms after treatment (7). Therefore, it is very important to determine the pathophysiological mechanisms and to explore the objective biomarkers of depression in order to improve the consistency of diagnosis and treatment.

Imaging genetics is an emerging field aimed at identifying the associations between genetic variants and neuroimaging, bringing considerable promise in understanding the role of genes in determining the pathophysiological mechanism of MDD (8). Resting-state functional MRI (rs-fMRI) is one of the most commonly used neuroimaging techniques in imaging genetics studies. In rs-fMRI, spontaneous blood oxygen level-dependent (BOLD) low frequency fluctuations (0.01–0.08 Hz) were first suggested to have physiological significance by Biswal and colleagues, and this marker has been demonstrated to be closely related to spontaneous neural activities (9). The amplitude of low-frequency fluctuation (ALFF) based on voxel-wise analysis of the whole brain has been proposed as a quantitative measure of local BOLD signal variation due to regional spontaneous brain activity, which is an index reflecting the intensity of spontaneous neural activity within a specific frequency range, with no filtering at baseline (10).

Abnormal activity in frontotemporal regions (the cognitive and emotional control system in the cortico-limbic network) plays an important role in the pathophysiology of depression. The calcium channel, voltage-dependent, L type, alpha 1C subunit (*CACNA1C*) gene is considered to be involved in the development and plasticity of frontotemporal regions (11). The CACNA1C gene, located on chromosome 12p13.3, encodes the major L-type voltage-dependent calcium channel, Cav1.2 (alpha-1C subunit) (12). This channel is found in many types of cells, regulating the activity-dependent influx of calcium and is important for the normal functioning of the heart and brain cells (12). Evidence from animal studies, clinical studies, and genome-wide association studies supports the findings that CACNA1C is closely associated with depression (3, 13).

Many studies have focused on the CACNA1C single nucleotide polymorphism (SNP) rs1006737, which is located in the third intron of CACNA1C. This SNP has been demonstrated to have a close association with the minor allele A (adenine) and MDD (12, 14). To date, there have been few studies on other CACNA1C SNPs. However, rs11832738 is an SNP that is close to rs1006737, and they are both introns. Our research group used a multiple regression method and found that rs11832738 could significantly affect the anhedonia-associated grey matter network of MDD (15). Therefore, considering the results of our previous study, we hypothesized that this SNP may also be closely related to MDD. To the best of our knowledge, aside from our previous study, the associations between rs11832738 and MDD as well as other psychiatric disorders have not been studied. In this study, we explored the relationship between the polymorphism of the CACNA1C gene locus rs11832738 and MDD and investigated whether the gene locus could affect the severity and therapeutic effect of MDD by influencing spontaneous brain activity (reflected by ALFF values). We suspect that this gene locus affects MDD by influencing frontotemporal activities. Considering the complex etiology of MDD, we believe that it is critical to explore alterations in spontaneous brain activity and their associations with gene polymorphisms and depression severity, as well as possible therapeutic effects. Such exploration would help to elucidate the pathogenesis of MDD and clarify appropriate antidepressants to improve therapeutic effects and reduce the burden of depression.

METHODS

Participants

A total of 182 participants were recruited, including 116 MDD patients (MDD group) and 66 normal controls (NC group). The MDD patients were recruited through the inpatient and outpatient departments of psychiatry in the Second Affiliated Hospital of Xinxiang Medical University (n = 61) and ZhongDa Hospital Affiliated with Southeast University (n = 55), while the NC subjects were recruited through media advertising and community posting and through completed MRI scans at the Second Affiliated Hospital of Xinxiang Medical University

(n = 39) and ZhongDa Hospital Affiliated with Southeast University (n = 27). All participants were of Chinese Han ethnicity and right-handed. All participants signed informed consent forms, as approved by the local institutional review boards, and all study procedures adhered to the Declaration of Helsinki. The participants underwent MRI scans at baseline. All patients were in the acute phase of the disease and received antidepressant treatment depending on the clinical judgment of the empirical senior psychiatrists after the first scan and the first clinical scale assessment. Among the 116 patients with MDD, 51 experienced their first episodes without a history of antidepressant use, and the rest were recurrent patients with a history of antidepressant use. On searching the SNP database, we found that the frequency of the rs11832738 A allele was 72.5% in the East Asian population, while that of the G allele (guanine) was 27.5% (https://www.ncbi.nlm.nih.gov/snp/rs11832738#frequency_tab). According to our data, the frequency of the G allele was 22% in NC and 32.3% in MDD. Therefore, the G allele was suggested to be the rare risk allele. Accordingly, we further divided the MDD and NC groups into two subgroups: an AA homozygous group (MDD group, n = 55; NC group, n = 40) and a G-carrier group (GG/GA genotypes; MDD group, n = 61; NC group, n = 26).

Inclusion and Exclusion Criteria

The inclusion criteria for the MDD group were as follows: individuals who (1) were aged ≥ 18 years; (2) met the criteria listed in the *Diagnostic and Statistical Manual of Mental Disorders, Fourth Edition*; (3) had a Hamilton Depression Scale-24 (HAMD-24) score ≥ 20; and (4) had no contraindication to MRI scanning. The exclusion criteria were as follows: individuals with (1) other major psychiatric disorders or neurodegenerative illness history; (2) substance abuse (drug, caffeine, nicotine, alcohol, or others), head trauma, or loss of consciousness; or (3) a cardiac or pulmonary disease which could influence the MRI scan.

NC subjects were required to have a HAMD-24 score of ≤7. The exclusion criteria included a history of neuropsychiatric disease, substance abuse or insobriety, or contraindications to MRI scanning.

Clinical Evaluation

We used the HAMD-24 to assess depression severity at baseline and used the HAMD-24 reductive rate, calculated as (baseline HAMD score – follow-up HAMD score)/baseline HAMD score × 100%, to evaluate the effect of MDD treatment at the end of the 2- and 8-week treatments.

Genotyping

DNA was extracted from blood using standard protocols. DNA genotyping was performed by Tianhao Biotechnology Company (Shanghai, China). SNP genotypes in CACNA1C genes (rs11832738) were determined using predesigned Illumina next sequencing and array technologies (Illumina Inc., San Diego, CA, USA). Hardy-Weinberg equilibrium (HWE) tests, linkage disequilibrium statistics, and allele and genotype frequencies were calculated using PLINK 1.9 software (16). The SNP did not deviate from the HWE ($r = 0.78$, $P = 0.44$).

MRI Data Acquisition

MRI data were acquired using a Siemens 3.0 Tesla scanner with a 12-channel head coil (Siemens, Erlangen, Germany) in the Department of Clinical Magnetic Resonance Imaging at the Second Affiliated Hospital of Xinxiang Medical University and the affiliated ZhongDa Hospital of Southeast University. The heads of the participants were stabilized with a cushion to minimize head motion. Earplugs were used to reduce the scanner noise. High-resolution three-dimensional T1-weighted scans were recorded as magnetization-prepared rapid-acquisition gradient echo sequence (repetition time [TR] = 1,900 ms; echo time [TE] = 2.48 ms; flip angle [FA] = 9°; acquisition matrix = 256 × 256; field of view [FOV] = 250 × 250 mm^2; thickness = 1.0 mm; gap = 0; time = 4 min 18 s, 176 volumes). The parameters of the rs-fMRI were as follows: TR = 2,000 ms, TE = 25 ms, FA = 90°, acquisition matrix = 64 × 64, FOV = 240 × 240 mm^2, thickness = 3.0 mm, gap = 0 mm, 36 axial slices, 240 volumes, 3.75 × 3.75 mm^2 in-plane resolution parallel to the anterior-posterior commissure line, and an acquisition time of 8 min. During scanning, the participants were instructed to lie still in the scanner, keep their eyes open, and refrain from falling asleep.

MRI Image Preprocessing

For quality control, all image data were checked by two experienced radiologists. The rs-fMRI images were preprocessed using the Data Processing Assistant for Resting-State Function (DPARSF 2.3 advanced edition) MRI toolkit (17), which synthesizes procedures based on the resting-state functional MRI toolkit (REST, http://www.restfmri.net) and statistical parametric mapping software package (SPM, http://www.l.ion.ucl.ac.uk/spm). The first 10 time points were excluded to ensure stable longitudinal magnetization and adaptation to inherent scanner noise. The remaining 230 images were processed sequentially according to the following steps: (1) slice time was used with the 36th slice as the reference slice, corrected for temporal differences and head motion (participants with a head motion with maximum displacement greater than 1.5 mm in any direction [x, y, or z] or 1.5° of angular motion were excluded from the analyses); (2) T1 was co-registered to functional images and subsequently reoriented; (3) for spatial normalization, T1-weighted anatomic images were segmented into white matter, grey matter, and cerebrospinal fluid, and subsequently normalized to the Montreal Neurological Institute space using transformation parameters estimated with a unified segmentation algorithm (18). These transformation parameters were applied to the functional images, and the images were resampled with isotropic voxels of 3 mm; (4) spatial smoothing was conducted with a 4-mm full-width at half-maximum (FWHM) isotropic Gaussian kernel; (5) the linear trend within each voxel's time series was removed; (6) nuisance signals (white matter, cerebrospinal fluid signals, and head motion parameters calculated using rigid body six correction) and spiked regressors were regressed out; and (7) finally, temporal bandpassing (0.01–0.08 Hz) was performed to minimize low-frequency drift and filter high-frequency noise.

ALFF Analysis

After preprocessing, ALFF was calculated using the DPARSF software. For a given voxel, the time series was transformed into the frequency domain, and the power spectrum was obtained. The square root of the power spectrum was subsequently computed and averaged across a predefined frequency interval. The average square root was taken as the ALFF, which was assumed to reflect the absolute intensity of spontaneous brain activity (17).

STATISTICAL ANALYSES

Demographic and Clinical Data

Independent one-sample or two-sample t-tests or the chi-square tests were employed to explore differences in the demographic and clinical data (SPSS 20.0, Chicago, USA). Continuous variables were presented as mean ± SD. The threshold for statistical significance was defined as $P < 0.05$.

Analysis of Covariance and Correlation Analyses

A two-way factorial analysis of covariance (ANCOVA: MDD, CACNA1C rs11832738 G allele) was performed using AlphaSim correction (FWHM = 4 mm, with $61 \times 73 \times 61$ mm^3 whole brain mask, which yielded a corrected threshold of $P < 0.001$, cluster sizes ≥6 mm^3), by controlling for age, sex, education, and head motion. Subsequently, numerical representation of the mean ALFF strength of each significant cluster was displayed to reflect ALFF alterations among groups.

To further identify the clinical significance of the altered ALFF, the average ALFF strength of each significant region observed in the ANCOVA analysis was extracted. Partial correlation analysis was employed to detect the relationship between the average regional ALFF strength from the interactive effect and depressive severity or therapeutic effect (2-week/8-week) as well as the genotype of rs11832738 (GG, GA, and AA genotypes with scores of 1, 0.5, and 0, respectively) in patients with MDD after controlling for covariates including sex, age, education, and duration of illness. The threshold of statistical significance was $P < 0.05$.

Mediation Analyses

We performed mediation analyses to further determine whether ALFF strength could mediate the association between CACNA1C rs11832738 and MDD. This approach was based on a standard three-variable mediation model and was in line with the current most widely accepted mediation analysis technique (19, 20). A detailed description of the method is provided in the **Supplementary Material**.

RESULTS

Demographic and Clinical Data

Demographic and clinical data are shown in **Table 1**. There were no significant differences in age, sex, or education among the different allele groups in the MDD and NC groups. There were no significant differences in age of onset, duration of illness, number of episodes, family history, HAMD-24 score (0-week/2-week/8-week) or HAMD-24 reductive rate (2-week/8-week) among the different allele groups in the MDD group.

ANCOVA Analysis

MDD had a main effect on regional ALFF distribution in the three brain regions: the right medial frontal gyrus (MFG_R), the left anterior cingulate cortex (ACC_L), and the right cerebellum posterior lobe (CPL_R; **Table 2** and **Figure 1**). CACNA1C showed a significant interactive effect with MDD on the ALFF of MFG_R (**Table 3** and **Figure 2**). No main effect of the gene on regional ALFF was found (corrected $P < 0.001$, determined by AlphaSim with voxel number ≥6 for multiple corrections).

TABLE 1 | Demographic and clinical data of different allele groups in the MDD and NC groups.

	MDD (n = 116)		NC (n = 66)		*P1*	*P2*	*P3*
	GG/GA (n = 61)	AA (n = 55)	GG/GA (n = 26)	AA (n = 40)			
Sex (M/F)	32/29	22/33	11/15	20/20	0.179	0.541	0.957
Age (years)	45.10 ± 14.10	43.82 ± 13.82	40.35 ± 13.52	42.18 ± 13.75	0.623	0.579	0.155
Education (years)	10.18 ± 4.65	8.89 ± 4.33	12.50 ± 4.48	11.38 ± 4.64	0.126	0.244	0.071
Age of onset (years)	40.70 ± 14.81	38.84 ± 15.02	—	—	0.605	—	—
Duration of illness (months)	53.17 ± 80.38	60.33 ± 87.17	—	—	0.881	—	—
Number of episodes	2.05 ± 1.54	2.34 ± 2.37	—	—	0.539	—	—
Family history (Y/N)	5/56	6/49	—	—	0.619	—	—
HAMD-24 (0 w)	31.20 ± 7.08	31.24 ± 4.77	1.19 ± 1.96	1.13 ± 1.96	0.972	0.822	0.000
HAMD-24 (2 w)	15.85 ± 7.80	15.82 ± 15.76	—	—	0.979	—	—
HAMD-24 (8 w)	4.72 ± 5.40	3.78 ± 4.51	—	—	0.350	—	—
Reductive rate (2 w)	0.51 ± 0.18	0.50 ± 0.17	—	—	0.762	—	—
Reductive rate (8 w)	0.84 ± 0.18	0.88 ± 0.15	—	—	0.242	—	—

MDD, major depressive disorder; NC, normal control; HAMD-24, Hamilton Depression Scale-24; M/F, male/female; Y/N, yes/no. P1, comparison between the GG/GA and AA genotypes in the MDD group; P2, comparison between the GG/GA and AA genotypes in the NC group; P3, comparison between the MDD and NC groups.

TABLE 2 | Main effect of MDD on regional brain ALFF values.

Brain regions	BA	Voxel number	MNI coordinates			t-score
			X	Y	Z	
Right cerebellum posterior lobe	—	52	42	−72	−24	26.985
Anterior cingulate cortex	32	855	−12	27	−9	33.0669
Right medial frontal gyrus	10	736	15	45	−12	29.0273

The significance threshold was set at a corrected P < 0.001 (corrected with AlphaSim correction and cluster volume ≥6 voxels). ALFF, amplitude of low-frequency fluctuation; BA, Brodmann area; MNI, Montreal Neurological Institute.

TABLE 3 | Interactive effect of MDD and gene on regional brain ALFF values.

Brain regions	BA	Voxel number	MNI coordinates			t-score
			X	Y	Z	
Right medial frontal gyrus	10	11	3	0	66	14.7147

The significance threshold was set at a corrected P < 0.001 (corrected with AlphaSim correction and cluster volume ≥6 voxels). ALFF, amplitude of low-frequency fluctuation; BA, Brodmann area; MNI, Montreal Neurological Institute.

Correlation Analysis

For CACNA1C G allele carriers, the ALFF of MFG_R was significantly positively correlated with the baseline HAMD-24 score (r = 0.335, P = 0.011; **Figure 3A**). In the MDD group, CACNA1C rsll832738 was significantly negatively correlated with the ALFF of MFG_R (r = −0.224, P = 0.017: **Figure 3B**).

Mediation Analysis

Exploratory mediation analysis revealed that the intrinsic ALFF in MFG_R had a significant mediation effect on the association between the CACNA1C rs11832738 polymorphism and baseline HAMD-24 score (**Figure 4**).

DISCUSSION

To the best of our knowledge, our study is the first to explore the relationship between the CACNA1C rs11832738 polymorphism and ALFF in patients with MDD. In the current study, we found that MFG_R was both the brain area that was mainly affected by the MDD as well as affected by rs11832738 and MDD interactively. Moreover, for CACNA1C G allele carriers, the ALFF of MFG_R was significantly positively correlated with depression severity. Finally, through further mediation analyses, we found that the relationship between the CACNA1C rs11832738 polymorphism and depression severity was mediated by the altered spontaneous activity of MFG_R.

The MFG, a region of the ventral lateral prefrontal cortex, is responsible for the top-down regulation of emotional processing and numerous cognitive functions, such as decision-making, working memory, and attentional processing, and its contribution to MDD has been documented (21, 22). Compared to the left side, MFG_R could modulate the cognitive shift between the internal and external environments due to the link between the ventral attention network and the dorsal attention network (21), and lesions in this area could lead to negatively biased attention in patients with MDD (23, 24). Importantly, considerable research has, to date, supported the idea that negatively biased attention predicts prolonged mood persistence in patients with MDD and future increases in depression severity (24–26). A recent study also suggested that abnormal spontaneous activity (reflected by ALFF) of MFG_R predicts improvement in depressive symptoms (27). Our study found a significant correlation between spontaneous activity of MFG_R and depression severity. Therefore, MFG_R might have a closer relationship with MDD than does the left MFG.

Previous studies have suggested that the CACNA1C SNP can alter the function of the frontal cortex (11) and that the knockdown of CACNA1C in the frontal cortex has an antidepressant-like effect (28), suggesting that CACNA1C might affect depression by altering frontal lobe function. Our study is consistent with these studies and showed that the effect

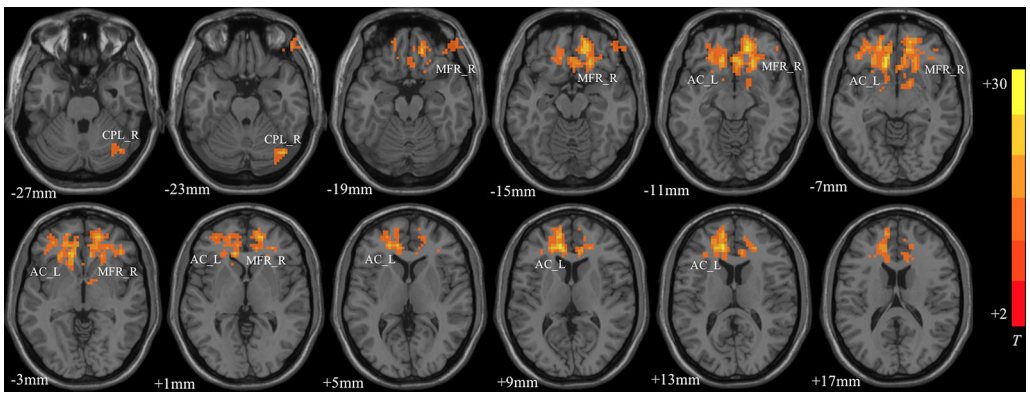

FIGURE 1 | The main effect of MDD on regional ALFF distributed in the three brain areas: the right medial frontal gyrus (MFG_R), left anterior cingulate cortex (ACC_L), and right cerebellum posterior lobe (CPL_R; corrected P < 0.001, determined by AlphaSim with voxel number ≥6 for multiple corrections). The color bar indicates the display window for the threshold t-value maps. More intense colors indicate higher ALFF values.

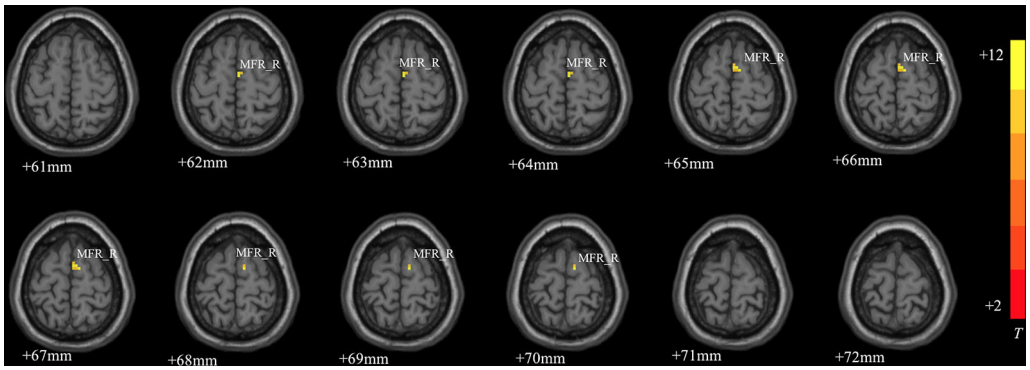

FIGURE 2 | The interactive effect of gene and MDD on the ALFF of the right medial frontal gyrus (MFG_R; corrected $P < 0.001$, determined by AlphaSim with voxel number ≥6 for multiple corrections). The color bar indicates the display window for the threshold t-value maps. More intense colors indicate higher ALFF values.

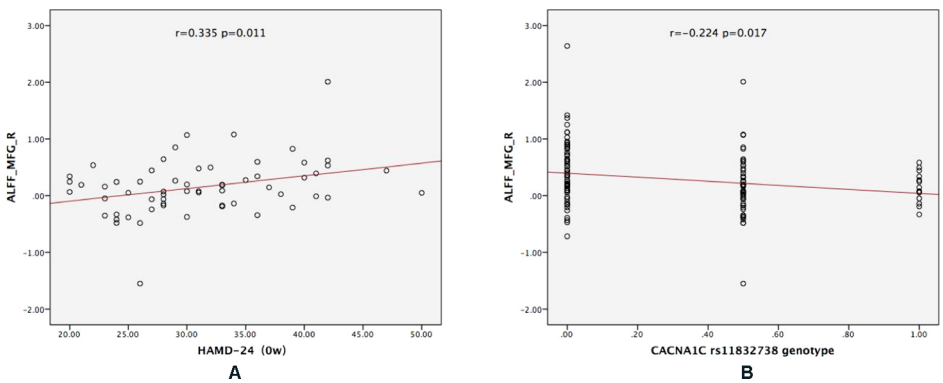

FIGURE 3 | The results of the partial correlation analyses. **(A)** For CACNA1C G allele carriers, ALFF_MFG_R was significantly positively correlated with the baseline HAMD-24 score ($r = 0.335$, $P = 0.011$); **(B)** in the MDD group, CACNA1C rsll832738 was significantly negatively correlated with ALFF_MFG_R ($r = -0.224$, $P = 0.017$). ALFF_MFG_R: amplitude of low-frequency fluctuation of the right medial frontal gyrus.

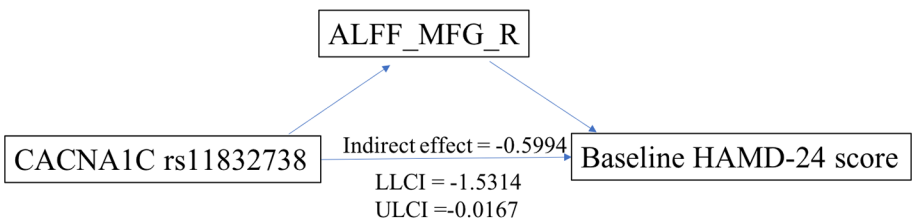

FIGURE 4 | ALFF_MFG_R had a significant positive mediation effect between the CACNA1C rs11832738 polymorphism and the baseline HAMD-24 score. ALFF_MFG_R, amplitude of low-frequency fluctuation of the right medial frontal gyrus; LLCI, lower-limit confidence interval; ULCI, upper-limit confidence interval.

of this gene on the severity of depression is mediated by changes in the spontaneous activity of MFG_R.

The underlying mechanism may be related to the contribution of Cav1.2 signaling. Cav 1.2 is encoded by CACNA1C and is the predominant calcium channel in the brain (accounting for approximately 90% of calcium channels), acting as the main pathway that mediates the entry of calcium into cells (29). Thus, it is of vital importance to intracellular signaling pathway activity, gene expression, synaptic plasticity, and neuronal and dendritic development, suggesting that perturbations in Cav1.2 signaling can lead to depressive phenotypes (28, 29). Cav1.2 modulates the calcium-dependent genes, including brain-derived neurotrophic factor and B-cell lymphoma 2, the protein products of which have been

demonstrated to have neurotrophic and neuroprotective effects in the context of corticolimbic frontotemporal structures and functions (30). Although not specifically about rs11832738, previous studies have suggested that SNPs could influence altered CACNA1C gene expression, which in turn would lead to the dysfunction of Cav1.2 and altered neural activity (12). Our results suggest that rs11832738 might contribute to depression severity through altered CACNA1C gene expression; however, this requires further research.

In addition to MFG_R, we found that the right CPL and ACC were also affected by MDD. The ACC is responsible for regulating stress and processing emotion and has repeatedly been shown to play an important role in MDD (31–33). The cerebellum is traditionally thought to be involved only in motor function, but in recent years, it has been increasingly recognized that the cerebellum is important for cognition and emotion (34). Therefore, an increasing number of studies have suggested that the cerebellum participates in the pathophysiological mechanism of depression (35). Moreover, a meta-analysis indicated that posterior and lateral cerebellar regions regulate cognition and emotion, whereas the anterior lobe is mainly involved in motor function (36). This is consistent with our results, demonstrating that the posterior lobe is associated with MDD.

There were two main limitations to our study. First, as with many other rs-fMRI studies, there was no way to constrain the subjects' thoughts during scanning, especially for MDD patients, making the cross-sectional resting ALFF comparison more difficult as there may already be differences in the patients' 'resting state'. Second, our data were collected from two sites, similar to many multicenter studies (37), and the site effect was an important problem which should not be ignored. However, to ensure the same scanning parameters and minimize the differences between the two sites, an indicated person (Chunming Xie) was invited to debug the MRI scan parameters of the two sites before we collected the data. One advantage of our study setup was the use of mediation analysis, which provided direct evidence of the neural basis of MDD.

CONCLUSIONS

This study provides initial evidence for CACNA1C genotype-related alterations in brain function among patients with MDD and contributes to a better understanding of the neurobiological mechanisms underlying MDD. This adds to the current state of knowledge regarding the effects of CACNA1C on brain function. Our study, together with previous studies, suggests that calcium channel dysfunction may, in part, contribute to the genetic etiology of MDD through alterations in the functional activity of the brain. In other words, MDD may be, in part, an ion channelopathy.

However, the present findings require replication with larger samples. Moreover, an important step in determining whether specific effects of the CACNA1C genotype exist in subgroups of patients with MDD is the investigation of different patient samples.

DATA AVAILABILITY STATEMENT

The datasets analyzed in this article are not publicly available. Requests to access the datasets should be directed to 1360809788@qq.com.

ETHICS STATEMENT

The studies involving human participants were reviewed and approved by the Medical Ethics Committee for Clinical Research of Zhongda Hospital Affiliated to Southeast University. The patients/participants provided their written informed consent to participate in this study.

AUTHOR CONTRIBUTIONS

XL was responsible for data collection, data processing and writing. YYi and ZH were responsible for data collection. CX, HaZ, HoZ and ZZ were responsible for data quality testing. YYu was responsible for the final examination of the paper.

FUNDING

This work was supported by the National Key Research and Development Program of China (2016YFC1306702), the National Natural Science Foundation of China (81971277), and the Scientific Research Foundation of Graduate School of Southeast University (YBPY1890).

SUPPLEMENTARY MATERIAL

The Supplementary Material for this article can be found online at: https://www.frontiersin.org/articles/10.3389/fpsyt.2020.00073/full#supplementary-material

REFERENCES

1. Freedman R, Lewis DA, Michels R, Pine DS, Schultz SK, Tamminga CA, et al. The initial field trials of DSM-5: new blooms and old thorns. *Am J Psychiatry* (2013) 170(1):1–5. doi: 10.1176/appi.ajp.2012.12091189
2. Ota KT, Liu RJ, Voleti B, Maldonado-Aviles JG, Duric V, Iwata M, et al. REDD1 is essential for stress-induced synaptic loss and depressive behavior. *Nat Med* (2014) 20(5):535–9. doi: 10.1038/nm.3513
3. Jaric I, Rocks D, Cham H, Herchek A, Kundakovic M. Sex and estrous cycle effects on anxiety- and depression-related phenotypes in a two-hit developmental stress model. *Front In Mol Neurosci* (2019) 12:74. doi: 10.3389/fnmol.2019.00074
4. Smith K. Mental health: a world of depression. *Nature* (2014) 515(7526):1. doi: 10.1038/515180a
5. Ben Forry J, Ashaba S, Rukundo GZ. Prevalence and associated factors of mental disorders among prisoners in Mbarara municipality, southwestern

Uganda: a cross-sectional study. *BMC Psychiatry* (2019) 19:178. doi: 10.1186/s12888-019-2167-7
6. Mathers CD, Loncar D. Projections of global mortality and burden of disease from 2002 to 2030. *PloS Med* (2006) 3(11):e442. doi: 10.1371/journal.pmed.0030442
7. Monteggia LM. Put therapies first. *Nat 2014;* (7526) 515:200–. doi: 10.1038/515200a
8. Hibar DP, Stein JL, Renteria ME, Arias-Vasquez A, Desrivieres S, Jahanshad N, et al. Common genetic variants influence human subcortical brain structures. *Nature* (2015) 520(7546):224–U16. doi: 10.1038/nature14101
9. Biswal B, Yetkin FZ, Haughton VM, Hyde JS. Functional connectivity in the motor cortex of resting human brain using echo-planar MRI. *Magn Reson In Med* (1995) 34(4):537–41. doi: 10.1002/mrm.1910340409
10. Zhuang LY, Liu XY, Shi YM, Liu XL, Luo BY. Genetic variants of PICALM rs541458 modulate brain spontaneous activity in older adults with amnestic mild cognitive impairment. *Front In Neurol* (2019) 10:494. doi: 10.3389/fneur.2019.00494
11. Wang F, McIntosh AM, He Y, Gelernter J, Blumberg HP. The association of genetic variation in CACNA1C with structure and function of a frontotemporal system. *Bipolar Disord* (2011) 13(7-8):696–700. doi: 10.1111/j.1399-5618.2011.00963.x
12. Backes H, Dietsche B, Nagels A, Konrad C, Witt SH, Rietschel M, et al. Genetic variation in CACNA1C affects neural processing in major depression. *J Psychiatr Res* (2014) 53:38–46. doi: 10.1016/j.jpsychires.2014.02.003
13. Rao SQ, Yao Y, Zheng C, Ryan J, Mao CQ, Zhang FQ, et al. Common variants in CACNA1C and MDD susceptibility: a comprehensive meta-analysis. *Am J Med Genet B* (2016) 171(6):896–903. doi: 10.1002/ajmg.b.32466
14. Gonzalez S, Xu C, Ramirez M, Zavala J, Armas R, Contreras SA, et al. Suggestive evidence for association between L-type voltage-gated calcium channel (CACNA1C) gene haplotypes and bipolar disorder in Latinos: a family-based association study. *Bipolar Disord* (2013) 15(2):206–14. doi: 10.1111/bdi.12041
15. Jang W. The Multivariate Data Driven Imaging Genetic Study on Anhedonia in Major Depressive Disorder. Doctoral Dissertation of Southeast University. (2018) (in Chinese).
16. Purcell S, Neale B, Todd-Brown K, Thomas L, Ferreira MAR, Bender D, et al. PLINK: a tool set for whole-genome association and population-based linkage analyses. *Am J Hum Genet* (2007) 81(3):559–75. doi: 10.1086/519795
17. Chaogan Yan YZ. DPARSF: a MATLAB toolbox for "pipeline" data analysis of resting-state fMRI. *Front In Syst Neurosci* (2010) 4:13. doi: 10.3389/fnsys.2010.00013
18. Ashburner J, Friston KJ. Unified segmentation. *Neuroimage* (2005) 26(3):839–51. doi: 10.1016/j.neuroimage.2005.02.018
19. Bolin JH. Introduction to mediation, moderation, and conditional process analysis: a regression-based approach. *J Educ Measurement* (2014) 51(3):335–7. doi: 10.1111/jedm.12050
20. Ma YN, Li BF, Wang CB, Shi ZH, Sun Y, Sheng F, et al. 5-HTTLPR polymorphism modulates neural mechanisms of negative self-reflection. *Cereb Cortex* (2014) 24(9):2421–9. doi: 10.1093/cercor/bht099
21. Geng JT, Yan R, Shi JB, Chen Y, Mo ZQ, Shao JN, et al. Altered regional homogeneity in patients with somatic depression: a resting-state fMRI study. *J Affect Disord* (2019) 246:498–505. doi: 10.1016/j.jad.2018.12.066
22. Wang Y, Lu WZ, Yan TQ, Zhou J, Xie YZ, Yuan JM, et al. Functional MRI reveals effects of high intraocular pressure on central nervous system in high-tension glaucoma patients. *Acta Ophthalmol* (2019) 97(3):E341–E8. doi: 10.1111/aos.14027
23. Beevers CG, Clasen PC, Enock PM, Schnyer DM. Attention bias modification for major depressive disorder: effects on attention bias, resting state connectivity, and symptom change. *J Abnormal Psychol* (2015) 124(3):463–75. doi: 10.1037/abn0000049
24. Clasen PC, Beevers CG, Mumford JA, Schnyer DM. Cognitive control network connectivity in adolescent women with and without a parental history of depression. *Dev Cogn Neurosci* (2014) 7:13–22. doi: 10.1016/j.dcn.2013.10.008
25. Beevers CG, Lee HJ, Wells TT, Ellis AJ, Telch MJ. Association of predeployment gaze bias for emotion stimuli with later symptoms of PTSD and depression in soldiers deployed in Iraq. *Am J Psychiatry* (2011) 168(7):735–41. doi: 10.1176/appi.ajp.2011.10091309
26. Sanchez A, Vazquez C, Marker C, LeMoult J, Joormann J. Attentional disengagement predicts stress recovery in depression: an eye-tracking study. *J Abnormal Psychol* (2013) 122(2):303–13. doi: 10.1037/a0031529
27. Du X, Mao Y, Ran Q, Zhang QL, Luo QH, Qiu J. Short-term group cognitive behavior therapy contributes to recovery from mild depression: Evidence from functional and structural MRI. *Psychiatry Res Neuroimaging* (2016) 251:53–9. doi: 10.1016/j.pscychresns.2016.04.010
28. Kabir ZD, Lee AS, Burgdorf CE, Fischer DK, Rajadhyaksha AM, Mok E, et al. Cacna1c in the prefrontal cortex regulates depression-related behaviors *via* REDD1. *Neuropsychopharmacology* (2017) 42(10):2032–42. doi: 10.1038/npp.2016.271
29. Zhang ZF, Wang YY, Zhang QM, Zhao W, Chen XY, Zhai JG, et al. The effects of CACNA1C gene polymorphism on prefrontal cortex in both schizophrenia patients and healthy controls. *Schizophr Res* (2019) 204:193–200. doi: 10.1016/j.schres.2018.09.007
30. Manji HK, Moore GJ, Rajkowska G, Chen G. Neuroplasticity and cellular resilience in mood disorders. *Mol Psychiatry* (2000) 5(6):578–93. doi: 10.1038/sj.mp.4000811
31. Godfrey KEM, Gardner AC, Kwon S, Chea W, Muthukumaraswamy SD. Differences in excitatory and inhibitory neurotransmitter levels between depressed patients and healthy controls: a systematic review and meta-analysis. *J Psychiatr Res* (2018) 105:33–44. doi: 10.1016/j.jpsychires.2018.08.015
32. Lai CH. Promising neuroimaging biomarkers in depression. *Psychiatry Invest* (2019) 16(9):662–70. doi: 10.30773/pi.2019.07.25.2
33. Tian S, Sun YR, Shao JN, Zhang SQ, Mo ZQ, Liu XX, et al. Predicting escitalopram monotherapy response in depression: the role of anterior cingulate cortex. *Hum Brain Mapp* (2019). 1–12. doi: 10.1002/hbm.24872
34. De Smet HJ, Paquier P, Verhoeven J, Marien P. The cerebellum: its role in language and related cognitive and affective functions. *Brain Lang* (2013) 127(3):334–42. doi: 10.1016/j.bandl.2012.11.001
35. Zhang Y, Yang Y, Wang Z, Bian R, Jiang W, Yin Y, et al. Altered regional cerebral blood flow of right cerebellum posterior lobe in asthmatic patients with or without depressive symptoms. *Front In Psychiatry* (2018) 9:225. doi: 10.3389/fpsyt.2018.00225
36. Stoodley CJ, Schmahmann JD. Functional topography in the human cerebellum: a meta-analysis of neuroimaging studies. *Neuroimage* (2009) 44(2):489–501. doi: 10.1016/j.neuroimage.2008.08.039
37. Yan CG, Chen X, Li L, Castellanos FX, Bai TJ, Bo QJ, et al. Reduced default mode network functional connectivity in patients with recurrent major depressive disorder. *Proc Natl Acad Sci United States America* (2019) 116(18):9078–83. doi: 10.1073/pnas.1900390116

Conflict of Interest: The authors declare that the research was conducted in the absence of any commercial or financial relationships that could be construed as a potential conflict of interest.

frontiers in Psychiatry

ORIGINAL RESEARCH
published: 17 March 2020
doi: 10.3389/fpsyt.2020.00198

Acute and Chronic Effects of Betel Quid Chewing on Brain Functional Connectivity

Adellah Sariah[1,2†], Shuixia Guo[3,4†], Jing Zuo[5†], Weidan Pu[6], Haihong Liu[7], Edmund T. Rolls[8,9], Zhimin Xue[1], Zhening Liu[1] and Xiaojun Huang[1]*

[1] Mental Health Institute of the Second Xiangya Hospital, Central South University, Changsha, China, [2] Department of Mental Health and Psychiatric Nursing, Hubert Kairuki Memorial University, Dar es Salaam, Tanzania, [3] MOE-LCSM, School of Mathematics and Statistics, Hunan Normal University, Changsha, China, [4] Key Laboratory of Applied Statistics and Data Science, Hunan Normal University, Changsha, China, [5] Department of Psychiatry, Brain Hospital of Hunan Province, Changsha, China, [6] Medical Psychological Institute, Second Xiangya Hospital, Central South University, Changsha, China, [7] Mental Health Center of Xiangya Hospital, Central South University, Changsha, China, [8] Oxford Centre for Computational Neuroscience, Oxford, England, [9] Department of Computer Science, University of Warwick, Coventry, England

OPEN ACCESS

Edited by:
Maorong HU,
Nanchang University, China

Reviewed by:
Xiangyu Long,
University of Calgary, Canada
Wen Qin,
Tianjin Medical University General Hospital, China
Yifeng Wang,
Sichuan Normal University, China

***Correspondence:**
Xiaojun Huang
xiaojunh9@csu.edu.cn

[†]*These authors share first authorship*

Specialty section:
This article was submitted to Neuroimaging and Stimulation, a section of the journal Frontiers in Psychiatry

Received: *11 October 2019*
Accepted: *02 March 2020*
Published: *17 March 2020*

Citation:
Sariah A, Guo S, Zuo J, Pu W, Liu H, Rolls ET, Xue Z, Liu Z and Huang X (2020) Acute and Chronic Effects of Betel Quid Chewing on Brain Functional Connectivity. Front. Psychiatry 11:198. doi: 10.3389/fpsyt.2020.00198

Background: The active alkaloid in Betel quid is arecoline. Consumption of betel quid is associated with both acute effects and longer-term addictive effects. Despite growing evidence that betel quid use is linked with altered brain function and connectivity, the neurobiology of this psychoactive substance in initial acute chewing, and long-term dependence, is not clear.

Methods: In this observational study, functional magnetic resonance imaging in a resting-state was performed in 24 male betel quid-dependent chewers and 28 male controls prior to and promptly after betel quid chewing. Network-based statistics were employed to determine significant differences in functional connectivity between brain networks for both acute effects and in long-term betel users versus controls. A support vector machine was employed for pattern classification analysis.

Results: Before chewing betel quid, higher functional connectivity in betel quid-dependent chewers than in controls was found between the temporal, parietal and frontal brain regions (right medial orbitofrontal cortex, right lateral orbital frontal cortex, right angular gyrus, bilateral inferior temporal gyrus, superior parietal gyrus, and right medial superior frontal gyrus). In controls, the effect of betel quid chewing was significantly increased functional connectivity between the subcortical regions (caudate, putamen, pallidum, and thalamus), and the visual cortex (superior occipital gyrus and right middle occipital gyrus).

Conclusion: These findings show that individuals who chronically use betel quid have higher functional connectivity than controls of the orbitofrontal cortex, and inferior temporal and angular gyri. Acute effects of betel quid are to increase the functional connectivity of some visual cortical areas (which may relate to the acute symptoms) and the basal ganglia and thalamus.

Keywords: functional brain imaging, basal ganglia, orbitofrontal cortex, betel quid, arecoline, resting-state fMRI

INTRODUCTION

Betel quid (BQ) is a psychotropic substance, extensively consumed by more than 600 million people worldwide (1). Right after consumption, users of BQ have reported experiencing decreased thinking ability, disturbed mental processes, increased vigilance, body relaxation, enhanced motor responses, and a boosted sense of wellness (2). Substance dependence features including tolerance, craving, and drug-seeking behaviors as well as withdrawal symptoms have been acknowledged by habitual users of BQ (3). Many psychoactive substances act on the brain's reward pathway during acute administration, an effect that may be different in habitual users (4). The basal ganglia, extended amygdala, and the prefrontal cortex have been implicated in the initial stages, development, and habitual use of addictive substances (5). During the initial stages, the individual engages in voluntary substance use behaviors (6). Such behaviors may be accompanied by intense feelings which once experienced, may enhance recurrent substance use (7). Arecoline is the principal active component in BQ (8). It facilitates the release of dopamine (DA) (9) by binding to M_5 muscarinic acetylcholine receptors on GABA terminals on DA neurons in the ventral tegmental area (VTA) (10). DA concentration is increased in the VTA and other projection areas through a series of mechanisms carried out by the mesocorticolimbic system [VTA, nucleus accumbens (NAc), and prefrontal cortex (PFC)], which is considered to be a principal pathway of drug reward (11). Additionally, cholinergic and inhibitory GABA'ergic inputs greatly regulate the mesolimbic dopaminergic neurons (12), which are known for their important role in processing rewards, reinforcement learning, (13) and dependence (14). Moreover, acute administration of psychoactive drugs has been found to activate brain areas connected to the mesocorticolimbic neural networks, implicated in drug rewards (15). Therefore, the need to use psychoactive substances repetitively and the compulsivity that is demonstrated in individuals addicted to drugs may be elucidated by the involvement of the reward and habit pathways in the brain (5). In contrast to the increased dopaminergic transmission in the NAc during acute exposure to drugs, chronic drug use is linked with less rewarding effects which result from reduced DA levels (16, 17). Chronic drug use is known to diminish the ability of the brain to control drug use behaviors, leading to increased risk for compulsive behavior that characterizes addiction (6). At first, it was believed that losing control over drug use stemmed from impairment in the subcortical reward brain region. However, findings from addiction studies have demonstrated the crucial role of the PFC in modulating the limbic reward regions and executive functions. Disruption of the PFC has been associated with loss of inhibitory control observed in drug-addicted individuals who have relapsed (18).

Resting-state functional connectivity (FC) studies have found that the majority of addictive drugs lead to reward, emotional and cognitive dysregulation (19). The mesocorticolimbic (MCL) system has been implicated to play an important role in drug addiction. The interaction among and between the MCL regions and other subcortical and cortical structures that manifests as circuit-level FC alterations have been observed in the reward circuit of drug addicts (19). The principal reward network is connected to other reward brain areas encompassing the subgenual anterior cingulate cortex (ACC), medial orbitofrontal cortex (mOFC), and medial PFC (mPFC) (20). For instance, increased resting-state FC was observed between NAc and the ventral mPFC (vmPFC) (rostral ACC and mPFC) of heroin addicts (21). Likewise, abstinent cocaine-users displayed greater resting-state FC between the ventral striatum and the vmPFC (22). Apart from increased striatal-PFC FC, a study investigating FC in prescription opioid users found reduced FC between NAc and the subcortical (hippocampus and amygdala) and cortical (cingulate, parietal, prefrontal) regions (23).

Drugs of addiction are also characterized by emotional dysregulation emanating from altered FC between the amygdala and PFC regions (19). Interaction of the amygdala with mPFC, hippocampus, cingulate, and insula regions has been linked with emotional processing and regulation, and generation of affective states (24). The hippocampus (involved in memory and learning) and the dorsal ACC (involved in cognitive control) are thought to be impaired in addiction, where a greater saliency value of drugs accompanied by a weaker inhibitory control leads to compulsive drug-seeking behavior (25, 26). The amygdala and its connections are fundamental elements perpetuating drug use, and previous studies propose that aberrant amygdala-mPFC FC may play a crucial role in emotional dysregulation frequently observed in drug addicts (19). Reduced FC strength was reported between the amygdala and regions of mPFC (including vmPFC and rostral ACC) in individuals addicted to cocaine (27), and heroin abusers (28). Similarly, extensive reduction of FC was displayed between the amygdala and several regions, including ventrolateral, medial, and dorsolateral PFC (dlPFC) regions in individuals addicted to prescription-opioid (23). In this study, longer periods of opioid use were linked with greater amygdala-vmPFC (specifically the subgenual ACC) FC reductions.

Apart from reward and emotional deficits, individuals addicted to psychoactive drugs are known to display neural dysfunction linked with cognitive control (29). The cognitive control network includes the ACC, lateral PFC, and parietal areas (19). For instance, decreased resting-state FC was observed between the ACC and dlPFC of heroin users relative to controls (21). Moreover, substantially decreased FC was observed within and between lateral PFC and parietal regions, such that decreased interhemispheric connectivity between lateral PFC areas was associated with a greater frequency of self-reported cognitive deficits (30) in cocaine addicts. A similar characteristic was displayed in abstinent heroin users such that FC was reduced between the lateral PFC and parietal regions. The observed reduction in FC matched a reduction in gray matter density in the same regions, with a longer duration of use predicting a greater reduction in both parameters (31).

A number of psychoactive substances have been linked with FC alterations in addicts. Specifically, compared to healthy controls,

Abbreviations: BQ, Betel quid; BQD, Betel quid dependence; HC, Healthy controls; FC, Functional connectivity; DA, Dopamine; OFC, Orbitofrontal cortex; CAU, Caudate; THA, Thalamus; PUT, Putamen; SOG, Superior occipital gyrus; MOG, Middle occipital gyrus; SPG, Superior parietal gyrus; SFG, Superior frontal gyrus; ITG, Inferior temporal gyrus; ACC, Anterior cingulate cortex.

cocaine users displayed decreased FC within corticostriatal reward circuitry (27, 32), which has been associated with compulsive use of drugs and relapse (32). Apart from the reward circuitry, users of cocaine demonstrated altered FC between vital regions in the salience network and cortical regions (involved in decision making) (33); and within cortical brain areas involved with executive control (such as the cognitive control and attentional salience networks) (30, 33). Similarly, cocaine dependence has been associated with disruption among the default mode, salience and emotional networks where cocaine-dependent individuals displayed decreased connectivity between rostral ACC and salience network; posterior cingulate cortex (PCC) and executive control network (ECN); and bilateral insula and default mode network (DMN) (34). Moreover, compared to controls, the ventral striatum of individuals with cocaine dependence exhibited reduced FC with the hippocampal, parahippocampal gyrus, vmPFC, and increased FC with the visual cortex (35). In alcohol dependence, individuals are often characterized by an impulsive drive to consume alcohol and a lack of self-control towards its consumption despite negative consequences (36). Evidence shows that individuals with alcohol dependence showed increased within-network FC in the salience network (SN) (including insula, hippocampus, and temporal lobe); anterior DMN (including superior frontal gyrus (SFG), ACC, medial frontal gyrus (MFG), and superior medial gyrus); posterior DMN (involving middle cingulate cortex, PCC, precuneus, insula, caudate, superior temporal gyrus (STG), and thalamus); orbitofrontal cortex (OFCN) (including middle and superior orbital gyrus, insula, amygdala); amygdala-striatum (ASN) (including putamen, amygdala, caudate, hippocampus, and inferior temporal gyrus (IFG); and left executive control (LECN) networks (consisting of the angular gyrus) (36). Relative to controls, cannabis abusers demonstrated increased resting-state FC of subcortical regions. Specifically, the cannabis abusers displayed greater local functional connectivity density (lFCD) than controls in the ventral striatum (NAc location), midbrain (SN/VTA location), brainstem, and thalamus (37). Results from a study investigating FC of the DMN revealed increased FC in the right hippocampus, while reduced FC was found in the right dorsal ACC and left caudate of chronic heroin users relative to controls (21). Increased FC was observed between dorsal ACC (dACC)-right anterior insula (AI), the dACC-thalamus, the dACC-left AI, and the right AI-left AI of nicotine addicts. Increased FC was associated with risky decision making (38).

The effect of BQ use on brain functional connectivity during acute administration is not well understood. Studies investigating the acute effects of BQ have largely focused on the frontal and default mode networks, giving subcortical regions less attention. For instance, based on previous findings from independent component analysis (ICA), acute use of BQ among naïve chewers was associated with increased and decreased FC in the frontal and default mode networks respectively (39). Evidence from addiction studies has linked initial drug use with activation of the reward pathway which primarily involves the interaction between subcortical and frontal cortical structures (6). Additionally, resting-state fMRI studies investigating chronic effects of BQ in the brain have yielded inconsistent results. For instance, compared to controls, individuals with betel quid dependence (BQD) had decreased FC in the DMN (40, 41), parietal network (42), and between the anterior cingulate cortex (ACC) and DMN (43); while increased connectivity was mostly displayed in networks including the visual (41), frontoparietal, occipital/parietal, frontotemporal, temporal/limbic, and frontotemporal/cerebellum (42), and between the ACC and regions of the reward network (41). The different FC results may have been influenced by differences in subjects across studies (sample size, age, gender, variations in BQ preparation, dependence level, duration of BQ exposure and the use of other substances, e.g., alcohol and tobacco) and use of different analysis methods, such as ICA (39, 40, 42), functional connectivity density mapping (44), graph theoretical analysis (GTA), and network-based statistics (NBS) (41).

Persistent psychoactive substance use has been linked with impaired brain function which disrupts the ability to wield self-control over drug use behaviors that typifies addiction (6).

Previous neuroimaging studies have investigated separately the acute and chronic effects of BQ on brain functional connectivity. Specifically, acute and chronic effects of BQ were mostly explored in the DMN and different parts of the brain respectively. This is the first study to examine both the acute and chronic effects of BQ concurrently. We explored the whole brain rather than predefined systems, with the aim of elucidating the impact of both initial and chronic BQ use on brain FC. Specifically, our first aim was to examine functional connectivity during initial BQ use among naïve chewers. Second, we aimed to explore the differences in FC between the naïve and BQ dependent chewers. We used NBS to identify FC differences (45). The results may provide further evidence and understanding of the neural mechanisms involved during initial BQ chewing and BQD.

MATERIALS AND METHODS

Aim, Design, and Setting of the Study

This is an observational neuroimaging study that aimed to examine the effects of both acute and chronic BQ chewing in the whole brain. Recruitment of participants and data collection was carried out between January 2015 and March 2016 at the Second Xiangya Hospital of Central South University, located in Changsha city, Hunan Province, China.

Characteristics of Participants

All participants in this study were male. The following criteria for inclusion and exclusion of participants have been described in our previous papers (39, 42). Twenty-five individuals with BQD had to meet the following inclusion criteria: (1) 18–40 years of age; (2) Han Chinese ethnicity; (3) accomplished nine or more years of education; (4) right-hand dominant; (5) diagnosed with BQD as individuals using BQ at least 1 day at a time for more than 3 years and with a score of 5 or higher on the Betel Quid Dependence Scale (BQDS). The BQDS is a 16-item self-

administered tool made up of three parts: physical and psychological urgent need, increasing dose and maladaptive use (46). Exclusion criteria included: (1) a history of neurological disorder or other serious physical illness; (2) a history of any mental disorders; (3) a history of substance abuse other than BQ; (4) a contraindication to MRI.

Thirty healthy controls were enrolled from the community in the Changsha City area. The inclusion and exclusion criteria for controls corresponded to those of the BQD group. The only exception was that controls would not have a diagnosis of BQD or have a family history of psychiatric illness amongst their first-degree relatives. All study participants were asked not to use any psychoactive substance during the 24-h period prior to scanning.

BQ can induce some physiological and psychological changes to users. But a half fruit of BQ is unlikely to induce severe adverse effects in healthy young men, even if used for the first time. We recorded the participants' heart rates and blood pressures just before the first scan and right after the second scan (about 30 min after using the betel quid) so as to monitor and rule out any physiological changes to users. Statistical analysis showed that there were no significant differences between the first and second measures of heart rate or blood pressure (**Table 1** below). It has been reported that "The onset (of physiological effect) was within 2 min after chewing, peak effect was reached within 4–6 min and the effect lasted for an average of 16.8 min (47)." The absence of changes in heart rate or blood pressure may have resulted from the long interval (about 30 min) between the betel quid chewing and the recording. We also administered behavior questionnaires including the Beck Depression Inventory and Beck Anxiety Inventory before betel quid chewing to assess the participants' emotional status.

This study was conducted in accordance with recommendations of the Helsinki Declaration established in 1964, and its later amendments or comparable ethical standards. Approval to conduct this study was obtained from the Ethics Committee of the Second Xiangya Hospital of Central South University. Before inclusion in the study, written informed consent was provided by each participant.

Image Acquisition and Preprocessing

HC1 and BQD1 were defined as controls and participants with BQD respectively, who were scanned before BQ chewing. HC2 and BQD2 were defined as controls and participants with BQD respectively scanned after BQ chewing. In theory, we can compare any pair of conditions. However, in the main text, we describe the results for HC1 versus HC2 and HC1 versus BQD1. The results for other comparisons are shown in the supplementary materials. The following explanation about image acquisition and preprocessing parameters have also been described in our previous papers (39, 42). Resting-state fMRI scans were carried out for all participants before and after BQ chewing. HC1 and BQD1 were asked to chew the dried BQ along with its husk and swallow the saliva quickly in no more than 3 min. The BQ was an industrially wrapped product that has been described before by (48). Subsequently, the residual BQ was spat out, and 3 min later participants underwent the second fMRI scan which resulted in HC2 and BQD2.

TABLE 1 | Demographics and clinical characteristic of participants.

	BQD (Mean ± SD)	HC (Mean ± SD)	t/χ^2	*P*-value
Age (years)	23.50 (3.88)	24.93 (2.60)	−1.58[a]	0.12
Gender (male/female)	24/0	28/0		
Education (years)	15.13 (1.73)	16.26 (1.32)	−2.66[a]	0.01*
Betel Quid Dependence Scale	7.58 (2.17)	N/A		
Duration of Betel Quid (years)	7.13 (3.79)	N/A		
Beck Depression Inventory	10.38 (6.75)	3.75 (4.60)	4.20[a]	0.00*
Beck Anxiety Inventory	28.588(6.25)	23.11 (2.64)	4.45[a]	0.00*

SD, standard deviations; N/A, not applicable.
[a]*Independent-samples t-test.*
**P < 0.05.*

Resting-state images were obtained from a Philips Gyroscan Achieva 3.0-T scanner in the axial direction. The following imaging parameters were used for the gradient-echo echo-planar imaging sequence: matrix size = 64 × 64, repetition time = 2,000 ms, echo time = 30 ms, flip angle = 90°, gap = 0 mm, field of view = 24 cm × 24 cm, number of slices = 36, and slice thickness = 4 mm. Earplugs and foam pads were utilized to lessen scanner noise and head motion respectively. Participants were asked to lie flat on their back motionless with their eyes closed. The maximum time for each resting-state fMRI scan was 500 s, and generally, 250 image volumes were acquired.

The Data Processing Assistant for Resting-State fMRI (DPARSF) toolbox (49) was utilized to preprocess the fMRI imaging data by way of Statistical Parametric Mapping (SPM8) (50). The first 10 images were removed to allow for scanner adjustment and for participants to gain familiarity with the scanner environment. Slice-timing correction and realignment for the head motion were performed to the residual 240 image volumes. The following measures were taken to minimize the effect of head motion on functional connectivity: First, the following criteria had to be met for realignment (1): a maximum displacement in the x, y, or z-axis of less than 2 mm and (2) angular rotation about each axis of less than 2°. Initially, the scan was performed among 25 BQD and 30 HCs, nevertheless, 1 BQD participant and 2 HCs had to be excluded from the study owing to greater than 2° and 2mm of rotations and translations respectively during fMRI scanning. Second, we utilized the Friston 24-parameter model (51) to regress out head motion effects from the realigned data (i.e., 6 head motion parameters, 6 head motion parameters one-time point before, and the 12 corresponding squared items) based on recent reports that higher-order models demonstrate benefits in removing head motion effects (52). Third, the head motion was also controlled at the group-level by using the mean framewise displacement (FD) as a covariate. These measures were strict enough to control artifacts caused by head movements. We compared head motion between the BQD1-2 and HC1-2, which was measured by mean FD derived from Jenkinson's formula (53), and no difference was detected between the groups. A scrubbing procedure was performed, where we calculated DVARS (a temporal derivative of time courses and variance across voxels) (54) to measure the rate of change of the BOLD signal across the entire brain for each frame of data. This revealed only a very small

proportion of our data had movement contamination. When we compared the results obtained from the original data and the movement scrubbed data, there were no notable differences. Thus, all the results are obtained from the original data in this paper.

The data were spatially normalized into standard coordinates using the Montreal Neurological Institute echo-planar imaging template in the SPM package and was then resampled into 3 mm × 3 mm × 3 mm voxels. The preprocessed images were smoothed using a 4mm Gaussian kernel before the statistics. Subsequently, the BOLD signal of each voxel was first detrended to eliminate any linear trend. These signals were then passed through a band-pass filter of 0.01–0.08 Hz to decrease low-frequency drift and high-frequency physiological noise. Lastly, nuisance covariates (Friston 24-head motion parameters, white matter and cerebrospinal signals) were regressed out from the BOLD signals.

Whole-Brain Functional Network Construction

The revised automated anatomical labeling atlas (AAL2) (55) was used to parcellate the brain into 94 regions of interest (ROI) (47 in each hemisphere). The mean time courses were obtained from each ROI by extracting the signal average of all voxels within the region. The AAL2 atlas provides an upgraded parcellation of the orbitofrontal cortex for the automated anatomical labeling atlas (56). The new parcellation of the orbitofrontal cortex is based on anatomical evidence (57). The anatomical regions defined in each hemisphere and their labels in the AAL2 are provided in the supplementary materials (**Table S4**).

Acute Impact of BQ

The acute impact of BQ was estimated by comparing HC1 versus HC2. Pearson correlation coefficients were calculated between all pairs of ROIs, to acquire 94 × 94 correlation matrices r_{ij},i, j = 1, 2….,94, indicating the FC strength for each pair (connectivity between any two brain regions) of regions for each participant. Then, the FC with significant differences (p-value of less than 0.05) before and after chewing BQ were selected by performing a paired t-test and the difference network was constructed. The number of all FCs for each node in the different network was defined as the degree of this brain region.

Differences of Functional Connectivity in Chronic BQ Users and Controls

These differences were estimated by comparing the difference between HC1 vs BQD1. The 94 × 94 Pearson correlation coefficients were initially calculated between all pairs of ROIs. Then, FCs with significant differences (p-value of less than 0.05) between HC1 and BQD1 were selected by performing a two-sample t-test and the difference network was constructed. The number of all FCs for each node in the difference network was defined as the degree of this brain region.

Network-Based Statistics

At present, studies using neuroimaging data to construct functional or structural networks are many, and most of them are aimed at finding different connections between the two groups of networks. When we test each connection in the graph of the network at the same time, the family-wise error rate is generated. The network-based statistic is an effective way to control the family-wise error rate, depending on the degree of association between the connections of interest (45). The specific steps are as follows. First, a Fisher's r to z transform for each connection in the network was performed, and a t-test was performed for the differences between the two groups for each connection. The test statistic computed for each pairwise association was then thresholded to formulate a set of suprathreshold links. Components present in the set of suprathreshold links were ascertained using a breadth-first search, and the number of links they comprise (or size) was stored. Thereafter, permutation testing was used to assign a p-value controlled for the FWE to each connected component based on its size. A total of M random permutations was created independently, where for each permutation, a random exchange was done for the group to which every participant belongs. The required test statistic for each permutation was recalculated, then the same threshold was applied to define a set of suprathreshold links. The maximal component size in the set of suprathreshold links extracted from each of the M permutations was ascertained and stored, thereby earning an empirical estimate of the null distribution of maximal component size. Lastly, to estimate the p-value of an observed component of size k, the total number of permutations was detected showing a greater maximal component size than k and normalizing by M. Networks with significant inter-group differences were detected if the p-value was smaller than the given 0.05 threshold.

Support Vector Machine (SVM) Classifier

In order to study how much difference there is between the different groups, we employed a widely used SVM classifier. SVM is a learning machine for two-class problems for pattern classification analysis.

We used an SVM toolkit called libsvm composed by Chih-Jen Lin from Taiwan University (58) (http://www.csie.ntu.edu.tw/~cjlin/libsvm/). Specifically, the whole brain FC was applied to the raw input matrix. Features that appeared statistically significant (a smaller p-value than the threshold for a two-sample t-test) were picked. Various types of kernel (linear, t=0; polynomial, t=1; radial basis function, t=2) and different trade-off parameter C (0.001, 0.01, 0.1, 1, 10, 100, 1,000, 10,000) were tried to attain the highest accuracy rate. A leave-one-subject-out cross-validation technique was applied to ascertain how the test performs as well as to validate the classifier, where the classifier was trained on all subjects except one, who was then used for the test data. The mean discrimination accuracy, sensitivity, specificity and AUC (area under ROC curve) were obtained for the entire sample.

Selecting the generalization rate as the statistic, permutation tests were employed to estimate the statistical significance of the observed classification accuracy. In the permutation testing, the class labels of the training data were randomly permuted prior to training. Cross-validation was then performed on the permuted

training set, and the permutation was repeated 100 times. The *p*-value represents the probability of observing a classification prediction rate in the permutation testing no less than the discrimination accuracy. If the *p*-value is smaller than the significance level, we reject the null hypothesis that the classifier could not learn the relationship between the data and the labels reliably and declare that the classifier learns the relationship with a probability of being wrong of at most *p*.

RESULTS

The mean age for BQD chewers and HC was 23.5 ± 3.88 years and 24.9 ± 2.60 years respectively. Individuals with BQD displayed a mean BQDS score of 7.58 ± 2.17 and a mean duration of BQ use of 7.13 ± 3.79 years (**Table 1**).

Acute Impact of BQ

We used the NBS method to assess specific network connections for acute impact. Compared with HC1, HC2 displayed higher functional connectivity strength between subcortical regions including the basal ganglia and thalamus, and occipital brain regions, after chewing BQ as shown in **Figure 1A**. The brain regions comprised of 37 nodes and 55 connections that included many connections involving the basal ganglia (corrected p value < 0.001). The ROIs with the highest degree are shown in **Figure 1B** including bilateral caudate (CAU), thalamus (THA), left putamen (PUT), bilateral superior occipital gyrus (SOG) and middle occipital gyrus (MOG). Because the right caudate has the biggest degree in **Figure 1**, it was used as an example to calculate the connectivity between the right caudate and the other voxels in the whole brain. We performed this analysis to show whether the voxel-wise analysis is consistent with the NBS analysis. We used a pairwise t-test to compare the difference between HC1 and HC2. The t map (link-wise FDR corrected, q=0.05) is shown in **Figure 2**. A significant difference was detected with connectivity involving the caudate and putamen. No association was found between the baseline scores and FCs.

Differences of Functional Connectivity in Chronic BQ Users and Controls

Using the NBS method, higher functional connectivity strength in BQD1 compared with HC1 was found between the temporal, parietal and prefrontal brain regions, as shown in **Figure 3**. The regions comprised of 55 nodes and 79 connections (corrected p-value is 0.035). The ROIs with the highest degree are shown in **Figure 3B** including the right medial OFC, right lateral OFC, angular gyrus, superior parietal gyrus (SPG), SFG, and bilateral ITG. There was no association between the baseline scores and FCs.

Significant links during acute and chronic BQ chewing are provided in supplementary materials 456 (**Figure S1** and **Table S2**).

Network-Based Classification

Receiver operating characteristic curves (ROC) were charted for network classification analysis, so as to ascertain whether graph-based network metrics might act as biomarkers for discriminating different groups. The ROC analysis was performed for each metric (i.e., one-dimensional characteristic) displaying significant differences between groups. For each particular metric, a range of thresholds was employed to allocate each participant into either the first or the second group. An initial linear discriminant analysis was carried out to yield an overall estimate of group separation. The highest degrees of separability (AUC) were observed between HC1 and HC2 (0.7551), as well as between HC1 and BQD2 (0.8646). HC2 versus BQD2 and BQD1 versus BQD2 portrayed the lowest AUC (**Table S3** and **Figure S2** in supplementary materials).

DISCUSSION

This study identifies the neurobiological effects involved in the initial acute effects of BQ chewing and in differences in those who are BQ dependent from controls when BQ was not being administered. For the purpose of this study, we only compared HC1 versus HC2, and HC1 versus BQD1, because our interest lies in the acute impact of BQ chewing, and in differences between long-term BQ and non-BQ users. NBS was used because it is a more sensitive approach than FDR.

The results from the SVM showed that the biggest difference between groups was observed between healthy controls who did not chew BQ and individuals who chewed BQ. For instance, HC1 versus BQD2 and HC1 versus HC2 have greater AUC values compared to those who chewed BQ (HC2 versus BQD2 and BQD1 versus BQD2). A small difference was detected between those who chewed BQ. Previous studies have also reported the difference in connectivity between BQ dependent chewers and healthy controls (41–43), as well as between non-chewer healthy controls and healthy controls who chewed BQ (39). This is consistent with the hypotheses that BQ can alter the brain once it is consumed; or with the hypothesis that there are differences between individuals that lead some to consume BQ. AUC has previously been suggested as the preferred measure of diagnostic accuracy in psychiatry and forensic psychology, with reports considering AUC values greater than 0.7 as having strong effects in test performance (59).

Effects of Acute BQ Chewing on Brain Functional Connectivity

Increased functional connectivity among naive BQ chewers was mostly observed between subcortical regions including the basal ganglia and thalamus (CAU, PUT.L, and THA) and the visual cortex (SOG and MOG.R). This effect of BQ is consistent with previous reports about increased activity in these regions during acute cocaine administration (60). For the majority of psychoactive drugs, the acute effects involve the activation of reward pathways (6). The reward pathways in the brain include the basal ganglia (including the striatum), the limbic system (amygdala) and parts of the PFC (61). The basal ganglia are known for modulating the rewarding effects of drug use and also play a role in habit formation (dorsal striatum) (5). The striatum

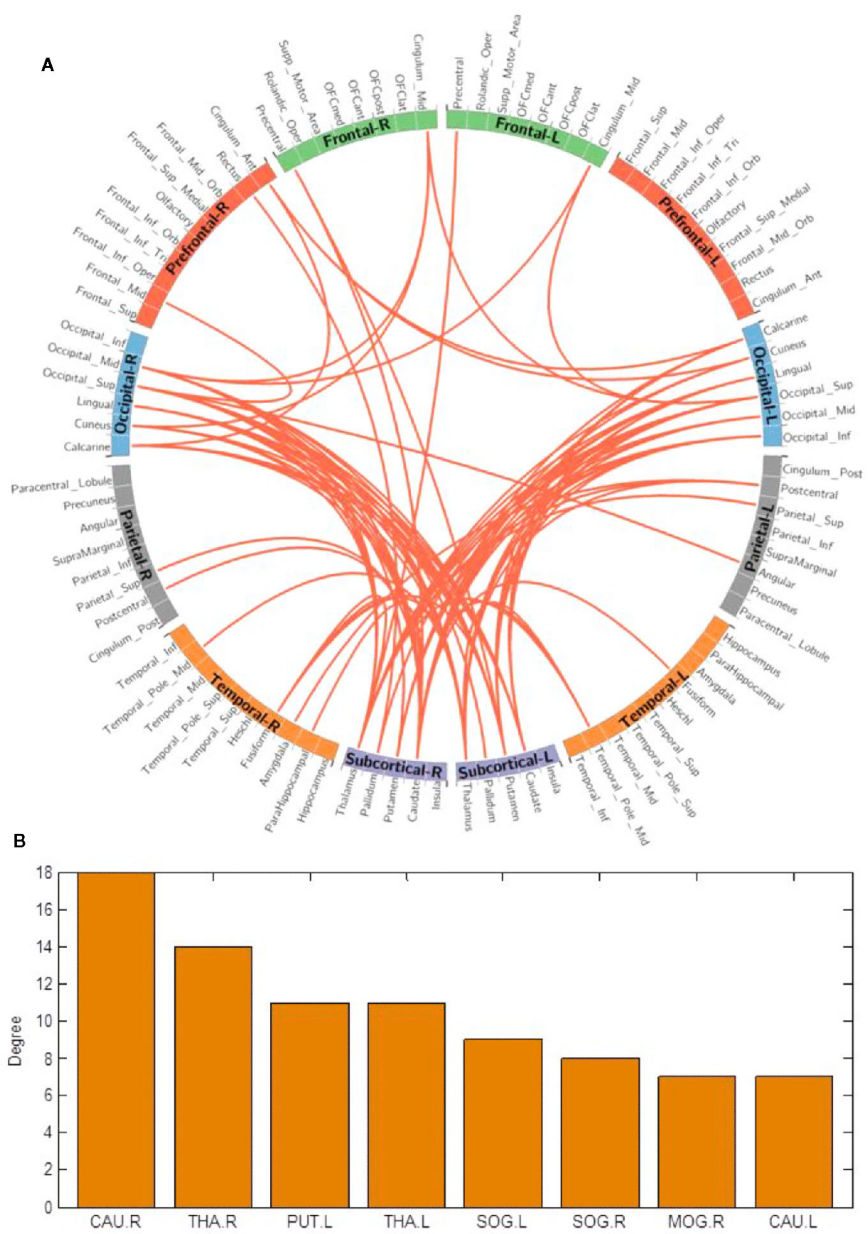

FIGURE 1 | (A) Network-based functional connectivity differences after acute administration of betel quid to naive participants. Orange indicates an increase in functional connectivity which was found between the subcortical and occipital brain regions. **(B)** The degree of different areas for acute use (ROIs with the highest degree). CAU, caudate; L/R, left/right; MOG, middle occipital gyrus; PUT, putamen; SOG, superior occipital gyrus; THA, thalamus.

is involved in reward-related learning, as well as contributing to the development and maintenance of addictive behaviors (62). In particular, the putamen and caudate of naive BQ chewers demonstrated significantly increased FC, portraying the role of the striatum in the reward pathway during acute drug administration (6). DA neurons in the VTA play an important role in processing drug rewards (63), and increased DA in the striatum has been linked with subjective feelings of pleasure, euphoria, or a "high" resulting from drug use (64) and alcohol-associated cues (65). Our results agree with previous studies where activation of the ventral striatum significantly correlated with smoking motivation for pleasurable relaxation (66), supporting the reported psychological effects experienced immediately after BQ chewing (2). Similarly, acute alcohol influences neuronal activity in the ventral striatum which is known to project to regions believed to regulate motor responses, motivation and executive functions (67). Compared to non-users, individuals with substance use disorders displayed

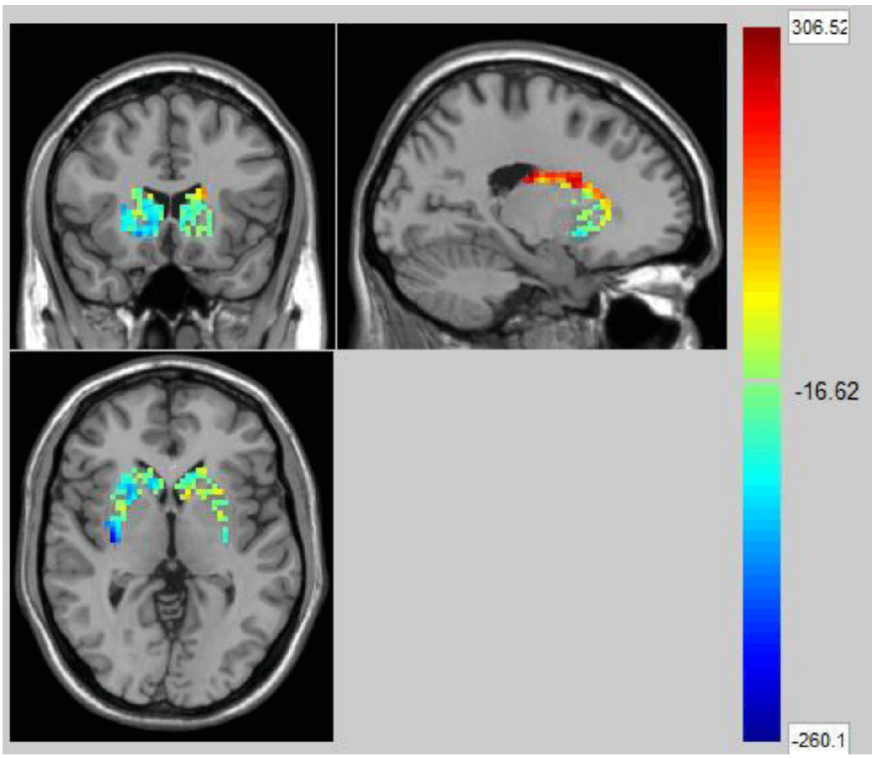

FIGURE 2 | The t map (link-wise FDR corrected, q=0.05) in Healthy Controls before and after acute betel quid chewing. A significant difference was detected with connectivity between the caudate and putamen. The colorbar represents the t value for each region of interest (ROI).

reduced functional connectivity between the nucleus accumbens and the frontal cortical regions responsible for controlling cognition (68). Such findings provide evidence that differences in the connections between the reward processing and cognitive-behavioral control areas may play a crucial role in the development of substance use disorders including betel quid dependence.

Compared to the frontal and striatal brain areas, the visual cortex (69) has received attention to a lesser degree in substance use and addiction neuroimaging studies. Our study found significantly increased FC involving the visual cortex of controls immediately after BQ chewing, which is consistent with results by Huang et al. (39) and also backing up the reported heightened alertness experienced by BQ chewers (8). Increased FC in the visual cortex has also been demonstrated after acute alcohol consumption (70). We suggest that BQ may enhance alertness which in turn activates the visual cortex, however, this requires further investigation. Drug cue exposure studies have also documented activation of the visual cortex in substance abusers when presented with visual drug cues as compared to neutral cues (71).

Differences of Functional Connectivity in Chronic BQ Users and Controls

Our study found significantly higher FC in the networks involving the right medial OFC, right lateral OFC, and right SFG of BQ dependent individuals. Analogous results have been reported by (39). The OFC, whose disruption leads to maladaptive and impulsive decision making (72), is known for its function in signaling the value of expected outcomes or consequences (73), motivational behavior (74), salience attribution (75), emotional regulation, and decision making (together with the amygdala and insula) (61, 76, 77). It has numerous projections to the striatum (75), and each of its sub-regions performs distinct functions; for example, the OFCmed is known for its role in monitoring reward stimuli whereas the lateral OFC evaluates punishing stimuli (78). For instance, individuals carrying out a monetary decision-making task exhibited activation of the OFCmed to positive reward outcome whereas activation of the lateral OFC was observed during monetary loss outcome (79). Addiction studies have also shown that the enhanced expectation value of a drug in the reward (ventral pallidum, NAc, and VTA), motivation (medial OFC, VTA, ventral ACC, dorsal striatum, SN, and motor cortex), and memory (medial OFC, amygdala, dorsal striatum, and hippocampus) circuits overcomes the control circuit (dlPFC, inferior frontal cortex, ACC, and lateral OFC) resulting in compulsive drug use and loss of control (80). Furthermore, compared to controls, individuals with cocaine dependency showed significantly decreased interhemispheric resting-state functional connectivity of the prefrontal cortex and the dorsal attention network encompassing medial premotor and posterior

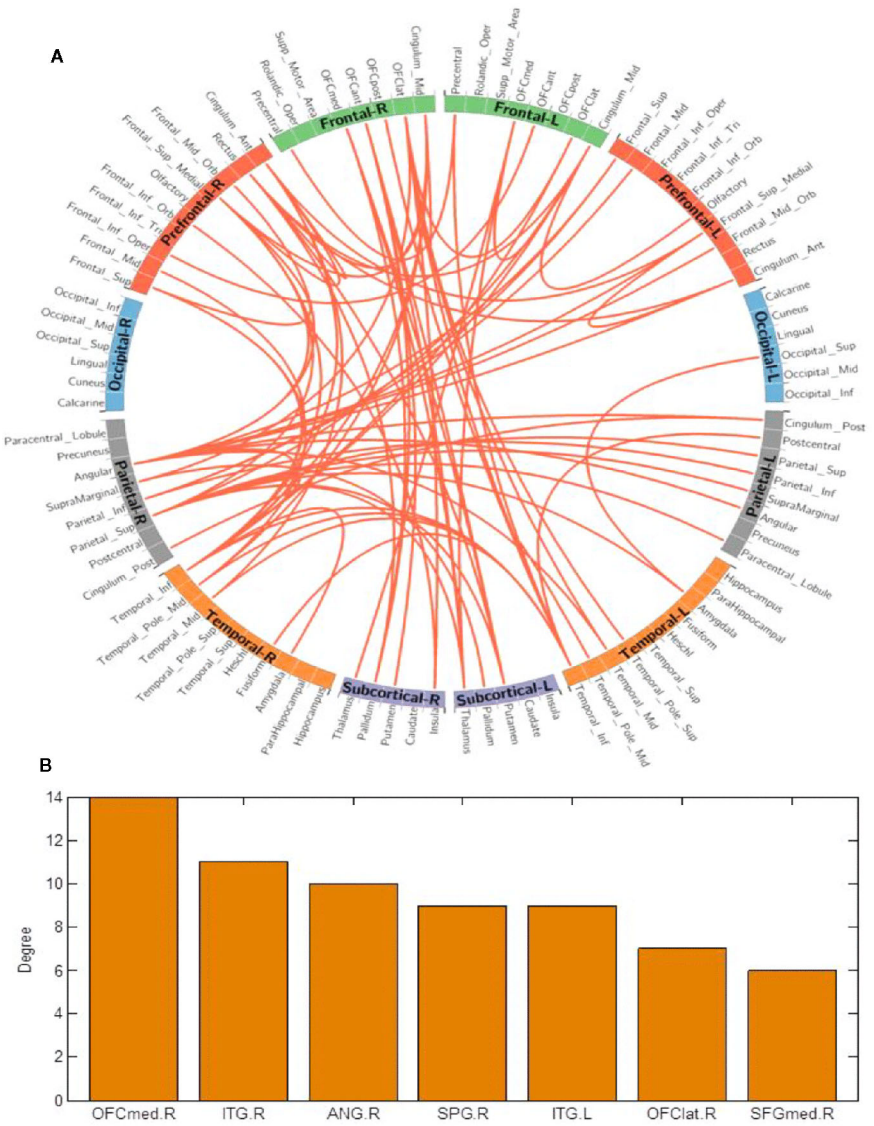

FIGURE 3 | (A) Network-based connection differences for chronic betel quid users minus controls. Orange indicates an increase in functional connectivity which was found between the frontal, parietal and temporal brain regions. **(B)** The degree of different areas for chronic use [regions of interest (ROIs) with the highest degree] The right OFCmed is the combination of the sum degree of rectus, OFCmed, OFCant, and OFCpost). ANG, angular gyrus; ant/post, anterior/posterior; ITG, inferior temporal gyrus; L/R, left/right; med/lat, medial/lateral; OFC, orbitofrontal cortex; SFG, superior frontal gyrus; SPG, superior parietal gyrus.

areas, as well as the bilateral frontal (30). Additionally, resting-state studies have portrayed dysfunctional network connectivity across the brain during both acute and chronic nicotine exposure, where the effects mostly appeared to involve the networks linked with attention, cognitive control, ACC, and insula (81). This relates to the enhanced attention that is commonly experienced by smokers (81) and continues to support the notion that substance use is associated with various alterations in connectivity between significant regions of the brain. The brain reward system is not only activated by the drugs, but also stimuli associated with the substance's rewarding effects, such as drug-associated cues. These stimuli can trigger the urge to use drugs (incentive salience) by activating the DA system on their own. The DA levels tend to persist even after the rewarding effects of the drugs have declined (5). Imaging studies of cocaine-addicted individuals have reported higher activity in the PFC during drug expectation than during drug administration (15, 60). This is in agreement with our hypothesis that the expectation value of BQ after 24 h of abstinence in dependent individuals was enhanced and may have contributed to the observed increased FC found in this investigation. Our study found increased FC in the amygdala whose key role is to control stress reactions and negative emotions (82). Therefore, the 24 h abstinence in BQ dependent individuals may have

triggered unpleasant feelings associated with withdrawal symptoms which are believed to originate from reduced activation in the reward network of the basal ganglia and increased activation of the stress system including stress neurotransmitters (corticotropin-releasing factor, norepinephrine, and dynorphin) (83) in the amygdala (84). There is evidence that all abused substances tend to disrupt the dopamine reward system when used for a long time (6). For instance, addicts in imaging studies have constantly demonstrated long-term decreased D2 dopamine receptor, compared with non-addicts (85). The overall loss of reward sensitivity may explain compulsive drug use seen in addicts as a way to experience the pleasurable feelings the reward system formerly exerted (86). The desire to get rid of the negative feelings accompanying withdrawal may therefore reinforce continual drug use like the one demonstrated in individuals with BQD. Additionally, compared to HC1 versus HC2, the FC observed in the subcortex between HC1 and BQD1 groups was not significantly increased. This may be due to reduced D2 dopamine receptors (85) in individuals with BQD, which makes them less sensitive to BQ and therefore increases their compulsivity.

We also found increased FC in the right medial SFG, which mirrors a reduced efficiency of response inhibition processes in the PFC (87). The SFG is involved in planning, and motivation, as well as contributing to both stimulation and inhibition of craving. Its activation during responding to smoking cues versus neutral cues is highly correlated with participants' reports of craving (88), suggesting that time spent without BQ may have stimulated craving and thus activated the SFG in the BQD group.

Increased FC was observed in the right angular gyrus and right SPG of BQ dependent individuals. Our results are similar to other cocaine studies that have demonstrated increased FC between frontal–temporal and frontal–parietal brain regions of abstinent chronic cocaine users (89). Similarly, compared to people who have never smoked and former nicotine smokers, current smokers had greater connectivity in the right superior parietal lobe located in the dorsal attention network (90). The dorsal attention network has been linked with attention processing, predominantly in employing top-down control over fundamental sensory operations including visual information and maybe a crucial location for distorting attention (91). Therefore, greater connectivity in this area may indicate an increased propensity to focus one's attention on external signals (90), which may make it harder to abstain from BQ. The angular gyrus plays a crucial role in comprehension, reasoning (92), attention, language memory and self-awareness as well as providing information about self-awareness in the default mode network (DMN) (93). Addicts with dysfunctional DMN may exhibit impairment in disease awareness, need for professional help, and/or drug-seeking behavior (94) which supports what is often depicted in BQD behavior.

The results from this study also demonstrated increased FC in the right ITG. The ITG and SPG are involved in visual and auditory processing (95), and the increased FC in these regions in this study may relate to a perceived improvement in visual and auditory abilities in chronic BQ chewers. Such experiences may facilitate maintenance of BQ chewing, thus leading to dependent behavior.

A number of limitations are noted. First, our study was cross-sectional: we only observed functional connectivity differences in naive and chronic BQ chewers, but cannot infer causality. Future longitudinal neuroimaging BQ studies are crucial to consider the mechanisms fundamental for the neuro-transition from initial BQ use to dependence. Second, the use of other substances, such as cigarettes or alcohol could have influenced the results even though all recruited participants met the inclusion and exclusion criteria. Third, for BQ dependent individuals, we did not take into account the influence of craving on functional connectivity and the duration since last BQ use; which might influence the results. Fourth, for the investigation of the acute effects of chewing betel, it would be useful in future studies to have a control group that did not chew betel but was otherwise scanned similarly.

CONCLUSION

This is the first study to examine the acute and chronic effects of BQ concurrently. In controls the effect of acute BQ chewing significantly increased functional connectivity between subcortical regions (including the caudate, putamen, pallidum and thalamus); and visual brain regions (including the bilateral superior occipital gyrus and right middle occipital gyrus networks). These increases may relate to the acutely rewarding and visual effects of betel produced by its arecoline. In habitual users of betel, networks comprising the right medial OFC, right lateral OFC, bilateral inferior temporal gyrus, right angular gyrus, superior parietal gyrus, and right medial superior frontal gyrus had higher functional connectivity as compared to the controls before BQ chewing. These differences may be related to the craving for betel.

DATA AVAILABILITY STATEMENT

The raw data supporting the conclusions of this article will be made available by the authors, without undue reservation, to any qualified researcher.

ETHICS STATEMENT

The studies involving human participants were reviewed and approved by the Ethics Committee of the Second Xiangya Hospital of Central South University. The patients/participants provided their written informed consent to participate in this study.

AUTHOR CONTRIBUTIONS

XH designed the study and collected data. XH and SG analyzed the data. AS, XH, and SG prepared the first draft of the manuscript. AS, XH, SG, ER, and ZL critically revised the content of the manuscript. WP, JZ, HL, and ZX actively participated in writing and revising the manuscript. All authors read and approved the final manuscript.

FUNDING

This study was supported by the China Precision Medicine Initiative (2016YFC0906300) and the National Natural Science Foundation of China (Grant nos. 81561168021, 81471362, 81671335, 81701325, 81801353, 11671129, 31671134).

ACKNOWLEDGMENTS

The authors gratefully acknowledge Professor Zhong He from the Department of Radiology, Second Xiangya Hospital, Central South University for his assistance in imaging data acquisition, and Professor Jianfeng Feng from the Centre for Computation Systems Biology, Fudan University, for revising this paper and his guidance in fMRI data analysis.

SUPPLEMENTARY MATERIAL

The Supplementary Material for this article can be found online at: https://www.frontiersin.org/articles/10.3389/fpsyt.2020.00198/full#supplementary-material

REFERENCES

1. Boucher BJ, Mannan N. Metabolic effects of the consumption of Areca catechu. *Addict Biol* (2002) 7(1):103–10. doi: 10.1080/13556210120091464
2. Osborne PG, Chou T-S, Shen T-W. Characterization of the Psychological, Physiological, psychological and EEG profiles of Acute Betel Quid Intoxication naive subjects. *PloS One* (2011) 6(8):1–11. doi: 10.1371/journal.pone.0023874
3. Garg A, Chaturvedi P, Mishra A, Datta S. A review on harmful effects of pan masala. *Indian J Cancer* (2015) 52(4):663. doi: 10.4103/0019-509X.178449
4. Nestler EJ. Is there a common molecular pathway for addiction? *Nat Neurosci* (2005) 8(11):1445–9. doi: 10.1038/nn1578
5. U.S. Department of Health and Human Services (HHS), Office of the Surgeon General. *Facing addiction in America: The Surgeon General's Report on Alcohol, Drugs, and Health*. Washington, DC: HHS; (2016), 1–413.
6. Volkow ND, Morales M. The Brain on Drugs: From Reward to Addiction. *Cell* (2015) 162(4):712–25. doi: 10.1016/j.cell.2015.07.046
7. Everitt BJ. Neural and psychological mechanisms underlying compulsive drug seeking habits and drug memories - indications for novel treatments of addiction. *Eur J Neurosci* (2014) 40(1):2163–82. doi: 10.1111/ejn.12644
8. Chu N-S. Effects of betel chewing on the central and autonomic nervous systems. *J Biomed Sci* (2001) 8(3):229–36. doi: 10.1007/BF02256596
9. Bendor J, Lizardi-Ortiz JE, Westphalen RI, Brandstetter M, Hemmings HC, Sulzer D, et al. AGAP1/AP-3-dependent endocytic recycling of M5 muscarinic receptors promotes dopamine release. *EMBO J* (2010) 29(16):2813–26. doi: 10.1038/emboj.2010.154
10. Yang K, Buhlman L, Khan GM, Nichols RA, Jin G, McIntosh JM, et al. Functional Nicotinic Acetylcholine Receptors Containing 6 Subunits Are on GABAergic Neuronal Boutons Adherent to Ventral Tegmental Area Dopamine Neurons. *J Neurosci* (2011) 31(7):2537–48. doi: 10.1523/JNEUROSCI.3003-10.2011
11. Sulzer D. How Addictive Drugs Disrupt Presynaptic Dopamine Neurotransmission. *Neuron* (2011) 69(4):628–49. doi: 10.1016/j.neuron.2011.02.010
12. Shina JH, Adrovera MF, Wessb J, Alvareza VA. Muscarinic regulation of dopamine and glutamate transmission in the nucleus accumbens. *PNAS* (2015) 112(26):8124–9. doi: 10.1073/pnas.1515368112
13. Saddoris MP. Rapid dopamine dynamics in the accumbens core and shell Learning and action. *Front Biosci* (2013) E5(1):273–88. doi: 10.2741/E615
14. Wise RA. Roles for nigrostriatal—not just mesocorticolimbic—dopamine in reward and addiction. *Trends Neurosci* (2009) 32(10):517–24. doi: 10.1016/j.tins.2009.06.004
15. Kufahl PR, Li Z, Risinger RC, Rainey CJ, Wu G, Bloom AS, et al. Neural responses to acute cocaine administration in the human brain detected by fMRI. *NeuroImage* (2005) 28(4):904–14. doi: 10.1016/j.neuroimage.2005.06.039
16. Wise RA. Dopamine, learning and motivation. *Nat Rev Neurosci* (2004) 5(6):483–94. doi: 10.1038/nrn1406
17. Tobler PN. Adaptive Coding of Reward Value by Dopamine Neurons. *Science* (2005) 307(5715):1642–5. doi: 10.1126/science.1105370
18. Goldstein RZ, Volkow ND. Dysfunction of the prefrontal cortex in addiction: neuroimaging findings and clinical implications. *Nat Rev Neurosci* (2011) 12(11):652–69. doi: 10.1038/nrn3119
19. Sutherland MT, McHugh MJ, Pariyadath V, Stein EA. Resting state functional connectivity in addiction: lessons learned and a road ahead. *NeuroImage* (2012) 62(4):2281–95. doi: 10.1016/j.neuroimage.2012.01.117
20. Koob GF, Volkow ND. Neurobiology of addiction: a neurocircuitry analysis. *Lancet Psychiatry* (2016) 3(8):760–73. doi: 10.1016/S2215-0366(16)00104-8
21. Ma N, Liu Y, Fu X-M, Li N, Wang C-X, Zhang H, et al. Abnormal Brain Default-Mode Network Functional Connectivity in Drug Addicts. *PloS One* (2011) 6(1):e16560. doi: 10.1371/journal.pone.0016560
22. Wilcox CE, Teshiba TM, Merideth F, Ling J, Mayer AR. Enhanced cue reactivity and fronto-striatal functional connectivity in cocaine use disorders. *Drug Alcohol Depend* (2011) 115(1–2):137–44. doi: 10.1016/j.drugalcdep.2011.01.009
23. Upadhyay J, Maleki N, Potter J, Elman I, Rudrauf D, Knudsen J, et al. Alterations in brain structure and functional connectivity in prescription opioid-dependent patients. *Brain* (2010) 133(7):2098–114. doi: 10.1093/brain/awq138
24. Stein JL, Wiedholz LM, Bassett DS, Weinberger DR, Zink CF, Mattay VS, et al. A validated network of effective amygdala connectivity. *NeuroImage* (2007) 36(3):736–45. doi: 10.1016/j.neuroimage.2007.03.022
25. Bechara A. Decision making, impulse control and loss of willpower to resist drugs: a neurocognitive perspective. *Nat Neurosci* (2005) 8(11):1458–63. doi: 10.1038/nn1584
26. Everitt BJ, Robbins TW. Neural systems of reinforcement for drug addiction: from actions to habits to compulsion. *Nat Neurosci* (2005) 8:1481–9. doi: 10.1038/nn1579
27. Gu H, Salmeron BJ, Ross TJ, Geng X, Zhan W, Stein EA, et al. Mesocorticolimbic circuits are impaired in chronic cocaine users as demonstrated by resting-state functional connectivity. *NeuroImage* (2010) 53(2):593–601. doi: 10.1016/j.neuroimage.2010.06.066
28. Wang W, Wang Y, Qin W. Changes in functional connectivity of ventral anterior cingulate cortex in heroin abusers. *Chin Med J* (2010) 123(12):1582–8. doi: 10.3760/cma.j.issn.0366-6999.2010.12.019
29. Goldstein RZ, Leskovjan AC, Hoff AL, Hitzemann R, Bashan F, Khalsa SS, et al. Severity of neuropsychological impairment in cocaine and alcohol addiction: association with metabolism in the prefrontal cortex. *Neuropsychologia* (2004) 42(11):1447–58. doi: 10.1016/j.neuropsychologia.2004.04.002
30. Kelly C, Zuo X-N, Gotimer K, Cox CL, Lynch L, Brock D, et al. Reduced Interhemispheric Resting State Functional Connectivity in Cocaine Addiction. *Biol Psychiatry* (2011) 69(7):684–92. doi: 10.1016/j.biopsych.2010.11.022
31. Yuan K, Qin W, Dong M, Liu J, Sun J, Liu P, et al. Gray matter deficits and resting-state abnormalities in abstinent heroin-dependent individuals. *Neurosci Lett* (2010) 482(2):101–5. doi: 10.1016/j.neulet.2010.07.005
32. Hu Y, Salmeron BJ, Gu H, Stein EA, Yang Y. Impaired Functional Connectivity Within and Between Frontostriatal Circuits and Its Association With Compulsive Drug Use and Trait Impulsivity in Cocaine Addiction. *JAMA Psychiatry* (2015) 72(6):584. doi: 10.1001/jamapsychiatry.2015.1
33. Cisler JM, Elton A, Kennedy AP, Young J, Smitherman S, Andrew James G, et al. Altered functional connectivity of the insular cortex across prefrontal

networks in cocaine addiction. *Psychiatry Res: Neuroimaging* (2013) 213 (1):39–46. doi: 10.1016/j.pscychresns.2013.02.007
34. Liang X, He Y, Salmeron BJ, Gu H, Stein EA, Yang Y. Interactions between the Salience and Default-Mode Networks Are Disrupted in Cocaine Addiction. *J Neurosci* (2015) 35(21):8081–90. doi: 10.1523/JNEUROSCI.3188-14.2015
35. Zhang S, Li C-SR. Ventral striatal dysfunction in cocaine dependence – difference mapping for subregional resting state functional connectivity. *Transl Psychiatry* (2018) 8(1):119. doi: 10.1038/s41398-018-0164-0
36. Zhu X, Cortes CR, Mathur K, Tomasi D, Momenan R. Model-free functional connectivity and impulsivity correlates of alcohol dependence: a resting-state study: Functional connectivity and impulsivity correlates of alcohol dependence. *Addict Biol* (2017) 22(1):206–17. doi: 10.1111/adb.12272
37. Manza P, Tomasi D, Volkow ND. Subcortical Local Functional Hyperconnectivity in Cannabis Dependence. *Biol Psychiatry: Cogn Neurosci Neuroimaging* (2018) 3(3):285–93. doi: 10.1016/j.bpsc.2017.11.004
38. Wei Z, Yang N, Liu Y, Yang L, Wang Y, Han L, et al. Resting-state functional connectivity between the dorsal anterior cingulate cortex and thalamus is associated with risky decision-making in nicotine addicts. *Sci Rep* (2016) 6(1):1–9. doi: 10.1038/srep21778
39. Huang X, Liu Z, Mwansisya TE, Pu W, Zhou L, Liu C, et al. Betel quid chewing alters functional connectivity in frontal and default networks: A resting-state fMRI study: Betel Quid Alters Network Connectivity. *J Magnetic Reson Imaging* (2016) 45(1):157–66. doi: 10.1002/jmri.25322
40. Zhu X, Zhu Q, Jiang C, Shen H, Wang F, Liao W, et al. Disrupted Resting-State Default Mode Network in Betel Quid-Dependent Individuals. *Front Psychol* (2017) 8:1–9. doi: 10.3389/fpsyg.2017.00084/full
41. Weng J-C, Chou Y-S, Huang G-J, Tyan Y-S, Ho M-C. Mapping brain functional alterations in betel-quid chewers using resting-state fMRI and network analysis. *Psychopharmacology* (2018) 1–15. doi: 10.1007/s00213-018-4841-8
42. Huang X, Pu W, Liu H, Li X, Greenshaw AJ, Dursun SM, et al. Altered Brain Functional Connectivity in Betel Quid-Dependent Chewers. *Front Psychiatry* (2017) 8:1–9. doi: 10.3389/fpsyt.2017.00239/full
43. Liu T, Li J, Zhao Z, Zhong Y, Zhang Z, Xu Q, et al. Betel quid dependence is associated with functional connectivity changes of the anterior cingulate cortex: a resting-state fMRI study. *J Trans Med* (2016) 14(1):1–13. doi: 10.1186/s12967-016-0784-1
44. Liu T, Li J, Zhang Z, Xu Q, Lu G, Huang S, et al. Altered Long- and Short-Range Functional Connectivity in Patients with Betel Quid Dependence: A Resting-State Functional MRI Study. *Cell Physiol Biochem* (2016) 40(6):1626–36. doi: 10.1159/000453212
45. Zalesky A, Fornito A, Bullmore ET. Network-based statistic: Identifying differences in brain networks. *NeuroImage* (2010) 53(4):1197–207. doi: 10.1016/j.neuroimage.2010.06.041
46. Lee C-Y, Chang C-S, Shieh T-Y, Chang Y-Y. Development and validation of a self-rating scale for betel quid chewers based on a male-prisoner population in Taiwan: The Betel Quid Dependence Scale. *Drug Alcohol Depend* (2012) 121 (1–2):18–22. doi: 10.1016/j.drugalcdep.2011.07.027
47. Chu N-S. Neurological aspects of areca and betel chewing. *Addict Biol* (2002) 7(1):111–4. doi: 10.1080/13556210120091473
48. Zhang X, Reichart PA. A review of betel quid chewing, oral cancer and precancer in Mainland China. *Oncol* (2007) 43(5):424–30. doi: 10.1016/j.oraloncology.2006.08.010
49. Yan. DPARSF: a MATLAB toolbox for "pipeline" data analysis of resting-state fMRI. *Front Syst Neurosci* (2010) 4(13):1–7. doi: 10.3389/fnsys.2010.00013/abstract
50. Flandin G, Friston KJ. Statistical parametric mapping. *Scholarpedia* (2008) 3 (4):6232. doi: 10.4249/scholarpedia.6232
51. Friston KJ, Williams S, Howard R, Frackowiak RSJ, Turner R. Movement-Related effects in fMRI time-series. *Magn Reson Med* (1996) 35(3):346–55. doi: 10.1002/mrm.1910350312
52. Yan C-G, Cheung B, Kelly C, Colcombe S, Craddock RC, Martino AD, et al. A Comprehensive Assessment of Regional Variation in the Impact of Head Micromovements on Functional Connectomics. (2014) 40:183–201. doi: 10.1016/j.neuroimage.2013.03.004
53. Jenkinson M, Bannister P, Brady M, Smith S. Improved Optimization for the Robust and Accurate Linear Registration and Motion Correction of Brain Images. *NeuroImage* (2002) 17(2):825–41. doi: 10.1006/nimg.2002.1132
54. Power JD, Barnes KA, Snyder AZ, Schlaggar BL, Petersen SE. Spurious but systematic correlations in functional connectivity MRI networks arise from subject motion. (2013) 28:2142–54. doi: 10.1016/j.neuroimage.2011.10.018
55. Rolls ET, Joliot M, Tzourio-Mazoyer N. Implementation of a new parcellation of the orbitofrontal cortex in the automated anatomical labeling atlas. *NeuroImage* (2015) 122:1–5. doi: 10.1016/j.neuroimage.2015.07.075
56. Tzourio-Mazoyer N, Landeau B, Papathanassiou D, Crivello F, Etard O, Delcroix N, et al. Automated Anatomical Labeling of Activations in SPM Using a Macroscopic Anatomical Parcellation of the MNI MRI Single-Subject Brain. *NeuroImage* (2002) 15(1):273–89. doi: 10.1006/nimg.2001.0978
57. Chiavaras MM, LeGoualher G, Evans A, Petrides M. Three-Dimensional Probabilistic Atlas of the Human Orbitofrontal Sulci in Standardized Stereotaxic Space. *NeuroImage* (2001) 13(3):479–96. doi: 10.1006/nimg.2000.0641
58. Chang C-C, Lin C-J. Training ν-Support Vector Classifiers: Theory and Algorithms. *Neural Comput* (2001) 13:2119–47. doi: 10.1162/089976601750399335
59. Rice ME, Harris GT. Comparing effect sizes in follow-up studies: ROC Area, Cohen's d, and r. *Law Hum Behav* (2005) 29(5):615–20. doi: 10.1007/s10979-005-6832-7
60. Kufahl P, Li Z, Risinger R, Rainey C, Piacentine L, Wu G, et al. Expectation Modulates Human Brain Responses to Acute Cocaine: A Functional Magnetic Resonance Imaging Study. *Biol Psychiatry* (2008) 63(2):222–30. doi: 10.1016/j.biopsych.2007.03.021
61. Rolls ET. *The Brain, Emotion, and Depression*. Oxford: Oxford University Press; (2018).
62. Gerfen CR, Surmeier DJ. Modulation of Striatal Projection Systems by Dopamine. *Annu Rev Neurosci* (2011) 34(1):441–66. doi: 10.1146/annurev-neuro-061010-113641
63. Wise RA. Dopamine and reward: The anhedonia hypothesis 30 years on. *Neurotoxicity Res* (2008) 14(2–3):169–83. doi: 10.1007/BF03033808
64. Volkow ND, Wang G-J, Fowler JS, Gatley SJ, Ding Y-S, Logan J, et al. Relationship between psychostimulant-induced "high" and dopamine transporter occupancy. *Proc Natl Acad Sci U S A* (1996) 93(19):10388–92. doi: 10.1073/pnas.93.19.10388
65. Heinz A. Correlation Between Dopamine D2 Receptors in the Ventral Striatum and Central Processing of Alcohol Cues and Craving. *Am J Psychiatry* (2004) 161(10):1783–9. doi: 10.1176/ajp.161.10.1783
66. Rose JE, Behm FM, Salley AN, Bates JE, Coleman RE, Hawk TC, et al. Regional brain activity correlates of nicotine dependence. *Neuropsychopharmacology* (2007) 32(12):2441. doi: 10.1038/sj.npp.1301379
67. Bjork JM, Gilman JM. The effects of acute alcohol administration on the human brain: Insights from neuroimaging. *Neuropharmacology* (2014) 84:101–10. doi: 10.1016/j.neuropharm.2013.07.039
68. Motzkin JC, Baskin-Sommers A, Newman JP, Kiehl KA, Koenigs M. Neural correlates of substance abuse: Reduced functional connectivity between areas underlying reward and cognitive control: Neuropsychological Correlates of SUD. *Hum Brain Mapp* (2014) 35(9):4282–92. doi: 10.1002/hbm.22474
69. Supèr H. Working Memory in the Primary Visual Cortex. *Arch Neurol* (2003) 60(6):809–12. doi: 10.1001/archneur.60.6.809
70. Shokri-Kojori E, Tomasi D, Wiers CE, Wang G-J, Volkow ND. Alcohol affects brain functional connectivity and its coupling with behavior: greater effects in male heavy drinkers. *Mol Psychiatry* (2017) 22(8):1185–95. doi: 10.1038/mp.2016.25
71. Hanlon CA, Dowdle LT, Naselaris T, Canterberry M, Cortese BM. Visual cortex activation to drug cues: A meta-analysis of functional neuroimaging papers in addiction and substance abuse literature. *Drug Alcohol Depend* (2014) 143:206–12. doi: 10.1016/j.drugalcdep.2014.07.028
72. Schoenbaum G, Shaham Y. The role of orbitofrontal cortex in drug addiction: a review of preclinical studies. *Biol Psychiatry* (2008) 63(3):256–62. doi: 10.1016/j.biopsych.2007.06.003
73. Schoenbaum G, Roesch MR, Stalnaker TA. Orbitofrontal cortex, decision-making and drug addiction. *Trends Neurosci* (2006) 29(2):116–24. doi: 10.1016/j.tins.2005.12.006
74. Rolls ET. The functions of the orbitofrontal cortex. *Brain Cognition* (2004) 55 (1):11–29. doi: 10.1016/S0278-2626(03)00277-X

75. Volkow ND, Fowler JS, Wang G-J, Swanson JM. Dopamine in drug abuse and addiction: results from imaging studies and treatment implications. *Mol Psychiatry* (2004) 9(6):557–69. doi: 10.1038/sj.mp.4001507
76. Rolls ET. The orbitofrontal cortex and emotion in health and disease, including depression. *Neuropsychologia* (2017) 1–63. doi: 10.1016/j.neuropsychologia.2017.09.021
77. Bechara A, Damasio H, Damasio AR. Emotion decision making and the orbital fontal cortex. *Cereb Cortex* (2000) 10:395–07. doi: 10.1093/cercor/10.3.295
78. Kringelbach M. The functional neuroanatomy of the human orbitofrontal cortex: evidence from neuroimaging and neuropsychology. *Prog Neurobiol* (2004) 72(5):341–72. doi: 10.1016/j.pneurobio.2004.03.006
79. Liu X, Powell DK, Wang H, Gold BT, Corbly CR, Joseph JE. Functional Dissociation in Frontal and Striatal Areas for Processing of Positive and Negative Reward Information. *J Neurosci* (2007) 27(17):4587–97. doi: 10.1523/JNEUROSCI.5227-06.2007
80. Volkow ND, Wang G-J, Fowler JS, Tomasi D, Telang F. Addiction: Beyond dopamine reward circuitry. *Proc Natl Acad Sci* (2011) 108(37):15037–42. doi: 10.1073/pnas.1010654108
81. Fedota JR, Stein EA. Resting-state functional connectivity and nicotine addiction: prospects for biomarker development: Resting-state functional connectivity and nicotine. *Ann NY Acad Sci* (2015) 1349(1):64–82. doi: 10.1111/nyas.12882
82. Davis M, Walker DL, Miles L, Grillon C. Phasic vs Sustained Fear in Rats and Humans: Role of the Extended Amygdala in Fear vs Anxiety. *Neuropsychopharmacology* (2010) 35(1):105–35. doi: 10.1038/npp.2009.109
83. Koob GF, Le Moal M. Plasticity of reward neurocircuitry and the "dark side" of drug addiction. *Nat Neurosci* (2005) 8(11):1442–4. doi: 10.1038/nn1105-1442
84. Koob GF, Volkow ND. Neurocircuitry of addiction. *Neuropsychopharmacology* (2010) 35(1):217. doi: 10.1038/npp.2009.110
85. Volkow ND, Tomasi D, Wang G-J, Logan J, Alexoff DL, Jayne M, et al. Stimulant-induced dopamine increases are markedly blunted in active cocaine abusers. *Mol Psychiatry* (2014) 19(9):1037–43. doi: 10.1038/mp.2014.58
86. Koob G. Drug Addiction, Dysregulation of Reward, and Allostasis. *Neuropsychopharmacology* (2001) 24(2):97–129. doi: 10.1016/S0893-133X(00)00195-0
87. Ding W, Sun J, Sun Y, Chen X, Zhou Y, Zhuang Z, et al. Trait impulsivity and impaired prefrontal impulse inhibition function in adolescents with internet gaming addiction revealed by a Go/No-Go fMRI study. *Behav Brain Functions* (2014) 10(1):20. doi: 10.1186/1744-9081-10-20
88. Rose JE, McClernon FJ, Froeliger B, Behm FM, Preud'homme X, Krystal AD. Repetitive Transcranial Magnetic Stimulation of the Superior Frontal Gyrus Modulates Craving for Cigarettes. *Biol Psychiatry* (2011) 70(8):794–9. doi: 10.1016/j.biopsych.2011.05.031
89. Ray S, Gohel S, Biswal BB. Altered Functional Connectivity Strength in Abstinent Chronic Cocaine Smokers Compared to Healthy Controls. *Brain Connectivity* (2015) 5(8):476–86. doi: 10.1089/brain.2014.0240
90. Claus ED, Weywadt CR. Resting-State Connectivity in Former, Current and Never Smokers. *Nicotine Tob Res* (2018) 1–32. doi: 10.1093/ntr/nty266
91. Vossel S, Geng JJ, Fink GR. Dorsal and Ventral Attention Systems: Distinct Neural Circuits but Collaborative Roles. *Neuroscientist* (2014) 20(2):150–9. doi: 10.1177/1073858413494269
92. Seghier ML. The Angular Gyrus: Multiple Functions and Multiple Subdivisions. *Neuroscientist* (2013) 19(1):43–61. doi: 10.1177/1073858412440596
93. Greicius MD, Krasnow B, Reiss AL, Menon V. Functional connectivity in the resting brain: A network analysis of the default mode hypothesis. *Proc Natl Acad Sci* (2003) 100(1):253–8. doi: 10.1073/pnas.0135058100
94. Goldstein RZ, Craig ADB, Bechara A, Garavan H, Childress AR, Paulus MP, et al. The Neurocircuitry of Impaired Insight in Drug Addiction. *Trends Cogn Sci* (2009) 13(9):372–80. doi: 10.1016/j.tics.2009.06.004
95. Battelli L, Alvarez GA, Carlson T, Pascual-Leone A. The Role of the Parietal Lobe in Visual Extinction Studied with Transcranial Magnetic Stimulation. *J Cogn Neurosci* (2009) 21(10):1946–55. doi: 10.1162/jocn.2008.21149

Conflict of Interest: The authors declare that the research was conducted in the absence of any commercial or financial relationships that could be construed as a potential conflict of interest.

frontiers in Psychiatry

ORIGINAL RESEARCH
published: 03 April 2020
doi: 10.3389/fpsyt.2020.00236

Anatomical Connectivity-Based Strategy for Targeting Transcranial Magnetic Stimulation as Antidepressant Therapy

Qi Tao[1,2,3,4†], Yongfeng Yang[5,6,7,8†], Hongyan Yu[5], Lingzhong Fan[9,10,11], Shuxin Luan[12,13], Lei Zhang[12,13], Hua Zhao[12], Luxian Lv[5,6,7], Tianzi Jiang[8,9,10,11] and Xueqin Song[1,2,3*]*

[1] Department of Psychiatry, The First Affiliated Hospital of Zhengzhou University, Zhengzhou, China, [2] Biological Psychiatry International Joint Laboratory of Henan, Zhengzhou University, Zhengzhou, China, [3] Henan Psychiatric Transformation Research Key Laboratory, Zhengzhou University, Zhengzhou, China, [4] Academy of Medical Sciences, Zhengzhou University, Zhengzhou, China, [5] Department of Psychiatry, Henan Mental Hospital, The Second Affiliated Hospital of Xinxiang Medical University, Xinxiang, China, [6] Henan Key Lab of Biological Psychiatry, Xinxiang Medical University, Xinxiang, China, [7] International Joint Research Laboratory for Psychiatry and Neuroscience of Henan, Xinxiang, China, [8] Key Laboratory for NeuroInformation of Ministry of Education, School of Life Science and Technology, University of Electronic Science and Technology of China, Chengdu, China, [9] Brainnetome Center, Institute of Automation, Chinese Academy of Sciences, Beijing, China, [10] National Laboratory of Pattern Recognition, Institute of Automation, Chinese Academy of Sciences, Beijing, China, [11] University of Chinese Academy of Sciences, Beijing, China, [12] Department of Physiology, College of Basic Medical Sciences, Jilin University, Jilin, China, [13] Department of Psychiatry, The First Bethune Hospital of Jilin University, Changchun, China

Objectives: Abnormal activity of the subgenual anterior cingulate cortex (sACC) is implicated in depression, suggesting the sACC as a potentially effective target for therapeutic modulation in cases resistant to conventional treatments (treatment-resistant depression, TRD). We hypothesized that areas in the prefrontal cortex (PFC) with direct fiber connections to the sACC may be particularly effective sites for treatment using transcranial magnetic stimulation (TMS). The aim of this study was to identify PFC sites most strongly connected to the sACC.

Methods: Two neuroimaging data sets were used to construct anatomic and functional connectivity maps using sACC as the seed region. Data set 1 included magnetic resonance (MR) images from 20 healthy controls and Data set 2 included MR images from 15 TRD patients and 15 additional healthy controls. PFC voxels with maximum values in the mean anatomic connection probability maps were identified as optimal sites for TMS.

Results: Both right and left PFC contained sites strongly connected to the sACC, but the coordinates (in Montreal Neurological Institute space) of peak anatomic connectivity differed slightly between hemispheres. The left PFC site connected directly to the sACC both anatomically and functionally, while the right PFC site was functionally connected to the posterior cingulate cortex (PCC).

OPEN ACCESS

Edited by:
Wenbin Guo,
Central South University, China

Reviewed by:
Céline Sonja Reinbold,
University of Oslo, Norway
Jiaojian Wang,
University of Electronic Science and Technology of China, China
Zhifen Liu,
First Hospital of Shanxi Medical University, China

***Correspondence:**
Tianzi Jiang
jiangtz@nlpr.ia.ac.cn
Xueqin Song
fccsongxq@zzu.edu.cn

†These authors have contributed equally to this work

Specialty section:
This article was submitted to Neuroimaging and Stimulation, a section of the journal Frontiers in Psychiatry

Received: *17 January 2020*
Accepted: *11 March 2020*
Published: *03 April 2020*

Citation:
Tao Q, Yang Y, Yu H, Fan L, Luan S, Zhang L, Zhao H, Lv L, Jiang T and Song X (2020) Anatomical Connectivity-Based Strategy for Targeting Transcranial Magnetic Stimulation as Antidepressant Therapy. Front. Psychiatry 11:236. doi: 10.3389/fpsyt.2020.00236

Conclusions: Both left and right PFC are functionally connected to regions implicated in depression, the sACC and PCC, respectively. These bilateral PFC sites may be effective TMS targets to treat TRD.

Keywords: treatment-resistant depression (TRD), transcranial magnetic stimulation (TMS), anatomical connectivity, subgenual anterior cingulated cortex (sACC), prefrontal cortex (PFC)

INTRODUCTION

Major depressive disorder (MDD) can be effectively treated in the majority of cases by medication, psychotherapy, or a combination of both, but more than one third of patients fail to respond to these standard interventions and other treatments, termed treatment-resistant depression or TRD cases (1). Chronic depression is associated with reduced productivity and quality of life as well as increased suicide risk, so alternative treatments for TRD are required.

Transcranial magnetic stimulation (TMS), deep brain stimulation (DBS), and vagus nerve stimulation (VNS) exert antidepressant effects by modulating activity within specific neural networks associated with emotional regulation and cognition (2–5). Vagus nerve stimulation has been approved by the United States Food and Drug Administration (FDA) for TRD treatment, although not for management of acute illness (6). Clinically significant antidepressive effects have also been observed following chronic DBS of the subcallosal cingulate white matter (4, 7) and subgenual anterior cingulate cortex (sACC) (8, 9) with good patient tolerability. However, DBS treatment is invasive and efficacy for TRD is still under investigation (10). Alternatively, TMS is non-invasive and well tolerated, with no evidence of cognitive impairment and few reports of medical complications. While TMS has been approved by the FDA for TRD, its effect size is generally modest compared to DBS (6). This lower efficacy may result from uncertainty regarding therapeutic mechanisms and the optimal regimens and target sites. For instance, while the prefrontal cortex (PFC) is widely regarded as an effective stimulation site, the precise subregions of left and right PFC evoking the optimal therapeutic response are unclear (11–13).

Depression involves dysfunction in a distributed network of cortical and limbic regions, including the ACC (2, 14–16). Previous studies have suggested that DBS of the sACC can effectively reverse symptoms of TRD (9), and is particularly effective against the associated cognitive deficits (3, 9, 15, 16). There is also evidence that functional connectivity of the sACC may predict treatment response to TMS (15, 16). An early review by Mayberg (3) suggested that normalization of sACC hyperactivity was a prerequisite for symptom remission (3). Indeed, reduced sACC activity has been reported following successful treatment with a variety of methods, including TMS (17, 18) and VNS (19). These studies suggest that the sACC acts as a hub within a critical depression-related circuit and that effects on activity within this circuit are strongly related to antidepressant efficacy.

The sACC and rostral ACC (rACC) differ in anatomic connectivity, cytology, and neurotransmitter receptor organization (20, 21). Further, studies comparing different left prefrontal cortex (PFC) stimulation sites found that antidepressant efficacy was related to the functional connectivity with deeper limbic regions, especially the sACC (22, 23). Fox and colleagues found that the sACC and dorsolateral PFC (DLPFC) are intrinsically anticorrelated, and suggested that the functional link between these two regions is strongly related to depression and treatment response (24). This anatomic connectivity with the sACC suggests that the PFC may be the optimal TMS site for neuromodulation. To our knowledge, most TMS studies for MDD have applied stimuli to the left dorsolateral PFC (DLPFC) (13, 25, 26). In present study, we identified PFC regions of strongest anatomic and functional connectivity to sACC as potential sites for optimal TMS treatment response.

MATERIALS AND METHODS

Participants and Clinical Diagnosis

Two independent data sets were used in the present study. Data set 1 consisted of twenty healthy, right-handed subjects (10 males and 10 females, mean age=18.5 ± 1.5 years old) recruited by advertisement from the University of Electronic Science and Technology of China, Chengdu. None of the participants had a history of psychiatric or neurological diseases, and none had any contraindications for magnetic resonance imaging (MRI). All participants signed a consent form approved by the Medical Research Ethics Committee of the University of Electronic Science and Technology of China after a full explanation of study objectives and procedures. The Ethics Committee of the First Affiliated Hospital of Jilin University (China) approved the study protocol.

Data set 2 consisted of fifteen right-handed TRD patients (6 males and 9 females, mean age 29.7 ± 7.5 years old) and 15 healthy right-handed controls (8 males and 7 females, mean age 37.3 ± 8.5 years old). Healthy controls had no history of psychiatric or neurological diseases. All patients were screened independently by two psychiatrists to ensure that they met criteria for TRD. All fifteen patients were diagnosed with a major depressive episode of at least 2 years' duration according to Diagnostic and Statistical Manual of Mental Disorders-Fourth Edition IV (DSM-IV) criteria, and all had a minimum score at entry of 35 (37.4 ± 3.0) on the 17-item Hamilton Depression Rating Scale (HDRS), indicating severe depression (27). A priori exclusion criteria were a) other psychiatric disorders with the exception of depression, such as schizophrenia, bipolar disorder, and obsessive–compulsive disorder; b) organic causes of

depression including heart, liver, and kidney diseases; c) surgically implanted electronic devices or metal frame supporting equipment precluding MRI scanning.

Data set 1 was used to construct a probabilistic tractography map showing fibers directly connecting the PFC and sACC and the x-y-z coordinates of peak connectivity as the optimal site for TMS. Data set 2 was used for functional connectivity analysis to test the reliability of the optimal TMS site generated from the anatomic connectivity map.

Using probabilistic fiber tractography, we were able to infer anatomic connectivity that progressed into gray matter, and gained a comprehensive description of the connections between the sACC and PFC. By comparing the pattern of functional connectivity between TRD patients and healthy controls, we then verified the rationality of the TMS sites.

Data Acquisition

All Data set 1 subjects were examined using a Signa HDx 3.0 Tesla MR scanner (General Electric, Milwaukee, WI, USA). The diffusion tensor imaging (DTI) scheme of Data set 1 yielded 64 images with non-collinear diffusion gradients (b=1000 s/mm^2) and 3 non-diffusion-weighed images (b=0 s/mm^2) using a single-shot echo planar imaging sequence (SE-EPI). An integrated parallel acquisition technique was used with an acceleration factor of 2 to reduce acquisition time and image distortion from susceptibility artifacts. From each participant, 75 slices were collected with FOV = 256×256 mm, acquisition matrix = 128×128, flip angle (FA) = 90°, and slice thickness = 2 mm with no gap. This method resulted in voxel-dimensions of 2×2×2 mm, TE = 67.6 ms, and TR = 8500 ms. Sagittal 3D T1-weighted images were also acquired with a brain volume (BRAVO) sequence (TR/TE= 8.1/3.1 ms, inversion time = 450 ms, FA = 13°, FOV = 256×256 mm, matrix = 128×128, slice thickness = 1 mm with no gap, 176 sagittal slices, and voxel size = 1×1×1 mm).

In Data set 2, imaging was performed using a Siemens 3.0-T MR system equipped with a SIEMENS MR HEADER coil. The protocol (ep2d.bold.REST.2000/30.4M.6MIN.FAST.0.49) included 64 phase encoding steps. The following acquisition parameters were used in the fMRI protocol: echo time = 30 ms, FOV = 256×256, field of view = 256 mm, acquisition matrix = 64×64, voxel size: 1×1×1 mm, slice thickness = 4 mm, no gap, 188 sagittal slices, TR = 2000 ms, TE = 30 ms, and FA = 90°.

Data Preprocessing and Analysis of Data Set 1

Diffusion tensor and T1-weighted images from Data set 1 were visually inspected independently by two radiologists for obvious artifacts arising from subject motion and instrument malfunction. Distortions in diffusion-weighted images caused by eddy currents and simple head motions were corrected using the FMRIB Diffusion Toolbox (FSL) 4.0 (http://www.fmrib.ox.ac.uk/fsl). Skull-stripped T1-weighted images of each subject were co-registered to the subject's non-diffusion-weighted image (b=0s/mm^2) using the Statistical Parametric Mapping 8 (SPM8) package (http://www.fil.ion.ucl.ac.uk/spm), yielding a set of co-registered T1 images (rT1) in DTI space. Then the rT1 images were transformed to Montreal Neurological Institute (MNI) space. Seed masks and target masks were transformed from MNI space to native DTI space using nearest-neighbor interpolation.

Tractography was performed in diffusion space using the FSLpackage. Voxel-wise estimates of fiber orientation distribution were calculated using Bedpostx. Probability distributions for two fiber directions at each voxel were calculated using the multiple fiber extension (28) of a previously published diffusion modeling approach (29). The connection probability value was recorded for every seed voxel. We also transformed the connection probability map to MNI space and averaged the 20 individual connection probability maps to obtain a mean probability connectivity map for the seed. We then found the coordinate of maximum value in the mean probability connectivity map. Fiber tracking was used to obtain the fibers connecting the two areas. To map the anatomic connections between the PFC and sACC, these brain areas were defined in MNI space. The sACC was defined as that part of the ACC located beneath the genu of the corpus callosum and corresponds primarily to Brodmann's area (BA)10 as well as the caudal portions of BA32 and BA24 (20). The sACC was drawn by hand based on BAs 10, 24, and 32. As the PFC as no clear anatomic boundary, we defined a liberal mask including middle frontal gyrus, superior frontal gyrus, and part of the orbitofrontal region to map the connections between sACC and PFC. The PFC was drawn on the structural template of MNI152. The inferior boundary was the inferior frontal sulcus, and the posterior boundary was the precentral sulcus.

Data Preprocessing and Analysis of Data Set 2

We used Data set 2 to assess the accuracy of the anatomic connectivity derived from Data set 1 and to reveal differences in functional connectivity between TRD patients and healthy controls. First, DTI analysis of Data set 2 was used to demonstrate similar anatomical connectivity to normal subjects in Dataset 1. To test the rationality of the TMS sites identified by probabilistic tractography analysis of Data set 1, functional connectivity preprocessing was conducted using SPM8 Data Processing Assistant for Resting-State fMRI (DPARSF) V2.0 Advanced Edition (30) and Resting-State fMRI Data Analysis Toolkit (REST, http://www.restfmri.net). For statistical analysis, the contrast images of TRD patients and healthy controls were analyzed using a two-sample *t* test to compare the differences in functional connectivity between the right and left stimulation site.

RESULTS

We used Data set 1 consisting of MRI scans from 20 healthy subjects to examine the anatomical connectivity (probabilistic tractography) between the sACC and PFC (**Supplementary Figure 1**). A probability connectivity map was derived for both hemispheres of each subject and mean probability connectivity

maps obtained (**Figure 1**), yielded bilateral maximum probability coordination (x-y-z in MNI space) as potential TMS sites. Slight differences in connectivity were observed between left and right PFC, with the right maximum anterior to the left (left MNIxyz, −15, 65, 14; right MNIxyz, −15, 65, 5). Potential PFC stimulation sites were identified as voxels with the highest probability of connectivity to the sACC (**Supplementary Figure 2**). Fiber tracking from the sACC to PFC indicated that the inferior fronto-occipital fasciculus ran through the sACC and the left PFC probability peak (**Figure 2**).

To explore the reproducibility of this PFC–sACC connectivity, Data set 2 derived from another group of 15 healthy controls, as well as 15 TRD patients using a different MRI scanner was subjected to similar analysis. Again, the PFC region demonstrated a strong probability of anatomic connectivity with sACC. Further, while absolute values differed, the connectivity map of TRD patients was similar to that of the healthy controls (**Figure 1**), including near overlapping maximum value coordinates. Thus, our tractography method was highly reproducible among different populations.

Since resting state functional connectivity may differ from anatomical connectivity, we constructed whole-brain functional connectivity maps using the average MNI coordinates of maximum value in Data set 2 as ROIs. Peak functional connectivity of the left PFC with the left sACC was located exactly at the position of peak anatomic connectivity in both patients and controls, but was significantly stronger among healthy controls than TRD patients (**Figure 3A**). In contrast, the right PFC was functionally connected to the posterior cingulate cortex (PCC) (**Figure 3B**). Between-group comparisons across the whole brains of Data set 2 at an AlphaSim corrected $p < 0.01$ height threshold ($t = 2.467$, df = 28) confirmed reproducibility with anatomic connectivity analysis across disease states and MRI scanners (**Table 1**).

DISCUSSION

In this study, we identified PFC sites with strong anatomical connectivity to the sACC, and PCC that may be optimal targets from TMS treatment of depression. Further, these sites were reproducible across different data sets and closely mirrored functional connectivity. In light of the strong evidence that modulation of sACC and PCC activity can mitigate symptoms of depression, we suggest that these PFC sites are optimal targets for TMS treatment.

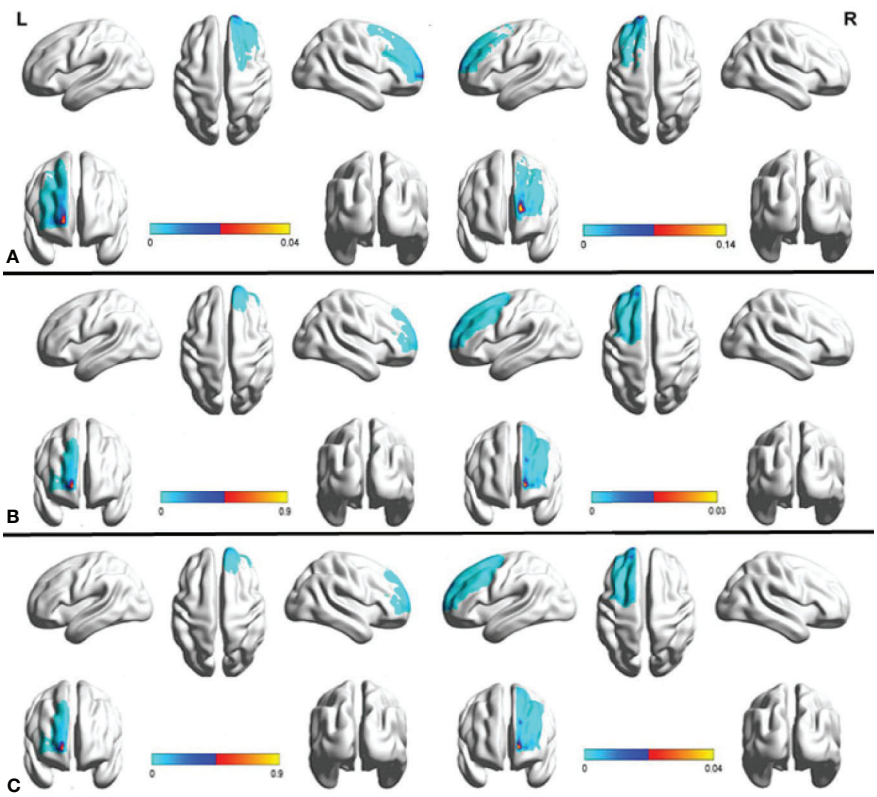

FIGURE 1 | Mean probabilistic anatomic connectivity maps derived from healthy controls **(A, B)** and treatment-resistant depression (TRD) patients **(C)** using the subgenual anterior cingulate cortex (sACC) as the seed region. The connectivity map of each individual (a, n=20; b, n=15; c, n=15) was transformed to MNI space and averaged. The prefrontal cortex (PFC) coordinate of maximum value in the mean connectivity map was identified as the optimal site for transcranial magnetic stimulation (TMS) to modulate sACC activity. The results based on Data set 1 **(A)** were reproducible in Data set 2 **(B, C)**.

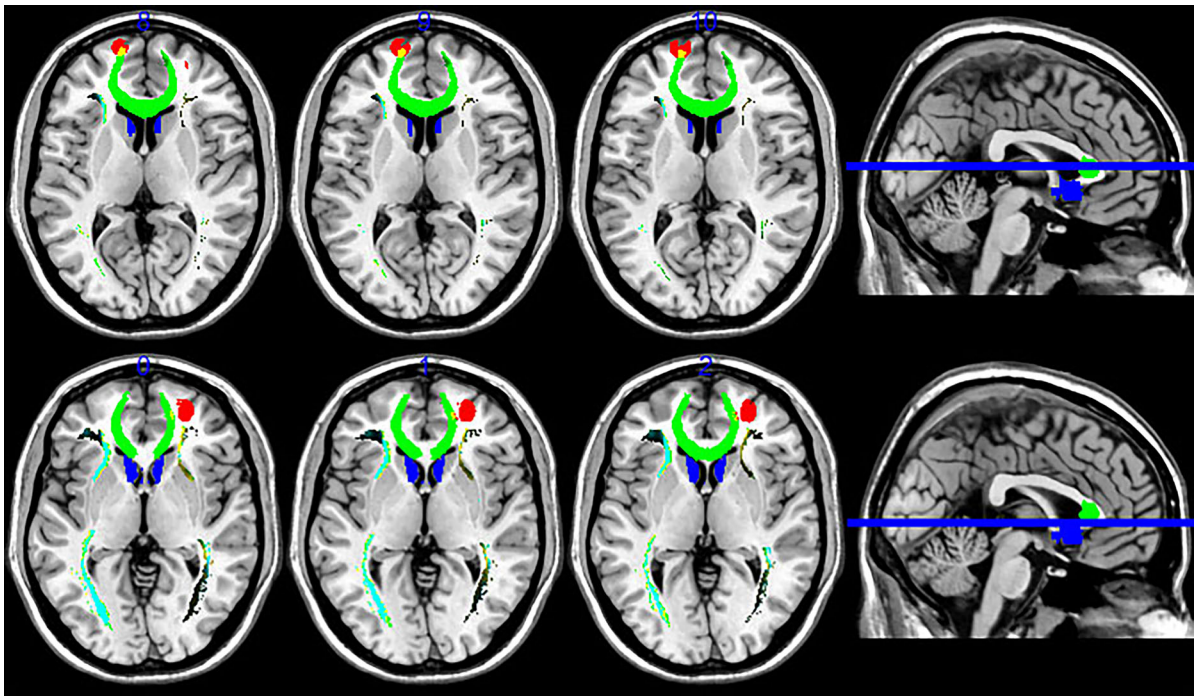

FIGURE 2 | Fiber tractography map, including the prefrontal cortex (PFC) and sACC (seed region). PFC targets are in red and the sACC seed region is in blue, while fibers running through the seed region are in green. Fiber tracts connected mainly to the medial frontal areas, but also included a site of strong connectivity in the left PFC.

Depression is linked to reduced activity of the left PFC (26, 31, 32). Recently, Wang et al. (33) reported that the effective connectivity from DLPFC to right angular gyrus predicts the antidepressant effects of electroconvulsive therapy (ECT) for MDD (33). Further, a recent functional connectivity study found that dysfunctional communication between the medial PFC and right ventral anterior insula is a major contributor to MDD pathogenesis (34). The application of repetitive (r)TMS for depression was initially driven by functional imaging data showing reduced left PFC activity in depression (35, 36). Based on empirical experience, the majority of the initial studies applied high-frequency rTMS to the left PFC (13, 25, 37, 38). However, low-frequency stimulation of the right PFC has also been used (17, 39) with clinically significant efficacy (37, 40). Grimm et al. (41) found that depressed patients exhibited hypoactivity in the left PFC during both unattended and attended emotional judgments but hyperactivity in the right PFC during attended emotional judgment (41), suggesting distinct forms of dysfunction in left and right PFC–ACC pathways Our current study also provides evidence that sites within both right and left PFC are strongly connected to regions involved in TRD, consistent with previous studies(13, 22, 23), and so may be effective TMS targets.

Repetitive TMS applied at a variety of sites and frequencies has proven highly effective for inducing mood changes in healthy controls and therapeutic effects in TRD patients. For instance, concomitant high-frequency rTMS stimulation of the left PFC and low-frequency rTMS of the right PFC was reported to have antidepressive effects. Alternatively, these regimens were ineffective when the stimulation side was reversed (37, 40, 42), suggesting an imbalance in frontal lobe activity (hypoactivity in the left frontal lobe and excessive inhibitory activity in the right frontal lobe) among MDD patients. Left and right PFC sites with strongest anatomic connectivity also appear to have non-overlapping functional targets, the sACC (left target) and PCC (right target), both of which are involved in depression (41). Therefore, analyzing the connectivity of sACC (43) and PCC (44) could reveal the mechanisms underlying therapeutic responses to TMS at these sites. Our study provides further evidence that the left PFC connects directly to the sACC and the right PFC connects to the PCC, consistent with previous studies (22, 43, 44). Therefore, this study suggests that the antidepressant mechanisms of TMS are mediated by modulation of left PFC–sACC neural circuit activity and right PFC–PCC activity.

Multiple targets have been used for rTMS treatment (26) as there is no current consensus on the optimal target for antidepressant efficacy. Tracing direct fiber pathways from deep regions implicated in depression, such as the ACC, to cortical areas accessible to modulation by TMS is a novel approach for targeting. We performed probabilistic tractography in healthy controls and TRD patients to determine the connectivity patterns of the sACC and PFC. The subcallosal cingulate is connected to many ipsilateral

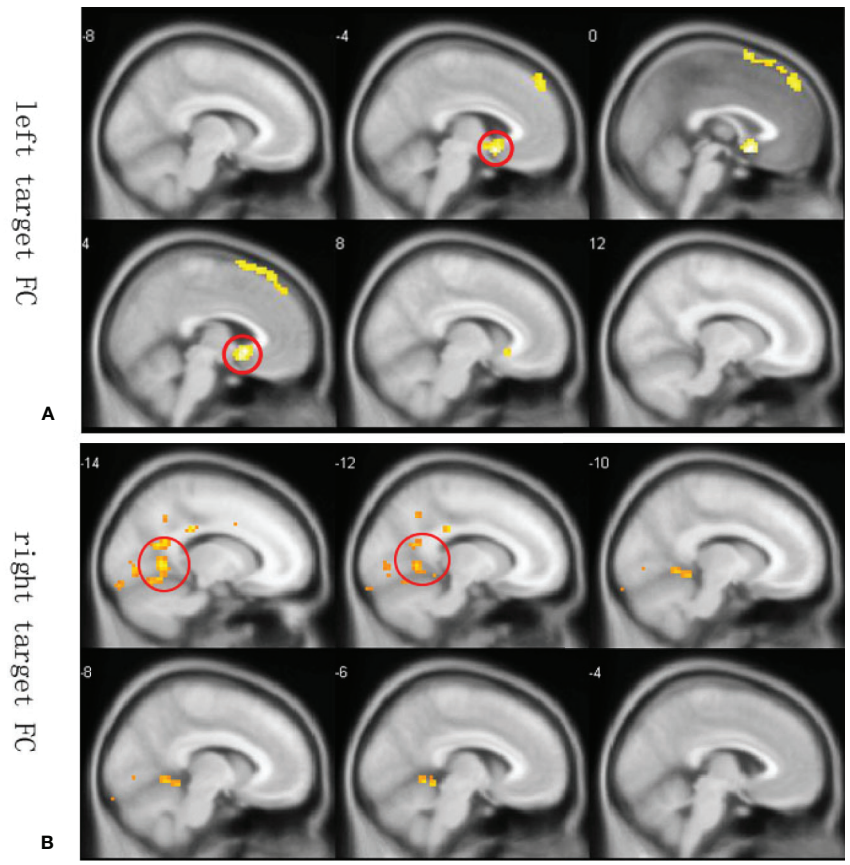

FIGURE 3 | Whole-brain resting state functional connectivity differences between healthy controls and TRD patients. Functional connectivity ROIs were taken from our anatomic connectivity results (coordinates shown in **Figure 3**). **(A)** Functional connectivity between the left target and sACC (seed region for the anatomic connectivity, red circles in **A**) was significantly stronger in the healthy group. Only negative results are shown because a previous study reported that anticorrelation between the PFC and subgenual cingulate (BA25) is related to depression networks (22). **(B)** Functional connectivity with the right PFC target. Only negative results are shown. Red circles in Figure 3B illustrate PCC areas involved in depression (41).

TABLE 1 | Functional connectivity results in healthy controls versus depression patients.

L/R	Region	cluster	Peak MNI coordinate			peak Z score	Peak intensity
			x	y	z		
L	Limbic Lobe	60					
L	Anterior Cingulate	54	0	9	-12	3.62	-4.30
L	Brodmann area 25	30					
R	Limbic Lobe	25					
R	Cerebelum_4_5_L (aal)	20					
R	Cerebelum_6_L (aal)	20	-15	-57	0	3.89	-4.30
R	Calcarine_L (aal)	16					
R	Posterior Cingulate	14					

Two sample t-test, Alphasim corrected, p < 0.01, cluster size = 19(left), cluster size = 11 (right).

regions, such as the medial frontal cortex, ACC, and PCC (4), but these regions have limited area for TMS. Here we identified strong connection with specific sites of the left and right PFC that may be superior targets for treating TRD. The left PFC site is located on the gyrus, while the right PFC target is located on the sulcus, so the left PFC target may be more readily activated by TMS. Nonetheless, stimulation of both sides with distinct frequency patterns may provide the best therapeutic effect (6, 37, 42–44).

The DLPFC position for TMS is often located using the electroencephalography (EEG)-based "5-cm rule" or by neuroimaging-based targeting of BA9 or BA46 (42, 45–47). While the 5-cm rule is an easy low-cost option, it does not account for individual differences in skull size. Further, targeting based on BA9 or BA46 locations on neuroimages did not substantially improve clinical efficacy compared to the 5-cm rule (22). We suggest that the optimal target can be identified using a TMS Navigation system and our MNI coordinates.

This study has several limitations. First, only 15 TRD patients were examined and MDD is a heterogeneous disorder, so certain abnormalities in anatomic or functional connectivity may have been missed. Second, the sACC subregions connected anatomically with the PFC were not examined.

CONCLUSIONS

This study identifies sites in right and left prefrontal cortex that may be optimal targets for transcranial magnetic stimulation treatment of depression based on strong functional connectivity with the posterior and subgenual anterior cingulate cortex.

DATA AVAILABILITY STATEMENT

The datasets generated for this study are available on request to the corresponding authors.

ETHICS STATEMENT

The studies involving human participants were reviewed and approved by The Ethical Committee of the First Affiliated Hospital of Jilin University. The patients/participants provided their written informed consent to participate in this study. Written informed consent was obtained from the individual(s) for the publication of any potentially identifiable images or data included in this article.

AUTHOR CONTRIBUTIONS

TJ and LL designed the study. SL, LZ, HZ, and YY collected the samples and participants' characteristics. YY, QT, HY, and LF analyzed and discussed the experimental results. QT, YY, XS, and TJ wrote the paper. All authors contributed to and have approved the final manuscript.

FUNDING

This work was supported by the National Natural Science Foundation of China (81671330 to LL, 81571318 to XS); Medical Science and Technology Research Project of Henan Province (2018020373 to HY); Health and Family Planning Commission of Henan Province (201501015 to XS), Department of Science and Technology of Henan Province (162102410061 to XS; No. 2017JQ023 to XS), and School and Hospital Co-incubation Funds (2017-BSTDJJ-04 to XS) and Research Council of Norway (223273).

ACKNOWLEDGMENTS

The authors thank the patient, their families, and the healthy volunteers for their participation, and the physicians who collect the MRI and clinical data. We thank International Science Editing (http://www.internationalscienceediting.com) for editing this manuscript.

SUPPLEMENTARY MATERIAL

The Supplementary Material for this article can be found online at: https://www.frontiersin.org/articles/10.3389/fpsyt.2020.00236/full#supplementary-material

SUPPLEMENTARY FIGURE 1 | Regions of interest (ROIs) for connectivity analysis. (a) Left prefrontal cortex (black) and right prefrontal cortex (yellow) ROIs. (b) The seed region (sACC, red) contains effective therapeutic target for DBS and VNS (7, 19).

SUPPLEMENTARY FIGURE 2 | Optimal TMS sites were defined as the coordinates of maximum values in the probability connectivity map (left MNI x-y-z -15, 65,14; right MNI x-y-z 24, 53, 1). The radius was 8 mm. These targets were also used as seed ROIs to conduct functional connectivity analysis.

REFERENCES

1. Souery D, Papakostas GI, Trivedi MH. Treatment-resistant depression. *J Clin Psychiatry* (2006) 67(Suppl 6):16–22.
2. Ressler KJ, Mayberg HS. Targeting abnormal neural circuits in mood and anxiety disorders: from the laboratory to the clinic. *Nat Neurosci* (2007) 10 (9):1116–24. doi: 10.1038/nn1944
3. Mayberg HS. Modulating dysfunctional limbic-cortical circuits in depression: towards development of brain-based algorithms for diagnosis and optimised treatment. *Br Med Bull* (2003) 65:193–207. doi: 10.1093/bmb/65.1.193
4. Gutman DA, Holtzheimer PE, Behrens TE, Johansen-Berg H, Mayberg HS. A tractography analysis of two deep brain stimulation white matter targets for depression. *Biol Psychiatry* (2009) 65(4):276–82. doi: 10.1016/j.biopsych.2008.09.021
5. Dougherty DD, Rauch SL. Somatic therapies for treatment-resistant depression: new neurotherapeutic interventions. *Psychiatr Clin North Am* (2007) 30(1):31–7. doi: 10.1016/j.psc.2006.12.006
6. Cusin C, Dougherty DD. Somatic therapies for treatment-resistant depression: ECT, TMS, VNS, DBS. *Biol Mood Anxiety Disord* (2012) 2 (1):14. doi: 10.1186/2045-5380-2-14
7. Lozano AM, Mayberg HS, Giacobbe P, Hamani C, Craddock RC, Kennedy SH. Subcallosal cingulate gyrus deep brain stimulation for treatment-resistant depression. *Biol Psychiatry* (2008) 64(6):461–7. doi: 10.1016/j.biopsych.2008.05.034
8. Riva-Posse P, Holtzheimer PE, Garlow SJ, Mayberg HS. Practical considerations in the development and refinement of subcallosal cingulate white matter deep brain stimulation for treatment-resistant depression. *World Neurosurg* (2013) 80(3-4):S27 e5–34. doi: 10.1016/j.wneu.2012.11.074
9. Mayberg HS, Lozano AM, Voon V, McNeely HE, Seminowicz D, Hamani C, et al. Deep brain stimulation for treatment-resistant depression. *Neuron* (2005) 45(5):651–60. doi: 10.1016/j.neuron.2005.02.014
10. Merkl A, Aust S, Schneider GH, Visser-Vandewalle V, Horn A, Kuhn AA, et al. Deep brain stimulation of the subcallosal cingulate gyrus in patients with treatment-resistant depression: A double-blinded randomized controlled study and long-term follow-up in eight patients. *J Affect Disord* (2018) 227:521–9. doi: 10.1016/j.jad.2017.11.024
11. Herwig U, Satrapi P, Schonfeldt-Lecuona C. Using the international 10-20 EEG system for positioning of transcranial magnetic stimulation. *Brain Topogr* (2003) 16(2):95–9. doi: 10.1023/b:brat.0000006333.93597.9d
12. Kumar S, Singh S, Kumar N, Verma R. The Effects of Repetitive Transcranial Magnetic Stimulation at Dorsolateral Prefrontal Cortex in the Treatment of Migraine Comorbid with Depression: A Retrospective Open Study. *Clin Psychopharmacol Neurosci* (2018) 16(1):62–6. doi: 10.9758/cpn.2018.16.1.62
13. Padberg F, George MS. Repetitive transcranial magnetic stimulation of the prefrontal cortex in depression. *Exp Neurol* (2009) 219(1):2–13. doi: 10.1016/j.expneurol.2009.04.020
14. Drevets WC, Price JL, Furey ML. Brain structural and functional abnormalities in mood disorders: implications for neurocircuitry models of

depression. *Brain Struct Funct* (2008) 213(1-2):93–118. doi: 10.1007/s00429-008-0189-x
15. Cash RFH, Zalesky A, Thomson RH, Tian Y, Cocchi L, Fitzgerald PB. Subgenual Functional Connectivity Predicts Antidepressant Treatment Response to Transcranial Magnetic Stimulation: Independent Validation and Evaluation of Personalization. *Biol Psychiatry* (2019) 86(2):e5–7.. doi: 10.1016/j.biopsych.2018.12.002
16. Weigand A, Horn A, Caballero R, Cooke D, Stern AP, Taylor SF, et al. Prospective Validation That Subgenual Connectivity Predicts Antidepressant Efficacy of Transcranial Magnetic Stimulation Sites. *Biol Psychiatry* (2018) 84 (1):28–37. doi: 10.1016/j.biopsych.2017.10.028
17. Kito S, Fujita K, Koga Y. Regional cerebral blood flow changes after low-frequency transcranial magnetic stimulation of the right dorsolateral prefrontal cortex in treatment-resistant depression. *Neuropsychobiology* (2008) 58(1):29–36. doi: 10.1159/000154477
18. Kito S, Hasegawa T, Koga Y. Neuroanatomical correlates of therapeutic efficacy of low-frequency right prefrontal transcranial magnetic stimulation in treatment-resistant depression. *Psychiatry Clin Neurosci* (2011) 65(2):175–82. doi: 10.1111/j.1440-1819.2010.02183.x
19. Nahas Z, Teneback C, Chae J-H, Mu Q, Molnar C, Kozel FA, et al. Serial vagus nerve stimulation functional MRI in treatment-resistant depression. *Neuropsychopharmacology* (2007) 32(8):1649–60. doi: 10.1038/sj.npp.1301288
20. Johansen-Berg H, Gutman D, Behrens T, Matthews P, Rushworth M, Katz E, et al. Anatomical connectivity of the subgenual cingulate region targeted with deep brain stimulation for treatment-resistant depression. *Cereb Cortex* (2008) 18(6):1374–83. doi: 10.1093/cercor/bhm167
21. Palomero-Gallagher N, Mohlberg H, Zilles K, Vogt B. Cytology and receptor architecture of human anterior cingulate cortex. *J Comp Neurol* (2008) 508 (6):906–26. doi: 10.1002/cne.21684
22. Fox MD, Buckner RL, White MP, Greicius MD, Pascual-Leone A. Efficacy of transcranial magnetic stimulation targets for depression is related to intrinsic functional connectivity with the subgenual cingulate. *Biol Psychiatry* (2012) 72 (7):595–603. doi: 10.1016/j.biopsych.2012.04.028
23. Fox MD, Liu H, Pascual-Leone A. Identification of reproducible individualized targets for treatment of depression with TMS based on intrinsic connectivity. *Neuroimage* (2013) 66:151–60. doi: 10.1016/j.neuroimage.2012.10.082
24. Fox MD, Liu H, Pascual-Leone A. Identification of reproducible individualized targets for treatment of depression with TMS based on intrinsic connectivity. *Neuroimage* (2012) 66:151–60. doi: 10.1016/j.neuroimage.2012.10.082
25. Teng S, Guo Z, Peng H, Xing G, Chen H, He B, et al. High-frequency repetitive transcranial magnetic stimulation over the left DLPFC for major depression: Session-dependent efficacy: A meta-analysis. *Eur Psychiatry* (2017) 41:75–84. doi: 10.1016/j.eurpsy.2016.11.002
26. Downar J, Daskalakis ZJ. New targets for rTMS in depression: a review of convergent evidence. *Brain Stimul* (2013) 6(3):231–40. doi: 10.1016/j.brs.2012.08.006
27. Hamilton M. A rating scale for depression. *J Neurol Neurosurg Psychiatry* (1960) 23(1):56. doi: 10.1136/jnnp.23.1.56
28. Behrens T, Berg HJ, Jbabdi S, Rushworth M, Woolrich M. Probabilistic diffusion tractography with multiple fibre orientations: What can we gain? *Neuroimage* (2007) 34(1):144–55. doi: 10.1016/j.neuroimage.2006.09.018
29. Behrens T, Johansen-Berg H, Woolrich M, Smith S, Wheeler-Kingshott C, Boulby P, et al. Non-invasive mapping of connections between human thalamus and cortex using diffusion imaging. *Nat Neurosci* (2003) 6(7):750–7. doi: 10.1038/nn1075
30. Chao-Gan Y, Yu-Feng Z. DPARSF: a MATLAB toolbox for "pipeline" data analysis of resting-state fMRI. *Front Syst Neurosci* (2010) 4:13. doi: 10.3389/fnsys.2010.00013
31. Bench C, Frackowiak R, Dolan R. Changes in regional cerebral blood flow on recovery from depression. *psychol Med* (1995) 25(2):247–62. doi: 10.1017/S0033291700036151
32. Drevets WC. Neuroimaging studies of mood disorders. *Biol Psychiatry* (2000) 48(8):813–29. doi: 10.1016/S0006-3223(00)01020-9
33. Wang L, Wei Q, Wang C, Xu J, Wang K, Tian Y, et al. Altered functional connectivity patterns of insular subregions in major depressive disorder after electroconvulsive therapy. *Brain Imaging Behav* (2019). doi: 10.1007/s11682-018-0013-z
34. Wang L, Yu L, Wu F, Wu H, Wang J. Altered whole brain functional connectivity pattern homogeneity in medication-free major depressive disorder. *J Affect Disord* (2019) 253:18–25. doi: 10.1016/j.jad.2019.04.040
35. Videbech P. PET measurements of brain glucose metabolism and blood flow in major depressive disorder: a critical review. *Acta Psychiatr Scand* (2000) 101 (1):11–20. doi: 10.1034/j.1600-0447.2000.101001011.x
36. Paus T, Barrett J. Transcranial magnetic stimulation (TMS) of the human frontal cortex: implications for repetitive TMS treatment of depression. *J Psychiatry Neurosci* (2004) 29(4):268.
37. Pascual-Leone A, Rubio B, Pallardo F, Catala MD. Rapid-rate transcranial magnetic stimulation of left dorsolateral prefrontal cortex in drug-resistant depression. *Lancet* (1996) 348(9022):233–7. doi: 10.1016/S0140-6736(96)01219-6
38. Hauer L, Scarano GI, Brigo F, Golaszewski S, Lochner P, Trinka E, et al. Effects of repetitive transcranial magnetic stimulation on nicotine consumption and craving: A systematic review. *Psychiatry Res* (2019) 281:112562. doi: 10.1016/j.psychres.2019.112562
39. Chen J, Zhou C, Wu B, Wang Y, Li Q, Wei Y, et al. Left versus right repetitive transcranial magnetic stimulation in treating major depression: a meta-analysis of randomised controlled trials. *Psychiatry Res* (2013) 210(3):1260–4. doi: 10.1016/j.psychres.2013.09.007
40. Januel D, Dumortier G, Verdon CM, Stamatiadis L, Saba G, Cabaret W, et al. A double-blind sham controlled study of right prefrontal repetitive transcranial magnetic stimulation (rTMS): therapeutic and cognitive effect in medication free unipolar depression during 4 weeks. *Prog Neuropsychopharmacol Biol Psychiatry* (2006) 30(1):126–30. doi: 10.1016/j.pnpbp.2005.08.016
41. Grimm S, Beck J, Schuepbach D, Hell D, Boesiger P, Bermpohl F, et al. Imbalance between left and right dorsolateral prefrontal cortex in major depression is linked to negative emotional judgment: an fMRI study in severe major depressive disorder. *Biol Psychiatry* (2008) 63(4):369–76. doi: 10.1016/j.biopsych.2007.05.033
42. Schutter DJ. Quantitative review of the efficacy of slow-frequency magnetic brain stimulation in major depressive disorder. *Psychol Med* (2010) 40 (11):1789–95. doi: 10.1017/S003329171000005X
43. Wu H, Sun H, Xu J, Wu Y, Wang C, Xiao J, et al. Changed Hub and Corresponding Functional Connectivity of Subgenual Anterior Cingulate Cortex in Major Depressive Disorder. *Front Neuroanat* (2016) 10:120. doi: 10.3389/fnana.2016.00120
44. Wang J, Becker B, Wang L, Li H, Zhao X, Jiang T. Corresponding anatomical and coactivation architecture of the human precuneus showing similar connectivity patterns with macaques. *Neuroimage* (2019) 200:562–74. doi: 10.1016/j.neuroimage.2019.07.001
45. Fitzgerald PB, Hoy K, McQueen S, Maller JJ, Herring S, Segrave R, et al. A randomized trial of rTMS targeted with MRI based neuro-navigation in treatment-resistant depression. *Neuropsychopharmacology* (2009) 34 (5):1255–62. doi: 10.1038/npp.2008.233
46. Rusjan PM, Barr MS, Farzan F, Arenovich T, Maller JJ, Fitzgerald PB, et al. Optimal Transcranial Magnetic Stimulation Coil Placement for Targeting the Dorsolateral Prefrontal Cortex Using Novel Magnetic Resonance Image-Guided Neuronavigation. *Hum Brain Mapp* (2010) 31(11):1643–52. doi: 10.1002/hbm.20964
47. Brunoni AR, Chaimani A, Moffa AH, Razza LB, Gattaz WF, Daskalakis ZJ, et al. Repetitive Transcranial Magnetic Stimulation for the Acute Treatment of Major Depressive Episodes. *JAMA Psychiatry* (2017) 74(2):143. doi: 10.1001/jamapsychiatry.2016.3644

Conflict of Interest: The authors declare that the research was conducted in the absence of any commercial or financial relationships that could be construed as a potential conflict of interest.

frontiers in Psychiatry

ORIGINAL RESEARCH
published: 29 April 2020
doi: 10.3389/fpsyt.2020.00358

Emotional Contexts Modulate Anticipatory Late Positive Component and Reward Feedback Negativity in Adolescents With Major Depressive Disorder

Wenhai Zhang[1,2,3†], Caizhi Liao[2†], Fanggui Tang[3†], Shirui Liu[3], Jing Chen[4], Lulu Zheng[2], Ping Zhang[5], Qiang Ding[6] and Hong Li[4]*

[1] Mental Health Center, Yancheng Institute of Technology, Yancheng, China, [2] College of Education Science, Chengdu University, Chengdu, China, [3] College of Education Science, Hengyang Normal University, Hengyang, China, [4] Institute for Brain and Psychological Sciences, Sichuan Normal University, Chengdu, China, [5] Research Center of Brain and Cognitive Neuroscience, Liaoning Normal University, Dalian, China, [6] Department of Psychological Medicine, Children's Hospital of Fudan University, Shanghai, China

OPEN ACCESS

Edited by:
Jeffrey Robert Strawn, University of Cincinnati, United States

Reviewed by:
Molly K. McVoy, Case Western Reserve University, United States
Deniz Doruk, Mayo Clinic, United States

***Correspondence:**
Hong Li
bmhlab@163.com

[†]These authors have contributed equally to this work

Specialty section:
This article was submitted to Neuroimaging and Stimulation, a section of the journal Frontiers in Psychiatry

Received: *12 January 2020*
Accepted: *08 April 2020*
Published: *29 April 2020*

Citation:
Zhang W, Liao C, Tang F, Liu S, Chen J, Zheng L, Zhang P, Ding Q and Li H (2020) Emotional Contexts Modulate Anticipatory Late Positive Component and Reward Feedback Negativity in Adolescents With Major Depressive Disorder. Front. Psychiatry 11:358. doi: 10.3389/fpsyt.2020.00358

Background: Neuroimaging research has determined deficits in the dopaminergic circuit of major depressive disorder (MDD) during adolescence. This study investigated how emotional contexts modulate the temporal dynamics of reward anticipation and feedback in adolescents.

Methods: EEG data from 35 MDD and 37 healthy adolescents were recorded when they conducted a gambling task after being presented with emotional pictures.

Results: The results demonstrated that both MDD and healthy adolescents exhibited the largest late positive component (LPC) in positive contexts at the frontal sites and the largest LPC in negative contexts at the central sites; however, MDD adolescents exhibited anticipatory LPC hypoactivation than healthy adolescents. However, MDD adolescents exhibited smaller gain feedback negativity (FN) than healthy adolescents independent of emotional contexts, positively correlating with the trait anhedonia according to the consummatory aspect of the Temporal Experience of Pleasure Scale. In contrast, MDD adolescents exhibited greater FN loss in positive and neutral contexts than healthy adolescents while no difference in FN loss was found between the two groups in negative contexts. Moreover, the FN loss amplitudes negatively correlated with hedonic tone according to the Snaith-Hamilton Pleasure Scale over the past week.

Conclusions: These findings suggest that MDD adolescents exhibited dissociable deficits in reward anticipation and gain or loss feedback that are distinctly modulated by emotional contexts, and they deepen our understanding of the modulation of emotional contexts on the temporal dynamic reorganization of the reward circuit in MDD adolescents.

Keywords: adolescents, feedback negativity, late positive component, major depressive disorder, reward anticipation

INTRODUCTION

Adolescence is a critical period of developmental transition in cognitive, affective, and social domains (1). During this period, adolescents undergo dramatic neuroplastic changes in neural structure and function (including the dopaminergic corticomesolimbic circuit) (2), coinciding with a high incidence of mental illnesses (e.g., depression with the subsequent reoccurrence of depressive episodes) (3). Particularly, adolescents in major depressive disorder (MDD) exhibit emotional disturbances and blunted reward sensitivity (4). As MDD impacts not only responses to emotional events, but extends to other cognitive processes (e.g., reward processing) carried out in the context of emotional engagement (5, 6), exploring the interaction between emotional contexts and reward processes is important for the understanding of the reward function reorganization in MDD across adolescence.

It is well-known that contextual factors (e.g., affective state/mood) might promote or subvert goal-directed behaviors (7). According to the appraisal tendency framework (8), contextual emotions generate specific anticipatory effects consistent with underlying appraisal tendencies and carry over to a new situation to alter sequent task performances (9–11). Changes in anticipatory effect might lead to goal reprioritization by modifying the salience of potential gains or loss: positive mood increases the value of reward motivation and activates corticostriatal pathways, including the nucleus accumbens, putamen, and ventromedial prefrontal cortex (9, 12–14). However, these effects are not found during reward outcome, loss anticipation, and loss outcome (14). Following positive mood induction, nucleus accumbens' activation decreases during reward anticipation (but not receipt) while its connectivity with the dorsolateral prefrontal cortex increases and these effects are modulated by anhedonia (15).

In contrast, negative mood leads to a greater degree of anchor biasing, which reduces reward-processing capacity and makes people avoid loss (16–18). Recently, Park et al. (19) proposed the valence compatibility hypothesis and found that positive emotional valence increases activity in typical reward-processing regions (e.g., ventral striatum) (reflecting additive value effect) while negative valence imposes increased task demands, eliciting conflict processes, which leads to the engagement of regions related to cognitive control (e.g., medial and lateral prefrontal cortex). Thus, how emotional contexts interact with reward processes during the distinct stages of reward anticipation and outcome remains an open question.

Event-related potentials with high temporal resolution easily capture rapid neural responses during different stages of reward processes. Late positive component (LPC) is a slow, positive component that lasts several hundred milliseconds after stimulus onset (20). Generally, positive and negative visual stimuli elicit enhanced LPC amplitudes compared with neutral stimuli (21), reflecting selective attention to motivationally salient stimuli (22). Particularly, during the anticipatory stage, the low positive affect trait was associated with reduced LPC by rewarding images and a blunted threat of eliciting LPC in adult depression, while the negative affect trait was not associated with the magnitude of neural responses to either threatening or rewarding pictures (23). Moreover, Howsley & Levita (24) found that only preadolescents exhibited heightened LPC in the reward block, whereas all preadolescents, adolescents, and late adolescents exhibited LPC potentiation to discriminative stimuli versus control stimuli in the avoidance block.

Feedback negativity (FN) is a negative-going waveform, and it reaches a maximum at the frontocentral sites approximately 300 ms after feedback presentation (25). Reflecting deeper striatal signals or prefrontal responses to changes in striatal activity (26–28), FN is sensitive to outcome evaluation and is correlated with the magnitude of the reward prediction error (29, 30). Following sadness induction, individuals reporting a greater state of sadness exhibited less differentiation between non-rewards and rewards in behavioral and FN responses (31). In contrast, positive emotional contexts enhanced reward-related FN sensitivity to outcomes compared with neutral and negative emotional contexts (9). Moreover, the FN amplitude to gain feedback (but not loss) in MDD adults was related to anhedonia severity (32). In adolescents, depressive symptoms were associated with reduced FN (33, 34), but the opposite trend has also been observed (35). After sadness induction, the reduced FN was also observed in adolescents with high familial risk for MDD (26). Taken together, positive and negative contexts might modulate the temporal dynamics of reward anticipation and outcome evaluation differently in MDD adolescents.

The present study aimed to investigate how emotional contexts interact with reward processes in MDD adolescents. In each trial, a positive, neutral, or negative picture was presented before MDD and healthy adolescents accomplished a simple gamble task, and then they received gain or loss feedback. Based on the appraisal tendency framework and the previous results (19, 23), we expected that positive contexts would increase anticipation-related LPC amplitudes and gain-related FN compared with neutral and negative contexts while negative contexts would amplify loss-related FN compared with positive and neutral contexts. Moreover, if MDD adolescents have impaired capacity to reward processing and greater perceptual biases to avoidance-related cues (24, 32–34), MDD adolescents would exhibit smaller LPC amplitudes and smaller FN amplitudes in gain trials, while MDD adolescents would exhibit larger FN amplitudes in loss trials relative to healthy adolescents.

METHODS

Participants

In total, we recruited 74 right-handed adolescent students (14–18 years old) from several secondary vocational schools in Dalian City, China. All participants had the normal or corrected vision and provided written informed consent under the approval of their parents. All adolescents completed clinical mini-interviews that were performed separately with adolescents and their parents. MDD adolescents were included if they had a primary MDD diagnosis based on DSM-IV criteria but no other mental disorders and had received no medication treatment for the past

3 months. Healthy adolescents were included if they had no current or past psychiatric diagnoses and serious head trauma. Two healthy adolescents were excluded due to poor EEG quality. Finally, the sample had 35 MDD adolescents (11 males; 15.26 ± 1.41years old) and 37 healthy adolescents (12 males; 15.53 ± 1.36 years old). This study was under the Declaration of Helsinki and was approved by the local ethics committee.

Stimuli

Two hundred and sixty-four pictures were selected from the Chinese Affective Picture System (36), including 88 positive, 88 neutral, and 88 negative pictures. There were no differences in arousal among positive, neutral, and negative pictures, but there were significant differences in valence among the three picture types ($p < 0.001$), as reported by another sample of 40 healthy adolescents from the same schools. E-prime 2.0 (Psychology Software Tools Inc., Pittsburgh) was used for stimulus presentation and response recording.

Measures

Beck Depression Inventory-II (BDI-II), a 21-item self-reporting inventory, measures symptoms of depression (past two weeks) (37). The version used for the present study has been validated in the Chinese population (32). Cronbach's alpha in the current sample was 0.86.

The Temporal Experience of Pleasure Scale (TEPS) was used to assess distinct components of the long-term pleasure experience (including anticipatory and consummatory aspects) (38). This study applied a 20-item Chinese version that was revised from the original English version (38, 39). In the current sample, Cronbach's alphas for the TEPS-ANT (anticipatory pleasure) and the TEPS-CON (consummatory pleasure) were 0.82 and 0.84, respectively.

The Snaith–Hamilton Pleasure Scale (SHAPS) was used to measure the hedonic tone over the past week (40). This scale contains 14 items and covers four aspects of hedonic experiences, i.e., interests/past times, sensory experience, social interaction, and food/drink. The Chinese version in the current study has good validity in Chinese samples (41). Cronbach's alpha in our sample was 0.90.

Procedure

In the laboratory, participants were seated in a sound-attenuated, electrically shielded room where they were attached to the sensors. As **Figure 1** shows, after receiving an understanding of the instructions, they conducted a simple gambling task. The task included 240 trials with 80 trials separately for positive, neutral, and negative pictures. At the beginning of each trial, participants were presented with a fixation for 1,000 ms and then a picture for 1,500 ms. Next, two doors appeared on the screen for 1,000 ms when participants were instructed to guess how to choose the door. They were told that they would win 1 or 5¥ in a winning trial or lose 1 or 5¥ in a loss trial. When the doors with the number of 1 or 5 appeared randomly on the left or right side for 1,000 ms, participants pressed the button to choose the door they guessed. The outcome was presented the next screen on which 1 or 5 appeared for a win or −1 or −5 appeared for a loss. During the task, 40 win and 40 loss trials for each picture type were presented in random order. Participants rested 15 s for every 40 trials.

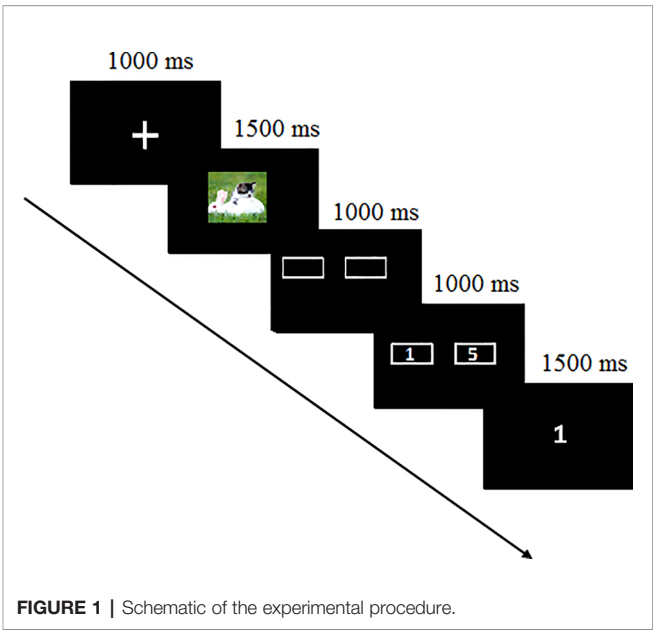

FIGURE 1 | Schematic of the experimental procedure.

Data Collection and Statistical Analysis

Continuous scalp EEG was collected from the Active Two system (BioSemi, Netherlands) with a 64-electrode elastic cap arranged according to the 10/20 guidelines. Electrooculogram (EOG) was recorded using four electrodes placed above and below the left eye and at the outer edge of the right eye to monitor horizontal and vertical eye movements. The impedance was brought below 10 kΩ. The data were sampled at 500 Hz with a bandpass of 0.10–100 Hz and a 24-bit A/D converter referenced to the vertex electrode (Cz). EEG data were offline re-referenced to the mean of the two mastoids using Brain Vision Analyzer 2.0 (Brain Product, Munich, Germany). The signals were bandpass-filtered using a second-order digital Butterworth filter (24 dB) of 0.10–30 Hz and adjusted for DC offset. EEG data were visually inspected for artifacts or extreme offsets. Oculomotor artifacts were eliminated using built-in ICA blink templates. Epochs were generated from −200 ms to 1,000 ms following the presentation of the stimuli or feedback and were baseline-corrected using the 200 ms pre-stimulus/feedback interval. Trials with voltage amplitudes over ±50 μV were discarded by an automatic procedure.

The ERP analysis focused on the two stages of anticipation and feedback. During the anticipatory stage, we selected the mean LLP amplitudes of three composite electrodes separately from the frontal (Fz, F1, and F2), frontocentral (FCz, FC1, and FC2), and central (Cz, C1, and C2) electrodes within the 600–800 ms time window. Similarly, during the outcome feedback stage, we selected the mean FN amplitudes of the three composite electrodes separately from the prefrontal (FPz, FP1, and FP2), frontal (Fz, F1, and F2), and frontocentral (FCz, FC1, and FC2) electrodes between 270 and 370 ms.

Repeated-measures analysis of variance (ANOVA) with two groups (MDD and control) × three valences (positive, neutral, and negative pictures) × three regions were conducted separately for LPC, FN in the gain trials, and FN in the loss trials. Independent-sample tests were executed for depressive symptoms and anhedonia severity. The Greenhouse–Geisser correction was used when the variance sphericity assumption was violated. All *post hoc* tests were corrected by the Bonferroni method. Pearson's correlation analysis was performed to investigate the association between behavioral and ERP data.

RESULTS

Behavioral Data

As **Table 1** shows, the independent-sample t-test indicated that MDD adolescents reported significantly higher symptoms of depression as measured by BDI-II than the healthy controls (t (71) = 17.41, $p < 0.001$). Moreover, MDD adolescents exhibited lower anticipatory pleasure experience as measured by TEPS-ANT (t (71) = 2.96, $p < 0.01$) and higher SHARP scores than the healthy controls (t (71) = 5.21, $p < 0.001$). However, there were no sex or age differences between the two groups (t (71) = 0.94, 0.61, p >0.05).

ERP Data

LPC at the Anticipatory Stage

The three-way repeated-measures ANOVA yielded significant main effects of group (F(1, 70) = 4.52, $p < 0.05$, $\eta^2 = 0.16$), valence (F(2, 140) = 29.41, $p < 0.001$, $\eta^2 = 0.30$), and region (F(2, 140) = 8.85, $p < 0.001$, $\eta^2 = 0.11$) (See **Figure 2** and **Table 2**). The *post hoc* tests indicated that the LPC amplitudes in MDD adolescents were lower than those in healthy adolescents ($p_{adj} = 0.0068$); the LPC amplitudes for positive pictures were greater than those for negative pictures, which were larger than those neutral pictures ($p_{adj} = 0.0008$); the LPC amplitudes at the frontocentral sites were the greatest ($p_{adj} = 0.0004$). Furthermore, there was a significant interaction between valence and region (F(4, 280) = 2.97, $p < 0.05$, $\eta^2 = 0.10$). The *post hoc* tests indicated that at the frontal sites, the LPC amplitudes for positive pictures were greater than those for negative and neutral pictures ($p_{adj} = 0.0274$); at the central sites, the LPC amplitudes for negative pictures were larger than those for positive and neutral pictures ($p_{adj} = 0.0165$); at the frontocentral sites, there were no differences in LPC amplitudes for the three type pictures (p_{adj} >0.05). No other significant effects were observed.

FN at the Feedback Stage

In the gain trials, the three-way repeated-measures ANOVA yielded significant main effects of group (F (1,70) = 8.51, $p < 0.01$, $\eta^2 = 0.31$) and region (F (2,140) = 23.46, $p < 0.001$, $\eta^2 = 0.25$; See **Figure 3** and **Table 2**). The *post hoc* tests indicated that MDD adolescents exhibited lower FN amplitudes than healthy adolescents ($p_{adj} = 0.0036$); the FN amplitudes were greatest at frontocentral sites and smallest at the prefrontal sites ($p_{adj} = 0.0048$). Additionally, there was a significant interaction between group and region (F (2,140) = 10.32, $p < 0.01$, $\eta^2 = 0.21$) (See **Figure 4**). The *post hoc* tests indicated that MDD adolescents exhibited lower FN amplitudes at the prefrontal sites ($p_{adj} = 0.0036$)

TABLE 1 | Demographic and sample characteristics.

Characteristic	MDD	HCL	Statistic	*p*-value
Age (years)	15.26 ± 1.41	15.53 ± 1.36	$t = 0.58$	0.61
Sex (M/F)	24/11	25/12	$\chi^2 = 0.00221$	0.94
BDI-II	33.32 ± 5.71	6.26 ± 1.72	$t = 17.41$	< 0.001
SHARP	28.45 ± 7.21	22.89 ± 5.78	$t = 5.21$	< 0.001
Age of first episode onset (years)	12.62 ± 1.70			
Duration (months)	25.82 ± 6.49			

MDD, major depressive disorder; HCL, healthy controls. BDI, Beck Depression Inventory-II; SHARP, the Snaith-Hamilton Pleasure Scale.

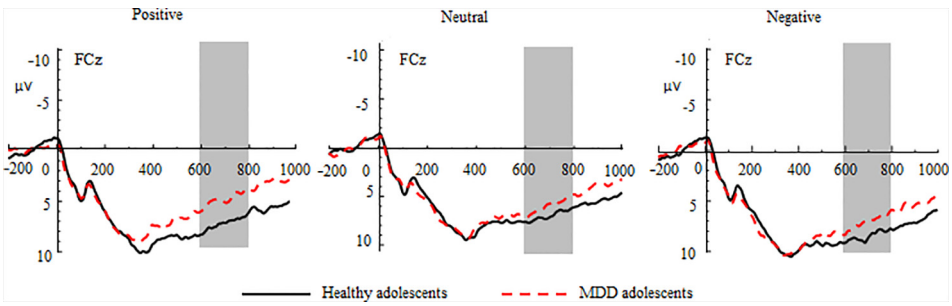

FIGURE 2 | Group waveforms of major depressive disorder (MDD) and healthy adolescents for positive, neutral, and negative pictures during the anticipatory stage at FCz. Late positive components are defined within 600–800 ms.

TABLE 2 | Results of the 3-factorial repeated-measures analysis of variance (ANOVA).

Dependent variables	Variables	*df*	*F* value	*p*-value
Anticipatory LPC	Group	1, 70	4.52	0.0132*
	Valence	2, 140	29.41	0.0005***
	Region	2, 140	8.85	0.0042**
	Group × valence	2, 140	2.51	0.2964
	Group × region	2, 140	2.21	0.3872
	Valence × region	4, 280	2.97	0.0312*
	Group × valence × region	4, 280	2.08	0.1245
FN in gain trials	Group	1, 70	8.51	0.0076**
	Valence	2, 140	1.68	0.5843
	Region	2, 140	23.46	0.0006***
	Group × valence	2, 140	2.31	0.3745
	Group × region	2, 140	10.32	0.0052**
	Valence × region	4, 280	2.10	0.1205
	Group × valence × region	4, 280	1.68	0.5026
FN in loss trials	Group	1, 70	14.87	0.0026**
	Valence	2, 140	3.97	0.0231*
	Region	2, 140	8.91	0.0039**
	Group × valence	2, 140	8.47	0.0061**
	Group × region	2, 140	1.97	0.5167
	Valence × region	4, 280	2.12	0.1201
	Group × valence × region	4, 280	1.49	0.6781

*LPC, late positive component; FN, feedback negativity. *p < 0.05, **p < 0.01, ***p < 0.001.*

while there were no differences in FN amplitudes at the frontal and frontocentral sites (p_{adj} >0.05).

In the loss trials, the three-way repeated-measures ANOVA revealed significant main effects of group (F (1,70) = 14.87, $p < 0.01$, $\eta^2 = 0.44$), valence (F (2,140) =3.97, $p < 0.05$, $\eta^2 = 0.11$), and region (F (2,140) = 8.91, $p < 0.01$, $\eta^2 = 0.11$) (See **Figure 5** and **Table 2**). The *post hoc* tests indicated that MDD adolescents exhibited greater FN amplitudes than healthy adolescents (p_{adj} = 0.0028); the FN amplitudes for negative pictures were more pronounced than those for positive and neutral pictures (p_{adj} = 0.0128); the FN amplitudes at the frontocentral sites were the highest (p_{adj} = 0.0051). Moreover, there was a significant interaction between group and valence (F (2,140) =8.47, $p < 0.01$, $\eta^2 = 0.21$) (See **Figure 4**). The *post hoc* tests indicated that MDD adolescents exhibited more pronounced FN amplitudes for positive and neutral pictures than healthy adolescents (p_{adj} = 0.0027, 0.0045), while we detected no differences in FN amplitudes for negative pictures between the two groups (p_{adj} = 0.1827).

Correlation Analysis

The correlation analyses indicated that the BDI scores were negatively correlated with LPC amplitudes for positive

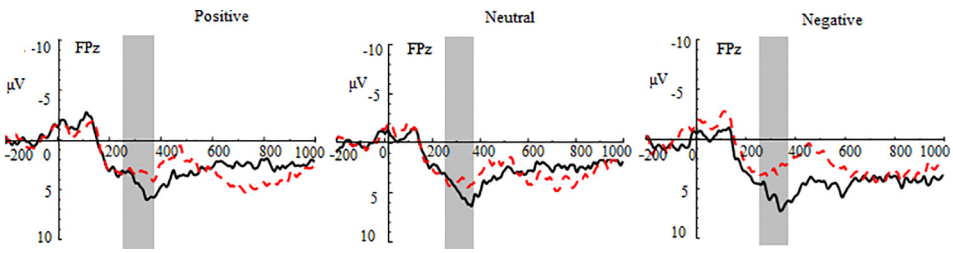

FIGURE 3 | Group waveforms of major depressive disorder (MDD) and healthy adolescents for positive, neutral, and negative pictures during the gain feedback stage at FPz. Feedback negativity is defined between 270 and 370 ms after the presentation of feedback.

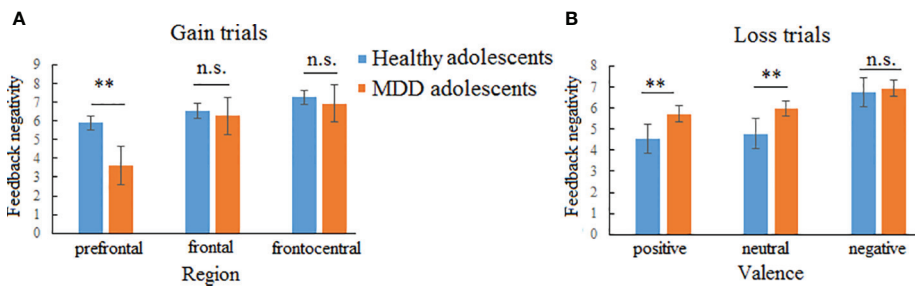

FIGURE 4 | Two-way interactions of feedback negativity (FN) in gain and loss trials. **(A)** Interaction between group and region in gain trials indicating that major depressive disorder (MDD) adolescents exhibited lower FN amplitudes than healthy adolescents at the prefrontal region while no group difference was found at the frontal and frontocentral regions. **(B)** Interaction between group and valences indicating that MDD adolescents exhibited larger FN amplitudes for positive and neutral pictures than healthy adolescents while no group difference was found for negative pictures. n.s., not significant. **p < 0.01.

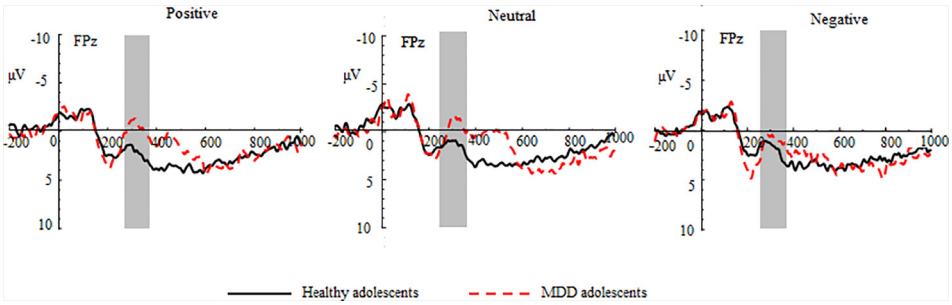

FIGURE 5 | Group waveforms of major depressive disorder (MDD) and healthy adolescents for positive, neutral, and negative pictures during the loss feedback stage at FPz.

(r = −0.26, p < 0.05) and negative pictures (r = −0.25, p < 0.05) but not for neutral pictures (r = −0.06, p >0.05). In the gain trials, the TEPS-CON scores were positively correlated with the FN amplitudes for positive, negative, and neutral pictures (r = 0.31, 0.31, 0.34, p < 0.01). In the loss trials, the SHARP scores were positively correlated with the FN amplitudes for positive, negative, and neutral pictures (r = 0.24, 0.24, 0.25, p < 0.05).

DISCUSSION

This study used LPC and FN as neural indices to examine how emotional contexts modulate reward anticipation and outcome evaluation in MDD adolescents. The behavioral results indicated that MDD adolescents had a lesser anticipatory pleasure experience (TEPS-ANT) and higher SHARP scores than healthy adolescents. The ERP results indicated that at the anticipatory stage MDD adolescents exhibited smaller LPC amplitudes than healthy adolescents; at the feedback stage, MDD adolescents exhibited smaller FN amplitudes for the gain trials than healthy adolescents while MDD adolescents exhibited greater FN amplitudes for the loss trials than healthy adolescents. Consistent with the previous fMRI and ERP results (32–34), these observations suggest that MDD adolescents exhibited impaired capacity toward reward processing (i.e., anhedonia) and greater perceptual biases toward negative outcomes. Moreover, the emotional contexts modulated LPC and FN in adolescents, discussed as follows, which is important implication for our understanding of the temporal dynamical organization and development of brain function during adolescence.

Many researchers have found that positive mood facilitates reward anticipation motivation, including increased corticostriatal circuit activation (9, 12–14) and anticipatory LPC amplitudes (24). In line with these results, our study found that the anticipation-related LPC amplitudes in positive picture contexts were larger than those in negative and neutral picture contexts at the frontal sites. In contrast, the negative picture contexts elicited larger LPC amplitudes than the positive and neutral picture contexts at the central sites. On the one hand, consistent with the appraisal tendency framework (8), positive mood further enhanced the value of reward motivation while negative mood increased avoidant motivation, which reduced the value of reward anticipation (16–18). On the other hand, Park et al. (19) found that reward trials by positive emotion did not enhance activity differently anywhere in the adult brain. Inconsistent with this, our results suggest that as LPCs seem to be modulated by anticipatory top-down signals from the frontoparietal neural network (42, 43), the adolescent brain is undergoing functional reorganization and exhibits cortical differences in top-down processing approach and avoidant motivation. For example, the previous adult study indicated that positive and negative stimuli activated different functional networks (44). Future research in adolescents should further verify the possibility of interaction between valences and cortical regions.

During reward receipt, the group × region interaction on FN amplitudes reached significance but independent of emotional contexts, indicating that MDD adolescents exhibited smaller FN amplitudes than healthy adolescents only at the prefrontal sites. Consistent with our results, the previous ERP and behavioral studies also found that emotional stimuli are processed independent of reward (45, 46). This might be attributed to the more pronounced gain-related FN amplitudes reflecting a phasic increase in dopaminergic activity in the reward pathways, which partly underpins the associations between gain-related FN and trait measures; for example, extraversion has higher scores on a dopaminergic function and is associated with enhanced FN waves compared with introversion (47). We also found that gain-related FN amplitudes were positively correlated with TEPS-CON scores (reflecting anhedonia trait). Another possibility is that emotional contexts are task-irrelevant and have a long internal with feedback presentation, which leads to the disappearance of the carryover effect. However, this did not explain why loss-related FN amplitudes are modulated by emotional contexts as discussed in the following.

Notably, we observed a significant group × valence interaction on loss-related FN amplitudes, indicating that MDD adolescents exhibited greater FN amplitudes in positive and neutral contexts than healthy adolescents while no FN difference was observed between the two groups in negative contexts. These results seemed to be consistent with the valence

compatibility hypothesis (19). During loss feedback that leads to an aversive signal, positive contexts elicited conflict processes with loss feedback consumption, which makes frontal control engage with conflict regulation. The previous results indicated that MDD individuals have impaired corticostriatal connectivity (e.g., dorsolateral prefrontal cortex and striatum) following positive mood induction (12, 15). Thus, MDD adolescents seemed to be incapable of modulating potential conflicts, which further amplifies the aversive effects of losing money. In contrast, there was no valence mismatch between negative contexts and transient loss manipulation, so that MDD adolescents exhibited the same FN amplitudes as healthy adolescents. Moreover, the loss-related FN amplitudes were positively correlated with the SHARP scores, possibly reflecting anhedonia. Overall, these results suggest that emotional contexts did not appear to modulate gain-related FN, reflecting a lower dopamine function (trait anhedonia) in MDD adolescents, whereas emotional contexts might modulate loss-related FN, partly reflecting anhedonia from disrupted regulating function in corticostriatal circuits.

The limitations must be mentioned as follows. First, it should be acknowledged that this study had a small sample. Future studies should perform a power analysis to estimate the effect size and select a larger sample to verify the results. Second, although there were 40 trials for gain and 40 loss trials for loss, there were insufficient trials to separate ±1 or 5 Y trials. Therefore, future studies should add the number of gains and losses to separately analyze whether rewards of different sizes have an impact on FN amplitudes.

In summary, MDD adolescents exhibited dissociable deficits in reward anticipation and outcome processing that are modulated by emotional contexts. Anticipation-related LPC hypoactivation in MDD adolescents might reflect aberrant functional reorganization in top-down cortical networks that show different sensitivity to positive and negative contexts. Emotional contexts did not modulate reduced gain-related FN in MDD adolescents, which might reflect trait-like reward deficits in MDD adolescents. However, positive (but not negative) contexts seem to amplify loss-related FN, revealing impaired conflict-regulating function from the lateral and medial prefrontal cortex in MDD adolescents. These observations provide important evidence for our understanding of the temporal dynamic reorganization of the reward functions in MDD adolescents during distinct emotional contexts.

DATA AVAILABILITY STATEMENT

The data that support the findings of this study are available from the corresponding author upon reasonable request.

ETHICS STATEMENT

This study was in accordance with the Declaration of Helsinki and was approved by the Ethics Committee of Liaoning Normal University. Written informed consent to participate in this study was provided by the participants' legal guardian/next of kin.

AUTHOR CONTRIBUTIONS

LZ, QD, SL, PZ, and WZ designed and performed the study and analyzed the data. WZ wrote the manuscript. CL, FT, HL, and JC reviewed and modified the manuscript.

FUNDING

This study was supported by the National Natural Science Foundation of China (31470997 and 81171289) and Jiangsu Provincial Social Science Foundation of China (19JYD009).

REFERENCES

1. Luna B, Marek S, Larsen B, Tervo-Clemmens B, Chahal R. An integrative model of the maturation of cognitive control. *Annu Rev Neurosci* (2015) 38:151–70. doi: 10.1146/annurev-neuro-071714-034054
2. Casey BJ. Beyond simple models of self-control to circuit-based accounts of adolescent behavior. *Annu Rev Psychol* (2015) 66:295–319. doi: 10.1146/annurev-psych-010814-015156
3. Wagner S, Müller C, Helmreich I, Huss M, Tadić A. A meta-analysis of cognitive functions in children and adolescents with major depressive disorder. *Eur Child Adolescent Psychiat* (2014) 24:5–19. doi: 10.1007/s00787-014-0559-2
4. Bress JN, Foti D, Kotov R, Klein DN, Hajcak G. Blunted neural response to rewards prospectively predicts depression in adolescent girls. *Psychophysiology* (2013) 50:74–81. doi: 10.1111/j.1469-8986.2012.01485.x
5. Dichter GS, Felder JN, Smoski MJ. Affective context interferes with cognitive control in unipolar depression: An fMRI investigation. *J Affect Disord* (2009) 114:131–42. doi: 10.1016/j.jad.2008.06.027
6. Rottenberg J, Hindash AC. Emerging evidence for emotion context insensitivity in depression. *Curr Opin Psychol* (2015) 4:1–5. doi: 10.1016/j.copsyc.2014.12.025
7. Roseman IJ. Motivations and emotivations: approach, avoidance, and other tendencies in motivated and emotional behavior. In: Elliot AJ, editor. *Handbook of Approach and Avoidance Motivation*. New York: Psychology Press (2008).
8. Lerner JS, Tiedens LZ. Portrait of the angry decision maker: How appraisal tendencies shape anger's influence on cognition. *J Behav Decision Making* (2006) 19(2):115–37. doi: 10.1002/bdm.515
9. Bandyopadhyay D, Pammi VSC, Srinivasan N. Incidental positive emotion modulates neural response to outcome valence in a monetarily rewarded gambling task. *Prog Brain Res* (2019) 247:219–51. doi: 10.1016/bs.pbr.2019.04.004
10. Han S, Lerner JS, Keltner D. Feelings and consumer decision making: The appraisal tendency framework. *J Consumer Psychol* (2007) 17:158–68. doi: 10.1016/S1057-7408(07)70023-2
11. Lerner JS, Small DA, Loewenstein G. Heart strings and purse strings: Carryover effects of emotions on economic decisions. *Psychol Sci* (2004) 15:337–41. doi: 10.1111/j.0956-7976.2004.00679.x
12. Admon R, Pizzagalli DA. Corticostriatal pathways contribute to the natural time course of positive mood. *Nat Commun* (2015) 6:10065. doi: 10.1038/ncomms10065
13. Knutson B, Bhanji JP, Cooney RE, Atlas LY, Gotlib IH. Neural responses to monetary incentives in major depression. *Biol Psychiatry* (2008) 63(7):686–92. doi: 10.1016/j.biopsych.2007.07.023

14. Young CB, Nusslock R. Positive mood enhances reward-related neural activity. *Soc Cogn Affect Neurosci* (2016) 11(6):934–44. doi: 10.1093/scan/nsw012
15. Green IW, Pizzagalli DA, Admon R, Kumar P. Anhedonia modulates the effects of positive mood induction on reward-related brain activation. *NeuroImage* (2019) 193:115–25. doi: 10.1016/j.neuroimage.2019.02.063
16. Bodenhausen GV, Gabriel S, Lineberger M. Sadness and susceptibility to judgmental bias: The case of anchoring. *psychol Sci* (2000) 11:320–3. doi: 10.1111/1467-9280.00263
17. Kuhnen CM, Knutson B. The neural basis of financial risk-taking. *Neuron* (2005) 47:763–70. doi: 10.1016/j.neuron.2005.08.008
18. Umemoto A, Holroyd CB. Neural mechanisms of reward processing associated with depression-related personality traits. *Clin Neurophysiol* (2017) 128(7):1184–96. doi: 10.1016/j.clinph.2017.03.049
19. Park HRP, Kostandyan M, Boehler CN, Krebs RM. Winning smiles: Signalling reward by overlapping and non-overlapping emotional valence differentially affects performance and neural activity. *Neuropsychologia* (2019) 122:28–37. doi: 10.1016/j.neuropsychologia.2018.11.018
20. Cuthbert BN, Schupp HT, Bradley MM, Birbaumer N, Lang PJ. Brain potentials in affective picture processing: Covariation with autonomic arousal and affective report. *Biol Psychol* (2000) 52(2):95–111. doi: 10.1016/S0301-0511(99)00044-7
21. Hajcak G, Dunning JP, Foti D. Automatic and controlled attention to emotion: Time-course of the late positive potential. *Clin Neurophysiol* (2009) 120:505–10. doi: 10.1016/j.clinph.2008.11.028
22. Schupp HT, Flaisch T, Stockburger J, Junghofer M. Emotion and attention: Event-related brain potential studies. *Prog Brain Res* (2006) 156:123–43. doi: 10.1016/S0079-6123(06)56002-9
23. Weinberg A, Sandre A. Distinct associations between low positive affect, panic, and neural responses to reward and threat during late stages of affective picture processing. *Cogn Neurosci Neuroimaging* (2017) 3:59–68. doi: 10.1016/j.bpsc.2017.09.013
24. Howsley P, Levita L. Anticipatory representations of reward and threat in perceptual areas from preadolescence to late adolescence. *Dev Cogn Neurosci* (2017) 25:246–59. doi: 10.1016/j.dcn.2017.03.001
25. Gehring WJ, Willoughby AR. The medial frontal cortex and the rapid processing of monetary gains and losses. *Science* (2002) 295:2279–82. doi: 10.1126/science.1066893
26. Foti D, Kotov R, Klein DN, Hajcak G. Abnormal neural sensitivity to monetary gains versus losses among adolescents at risk for depression. *J Abnormal Child Psychol* (2011) 39:913–24. doi: 10.1007/s10802-011-9503-9
27. Hajcak G, Moser JS, Holroyd CB, Simons RF. It's worse than you thought: The feedback negativity and violations of reward prediction in gambling tasks. *Psychophysiology* (2007)) 44:905–12. doi: 10.1111/j.1469-8986.2007.00567.x
28. Holroyd CB, Coles MGH. The neural basis of human error processing: Reinforcement learning, dopamine, and the error-related negativity. *psychol Rev* (2002) 109:679–709. doi: 10.1037/0033-295X.109.4.679
29. San Martin R, Manes F, Hurtado E, Isla P, Ibanez A. Size and probability of rewards modulate the feedback error-related negativity associated with wins but not losses in a monetarily rewarded gambling task. *NeuroImage* (2010) 51:1194–204. doi: 10.1016/j.neuroimage.2010.03.031
30. Wu Y, Zhou X. The P300 and reward valence, magnitude, and expectancy in outcome evaluation. *Brain Res* (2009) 1286:114–22. doi: 10.1016/j.brainres.2009.06.032
31. Foti D, Hajcak G. State sadness reduces neural sensitivity to non-rewards versus rewards. *NeuroRep Rapid Commun Neurosci Res* (2010) 21(2):143–7. doi: 10.1097/WNR.0b013e3283356448
32. Liu W, Wang LZ, Shang HR, Shen Y, Li Z, Cheung EFC, et al. The influence of anhedonia on feedback negativity in major depressive disorder. *Neuropsychologia* (2014) 53(4):213–20. doi: 10.1016/j.neuropsychologia.2013.11.023
33. Bress JN, Smith E, Foti D, Klein DN, Hajcak G. Neural response to reward and depressive symptoms in late childhood to early adolescence. *Biol Psychol* (2012) 89:156–62. doi: 10.1016/j.biopsycho.2011.10.004
34. Bress JN, Meyer A, Hajcak G. Differentiating anxiety and depression in children and adolescents: Evidence from event-related brain potentials. *J Clin Child Adolesc Psychol* (2015) 44:238–49. doi: 10.1080/15374416.2013.814544
35. Webb CA, Auerbach RP, Bondy E, Stanton CH, Foti D, Pizzagalli DA. Abnormal neural responses to feedback in depressed adolescents. *J Abnormal Psychol* (2017) 126:19–31. doi: 10.1037/abn0000228
36. Bai L, Ma H, Huang YX, Luo YJ. The development of native Chinese affective picture system—a pretest in 46 college students. *Chin Ment Health J* (2005) 19:719–22. doi: 10.1016/j.molcatb.2005.02.001
37. Beck AT, Steer RA, Brown GK. *Beck Depression Inventory.* 2nd Ed Manual. San Antonio, TX: The Psychological Corporation (1996).
38. Gard DE, Gard MG, Kring AM, John OP. Anticipatory and consummatory components of the experience of pleasure: A scale development study. *J Res Pers* (2006) 40(6):1086–102. doi: 10.1016/j.jrp.2005.11.001
39. Liu W, Chan RC, Wang L, Huang J, Cheung E, Gong Q, et al. Deficits in sustaining reward responses in subsyndromal and syndromal major depression. *Prog Neuropsychopharmacol Biol Psychiatry* (2011) 35:1045–52. doi: 10.1016/j.pnpbp.2011.02.018
40. Snaith RP, Hamilton M, Morley S, Humayan A, Hargreaves D, Trigwell P. A scale for the assessment of hedonic tone the Snaith-Hamilton Pleasure Scale. *Br J Psychiatry* (1995) 167(1):99–103. doi: 10.1192/bjp.167.1.99
41. Liu W, Wang L, Zhu Y, Li M, Chan RC. Clinical utility of the Snaith-Hamilton-Pleasure Scale in Chinese settings. *BMC Psychiatry* (2012) 12:184. doi: 10.1186/1471-244X-12-184
42. Ferrari V, Codispoti M, Cardinale R, Bradley MM. Directed and motivated attention during the processing of natural scenes. *J Cogn Neurosci* (2008) 20 (10):1753–61. doi: 10.1162/jocn.2008.20121
43. Moratti S, Saugar C, Strange BA. Prefrontal-occipitoparietal coupling underlies late latency human neuronal responses to emotion. *J Neurosci* (2011) 31(47):17278–86. doi: 10.1523/JNEUROSCI.2917-11.2011
44. Zhang W, Li H, Pan X. Positive and negative affective processing exhibit dissociable functional hubs during the viewing of affective pictures. *Hum Brain Mapp* (2015) 36(2):415–26. doi: 10.1002/hbm.22636
45. Kaltwasser L, Ries S, Sommer W, Knight R, Willems RM. Independence of valence and reward in emotional word processing: Electrophysiological evidence. *Front Psychol* (2013) 4:168. doi: 10.3389/fpsyg.2013.00168
46. Wei P, Kang G. Task relevance regulates the interaction between reward expectation and emotion. *Exp Brain Res* (2014) 232:1783–91. doi: 10.1007/s00221-014-3870-8
47. Cooper AJ, Duke E, Pickering AD, Smillie LD. Individual differences in reward prediction error: Contrasting relations between feedback-related negativity and trait measures of reward sensitivity, impulsivity and extraversion. *Front Hum Neurosci* (2014) 8:248. doi: 10.3389/fnhum.2014.00248

Conflict of Interest: The authors declare that the research was conducted in the absence of any commercial or financial relationships that could be construed as a potential conflict of interest.

frontiers in Psychiatry

ORIGINAL RESEARCH
published: 30 April 2020
doi: 10.3389/fpsyt.2020.00338

Changes of Altruistic Behavior and Kynurenine Pathway in Late-Life Depression

Yujie Wu[1,2], *Naikeng Mai*[2], *Xuchu Weng*[1,3], *Jiuxing Liang*[3] *and Yuping Ning*[2,4,5*]

[1] School of Psychology, South China Normal University, Guangzhou, China, [2] Department of Neurology, The Affiliated Brain Hospital of Guangzhou Medical University (Guangzhou Huiai Hospital), Guangzhou, China, [3] Institute for Brain Research and Rehabilitation, South China Normal University, Guangzhou, China, [4] The First School of Clinical Medicine, Southern Medical University, Guangzhou, China, [5] Guangdong Engineering Technology Research Center for Translational Medicine of Mental Disorders, Guangzhou, China

Background: Depressive patients show less altruistic behavior. While, older adults present higher tendencies for altruism than younger adults. Depression and age are two of the influencing factors of altruism, kynurenine (KYN), and its metabolites. However, the characteristics of altruism in late-life depression (LLD) and its possible underlying mechanism have not been studied.

Objective: We aimed to explore the characteristics of altruism in LLD patients and its neurobiological mechanism and structural brain network. We investigated whether the levels of metabolites in kynurenine pathway (KP) and white matter (WM) network topological features would influence the altruistic behavior in LLD patients.

Methods: Thirty-four LLD patients and 36 heathy controls (HCs) were included. Altruism was evaluated by the Dictator Game (DG) paradigm. Serum concentrations of KP metabolites were detected by the liquid chromatography-tandem mass spectrometry method. The topological features of the WM network were calculated from diffusion tensor imaging data in conjunction with graph-theoretical analysis.

Results: The LLD participants exhibited a higher level of altruism and WM global network properties than the HCs. Kynurenic acid to kynurenine (KYNA/KYN) ratio was associated with the DG performance in LLD group. KYNA/KYN ratio was associated with the WM network properties in HC group.

Conclusions: KYN metabolism played an important role in altruistic behavior in LLD.

Keywords: altruism, kynurenine pathway, late-life depression, Dictator Game, diffusion tensor imaging, graph-theoretical analysis

OPEN ACCESS

Edited by:
Ping Li,
Qiqihar Medical University, China

Reviewed by:
Yosuke Morishima,
University of Bern, Switzerland
Wi Hoon Jung,
Daegu University, South Korea

***Correspondence:**
Yuping Ning
ningjeny@126.com

Specialty section:
This article was submitted to Neuroimaging and Stimulation, a section of the journal Frontiers in Psychiatry

Received: *11 January 2020*
Accepted: *03 April 2020*
Published: *30 April 2020*

Citation:
Wu Y, Mai N, Weng X, Liang J and Ning Y (2020) Changes of Altruistic Behavior and Kynurenine Pathway in Late-Life Depression. Front. Psychiatry 11:338. doi: 10.3389/fpsyt.2020.00338

INTRODUCTION

Depression is the most common mental disorder in the growing geriatric population (1). Late-life depression (LLD) is associated with physical and cognitive deficits and the poor treatment responses of these patients, which results in a heavy economic and emotion burden to their families (2–5). Moreover, deficits of social functioning commonly occur in patients with depression, which have an

impact on their work performances and marriages (6). However, seldom investigations shed light on social impairments in LLD. Hence, we attempted to focus on the social functioning in LLD from the perspective of neural, biological, and behavioral factors.

Altruistic behavior is a kind of typical prosocial behavior in human societies, influencing the interactions and cooperations among individuals (7). Altruism is a characteristic in which people are willing to help others even when there is no expectation of receiving any help or reward in return. Altruism has been modeled using the Dictator Game (DG) (8). Based on previous studies, depression and age are two of the primary influencing factors of altruistic behavior. Depression patients at midlife would avoid altruistic behaviors (9). Furthermore, older adults show higher tendencies for altruism than younger adults (10). However, altruistic behavior in depression in old age and its possible underlying mechanism have not been studied.

There are many possible factors can influence altruistic behavior, such as social environment, economic condition and hormones (11). According to a literature review, 5-hydroxytryptamine (5-HT) plays an important role in altruism. Depletion of 5-HT is associated with decreased activity in the striatum by affecting dopaminergic terminal function (6). While, the level of dopamine in the ventral striatum is one of vital factors that influences altruism decision (8). Kynurenine pathway (KP) plays an important role in 5-HT synthesis. Kynurenine (KYN) and its metabolites can cross the blood-brain barrier and have effects on the central nervous system and several psychiatric disorders, such as depression and schizophrenia (12). Tryptophan (TRP) is considered as the beginning of KP. The shunt of TRP from 5-HT formation to KYN formation is a major etiological factor of depression (13, 14). We aimed to explore the relationship between several main metabolites in the upstream and downstream of KP and altruistic behavior in patients with LLD.

KP changes are associated with the development of LLD (15). There are two distinct routes in KYN metabolism. One such route is the kynurenic acid (KYNA) pathway. The other is the quinolinic acid (QUIN) pathway, which forms the N-methyl-D-aspartate receptor (NMDA-R) agonists that make the astrocyte-microglia-neuronal network vulnerable. KYNA exerts a neuroprotective role and is the only known endogenous antagonist to NMDA-R, which can inhibit the toxic effect of QUIN (16). However, the abnormal accumulation of KYNA beyond physiological levels could induce glutamatergic hypofunctioning and cause cognitive dysfunction, since KYNA is an antagonist for all of the ionotropic excitatory amino acid receptors (17). The severity of depression is associated with the level of KP imbalance (18). TRP metabolism has been related to depressive symptoms in old age (19). According to our consideration, if LLD patients display different altruism levels, KP alterations, especially the KYN metabolism changes, may represent one neurobiological explanation and associated with the level of altruism.

Previous studies mention that KP is associated with the disrupted white matter (WM) in bipolar disorders (20), schizophrenia (21), and multiple sclerosis (22). However, the study on the relationship between KP and changes of WM in LLD is not been found. Some scholars have found that LLD is characterized by WM lesions that affect the WM tract integrity and alter the rich-club organization, which disrupt cognition function and mental health in LLD patients (23, 24). In addition, we suspected that KP possibly has an impact on the WM connectivity in LLD, which may underlie the development of the cognitive and social functioning deficits of LLD. Furthermore, the neural pathway of altruistic behavior is not fully understood. According to the previous study of functional connectivity, the engagement of the medial prefrontal and temporo-parietal cortices is associated with prosocial behavior (25). While the changes of function is related with the changes of structure (26). Thus, we considered the changes of altruistic behavior in LLD might blame to some abnormal brain structural network connectivity.

Diffusion tensor imaging (DTI), a technique that is used to quantify water diffusion in tissue, is sensitive to tissue damage and can detect damage in the WM (23). The human brain serves as a highly complex and integrated network system. The graph-theoretical analysis of this complex network has resulted in a potent mathematical tool to quantify the collection of the comprehensive topological dynamics in these human structural connectomes (27). Considering the light of corresponding relationship between the function and structure of our brain (26), the structural foundation of the altruism changes that occur in older people is another question we want to investigate. DTI data in conjunction with graph-theoretical analysis makes it possible to quantitatively describe the brain's overall organization and communicative processes through a variety of physical topological properties.

In this study, we aimed to investigate the characteristics of altruistic behavior, KP metabolism, and WM network connectivity in LLD, and further explore whether KP metabolism and WM network topological features would influence altruistic behavior in LLD patients. We collected DG performance, serum sample, and DTI data from each participant. The DG task was conducted to assess altruistic behavior. Serum concentrations of TRP, KYN, and KYNA were determined by a high-performance liquid chromatography-tandem mass spectrometry (LC-MS/MS) method. A graph-theoretical analysis was utilized to calculate the global network properties that describe the WM topological features. We hypothesized that disruptions of KP metabolism and WM network topological features would occur in patients with LLD, and these disruptions would relate to altruism in LLD.

MATERIALS AND METHODS

Participants

This study was approved by the ethics committee of the Affiliated Brain Hospital of Guangzhou Medical University (Guangzhou Huiai Hospital). We obtained written informed consent from each participant after a complete description of this study. All of the patients were recruited from the outpatient and inpatient

departments of the Affiliated Brain Hospital of Guangzhou Medical University, Guangzhou, Guangdong, China, and the healthy controls (HCs) were recruited from the community.

All participants were interviewed by well-trained psychiatrists during a clinical interview that was structured to meet the inclusion and exclusion criteria. LLD was diagnosed based on *Diagnostic and Statistical Manual of Mental Disorders, fourth edition*. Cognition performance was evaluated by a Mini-Mental State Examination (MMSE). The presence of depressive symptoms was evaluated by the 17-item Hamilton Rating Scale for Depression (HAMD-17). Exclusion criteria were as follows: (1) serious suicidal behavior; (2) serious medical conditions or concomitant medications likely to influence the central nervous system or immunological function, including cardiovascular, respiratory, endocrine and neurological diseases; (3) a history of drug or alcohol abuse in the past 6 months or a history of drug or alcohol dependence within the past year; (4) < 55 years old. In addition, the gender- and age-matched HCs were required to have no first-degree relative with a psychiatric disorder (15, 28).

Finally, we recruited investigated 34 patients with a diagnosis of LLD and 36 healthy elderly subjects as HCs, and all of the participants were of Han Chinese ethnicity and were right-handed.

Experimental Procedures

Upon participants' arrival to the outpatient department, we collected peripheral blood samples and measured the body mass index (BMI) of every participant between 8:00 and 9:00 a.m. after an overnight fast. The blood samples were collected in vacutainers without additional additives. After 0.5 h of coagulation, the samples were centrifuged at 3,000 r/min for 10 min, and the supernatant was aliquoted into Eppendorf tubes (Eppendorf, Hamburg, Germany) and frozen at −80°C immediately until the time of the assay. Then, the DG task and neuropsychological tests were performed.

In DG procedures, we told participant that there were other participants who also took part in this game simultaneously but they did not know each another. The another old person played a passive recipient in DG task, and the participant played a proposer could choose how to allocate 1,000 monetary units (Yuan) between himself/herself and another old person. In the current study, DG task was anonymous paradigm in case of bias choice. Each participant played 30 rounds one-shot DG task against 30 anonymous players. With no material incentive to offer anything, a proposer who offers a nonzero amount is considered to be altruistic and the magnitude of their proposal reflects the degree of altruism from the proposer toward the passive recipient (8).

Laboratory Analyses

We used an LC-MS/MS method to detect the TRP, KYN, and KYNA serum concentrations. L-TRP, L-KYN, KYNA, and activated charcoal were purchased from Sigma-Aldrich, and Kyna-d5 was supplied by Toronto Research Chemicals, Inc. (Toronto, Canada). Methanol was obtained from Merck KGaA (Darmstadt, Germany) and ammonium formate was purchased from Sigma-Aldrich Corporation (Bangalore, India). Purified water was produced by a Milli-Q water purification system (Millipore Corporation, Billerica, MA, USA) (29).

MRI Acquisition

Participants were scanned by a 3.0-Tesla Philips Achieva scanner (Philips, Best, Netherlands). The T2-weighted image was applied to rule out cerebral infarction, tumors, and major WM lesions. Foam padding and earplugs were used to reduce head moving and scanner noise. The DTI scanning parameters were as follows: direction = 32, b_0 = 1,000 s/mm^2, repetition time (TR) = 10,015 ms, echo time (TE) = 92 ms, flip angle = 90°, matrix = 128 × 128 mm^2, FOV = 256 × 256 mm^2, 75 contiguous slices, voxel size = 2 × 2 × 2 mm^3. High-resolution T1-weighted images were acquired from a 3D spoiled gradient echo sequence: TR = 8.2 ms, TE = 3.8 ms, matrix= 256 × 256 × 188, FOV = 256 × 256 mm^2, voxel size = 1 × 1 × 1 mm^3.

Data Preprocessing

Data preprocessing was performed using the FMRIB's Diffusion Toolbox (FMRIB's Software Library, FSL) for the following procedures. First, the eddy current correction was used to correct the distortions from stretches and shears in the DTI as well as correct for simple head motion. Second, b_0 image extraction and brain extraction (fractional intensity threshold = 0.2) were performed. Third, a Bayesian Estimation of Diffusion Parameters Obtained using Sampling Techniques (Bedpostx) was used to set up the distribution of fiber orientation at each voxel. In the T1 images, BET was utilized for the brain extraction (fractional intensity threshold = 0.3).

Network Construction

The brain network contains nodes and edges. To determine the nodes in the network, we selected 90 gray matter regions of the cerebrum with Anatomical Automatic Labeling (AAL), which included 45 regions of cortical and subcortical structures in each hemisphere. Edge definition was accomplished using the connectivity probability between each pair of nodes in the network. Network construction was performed by PANDA (30). The details of network construction were as follows.

Node Definition

The procedure was completed following Gong's description (31). Briefly, T1 images were nonlinearly coregistered to the Montreal Neurological Institute (MNI) 152_T1_Template. The inverse warp was obtained from a previous step and the transformation matrixes from T1 to b_0 were combined to warp the AAL regional mask from the MNI space to the individual T1 space and b_0 space successively. In total, 90 AAL regions were executed using the procedures described above to establish the seed mask. For each of the seed masks, the remaining 89 regional masks were merged to form the terminal mask.

Edge Definition

As aforementioned, probabilistic tractography (FSL 5.09) was used to define the edge of the brain network. For each voxel in the seed mask, 5,000 streamlines were sampled. Each fiber was drawn depending on the distribution of the orientation set up by

Bedpostx. The tract was established every 0.5 mm to the other 89 masks and terminated in a terminal mask to prevent tracking in the loop with parameters of 0.2 curvature threshold, 2,000 steps with length of 0.5 mm. Then, the connectivity probabilities from the seed mask to the remaining 89 target masks were established. The probability was defined as weight. After 90 seed masks were performed, the same procedure that was described above was performed, and a 90 × 90 connective matrix was constructed for each participant.

As it is impossible to determine the directionality between node A and node B by probabilistic tractography, we defined the unidirectional connective matrix using Schmidt's description (32), the probabilities of node A and node B were calculated by the average of $weight_{AB}$ and $weight_{BA}$.

Network Analysis

To describe the topological features of the WM network at a global level, we calculated several global network properties: clustering coefficient (Cp), shortest path length (Lp), efficiency (E), connective strength (S), fault tolerant efficiency (E_{loc}), density of network (Density), small world properties, modularity (Q), hierarchy (β), and assortativity (r). All of the global network properties were calculated with the GRETNA toolkit (33) or our custom-made MATLAB program. To rule out spurious connections, a connection was excluded from the connective matrix before calculating the global network properties if it existed in fewer than 20% of the group subjects (24).

Global Clustering Coefficient (Global Cp)

The global clustering coefficient is defined as the average of the likelihood of a neighbor-to-neighbor connection. A greater value represented a larger extent of the local interconnectivity of a network. For a network G, the equation is:

$$\text{Global } C_p = (1/N) \times \{ \sum_{A \in G} [2/k_A(k_A - 1) \sum_{B,k} (\omega_{AB}\omega_{Bk}\omega_{kA})^{\frac{1}{3}}] \}$$

k_A is the degree of node A and ω_{AB} is the weight between node A and node B. N = 90.

Global Shortest Path Length (Global Lp)

The global shortest path length is defined as the average of all of the shortest lengths between each pair of nodes in the network. A smaller value represented a faster transfer speed of information in the brain. For a network G, the equation is:

$$\text{Global } L_p = [1/N(N-1)] \times \sum_{A \neq B \in G} L_{AB}$$

L_{AB} is the shortest path length between node A and node B and N = 90.

Small World Properties

Before the calculation of the small-world property, 1,000 random networks that maintained the same nodes and edges as the original network but also maintained the differences in distribution were generated. The small-world properties consisted of the normalized global clustering coefficient Gamma (γ) and the normalized global shortest path length Lambda (λ), which represented the means of 1,000 random network global clustering coefficients and the global shortest path length respectively.

$$\gamma = \text{Global } C_p^{real} / \text{Global } C_p^{rand} \ \ldots \ \lambda = \text{Global } L_p^{real} / \text{Global } L_p^{rand}$$

The small-world measurement sigma (σ), where $\sigma = \gamma/\lambda$, $\gamma > 1$, $\lambda \approx 1$ and $\sigma > 1$, indicate the existence of small-world properties.

Network Connective Strength (Global S)

The connective strength of node A is defined as the sum of the connective weight, which is the weight that directly connects to node A. Network connective strength is the average of all of the nodal connective strengths in the network. For a network G, the equation is:

$$S = (1/N) \times [\Sigma_{A \in G}(\Sigma_{B \in G}\omega_{AB})]$$

The variable ω_{AB} represents the weight between node A and node B. A greater network connective strength is represented by a greater connection connective strength in the network.

Global Efficiency (E_{glob})

The global efficiency is represented as the information transfer efficiency of the network. For a network G, the equation is:

$$E_{glob} = [1/N(N-1)] \times \sum_{A \neq B \in G} 1/L_{AB}$$

where L_{AB} is the shortest path length between node A and node B.

Global Fault Tolerant Efficiency (E_{loc})

The E_{loc} of node A is defined as how much of the network is fault-tolerant when the first neighbors of node A are removed from the network. The global E_{loc} is the average of the nodal E_{loc} values in the network. A greater global E_{loc} represents a greater fault tolerance of the network. For a network G, the equation is:

$$E_{loc} = (1/N) \times \sum_{A \in G} E_{glob}(G_A)$$

Density of Network (Density)

The density of a network is the fraction of present connections to possible connections. In this study, the possible connections are equal to N(N-1)/2.

Hierarchy (β)

Many real networks, particularly brain networks, commonly share a natural topological property that is called a hierarchical organization. In a hierarchical network, the low-degree nodes in the graph typically exhibit a higher clustering coefficient compared with high-degree nodes and vice versa, yielding an efficient network communication. For reasons of the strict

scaling law and scale-free properties, the hierarchical coefficient could be described by the distribution of the ratio, the equation is:

$$C \sim k^{-\beta}$$

in which the C represents the clustering and k indicates the degree of a node in a network β; the coefficient of hierarchical organization was calculated by fitting a linear regression with the ratio of the log-transformed C to the log-transformed k.

Assortativity (r)

Assortativity is defined as the degree to which one node tends to connect with other similar nodes in the network. In this study, we calculated assortativity with the Pearson correlation coefficients of the connective strength between each pair of linked nodes in the network, as described by Leung and Chau (34). The equation is:

$$r^{\omega} = \frac{H^{-1}\Sigma_{\phi}(\omega_{\phi}\Pi_{A\in F(\phi)}k_A - [\frac{H^{-1}}{2}\Sigma_{\phi}(\omega_{\phi}\Sigma_{A\in F(\phi)}k_A)]^2}{\frac{H^{-1}}{2}\Sigma_{\phi}(\omega_{\phi}\Sigma_{A\in F(\phi)}k_A^2 - [\frac{H^{-1}}{2}\Sigma_{\phi}(\omega_{\phi}\Sigma_{A\in F(\phi)}k_A)]^2}$$

where the edge of the network is sorted by ascending values, H is the total weight of all the edges in the network, ω_φ is the weight of the φth edge and F(φ) is the pair of nodes that is connected by the φth edge. If M represents the total degree of the network, then φ = 1~M.

Modularity (Q)

To describe the patterns of integration within the module and the segregation between them, modularity was calculated. Modularity is also called Q, a larger Q indicates more connection than was expected within the chosen communities. The definition of the modularity pattern was determined by a method that was previously described by Reichardt and Bornholdt (35) that aims to maximize the number of within-group edges and minimize the number of between-group edges. The equation is:

$$Q = \frac{1}{2m}\sum_{AB}\left[E_{AB} - \frac{k_A k_B}{2m}\right]\delta_{c_A,c_B}$$

where m refers to the total weight of the edges in the network, E_{AB} is the connectivity between node A and node B; k_A is the degree of node A; δ_{AB} is the Kronecker delta symbol; C_A is the mode to which node A is assigned.

Statistical Analyses

The statistical analysis was performed with Statistical Package for Social Sciences software version 22.0 (SPSS IBM, Chicago, Illinois, USA). The demographic and clinical variables were analyzed using a Chi-square (χ^2) test for the categorical variables and two-sample *t*-tests were used for the continuous variables. Further, we used a general linear model (GLM) with diagnosis as the independent factor and age, gender, and education years as covariates to determine the group differences in neuropsychological scores and WM global network properties. To determine the group differences in the serum levels of TRP, KYN, and KYNA, we used a GLM with diagnosis as the independent factor and age, gender and BMI (36) as covariates. The level of significance was set as a two-tailed *P* value of 0.05.

To determine the significant differences in the subnetwork connection between the LLD and the HC groups, network-based statistics (NBS) were utilized (37, 38). First, the *t* test statistical threshold was chosen by the primary threshold ($P < 0.01$). Second, a two-sample one-tail *t* test (LLD < HC and LLD > HC) was computed for difference in the edges between the LLD and HC groups. A set of suprathreshold links was constructed according to the statistical threshold. Third, a connected graph component was determined by breadth search and the component size M was established by the sum of the test statistical values across all connections in the component. A permutation test (5,000 permutations) was used to correct for multiple comparisons ($P < 0.05$ with a FWE rate approach). The size of the largest component was recorded in each permutation and generated a random component size distribution. Finally, the correct *P* value was determined from the position of M in the random component size distribution. A significantly different subnetwork between the LLD and HC groups was obtained. The connective strength of the NBS subnetwork was calculated.

Furthermore, Pearson correlation was applied to determine relationships between DG performance and clinical variates and KP metabolism, DG performance and WM network properties, and KP metabolites and WM network properties in LLD and HC groups respectively.

RESULTS

Demographic and Clinical Characteristics

There is no significant difference in the gender, age, BMI, education years, or MMSE scores between the LLD and HC groups (all $P > 0.05$). The HAMD-17 scores and DG performance were significantly different between these two groups (both $P < 0.05$). Serum concentrations of TRP and the KYN/TRP ratio were significantly different between these two groups (both $P < 0.05$). The details are shown in **Table 1**. In the LLD group, 3 patients were medication-free, 2 patients received serotonin noradrenaline reuptake inhibitors, 15 patients received selective serotonin reuptake inhibitors, no patients received tricyclic antidepressants, 8 patients received noradrenergic and specific serotonergic antidepressants, and 20 patients received benzodiazepines as a combination treatment within the last 3 months.

Global Network Properties

The global topologies of the WM network are shown in **Table 2**. Small-world organization ($\gamma > 1$, $\lambda \approx 1$, $\sigma > 1$) was observed in both the LLD and HC groups' connectivity networks. Intergroup differences were found in the global Cp, global Lp, small-world properties, global S, E_{glob}, and density between the LLD and HC groups (all $P < 0.05$).

TABLE 1 | Demographic and clinical characteristics, TRP, KYN, and KYNA) levels of MDD patients and HCs.

	LLD	HCs	Statistics	*P* value
	(*n* = 34)	(*n* = 36)	(*z*/*t*)	
Gender (male/female)	11/23	6/30	2.340[a]	0.126
Age (years)	65.000 ± 5.592	65.830 ± 7.296	0.534[b]	0.595
Education (years)	8.764 ± 3.447	9.681 ± 3.366	1.125[b]	0.265
BMI	21.867 ± 2.918	22.519 ± 2.779	0.957[b]	0.342
MMSE	25.680 ± 2.184	26.670 ± 2.098	2.900[c]	0.093
HAMD-17	9.560 ± 7.439	1.390 ± 2.979	34.085[c]	<0.001
DG	682.350 ± 266.823	502.780 ± 171.524	11.236[c]	0.001
TRP (ng/ml)	11,194.851 ± 2,141.914	12,598.841 ± 1,793.315	8.053[d]	0.006
KYN (ng/ml)	326.566 ± 67.562	329.790 ± 44.917	0.004[d]	0.985
KYNA (ng/ml)	7.068 ± 2.328	7.691 ± 2.649	0.999[d]	0.321
KYN/TRP	0.030 ± 0.009	0.026 ± 0.004	4.575[d]	0.036
KYNA/KYN	0.021 ± 0.006	0.023 ± 0.007	1.236[d]	0.270

LLD, late-life depression; HCs, healthy controls; BMI, body mass index; MMSE, Mini-Mental State Examination; HAMD-17, 17-item Hamilton Depression Scale; DG, Dictator Game; TRP, tryptophan; KYN, kynurenine; KYNA, kynurenic acid; KYN/TRP, kynurenine to tryptophan ratio; KYNA/KYN, kynurenic acid to kynurenine ratio.
[a]P-value was obtained using a Chi-square (χ^2) test.
[b]P-values were obtained using two-sample t-tests.
[c]P-values were obtained using GLMs with diagnosis as the independent factor and gender, age and education as covariates.
[d]P-values were obtained using GLMs with diagnosis as the independent factor and gender, age and BMI as covariates.

TABLE 2 | Global network properties of white matter network of LLD patients and HCs.

	LLD	HCs	Statistics	*P* value
	(*n* = 34)	(*n* = 36)	(*t*)	
Global Cp	0.004 ± 0.0001	0.005 ± 0.0001	13.707	<0.001
Global Lp	45.513 ± 3.525	47.148 ± 3.348	6.553	0.013
Gamma, γ	2.072 ± 0.235	2.236 ± 0.229	11.355	0.001
Lamda, λ	1.266 ± 0.014	1.276 ± 0.014	11.950	0.001
Sigma, σ	1.635 ± 0.172	1.751 ± 0.170	10.321	0.002
Global S	0.416 ± 0.033	0.402 ± 0.027	6.190	0.015
E_{glob}	0.022 ± 0.001	0.021 ± 0.001	6.619	0.012
E_{loc}	0.022 ± 0.001	0.022 ± 0.001	2.944	0.091
Density	0.562 ± 0.021	0.536 ± 0.018	37.823	<0.001
β	−0.345 ± 2.103	−0.0413 ± 2.032	0.682	0.412
r	−0.029 ± 0.009	−0.031 ± 0.012	0.345	0.559
Q	0.593 ± 0.011	0.593 ± 0.117	0.255	0.615

LLD, late-life depression; HCs, healthy controls; Cp, clustering coefficient; Lp, shortest path length; γ, normalized clustering coefficient; λ, normalized shortest path length; σ, small-worldness; S, network connective strength; Eglob, global efficiency; Eloc, fault tolerant efficiency; Density, density of network; β, hierarchy; r, assortativity; Q, modularity. P-values were obtained using GLMs with diagnosis as the independent factor and gender, age and education years as covariates.

NBS Analysis

We found that the subnetwork strength detected by NBS of the LLD group was 0.307 ± 0.0248, the NBS subnetwork strength of HC group was 0.282 ± 0.0214. The difference of the NBS strength measurements between these two groups was significant (F = 24.625, df = 1, P < 0.001). We found a disrupted subnetwork composing of 14 nodes and 15 connections in LLD group (HC < LLD, P = 0.036). The involved nodes in this NBS-based subnetwork mainly included the frontal (Frontal_Inf_Oper_L), parietal (Rolandic_Oper_R, Supp_Motor_Area_R), paralimbic (Insula_L, Hippocampus_R, Calcarine_R, Lingual_L, Precuneus_R, Thalamus_R), and temporal (Temporal_Sup_R, Temporal_Pole_Sup_L, Temporal_Pole_Sup_R, Temporal_Mid_R, Temporal_Pole_Mid_R) gyrus. This NBS's subnetwork is shown in **Figure 1**.

Correlation Analysis

A partial correlation was conducted with the DG task, KYN/TRP ratio and KYNA/KYN ratio, gender, age, education, and BMI as covariates. We considered KYN/TRP ratio and the KYNA/KYN ratio could represent the changes of KP metabolism most. We found that, in the LLD group, the DG task was correlated with KYNA/KYN ratio (r = −0.371, P = 0.037). In addition, the HC participants who performed the DG task also showed a trend toward the KYNA/KYN ratio (r = −0.334, P = 0.053). Furthermore, a partial correlation was conducted with the MMSE, HAMD-17, KYN/TRP ratio, and KYNA/KYN ratio, gender, age, education and BMI as covariates. In LLD group, HAMD-17 was significantly correlated with KYNA/KYN ratio (r = 0.507, P = 0.003). In HC group, HAMD-17 was significantly correlated with KYN/TRP ratio (r = 0.362, P = 0.049). No significant relationships were observed among DG task, MMSE and HAMD-17 scores in LLD group and HC groups respectively.

A partial correlation was performed between the WM network properties and DG task, gender, age, and education years as covariates. In LLD group and HC group, no significant correlations were observed between WM network properties and DG task. Moreover, a partial correlation was performed between the WM network properties and KP metabolism, gender, age, education and BMI as covariates. KYNA/KYN ratio was significantly correlated with Density (r = −0.576, P < 0.001, q = 0.024), small world properties [γ (r = 0.467, P = 0.007, q = 0.028) and σ (r = 0.442, P = 0.011, q = 0.033)] and Q (r = 0.468, P = 0.007, q = 0.028) in HC group. No significant correlations were observed between KP metabolism and network properties in LLD group.

A partial correlation was performed between the DG task and the WM subnetwork strength detected by NBS, gender, age, and

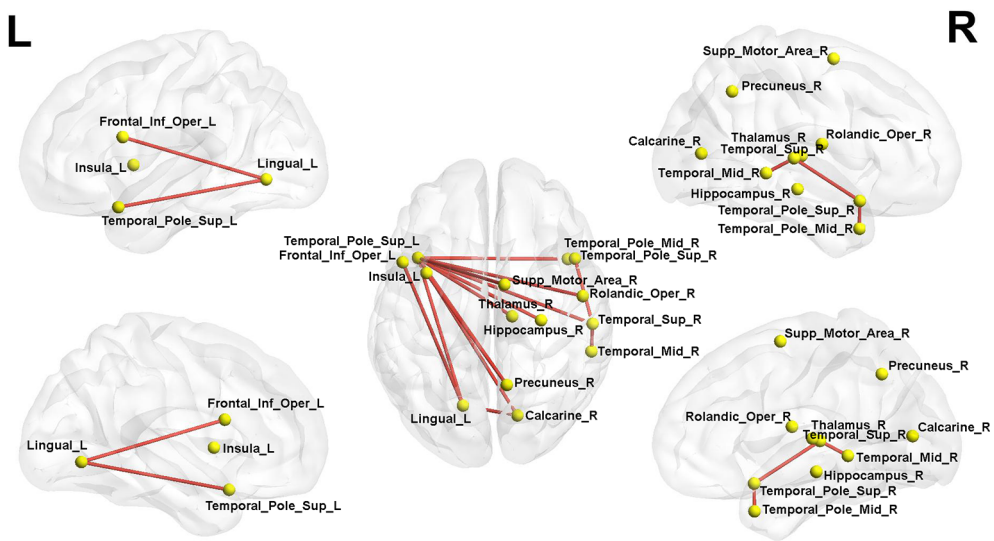

FIGURE 1 | Network-based statistics (NBS) analysis showed a single subnetwork composing of 14 nodes and 15 edges in LLD patients compared with the HCs. Red lines represent the edges of the subnetwork connections. L, left; R, right; LLD, late-life depression; HCs, healthy controls. The nodes and connections were mapped using Brain Net Viewer software (http://www.nitrc.org/projects/bnv/).

education as covariates. We did not observe any significant correlations between the DG task and the WM subnetwork strength in the LLD group and HC group respectively. In addition, a partial correlation was conducted with the KYN/TRP ratio, KYNA/KYN ratio, and the NBS subnetwork strength, gender, age, education, and BMI as covariates. We did not observe any significant correlations between the KYN/TRP ratio, KYNA/KYN ratio and the WM subnetwork strength in the LLD group and HC group, respectively.

DISCUSSION

To the best of our knowledge, the current study is the first to explore the neurobiological mechanism and structural brain network that underlies altruism in older people with depression. We compared the altruistic behavior in the DG task, serum concentrations of TRP, KYN, and KYNA, and the WM network topological features between the LLD and HC participants. The preliminary findings of the current study were as follows: (1) LLD participants exhibited a higher altruism level than HC participants; (2) in LLD group, DG performance was negatively correlated with the KYNA/KYN ratio, while HAMD-17 was positively correlated with KYNA/KYN ratio; (3) in their global network properties, the LLD participants displayed decreased global Cp, global Lp, and small-world properties, increased global S and E_{glob} and density compared to the HCs; (4) KYNA/KYN ratio was correlated with density, small world properties (γ and σ) and Q in HC group.

In the current study, LLD participants demonstrated a higher level of altruism. If people are motivated by self-interest in response to the passive recipient in the DG, the proposer will offer the smallest amount, even zero, as this is the optimal, 'smartest' decision they can make (8). Previous studies showed that MDD patients would not exhibit higher altruism due to the stress from the cost of helping others (9), reducing the use of task representations and hindering performance during exploratory decision-making (39) and undervaluation of actions leading to rewarding outcomes (40). However, the LLD patients shared more than their fair share in this study. The ability to make a 'smart' decision becomes vulnerable in patients with neuropsychiatric disorders and in the aftermath of chronic stress; this phenomenon has been observed in the prefronto-striatal circuit dynamics in rodents exposed to chronic stress (41). However, the level of dopamine in the ventral striatum is one of vital factors that influences altruism decision (8). Furthermore, we found that the breakdown of KYN was closely related to depression, had an effect on altruistic decision-making in the LLD patients of the current study.

The KYNA/KYN ratio had an impact on DG performance in the LLD participants. The KYNA/KYN ratio is closely related to cognition. In the presence of inflammation, the formation of QUIN is enhanced, which result in excitotoxic neurodegenerative changes and cognitive deficits. In addition, KYN/TRP ratio was increased inpatients with LLD, enhanced KYN synthesis might induce an abnormality in KYNA formation that is also harmful to cognition. If KYNA formation is beyond the physiological level, it can lead to glutamatergic hypofunctioning. KYNA is an antagonist of all ionotropic excitatory amino acid receptors; specifically, KYNA has a higher affinity for the alpha-7-nicotinic acetylcholine receptor than for the NMDA-R, this disrupts auditory sensory gating.

Furthermore, the level of KYNA produces is associated with the extracellular dopamine concentrations, this influences dopaminergic neurotransmission (17, 42). However, the dopamine in the ventral striatum is involved in the reward process, by which people feel rewarded from helping others (7, 8, 43). Briefly, in the current study, we found that an imbalance of KYN metabolism would have a negative impact on altruistic behavior, which might be caused by cognitive deficits or abnormal dopamine level. Future study should aim at the role of cognitive function and the effects of the level of dopamine in the altruistic behavior of LLD.

In addition, we found that the serum level of TRP was lower in the LLD patients than in the HCs, reflecting the conversion of TRP to KYN and its insufficient quantity for 5-HT synthesis. These results are in line with the mechanism of depression. According to our partial correlation analysis, we found that HAMD-17 was positive associated with KYNA/KYN ratio in LLD. It is not consistent with our previous findings in late-onset depression, which showed negative correlated with depressive factor (15). In the current study, we did not divide HAMD-17 into serval factors, due to the limited sample size. This might be the reason of the opposite finding in the current study. However, the main topic of this study was to explore whether KP metabolism and WM deficits have an effect on altruistic behaviors in LLD. The association of KP metabolism and LLD had been fully discussed in our previous studies (15, 44), which was not our main concern in this study. Thus, we are confident with our current findings in altruistic behavior in LLD. However, a larger sample study is still needed in future study.

In the analysis of their global network properties, LLD participants displayed decreased Cp, Lp and small-world properties, increased strength, E_{glob} and density compared with the HC participants. We determined that LLD participants presented with an increased global network efficiency rather than a decreased regional efficiency, as suggested by the findings of the previous study (45). In addition, some network properties were associated with KYNA/KYN ratio in HCs. While, such relations were lacked in LLD and no difference was found between LLD and HC in KYNA/KYN ratio, indicated that the WM damage of LLD might be not relevant with the changes of KP. Notably, left superior temporal pole was the important node based on NBS analysis. According to the previous studies, superior temporal pole involved in process of depression (46), cognitive impairment (47), and decision-making (48). To some extent, LLD patients have a higher risk of cognitive deficits. The current study hinted that superior temporal pole played an important role in the abnormal altruistic behavior in LLD, but the specific mechanism is needed to be explored in further experiments.

Several limitations must be addressed here. First, we did not quantifiably detect the level of dopamine and calculate relationships among the altruistic, levels of dopamine and KP metabolites in this study. We will make our efforts in future studies. Then, the sample size was small, but it was still statistically significant. We will increase the sample size in future research.

CONCLUSION

Our exploratory findings showed that LLD participants exhibited a higher level of altruism than the HC participants. The LLD participants manifested profound shifts in KP that influenced their altruistic behavior. KYNA/KYN ratio influenced altruistic behavior and depressive severity in LLD patients, WM global network properties in HCs.

DATA AVAILABILITY STATEMENT

The data used to support the findings of this study are available from the corresponding author upon request.

ETHICS STATEMENT

The studies involving human participants were reviewed and approved by the ethics committee of the Affiliated Brain Hospital of Guangzhou Medical University (Guangzhou Huiai Hospital). The patients/participants provided their written informed consent to participate in this study.

AUTHOR CONTRIBUTIONS

YW and NM were responsible for the data collection, data analysis. YW was responsible for writing the drafts of manuscript. YN supervised experiment design, and the drafts of the manuscript. XW and JL were involved in revising the drafts. All authors approved the final version of the manuscript.

FUNDING

This work was supported by Science and Technology Plan Project of Guangdong Province (No.2019B030316001); Guangzhou Municipal Psychiatric Disease Clinical Transformation Laboratory (No. 201805010009); Key Laboratory for Innovation platform Plan, Science and Technology Program of Guangzhou, China; Guangzhou municipal key discipline in medicine (2017-2019). The funding agency had no role in study design, data collection, analysis, decision to publish, or preparation of the manuscript.

ACKNOWLEDGMENTS

We would like to thank all LLD patients, and HC participants engaged in the current study.

REFERENCES

1. Leles da Costa Dias F, Teixeira AL, Cerqueira Guimaraes H, Borges Santos AP, Rios Fonseca Ritter S, Barbosa Machado JC, et al. Prevalence of late-life depression and its correlates in a community-dwelling low-educated population aged 75+ years: The Pieta study. *J Affect Disord* (2019) 242:173–9. doi: 10.1016/j.jad.2018.08.012
2. Tedeschini E, Levkovitz Y, Iovieno N, Ameral VE, Nelson JC, Papakostas GI. Efficacy of antidepressants for late-life depression: a meta-analysis and meta-regression of placebo-controlled randomized trials. *J Clin Psychiatry* (2011) 72 (12):1660–8. doi: 10.4088/JCP.10r06531
3. Sheline YI, Barch DM, Garcia K, Gersing K, Pieper C, Welsh-Bohmer K, et al. Cognitive function in late life depression: relationships to depression severity, cerebrovascular risk factors and processing speed. *Biol Psychiatry* (2006) 60 (1):58–65. doi: 10.1016/j.biopsych.2005.09.019
4. Marin RS, Butters MA, Mulsant BH, Pollock BG, Reynolds CF 3rd, et al. Apathy and executive function in depressed elderly. *J Geriatr Psychiatry Neurol* (2003) 16(2):112–6. doi: 10.1177/0891988703016002009
5. Tavares LR, Barbosa MR. Efficacy of group psychotherapy for geriatric depression: A systematic review. *Arch Gerontol Geriatr* (2018) 78:71–80. doi: 10.1016/j.archger.2018.06.001
6. Kupferberg A, Bicks L, Hasler G. Social functioning in major depressive disorder. *Neurosci Biobehav Rev* (2016) 69:313–32.doi: 10.1016/j.neubiorev.2016.07.002
7. Fehr E, Fischbacher U. The nature of human altruism. *Nature* (2003) 425 (6960):785–91. doi: 10.1038/nature02043
8. Rilling JK, Sanfey AG. The neuroscience of social decision-making. *Annu Rev Psychol* (2011) 62:23–48. doi: 10.1146/annurev.psych.121208.131647
9. Fujiwara T. The role of altruistic behavior in generalized anxiety disorder and major depression among adults in the United States. *J Affect Disord* (2007) 101(1-3):219–25. doi: 10.1016/j.jad.2006.11.024
10. Sparrow EP, Armstrong BA, Fiocco AJ, Spaniol J. Acute stress and altruism in younger and older adults. *Psychoneuroendocrinology* (2019) 100:10–7. doi: 10.1016/j.psyneuen.2018.09.025
11. Gintis H, Bowles S, Boyd R, Fehr E. Explaining altruistic behavior in humans. *Evol Hum Behav* (2003) 24(3):153–72. doi: 10.1016/S1090-5138(02)00157-5
12. Cervenka I, Agudelo LZ, Ruas JL. Kynurenines: Tryptophan's metabolites in exercise, inflammation, and mental health. *Science* (2017) 357(6349):369–369. doi: 10.1126/science.aaf9794
13. Wichers MC, Koek GH, Robaeys G, Verkerk R, Scharpe S, Maes M. IDO and interferon-alpha-induced depressive symptoms: a shift in hypothesis from tryptophan depletion to neurotoxicity. *Mol Psychiatry* (2005) 10(6):538–44. doi: 10.1038/sj.mp.4001600
14. Gabbay V, Klein RG, Katz Y, Mendoza S, Guttman LE, Alonso CM, et al. The possible role of the kynurenine pathway in adolescent depression with melancholic features. *J Child Psychol Psychiatry* (2010) 51(8):935–43. doi: 10.1111/j.1469-7610.2010.02245.x
15. Wu Y, Zhong X, Mai N, Wen Y, Shang D, Hu L, et al. Kynurenine pathway changes in late-life depression. *J Affect Disord* (2018) 235:76–81. doi: 10.1016/j.jad.2018.04.007
16. Oxenkrug GF. Tryptophan kynurenine metabolism as a common mediator of genetic and environmental impacts in major depressive disorder: the serotonin hypothesis revisited 40 years later. *Isr J Psychiatry Relat Sci* (2010) 47(1):56–63. doi: 10.3109/09540261.2010.535509
17. Myint AM. Kynurenines: from the perspective of major psychiatric disorders. *FEBS J* (2012) 279(8):1375–85. doi: 10.1111/j.1742-4658.2012.08551.x
18. Reus GZ, Jansen K, Titus S, Carvalho AF, Gabbay V, Quevedo J. Kynurenine pathway dysfunction in the pathophysiology and treatment of depression: Evidences from animal and human studies. *J Psychiatr Res* (2015) 68:316–28. doi: 10.1016/j.jpsychires.2015.05.007
19. Capuron L, Schroecksnadel S, Feart C, Aubert A, Higueret D, Barberger-Gateau P, et al. Chronic low-grade inflammation in elderly persons is associated with altered tryptophan and tyrosine metabolism: role in neuropsychiatric symptoms. *Biol Psychiatry* (2011) 70(2):175–82. doi: 10.1016/j.biopsych.2010.12.006
20. Poletti S, Myint AM, Schuetze G, Bollettini I, Mazza E, Grillitsch D, et al. Kynurenine pathway and white matter microstructure in bipolar disorder. *Eur Arch Psychiatry Clin Neurosci* (2018) 268(2):157–68. doi: 10.1007/s00406-016-0731-4
21. Chiappelli J, Postolache TT, Kochunov P, Rowland LM, Wijtenburg SA, Shukla DK, et al. Tryptophan Metabolism and White Matter Integrity in Schizophrenia. *Neuropsychopharmacology* (2016) 41(10):2587–95. doi: 10.1038/npp.2016.66
22. Lovelace MD, Varney B, Sundaram G, Lennon MJ, Lim CK, Jacobs K, et al. Recent evidence for an expanded role of the kynurenine pathway of tryptophan metabolism in neurological diseases. *Neuropharmacology* (2017) 112(Pt B):373–88. doi: 10.1016/j.neuropharm.2016.03.024
23. Charlton RA, Lamar M, Zhang A, Yang S, Ajilore O, Kumar A. White-matter tract integrity in late-life depression: associations with severity and cognition. *Psychol Med* (2014) 44(7):1427–37. doi: 10.1017/S0033291713001980
24. Mai N, Zhong X, Chen B, Peng Q, Wu Z, Zhang W, et al. Weight Rich-Club Analysis in the White Matter Network of Late-Life Depression with Memory Deficits. *Front Aging Neurosci* (2017) 9:279. doi: 10.3389/fnagi.2017.00279
25. Zanon M, Novembre G, Zangrando N, Chittaro L, Silani G. Brain activity and prosocial behavior in a simulated life-threatening situation. *NeuroImage* (2014) 98:134–46. doi: 10.1016/j.neuroimage.2014.04.053
26. Sporns O. The human connectome: a complex network. *Ann N Y Acad Sci* (2011) 1224:109–25. doi: 10.1111/j.1749-6632.2010.05888.x
27. Chen Z, Hu X, Chen Q, Feng T. Altered structural and functional brain network overall organization predict human intertemporal decision-making. *Hum Brain Mapp* (2019) 40(1):306–28. doi: 10.1002/hbm.24374
28. Savitz J, Dantzer R, Meier TB, Wurfel BE, Victor TA, McIntosh SA, et al. Activation of the kynurenine pathway is associated with striatal volume in major depressive disorder. *Psychoneuroendocrinology* (2015) 62:54–8. doi: 10.1016/j.psyneuen.2015.07.609
29. Hu LJ, Li XF, Hu JQ, Ni XJ, Lu HY, Wang JJ, et al. A Simple HPLC-MS/MS Method for Determination of Tryptophan, Kynurenine and Kynurenic Acid in Human Serum and its Potential for Monitoring Antidepressant Therapy. *J Anal Toxicol* (2017) 41(1):37–44. doi: 10.1093/jat/bkw071
30. Cui Z, Zhong S, Xu P, He Y, Gong G. PANDA: a pipeline toolbox for analyzing brain diffusion images. *Front Hum Neurosci* (2013) 7:42. doi: 10.3389/fnhum.2013.00042
31. Gong G, He Y, Concha L, Lebel C, Gross DW, Evans AC, Beaulieu C. Mapping anatomical connectivity patterns of human cerebral cortex using in vivo diffusion tensor imaging tractography. *Cereb Cortex* (2009) 19(3):524–36. doi: 10.1093/cercor/bhn102
32. Schmidt A, Crossley NA, Harrisberger F, Smieskova R, Lenz C, Riecher-Rossler A, et al. *Structural Network Disorganization in Subjects at Clinical High Risk for Psychosis*. *Schizophr Bull* (2017) 43(3):583–91. doi: 10.1093/schbul/sbw110
33. Wang J, Wang X, Xia M, Liao X, Evans A, He Y. *GRETNA: a graph theoretical network analysis toolbox for imaging connectomics*. *Front Hum Neurosci* (2015) 9:386. doi: 10.3389/fnhum.2015.00458
34. Leung CC, Chau HF. *Weighted assortative and disassortative networks model*. *Physica A: Stat Mech Appl* (2007) 378(2):591–602. doi: 10.1016/j.physa.2006.12.022
35. Reichardt J, Bornholdt S, Bornholdt S. Statistical Mechanics of Community Detection. *Phys Rev E* (2006) 7474(1):016110. doi: 10.1103/PhysRevE.74.016110
36. Kennedy PJ, Cryan JF, Dinan TG, Clarke G. Kynurenine pathway metabolism and the microbiota-gut-brain axis. *Neuropharmacology* (2017) 112(Pt B):399–412. doi: 10.1016/j.neuropharm.2016.07.002
37. Zalesky A, Fornito A, Bullmore ET. Network-based statistic: identifying differences in brain networks. *Neuroimage* (2010) 53(4):1197–207. doi: 10.1016/j.neuroimage.2010.06.041
38. Li X, Steffens DC, Potter GG, Guo H, Song S, Wang L. Decreased between-hemisphere connectivity strength and network efficiency in geriatric depression. *Hum Brain Mapp* (2017) 38(1):53–67. doi: 10.1002/hbm.23343
39. Blanco NJ, Otto AR, Maddox WT, Beevers CG, Love BC. The influence of depression symptoms on exploratory decision-making. *Cognition* (2013) 129 (3):563–8. doi: 10.1016/j.cognition.2013.08.018

40. Paulus MP, Yu AJ. Emotion and decision-making: affect-driven belief systems in anxiety and depression. *Trends Cognit Sci* (2012) 16(9):476–83. doi: 10.1016/j.tics.2012.07.009
41. Friedman A, Homma D, Bloem B, Gibb LG, Amemori KI, Hu D, et al. Chronic Stress Alters Striosome-Circuit Dynamics, Leading to Aberrant Decision-Making. *Cell* (2017) 171(5):1191–205:e28. doi: 10.1016/j.cell.2017.10.017
42. Stone TW, Stoy N, Darlington LG. An expanding range of targets for kynurenine metabolites of tryptophan. *Trends Pharmacol Sci* (2013) 34 (2):136–43. doi: 10.1016/j.tips.2012.09.006
43. Schultz W. Predictive reward signal of dopamine neurons. *J Neurophysiol* (1998) 80(1):1–27. doi: 10.1152/jn.1998.80.1.1
44. Wu Y, Mai N, Zhong X, Wen Y, Zhou Y, Li H, et al. Kynurenine pathway changes in late-life depression with memory deficit. *Psychiatry Res* (2018) 269:45–9. doi: 10.1016/j.psychres.2018.08.041
45. Bai F, Shu N, Yuan Y, Shi Y, Yu H, Wu D, et al. Topologically convergent and divergent structural connectivity patterns between patients with remitted geriatric depression and amnestic mild cognitive impairment. *J Neurosci* (2012) 32(12):4307–18. doi: 10.1523/JNEUROSCI.5061-11.2012
46. Fitzgerald P, Maller J, Hoy K, Oxley T, Daskalakis Z, Laird A. A meta-analytic study of changes in brain activation in depression. *Acta Neuropsychiatr* (2006) 18(6):286–7. doi: 10.1017/S0924270800031173
47. Li M, Meng Y, Wang M, Yang S, Wu H, Zhao B, Wang G. Cerebral gray matter volume reduction in subcortical vascular mild cognitive impairment patients and subcortical vascular dementia patients, and its relation with cognitive deficits. *Brain Behav* (2017) 7(8):e00745. doi: 10.1002/brb3.745
48. Yang XH, Huang J, Lan Y, Zhu CY, Liu XQ, Wang YF, et al. Diminished caudate and superior temporal gyrus responses to effort-based decision making in patients with first-episode major depressive disorder. *Prog Neuropsychopharmacol Biol Psychiatry* (2016) 64:52–9. doi: 10.1016/j.pnpbp.2015.07.006

Conflict of Interest: The authors declare that the research was conducted in the absence of any commercial or financial relationships that could be construed as a potential conflict of interest.

frontiers in Psychiatry

ORIGINAL RESEARCH
published: 20 May 2020
doi: 10.3389/fpsyt.2020.00450

Pineal Gland Volume in Major Depressive and Bipolar Disorders

Tsutomu Takahashi[1], Daiki Sasabayashi[1], Murat Yücel[2], Sarah Whittle[3], Valentina Lorenzetti[4], Mark Walterfang[3,5,6], Michio Suzuki[1], Christos Pantelis[3], Gin S. Malhi[7,8] and Nicholas B. Allen[9]*

[1] Department of Neuropsychiatry, University of Toyama School of Medicine, Toyama, Japan, [2] School of Psychological Sciences, Turner Institute for Brain and Mental Health, Monash University, Clayton, VIC, Australia, [3] Melbourne Neuropsychiatry Centre, Department of Psychiatry, The University of Melbourne and Melbourne Health, Melbourne, VIC, Australia, [4] Faculty of Health Sciences, School of Psychology, Australian Catholic University, Melbourne, VIC, Australia, [5] Department of Neuropsychiatry, Royal Melbourne Hospital, Melbourne, VIC, Australia, [6] Florey Institute of Neuroscience and Mental Health, University of Melbourne, Melbourne, VIC, Australia, [7] Discipline of Psychological Medicine, Northern Clinical School, University of Sydney, Sydney, NSW, Australia, [8] CADE Clinic, Department of Psychiatry, Royal North Shore Hospital, Sydney, NSW, Australia, [9] Department of Psychology, University of Oregon, Eugene, OR, United States

OPEN ACCESS

Edited by:
Ping Li,
Qiqihar Medical University, China

Reviewed by:
Veena Kumari,
Brunel University London, United Kingdom
Ning Sun,
First Hospital of Shanxi Medical University, China
Miao Chang,
The First Affiliated Hospital of China Medical University, China

***Correspondence:**
Tsutomu Takahashi
tsutomu@med.u-toyama.ac.jp

Specialty section:
This article was submitted to Neuroimaging and Stimulation, a section of the journal Frontiers in Psychiatry

Received: *10 January 2020*
Accepted: *04 May 2020*
Published: *20 May 2020*

Citation:
Takahashi T, Sasabayashi D, Yücel M, Whittle S, Lorenzetti V, Walterfang M, Suzuki M, Pantelis C, Malhi GS and Allen NB (2020) Pineal Gland Volume in Major Depressive and Bipolar Disorders. Front. Psychiatry 11:450. doi: 10.3389/fpsyt.2020.00450

Abnormal melatonin secretion has been demonstrated in patients with affective disorders such as major depressive disorder (MDD) and bipolar disorder (BD). However, magnetic resonance imaging (MRI) studies that previously investigated the volume of the pineal gland, which regulates circadian rhythms by secreting melatonin, in these patients reported inconsistent findings. The present study employed MRI to examine pineal gland volumes and pineal cyst prevalence in 56 MDD patients (29 currently depressed and 27 remitted patients), 26 BD patients, and matched controls (33 for MDD and 24 for BD). Pineal volumes and cyst prevalence in the current MDD, remitted MDD, and BD groups did not significantly differ from those of the healthy controls. However, pineal gland volumes were significantly smaller in the current MDD subgroup of non-melancholic depression than in the melancholic MDD subgroup. Interestingly, pineal volumes correlated negatively with the severity of *loss of interest* in the current MDD group. Medication and the number of affective episodes were not associated with pineal volumes in the MDD or BD group. While these results do not suggest that pineal volumes reflect abnormal melatonin secretion in affective disorders, they do point to the possibility that pineal abnormalities are associated with clinical subtypes of MDD and its symptomatology.

Keywords: pineal gland, melatonin, magnetic resonance imaging, major depressive disorder, bipolar disorder

INTRODUCTION

Hormonal evidence has suggested abnormal melatonin secretion in patients with affective disorders, such as major depressive disorder (MDD) and bipolar disorder (BD), which may contribute to the circadian rhythm dysfunctions commonly observed in these patients (1, 2). While low melatonin secretion irrespective of the mood status (i.e., manic, depressive, and euthymic) in BD appears to support its role as a trait marker (2, 3), previous findings on serum melatonin levels in MDD have

been inconsistent (i.e., decreased, normal, or even increased) (1), which may be partly attributed to the heterogeneity of MDD (e.g., melancholic *vs.* atypical subtypes) (4). Previous studies also suggested different alterations in the timing of melatonin secretion that were dependent on the mood status in MDD and BD patients (1, 2). These findings suggest different roles for melatonin abnormalities in the diagnosis (MDD *vs.* BD), MDD subtypes, and mood status of affective disorders.

To date, only a few magnetic resonance imaging (MRI) studies have examined the pineal gland, a neuroendocrine organ involved in circadian regulation through melatonin secretion (5, 6), in affective disorders. Although not consistently replicated, current evidences generally support the notion that the pineal volume, especially its parenchymal (i.e., non-cystic) volume, likely reflects melatonin levels or melatonin secretion patterns for both healthy subjects (7, 8) and patients with affective disorders (9). A recent study demonstrated smaller pineal volumes and a higher prevalence of pineal cysts, which asymptomatically exist in 20%–40% of healthy adults (10, 11), in MDD patients than in healthy controls (12). However, normal pineal volumes have also been reported in MDD (13) and BD (13, 14) patients, in whom pineal volumes were not related to clinical symptoms (9). These inconsistent findings may be partly attributed to different imaging techniques and exclusion criteria for pineal cysts; previous studies (13, 14) estimated pineal volumes two-dimensionally and also excluded patients with pineal cysts. The heterogeneity of MDD cohorts and/or different mood status (e.g., depressive or euthymic) between studies also appear to have biased the findings obtained; however, this hypothesis warrants further study on a well-defined group of MDD patients with different subtypes and illness stages.

The present MRI study examined pineal volumes and pineal cyst prevalence in patients with MDD (currently depressed and euthymic subgroups) and BD and compared them with those in matched controls. The influence of clinical characteristics (e.g., medication, mood status, and symptom severity, and the melancholic *vs.* non-melancholic subtypes of MDD) on pineal volumes in the patient groups was also investigated. Based on previous hormonal and neuroimaging findings that support the heterogeneity of MDD and potential role of melatonin in the mood status, we predicted that MDD but not BD patients have smaller pineal glands and a higher prevalence of pineal cysts, at least in specific subtypes or mood status, which may be associated with symptom severity.

MATERIALS AND METHODS

Participants

Fifty-six MDD patients, 26 BD patients, and 57 healthy matched subjects were included. The local Internal Review Boards (The Prince of Wales Hospital and University of New South Wales research ethics committees and Mental Health Research & Ethics Committee, Melbourne Health, Melbourne, Australia) approved the study protocol, and all study participants provided written informed consent in accordance with the Declaration of Helsinki. Sample characteristics (**Tables 1** and **2**) and inclusion/exclusion criteria were described previously for the MDD (15–17) and BD (18–20) cohorts, who were screened for head trauma, neurological illness, substance misuse, or other serious physical diseases.

Briefly, the MDD cohort was recruited through an advertisement in the local media and *via* outpatient psychiatric clinics in Melbourne, Australia, and comprised 29 patients currently under a depressive state (cMDD), 27 with a history of MDD but currently in remission (rMDD), and 33 healthy controls with no personal history of neuropsychiatric diseases. All participants underwent clinical and neuropsychological assessments by experienced research psychologists at ORYGEN Youth Health, Melbourne, with the Structured Clinical Interview for DSM-IV (SCID-IV-TR) (21), the Beck Depression Inventory (BDI) (22), Mood and Anxiety Symptom Questionnaire (MASQ) (23), and Positive Affect and Negative Affect Scale (PANAS) (24). The medication status, case history, and comorbid anxiety disorder were also examined. Depression subtype (melancholic *vs.* non-melancholic) was assessed only for the cMDD group; the melancholic depressed patients fulfilled the SCID criteria (21) based on the eight symptoms of the melancholic specifier (i.e., a loss of pleasure, lack of reactivity to usually pleasurable stimuli, distinct quality of depressed mood, mood regularly worse in the morning, insomnia, psychomotor retardation or agitation, significant anorexia or weight loss, and excessive or inappropriate guilt).

Twenty-six patients with bipolar I disorder under euthymic conditions were recruited from the Mood Disorders Unit at the Prince of Wales Hospital, Sydney, Australia, at which research psychiatrists made diagnoses using the SCID-IV patient version (25) supplemented by chart reviews. Twenty-four healthy subjects, screened using the SCID-IV non-patient version (25), were recruited through the advertisement. Ten BD patients had a family history of affective disorders, such as BD (N = 3), MDD (N = 5), and both (N = 2), whereas 12 did not and four had an unknown family illness history. Sixteen BD patients had experienced psychotic symptoms (hallucinations and/or delusions) during affective episodes.

MRI Acquisition and Data Processing

MR scans of MDD cohort were acquired using a 1.5T Siemens scanner (Magnetom Avanto) at Saint Vincent's Hospital Melbourne, Victoria (16, 17). Structural T1-weighted axial images were obtained using the following parameters: time to echo = 2.3 ms, time repetition = 2.1 ms, flip angle = 15°, matrix size = 256 × 256, voxel dimension = 1 × 1 × 1 mm.

T1-weighted images of BD cohort were acquired in the coronal orientation using a 1.5-T GE Signa scanner located at the Royal Prince Alfred Hospital, Sydney, Australia, with a fast-spoiled gradient echo sequence (time to echo = 5.3 ms, time repetition = 12.2 ms, flip angle = 25°, matrix size = 256 × 256, and voxel dimensions = 0.98 × 0.98 × 1.6 mm) (18, 19).

Brain images were realigned in three dimensions using Dr. View software (Infocom, Tokyo, Japan), and then reconstructed into 1.0-mm (MDD cohort)- or 0.98-mm (BD cohort)-thick entire contiguous coronal images. Voxels were segmented into brain tissue components and cerebrospinal fluid (CSF) based on

TABLE 1 | Demographic/clinical characteristics and brain measurements of the major depression cohort.

	Controls	cMDD	rMDD	Group comparisons[a]
	(*N* = 33)	(*N* = 29)	(*N* = 27)	
Age (years)	34.0 ± 9.9	32.5 ± 8.3	35.1 ± 10.0	F (2, 86) = 0.52, p = 0.595
Male/female	12/21	7/22	9/18	Chi-squared = 1.13, p = 0.568
Current IQ	111.1 ± 10.9	104.9 ± 8.7	111.4 ± 9.9	F (2, 85) = 4.03, p = 0.021; not significant (Scheffé's test)
Premorbid IQ	111.6 ± 12.3	107.5 ± 11.4	111.7 ± 8.9	F (2, 86) = 1.41, p = 0.250
Age of onset	–	21.1 ± 8	26.0 ± 9.4	F (1, 54) = 4.56, p = 0.037; cMDD < rMDD
Number of episodes	–	3.7 ± 3.4	3.1 ± 2.6	F (1, 38) = 0.37, p = 0.547
First episode/recurrent	–	7/22	–	-
Melancholic/non-melancholic[b]	–	10/18	–	-
Medication past 6 months: yes/no	–	21/6	12/13	Chi-squared = 4.96, p = 0.026
Current anxiety disorder: yes/no	–	18/10	4/23	Chi-squared = 14,02 p < 0.001
Beck Depression Inventory	3.6 ± 4.1	36.8 ± 8.9	13.0 ± 11.7	F (2, 86) = 120.57, p < 0.001; cMDD > rMDD > controls
MASQ general distress	27.9 ± 8.3	50.5 ± 7.8	40.4 ± 10.3	F (2, 81) = 49.21, p < 0.001; cMDD > rMDD > controls
MASQ general depression	19.5 ± 7.2	47.3 ± 9.2	35.0 ± 11.7	F (2, 82) = 66.85, p < 0.001; cMDD > rMDD > controls
MASQ general anxiety	16.4 ± 6.4	32.3 ± 8.7	24.7 ± 7.7	F (2, 82) = 32.31, p < 0.001; cMDD > rMDD > controls
MASQ anxious arousal	22.0 ± 4.4	42.0 ± 12.2	28.9 ± 7.7	F (2, 79) = 40.47, p < 0.001; cMDD > rMDD > controls
MASQ high positive affect	81.1 ± 14.3	43.6 ± 13.5	65.0 ± 12.4	F (2, 80) = 57.19, p < 0.001; cMDD < rMDD < controls
MASQ loss of interest	14.7 ± 5.0	31.6 ± 6.4	23.5 ± 6.8	F (2, 82) = 58.68, p < 0.001; cMDD > rMDD > controls
PANAS positive affect	32.9 ± 7.3	21.6 ± 6.5	28.7 ± 8.0	F (2, 82) = 18.57, p < 0.001; cMDD < rMDD, controls
PANAS negative affect	11.2 ± 1.6	21.2 ± 8.5	14.2 ± 4.7	F (2, 83) = 24.98, p < 0.001; cMDD > rMDD, controls
Total pineal volume [mm^3 (Cohen's d relative to controls)]	145.2 ± 84.9	119.2 ± 51.5 (-0.37)	119.7 ± 53.7 (-0.36)	F (2, 81) = 0.65, p = 0.526
Pineal parenchymal volume [mm^3 (Cohen's d relative to controls)]	138.8 ± 71.7	115.0 ± 45.1 (-0.40)	116.5 ± 48.2 (-0.37)	F (2, 81) = 0.84, p = 0.435
Cyst (≥ 2 mm) [*N*(%)]	9 (27.3%)	11 (37.9%)	7 (25.9%)	Chi-squared = 1.19, p = 0.553
Small cystic change (< 2 mm) [*N*(%)]	7 (21.2%)	5 (17.2%)	7 (25.9%)	Chi-squared = 0.63, p = 0.730
Intracranial volume (cm^3)	1493 ± 143	1477 ± 138	1470 ± 150	F (2, 85) = 0.20, p = 0.816[c]

Values represent means ± SD.

cMDD, currently depressed patients; MASQ, Mood and Anxiety Symptom Questionnaire; PANAS, Positive and Negative Affect Schedule; rMDD, remitted depressed patients.

[a]*Differences between the degree of freedom across measures were due to missing data.*

[b]*Assessed only for cMDD patients. Information missing for one patient.*

[c]*ANCOVA with age as a covariate and group as a between-subject factor.*

the signal-intensity histogram distribution of each T1-weighted image (26, 27). The intracranial volume (ICV) was measured on a sagittal reformat of the original 3D data (28), and did not significantly differ among the groups examined (**Tables 1 and 2**).

Pineal Gland Measurements

As reported previously (26, 27), one rater (TT), who was blinded to subject identities, manually traced the pineal gland, a small pinecone-shaped endocrine gland surrounded by CSF, except at the connection to the habenulae (**Figure 1**), on consecutive coronal slices. The parenchyma (i.e., segmented brain tissue component) of the pineal gland and internal cystic changes (pineal cyst ≥ 2 mm or small cystic change < 2 mm in diameter), observed as circular areas of iso-intensity relative to CSF (10), were differentiated by the signal intensity of each image. Therefore, we obtained total (cyst included) and parenchymal (non-cystic) pineal volumes. Intra- (TT) and inter-rater (TT and DS) intraclass correlation coefficients in a subset of 12 randomly selected brains (7 from the MD cohort and 5 from the BD cohort) were all > 0.90.

Statistical Analysis

Demographic and clinical differences between groups (cMDD *vs.* rMDD *vs.* controls, BD *vs.* controls) were assessed using a one-way analysis of variance (ANOVA) or the chi-squared test.

An analysis of covariance (ANCOVA) was performed on pineal volumes (total and parenchymal volumes) using age and ICV as covariates and group (cMDD *vs.* rMDD *vs.* controls, BD *vs.* controls) and gender as between-subject factors. The same ANCOVA model was used for assessing the effect of MDD subgroups [i.e., melancholic features (information available only for cMDD patients), co-morbid anxiety disorder, medication

TABLE 2 | Demographic/clinical characteristics and brain measurements of the bipolar disorder cohort.

	Controls	Bipolar disorder	Group comparisons
	(*N* = 24)	(*N* = 26)	
Age (years)	38.7 ± 11.1	38.4 ± 10.9	F (1, 48) = 0.01, p = 0.928
Male/female	7/17	8/18	Chi-squared = 0.02, p = 0.902
NART-estimated IQ[a]	115.1 ± 9.6	113.8 ± 7.1	F (1, 47) = 0.28, p = 0.597
Education (years)	14.6 ± 2.1	14.7 ± 2.8	F (1, 48) = 0.02, p = 0.899
Illness duration (years)	–	13.5 ± 10.1	–
Number of manic episodes	–	8.8 ± 10.2	–
Number of depressive episodes	–	11.1 ± 10.8	–
Lithium dosage (mg, *N* = 12)	–	975 ± 213	–
Valproate dosage (mg, *N* = 12)	–	1437 ± 594	–
Total pineal volume [mm^3 (Cohen's *d* relative to controls)]	129.8 ± 62.0	121 ± 79.0 (-0.13)	F (1, 44) = 0.64, p = 0.430
Pineal parenchymal volume [mm^3 (Cohen's *d* relative to controls)]	126.4 ± 57.6	119.6 ± 76.8 (-0.10)	F (1, 44) = 0.60, p = 0.442
Cyst (≥ 2 mm) [*N*(%)]	6 (25%)	5 (19.2%)	Chi-squared = 0.24, p = 0.623
Small cystic change (< 2 mm) [*N*(%)]	6 (25%)	11 (42.3%)	Chi-squared = 1.67, p = 0.197
Intracranial volume (cm^3)	1461 ± 148	1476 ± 126	F (1, 47) = 0.13, p = 0.715[b]

Values represent means ± SD.
NART, National Adult Reading Test.
[a]*Data missing for one bipolar patient.*
[b]*ANCOVA with age as a covariate and group as a between-subject factor.*

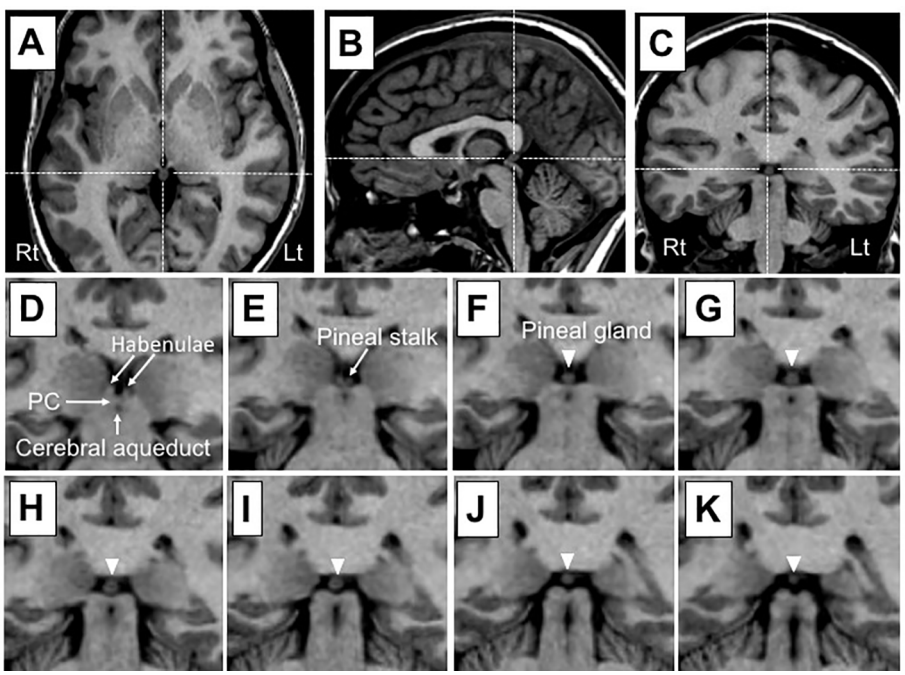

FIGURE 1 | Sample T1 images of the pineal gland in a subject with a small cystic change. Dotted lines in **(A)** (axial), **(B)** (sagittal), and **(C)** (coronal) show pineal gland coordinates. The pineal gland (arrowhead) and neighboring anatomical landmarks are shown on consecutive 1-mm-thick coronal slices from an anterior **(D)** to posterior **(K)** direction. The pineal gland is located posterior to the habenular nucleus and may be readily delineated on voxels as a brain tissue component largely surrounded by cerebrospinal fluid, except at its attachment to the stalk. The pineal stalk was excluded from the measurement of pineal gland volumes. PC, posterior commissure.

status, and first-episode or recurrent cMDD group] on the pineal volumes. Scheffé's test was used to follow-up any significant main effects or interactions. Group differences in the prevalence of pineal cysts (≥ 2 mm) and small cystic changes (< 2 mm) were examined using the chi-squared test. Relationships between pineal volumes and clinical variables were investigated by Pearson's partial correlation coefficients, with adjustments for age and ICV. To reduce the rate of Type I errors due to multiple comparisons, only parenchymal (non-cystic) volumes, which more accurately reflect the levels of melatonin secreted than total pineal volumes (7, 8), were used in correlational analyses. Pineal volumes and clinical variables (number of episodes,

medication, and symptom measures) were log-transformed for statistical analyses because of their skewed distribution (tested by the Kolmogorov– Smirnov test). A p-value of < 0.05 was considered to be significant.

RESULTS

Demographic and Clinical Characteristics

The MDD (**Table 1**) and BD (**Table 2**) groups were matched for age, gender, and intelligence or education with healthy controls. The cMDD group was characterized by an earlier onset age, higher proportion of medicated patients, higher rate of comorbid anxiety disorder, and more severe depressive/anxiety symptoms than the rMDD group (**Table 1**).

Pineal Gland Volume

Total and parenchymal pineal volumes in the cMDD and rMDD groups did not differ significantly from those of the healthy controls without any significant effect involving gender. However, these MDD groups exhibited non-significant pineal atrophy to the same degree as compared with healthy controls (Cohen's d relative to controls = -0.36 to -0.40) (**Table 1**). Comparisons between cMDD patients with and without melancholic features showed a significant difference in total [F (1, 24) = 4.98, p = 0.035] and parenchymal [F (1, 24) = 4.74, p = 0.040] volumes; the non-melancholic group had a significantly smaller volume than the melancholic group (p = 0.014 for both total and parenchymal volumes) (**Figure 2**). Total and parenchymal pineal volumes did not significantly differ between MDD patients with and without co-morbid anxiety disorder, those with and without medication in the past 6 months, or first-episode and recurrent cMDD patients.

No significant differences were observed in total (Cohen's d = -0.13) or parenchymal (Cohen's d = -0.10) pineal volumes between the BD group and healthy controls (**Table 2**). No significant effect involving gender was found. Furthermore, total and parenchymal pineal volumes did not significantly differ between the patient subgroups based on psychotic symptoms, family history, and medication status (lithium and valproate).

Pineal Cyst and Small Cystic Change

No significant differences were observed in the prevalence of pineal cysts and small cystic changes between the groups in the MDD (**Table 1**) and BD (**Table 2**) cohorts.

Correlational Analyses

Pineal parenchymal volumes in cMDD patients negatively correlated with the MASQ loss of interest score (r = -0.571, p = 0.002; **Figure 3**) even after the Bonferroni correction for multiple comparisons [10 clinical variables in two groups; $p < 0.0025$ (0.05/20)], but not with the number of episodes, total BDI score, and other MASQ and PANAS subscale scores. These clinical variables did not correlate with pineal parenchymal volumes in the rMDD group.

In the BD cohort, pineal parenchymal volumes did not correlate with illness duration, the number of manic/depressive episodes, or medication dose (lithium and valproate).

DISCUSSION

In the present study, no significant differences were observed in pineal volumes or cyst prevalence between the currently depressed and remitted MDD subgroups, bipolar I disorder group, and their matched controls. However, pineal volumes were specifically reduced in non-melancholic MDD patients and also negatively correlated with the severity of *loss of interest* in MDD patients under an active depressive state, thereby

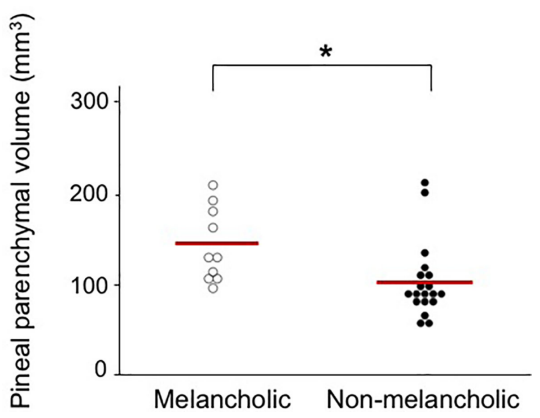

FIGURE 2 | Absolute pituitary parenchymal volume in currently depressed patients with melancholic (142.0 ± 40.7mm^3, Cohen's d relative to controls = 0.05) and non-melancholic (101.9 ± 42.4 mm^3, Cohen's d relative to controls = -0.63) subtypes. Scheffé's test: *$p < 0.05$.

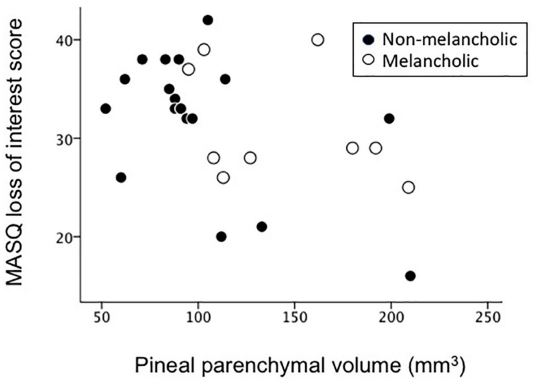

FIGURE 3 | Relationship between pineal parenchymal volumes and Mood and Anxiety Symptom Questionnaire (MASQ) loss of interest scores in currently depressed patients.

supporting the role of pineal abnormalities in certain clinical aspects of MDD.

Consistent with previous findings reported by Fındıklı et al. (13), the pineal volumes of MDD patients in the present study did not significantly differ from those of control subjects. However, these findings and the present results suggest non-significant pineal atrophy in MDD with the degree of a small to medium effect size (Cohen's *d* relative to controls = approximately -0.4 for both studies; see **Table 1**), which was smaller than, but similar to a recent study by Zhao et al. (9) (Cohen's *d* = -0.57) that reported significantly decreased pineal volumes in MDD. While Fındıklı et al. (13) estimated pineal volumes using a two-dimensional approximation formula (29) in a relatively small sample of MDD patients who had no pineal cysts ($N = 16$), Zhao et al. (12) and the present study manually measured true parenchymal (non-cystic) volumes, which appear to reflect pineal function more accurately than total (cyst included) pineal volumes (7, 8), in larger MDD cohorts regardless of the presence or absence of pineal cysts ($N \geq 50$). Thus, inconsistent pineal findings among studies (i.e., degree of volume reductions in MDD) cannot only be explained by differences in imaging techniques, approaches to pineal cysts, or sample sizes. However, the heterogeneity of MDD discussed below may be relevant.

The present results showing different pineal volumes between the melancholic and non-melancholic subtypes of depression support MDD being a heterogeneous disorder with different phenotypes caused by various neuropathological alterations (30, 31). Since the melancholic features of depression, such as diurnal variations in mood and insomnia (21), imply melatonin abnormalities and related circadian rhythm dysfunctions, the present results showing greater pineal atrophy in the non-melancholic MDD subtype were unexpected. On the other hand, we demonstrated that the severity of *loss of interest*, one of the core factors of melancholic depression (32), correlated with the degree of pineal reduction. While some neuroimaging [e.g., hippocampal atrophy (33) and hypofrontality (34)] and neuroendocrine [e.g., abnormal dexamethasone suppression pattern (35)] findings appear to be associated with the pathophysiology of melancholia, there have been no definitive biological markers of different subtypes of depression (35). However, the present results support pineal abnormalities potentially contributing to the clinical subtype and symptomatology of MDD.

In the present study, the illness stages (i.e., number of episodes, first-episode *vs.* multiple episodes) and mood status (currently depressed or remitted) of MDD patients did not affect pineal volumes, supporting its role as a stable trait marker. This appears to be consistent with previous clinical/hormonal findings showing that altered patterns of melatonin secretion (36) and circadian deregulation (37) were also present in the remission phases of depression, which may be relevant to residual symptoms or vulnerability to relapse. While this structural MRI study did not investigate the mechanisms underlying potential pineal volume changes, pineal dysfunctions in MDD are considered to be primarily caused by serotoninergic and norepinephrinergic deficits (36). However, the pineal pathology of depression has not yet been elucidated in detail; active structural/functional alterations in the pineal gland may occur around the first manifestation of depressive symptoms, while the genetic control of circadian rhythms in mood disorders (37) and animal findings of the significant contribution of intrauterine (maternal) melatonin deprivation to depressive symptoms in adult offspring (38) appear to support its neurodevelopmental aspects. Longitudinal studies on pineal volumes and melatonin secretion are required to clarify the nature of pineal abnormalities in MDD, particularly in the early course of the illness.

In contrast to a previous MRI study showing a higher prevalence of pineal cysts in MDD patients (62%) than in healthy subjects (40%) (12), our cohort had a prevalence of approximately 50% [combined rate of macroscopic cysts (≥ 2 mm in diameter) and small cystic changes (< 2 mm in diameter)] in the MDD and control groups (**Table 1**). Since macroscopic pineal cysts may affect melatonin (39) as well as cortisol (40) secretion profiles, the higher prevalence of pineal cysts may have induced neuroendocrine disturbances and consequent depressive symptomatology (41). However, Zhao et al. (12) did not differentiate pineal cysts and small cystic changes and we were unable to reliably evaluate exact cyst sizes in all cases using MR images due to the partial volume effect; therefore, future studies using higher-resolution images are needed to clarify the role of pineal cysts in the pathophysiology of major depression.

BD patients in the present study showed no abnormal morphological changes (i.e., total or parenchymal volumes and cyst prevalence) in the pineal gland, and the pineal morphology was not associated with clinical variables. Previous MRI studies reported a normal pineal volume in BD (13, 14), suggesting no significant role for pineal volume in the pathophysiology of BD. However, other hormonal studies have suggested that abnormal melatonin secretion is a heritable trait marker of BD (2, 42). Potential treatment effects of melatonin for mood symptoms and relapse prevention in BD (2) also support melatonin dysregulation in these patients. Thus, the normal relationship between the volume of the pineal gland and its secretion of melatonin (7, 8) may be disrupted under pathological conditions, such as BD.

The present study had several limitations. First, we did not assess melatonin levels or circadian rhythms in study participants. Therefore, it currently remains unclear whether the pineal results obtained reflect its function and disturbances in the circadian rhythms of MDD patients. Further, given the association between the pineal activation and physical/mental relaxation (43), potential role of its abnormality in affective disorders needs to be tested in future functional neuroimaging studies. Second, the sample size of the study participants was rather small, especially for each MDD subgroup [e.g., melancholic cMDD group ($N = 10$), first-episode cMDD group ($N = 7$)]. In addition, the information of melancholic/non-

melancholic subtype was not available for the rMDD group in this study. It should be also noted that the MDD and BD cohorts were scanned using different scanners/parameters in the present study, which disabled direct comparisons of pineal volumes between the MDD and BD groups. Control matched groups for the MDD and BD groups showed markedly different pineal volumes (**Tables 1** and **2**), which may reflect the influence of the different imaging settings. Thus, our preliminary results need to be replicated in a larger sample of various affective disorders scanned using the same setting. Third, as discussed previously (26), T1-weighted MR images cannot reliably assess pineal calcification, which may be associated with melatonin secretion (44) and treatment responses in bipolar patients (45). Another technical issue is that the error caused by manual measurement cannot be avoided especially for a small structure such as the pineal gland. While the measurement in this study required only minimal manual editing (**Figure 1**) and the inter- and intra-rater reliabilities were rather high (> 0.90), future studies using non-manual automated measurement methods would increase the accuracy of the pineal gland assessment. Finally, while the present study found no effect of medication on pineal volumes in the MDD and BD cohorts, their complete medication data (e.g., lifetime medication) were not available. Since mood stabilizers (46, 47) and antidepressants (48) have been shown to affect melatonin secretion patterns or brain melatonin receptor expression, the potential effects of prolonged medication on pineal morphology/functions warrant further study.

In summary, the present study found that pineal gland volumes were not significantly altered in patients with MDD and BD. These results do not support the association of pineal volumes with abnormal melatonin secretion in affective disorders (1, 2). However, significant reductions were observed in pineal volumes in specific depression subtypes, and these changes correlated with specific symptoms of depression, suggesting an association between pineal abnormalities and clinical subtype and/or symptomatology of major depression.

DATA AVAILABILITY STATEMENT

The datasets generated for this study will not be made publicly available because we do not have permission to share the data. Requests to access the datasets should be directed to the corresponding author.

ETHICS STATEMENT

The studies involving human participants were reviewed and approved by The Prince of Wales Hospital and University of New South Wales research ethics committees and Mental Health Research & Ethics Committee, Melbourne Health, Melbourne, Australia. The patients/participants provided their written informed consent to participate in this study.

AUTHOR CONTRIBUTIONS

MY, MS, CP, GM, and NA conceived the concept for and methodology of the study. TT conducted statistical analyses and wrote the manuscript. MY, SW, VL, MW, GM, and NA recruited subjects and were involved in clinical and diagnostic assessments. TT and DS analyzed MRI data. MY, MS, CP, GM, and NA contributed to the writing and editing of the manuscript. All authors contributed to and have approved the final manuscript.

FUNDING

This work was supported in part by JSPS KAKENHI Grant Number No. JP18K07550 to TT, JP18K15509 to DS, and by Health and Labour Sciences Research Grants for Comprehensive Research on Persons with Disabilities from the Japan Agency for Medical Research and Development (AMED) Grant Number 16dk0307029h0003 to MS.

REFERENCES

1. Dmitrzak-Weglarz M, Reszka E. Pathophysiology of depression: molecular regulation of melatonin homeostasis - current status. *Neuropsychobiology* (2017) 76(3):117–29. doi: 10.1159/000489470
2. Takaesu Y. Circadian rhythm in bipolar disorder: A review of the literature. *Psychiatry Clin Neurosci* (2018) 72(9):673–82. doi: 10.1111/pcn.12688
3. Kennedy SH, Kutcher SP, Ralevski E, Brown GM. Nocturnal melatonin and 24-hour 6-sulphatoxymelatonin levels in various phases of bipolar affective disorder. *Psychiatry Res* (1996) 63(2-3):219–22. doi: 10.1016/0165-1781(96)02910-1
4. Lamers F, Cui L, Hickie IB, Roca C, Machado-Vieira R, Zarate CAJr, et al. Familial aggregation and heritability of the melancholic and atypical subtypes of depression. *J Affect Disord* (2016) 204:241–6. doi: 10.1016/j.jad.2016.06.040
5. Cajochen C, Kräuchi K, Wirz-Justice A. Role of melatonin in the regulation of human circadian rhythms and sleep. *J Neuroendocrinol* (2003) 15(4):432–7. doi: 10.1046/j.1365-2826.2003.00989.x
6. Borjigin J, Zhang LS, Calinescu AA. Circadian regulation of pineal gland rhythmicity. *Mol Cell Endocrinol* (2012) 349(1):13–9. doi: 10.1016/j.mce.2011.07.009
7. Nölte I, Lütkhoff AT, Stuck BA, Lemmer B, Schredl M, Findeisen P, et al. Pineal volume and circadian melatonin profile in healthy volunteers: an interdisciplinary approach. circadian melatonin profile. *J Magn Reson Imaging* (2009) 30(3):499–505. doi: 10.1002/jmri.21872
8. Liebrich LS, Schredl M, Findeisen P, Groden C, Bumb JM, Nölte IS. Morphology and function: MR pineal volume and melatonin level in human saliva are correlated. *J Magn Reson Imaging* (2014) 40(4):966–71. doi: 10.1002/jmri.24449
9. Carpenter JS, Abelmann AC, Hatton SN, Robillard R, Hermens DF, Bennett MR, et al. Pineal volume and evening melatonin in young people with affective disorders. *Brain Imaging Behav* (2017) 11(6):1741–50. doi: 10.1007/s11682-016-9650-2
10. Pu Y, Mahankali S, Hou J, Li J, Lancaster JL, Gao JH, et al. High prevalence of pineal cysts in healthy adults demonstrated by high-resolution, noncontrast brain MR imaging. *AJNR Am J Neuroradiol* (2007) 28(9):1706–9. doi: 10.3174/ajnr.A0656
11. Nolte I, Brockmann MA, Gerigk L, Groden C, Scharf J. TrueFISP imaging of the pineal gland: more cysts and more abnormalities. *Clin Neurol Neurosurg* (2010) 112(3):204–8. doi: 10.1016/j.clineuro.2009.11.010
12. Zhao W, Zhu DM, Zhang Y, Zhang C, Wang Y, Yang Y, et al. Pineal gland abnormality in major depressive disorder. *Psychiatry Res Neuroimaging* (2019) 289:13–7. doi: 10.1016/j.pscychresns.2019.05.004
13. Fındıklı E, Inci MF, Gökçe M, Fındıklı HA, Altun H, Karaaslan MF. Pineal gland volume in schizophrenia and mood disorders. *Psychiatr Danub* (2015) 27(2):153–8.

14. Sarrazin S, Etain B, Vederine FE, d'Albis MA, Hamdani N, Daban C, et al. MRI exploration of pineal volume in bipolar disorder. *J Affect Disord* (2011) 135(1-3):377–9. doi: 10.1016/j.jad.2011.06.001
15. Lorenzetti V, Allen NB, Fornito A, Pantelis C, De Plato G, Ang A, et al. Pituitary gland volume in currently depressed and remitted depressed patients. *Psychiatry Res Neuroimaging* (2009) 172(1):55–60. doi: 10.1016/j.pscychresns.2008.06.006
16. Walterfang M, Yücel M, Barton S, Reutens DC, Wood AG, Chen J, et al. Corpus callosum size and shape in individuals with current and past depression. *J Affect Disord* (2009) 115(3):411–20. doi: 10.1016/j.jad.2008.10.010
17. Takahashi T, Nishikawa Y, Yücel M, Whittle S, Lorenzetti V, Walterfang M, et al. Olfactory sulcus morphology in patients with current and past major depression. *Psychiatry Res Neuroimaging* (2016) 255:60–5. doi: 10.1016/j.pscychresns.2016.07.008
18. Javadapour A, Malhi GS, Ivanovski B, Chen X, Wen W, Sachdev P. Hippocampal volumes in adults with bipolar disorder. *J Neuropsychiatry Clin Neurosci* (2010) 22(1):55–62. doi: 10.1176/appi.neuropsych.22.1.55
19. Takahashi T, Malhi GS, Wood SJ, Yücel M, Walterfang M, Kawasaki Y, et al. Gray matter reduction of the superior temporal gyrus in patients with established bipolar I disorder. *J Affect Disord* (2010) 123(1-3):276–82. doi: 10.1016/j.jad.2009.08.022
20. Takahashi T, Malhi GS, Nakamura Y, Suzuki M, Pantelis C. Olfactory sulcus morphology in established bipolar affective disorder. *Psychiatry Res Neuroimaging* (2014) 222(1-2):114–7. doi: 10.1016/j.pscychresns.2014.02.005
21. First MB, Spitzer RL, Gibbon M, Williams JBW. *Structured Clinical Interview for Axis 1 DSM-IV Disorders*. New York: New York State Psychiatric Institute (2001).
22. Beck AT, Steer RT. *Beck Depression Inventory Manual*. San Antonio: Harcourt Brace Jovanovich (1987).
23. Watson D, Clark L, Weber K, Assenheimer J, Strauss M, McCormick R. Testing a tripartite model: I. Evaluating the convergent and discriminant validity of anxiety and depression symptom scales. *J Abnorm Psychol* (1995) 104:3–14. doi: 10.1037/0021-843X.104.1.3
24. Watson D, Clark L, Tellegen A. Development and validation of brief measures of positive and negative affect: the PANAS scales. *J Pers Soc Psychol* (1988) 54:1063–70. doi: 10.1037/0022-3514.54.6.1063
25. First MB, Spitzer RL, Gibbon M, Williams JB. *Structured Clinical Interview for DSM-IV*. Washington DC: American Psychiatric Press (1998).
26. Takahashi T, Nakamura M, Sasabayashi D, Nishikawa Y, Takayanagi Y, Nishiyama S, et al. Reduced pineal gland volume across the stages of schizophrenia. *Schizophr Res* (2019a) 206:163–70. doi: 10.1016/j.schres.2018.11.032
27. Takahashi T, Nakamura M, Sasabayashi D, Nishikawa Y, Takayanagi Y, Furuichi A, et al. Reduced pineal gland volume in schizotypal disorder. *Schizophr Res* (2019b) 209:289–91. doi: 10.1016/j.schres.2019.05.004
28. Eritaia J, Wood SJ, Stuart GW, Bridle N, Dudgeon P, Maruff P, et al. An optimized method for estimating intracranial volume from magnetic resonance images. *Magn Reson Med* (2000) 44:973–7. doi: 10.1002/1522-2594(200012)44:6<973::aid-mrm21>3.0.co;2-h
29. Sumida M, Barkovich AJ, Newton TH. Development of the pineal gland: measurement with MR. *AJNR Am J Neuroradiol* (1996) 17(2):233–6.
30. Savitz JB, Drevets WC. Imaging phenotypes of major depressive disorder: genetic correlates. *Neuroscience* (2009) 164(1):300–30. doi: 10.1016/j.neuroscience.2009.03.082
31. Stringaris A. Editorial: What is depression? *J Child Psychol Psychiatry* (2017) 58(12):1287–9. doi: 10.1111/jcpp.12844
32. Biro M, Till E. Factor analytic study of depressive disorders. *J Clin Psychol* (1989) 45:369–73. doi: 10.1002/1097-4679(198905)45:3<369::AID-JCLP2270450304>3.0.CO;2-D
33. Hickie I, Naismith S, Ward PB, Turner K, Scott E, Mitchell P, et al. Reduced hippocampal volumes and memory loss in patients with early- and late-onset depression. *Br J Psychiatry* (2005) 186:197–202. doi: 10.1192/bjp.186.3.197
34. Pizzagalli DA, Oakes TR, Fox AS, Chung MK, Larson CL, Abercrombie HC, et al. Functional but not structural subgenual prefrontal cortex abnormalities in melancholia. *Mol Psychiatry* (2004) 9(4):393–405. doi: 10.1038/sj.mp.4001501
35. Leventhal AM, Rehm LP. The empirical status of melancholia: implications for psychology. *Clin Psychol Rev* (2005) 25(1):25–44. doi: 10.1016/j.cpr.2004.09.001
36. Pacchierotti C, Iapichino S, Bossini L, Pieraccini F, Castrogiovanni P. Melatonin in psychiatric disorders: a review on the melatonin involvement in psychiatry. *Front Neuroendocrinol* (2001) 22(1):18–32. doi: 10.1006/frne.2000.0202
37. Etain B, Milhiet V, Bellivier F, Leboyer M. Genetics of circadian rhythms and mood spectrum disorders. *Eur Neuropsychopharmacol* (2011) 21(Suppl 4): S676–82. doi: 10.1016/j.euroneuro.2011.07.007
38. Voiculescu SE, Rosca AE, Zeca V, Zagrean L, Zagrean AM. Impact of maternal melatonin suppression on forced swim and tail suspension behavioral despair tests in adult offspring. *J Med Life* (2015) 8(2):202–6.
39. Karadaş O, Ipekdal IH, Ulaş UH, Odabaşi Z. Nocturnal headache associated with melatonin deficiency due to a pineal gland cyst. *J Clin Neurosci* (2012) 19 (2):330–2. doi: 10.1016/j.jocn.2011.05.022
40. Májovský M, Řezáčová L, Sumová A, Pospíšilová L, Netuka D, Bradáč O, et al. Melatonin and cortisol secretion profile in patients with pineal cyst before and after pineal cyst resection. *J Clin Neurosci* (2017) 39:155–63. doi: 10.1016/j.jocn.2017.01.022
41. Malhi GS, Mann JJ. Depression. *Lancet* (2018) 392(10161):2299–312. doi: 10.1016/S0140-6736(18)31948-2
42. Hallam KT, Olver JS, Chambers V, Begg DP, McGrath C, Norman TR. The heritability of melatonin secretion and sensitivity to bright nocturnal light in twins. *Psychoneuroendocrinology* (2006) 31(7):867–75. doi: 10.1016/j.psyneuen.2006.04.004
43. Liou CH, Hsieh CW, Hsieh CH, Chen JH, Wang CH, Lee SC. Studies of chinese original quiet sitting by using functional magnetic resonance imaging. *Conf Proc IEEE Eng Med Biol Soc* (2005) 2005:5317–9. doi: 10.1109/IEMBS.2005.1615681
44. Tan DX, Xu B, Zhou X, Reiter RJ. Pineal Calcification, Melatonin Production, Aging, Associated Health Consequences and Rejuvenation of the Pineal Gland. *Molecules* (2018) 23(2):E301. doi: 10.3390/molecules23020301
45. Sandyk R, Pardeshi R. The relationship between ECT nonresponsiveness and calcification of the pineal gland in bipolar patients. *Int J Neurosci* (1990) 54(3-4):301–6. doi: 10.3109/00207459008986648
46. Hallam KT, Olver JS, Norman TR. Effect of sodium valproate on nocturnal melatonin sensitivity to light in healthy volunteers. *Neuropsychopharmacology* (2005) 30(7):1400–4. doi: 10.1038/sj.npp.1300739
47. Moreira J, Geoffroy PA. Lithium and bipolar disorder: Impacts from molecular to behavioural circadian rhythms. *Chronobiol Int* (2016) 33 (4):351–73. doi: 10.3109/07420528.2016.1151026
48. Hirsch-Rodriguez E, Imbesi M, Manev R, Uz T, Manev H. The pattern of melatonin receptor expression in the brain may influence antidepressant treatment. *Med Hypotheses* (2007) 69(1):120–4. doi: 10.1016/j.mehy.2006.11.012

Conflict of Interest: The authors declare that this research was conducted in the absence of any commercial or financial relationships that may be construed as a potential conflict of interest.

frontiers in Psychiatry

ORIGINAL RESEARCH
published: 20 May 2020
doi: 10.3389/fpsyt.2020.00439

Gray Matter Deficits and Dysfunction in the Insula Among Individuals With Intermittent Explosive Disorder

Ji-Woo Seok[1,2] *and Chaejoon Cheong*[3]*

[1] Department of Psychiatry, University of Nebraska Medical Center, Omaha, NE, United States, [2] Department of Rehabilitation Counseling Psychology, Seoul Hanyoung University, Seoul, South Korea, [3] Bioimaging Research Team, Korean Basic Science Institute, Cheongju, South Korea

Although numerous neuroimaging studies have evaluated the characteristics of intermittent explosive disorder (IED), studies on the structural alterations and focal dysfunction in the brain in this condition are limited. This study aimed to identify gray matter deficits and functional alterations in individuals with IED using voxel-based morphometry (VBM) and functional magnetic resonance imaging (fMRI) analyses. Fifteen men with IED and 15 age- and sex-matched healthy controls participated in this study. Gray matter volume and brain activation while viewing the anger-inducing films were measured using 7T MRI. VBM results indicated that individuals with IED had significantly reduced gray matter volume in the insula, amygdala, and orbitofrontal area, relative to controls. Gray matter volume in the left insula was negatively correlated with composite aggression scores. fMRI results demonstrated that relative to healthy controls, individuals with IED showed greater activation in the insula, putamen, anterior cingulate cortex, and amygdala during anger processing. Left insular activity was positively correlated with composite aggression scores. Collectively, these findings suggest that structural and functional alterations in the left insula are linked to IED; this provides insight into the neural mechanisms underlying IED.

Keywords: 7T magnetic resonance imaging, functional magnetic resonance imaging, insula, intermittent explosive disorder, voxel-based morphometry

OPEN ACCESS

Edited by:
Ping Li,
Qiqihar Medical University, China

Reviewed by:
Royce J. Lee,
University of Chicago, United States
Emil Frank Coccaro,
University of Chicago, United States
Fengyu Zhang,
Global Clinical and Translational Research Institute, United States

***Correspondence:**
Chaejoon Cheong
cheong@kbsi.re.kr;
cheong@ust.ac.kr

Specialty section:
This article was submitted to Neuroimaging and Stimulation, a section of the journal Frontiers in Psychiatry

Received: *07 October 2019*
Accepted: *28 April 2020*
Published: *20 May 2020*

Citation:
Seok J-W and Cheong C (2020) Gray Matter Deficits and Dysfunction in the Insula Among Individuals With Intermittent Explosive Disorder. Front. Psychiatry 11:439. doi: 10.3389/fpsyt.2020.00439

INTRODUCTION

Self-protective aggression lies within the normal range of human behavior. However, impulsive and intentional aggression behaviors are viewed as pathological. Impulsive and intentional aggression behaviors are known to have significant physical and psychosocial effects on the aggressive individual, victims of the aggression, and society (1). Pathological impulsive aggression, despite its serious negative consequences, is defined as intermittent explosive disorder (IED) in the Diagnostic and Statistical Manual of Mental Disorders, Fifth Edition (DSM-5) (2). Previous research demonstrates that the lifetime prevalence of IED is 3%–5% (1) and that the average age of onset is 14 years (3). Studies on IED identified that individuals with IED display 65–70 acts of assault and property destruction on an average, and this frequency of aggressive acts is much higher than that among individuals without IED (3, 4). These studies also demonstrated that IEDs incur

large costs including over $1,000 in damage, and lead to multiple hospitalizations (3, 4). Owing to the adverse personal and social problems arising from IED, research is needed into the behavioral and neurobiological underpinnings of IED to identify the theoretical and clinical implications of this disorder, and to discover effective treatments.

Neuroimaging studies demonstrate that IED is related to possible brain impairments (5–11). In a functional magnetic resonance imaging (fMRI) study on face processing, individuals with IED showed a stronger amygdala response to angry faces than did healthy controls (6, 8, 10), and amygdala activation to angry faces was correlated with a lifetime history of aggression (6) and the number of prior aggressive acts (10). Compared with controls, individuals with IED exhibit diminished functional connectivity between the amygdala and orbitofrontal cortex, suggesting reduced regulatory control of the prefrontal cortex (10). Other fMRI studies on regulation ability among patients with IED demonstrated that these individuals displayed more errors on the color-word Stroop task than did controls, and revealed that this inhibitory dysregulation was related to impairments in the dorsolateral prefrontal cortex (11).

Structural brain imaging has been used extensively in recent years to examine the morphology of brain tissues. In particular, structural brain imaging of individuals with mental disorders provides information regarding cortical atrophy, thinning, and deformation that occurs in response to psychiatric disorders. Mounting evidence from structural brain imaging studies has revealed that IED may be linked to possible anatomical changes within the brain (5, 9). Lee et al. (9) suggested that IED is associated with the degeneration of white matter tracts in long-range connections between frontal and temporoparietal regions. In addition, another structural study using voxel-based morphometry (VBM) revealed significantly reduced gray matter volume in patients with IED relative to controls in frontolimbic systems including the orbitofrontal cortex, ventral medial prefrontal cortex, anterior cingulate cortex, amygdala, insula, and uncus (5).

VBM analysis is used to investigate the focal differences in brain anatomy *in vivo* using structural MRI. This type of analysis is useful for detecting small-scale regional alterations across the volume of the whole brain or its subparts in individuals with neurological and psychiatric disorders (12). However, as VBM depends entirely on accurate registration and normalization, it is likely to increase false estimates (13, 14). Diffeomorphic Anatomical Registration Through Exponentiated Lie Algebra (DARTEL) algorithms have been proposed to reduce false estimates by improving intersubject registration of brain images (15). DARTEL can consequently strengthen the robustness and reliability of VBM results (16, 17).

Although several neuroimaging studies have reported impaired brain function and structure in IED, few studies have used both, structural and functional analyses to focus on the functional and structural alterations in IED. Integrating measures of structural and functional brain imaging provides profound insights into the neurobiological underpinnings of IED and may lead to the detection of clinically useful biomarkers for IED. Therefore, in this study, we used 7T MRI to identify alterations in brain structure and function among individuals with IED, by measuring gray matter volume and brain function during anger processing from combined fMRI and automated whole-brain VBM DARTEL analyses. In particular, we focused on gray matter volume in the frontolimbic system, including the amygdala, prefrontal cortex, and insula, and investigated alterations in brain function in areas exhibiting reduced gray matter volume.

MATERIALS AND METHODS

Participants

Fifteen right-handed men diagnosed with IED and 15 right-handed healthy controls with no history of any psychiatric or personality disorder participated in the study. All participants were 25–35 years old and were recruited from local psychiatric clinics and counseling centers, as well as through website postings. All participants in the IED group met DSM-5 criteria for current IED. Additional diagnoses were also used based on the Structured Clinical Interview for DSM-IV Axis I Disorders (SCID-I) and Symptom Check List-90-Revised (SCL-90-R). To identify the specific characteristics for IED, the IED participants were excluded from the study if they reported any of the following: (1) on current psychopharmacological medication, (2) a history of bipolar or psychotic disorder, (3) a traumatic head injury, or (4) a current major depressive episode or substance dependence.

For the control group, 15 participants with matching demographic characteristics (age, gender, education level, and income level) were selected and none of the 15 control participants fulfilled the criteria for any psychiatric disorder. None of the participants had any history of brain injury or abuse of psychoactive drugs within the past year. The patients with IED were not on any medication related to IED at the time of the study. All participants provided written informed consent according to the Declaration of Helsinki (18) after being thoroughly informed about the details of the experiment. The experimental procedures were approved by the Chungnam National University Institutional Review Board (approval number: 201803-SB-041-01).

Psychological Assessments

To assess the severity of aggression, a composite aggression score was obtained by measuring the three aggression scales including the Life History of Aggression (19), Buss-Perry Aggression Questionnaire (20), and State-Trait Anger Expression Inventory-2 (21) in all participants. The Life History of Aggression assesses a lifetime history of actual aggressive behavior, and the Buss-Perry Aggression Questionnaire assesses aggressive tendency by measuring the four components of physical aggression, verbal aggression, anger, and hostility. The State-Trait Anger Expression Inventory-2 assessment evaluates the temporary condition of anger experience (state anger) and the more long-standing propensity of anger experience (trait anger).

As there are strong correlations between the three aggression scales ($r > 0.8$, $p < 0.01$), we created composite variables for aggression in a data-reduction step summing the z-scores on these three scales (22). The Beck Depression Inventory (23), Beck Anxiety Inventory (24), and Barratt Impulsiveness Scale II (25) were administered to identify other psychological characteristics among all the participants. Statistical analyses were conducted with SPSS 25 (SPSS Inc., Chicago, IL, USA). The independent t test and Mann-Whitney U test were used for between-group comparisons of demographic and clinical variables. Data on the demographic and clinical characteristics of all participants have been presented in **Table 1** and **Table S1**.

Stimuli and Experimental Paradigm

Two types of film clips (anger and neutral) were presented to the participants. Each film clip was a scene selected from movies, dramas, news, and/or documentaries. Anger-inducing clips included stories of child abuse, mocking a person with disabilities, racism, unfair treatment, and bullying. Neutral clips showed nonaffective nature scenes and were similar in color and hue to those of anger-inducing clips. Seok and Cheong (26) have previously employed these stimuli (**Figure 1**) (26).

The fMRI task was divided into 10 blocks, with five neutral and five anger-inducing blocks. Each block included a film clip and an interstimulus interval, and each film clip presented for 30 s in random order to eliminate order effects. A 12-s interstimulus interval was presented between blocks to reduce possible carry over effects. The duration of the entire scanning session was approximately 7 min (**Figure 1**).

After the scanning procedure, participants were asked the following question to assess suitability, frequency and intensity of anger during viewing the film clips; "Does this film clip provoke the anger? Please answer yes or no," "How often did you get angry during viewing this film clip? Please answer the number," "How angry you were while watching this film clip? Please rate the intensity on below scale ranging from 0 (not angry at all) to 5 (extremely angry)."

Data Acquisition

A 7T Philips Achieva MRI scanner (Philips Medical Systems, Best, Netherlands) was used for image acquisition. High-

TABLE 1 | Demographic and clinical characteristics of the IED and control groups.

Variables (mean ± SD)	IED	HC	p	Effect Size
Age (year)	28.53 ± 2.36	28.60 ± 4.40	0.95	0.02
Onset age of FAA	13.93 ± 1.79	N.A.	N.A	N.A.
Cigarettes per day (Last 3 months)	5.53 ± 2.56	4.53 ± 2.85	0.32	0.37
Num. of alcohol use day* (Last 3 months)	2.00 [1.00, 3.00]	2.00 [1.00, 3.00]	0.91	0.001
Num. of AO per week* (Last 3 month)	4.00 [3.00, 5.00]	0.00 [0.00, 0.50]	0.00	0.72
BDI*	9.00 [3.50, 16.50]	2.00 [0.50, 9.00]	0.04	0.14
BAI*	8.00 [4.00, 12.00]	3.00 [1.00, 4.50]	0.09	0.09
BIS-II	67.00 ± 6.77	60.07 ± 8.35	0.02	0.91
LHA	11. 67 ± 3.64	4.73 ± 3.41	0.00	1.95
SA	21.93 ± 4.13	15.13 ± 2.90	0.01	0.95
TA	23.00 ± 4.58	16.00 ± 3.95	0.00	1.63
AQ	70.07 ± 5.34	47.93 ± 15.31	0.00	1.93

AO, aggressive outbursts; AQ, aggression questionnaire; BAI, Beck Anxiety Inventory; BDI, Beck Depression Inventory; BIS, Barrett's Impulsiveness Scale II; FAA, First Anger Attack HC, healthy controls; IED, intermittent explosive disorder; LHA, Life History of Aggression Questionnaire; Num, Number; SA, state anger; TA, trait anger.

**The variables are nonnormal distributed and are described as median and interquartile range. The Mann-Whitney U test was used to compare between groups for the variables.*

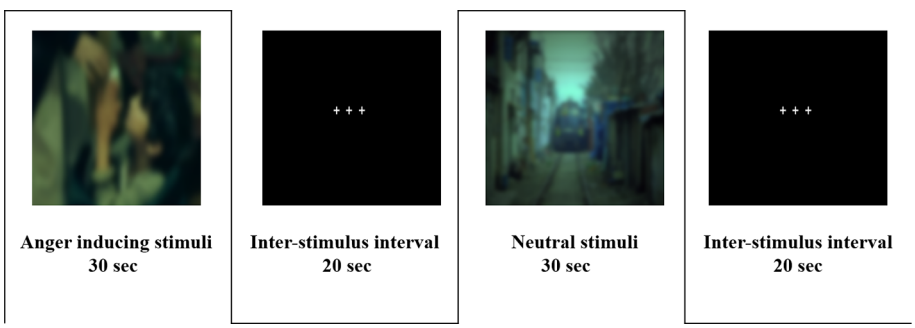

FIGURE 1 | Experimental paradigm for functional magnetic resonance imaging.

resolution structural images were obtained using a three-dimensional T1-weighted sequence (repetition time = 5.5 ms, echo time = 2.6 ms, flip angle = 7, field of view = 234 × 234 mm^2, voxel size = 0.7 × 0.7 × 0.7 mm^3). During the fMRI experiment, blood oxygenation level dependent images were acquired using a T2*-weighted gradient echo-planar imaging sequence with the following parameters: repetition time = 2000 ms, echo time = 17 ms, flip angle = 70°, bandwidth = 1856 Hz/pixel, field of view = 192 × 192 mm^2, voxel size = 2.0 × 2.0 × 3.5 mm^3, and 32 interleaved slices with no slice gap.

VBM Analysis

VBM analysis was conducted using SPM12 (http://www.fil.ion.ucl.ac.uk/spm) implemented in Matlab R2017a (MathWorks, Natick, MA). First, T1-weighted images were segmented into gray and white matter using the standard unified segmentation model. Second, gray matter templates were made from the entire image dataset using the diffeomorphic nonlinear registration algorithm (DARTEL) technique to increase the accuracy of intersubject registration by estimating the nonlinear deformation method (13, 15). Third, each participant's gray matter image was normalized to Montreal Neurological Institute space (http://www.mni.mcgill.ca/) using an initial affine registration and nonlinear warping. Fourth, modulation was performed to ensure that relative volumes of gray matter were preserved after the spatial normalization procedure. Lastly, images were smoothed with an 8-mm, full-width-at-half-maximum Gaussian kernel to decrease spatial noise.

After data preprocessing, between-group comparisons were conducted using analysis of covariance (ANCOVA), with age, education, BDI score, BAI score, BIS scores, and intracranial volume (i.e., the sum of gray matter, white matter, and cerebrospinal fluid, as derived from the segmentation process) as nuisance variables. To estimate the relationship between the severity of aggression and structural abnormalities linked to depression, anxiety, and impulsivity, whole-brain analyses using multiple linear regression were performed between the gray matter volume and the composite aggression score. The exploratory lenient significance threshold was set at $p < 0.001$ (uncorrected at the voxel level) and $p < 0.05$ (corrected for spatial extent).

To confirm the validity of the results acquired using the whole-brain analysis, *post hoc* analysis was conducted with the extracted gray matter volume from each brain area using SPSS 25.

Functional MRI Analysis

We used SPM12 (http://www.fil.ion.ucl.ac.uk/spm) implemented in Matlab R2017a (MathWorks) for preprocessing and statistical analyses. The first three image volumes were discarded to prevent instability of the initial MRI signal. Correction of slice acquisition timing, realignment to the first functional image using an affine (six parameter) spatial transformation, correction of geometric distortion by the unwarp function, coregistration with the high-resolution anatomical image, and normalization to the standard brain of the Montreal Neurological Institute were executed after the origin coordinates were adjusted to the anterior commissure. Lastly, smoothing was performed with a 6-mm full-width-at-half-maximum Gaussian kernel.

A design matrix was constructed for the anger-evoking and neutral conditions using a box-car function convolved with the canonical hemodynamic response function and its temporal derivative. The six movement parameters of rigid body transformation applied by the realignment procedure were included as nuisance variables in the model. A high-pass filter was implemented using a discrete cosine transform set with a cutoff frequency of 1/128 Hz in the design matrix. Since 7T MRI data have several limitations including signal dropout, distortions, and susceptibility, we used the following methods to compensate for them: (1) applying second-order B0 shimming, (2) using barium titanate–based dielectric pads (27), and (3) eliminating data with over 20% signal dropout in the ventromedial prefrontal cortex.

T-contrasts were calculated for each participant to identify anger-specific neural substrates by comparing the anger-inducing and neutral conditions. To measure group-level activation of the blood oxygenation level-dependent response during anger processing, the contrast images of all participants in each group were subjected to a standard random-effects analysis. ANCOVA analysis was applied to control for potential confounding variables using BDI, BAI, and BIS scores as covariates. The threshold for statistical significance was set at $p < 0.001$ or $p < 0.05$ with false discovery rate (FDR) correction. Additionally, multiple linear regression was conducted to determine the regions of activation that correlated with the severity of aggression (i.e., composite aggression score) after adjusting for depression (i.e., BDI score), anxiety (i.e., BAI score), and impulsivity (i.e., BIS score) effects.

To confirm the validity of the results acquired using ANCOVA and multiple linear regression analyses, *post hoc* analysis was conducted with the percent signal change from regions of interest (ROIs) using SPSS 25. The percent signal change was extracted from the ROIs based on the results of the between-group and correlation analyses (i.e., bilateral putamen, bilateral insula, right amygdala, right anterior cingulate cortex). The ROIs were created by placing a 5-mm sphere around the described coordinates in **Tables 2** and **3**.

TABLE 2 | The result of anger induction.

Variables (mean ± SD)	IED	HC	p
Frequency of anger induction (%)[a]	40.00 [40.00, 50.00]	40.00 [30.00, 50.00]	0.43
Intensity of anger[b]	18.53 ± 3.31	14.67 ± 5.40	0.03

HC, healthy controls; IED, intermittent explosive disorder.

[a]*Represented as percentage of anger inducing stimuli that evoked anger among five anger-inducing clips. The variable is nonnormal distributed and is described as median and interquartile range. The Mann-Whitney U test was used to compare between groups for the variable.*

[b]*Degree of anger triggered by the anger-inducing cues on a five-point Likertscale.*

TABLE 3 | Differences in gray matter volume between the IED and control groups and brain regions negatively correlated with the severity of aggression.

Brain region	MNI coordinates			t_{max}	Cluster size (voxels)
	x	y	z		
IED < HC[1]					
Left OFC	−15	60	0	4.04	171
Left insula (BA 13)	−28	27	0	4.29	204
Right insula (BA 13)	33	30	−5	3.91	102
Left amygdala	−21	-6	−9	3.55	39
Correlation with the severity of aggression[2]					
Left insula	−24	33	−2	3.61	43

BA, Brodmann area; HC, healthy control; IED, intermittent explosive disorder; MNI, Montreal Neurological Institute; OFC, orbitofrontal cortex.

MNI coordinates of the maximum t-scores are shown for each cluster.

[1]Results are reported at p < 0.001, uncorrected for the whole-brain analysis. The regions exhibited the greater activity in the IED group compared to healthy controls during the anger-inducing condition compared to the neutral condition. There was no brain region in which healthy controls exhibited greater activation than the IED group.

[2]Results are reported at p < 0.001, uncorrected for the whole-brain analysis.

RESULTS

Participant Characteristics and Psychological Assessments

Healthy controls and individuals with IED did not differ significantly in age (t = 0.05, p > 0.05, Cohen's d = 0.02) or Beck Anxiety Inventory score (Mann-Whitney U =153, p > 0.05, η^2 = 0.09). Individuals with IED scored higher on the Barratt Impulsiveness Scale II (t = 2.50, p < 0.05, Cohen's d = 0.91), Beck Depression Inventory (Mann-Whitney U =162.5, p < 0.05, η^2 = 0.14), Life History of Aggression (t = 5.34, p < 0.001, Cohen's d = 1. 95), state anger (t = 2.61, p < 0.05, Cohen's d = 0.95), trait anger (t = 4.48, p < 0.001, Cohen's d = 1.63), and Buss-Perry Aggression Questionnaire (t = 5.29, p < 0.001, Cohen's d = 1.93) than healthy controls (**Table 1**).

Anger Induction

All participants reported that they had been angry during the anger-inducing conditions and had not felt any emotion while viewing the neutral pictures. The result of the Mann-Whitney U test did not show group differences in the frequency of occurrence of angry feelings when viewing the five anger-inducing stimuli (Mann-Whitney U = 131, p > 0.05, η^2 = 0.28). However, Independent t-tests of the intensity of angry feelings indicated that compared to healthy controls, individuals with IED exhibited anger that was more intense in response to anger-inducing stimuli (t = 2.29, p < 0.05, Cohen's d = 0.71) (**Table 2**).

VBM Analysis

VBM analysis was conducted to detect structural differences between individuals with IED and healthy controls. As shown in **Table 3** and **Figure 2A**, individuals with IED had significantly reduced gray matter volume in the left amygdala, left orbitofrontal cortex, and left anterior insula when compared with healthy controls (p < 0.001, uncorrected). No areas were identified where healthy controls showed reduced gray matter volume relative to that of the IED group. A significant negative correlation was detected between the gray matter volume in the left insula and the severity of aggression (i.e., composite aggression scores) as shown in **Figure 2B** (p < 0.001, uncorrected). The results of *post hoc* analyses using multiple linear regression revealed that the gray matter volume in the left insula was negatively linked to the composite aggression score in IED group.

fMRI Analysis

In both groups, activation was observed in the bilateral middle/inferior frontal gyri (Brodmann area [BA] 9), cuneus/precuneus (BA 7, 18, 19), thalamus, cingulate gyri (BA 24, 32), anterior insula (BA 13), putamen, amygdala, and superior/middle temporal gyri in response to the anger-inducing vs. neutral condition (p < 0.05, FDR corrected). Between-group analyses revealed that compared to healthy controls, individuals with IED showed significantly more activation in the bilateral putamen, bilateral anterior insula (BA 13), right amygdala, and right anterior cingulate cortex (BA 24) during the anger-inducing vs. neutral condition. There was no brain region in which healthy controls exhibited greater activation than the IED group (**Table 4**, **Figure 3A**) (p < 0.05, FDR corrected). **Figure 3A** illustrates the percent signal changes in the selected ROIs based on the results of the between-group analyses in healthy controls and individuals with IED for each experimental condition (i.e., anger-inducing and neutral conditions).

Multiple linear regression analysis was conducted to identify brain regions positively associated with the severity of aggression after adjusting for depression, anxiety, and impulsivity effects. The results were significant for the left anterior insula (BA 13) (p < 0.001, uncorrected) during anger-inducing conditions (**Table 5**). Post-hoc analyses using multiple linear regression revealed that only the composite aggression score was significantly positively correlated with the extracted percent signal change from the left insula during the anger-inducing condition, and the factors explained the variability of the left insula activation by 42.38%, as shown in **Figure 3B** and **Figure S1**.

DISCUSSION

To the best of our knowledge, this is the first study to apply combined structural and functional MRI to identify altered brain regions in individuals with IED. We demonstrated that individuals with IED had significantly diminished gray matter volume in the anterior insula, amygdala, and orbitofrontal area, after statistically controlling for age and years of education, relative to controls. Gray matter volume in the left insula was negatively correlated with the severity of IED, as measured by the composite aggression score. We also examined altered brain function during anger processing among individuals with IED. fMRI revealed that patients with IED showed greater activation in the anterior insula, putamen, anterior cingulate cortex, and amygdala in response to anger-inducing films than did healthy

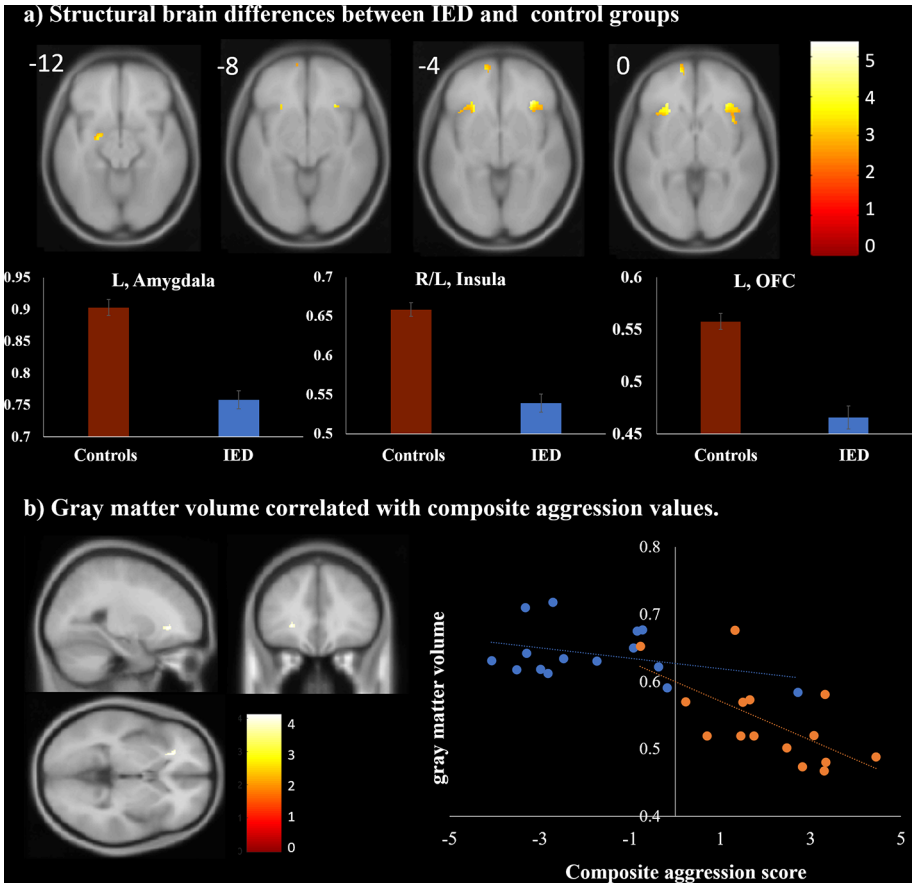

FIGURE 2 | Structural magnetic resonance imaging findings of individuals with intermittent explosive disorder (IED) and healthy controls. **(A)** Regions showing gray matter reduction in individuals with IED relative to controls [$p < 0.05$, false discovery rate (FDR) corrected]. **(B)** Brain region map and scatter plots of the correlation between the composite aggression score and the gray matter volume in the left insula ($p < 0.001$, uncorrected). Each orange and blue circle represents the data of an IED and control participant, respectively.

TABLE 4 | Functional magnetic resonance imaging (fMRI) results from analysis of covariance.

Brain region	MNI coordinates			t_{max}	Cluster size (voxels)
	x	y	z		
IED > HC					
Left putamen	–26	8	8	6.70	650
Right putamen	24	10	6	8.47	809
Left insula (BA 13)	–38	–2	8	5.83	248
Right insula (BA 13)	34	12	10	5.43	166
Right amygdala (BA 24)	22	–2	–22	4.11	99
Right ACC	2	34	12	4.83	139

ACC, anterior cingulate cortex; BA, Brodmann area; HC, healthy control; IED, intermittent explosive disorder; MNI, Montreal Neurological Institute.
The regions exhibited the greater activity in the IED group compared to healthy controls during the anger-inducing condition compared to the neutral condition. There was no brain region in which healthy controls exhibited greater activation than the IED group.
MNI coordinates of the maximum t-scores are shown for each cluster.
Results are reported at $p < 0.05$, false discovery rate-corrected for the whole-brain analysis.

controls. In addition, activation in the left insula during anger processing was associated with IED severity.

The regions we identified as exhibiting significantly greater activation in the IED group are known to be related to emotion processing functions such as emotional perception, experience, regulation, and reactions to anger (28, 29). The putamen, one of the structures comprising the basal ganglia, is linked to motor control, cognition, emotion, and somatosensory functions (30). According to previous neuroimaging studies on emotion, the putamen is associated with the recognition of emotional facial expressions (31–33). A growing body of evidence from animal studies (34, 35), lesion studies (36), and neuroimaging studies (37, 38) has suggested that the amygdala is associated with the subliminal perception of emotional stimuli, which includes the decoding of emotional reactions according to their significance. Several studies have implicated the anterior cingulate cortex in emotional regulation. According to a meta-analysis study, the anterior cingulate cortex is activated when detecting emotional

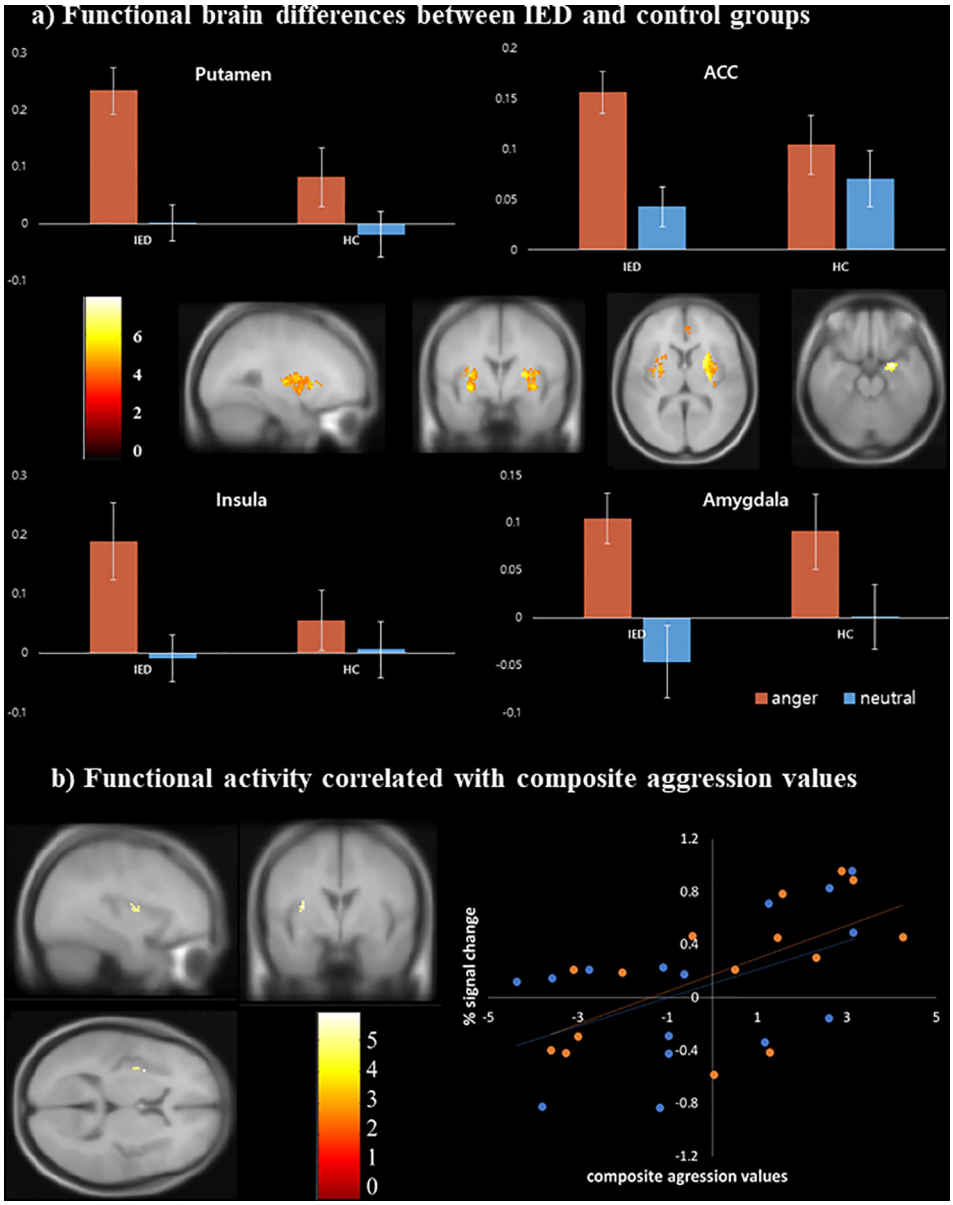

FIGURE 3 | Functional magnetic resonance imaging findings of individuals with intermittent explosive disorder (IED) and healthy controls. **(A)** Brain areas showing increased activity in response to anger stimuli among individuals with IED compared to healthy controls [$p < 0.05$, false discovery rate (FDR) corrected]. **(B)** Scatter plots of the correlation between the composite aggression score and functional activity in the left insula ($p < 0.001$, uncorrected). Each orange and blue circle represents the data of an IED and control participant, respectively.

TABLE 5 | Functional magnetic resonance imaging (fMRI) result of whole-brain multiple regression analysis. The composite aggression value was positively correlated with the left insula.

Brain region	MNI coordinates			t_{max}	Cluster size (voxels)
	x	y	z		
Left insula	–34	–2	4	4.88	35

MNI, Montreal Neurological Institute.
MNI coordinates of the maximum t-scores are shown for a cluster.
Results are reported at $p < 0.001$, uncorrected for the whole-brain analysis.

conflicts and emotion appraisal (39). Moreover, the extent of reappraisal-mediated changes in the anterior cingulate cortex predicts the extent of negative affect attenuation (40). Therefore, the greater activation of these regions in the IED group than controls in the present cohort may suggest that anger arousal was stronger in the IED group.

Previous fMRI studies on pathological aggression have suggested a cortico-limbic model that implicates hyperreactivity in brain areas related to emotional expression (e.g., amygdala and insula) and hyporeactivity in brain regions involved in emotional regulation

(e.g., orbitofrontal cortex and anterior cingulate cortex) (7, 41, 42). Our fMRI results partially support the cortico-limbic model of pathological aggression with respect to the hyperresponsivity of subcortical regions. We found hyperreactivity in brain regions involved in both, emotional expression, and regulation. The activation of certain brain areas in our fMRI study may be related to task-related behavioral aggression rather than pathological aggression. Since these types of aggression may be confounded, we cannot be certain whether the present fMRI results are restricted to the neural correlates of pathological aggression in IED. KrKr K et al. (2007) demonstrated that individuals who reported greater anger during the task showed greater provocation-related activity in brain regions that support emotional expression (insula) and increased activity in emotional regulation regions (i.e., inferior frontal gyrus, anterior cingulate cortex) (43). In the current study, the IED group reported experiencing anger that was more intense relative to that reported by controls in response to anger-inducing stimuli. Therefore, to identify the areas specifically linked to pathological aggression rather than task-related behavioral aggression among these activated brain regions, we also examined whether IED severity was correlated with activity in these clusters. The finding suggested that the insula was positively correlated with pathological aggression in IED. The results of our correlation analysis provide supportive evidence regarding the important role played by the insula in IED.

VBM analysis in our cohort revealed reduced gray matter volumes in the left insula, amygdala, and orbitofrontal area among individuals with IED compared with controls. Similar to the fMRI results, alterations in the insula were associated with the severity of IED, as measured by the composite aggression score. These VBM results correspond to the findings of a previous VBM study on IED (5). In agreement with our VBM results, the findings from recent studies have provided new information on the role of the insula in impulsive aggression (5, 44–46). Tiihonen et al. (2008) observed reductions of focal gray matter volumes in the right insula among violent offenders when compared to healthy individuals (44). A study on substance use disorders reported that individuals with substance use disorders who exhibit violent behavior display smaller gray matter volumes in the left insula than those who do not (45). Other studies in aggressive individuals reported reductions in gray matter volume in the anterior insula and amygdala (46).

In our combined study, the core overlap of neural substrates was located in the anterior insula, suggesting anterior insula involvement in IED. The insula has afferent and efferent connections with the orbitofrontal cortices, anterior cingulate, and amygdala (47). Craig (2009) suggested that the anterior insula is a crucial node in the human awareness network (i.e., awareness of bodily sensations, interoception, and awareness of affective feelings), the main role of which is the subjective regulation of psychological and physiological responses to cognitively challenging conditions (48). More recently, Dambacher et al. (2014) and Dambacher, et al. (2015) suggested strong and constant involvement of the anterior insula in motor impulsivity and reactive aggression (49, 50). They found an overlap of activity in the anterior insula between failed motor response inhibition and reactive aggression in healthy men using functional imaging. By providing an overarching role of the anterior insula across different modalities of self-control, they suggested that the insula functions in a comprehensive model of impulsivity as an integrator of cognitive, social, and emotional factors (49, 50). Based on our findings and the known roles of the insula, we speculate that alterations in the insula, such as a reduction in gray matter volume and increased activity during anger processing, may be associated with the observed anger regulation deficits in individuals with IED. In particular, we found left lateralization for IED in the insula. The correlation results showed that the left insula was structurally and functionally impaired. This finding agrees with that of a recent meta-analysis, which demonstrated hemispheric asymmetry in the functional activation of the insula during emotional processing (30). This study showed left-lateralized insula activation during emotional perception and experience. Another study on emotional intelligence reported that its score was significantly correlated with the activity of the left insula during social judgment of fearful faces. These studies suggest that the alterations of the left insula may lead to psychiatric disorders by affecting changes in social and emotional functioning (51). Thus, it is possible that the left lateralized alteration of the insula in the IED group may link with a lower ability to process oneonetion of the insula in the IED group may link with a lowesocially inappropriate behavior characteristics.

This study has several limitations. First, we conducted a cross-sectional study; therefore, we could not identify any causal relationship between IED and alterations in the insula. Our study design prevented the evaluation of association between alterations in the insula and the development of IED, and insular changes consequent to impulsive and frequent aggression. Longitudinal studies will be necessary to identify causal relationships between alterations in the insula and development of IED. Second, we used 7T MRI to acquire anatomical data with high spatial resolution and functional data with high signal to noise. However, 7T MRI has certain limitations related to susceptibility, signal dropout, and distortion. We used several methods to compensate for these limitations; however, that did not ensure full compensation. Third, a relatively small number of individuals participated in the study. The small sample size and low statistical power may have affected the reliability of the findings. For this study, the sample size was calculated by evaluating in the study. The small sample size and low statistical power may 1, as determined by a previous 7T fMRI study (26). With G Power of 3.1.9.2 (52), the sample size 14 participants in each group was calculated to be appropriate. To allow for a 10% dropout rate per group, we enrolled 30 patients in total. However, to increase external validity and provide insights into IED that are more generalizable, larger sample sizes should be used in future studies. A hypothesis-generating study is necessary to gain an

understanding of the population and determine the optimal sample size (53). Finally, to identify functional connections and interactions between the insula and other regions in the resting state, resting-state fMRI will be needed. Task-based fMRI studies may provide information on specific functional disturbances, while resting-state fMRI studies may elucidate different and potentially broader alterations, such as distributed circuit abnormalities in individuals with neuropsychiatric illnesses (54). Therefore, to validate the cortico-limbic model proposed by previous research on IED, resting-state functional connectivity analysis will be required.

Despite these limitations, the strength of our study lies in the combined use of fMRI and VBM to examine patients with IED, as such studies on brain changes in these patients using both approaches are scarce. By conducting this combined functional and structural brain imaging study, we were able to demonstrate that impulsive and frequent aggression are linked to changes in brain structure and function, thereby clarifying aspects of the underlying neurobiology of IED.

In summary, the present structural and functional study revealed gray matter deficits and altered functional activity in the insula among individuals with IED relative to healthy controls. In particular, the diminished structure and increased functional activity in the insula in response to anger stimuli were significantly associated with the severity of IED. These findings provide new insights into the underlying neural mechanisms of IED and suggest that alterations in the insula may act as neuroimaging markers of IED.

DATA AVAILABILITY STATEMENT

The data are not publicly available due to their containing information that could compromise the privacy of research participants. Requests to access these datasets should be directed to the corresponding author.

ETHICS STATEMENT

All participants provided their written informed consent to participate in this study after being thoroughly informed about the details of the experiment. The studies involving human participants were reviewed and approved by: The experimental procedures were approved by the Chungnam National University Institutional Review Board (approval number: 201803-SB-041-01; Daejeon, South Korea).

AUTHOR CONTRIBUTIONS

J-WS made substantial contributions to conception and design, acquisition of the data, and analysis and interpretation of the data. J-WS and CC were involved in drafting the manuscript and revising it critically for important intellectual content. J-WS and CC agree to be accountable for all aspects of the work in ensuring that questions related to the accuracy or integrity of any part of the work are appropriately investigated and resolved. All authors gave final approval of the version to be published.

ACKNOWLEDGMENTS

This work was supported by the Ministry of Education of the Republic of Korea and the National Research Foundation of Korea (NRF-2018S1A5A8029877 and NRF-2017R1A2B4012546) and Korea Basic Science Institute (C030222).

SUPPLEMENTARY MATERIAL

The Supplementary Material for this article can be found online at: https://www.frontiersin.org/articles/10.3389/fpsyt.2020.00439/full#supplementary-material

REFERENCES

1. Coccaro EF. Intermittent Explosive Disorder as a Disorder of Impulsive Aggression for DSM-5. *Am J Psychiatry* (2012) 169:577–88. doi: 10.1176/appi.ajp.2012.11081259
2. American Psychiatric Association. *Diagnostic and Statistical Manual of Mental Disorders. Fifth Edition*. Washington, DC (2013) doi: 10.1176/appi.books.9780890425596
3. Kessler RC, Coccaro EF, Fava M, Jaeger S, Jin R, Walters E. The Prevalence and Correlates of DSM-IV Intermittent Explosive Disorder in the National Comorbidity Survey Replication. *Arch Gen Psychiatry* (2006) 63:669. doi: 10.1001/archpsyc.63.6.669
4. Coccaro EF. Intermittent explosive disorder. In: Coccaro EF (eds) *Aggression, psychiatric treatment and assessment*. New York, NY: Marcel Dekker (2003).
5. Coccaro EF, Fitzgerald DA, Lee R, McCloskey M, Phan KL. Frontolimbic Morphometric Abnormalities in Intermittent Explosive Disorder and Aggression. *Biol Psychiatry Cognit Neurosci Neuroimaging* (2016) 1:32–8. doi: 10.1016/j.bpsc.2015.09.006
6. Coccaro EF, McCloskey MS, Fitzgerald DA, Phan KL. Amygdala and Orbitofrontal Reactivity to Social Threat in Individuals with Impulsive Aggression. *Biol Psychiatry* (2007) 62:168–78. doi: 10.1016/j.biopsych.2006.08.024
7. Coccaro EF, Sripada CS, Yanowitch RN, Phan KL. Corticolimbic Function in Impulsive Aggressive Behavior. *Biol Psychiatry* (2011) 69:1153–9. doi: 10.1016/j.biopsych.2011.02.032
8. Cremers H, Lee R, Keedy S, Phan KL, Coccaro E. Effects of Escitalopram Administration on Face Processing in Intermittent Explosive Disorder: An fMRI Study. *Neuropsychopharmacology* (2016) 41:590–7. doi: 10.1038/npp.2015.187
9. Lee R, Arfanakis K, Evia AM, Fanning J, Keedy S, Coccaro EF. White Matter Integrity Reductions in Intermittent Explosive Disorder. *Neuropsychopharmacology* (2016) 41:2697–703. doi: 10.1038/npp.2016.74
10. McCloskey MS, Phan KL, Angstadt M, Fettich KC, Keedy S, Coccaro EF. Amygdala hyperactivation to angry faces in intermittent explosive disorder. *J Psychiatr Res* (2016) 79:34–41. doi: 10.1016/j.jpsychires.2016.04.006
11. Moeller SJ, Froböse MI, Konova AB, Misyrlis M, Parvaz MA. Goldstein RZ et.al. Common and distinct neural correlates of inhibitory dysregulation: Stroop fMRI study of cocaine addiction and intermittent explosive disorder. *J Psychiatr Res* (2014) 58:55–62. doi: 10.1016/j.jpsychires.2014.07.016
12. Mechelli A, Price C, Friston K, Ashburner J. Voxel-Based Morphometry of the Human Brain: Methods and Applications. *Curr Med Imaging Rev* (2005) 1:105–13. doi: 10.2174/1573405054038726
13. Ashburner J, Friston KJ. Why Voxel-Based Morphometry Should Be Used. *NeuroImage* (2001) 14:1238–43. doi: 10.1006/nimg.2001.0961

14. Bookstein FL. "Voxel-Based Morphometry" Should Not Be Used with Imperfectly Registered Images. *NeuroImage* (2001) 14:1454–62. doi: 10.1006/nimg.2001.0770
15. Ashburner J. A fast diffeomorphic image registration algorithm. *NeuroImage* (2007) 38:95–113. doi: 10.1016/j.neuroimage.2007.07.007
16. Li W, He H, Lu J, Lv B, Li M, Jin Z. Evaluation of Multiple Voxel-Based Morphometry Approaches and Applications in the Analysis of White Matter Changes in Temporal Lobe Epilepsy. In: Liao H, Linte CA, Masamune K, Peters TM, Zheng G, editors. *Augmented Reality Environments for Medical Imaging and Computer-Assisted Interventions Lecture Notes in Computer Science*. Berlin, Heidelberg: Springer Berlin Heidelberg (2010). p. 268–76. doi: 10.1007/978-3-642-40843-4_29
17. Yassa M, Stark C. A quantitative evaluation of cross-participant registration techniques for MRI studies of the medial temporal lobe☆. *NeuroImage* (2009) 44:319–27. doi: 10.1016/j.neuroimage.2008.09.016
18. World Medical Association Declaration of Helsinki: Recommendations Guiding Physicians in Biomedical Research Involving Human Subjects. *JAMA* (1997) 277:925. doi: 10.1001/jama.1997.03540350075038
19. Coccaro EF, Berman ME, Kavoussi RJ. Assessment of life history of aggression: development and psychometric characteristics. *Psychiatry Res* (1997) 73:147–57. doi: 10.1016/S0165-1781(97)00119-4
20. Buss AH, Perry M. The Aggression Questionnaire. *J Pers Soc Psychol* (1992) 63:452–9. doi: 10.1037/0022-3514.63.3.452
21. Spielberger CD. *STAXI-2 : State-Trait Anger Expression Inventory-2: professional manual*. Odessa, FL (P.O. Box 998, Odessa 33556): Psychological Assessment Resources (1999).
22. Coccaro EF, Lee R, Coussons-Read M. Elevated Plasma Inflammatory Markers in Individuals With Intermittent Explosive Disorder and Correlation With Aggression in Humans. *JAMA Psychiatry* (2014) 71:158. doi: 10.1001/jamapsychiatry.2013.3297
23. Beck AT, Steer RA, Brown GK. *Beck depression inventory-II* Vol. 78. San Antonio, TX: Psychological Corporation (1996). p. 490–8.
24. Beck AT, Steer RA. Beck Anxiety Inventory manual. San Antonio, TX: Psychological Corporation (1993).
25. Patton JH, Stanford MS, Barratt ES. Factor structure of the Barratt impulsiveness scale. *J Clin Psychol* (1995) 51:768–74. doi: 10.1002/1097-4679(199511)51:6<768::AID-JCLP2270510607>3.0.CO;2-1
26. Seok J-W, Cheong C. Dynamic Causal Modeling of Effective Connectivity During Anger Experience in Healthy Young Men: 7T Magnetic Resonance Imaging Study. *Adv Cognit Psychol* (2019) 15:52–62. doi: 10.5709/acp-0256-7
27. Teeuwisse WM, Brink WM, Haines KN, Webb AG. Simulations of high permittivity materials for 7 T neuroimaging and evaluation of a new barium titanate-based dielectric. *Magn Reson Med* (2012) 67:912–8. doi: 10.1002/mrm.24176
28. Adolphs R. Neural systems for recognizing emotion. *Curr Opin Neurobiol* (2002) 12:169–77. doi: 10.1016/S0959-4388(02)00301-X
29. Phillips ML, Drevets WC, Rauch SL, Lane R. Neurobiology of emotion perception II: implications for major psychiatric disorders. *Biol Psychiatry* (2003) 54:515–28. doi: 10.1016/S0006-3223(03)00171-9
30. Arsalidou M, Duerden EG, Taylor MJ. The centre of the brain: Topographical model of motor, cognitive, affective, and somatosensory functions of the basal ganglia: Topographical Model of the Basal Ganglia. *Hum Brain Mapp* (2013) 34:3031–54. doi: 10.1002/hbm.22124
31. Calder AJ. Impaired recognition of anger following damage to the ventral striatum. *Brain* (2004) 127:1958–69. doi: 10.1093/brain/awh214
32. Calder AJ, Keane J, Manes F, Antoun N, Young AW. Impaired recognition and experience of disgust following brain injury. *Nat Neurosci* (2000) 3:1077–8. doi: 10.1038/80586
33. Phillips ML, Young AW, Scott SK, Calder AJ, Andrew C, Giampietro V, et al. Neural responses to facial and vocal expressions of fear and disgust. *Proc R Soc Lond B Biol Sci* (1998) 265:1809–17. doi: 10.1098/rspb.1998.0506
34. Maeda H, Morimoto H, Yanagimoto K. Response characteristics of amygdaloid neurons provoked by emotionally significant environmental stimuli in cats, with special reference to response durations. *Can J Physiol Pharmacol* (1993) 71:374–8. doi: 10.1139/y93-057
35. Ono T, Nishijo H. Neurophysiological basis of the Klüver-Bucy syndrome: Responses of monkey amygdaloid neurons to biologically significant objects. In: Aggleton JP, editor. *The amygdala: Neurobiological aspects of emotion, memory, and mental dysfunction*. New York, NY, US: Wiley-Liss (1992). p. 167–90.
36. Aggleton JP, Young AW. The enigma of the amygdala: On its contribution to human emotion. In: Lane RD, Nadel L, editors. *Cognitive neuroscience of emotion. Series in affective science*. New York, NY, US: Oxford University Press. (2000) p. 106–28.
37. Morris JS, Öhman A, Dolan RJ. Conscious and unconscious emotional learning in the human amygdala. *Nature* (1998) 393:467–70. doi: 10.1038/30976
38. Whalen PJ, Rauch SL, Etcoff NL, McInerney SC, Lee MB, Jenike MA. Masked Presentations of Emotional Facial Expressions Modulate Amygdala Activity without Explicit Knowledge. *J Neurosci* (1998) 18:411–8. doi: 10.1523/JNEUROSCI.18-01-00411.1998
39. Etkin A, Egner T, Kalisch R. Emotional processing in anterior cingulate and medial prefrontal cortex. *Trends Cognit Sci* (2011) 15:85–93. doi: 10.1016/j.tics.2010.11.004
40. Ochsner KN, Bunge SA, Gross JJ, Gabrieli JDE. Rethinking Feelings: An fMRI Study of the Cognitive Regulation of Emotion. *J Cognit Neurosci* (2002) 14:1215–29. doi: 10.1162/089892902760807212
41. Bufkin JL, Luttrell VR. Neuroimaging Studies of Aggressive and Violent Behavior: Current Findings and Implications for Criminology and Criminal Justice. *Trauma Violence Abuse* (2005) 6:176–91. doi: 10.1177/1524838005275089
42. Fanning JR, Keedy S, Berman ME, Lee R, Coccaro EF. Neural Correlates of Aggressive Behavior in Real Time: a Review of fMRI Studies of Laboratory Reactive Aggression. *Curr Behav Neurosci Rep* (2017) 4:138–50. doi: 10.1007/s40473-017-0115-8
43. Krämer UM, Jansma H, Tempelmann C, Münte TF. Tit-for-tat: The neural basis of reactive aggression. *NeuroImage* (2007) 38:203–11. doi: 10.1016/j.neuroimage.2007.07.029
44. Tiihonen J, Rossi R, Laakso MP, Hodgins S, Testa C, Perez J, et al. Brain anatomy of persistent violent offenders: More rather than less. *Psychiatry Res Neuroimaging* (2008) 163:201–12. doi: 10.1016/j.pscychresns.2007.08.012
45. Schiffer B. Disentangling Structural Brain Alterations Associated With Violent Behavior From Those Associated With Substance Use Disorders. *Arch Gen Psychiatry* (2011) 68:1039. doi: 10.1001/archgenpsychiatry.2011.61
46. Sterzer P, Stadler C, Poustka F, Kleinschmidt A. A structural neural deficit in adolescents with conduct disorder and its association with lack of empathy. *NeuroImage* (2007) 37:335–42. doi: 10.1016/j.neuroimage.2007.04.043
47. Augustine J. Circuitry and functional aspects of the insular lobe in primates including humans. *Brain Res Rev* (1996) 22:229–44. doi: 10.1016/S0165-0173(96)00011-2
48. Craig AD. (Bud). Emotional moments across time: a possible neural basis for time perception in the anterior insula. *Philos Trans R Soc B Biol Sci* (2009) 364:1933–42. doi: 10.1098/rstb.2009.0008
49. Dambacher F, Sack AT, Lobbestael J, Arntz A, Brugman S, Schuhmann T. Out of control: Evidence for anterior insula involvement in motor impulsivity and reactive aggression. *Soc Cognit Affect Neurosci* (2014) 10:508–16. doi: 10.1093/scan/nsu077
50. Dambacher F, Schuhmann T, Lobbestael J, Arntz A, Brugman S, Sack AT. No Effects of Bilateral tDCS over Inferior Frontal Gyrus on Response Inhibition and Aggression. *PloS One* (2015) 10:e0132170. doi: 10.1371/journal.pone.0132170
51. Quarto T, Blasi G, Maddalena C, Viscanti G, Lanciano T, Soleti E, et al. Association between ability emotional intelligence and left insula during social judgment of facial emotions. *PloS One* (2016) 11(2):e0148621. doi: 10.1371/journal.pone.0148621
52. Faul F, Erdfelder E, Lang A-G, Buchner A. G*Power 3: A flexible statistical power analysis program for the social, behavioral, and biomedical sciences. *Behav Res Methods* (2007) 39:175–91. doi: 10.3758/BF03193146
53. Kraemer H. A Comment on "Beyond P-value: the Rigor and Power of Study". *Glob Clin Transl Res* (2020) 2(1):7–9. doi: 10.36316/gcatr.02.0022
54. Ko C-H, Hsieh T-J, Wang P-W, Lin W-C, Yen C-F, Chen C-S, et al. Altered gray matter density and disrupted functional connectivity of the amygdala in

adults with Internet gaming disorder. *Prog Neuropsychopharmacol Biol Psychiatry* (2015) 57:185–92. doi: 10.1016/j.pnpbp.2014.11.003

Conflict of Interest: The authors declare that the research was conducted in the absence of any commercial or financial relationships that could be construed as a potential conflict of interest.

frontiers in Psychiatry

ORIGINAL RESEARCH
published: 14 July 2020
doi: 10.3389/fpsyt.2020.00643

Decreased Relative Cerebral Blood Flow in Unmedicated Heroin-Dependent Individuals

*Wenhan Yang[1], Ru Yang[1], Fei Tang[1], Jing Luo[1], Jun Zhang[2], Changlong Chen[3,4], Chunmei Duan[5], Yuan Deng[5], Lidan Fan[1] and Jun Liu[1]**

[1] Department of Radiology, Second Xiangya Hospital of Central South University, Changsha, China, [2] Hunan Judicial Police Vocational College, Changsha, China, [3] School of Computer Science and Engineering, Central South University, Changsha, China, [4] Hunan Province Engineering Technology Research Center of Computer Vision and Intelligent Medical Treatment, Changsha, China, [5] Yunnan Institute for Drug Abuse, Kunming, China

Understanding the brain mechanisms of heroin dependence is invaluable for developing effective treatment. Measurement of regional cerebral blood flow (CBF) provides a method to visualize brain circuits that are functionally impaired by heroin dependence. This study examined regional CBF alterations and their clinical associations in unmedicated heroin-dependent individuals (HDIs) using a relatively large sample. Sixty-eight (42 males, 26 females; age: 40.9 ± 7.3 years) HDIs and forty-seven (34 males, 13 females; age: 39.3 ± 9.2 years) matched healthy controls (HCs) underwent high-resolution T1 and whole-brain arterial spin labeling (ASL) perfusion magnetic resonance imaging (MRI) scans. Additionally, clinical characteristics were collected for neurocognitive assessments. HDIs showed worse neuropsychological performance than HCs and had decreased relative CBF (rCBF) in the bilateral middle frontal gyrus (MFG), inferior temporal gyrus, precuneus, posterior cerebellar lobe, cerebellar vermis, and the midbrain adjacent to the ventral tegmental area; right posterior cingulate gyrus, thalamus, and calcarine. rCBF in the bilateral MFG was negatively correlated with Trail Making Test time in HDIs. HDIs had limbic, frontal, and parietal hypoperfusion areas. Low CBF in the MFG indicated cognitive impairment in HDIs. Together, these findings suggest the MFG as a critical region in HDIs and suggest ASL-derived CBF as a potential marker for use in heroin addiction studies.

Keywords: heroin addiction, magnetic resonance perfusion imaging, arterial spin labeling, neurocognitive, reward circuits

OPEN ACCESS

Edited by:
Maorong Hu,
Nanchang University, China

Reviewed by:
Niklaus Denier,
University of Bern, Switzerland
Kai Yuan,
Xidian University, China

****Correspondence:***
Jun Liu
junliu123@csu.edu.cn

Specialty section:
This article was submitted to Neuroimaging and Stimulation, a section of the journal Frontiers in Psychiatry

Received: *20 December 2019*
Accepted: *19 June 2020*
Published: *14 July 2020*

Citation:
Yang W, Yang R, Tang F, Luo J, Zhang J, Chen C, Duan C, Deng Y, Fan L and Liu J (2020) Decreased Relative Cerebral Blood Flow in Unmedicated Heroin-Dependent Individuals. Front. Psychiatry 11:643. doi: 10.3389/fpsyt.2020.00643

INTRODUCTION

Heroin addiction has been a large societal and health problem worldwide for many decades. Long-term use of heroin induces progressive spongiform leukodystrophy, or heroin encephalopathy, resulting in a range of mental symptoms and somatic activity disorders. It is also a major causal factor for the accelerated spread of AIDS, hepatitis C and other major infectious diseases due to the sharing of syringes among patients with addiction (1). While tremendous research advances in heroin addiction have been achieved over the past decades,

heroin addiction treatment still has a high relapse rate. A total of 55.8–80% (2, 3) of patients relapsed to heroin use after being abstinent from drug use for 1–3 years at a 12-month follow-up. A major reason for the lack of an effective method for preventing relapse is the lack of a clear picture of heroin addiction-related brain mechanisms (4).

Neuroimaging has been a major tool used to examine brain alterations in heroin addiction/dependence. Brain function involves regional metabolism, which is tightly coupled with cerebral blood flow (CBF) (5). Therefore, measuring regional CBF can enable direct visualization of regional functional brain alterations (6) in heroin-dependent individuals (HDIs). A few studies (7–9) reported decreased CBF in the frontal and parietal lobes in HDIs. While these hypoperfusion patterns are consistent with the frontal and parietal functional impairments often observed in HDIs, relevant findings show large discrepancies across studies, which might be related to the sample sizes included. Some of the hypoperfusion patterns lacked explicit clinical associations. Another major issue is that early studies were based on [18F]-fluoro-deoxy-D-glucose (18F-FDG) positron emission tomography-computed tomography (PET-CT) or single-photon emission computed tomography (SPECT), which require injection of radioactive tracers and are not acceptable to all subjects.

Arterial spin labeling (ASL) perfusion magnetic resonance imaging (MRI) (10, 11) is an MR-based, entirely non-invasive technique for quantifying CBF. ASL uses magnetically labeled arterial blood as an endogenous tracer (12). The perfusion signal is extracted from MR images with labeled arterial blood compared to those without labeling (13). CBF was calculated using the one-compartment model (14) implemented in ASLtbx (15):

$$f = \frac{\Delta M}{2\alpha \cdot M_{0b} \cdot TI_1 \cdot e^{-TI_2/T_{1b}}} \quad (1)$$

where f is the CBF in ml/100 g-min, α is the labeling efficiency (0.9), and TI1 and TI2 are the time of saturation and the time of imaging after applying the spin labeling pulse, respectively. Their values were given above. T1b is the T1 of blood (1.67 s) (16). M0b is the equilibrium magnetization of blood. Because we did not acquire separate M0 images, M0b was approximated by the control image intensity in this study.

CBF measured with ASL MRI has been shown to closely resemble that measured by PET or dynamic susceptibility contrast (DSC) and has high test-retest stability (17, 18). Over time, ASL MRI has been increasingly used in neuropsychiatric studies (19, 20) including drug addiction (9). However, the technique has rarely been used to study heroin addiction.

The purpose of this work was to examine baseline CBF alterations in heroin addiction using ASL perfusion MRI as well as associations of ASL-derived CBF with functional impairments observed in HDIs. Because functional deficits in the prefrontal cortex and the limbic dopamine systems are common in heroin addiction, we hypothesized that HDIs have reduced CBF in those regions, which would be correlated with the behavioral measures of their functional impairments.

MATERIALS AND METHODS

Participant Characteristics

All human studies were approved by the local Institutional Review Board (IRB) of the Second Xiang-Ya Hospital of Central South University. All subjects provided signed written consent forms before participating in any experiments. A total of 72 unmedicated HDIs and 52 demographically matched healthy controls (HCs) were recruited. HDIs were recruited from drug rehabilitation centers in Changsha, Zhuzhou, and Yue Yang (three different cities in Hunan Province), following a positive urine test for heroin, the HDIs underwent compulsory abstinence for no more than 6 months. The HDIs were not taking medications before or during the current study. In total, four HDIs and five HCs were excluded due to poor MR image quality caused by severe head motion and image artifacts. All participants were right-handed Han people. Most participants were smokers, and some also reported alcohol use. The inclusion criteria for the heroin group were as follows: (1) a positive urine test for heroin; (2) a diagnosis of dependence based on criteria outlined in the fourth edition of the Diagnostic and Statistical Manual of Mental Disorders (DSM-IV); (3) a negative urine test for methamphetamine and ketamine; (4) no history of structural brain disease, epilepsy, or head trauma; (5) no contraindications to MRI; and (6) no history of mental or psychiatric illness.

Demographically matched control subjects were recruited through WeChat, flyers, etc., and subjects had to meet the aforementioned inclusion criteria (4), (5), and (6) and have a negative urine test for heroin, methamphetamine, and ketamine. **Table 1** provides the demographic data of the enrolled HDIs and HCs.

TABLE 1 | Participant characteristics.

	HDIs (n = 68) (mean ± SD)	HCs (n = 47) (mean ± SD)	t/χ^2/Z value	*p*
Age (years)	40.9 ± 7.3	39.3 ± 9.2	t = 1.064	0.290
Gender				
Male	42	34		
Female	26	13	χ^2 = 1.387	.239
Education				
Primary school	3	2	Z = –0.857	.391
Junior high school	50	31		
Senior high school	15	14		
Age of first use (years)	27.69 ± 9.36	–	–	–
Duration of drug use (years)	14.19 ± 7.08	–	–	–
Nicotine use				
Y	62	37		
N	6	10	χ^2 = 3.598	0.100
Alcohol use				
Y	27	22		
N	41	25	χ^2 = 0.573	0.450
Handedness	68R	47R	–	–

HDIs, heroin-dependent individuals; HCs, healthy controls.

Acquisition/Analysis of ASL Data

MRI data acquisitions were conducted in a 3T MRI scanner (MAGNETOM Skyra, Siemens) equipped with a 32-channel receiver coil. Foam padding and a forehead restraining strap were utilized to limit head movement during the scanning procedure. To obtain high-quality ASL data, participants were instructed to remain still with their eyes open during the MRI scan. All participants were allowed a moment to relax and move their hands/feet prior to scanning to ensure the quality of MR images.

T1-weighted high-resolution MRI was acquired using a three-dimensional fast gradient echo sequence with the following parameters: repetition time (TR) = 1450 ms, echo time (TE) = 2.0 ms, inversion time (TI) = 900 ms, field-of-view (FOV) = 256 × 256 mm, slice thickness = 1 mm, and flip angle = 12°. A 5-min 3D ASL scan was performed using a pulsed-ASL sequence from a Siemens device with the following parameters: TR/TE/TI1/TI2 = 2290/16/700/1990 ms, and voxel size = 4 × 4 × 5 mm^3. Background suppression was applied.

ASL images were preprocessed by ASLtbx (15) using the following steps: motion correction (MoCo) (20, 21), temporal denoising, spatial smoothing, CBF quantification, outlier cleaning, partial volume correction (PVC), spatial registration to the Montreal Neurology Institute (MNI) standard brain space, and CBF extraction for regions of interest (ROIs). Temporal filtering used a high-pass Butterworth filter (cutoff frequency = 0.01 Hz) and temporal nuisance cleaning. Temporal nuisance variables, including the time courses of head motion (three translations and three rotations), the global signal, and the mean CSF signal, were regressed out from the ASL image series at each voxel. The CSF mask was defined during the T1-weighted structural image segmentation. Spatial smoothing was performed with an isotropic Gaussian kernel with a full-width-at-half-maximum (FWHM) of 4 mm. The preprocessed ASL label and control image pairs were then successively subtracted to obtain the perfusion map. The detailed model parameters can be found in previous publications (15, 16). The mean ASL image was registered to the high-resolution structural image. Structural images were segmented into gray matter (GM), white matter (WM), and cerebrospinal fluid (CSF) using the segmentation tool provided in Statistical Parametric Mapping (https://www.fil.ion.ucl.ac.uk/spm/software/spm12/), projected into the ASL image space based on the registration transform between the mean ASL control image and the structural image and subsequently used to extract the CBF signals for temporal denoising and PVC. The relative CBF (rCBF) map (22, 23) was calculated by dividing the perfusion maps by the global mean perfusion value from the GM and WM.

Voxel-wise CBF differences between the two groups were computed using two-sample t-tests, the result was showed in **Figure 1**, age, gender, education, smoking, and drinking as covariates. Differences in the rCBF from group comparisons were corrected for multiple comparisons to a significance level of $p < 0.05$ by false discovery rate (FDR) correction. The ROIs from whole-brain voxel-wise comparisons (**Figure 1**) mainly include nine cerebral regions according to the automated anatomical labeling (AAL) template: the bilateral middle frontal gyrus (MFG), inferior temporal gyrus (ITG), and precuneus (PCUN); the right posterior cingulate gyrus (PCG), calcarine area (CAL), and thalamus. Then, nine sub-ROIs were

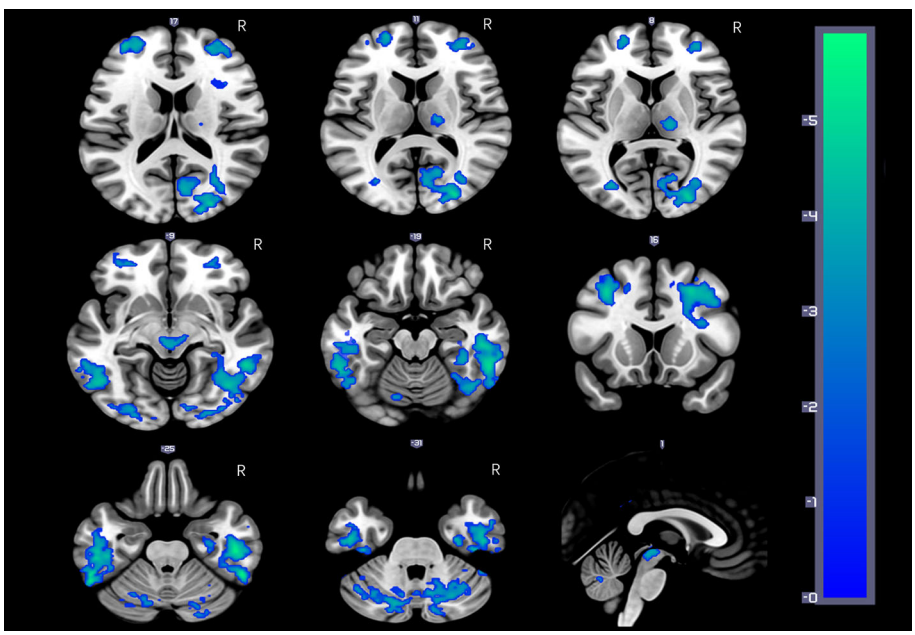

FIGURE 1 | HDIs show significantly reduced rCBF in the bilateral inferior temporal gyrus (ITG), middle frontal gyrus (MFG), cerebellar vermis, and posterior cerebellar lobe, precuneus; the right posterior cingulate gyrus (PCG) and thalamus; and the midbrain adjacent to the ventral tegmental area (VTA) (FDR correction, q = 0.05, p = 0.00158, t = 3.012).

generated from the intersection of voxel-wise ROIs and each regional AAL template, and each sub-ROI of rCBF values was calculated for the two groups. The rCBF values extracted by each sub-ROI between the two groups were compared using two-sample t-tests (**Table 3**) and evaluated for possible associations with neuropsychological characteristics.

Clinical Characteristics and Neurocognitive Measures

The duration of heroin use, the dose consumed, and other clinical characteristics was also collected from the HDIs. Cognitive function tests, including the Wechsler Adult Intelligence Scale Third Edition (WAIS-3) Digit Symbol Test (including the first and second minutes), forward and backward digit memory span tasks, and Trail Making Test (TMT) were completed by all patients following MRI examination. The Digit Symbol Test score is a part of the WAIS and an indicator of the executive function of the frontal lobe based on visual, spatial and motor processing speed. Participants were asked to write as many numbers as possible that were paired with symbols within 2 min (24–26). The forward and backward digit memory span tasks have been widely used for simple clinical measurements of working memory. The digit span task required the subjects to remember the numbers on an answer sheet in both forward and backward order. This test involves working memory, which can reflect particular aspects of the cognitive function of the brain (27–29). The TMT (30) required the subjects to connect scattered numbers in the correct sequence on a sheet of paper quickly and accurately. They could not skip numbers. The TMT was used to evaluate psychomotor performance (31).

Statistical Analysis

Statistical analyses were performed using SPSS 18.0. The HDI and HC groups were compared using a two-sample t-test for age, the chi-square test for smoking and drinking and rank sum tests for education levels, and the significance level was set to $p < 0.05$. The data distributions were tested for normality using the Kolmogorov-Smirnov test. Normally distributed data were analyzed using independent-samples t-tests, while non-normally distributed data were analyzed using rank sum tests.

Voxel-wise CBF differences between the two groups were computed using two-sample t-tests. Differences in rCBF from group comparisons were corrected for multiple comparisons to a significance level of $p < 0.05$ by FDR correction [$q = 0.05$, $p = 0.00158$, $t(113) = -3.012$] and a cluster size threshold of 100. Correlations between rCBF levels and clinical characteristics were evaluated using Pearson's correlation coefficients. The level of statistical significance was set at $p < 0.05$.

RESULTS

ASL Results

Figure 1 and **Table 2** show the whole-brain cross-sectional rCBF comparison results. The statistical threshold of $p = 0.00158$ was corrected for multiple comparisons with False FDR correction.

TABLE 2 | Brain areas with significantly lower rCBF in HDIs.

Brain areas (AAL)	R/L	MNI coordinates			Voxels	Peak intensity
		x	y	z		
Middle frontal gyrus /medial frontal gyrus/OMFC	R	26	12	46	2450	−5.1791
Middle frontal gyrus /medial frontal gyrus/OMFC	L	−34	18	46	644	−5.5855
Inferior temporal gyrus	R	50	−22	−24	2081	−5.7475
Inferior temporal gyrus /fusiform gyrus	L	−56	−52	−24	1047	−5.5997
Posterior cingulate cortex/calcarine	R	16	−66	12	161	−3.9249
Cerebellar posterior lobe /cerebellar declive	L	−16	−76	−28	262	−4.2837
Thalamus	R	6	−22	−4	260	−3.9918
Cerebellar posterior lobe /cerebellar declive	R	26	−68	−30	150	−3.7962
Precuneus	R	28	−62	−38	220	−4.3007
Precuneus	L	−10	−54	44	414	−4.4647
Midbrain (VTA)/right thalamus	B/R	0	−28	−8	118	−3.9221

The statistical threshold of $p = 0.00158$ was corrected for multiple comparisons with false discovery rate (FDR) correction, and the cluster size = 100; coordinates are located in Montreal Neurological Institute (MNI) space; OMFC, orbital medial frontal cortex; VTA, ventral tegmental area; B, bilateral; AAL, automated anatomical labeling template.

Compared to HCs, HDIs showed significant rCBF decreases in the bilateral cortical and subcortical ITG, MFG, cerebellar vermis, posterior cerebellar lobe, and PCUN; the right PCG and thalamus; and the midbrain adjacent to the ventral tegmental area (VTA) (**Figure 1**, **Table 2**). Many significant differences were shown in the rCBF values extracted from overlapping ROI masks, and 3 rCBF values were excluded due to negative values (1 in the bilateral PCUN and 1 in the right thalamus) (**Table 3**). No increased regional rCBF areas were detected in HDIs compared with the control group (FDR correction).

Neuropsychological Tests

Compared to HCs, HDIs showed significant differences in the WAIS-R Digit Symbol Test 2nd-minute scores [$t_{(73)} = -2.663$, $p = 0.011$], backward digit memory span [$t_{(70)} = -2.557$, $p = 0.013$],

TABLE 3 | rCBF of ROI mask.

Brain areas	Patients (mean ± SD)	Controls (mean ± SD)	*t*	*p*
MFG.L	1.28 ± 0.40	1.69 ± 0.27	t (113) = −6.66	.000
MFG.R	1.35 ± 0.41	1.72 ± 0.25	t (113) = −6.11	.000
ITG.L	1.15 ± 0.39	1.51 ± 0.32	t (113) = −5.37	.000
ITG.R	1.22 ± 0.36	1.58 ± 0.28	t (113) = −5.92	.000
PCUN.L	1.60 ± 0.44	1.96 ± 0.31	t (112) = −5.27	.000
PCUN.R	1.78 ± 0.48	2.15 ± 0.37	t (112) = −4.42	.000
THA.R	1.41 ± 0.47	1.68 ± 0.33	t (113) = −3.68	.000
PCG.R	1.09 ± 0.32	1.27 ± 0.31	t (112) = −3.05	.003
CAL.R	1.74 ± 0.64	2.18 ± 0.40	t (113) = −4.48	.000

MFG.L, left middle frontal gyrus (47 HCs + 68 HDIs); MFG.R, right middle frontal gyrus (47 HCs + 68 HDIs); ITG.L, left inferior temporal gyrus (47 HCs + 68 HDIs); ITG.R, right inferior temporal gyrus (47 HCs + 68 HDIs); PCUN.L, left precuneus (46 HCs + 68 HDIs); PCUN.R, right precuneus (46 HCs + 68 HDIs); THA.R, right thalamus (47 HCs + 68 HDIs); PCG.R, right posterior cingulate gyrus (46 HCs + 68 HDIs); CAL.R, right calcarine (47 HCs + 68 HDIs).

and TMT times [$t_{(76)} = 3.556$, p = 0.001]. No significant differences were observed between forward digit memory span [$t_{(70)} = -1.730$, p = 0.086] and Digit Symbol Test 1st-minute scores [$t_{(73)} = -1.689$, p = 0.095].

Correlations Between CBF and Neuropsychological Test Performance

Data from the neuropsychological tests completed by 36 patients and 42 HCs were used to assess the significance of correlations between test performance and rCBF. rCBF in the left MFG and right MFG was negatively correlated with the TMT times (left: r = −0.413, p < 0.001; right: r = −0.466, p < 0.001) (**Figures 2** and **3**). No significant correlation was observed between rCBF in the bilateral MFG/ITG and the other neuropsychological test results.

DISCUSSION

Using ASL perfusion MRI, we identified hypoperfusion in frontal, temporal, and parietal areas in HDIs, which was correlated with neuropsychological impairments in the patients.

Hypoperfusion in HDIs has been reported in several studies. Denier et al. (9) found hypoperfusion in frontal and temporal areas following acute administration of heroin to HDIs. Using SPECT, Gilberto et al. (7) demonstrated reduced CBF in the right frontal and left temporal lobes in opioid-dependent subjects with comorbid depression. Lukas et al. (8) investigated opioid-dependent subjects with SPECT and reported decreased CBF in the bilateral cortical prefrontal lobe, right thalamus and hippocampus in opioid-dependent patients. While our hypoperfusion findings in HDIs were partially consistent with those of previous studies, we used ASL MRI, which is non-invasive and does not require radioactive materials. Another merit of our study was the relatively large sample size.

Mesolimbic system dysfunction is a hallmark change in drug addiction (32, 33), including heroin addiction (34–36). By binding to the μ-opioid receptors on GABA neurons in the midbrain, heroin suppresses the inhibitory effects of GABA on dopamine neurons, which subsequently promotes the release of dopamine, leading to elevated reward effects (37). Reduced rCBF in mesolimbic areas in HDIs may be a result of that hallmark change and is consistent with various dysfunctions (such as increased impulsivity and altered reward processing) involving those regions as identified by previous neuroimaging and neurobiological studies (33).

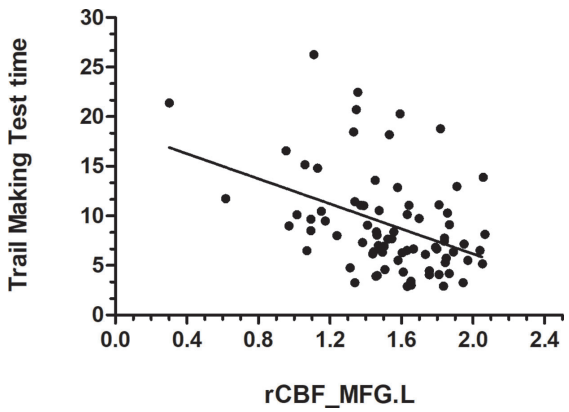

FIGURE 2 | rCBF value in MFG.L was negatively correlated with Trail Making Test completion time (s) (r = −0.413, p < 0.001; N=36 HDIs + 42 HCs); MFG. L, left middle frontal gyrus.

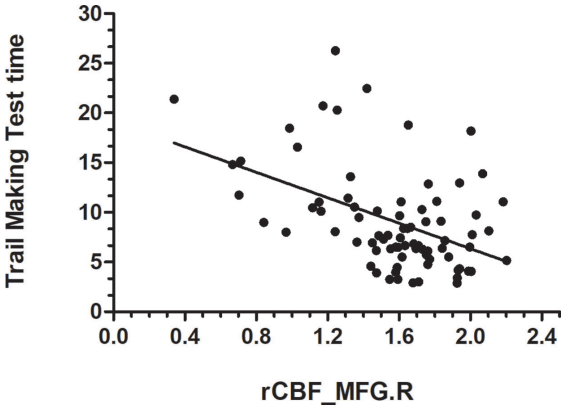

FIGURE 3 | rCBF value in MFG.R was negatively correlatedwith Trail Making Test Time completion time (r = −0.466, p < 0.001; N=36 HDIs + 42 HCs); MFG.R, right middle frontal gyrus.

Frontal brain alterations represent a second hallmark symptom of drug addiction, which is often characterized by a loss of executive function, especially inhibition (38). Our frontal hypoperfusion findings in HDIs align with that symptom, which also establishes ASL MRI as a useful tool for measuring such frontal brain dysfunction in drug addiction. The clinical relevance of the frontal hypoperfusion patterns was further demonstrated by the rCBF vs TMT correlations. The TMT reflects the capabilities of mental flexibility, working memory, and executive function (38, 39). The negative frontal rCBF vs TMT processing time in HDIs indicates that patients with lower rCBF in the frontal cortex have more-impaired executive functions.

We found significantly reduced rCBF in the precuneus and ITG in HDIs. The precuneus and ITG are part of the default mode network (DMN). Hypoperfusion in the ITG and precuneus might be a result of altered facilitation function of the DMN, which has been shown to be affected by many neuropsychiatric diseases (40, 41). Reduced rCBF in the precuneus is consistent with the reduced structural and functional connectivity of the precuneus in HDIs, as reported in (42–44), and may reflect functional alterations regarding memory consolidation and information processing, especially in relation to drug cues (45–47). The ITG plays an important role in the connection of visual, linguistic and multisensory processing (47, 48). However, the role of the ITG in heroin addiction remains unclear. Our finding of reduced ITG rCBF is consistent with the hypoperfusion in the bilateral temporal gyrus as measured with SPECT (single photon emission computed tomography) (49).

Decreased CBF was detected in the cerebellar vermis and cerebellar posterior lobe. Studies have shown that the vermis is involved in the regulation of both emotional and cognitive processes (49–52). Thus, further research is needed to clarify the relationship between alterations in CBF and cognitive function in HDIs.

Using ASL, we demonstrated that frontal cognitive impairment is a major element of dysfunction in abstinent HDIs. The limitation of this study is that it had a cross-sectional design. Further studies are required to confirm the relationship between alterations in brain CBF and impaired cognitive function after abstinence.

CONCLUSIONS

In summary, using a relatively large sample, we identified hypoperfusion patterns in mesolimbic, frontal, parietal, and temporal regions in HDIs. Hypoperfusion in frontal brain regions might be a primary marker for heroin addiction as supported by the cross-sectional differences and correlations with cognitive impairment identified.

DATA AVAILABILITY STATEMENT

All datasets generated for this study are included in the article/supplementary material.

ETHICS STATEMENT

The studies involving human participants were reviewed and approved by Institutional Review Board of the Second Xiang-Ya Hospital of Central South University. The patients/participants provided their written informed consent to participate in this study. Written informed consent was obtained from the individual(s) for the publication of any potentially identifiable images or data included in this article.

AUTHOR CONTRIBUTIONS

WY, JiL, JZ, and JuL conceptualized and designed the study. WY, JiL, FT, and LF conducted the behavioral and imaging analyses. RY, CC, CD, and YD conducted the assessments. JuL modified the manuscript and supervised the study. WY wrote the first draft and all authors provided input on the final version of the manuscript.

FUNDING

The National Key Research and Development Program of China (Grant number: 2016YFC0800908) and the National Natural Science Foundation of China (U1052225). National Natural Science Foundation of China, Grant Number: 61971451; Innovative Province special construction foundation of Hunan Province, China, Grant Number: 2019SK2131.

ACKNOWLEDGMENTS

This work was funded by the National Key Research and Development Program of China (Grant number: 2016 YFC0800908) and the National Natural Science Foundation of China (U1052225). The authors express their appreciation to their patients and volunteers for participating in this study.

REFERENCES

1. Benyamin R, Trescot AM, Datta S, Buenaventura R, Adlaka R, Sehgal N, et al. Opioid complications and side effects. *Pain Physcian* (2008) 11:S105–20.
2. Wang W. Illegal drug abuse and the community camp strategy in China. *J Drug Educ* (1999) 29:97–114. doi: 10.2190/J28R-FH8R-68A9-L288
3. Tang YL, Zhao D, Zhao C, Cubells JF. Opiate addiction in China: current situation and treatments. *Addiction* (2006) 101:657–65. doi: 10.1111/j.1360-0443.2006.01367.x
4. Wang Z, Suh J, Duan D, Darnley S, Jing Y, Zhang J, et al. A hypo-status in drug-dependent brain revealed by multi-modal MRI. *Addict Biol* (2017) 22:1622–31. doi: 10.1111/adb.12459
5. Detre JA, Wang J, Wang Z, Rao H. Arterial spin-labeled perfusion MRI in basic and clinical neuroscience. *Curr Opin Neurol* (2009) 22:348–55. doi: 10.1097/WCO.0b013e32832d9505
6. Adinoff B, Gu H, Merrick C, McHugh M, Jeon-Slaughter H, Lu H, et al. Basal Hippocampal Activity and Its Functional Connectivity Predicts Cocaine Relapse. *Biol Psychiatry* (2015) 78:496–504. doi: 10.1016/j.biopsych.2014.12.027
7. Gerra G, Calbiani B, Zaimovic A, Sartori R, Ugolotti G, Ippolito L, et al. Regional cerebral blood flow and comorbid diagnosis in abstinent opioid addicts. *Psychiatry Res* (1998) 83:117–26. doi: 10.1016/S0925-4927(98)00030-4
8. Pezawas L, Fischer G, Podreka I, Schindler S, Brücke T, Jagsch R, et al. Opioid addiction changes cerebral blood flow symmetry. *Neuropsychobiology* (2002) 45:67–73. doi: 10.1159/000048679
9. Denier N, Schmidt A, Gerber H, Schmid O, Riecher-Rössler A, Wiesbeck GA, et al. Association of frontal gray matter volume and cerebral perfusion in heroin addiction: a multimodal neuroimaging study. *Front Psychiatry* (2013) 4:135. doi: 10.3389/fpsyt.2013.00135
10. Alsop DC, Detre J, Golay X. Recommended implementation of arterial spin-labeled perfusion MRI for clinical applications: A consensus of the ISMRM perfusion study group and the European consortium for ASL in dementia. *Magn Reson Med* (2015) 73:102–16. doi: 10.1002/mrm.25607
11. Wang Z, Faith M, Patterson F, Tang K, Kerrin K, Wileyto EP, et al. Neural substrates of abstinence-induced cigarette cravings in chronic smokers. *J Neurosci* (2007) 27:14035–40. doi: 10.1523/JNEUROSCI.2966-07.2007
12. Franklin TR, Wang Z, Wang J, Sciortino N, Harper D, Li Y, et al. Limbic activation to cigarette smoking cues independent of nicotine withdrawal: a perfusion fMRI study. *Neuropsychopharmacol* (2007) 32:2301–9. doi: 10.1038/sj.npp.1301371
13. Chen Y, Wang DJ, Detre JA. Test-retest reliability of arterial spin labeling with common labeling strategies. *J mMagn Reson Imaging* (2011) 33:940–9. doi: 10.1002/jmri.22345
14. Buxton RB, Frank LR, Wong EC, Siewert B, Warach S, Edelman RR. A general kinetic model for quantitative perfusion imaging with arterial spin labeling. *Magn Reson Med* (1998) 40:383–96. doi: 10.1002/mrm.1910400308
15. Wang Z, Aguirre GK, Rao H, Wang J, Fernández-Seara MA, Childress AR, et al. Empirical optimization of ASL data analysis using an ASL data processing toolbox: ASLtbx. *Magn Reson Imaging* (2008) 26:261–9. doi: 10.1016/j.mri.2007.07.003

16. Cavusoglu M, Pfeuffer J, Ugurbil K, Uludag K. Comparison of pulsed arterial spin labeling encoding schemes and absolute perfusion quantification. *Magn Reson Imaging* (2009) 27:1039–45. doi: 10.1016/j.mri.2009.04.002
17. Qiao PG, Han C, Zuo ZW, Wang YT, Pfeuffer J, Duan L, et al. Clinical assessment of cerebral hemodynamics in Moyamoya disease via multiple inversion time arterial spin labeling and dynamic susceptibility contrast-magnetic resonance imaging: A comparative study. *J Neuroradiol* (2017) 44:273–80. doi: 10.1016/j.neurad.2016.12.006
18. Detre JA, Rao H, Wang DJ, Chen YF, Wang Z. Applications of arterial spin labeled MRI in the brain. *J Magn Reson Imaging* (2012) 35:1026–37. doi: 10.1002/jmri.23581
19. Delgado AF, De Luca F, Hanagandi P, van Westen D, Delgado AF. Arterial Spin-Labeling in Children with Brain Tumor: A Meta-Analysis. *AJNR Am J Neuroradiol* (2018) 39:1536–42. doi: 10.3174/ajnr.A5727
20. Schneider K, Michels L, Hartmann-Riemer MN, Burrer A, Tobler PN, Stampfli P, et al. Cerebral blood flow in striatal regions is associated with apathy in patients with schizophrenia. *J Psychiatry Neurosci* (2019) 44:102–10. doi: 10.1503/jpn.170150
21. Wang Z. Improving cerebral blood flow quantification for arterial spin labeled perfusion MRI by removing residual motion artifacts and global signal fluctuations. *Magn Reson Imaging* (2012) 30:1409–15. doi: 10.1016/j.mri.2012.05.004
22. Tsien C, Galban CJ, Chenevert TL, Johnson TD, Hamstra DA, Sundgren PC, et al. Parametric response map as an imaging biomarker to distinguish progression from pseudoprogression in high-grade glioma. *J Clin Oncol* (2010) 28:2293–9. doi: 10.1200/JCO.2009.25.3971
23. Galban CJ, Chenevert TL, Meyer CR, Tsien C, Lawrence TS, Hamstra DA, et al. The parametric response map is an imaging biomarker for early cancer treatment outcome. *Nat Med* (2009) 15:572–6. doi: 10.1038/nm.1919
24. Loprinzi PD. Epidemiological investigation of muscle-strengthening activities and cognitive function among older adults. *Chronic Illn* (2016) 12:157–62. doi: 10.1177/1742395316641998
25. Nakahachi T, Ishii R, Iwase M, Canuet L, Takahashi H, Kurimoto R, et al. Frontal activity during the digit symbol substitution test determined by multichannel near-infrared spectroscopy. *Neuropsychobiology* (2008) 57:151–8. doi: 10.1159/000147467
26. Frith E, Loprinzi PD. Physical Activity and Cognitive Function Among Older Adults with an Elevated Gamma Gap. *Med Princ Pract* (2018) 27:531–6. doi: 10.5455/JCBPR.284072
27. Jensen AR, Figueroa RA. Forward and backward digit span interaction with race and IQ: predictions from Jensen's theory. *J Educ Psychol* (1975) 67:882–93. doi: 10.1037/0022-0663.67.6.882
28. Hester RL, Kinsella GJ, Ong B. Effect of age on forward and backward span tasks. *J Int Neuropsychol Soc* (2004) 10:475–81. doi: 10.1017/S1355617704104037
29. Wechsler D. *Technical manual for the Wechsler Adult Intelligence and Memory Scale. 3rd ed.* New York: The Psychological Corporation. (1997).
30. Wilckens KA, Tudorascu DL, Snitz BE, Price JC, Aizenstein HJ, Lopez OL, et al. Sleep moderates the relationship between amyloid beta and memory recall. *Neurobiol Aging* (2018) 71:142–8. doi: 10.1016/j.neurobiolaging.2018.07.011
31. Yu Y, Zhao Y, Si Y, Ren Q, Ren W, Jing C, et al. Estimation of the cool executive function using frontal electroencephalogram signals in first-episode schizophrenia patients. *BioMed Eng Online* (2016) 15:131. doi: 10.1186/s12938-016-0282-y
32. Koob GFAV. Neurocircuitry of addiction. *Neuropsychopharmacology* (2013) 35:217–38. doi: 10.1016/B978-0-444-62619-6.00003-3
33. Schluter RS, Daams JG, van Holst RJ, Goudriaan AE. Effects of Non-invasive Neuromodulation on Executive and Other Cognitive Functions in Addictive Disorders: A Systematic Review. *Front Neurosci* (2018) 12:642. doi: 10.3389/fnins.2018.00642
34. Karila L, Marillier M, Chaumette B, Billieux J, Nicolas F, Amine B. New synthetic opioids: Part of a new addiction landscape. *Neurosci Biobehav Rev* (2018) 106:133–40. doi: 10.1016/j.neubiorev.2018.06.010
35. Valentino RJ, Volkow N. Untangling the complexity of opioid receptor function. *Neuropsychopharmacol* (2018) 43:2514–20. doi: 10.1038/s41386-018-0225-3
36. Jay GW, Barkin RL. Perspectives on the opioid crisis from pain medicine clinicians. *Dis Mon* (2018) 64:451–66. doi: 10.1016/j.disamonth.2018.07.002
37. Darcq E, Kieffer BL. Opioid receptors: drivers to addiction? *Nat Rev Neurosci* (2018) 19:499–514. doi: 10.1038/s41583-018-0028-x
38. Ryu K, Kim Y, Kwon M, Kim H, Kim J. The frontal executive function in exercise addicts, moderate exercisers, and exercise avoiders. *Am J Addict* (2016) 25:466–71. doi: 10.1111/ajad.12422
39. Varjacic A, Mantini D, Demeyere N, Gillebert CR. Neural signatures of Trail Making Test performance: Evidence from lesion-mapping and neuroimaging studies. *Neuropsychologia* (2018) 115:78–87. doi: 10.1016/j.neuropsychologia.2018.03.031
40. Hu ML, Zong XF, Mann JJ, Zheng JJ, Liao YH, Li ZC, et al. A Review of the Functional and Anatomical Default Mode Network in Schizophrenia. *Neurosci Bull* (2017) 33:73–84. doi: 10.1007/s12264-016-0090-1
41. Malhi GS, Das P, Outhred T, Bryant RA, Calhoun V, Mann JJ. Default mode dysfunction underpins suicidal activity in mood disorders. *Psychol Med* (2019) 50:1–10. doi: 10.1017/S0033291719001132
42. Yuan K, Qin W, Dong M, Liu J, Liu P, Zhang Y, et al. Combining spatial and temporal information to explore resting-state networks changes in abstinent heroin-dependent individuals. *Neurosci Lett* (2010) 475:20–4. doi: 10.1016/j.neulet.2010.03.033
43. Li Q, Li Z, Li W, Zhang Y, Wang Y, Zhu J, et al. Disrupted Default Mode Network and Basal Craving in Male Heroin-Dependent Individuals: A Resting-State fMRI Study. *J Clin Psychiatry* (2016) 77:e1211–7. doi: 10.4088/JCP.15m09965
44. Ma X, Qiu Y, Tian J, Wang J, Li S, Zhan W, et al. Aberrant default-mode functional and structural connectivity in heroin-dependent individuals. *PloS One* (2015) 10:e120861. doi: 10.1371/journal.pone.0120861
45. Rugg MD, Vilberg KL. Brain networks underlying episodic memory retrieval. *Curr Opin Neurobiol* (2013) 23:255–60. doi: 10.1016/j.conb.2012.11.005
46. Chen J, Honey CJ, Simony E, Arcaro MJ, Norman KA, Hasson U. Accessing Real-Life Episodic Information from Minutes versus Hours Earlier Modulates Hippocampal and High-Order Cortical Dynamics. *Cereb Cortex (New York N Y 1991)* (2016) 26:3428–41. doi: 10.1093/cercor/bhv155
47. Engelmann JM, Versace F, Robinson JD, Minnix JA, Lam CY, Cui Y, et al. Neural substrates of smoking cue reactivity: a meta-analysis of fMRI studies. *Neuroimage* (2012) 60:252–62. doi: 10.1016/j.neuroimage.2011.12.024
48. Onitsuka T, Shenton ME, Salisbury DF, Dickey CC, Kasai K, Toner SK, et al. Middle and inferior temporal gyrus gray matter volume abnormalities in chronic schizophrenia: an MRI study. *Am J Psychiatry* (2004) 161:1603–11. doi: 10.1176/appi.ajp.161.9.1603
49. Botelho MF, Relvas JS, Abrantes M, Cunha MJ, Marques TR, Rovira E, et al. Brain blood flow SPET imaging in heroin abusers. *Ann N Y Acad Sci* (2006) 1074:466–77. doi: 10.1196/annals.1369.047
50. Schmahmann JD. Disorders of the cerebellum: ataxia, dysmetria of thought, and the cerebellar cognitive affective syndrome. *J Neuropsychiatr Clin Neurosci* (2004) 16:367–78. doi: 10.1176/jnp.16.3.367
51. Schmahmann JD. The cerebellum and cognition. *Neurosci Lett* (2018) 30:1409–15. doi: 10.1016/j.neulet.2018.07.005
52. Yucel K, Nazarov A, Taylor VH, Macdonald K, Hall GB, Macqueen GM. Cerebellar vermis volume in major depressive disorder. *Brain Struct Funct* (2013) 218:851–8. doi: 10.1007/s00429-012-0433-2

Conflict of Interest: The authors declare that the research was conducted in the absence of any commercial or financial relationships that could be construed as a potential conflict of interest.

frontiers in Psychiatry

ORIGINAL RESEARCH
published: 31 July 2020
doi: 10.3389/fpsyt.2020.00732

Repetitive Transcranial Magnetic Stimulation Improves Amygdale Functional Connectivity in Major Depressive Disorder

Fu-jian Chen[1], Chuan-zheng Gu[2]*, Ning Zhai[3], Hui-feng Duan[4], Ai-ling Zhai[5] and Xiao Zhang[2]**

[1] Medical Imaging Department, Jining Psychiatric Hospital, Jining, China, [2] Psychiatric Department, Jining Psychiatric Hospital, Jining, China, [3] Medical Imaging Department, Affiliated Hospital of Jining Medical College, Jining, China, [4] Mental Diseases Prevention and Treatment Institute of Chinese PLA, No. 988 Hospital of Joint Logistic Support Force, Jiaozuo, China, [5] Mental Rehabilitation Department, Jining Psychiatric Hospital, Jining, China

Emotional abnormality in major depressive disorder (MDD) is generally regarded to be associated with functional dysregulation in the affective network (AN). The present study examined the changes in characteristics of AN connectivity of MDD patients before and after repetitive transcranial magnetic stimulation (rTMS) treatment over the left dorsolateral prefrontal cortex, and to further assess how these connectivity changes are linked to clinical characteristics of patients. Functional connectivity (FC) in the AN defined by placing seeds in the bilateral amygdale was calculated in 20 patients with MDD before and after rTMS, and in 20 healthy controls (CN). Furthermore, a linear regression model was used to obtain correlations between FC changes and Hamilton depression scale (HAMD) changes in MDD before and after rTMS. Before rTMS, compared with CN, MDD exhibited significantly lower FC between left insula (INS.L), right superior and inferior frontal gyrus (SFG.R and IFG.R), right inferior parietal lobule (IPL.R), and amygdala, and showed an increment of FC between the bilateral precuneus and amygdala in AN. After rTMS, MDD exhibited a significant increase in FC in the INS.L, IFG.R, SFG.R, IPL.R, and a significant reduction in FC in the precuneus. Interestingly, change in FC between INS.L and left amygdala was positively correlated with change in HAMD scores before and after rTMS treatment. rTMS can enhance affective network connectivity in MDD patients, which is linked to emotional improvement. This study further suggests that the insula may be a potential target region of clinical efficacy for MDD to design rationale strategies for therapeutic trials.

Keywords: major depressive disorder, affective network, repetitive transcranial magnetic stimulation, fMRI, amygdala

OPEN ACCESS

Edited by:
Ping Li,
Qiqihar Medical University, China

Reviewed by:
Jennifer Barredo,
Providence VA Medical Center, United States
Qiwen Mu,
North Sichuan Medical College, China
Katharine Dunlop,
University of Toronto, Canada
Ephrem Takele Zewdie,
University of Calgary, Canada

****Correspondence:***
Fu-jian Chen
chen3165659@163.com
Chuan-zheng Gu
guchuanzheng120@163.com
Xiao Zhang
woshixiao_81@163.com

Specialty section:
This article was submitted to Neuroimaging and Stimulation, a section of the journal Frontiers in Psychiatry

Received: *24 March 2020*
Accepted: *13 July 2020*
Published: *31 July 2020*

Citation:
Chen F-j, Gu C-z, Zhai N, Duan H-f, Zhai A-l and Zhang X (2020) Repetitive Transcranial Magnetic Stimulation Improves Amygdale Functional Connectivity in Major Depressive Disorder. Front. Psychiatry 11:732. doi: 10.3389/fpsyt.2020.00732

INTRODUCTION

Emotional abnormality is a crucial feature of major depressive disorder (MDD) and is also associated with functional dysregulation in the amygdala affective network (AN) (1–3). Furthermore, numerous studies have indicated that brain circuits and network dysfunction can cause depressive symptoms and disability (4, 5). Magnetic resonance imaging (MRI) has been considered to be a non-invasive imaging technology that can help establish relationships between brain circuit and human behavior (5). Therefore, it is essential to understand the relationship between depressive symptom and imaging feature for amelioration in the clinic in the course of MDD.

In resting-state functional connectivity (FC) MRI of MDD, the AN have attracted a great deal of interest. The AN is a frontolimbic circuit comprising brain areas in the amygdala, the subgenual anterior cingulate cortex, the hippocampus, the hypothalamus, orbitofrontal cortex (6, 7), the fusiform gyrus, and the medial frontal gyrus (3). The role of the AN is considered to be the processing emotions and mediating motivated behaviors (6, 7). Recently, numerous MRI studies have reported that MDD patients present dysfunctional AN, including lower FC between the bilateral precuneus and the left amygdala (3), lower FC between the orbitofrontal cortex and the amygdala that are negatively associated with depression scores (8), lower FC between amygdala and posterior insula that are negatively related to increasing severity of behavioral and emotional dysregulation (9), and reduced connectivity between the amygdala and the "positive network" (10). These studies suggest that some crucial brain areas are specifically related to processing and regulating emotions. Indeed, a recently published article has identified symptom-specific targets for MDD, and they thought that different depression symptom had different specific brain circuits (11). However, little is known about the consensus circuit, or the relationship between depressive symptom and AN circuits for amelioration in the clinic.

Transcranial magnetic stimulation (TMS) has been widely used in recent years. Previous studies have widely applied TMS to promote the improvement of cognition, enhancement of neural activity, restoration of network connectivity, and amelioration of negative symptom in neuropsychiatric disorders (4, 12–15), but the mechanism of TMS action is still mostly unclear. Furthermore, some studies have begun to investigate causal relationships between network markers and clinical phenomena in schizophrenia (4). Repetitive transcranial magnetic stimulation (rTMS) is considered as a non-invasive brain stimulation method to modulate cortical excitability (12). Furthermore, rTMS has been approved by the food and drug administration (FDA) to treat the symptoms of MDD. However, it is mostly unknown if AN network target pathology is causally linked to psychiatric symptoms and if the TMS manipulation of network target can reflect the symptom modification of patients with MDD.

The present study examined the changes in the patterns of AN connectivity of patients with MDD before and after rTMS treatment, and further assessed how these connectivity changes are linked to clinical characteristics of patients. We hypothesized that MDD patients would exhibit lower affective network connectivity (for example, lower FC between the amygdala and the insula). We also hypothesized that high-frequency excitatory rTMS could enhance the emotional network connectivity (for example, increase the FC the amygdala and the insula) in MDD patients. Furthermore, it was further hypothesized that changes in AN induced by rTMS are linked to modifications of depressive symptoms of MDD.

MATERIALS AND METHODS

Subjects

Forty MDD patients (who met DSM-5 criteria, right-handed) and 20 healthy controls (CN, right-handed) were recruited from inpatients at the Medical Imaging Department of Jining Psychiatric Hospital (**Table 1**). The inclusion and exclusion criteria of subjects can be seen in the published studies (3, 16, 17). The depressed group consisted of consecutively recruited subjects who met the Diagnostic and Statistical Manual of Mental Disorders, 5th Edition (DSM-5) criteria for major depression without psychotic features and had a score of 20 or higher on the 17-item Chinese Hamilton Depression Scale (HAMD) (18). The healthy controls (CN) were recruited through advertisement and were required to have no history or presence of any psychiatric disorder. The subjects signed written informed consent was taken from all subjects. This study was

TABLE 1 | Demographics and clinical measures of CN, bef-MDD and aft-MDD.

Items	CN	real rTMS MDD		sham rTMS MDD		*F* values (χ^2)	*p* values
		bef- MDD	aft-MDD	bef- MDD	aft-MDD		
	n = 20	n = 20	n = 20	n = 20	n = 20		
Age (years)	45.95 (8.02)	46.75 (5.52)	46.75 (5.52)	46.30 (4.76)	46.30 (4.76)	0.068	0.991
Sex (male/female)	8/12	9/11	9/11	12/8	12/8	1.735	0.420
Education (years)	11.10 (2.83)	10.40 (1.10)	10.40 (1.10)	10.45 (1.18)	10.45 (1.18)	0.600	0.663
HAMD scores	3.30 (1.53)	26.95 (2.04)[a]	5.75 (2.24)[b,c]	25.50 (2.01)	24.95 (2.24)[d]	666.333	0.000*
Duration of illness (months)	NA	25.00 (5.98)	25.00 (5.98)	24.50 (4.76)	24.50 (4.76)	NA	NA
Antidepressant comedication	NA	20(100%)	20 (100%)	20 (100%)	20 (100%)	NA	NA

*Data are presented as the mean (with standard deviation, SD). CN, controls; MDD, major depressive disorder; bef-MDD, MDD before treatment; aft-MDD, MDD after treatment; HAMD, Hamilton depression scale. *representing significant differences; [a]bef-MDD v.s. CN; [b]aft-MDD v.s. CN; [c]bef-MDD v.s. aft-MDD; [d]real rTMS MDD v.s. sham rTMS MDD.*

approved by the Human Participants Ethics Committee at the Medical Imaging Department of Jining Psychiatric Hospital. All patients were randomly assigned to the rTMS group (N = 20) and the sham group (N = 20). The rTMS (or sham) was applied daily on weekdays between Monday and Friday, at the same time of the day, in a course comprising of 25 sessions. Participants received treatment of rTMS or sham over four weeks. Note: the CN subjects were only used to identify brain regions affected by MDD by comparing the network connectivity between CN and MDD and didn't receive rTMS.

Neuropsychological and MRI assessments were performed on Monday 1 morning at baseline and after 4-week treatment (rTMS or sham). All researchers performing patients' evaluations were blind to their experimental arm belonging.

Individuals were excluded if they had severe suicide risk, a history of stroke, impaired thyroid function, multiple sclerosis, or degenerative diseases; metastatic cancer, brain tumors, unstable cardiac, hepatic, or renal disease, myocardial infarction, or stroke within the three months preceding the study; metal implants. MDD subjects with history of comorbid Axis I diagnosis were excluded.

MRI Data Acquisition

MRI images were acquired using a 1.5T Avanto Siemens scanner (Siemens, Erlangen, Germany) with a 12-channel head coil. Resting-state functional images including 240 volumes were obtained by gradient-recalled echo-planar imaging (GRE-EPI) sequence (EPI: TR = 2,000 ms, TE = 25 ms, FA = 90°, matrix = 64 × 64, FOV = 240 mm × 240 mm, thickness = 4.0 mm, no gap, number of slices = 36, voxel size = 3.75 × 3.75 × 4 mm^3). High-resolution T1-weighted axial images covering the whole brain were acquired by 3D magnetization prepared rapid gradient echo (MPRAGE) sequence (TR = 1,900 ms, TE = 2.48 ms; FA = 9°, matrix = 256 × 256, FOV = 250 × 250 mm, thickness = 1.0 mm, no gap, number of slices = 176, voxel size = 1 × 1 × 1 mm^3).

rTMS Protocol

rTMS was delivered using a Magstim Rapid2 magnetic stimulator with a 70-mm figure-8-shaped coil. In all participants, rTMS was applied over the left dorsolateral prefrontal cortex (DLPFC). For stimulation of the DLPFC, the tip of the intersection of the two coil loops was lined up with the F3 sites of the 10–20 electroencephalogram system (19).

The rTMS was applied, using trains of 1,000 stimuli at 10 Hertz (Hz) frequency and an intensity of 90% of the motor threshold (MT). The MT was defined as the lowest intensity (as assessed with single-pulse TMS) producing motor evoked potentials of greater than 50 μV in at least five out of 10 trials in the relaxed first dorsal interosseous (FDI) muscle of the contralateral (right) hand (20). No significant differences were found in MT values between CNs (61 ± 6.3%) and MDD patients (60 ± 7.0%) (CN only perform an MT to compare to MDD and didn't receive rTMS treatment). Participants received 25 sessions of either rTMS or sham stimulation over the left DLPFC. Each daily stimulation session consisted of 40 trains of 4 s duration with an interval of 56 s. The entire session lasted approximately 25 min twice each day (once at 8 o'clock morning and once at 4 o'clock afternoon), and the interval between daily sessions is 8 h. The total sessions are 1,000 (25 sessions/time * 2 times /day * 5 days/week * 4 weeks), and The total trains are 40000 (40 trains/session * 25 sessions/time * 2 times /day * 5 days/week * 4 weeks). The sham rTMS blocks were conducted, with the coil held close to the DLPFC, but angled away. We chose 90% of MT, although the FDA approved protocol suggests 120% of MT. This reason specified regarding this choice as follows: our subjects were made up of people with 17-item HAMD scores greater than 20, that is, all subjects are major depressive disorder. In the early stages, the use of 120% of MT in some of the patients was attempted, but these subjects felt uncomfortable or emotionally disturbed. Furthermore, some studies have also shown that 90% of MT can improve HAMD scores significantly (21, 22). Finally, to meet safety recommendations, 90% of MT was found most suitable for use.

The sham rTMS group were conducted, with the coil held close to the left DLPFC but angled away (13).

Image Preprocessing

Data analyses of groups were conducted with Matlab (Math Works Inc., Natick, MA, USA), and Data Processing & Analysis for Brain Imaging (DPABI) (23) based on SPM8. To eliminate T1 equilibration effects, the first ten volumes were discarded. Images were then time-shifted and motion-corrected (24, 25). Participants with head motion more than 2 mm maximum displacement in any direction of x, y, and z or 2∘ of any angular motion throughout the course of scan were excluded from the present study. The resulting images were linearly normalized into Montreal Neurological Institute (MNI) space using a 12-parameter affine approach and an EPI template image. Functional images were resampled to 2 × 2 × 2 mm^3 voxels and spatially smoothed (6 mm full-width half-maximum Gaussian kernel). Linear detrending and temporal band-pass filtering (0.01–0.08 Hz) were applied to reduce the effect of low-frequency drifts and high-frequency physiological noise. Finally, several nuisance variables, including six head motion parameters, global mean signal (26), CSF signal, and WM signal were removed by multiple linear regression analysis. There were no significant differences between groups in head motion parameters ($t = 0.12$, $p > 0.05$ for CN vs. MDD; $t = 1.16$, $p > 0.05$ for pre-rTMS group vs. post- rTMS group; $t = 1.34$, $p > 0.05$ for pre-sham group vs. post-sham group)) (24, 25).

Functional Connectivity Analysis

The seed region of interest (ROI) located in the left and right amygdala (**Figures 1A** and **2A**) was determined by using automated anatomic labelling template (27) implemented with wfu_PickAtlas software and functional connectivity analysis was referred to the previously published study (3). We extracted the individual time courses for each seed as the reference time course, and then performed a voxelwise cross-correlation analysis between the seed region and the whole brain within the grey matter (GM) mask.

Statistical Analysis

Demographic and Neuropsychological Data

The demographic data and clinical variables were compared using two-tailed analysis of variance, Two-samples t-test and chi-square test between MDD and CN.

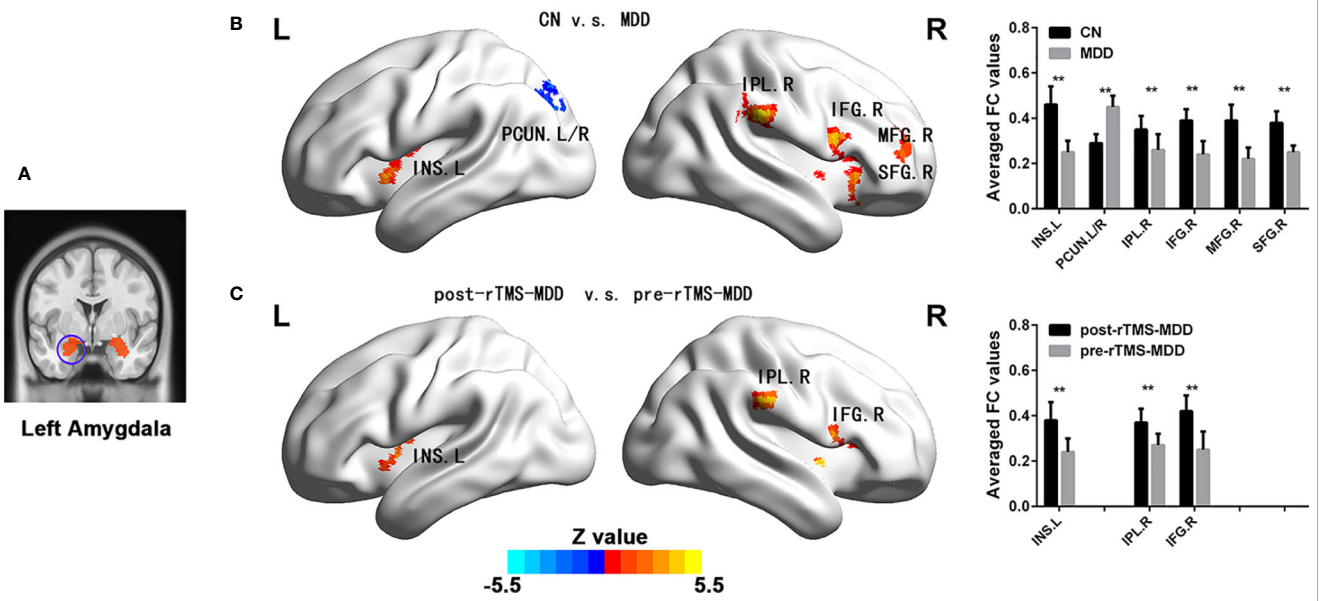

FIGURE 1 | Comparisons of functional connectivity of the left affective network between MDD patients before and after treatment and CN subjects. **(A)** indicating left amygdala ROI. **(B)** brain different regions of the left amygdala functional connectivity between CN and MDD, and pre-rTMS-MDD and post-rTMS-MDD. **(C)** The bar chart shows quantitative differences in left amygdala functional connectivity of these differential brain regions. The statistical maps were managed by False Discovery Rate (FDR) for multiple comparisons to a significant level of p <0.01, with cluster size over 160 mm^3. CN, controls; MDD, major depressive disorder; pre-rTMS-MDD, MDD before rTMS treatment; post-rTMS-MDD, MDD after rTMS treatment; PCUN.L/R, left/right Precuneus; INS.L, left Insula; IFG.R, right Inferior Frontal Gyrus; IPL.R,right Inferior Parietal Lobule; SFG.R, right Superior Frontal Gyrus. **p <0.01 with FDR for multiple comparisons.

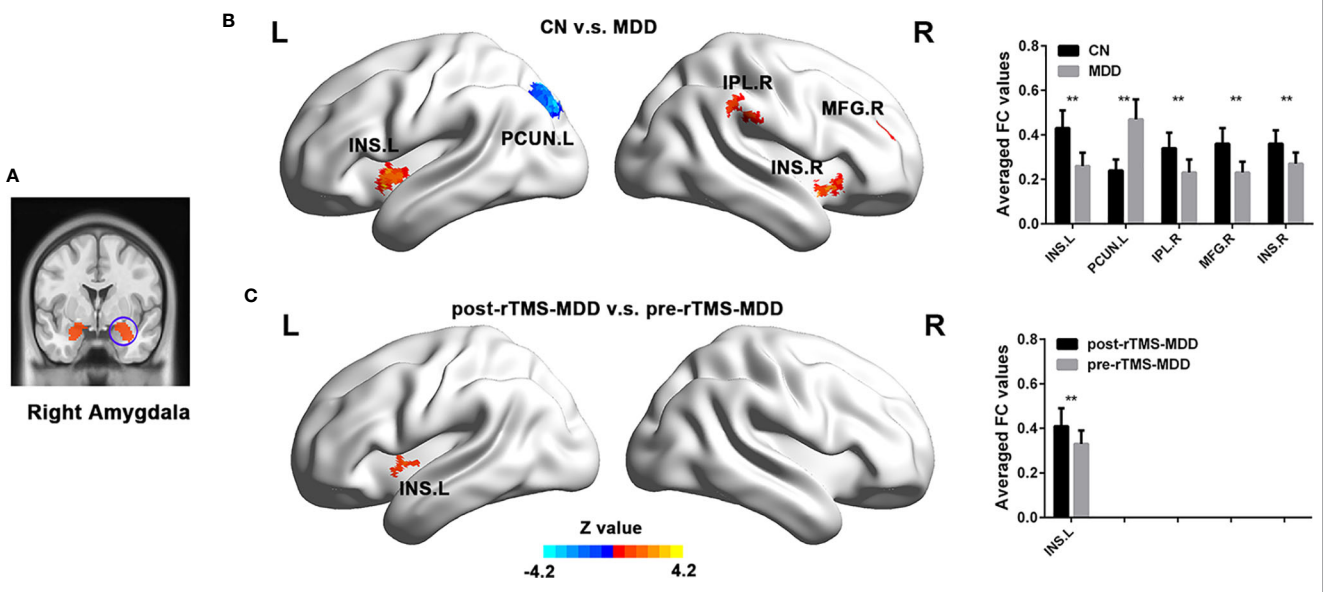

FIGURE 2 | Comparisons of functional connectivity of the right affective network between MDD patients before and after treatment and CN subjects. **(A)** indicating the right amygdala ROI. **(B)** brain different regions of the right amygdala functional connectivity between CN and MDD, and pre-rTMS-MDD and post-rTMS-MDD. **(C)** The bar chart shows quantitative differences in right amygdala functional connectivity of these differential brain regions. The statistical maps were managed by FDR for multiple comparisons to a significant level of p <0.01, with cluster size over 160 mm^3. CN, controls; MDD, major depressive disorder; pre-rTMS-MDD, MDD before rTMS treatment; post-rTMS-MDD, MDD after rTMS treatment; PCUN.L, left Precuneus; INS.L, left Insula; INS.R, right Insula; IPL.R, right Inferior Parietal Lobul. **p <0.01 with FDR for multiple comparisons.

Comparisons of Affective Network Connectivities Between CN and all MDD Subjects

To explain the changes that are related to MDD during rTMS treatment, we performed a voxel-wise analysis. Using a voxel-wise analysis, we compare CN to all 40 MDD (both the rTMS group and the sham group before rTMS) to identify brain regions affected by MDD. Using general mixed linear model analysis, we assessed the differences of the affective network connectivities between all MDD subjects and CN with age, gender, education level and voxel-wise GM volume map treated as covariates. Then a mask was made based on these different brain regions related to MDD. The statistical maps were managed by False Discovery Rate (FDR) for multiple comparisons to a significant level of $p < 0.01$, with cluster size over 160 mm^3.

Comparisons of Affective Network Connectivities Between Pre-rTMS (or Sham) Group and Post- rTMS (or Sham) Group

Using general linear mixed model analysis, we assessed the differences of the affective network connectivities between pre-rTMS group and post- rTMS group (or pre-sham group v.s. post-sham group) within the above-referenced mask with age, gender, education level and voxel-wise GM volume map treated as covariates. The statistical maps were managed by FDR for multiple comparisons to a significant level of $p < 0.01$, with cluster size over 160 mm^3.

Correlations Between Changes of Connectivity and HAMD Scores Pre- Versus Post-rTMS

For each participant, the change in affective network connectivity was calculated to examine the correlations between FC changes post- versus pre-rTMS and HAMD scores pre- versus post-rTMS. The relationships between FC changes and HAMD changes in MDD before and after rTMS was also investigated using a linear regression model (independent variable: FC changes, dependent variable: HAMD changes).

RESULTS

Demographic and Neuropsychological Characteristics

No significant differences were observed in age, gender, or education level between the MDD patients and CN groups (all $p > 0.05$, **Table 1**).

Comparison of Affective Network Connectivities Between CN and All MDD Subjects

In the left affective network, compared with CN, MDD subjects showed significantly lower FC between left insula (INS.L), right inferior frontal gyrus (IFG.R), right superior frontal gyrus (SFG.R), right inferior parietal lobule (IPL.R), right middle frontal gyrus (MFG.R) and left amygdala, and showed significantly higher FC between bilateral PreCUN and left amygdala (**Figures 1A, B** and **Table 2**).

In the right affective network, compared with CN, MDD subjects exhibited significantly lower FC between INS.L, IFG.R/ INS.R, IPL.R, MFG.R and right amygdala, and exhibited a significantly higher FC between left precuneus (PCUN.L) and right amygdala (**Figure 2B** and **Table 2**).

Comparison of Affective Network Connectivities Between Pre-rTMS (or Sham) and Post-rTMS (or Sham) in MDD Patients

In the left affective network, compared with pre-rTMS-MDD, post-rTMS-MDD exhibited a significant increase of FC between INS.L, IFG.R/ right insula (INS.R), IPL.R and left amygdala (**Figures 1A, C** and **Table 2**). Compared with post-sham-rTMS-MDD, post-rTMS-MDD exhibited a significant rise in FC between INS.L, IFG.R/ right insula (INS.R), IPL.R and left amygdale.

In the right affective network, compared with pre-rTMS-MDD, post-rTMS-MDD exhibited a significant increase of FC between INS.L and right amygdala (**Figures 2A, C** and **Table 2**). Compared with post-sham-rTMS-MDD, post-rTMS-MDD exhibited a significant increase of FC between INS.L and right amygdala.

Furthermore, there were no changes for AN functional connectivity between pre-sham group vs. post-sham group.

Correlations Between Changes of Connectivity and HAMD Scores Pre-Versus Post-rTMS or Pre-Sham Versus Post-Sham-rTMS

As shown in **Figure 3**, the change in FC between INS.L and left amygdala was positively correlated with the changes in HAMD scores before and after TMS treatment ($p < 0.001$). Furthermore, there were no correlations between changed FC and the changes in HAMD scores (25.50 v.s. 24.95) before and after sham TMS treatment ($p > 0.05$).

DISCUSSION

This study investigated the changing patterns of amygdala connectivity of MDD patients before and after rTMS treatment, and illuminated brain circuit or the relationship between the network and human behaviour in MDD. Firstly, compared to CN, MDD subjects showed significantly lower FC between INS.L, IPL.R, IFG.R, MFG.R, SFG.R and amygdala, and exhibited significantly higher FC between the bilateral precuneus and the left amygdala before rTMS. Secondly, after rTMS, MDD showed a significant increased FC in the INS.L, IFG.R/INS.R, and IPL.R. Finally, changes in FC between INS.L and left amygdala were positively correlated with changes in HAMD scores before and after rTMS treatment. Altogether, this study promotes our further understanding of the possible anatomical basis of MDD associated with emotional dysregulation.

Before rTMS treatment, this study exhibited lower FC between the left insula and amygdala in MDD patients, which are in

TABLE 2 | Functional connectivity of the affective network between MDD and CN, and bef-MDD and aft-MDD.

Brain region	BA area	Peak MNI coordinate			Peak *Z* value	Cluster size (mm^3)
		x	y	z		
The left affective network						
(1) CN < MDD						
L Precuneus	19	−24	−78	48	−4.9316	156
R Precuneus	30	15	−45	9	−5.3528	278
CN > MDD						
L Insula	13	−36	9	−3	4.3346	159
R Inferior Frontal Gyrus/Insula	13	39	15	12	5.3433	477
R Superior Frontal Gyrus	8	3	30	45	4.2349	171
R Inferior Parietal Lobule	40	57	−27	30	4.7245	193
R Middle Frontal Gyrus	10	42	39	−6	3.8478	64
(2) bef- MDD < aft- MDD						
L Insula	13	−36	3	0	4.136	55
R Inferior Frontal Gyrus/Insula	13	48	15	−3	5.0377	146
R Inferior Parietal Lobule	40	60	−24	30	4.7197	55
The right affective network						
(1) CN < MDD						
L Precuneus	19	−24	−78	51	−4.1022	175
CN > MDD						
L Insula	13	−36	6	−9	4.0263	54
R Inferior Frontal Gyrus/Insula	13	36	9	−12	3.346	32
R Inferior Parietal Lobule	40	63	−33	27	3.9365	82
R Middle Frontal Gyrus	10	36	51	21	3.0563	30
(2) bef -MDD < aft- MDD						
L Insula	13	−36	3	0	3.4073	30

CN, controls; MDD, major depressive disorder; bef-MDD, MDD before treatment; aft-MDD, MDD after treatment.

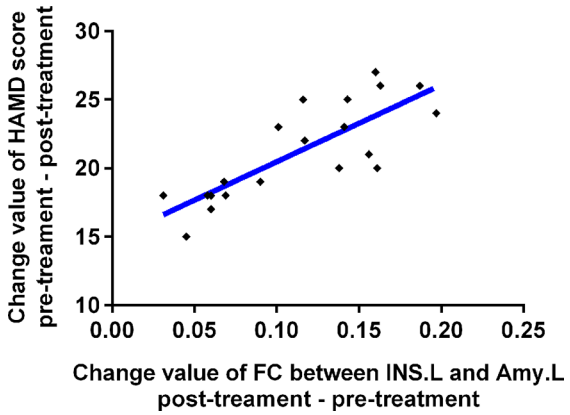

FIGURE 3 | Relationships between change value of HAMD scores and change value of affective network connectivity between MDD patients before and after treatment. MDD, major depressive disorder; FC, functional connectivity; bef-MDD, MDD before treatment; aft-MDD, MDD after treatment; INS.L, left Insula; Amy.L, left Amygdala; HAMD, Hamilton depression scale.

substantial agreement with previous studies (9). It has been indicated that emotional dysregulation in MDD patients is related to FC between amygdala and insula supporting emotion regulation (28). Some anatomical studies have reported that anterior insula is connected with the amygdala by subgenual ACC, which plays a crucial role in generating negative mood states (29). Functional neuroimaging studies in the resting brain have also demonstrated that the anterior insular cortex subserves the emotional functions (30, 31). Furthermore, the present study also exhibited lower FC between the right superior and inferior frontal gyrus, right inferior parietal lobule and amygdala. Our findings also suggest that MDD patients show an impairment of salience and emotion perception, and impairment of emotional controlling and goal-directed behavior, which is in concordance with previous studies (30, 32, 33). Indeed, some recent studies have also reported the therapeutic effects in AN (34) and frontostriatal network (35) in patients with MDD. However, our findings are inconsistent with a recent study (34), who investigated the effect of rTMS on neural connections in depressed patients. Although they also showed changes in amygdala connectivity, their findings showed the more subgenual anterior cingulate cortex role while our study mainly found reduced connectivities of the left insula, right superior and inferior frontal gyrus, right inferior parietal lobule in AN. This reason for the differences may be as follows. The disease severity of our subjects (mean HAMD-17 score: 26.95 for active rTMS, and 25.5 for sham rTMS) were more severe than those of their study (mean HRSD-17 score: 16 for active rTMS, and 13.1 for sham rTMS). Indeed, a series of studies have shown different emotional processing between minor depression and major depression and different mechanisms of electrophysiological damage (36).

Interestingly, our study showed increased FC between the bilateral precuneus and amygdala in MDD patients, which indicates increased connectivity could be associated with the persistently negative mood state and rumination (3). The

precuneus is consistently considered to participate in the processing of episodic memory (37) and to be implicated in the encoding of self-relevant information (38, 39). A large number of studies have indicated that the precuneus is a crucial node of the so-called default mode network (DMN) (40, 41). Accumulating evidence has indicated that the DMN is involved in self-referential processing, including self-prospecting and internal monitoring, autobiographical memory retrieval, future planning, and theory of mind (40, 42, 43). Therefore, our findings further suggest that patients with MDD may fail to restrain negative self-thoughts (44). This finding is inconsistent with our earlier results done at another research centre, which showed reduced FC between the left amygdala and the bilateral precuneus in MDD patients (3). It could be due to the difference in the mean age of subjects in the current study (46.75 years) v.s. the previous studies (32.11 years). Indeed, previous studies have reported that MDD presented age-related abnormalities of grey and white matter (45), and age-related changes in physiological functioning (46). Furthermore, the mean duration of illness in this study (25.00 months) was longer than those of previous studies (mean = 0.7 years). Previous studies have also indicated that duration of illness can affect adverse consequences in terms of outcome for individuals with MDD (47). Therefore, it is reasonable to assume that these inconsistencies in results are due to differences in age of subjects and the duration of their illness.

After rTMS treatment, our study showed significantly increased FC in these above-mentioned brain regions (INS.L, IFG.R, SFG.R, and IPL.R) showing altered connectivity in the affective network. Furthermore, these frontoparietal structures are classified as domain-general control regions, that is so-called cognitive control network (48, 49). Our findings suggest that rTMS can improve functional connectivities of brain regions in interaction hubs between the affective network and executive function network in MDD patients, which provides a potentially reproducible model of TMS-based rescue of a breakdown of connectivity. Some studies have reported that insula is connected with prefrontal cortices, which plays a role in emotional controlling and goal-directed behaviour (33). AN is considered to participate in emotional processing and mediating motivated behaviors (7, 50), emotional controlling and goal-directed behaviour (33). Meanwhile, orbital fronto-insular cortices are part of both the salience network and the AN (51). A recently published article has identified symptom-specific targets for MDD, and they thought that different depression symptom had different specific brain circuits (11). It is reasonable to speculate that the AN might be partially connected with the salience network in MDD patients. The excitatory rTMS plays a therapeutic improvement role in through stimulation of the DLPFC, which is connected with the salience network and the AN. Altogether, our findings suggest that non-invasive treatment of AN network dysfunction by stimulating the DLPFC is an effective strategy to improve depressive symptoms in MDD patients.

Interestingly, this study also found that changes in FC between INS.L and left amygdala was positively correlated with changes in HAMD scores before and after rTMS treatment, which indicates the existence of at least one network circuit linked directly to depressive symptoms. Indeed, it has been hypothesized that emotional dysregulation is considered to contribute to altered FC between the amygdala and insula (28), and it is reported that an insula-centered neural network is considered to support salience and emotion perception (30, 32). The insula is also believed to be connected with prefrontal cortices, which plays a role in emotional controling and goal-directed behavior (33). Therefore, it is reasonable to speculate that the rTMS-induced improvement of depressive symptoms supports the standpoint that DLPFC is directly implicated in the onset of depressive symptom in MDD patients. According to a neurobiological view, rTMS may induce relevant modulations to activate the changes in synaptic plasticity over a DLPFC–amygdala–insula circuit, which leads to clinical improvement. Therefore, the precise localiZation of a DLPFC–amygdala–insula circuit is critical in identifying the underlying neural substrates of the disabling depressive symptoms in patients with MDD. Our results provide experimental evidence in support of such a circuit, which, when directly modulated, rescues these deficits.

However, this has some limitations. Firstly, the longitudinal data was not available for the controls. In future studies, the longitudinal data of controls should be designed to ensure that the network changes observed pre/post-treatment are due to rTMS and not merely within the range of normal variation in FC, although FC is not expected to change within a short period. Secondly, this sham stimulation may affect our findings. The current sham rTMS studies are conducted using coils specially designed to deliver sham stimulation. However, tilting the coil away from DLPFC still provides low-intensity stimulation due to the magnetic field at the edge of the coil. Therefore, this limitation should be kept in mind. Finally, amygdala network connectivity is not the same as AN connectivity. The amygdala is associated with multiple functional networks, including the so-called salience network, which is involved in attentional and cognitive control in domains beyond affect. Although we have explained that TMS can improve functional connectivities of brain regions in interaction hubs between amygdala affective network and other networks (i.e. executive function network, DMN, and salience network and so on) in MDD patients, our interpretation of the results needs to be cautious.

The present study provides novel evidence that rTMS may be an effective strategy for improving the depressive symptom of patients with MDD, which may be useful in further characterizing network–symptom relationship in MDD. While our results demonstrate a target biological substrate for the treatment of depressive symptoms, we do not suggest that DLPFC–amygdala–insula-targeted TMS is the sole intervention that can do so. Our results raise the possibility that functional connectivity may be a useful marker of efficacy for other therapeutic interventions in the treatment of depressive symptoms. It further suggests that the amygdala–insula circuit may be a potential interventional target circuit of clinical efficacy for MDD to design rationale strategies for therapeutic trials.

DATA AVAILABILITY STATEMENT

The datasets generated for this study are available on request to the corresponding authors.

ETHICS STATEMENT

The studies involving human participants were reviewed and approved by Human Participants Ethics Committee at the Medical Imaging Department of Jining Psychiatric Hospital. The patients/participants provided their written informed consent to participate in this study.

AUTHOR CONTRIBUTIONS

F-JC, C-ZG, H-FD, and XZ contributed study concept and design. NZ, H-FD, A-LZ, and XZ acquired, analyzed, or interpreted data. F-JC and H-FD drafted and revised the manuscript. All authors contributed to the article and approved the submitted version.

REFERENCES

1. Mayberg HS. Modulating dysfunctional limbic-cortical circuits in depression: towards development of brain-based algorithms for diagnosis and optimised treatment. *Br Med Bull* (2003) 65:193–207. doi: 10.1093/bmb/65.1.193
2. Rigucci S, Serafini G, Pompili M, Kotzalidis GD, Tatarelli R. Anatomical and functional correlates in major depressive disorder: the contribution of neuroimaging studies. *World J Biol Psychiatry* (2010) 11:165–80. doi: 10.1080/15622970903131571
3. Wang YL, Yang SZ, Sun WL, Shi YZ, Duan HF. Altered functional interaction hub between affective network and cognitive control network in patients with major depressive disorder. *Behav Brain Res* (2016) 298:301–9. doi: 10.1016/j.bbr.2015.10.040
4. Brady ROJr., Gonsalvez I, Lee I, Ongur D, Seidman LJ, Schmahmann JD, et al. Cerebellar-Prefrontal Network Connectivity and Negative Symptoms in Schizophrenia. *Am J Psychiatry* (2019) 176:512–20. doi: 10.1176/appi.ajp.2018.18040429
5. Bebko G, Bertocci MA, Fournier JC, Hinze AK, Bonar L, Almeida JR, et al. Parsing dimensional vs diagnostic category-related patterns of reward circuitry function in behaviorally and emotionally dysregulated youth in the Longitudinal Assessment of Manic Symptoms study. *JAMA Psychiatry* (2014) 71:71–80. doi: 10.1001/jamapsychiatry.2013.2870
6. Yeo BT, Krienen FM, Sepulcre J, Sabuncu MR, Lashkari D, Hollinshead M, et al. The organization of the human cerebral cortex estimated by intrinsic functional connectivity. *J Neurophysiol* (2011) 106:1125–65. doi: 10.1152/jn.00338.2011
7. Lindquist KA, Wager TD, Kober H, Bliss-Moreau E, Barrett LF. The brain basis of emotion: a meta-analytic review. *Behav Brain Sci* (2012) 35:121–43. doi: 10.1017/S0140525X11000446
8. Kim SM, Park SY, Kim YI, Son YD, Chung US, Min KJ, et al. Affective network and default mode network in depressive adolescents with disruptive behaviors. *Neuropsychiatr Dis Treat* (2016) 12:49–56. doi: 10.2147/NDT.S95541
9. Bebko G, Bertocci M, Chase H, Dwojak A, Bonar L, Almeida J, et al. Decreased amygdala-insula resting state connectivity in behaviorally and emotionally dysregulated youth. *Psychiatry Res* (2015) 231:77–86. doi: 10.1016/j.pscychresns.2014.10.015
10. Luking KR, Repovs G, Belden AC, Gaffrey MS, Botteron KN, Luby JL, et al. Functional connectivity of the amygdala in early-childhood-onset depression. *J Am Acad Child Adolesc Psychiatry* (2011) 50:1027–1041 e1023. doi: 10.1016/j.jaac.2011.07.019
11. Siddiqi SH, Taylor SF, Cooke D, Pascual-Leone A, George MS, Fox MD. Distinct Symptom-Specific Treatment Targets for Circuit-Based Neuromodulation. *Am J Psychiatry* (2020) 177:435–46. doi: 10.1176/appi.ajp.2019.19090915
12. Rossi S, Hallett M, Rossini PM, Pascual-Leone ASafety of TMSCG. Safety, ethical considerations, and application guidelines for the use of transcranial magnetic stimulation in clinical practice and research. *Clin Neurophysiol* (2009) 120:2008–39. doi: 10.1016/j.clinph.2009.08.016
13. Turriziani P, Smirni D, Zappala G, Mangano GR, Oliveri M, Cipolotti L. Enhancing memory performance with rTMS in healthy subjects and individuals with Mild Cognitive Impairment: the role of the right dorsolateral prefrontal cortex. *Front Hum Neurosci* (2012) 6:62:62. doi: 10.3389/fnhum.2012.00062
14. Koch G, Bonni S, Pellicciari MC, Casula EP, Mancini M, Esposito R, et al. Transcranial magnetic stimulation of the precuneus enhances memory and neural activity in prodromal Alzheimer's disease. *Neuroimage* (2017) 169:302–11. doi: 10.1016/j.neuroimage.2017.12.048
15. Rabey JM, Dobronevsky E. Repetitive transcranial magnetic stimulation (rTMS) combined with cognitive training is a safe and effective modality for the treatment of Alzheimer's disease: clinical experience. *J Neural Transm (Vienna)* (2016) 123:1449–55. doi: 10.1007/s00702-016-1606-6
16. Chen J, Ma W, Zhang Y, Yang LQ, Zhang Z, Wu X, et al. Neurocognitive impairment of mental rotation in major depressive disorder: evidence from event-related brain potentials. *J Nerv Ment Dis* (2014) 202:594–602. doi: 10.1097/NMD.0000000000000167
17. Chen J, Yang L, Ma W, Wu X, Zhang Y, Wei D, et al. Ego-rotation and object-rotation in major depressive disorder. *Psychiatry Res* (2013) 209:32–9. doi: 10.1016/j.psychres.2012.10.003
18. Zheng YP, Zhao JP, Phillips M, Liu JB, Cai MF, Sun SQ, et al. Validity and reliability of the Chinese Hamilton Depression Rating Scale. *Br J Psychiatry* (1988) 152:660–4. doi: 10.1192/bjp.152.5.660
19. Turriziani P, Smirni D, Oliveri M, Semenza C, Cipolotti L. The role of the prefrontal cortex in familiarity and recollection processes during verbal and non-verbal recognition memory: an rTMS study. *Neuroimage* (2010) 52:348–57. doi: 10.1016/j.neuroimage.2010.04.007
20. Rossini PM, Burke D, Chen R, Cohen LG, Daskalakis Z, Di Iorio R, et al. Non-invasive electrical and magnetic stimulation of the brain, spinal cord, roots and peripheral nerves: Basic principles and procedures for routine clinical and research application. An updated report from an I.F.C.N. Committee. *Clin Neurophysiol* (2015) 126:1071–107. doi: 10.1016/j.clinph.2015.02.001
21. Williams NR, Sudheimer KD, Bentzley BS, Pannu J, Stimpson KH, Duvio D, et al. High-dose spaced theta-burst TMS as a rapid-acting antidepressant in highly refractory depression. *Brain* (2018) 141:e18. doi: 10.1093/brain/awx379
22. Sonmez AI, Camsari DD, Nandakumar AL, Voort JLV, Kung S, Lewis CP, et al. Accelerated TMS for Depression: A systematic review and meta-analysis. *Psychiatry Res* (2019) 273:770–81. doi: 10.1016/j.psychres.2018.12.041
23. Yan CG, Wang XD, Zuo XN, Zang YF. DPABI: Data Processing & Analysis for (Resting-State) Brain Imaging. *Neuroinformatics* (2016) 14:339–51. doi: 10.1007/s12021-016-9299-4
24. Power JD, Barnes KA, Snyder AZ, Schlaggar BL, Petersen SE. Spurious but systematic correlations in functional connectivity MRI networks arise from subject motion. *Neuroimage* (2012) 59:2142–54. doi: 10.1016/j.neuroimage.2011.10.018
25. Van Dijk KR, Sabuncu MR, Buckner RL. The influence of head motion on intrinsic functional connectivity MRI. *Neuroimage* (2012) 59:431–8. doi: 10.1016/j.neuroimage.2011.07.044
26. Fox MD, Zhang D, Snyder AZ, Raichle ME. The global signal and observed anticorrelated resting state brain networks. *J Neurophysiol* (2009) 101:3270–83. doi: 10.1152/jn.90777.2008
27. Tzourio-Mazoyer N, Landeau B, Papathanassiou D, Crivello F, Etard O, Delcroix N, et al. Automated anatomical labeling of activations in SPM using a macroscopic anatomical parcellation of the MNI MRI single-subject brain. *Neuroimage* (2002) 15:273–89. doi: 10.1006/nimg.2001.0978

28. Phillips ML, Ladouceur CD, Drevets WC. A neural model of voluntary and automatic emotion regulation: implications for understanding the pathophysiology and neurodevelopment of bipolar disorder. *Mol Psychiatry* (2008) 13:829, 833–857. doi: 10.1038/mp.2008.65
29. Mayberg HS, Liotti M, Brannan SK, McGinnis S, Mahurin RK, Jerabek PA, et al. Reciprocal limbic-cortical function and negative mood: converging PET findings in depression and normal sadness. *Am J Psychiatry* (1999) 156:675–82. doi: 10.1176/ajp.156.5.675
30. Dupont S, Bouilleret V, Hasboun D, Semah F, Baulac M. Functional anatomy of the insula: new insights from imaging. *Surg Radiol Anat* (2003) 25:113–9. doi: 10.1007/s00276-003-0103-4
31. Cauda F, D'Agata F, Sacco K, Duca S, Geminiani G, Vercelli A. Functional connectivity of the insula in the resting brain. *Neuroimage* (2011) 55:8–23. doi: 10.1016/j.neuroimage.2010.11.049
32. Dolan RJ. Emotion, cognition, and behavior. *Science* (2002) 298:1191–4. doi: 10.1126/science.1076358
33. Cloutman LL, Binney RJ, Drakesmith M, Parker GJ, Lambon Ralph MA. The variation of function across the human insula mirrors its patterns of structural connectivity: evidence from in vivo probabilistic tractography. *Neuroimage* (2012) 59:3514–21. doi: 10.1016/j.neuroimage.2011.11.016
34. Taylor SF, Ho SS, Abagis T, Angstadt M, Maixner DF, Welsh RC, et al. Changes in brain connectivity during a sham-controlled, transcranial magnetic stimulation trial for depression. *J Affect Disord* (2018) 232:143–51. doi: 10.1016/j.jad.2018.02.019
35. Kang JI, Lee H, Jhung K, Kim KR, An SK, Yoon KJ, et al. Frontostriatal Connectivity Changes in Major Depressive Disorder After Repetitive Transcranial Magnetic Stimulation: A Randomized Sham-Controlled Study. *J Clin Psychiatry* (2016) 77:e1137–43. doi: 10.4088/JCP.15m10110
36. Wu X, Chen J, Jia T, Ma W, Zhang Y, Deng Z, et al. Cognitive Bias by Gender Interaction on N170 Response to Emotional Facial Expressions in Major and Minor Depression. *Brain Topogr* (2016) 29:232–42. doi: 10.1007/s10548-015-0444-4
37. Cavanna AE, Trimble MR. The precuneus: a review of its functional anatomy and behavioural correlates. *Brain* (2006) 129:564–83. doi: 10.1093/brain/awl004
38. Kjaer TW, Nowak M, Lou HC. Reflective self-awareness and conscious states: PET evidence for a common midline parietofrontal core. *Neuroimage* (2002) 17:1080–6. doi: 10.1006/nimg.2002.1230
39. Amft M, Bzdok D, Laird AR, Fox PT, Schilbach L, Eickhoff SB. Definition and characterization of an extended social-affective default network. *Brain Struct Funct* (2015) 220:1031–49. doi: 10.1007/s00429-013-0698-0
40. Buckner RL, Andrews-Hanna JR, Schacter DL. The brain's default network: anatomy, function, and relevance to disease. *Ann N Y Acad Sci* (2008) 1124:1–38. doi: 10.1196/annals.1440.011
41. Raichle ME, MacLeod AM, Snyder AZ, Powers WJ, Gusnard DA, Shulman GL. A default mode of brain function. *Proc Natl Acad Sci U S A* (2001) 98:676–82. doi: 10.1073/pnas.98.2.676
42. Spreng RN, Mar RA, Kim AS. The common neural basis of autobiographical memory, prospection, navigation, theory of mind, and the default mode: a quantitative meta-analysis. *J Cognit Neurosci* (2009) 21:489–510. doi: 10.1162/jocn.2008.21029
43. Northoff G, Bermpohl F. Cortical midline structures and the self. *Trends Cognit Sci* (2004) 8:102–7. doi: 10.1016/j.tics.2004.01.004
44. Aghajani M, Veer IM, van Tol MJ, Aleman A, van Buchem MA, Veltman DJ, et al. Neuroticism and extraversion are associated with amygdala resting-state functional connectivity. *Cognit Affect Behav Neurosci* (2014) 14:836–48. doi: 10.3758/s13415-013-0224-0
45. Soriano-Mas C, Hernandez-Ribas R, Pujol J, Urretavizcaya M, Deus J, Harrison BJ, et al. Cross-sectional and longitudinal assessment of structural brain alterations in melancholic depression. *Biol Psychiatry* (2011) 69:318–25. doi: 10.1016/j.biopsych.2010.07.029
46. Sacchet MD, Camacho MC, Livermore EE, Thomas EAC, Gotlib IH. Accelerated aging of the putamen in patients with major depressive disorder. *J Psychiatry Neurosci* (2017) 42:164–71. doi: 10.1503/jpn.160010
47. Dell'Osso B, Cremaschi L, Grancini B, De Cagna F, Benatti B, Camuri G, et al. Italian patients with more recent onset of Major Depressive Disorder have a shorter duration of untreated illness. *Int J Clin Pract* (2017) 71:e12926. doi: 10.1111/ijcp.12926
48. Seeley WW, Menon V, Schatzberg AF, Keller J, Glover GH, Kenna H, et al. Dissociable intrinsic connectivity networks for salience processing and executive control. *J Neurosci* (2007) 27:2349–56. doi: 10.1523/JNEUROSCI.5587-06.2007
49. Smith SM, Fox PT, Miller KL, Glahn DC, Fox PM, Mackay CE, et al. Correspondence of the brain's functional architecture during activation and rest. *Proc Natl Acad Sci U S A* (2009) 106:13040–5. doi: 10.1073/pnas.0905267106
50. Grillner S, Hellgren J, Menard A, Saitoh K, Wikstrom MA. Mechanisms for selection of basic motor programs–roles for the striatum and pallidum. *Trends Neurosci* (2005) 28:364–70. doi: 10.1016/j.tins.2005.05.004
51. Elton A, Gao W. Divergent task-dependent functional connectivity of executive control and salience networks. *Cortex* (2014) 51:56–66. doi: 10.1016/j.cortex.2013.10.012

Conflict of Interest: The authors declare that the research was conducted in the absence of any commercial or financial relationships that could be construed as a potential conflict of interest.

frontiers in Psychiatry

ORIGINAL RESEARCH
published: 17 November 2020
doi: 10.3389/fpsyt.2020.548904

Regional White Matter Integrity Predicts Treatment Response to Escitalopram and Memantine in Geriatric Depression: A Pilot Study

*Beatrix Krause-Sorio[1], Prabha Siddarth[1], Michaela M. Milillo[1], Roza Vlasova[1], Linda Ercoli[1], Katherine L. Narr[2] and Helen Lavretsky[1]**

[1] Jane and Terry Semel Institute for Neuroscience and Human Behavior, University of California, Los Angeles, Los Angeles, CA, United States, [2] Department of Neurology, University of California, Los Angeles, Los Angeles, CA, United States

Background: Geriatric depression with subjective memory complaints increases the risk for Alzheimer's Disease. Memantine, a neuroprotective drug, can improve depression and help prevent cognitive decline. In our 6-months clinical trial, escitalopram/memantine (ESC/MEM) improved mood and cognition compared to escitalopram/placebo treatment (ESC/PBO; NCT01902004). In this report, we investigated whether baseline brain white matter integrity in fronto-limbic-striatal tracts can predict clinical outcomes using fractional anisotropy (FA).

Methods: Thirty-eight older depressed adults (mean age = 70.6, SD = 7.2) were randomized to ESC/MEM or ESC/PBO and underwent diffusion-weighted imaging (DWI) at 3 Tesla at baseline. Mood was assessed using the Hamilton Depression Rating Scale (HAMD), apathy using the Apathy Evaluation Scale (AES) and anxiety using the Hamilton Anxiety Scale (HAMA) at baseline and 6-months follow-up. FA was extracted from seven tracts of interest (six in each hemisphere and one commissural tract) associated with geriatric depression. Non-parametric General Linear Models were used to examine group differences in the association between FA and symptom improvement, controlling for age, sex, baseline symptom scores and scanner model, correcting for false discovery rate (FDR). *Post-hoc* tests further investigated group differences in axial, mean and radial diffusivity (AD, MD, and RD, respectively). Lastly, we performed an exploratory whole-brain model to test whether FA might be related to treatment response with memantine.

Results: There were no differences in remission rates or HAMD change between groups. In bilateral anterior and posterior internal capsule tracts and bilateral inferior and right superior fronto-occipital (IFO and SFO) fasciculus, higher FA was associated with larger improvements in depressive symptoms for ESC/MEM, but not ESC/PBO, correcting for FDR. Lower MD in the left IFO and RD in the right anterior internal capsule were associated with improved treatment responses. We found no significant associations in the whole-brain analysis.

Limitations: Included small sample size and high dropout.

OPEN ACCESS

Edited by:
Fengyu Zhang,
Global Clinical and Translational Research Institute, United States

Reviewed by:
Sara L. Weisenbach,
Stony Brook Medicine, United States
Stijn Michielse,
Maastricht University, Netherlands

****Correspondence:***
Helen Lavretsky
hlavretsky@mednet.ucla.edu

Specialty section:
This article was submitted to Neuroimaging and Stimulation, a section of the journal Frontiers in Psychiatry

Received: *03 April 2020*
Accepted: *19 October 2020*
Published: *17 November 2020*

Citation:
Krause-Sorio B, Siddarth P, Milillo MM, Vlasova R, Ercoli L, Narr KL and Lavretsky H (2020) Regional White Matter Integrity Predicts Treatment Response to Escitalopram and Memantine in Geriatric Depression: A Pilot Study. Front. Psychiatry 11:548904. doi: 10.3389/fpsyt.2020.548904

Conclusions: Higher baseline FA and lower RD and MD in hypothesized fronto-limbic-striatal tracts predicted greater improvement in mood and anxiety with ESC/MEM compared to ESC/PBO in geriatric depression. FA as a biomarker for white matter integrity may serve as a predictor of treatment response but requires confirmation in larger future studies.

Keywords: geriatric depression, cognitive decline, memantine, magnetic resonance imaging, diffusion weighted imaging, white matter integrity, fractional anisotropy, treatment response

INTRODUCTION

Depression is among the most common and disabling conditions in older adults (1–4). While 70% of depressed older adults successfully respond to the first-line antidepressant therapy with selective serotonin reuptake inhibitors (SSRIs) after 8–12 weeks of treatment (5), only 30–40% achieve remission (6). Geriatric depression is associated with reduced remission rates compared to younger depressed adults, which may be due to comorbid cognitive impairments with subjective memory decline and diminished executive functions (7–10). Comorbid cognitive impairments can worsen disease prognosis and increase the risk of developing Alzheimer's disease (11–13). Other frequent comorbid symptoms are anxiety and apathy, which can also moderate the antidepressant response (14, 15). Thus, it is important to develop new therapeutic approaches that target mood, anxiety, and cognitive symptoms, taking into consideration the symptom profile of geriatric depression.

Memantine is a fast-acting, well-tolerated, uncompetitive N-methyl-D-aspartate (NMDA) receptor antagonist and is FDA-approved for the treatment of Alzheimer's disease. NMDA receptors are ionotropic and bind glutamate, the major excitatory neurotransmitter in the nervous system. Increased glutamate concentrations have been detected in younger adults with major depressive disorder (MDD), and prefrontal cortex glutamate was found increased in geriatric depression (16, 17). Excessive glutamate can lead to excitotoxicity, leading to both acute neural injury and chronic neuronal degeneration (18). Therefore, memantine can be promising as an adjunct treatment for late-life depression, and potentially for the prevention of Alzheimer's disease in this high-risk population. While memantine has previously been tested for the treatment of depression, a systematic review reported contradictory findings, and a more recent meta-analysis was unable to confirm beneficial effects of memantine on mood in depression in younger populations (19–21).

In the parent double-blind randomized placebo-controlled trial (RCT) of geriatric depression with subjective memory complaints [(22), [NCT01902004]], we compared treatment response to escitalopram combined with memantine (ESC/MEM) to escitalopram combined with placebo (ESC/PBO). We did not find group differences in changes in mood at 6 or 12 months, but found improved cognition at 12-months follow-up in the ESC/MEM group. The use of brain biomarkers can address variability in treatment response and potentially identify subgroups that are more likely to respond to the targeted treatment, thus providing a more personalized approach to treatment selection. For example, we have found that higher baseline amyloid and tau markers in the frontal lobe, assessed with (2-(1-{6-[(2-[fluorine-18]fluoroethyl)(methyl)amino]-2-naphthyl}-ethylidene)) [^{18}F]FDDNP positron emission tomography (PET), was associated with greater improvement in executive functions at 6 months in both treatment group, thus identifying a potential biomarker of cognitive improvement with antidepressant use (23).

Prior studies demonstrated that both gray and white matter atrophy observed in geriatric depression mostly affected fronto-limbic-striatal regions and their structural connections (24–28). This included longitudinal volume reductions in frontal and association regions in geriatric depression compared to healthy controls, as well as white matter decreases within the superior frontal gyrus, posterior thalamic radiation, corpus callosum, and the superior longitudinal fasciculus over a 2-years period (29). A systematic review from 15 existing studies supports that fractional anisotropy (FA), a marker for white matter integrity, is consistently reduced in geriatric depression compared to healthy controls in frontal and fronto-limbic tracts (30, 31). One prior study comparing FA at baseline between remitted and non-remitted older adults with depression treated with escitalopram for 12 weeks demonstrated reduced FA in fronto-limbic tracts including sub-regions of the anterior cingulate gyrus (ACC) and the posterior cingulate (PCC), the dorsolateral prefrontal cortex, the genu of the corpus callosum, and in white matter regions adjacent to the hippocampus and the insula in non-remitters compared to those that achieved remission (32). To summarize, reductions in the diffusion tensor imaging measure FA have been reported in fronto-limbic fiber pathways in geriatric depression with some consistency. However, the majority of published studies in this field have only examined cross-sectional differences in diffusion imaging measures between geriatric depression and healthy controls. Although one prior report suggests that pre-treatment FA may serve as an indicator of successful therapeutic outcome (32), associations between FA and treatment-related changes in symptoms in geriatric depression remain unaddressed. Further, how escitalopram combined with memantine interacts with white matter integrity in association with symptom improvement remains unknown.

In this exploratory study, we tested whether FA can be used prospectively as a biomarker of treatment response in geriatric depression. Specifically, we investigated whether baseline FA, a biomarker of white matter integrity measured with diffusion-weighted imaging (DWI), could predict treatment response to

combined escitalopram and memantine (ESC/MEM) compared to escitalopram and placebo (ESC/PBO). To further identify the underlying structural mechanisms of the observed relationships between FA and symptom improvement, we investigated axial diffusivity (AD; reflecting axonal density), radial diffusivity (RD; myelination) and mean diffusivity (MD; magnitude of overall diffusion associated with tissue atrophy) in a *post-hoc* analysis.

MATERIALS AND METHODS

Participants

Participants included a sub-sample of 38 older adults (mean age = 70.6, SD = 7.2; 14 men/24 women) diagnosed with MDD (mean age = 70.6, SD = 7.2; 14 male/24 female) who participated in a larger clinical randomized placebo-controlled trial [RCT-NCT01902004, (22)] comparing the efficacy of ESC/MEM compared to ESC/PBO in treating geriatric depression with subjective memory complaints. Only 38 out of 95 were eligible for magnetic resonance imaging (MRI) scanning due to exclusion criteria of claustrophobia, or metallic implants that were deemed unsafe for scanning at 3 Tesla. These participants underwent diffusion-weighted imaging (DWI) at baseline (for patient characteristics, see **Table 1**) and based on the randomization of the parent clinical trial, 22 participants were randomized to receive ESC/MEM, while 16 received ESC/PBO (**Figure 1**). Only 26 participants completed MRI at follow-up and were included in this analysis. Inclusion criteria were: age ≥ 60 years; a DSM-5 (Diagnostic and Statistical Manual) diagnosis of MDD (33), and a Hamilton Rating Scale for Depression score of 16 or greater [HAMD-24; (34)], a Mini-Mental State Examination score of 23 or greater [MMSE; (35)] and a subjective report of memory impairment. Subjective memory complaints were assessed during the phone screening as an affirmative response to the question "Have you experienced memory problems over the past 6 months?" Exclusion criteria were a history of psychiatric disorders, including substance abuse disorder, suicidal behavior or suicide attempts within the past year; acute or severe current or recent medical illness; a history of allergies or intolerance to either escitalopram or memantine. The study was approved by the Institutional Review Board at the University of California Los Angeles (UCLA). Participants signed written informed consent prior to the beginning study procedures.

TABLE 1 | Participant demographics and baseline clinical scores of the subsample of 38 participants used in the current study.

	ESC/MEM Mean (standard deviation) *N* = 22	ESC/PBO Mean (standard deviation) *N* = 16	*Kruskal-Wallis test statistic*	*p*-value
Sex (m/f)	8/14	6/10		Fisher's exact $p = 1.0$
MCI diagnosis	5	2		Fisher's exact $p = 0.68$
Age	70.05 (7.33)	71.25 (7.15)	0.32	0.57
Education in years	15.82 (2.17)	16.13 (2.13)	0.37	0.54
MMSE	28.45 (1.53)	28.19 (1.72)	0.16	0.69
HAMD	17.64 (2.34)	17.69 (2.24)	<0.0001	1.0

There were no significant differences between treatment groups at baseline.
HAMD = Hamilton Depression Rating Scale; MMSE = Mini Mental State Examination.

Clinical and Cognitive Assessment

Remission was defined as a HAMD score of six or lower at follow-up (36). Participants completed the Clinical Dementia Rating Scale [CDR; (37)], and the MMSE (35) at baseline to exclude those with dementia. Mild cognitive impairment (MCI) was defined as the stage between normal cognition and dementia (CDR = 0.5), subjective reports of cognitive decline as experienced by the participant or a collateral, objective neurocognitive impairment, but the absence of significant functional impairment (38). The Wechsler Memory Scale Third Edition, WMS-III, including the verbal paired associates subtest [Total or Delayed scores; (39)] and the Hopkins Verbal Learning Test [HVLT; (40)] were additionally administered. Objective neurocognitive impairment was defined as a score below at least one standard deviation (SD) of age- and education-specific norms on two or more screening memory tests: HVLT Total or Delayed memory, and Wechsler Memory Scale Third Edition, WMS-III, verbal paired associates [Total or Delayed scores; (41, 42)]. In addition, we administered the Hamilton Anxiety Scale [HAMA, (43)] and the Apathy Evaluation Scale [AES, (44)].

Medication Administration and Adherence

During the first 4 weeks of treatment, the daily dose of escitalopram was 10 mg, while daily memantine or matched placebo doses were titrated up from 5 to 20 mg over the course of the first 4 weeks. The Clinical Global Impression Scale [CGI; (45)] was administered at baseline and follow-up to track the severity and improvement of depressive symptoms. If the CGI score was ≥3 after week four, escitalopram was increased to 20 mg. Memantine was adjusted to a minimum of 5 mg and escitalopram to 10 mg based on tolerability.

Neuroimaging Protocol

DWI images were collected using either a 3T Siemens TIM Trio or Prisma system (Siemens, Erlangen, Germany) due to a hardware upgrade mid-study with a 32-channel head coil at the UCLA Ahmanson & Lovelace Brain Mapping Center. Consequently, 4/15 participants in the ESC/MEM and 4/11 participants in the ESC/PBO group were scanned on the Trio. For co-registration, a T1-weighted image was acquired with parameters matched across scanners: a multi-echo magnetization-prepared rapid acquisition gradient echo (MPRAGE) scan: 1 mm^3 with isotropic voxel dimensions, 176 slices, repetition time = 2,150 ms, echo time = 1.74, 3.6, 5.46, and 7.32 ms, inversion time = 1,260, field of view (FOV) = 256 mm, matrix size = 256 × 256 mm, and a flip angle of 7 degrees. DWI parameters were: Trio: multi-band factor = 3; 72 slices; 144 gradient directions; 1.8 mm^3 isotropic voxel size; field of view = 190 mm; repetition time = 3.245 ms; echo time = 84 ms; 12 b0's; 90-degree flip angle; b-factor = 1,000 s/mm^2. Prisma: multi-band factor = 4; 98 gradient directions; 92 slices;

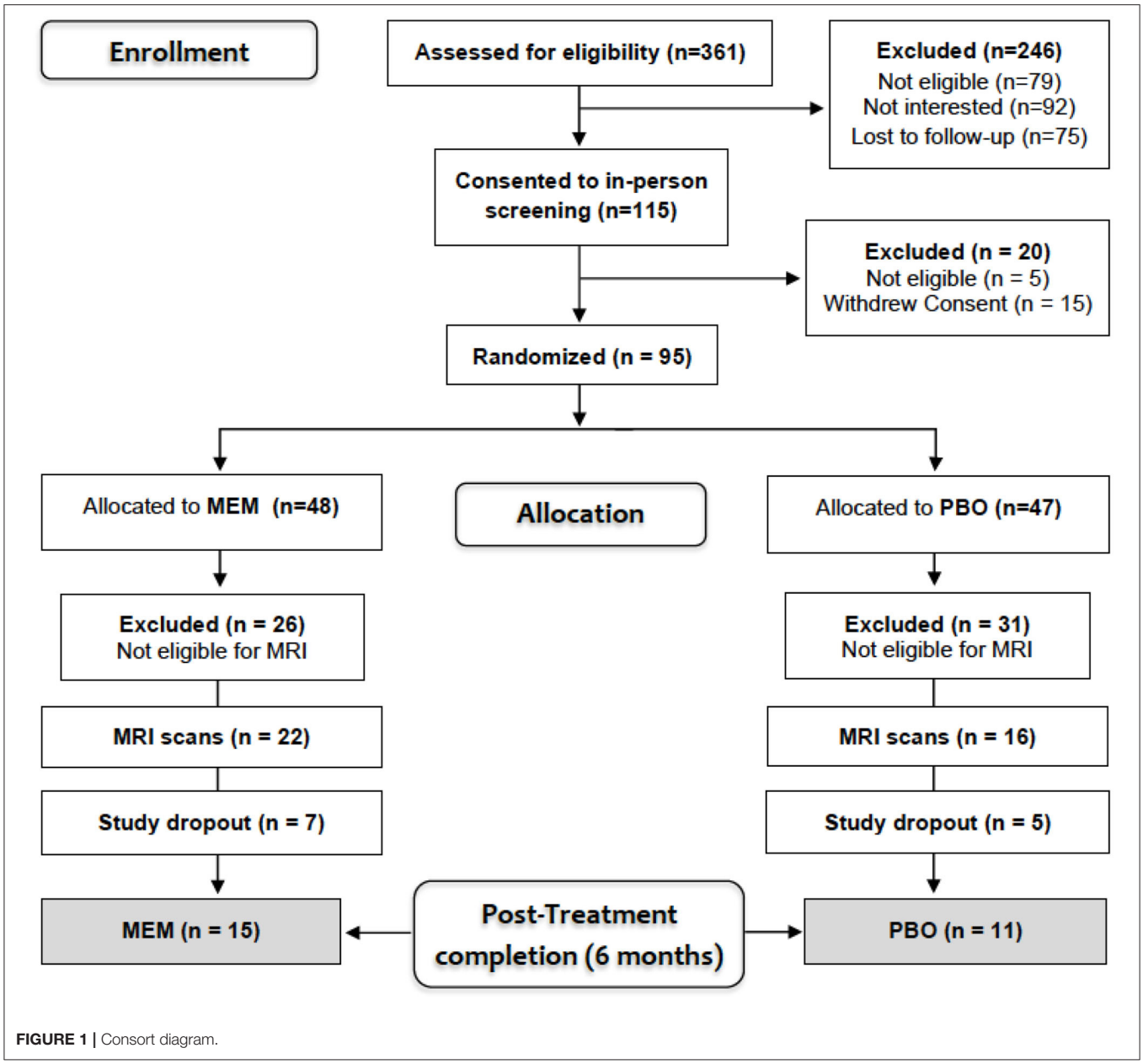

FIGURE 1 | Consort diagram.

1.5 mm^3 isotropic voxel size; field of view = 210 mm; repetition time = 3.23; echo time = 89.2 ms; 7 b0's; flip angle = 78 degrees; and b-factor = 1,500 s/mm^2.

DWI Data Processing

DWI images were processed using FSL software (http://fsl.fmrib.ox.ac.uk/fsl/fslwiki/) after visual inspection of gradient direction images for artifacts or excessive movement. DWI data underwent anatomical distortion correction (46), eddy-current and movement artifact correction. Further processing steps were equal for both scanner acquisition protocols: eddy-current and movement artifact correction. The gradient direction vectors (b-vectors) were adjusted accordingly. Subsequently, we separated the brain from its surrounding tissues, including cerebrospinal fluid, bone, fat and skin, and the non-brain tissue was removed from the images using the brain-extraction tool (47). A diffusion tensor model was fitted to the resulting data. Using FSL's Tract-based Spatial Statistics workflow [TBSS; (48)] individual FA maps were warped into 1 mm Montreal Neurological Institute (MNI) space and a study-specific white matter skeleton was created from all participants' images with a FA threshold of 0.2. Individual subjects' FA values were then projected onto the group white matter skeleton. This skeletonized data was used to extract mean FA values for each participant for seven tract regions-of-interest (ROIs). ROIs were derived from the ICBM-DTI-81 probabilistic white matter label atlas (https://fsl.fmrib.ox.ac.uk/fsl/fslwiki/Atlases) and comprised the cross-hemisphere genu of the corpus callosum (GCC), and the

left and right anterior and posterior limb of the internal capsule (ALIC, PLIC, respectively), cingulum bundle of the cingulate gyrus (CGC), the fornix (FX, left, right and the commissural body), inferior and superior fronto-occipital (IFO, SFO) and superior longitudinal fasciculi (SLF). The same procedure was applied to extract AD, MD, and RD metrics from each tract ROI, respectively.

Statistics

Due to the small sample size, non-parametric methods were used for all analyses (49). We used Kruskal-Wallis test to test baseline group differences in mean FA for all ROIs (six for each hemisphere plus one commissural) between Siemens Trio and Prisma scanners. For the following analyses, as recommended by Conover and Iman (50) and Conover (51), we used a rank transformation on all of the variables and then estimated standard general linear models (GLMs). Between-group differences in HAMD changes were examined with a rank-based GLM, with treatment group (ESC/MEM vs. ESC/PBO) as the predictor, controlling for the baseline score, age and sex. Similar rank-based GLMs were estimated to examine group differences in associations of HAMD change and mean FA in the ROIs of interest (L and R of ALIC, PLIC, CGC, IFO, FX, SFO, and SLF as well as FX body GCC), by including the mean FA and their interaction with treatment group as additional predictors, as well as scanner model (Trio vs. Prisma). We used the Benjamini-Hochberg procedure (with a false discovery rate of 10%) to correct for multiple comparisons. We also report Spearman rank correlation coefficients for all significant associations. As follow-up analyses, we estimated similar models on AD, MD, and RD for those tracts showing significant FA effects. While the tracts of interest comprised our main analysis, we additionally performed a GLM (group × change in HAMD on FA) exploratory voxel-wise whole skeleton analysis using 10,000 permutations and threshold-free cluster correction (TFCE) correction at an alpha level of 0.05.

RESULTS

Baseline

Baseline demographics, as well as clinical scores and symptoms are detailed in **Table 1** for the subset of 38 participants included in this study (also see **Supplementary Table 1**). The parent clinical trial included 95 participants, described in the primary article (22). The groups in this subsample also did not differ in demographic and clinical scores at baseline (**Table 1**). No images were excluded for motion or other artifacts and there was no difference in baseline FA averaged across ROIs between Trio and Prisma scanners [left FA: $x^2(1) = 0.03$, $p = 0.87$; right FA: $x^2(1) = 3.09$, $p = 0.15$].

Treatment Effects

Of the 38 participants who underwent an MRI at baseline, 26 (15 in the ESC/MEM group and 11 in the ESC/PBO group) completed the study. The groups of completers (ESC/MEM vs. ESC/PBO) did not differ in demographic and clinical data at baseline [sex: Fisher's exact $p = 0.7$; age: Kruskal-Wallis $x^2(1) = 0.02$, $p = 0.9$; education: $x^2(1) = .<0.01$, $p = 1.0$; MMSE: $x^2(1) = 0.1.73$, $p = 0.2$; HAMD: $x^2(1) = 0.3$, $p = 0.6$]. Remission was achieved by 11/15 completers (73%) in the ESC/MEM group, and 6/11 completers (55%) in the ESC/PBO group. There was no significant difference in remission rates between treatment groups at 6 months (Fisher's exact $p = 0.42$). There was also no significant difference between groups for 6-months change in HAMD [$F_{(1, 21)} = 0.92$, $p = 0.3$; **Table 2**, **Supplementary Table 2**].

Neuroimaging Results

Correcting for multiple comparisons, significant group x FA interactions were obtained for baseline FA and change in HAMD in the left and right ALIC, PLIC, and IFO, as well as in the right SFO (**Table 3**). For all of these significant interactions, follow-up analyses revealed that higher baseline FA was associated with a larger improvement in depressive symptoms in the ESC/MEM group (**Figure 2**). In the right PLIC, the effect within the ESC/MEM group did not reach significance ($t = -1.84$, $p = 0.08$). None of the associations between baseline FA and HAMD change were significant for the ESC/PBO group. The follow-up exploratory analyses on AD and RD revealed no significant interactions in the ALIC, PLIC, IFO, and right SFO, while RD showed a similar group x RD interaction in the right ALIC ($F_{(1, 18)} = 5.07$, $p = 0.04$) which did not reach significance in the left ALIC [$F_{(1, 18)} = 3.97$, $p = 0.06$; see **Supplementary Table 3**]. This was due to a negative association of RD with HAMD change in the ESC/MEM ($t = -3.27$, $p = 0.004$) but not the ESC/PBO group ($t = 0.31$, $p = 0.76$). For MD, there were trends in bilateral ALIC and PLIC, the right SFO (**Table 3**) and a significant interaction in the left [$F_{(1, 18)} = 0.66$, $p = 0.43$], but not the right IFO [$F_{(1, 18)} = 1.06$, $p = 0.32$]. Contrary to the results for FA, higher left IFO MD was associated with a poorer improvement in depressive symptoms in the ESC/MEM ($t = 2.23$, $p = 0.04$), but not the ESC/PBO group ($t = -1.17$, $p = 0.26$). There were no significant clusters for FA, AD, MD or RD in the voxel-wise whole-brain analysis of group differences. **Supplementary Table 4** and **Supplementary Figure 1** show FA × ROI interactions for anxiety (HAMA) and apathy (AES).

DISCUSSION

This pilot study is the first to demonstrate that higher baseline measures of brain white matter integrity may predict changes in symptoms of depression in a 6-months trial of escitalopram combined with memantine compared Toto placebo. Similar to results from the parent trial, in the current subset of participants who underwent MRI scanning, mood symptoms improved in both treatment groups (22). In bilateral ALIC, PLIC, and IFO, as well as the right SFO, components of the fronto-limbic-striatal network, baseline FA was associated with improvements in mood in the memantine, but not the placebo group. RD showed trends in the same direction in bilateral PLIC and the left ALIC, though only changes in RD in the right ALIC reached significance. This suggests that the mechanism underlying poorer treatment response to memantine in patients with higher RD may be attributed to demyelination processes (52). We did not observe

TABLE 2 | HAMD scores at baseline and 6 months by treatment group for the 26 completers of the trial.

Variable	ESC/MEM Mean (standard deviation) $N = 15$			ESC/PBO Mean (standard deviation) $N = 11$			Between-group change	
	Baseline	6 months	Change	Baseline	6 months	Change	$F_{(1, 21)}$ statistic	p-value
HAMD	17.6 (2.61)	5.67 (5.72)	−11 (6.16)	17.73 (1.95)	7.18 (5.04)	−10.55 (4.23)	0.92	0.3

There were no significant group differences in HAMD change. The results presented here stem from the rank-based general linear models.
HAMD, Hamilton Depression Rating Scale.

TABLE 3 | Relationship between change in HAMD and baseline FA in ESC/MEM and ESC/PBO.

FA	Left			Right		
	Interaction group x FA	ESC+MEM	ESC+PBO	Interaction group x FA	ESC+MEM	ESC+PBO
HAMD						
ALIC	$F_{(1, 18)} = 4.66$, $p = 0.04$*	T = −3.63, $p = 0.002$; r = −0.77	T = −0.56, $p = 0.58$	$F_{(1, 18)} = 7.7$, $p = 0.01$*	T = −5.11, $p \leq 0001$; r = −0.78	T = −0.76, $p = 0.45$
PLIC	$F_{(1, 18)} = 7.71$, $p = 0.01$	T = −2.73, $p = 0.01$; r = −0.51	T = 1.35, $p = 0.19$	$F_{(1, 18)} = 5.76$, $p =$ 0.03*	T = −1.84, $p = 0.08$; r = −0.31	T = 1.09, $p = 0.29$
CGC	$F_{(1, 18)} = 0.34$, $p = 0.56$			$F_{(1, 18)} = 2.11$, $p = 0.16$		
IFO	$F_{(1, 18)} = 4.65$, $p = 0.04$*	T = −2.57, $p = 0.02$; r = −0.59	T = 0.23, $p = 0.82$	$F_{(1, 18)} = 4.69$, $p = 0.04$*	T = −3.58, $p = 0.002$; r = −0.63	T = 0.18, $p = 0.86$
SFO	$F_{(1, 18)} = 0.17$, $p = 0.69$			$F_{(1, 18)} = 8.48$, $p = 0.009$**	T = −3.63, $p = 0.002$; r = −0.75	T = −0.04, $p = 0.97$
SLF	$F_{(1, 18)} = 1.49$, $p = 0.24$			$F_{(1, 18)} = 3.31$, $p = 0.09$		
FX	$F_{(1, 18)} = 0.24$, $p = 0.63$			$F_{(1, 18)} = 0.01$, $p = 0.94$		
FX Body	Interaction: $F_{(1, 18)} = 0.06$, $p = 0.80$					
GCC	Interaction: $F_{(1, 18)} = 0.13$, $p = 0.73$					

The results stem from the rank-based general linear models including the treatment group, FA and the interaction between group and FA as the predictors, while controlling for the respective baseline score, age, sex and scanner.
*HAMD, Hamilton Depression Scale. *Significant after FDR correction.*

any trends or effects in AD. MD, reflecting tissue atrophy rather than integrity, showed the opposite directionality of FA in the left IFO, but no effect in the right hemisphere. This further implicates that those with reduced white matter integrity in this region may respond less well to treatment with memantine. In contrast to the effects for improvement in depressive symptoms in bilateral ALIC, PLIC, IFO, and right SFO, larger improvements in anxiety were linked to higher FA in the left ALIC and SLF, as well as in bilateral CGC and IFO in the ESC/MEM but not the ESC/PBO group (**Supplementary Table 4**). For apathy, higher FA in the right SFO was associated with better treatment outcomes in the ESC/MEM group. While the limited sample size does not allow for broader generalizations, it appears from our results that white matter prediction effects might be symptom-, tract- and treatment-specific.

The use of non-invasive neuroimaging markers for prediction of treatment response has been previously recommended (53), further supporting the usefulness of FA in predicting the effects of combined antidepressant treatment with memantine in geriatric depression. For instance, it has been suggested that abnormalities in fronto-limbic white matter connectivity in geriatric depression plays a role in the reduced antidepressant response based on genetic factors for neuroprotective mechanisms (54). Another study on 12 weeks of escitalopram treatment found that remitters could be distinguished from non-remitters at baseline based on FA in fronto-limbic tracts including some of our selected ROIs (32). Furthermore, escitalopram effects on apathy have been found to be independent of its effects on mood in geriatric depression and could be predicted by baseline FA in the left uncinate fasciculus, a tract we did not examine in the current study (55). White matter integrity declines with aging and can affect treatment response in geriatric depression. It should be investigated whether the neuroprotective drug memantine can increase white matter connectivity in impaired circuits.

There are several limitations to the current study. First, the small sample size limited our statistical power. This

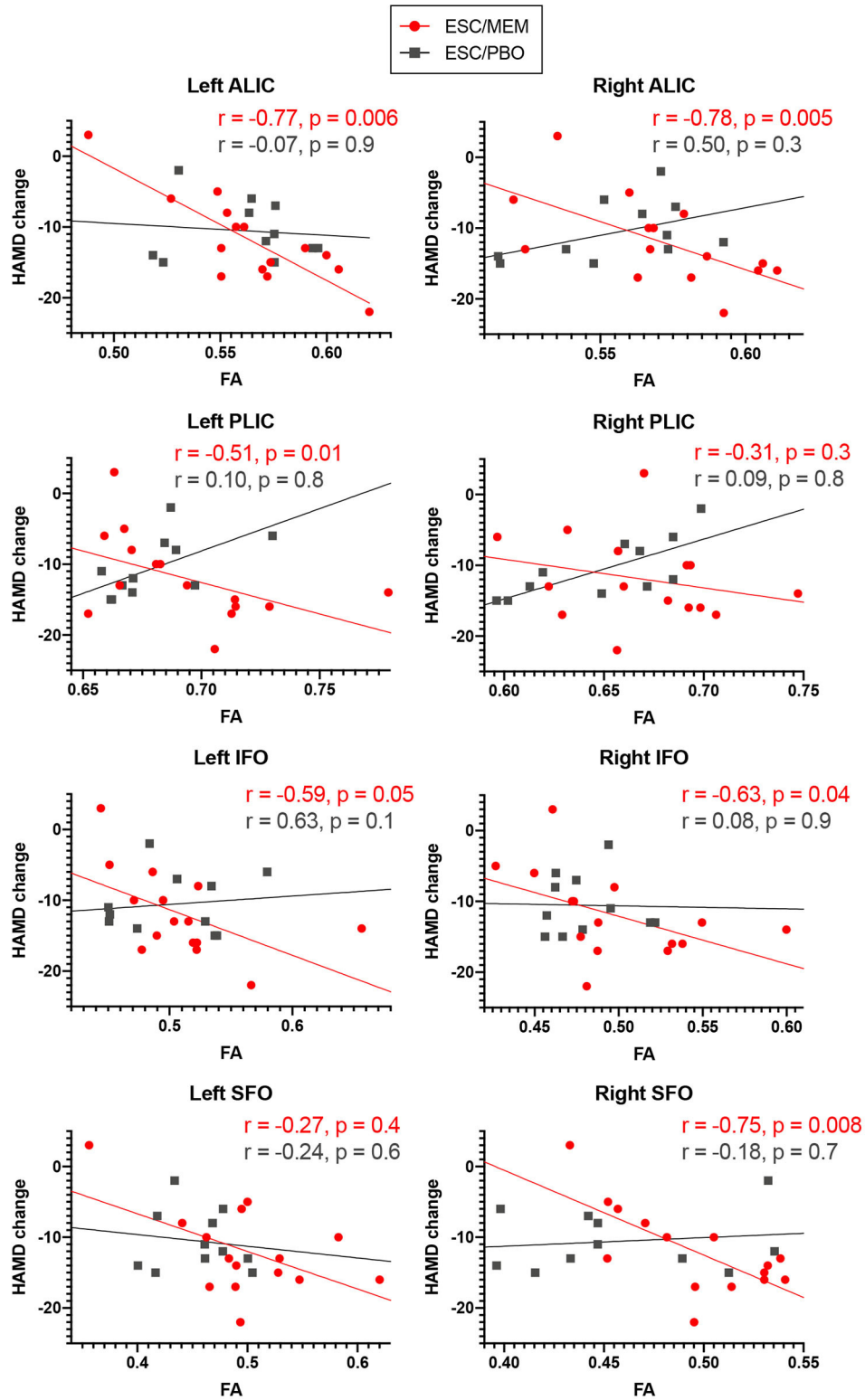

FIGURE 2 | Higher baseline FA in ROIs was associated with larger clinical improvements with memantine but not placebo treatment. Higher baseline FA in regions associated with geriatric depression was associated with greater improvement in depressive symptoms in bilateral ALIC, PLIC, and IFO and the right SFO in ESC/MEM treated participants. There was no relationship between FA and clinical improvement in the placebo group. While partial Spearman correlation coefficients (controlling for age, sex, baseline HAMD score, and scanner) were used, the plots depict (non-ranked) original values for better interpretability. HAMD, Hamilton Depression Scale.

study was intended as a hypothesis-generating pilot study and findings presented here must be replicated in larger longitudinal studies. Nonetheless, we demonstrated the feasibility of using MRI markers for fronto-limbic-striatal tract integrity as a possible predictor of antidepressant and cognitive enhancement treatment response in geriatric depression. The limited sample size was mainly due to contraindications to MRI scanning, such as implanted devices deemed unsafe for MRI scanning at 3 Tesla, as well as high dropout rates that might limit the generalizability of our findings. Third, we did not investigate change in FA from baseline to the 6-montha follow-up, such that we were unable to test the association between treatment-related change in clinical improvements and FA changes. Fourth, this was a secondary analysis of the primary RCT and used only a subset of the sample who completed the RCT and also had neuroimaging data. Fifth, our selection of tracts of interest was not inclusive of all major white matter pathways in the brain, but instead focused on those pathways previously implicated in geriatric depression. As reflected in the absence of results from our whole-brain analysis, we likely lack the power to detect effects at the voxel-wise level and larger studies using whole-brain models can investigate whether clusters appear to indicate more regional specificity. Lastly, it is important to note that FA has limited value as a proxy for white matter integrity, as it is highly sensitive to changes at the microstructural level (56).

In summary, in our pilot study of geriatric depression, we demonstrated the ability of baseline regional white matter tract integrity to predict treatment outcomes in a randomized placebo-controlled trial of escitalopram and memantine or placebo. While we were unable to detect significant differences in clinical response to memantine, we demonstrated that white matter health in fronto-limbic-striatal tracts was associated with symptom improvement favoring memantine. Our results suggest that even in the absence of clinical effects, FA in components of fronto-limbic-striatal tracts might be a biomarker of treatment response with memantine in older populations with depression, whereby higher indicators of white matter integrity were associated with improved treatment responses. Future studies might focus on treatment-related changes in structural and functional connectivity in larger prospective samples.

DATA AVAILABILITY STATEMENT

The raw data supporting the conclusions of this article will be made available by the authors, without undue reservation.

ETHICS STATEMENT

The studies involving human participants were reviewed and approved by University of California Los Angeles Institutional Review Board. The patients/participants provided their written informed consent to participate in this study.

AUTHOR CONTRIBUTIONS

HL conceived the study, obtained funding, and led the study. PS performed the statistical analysis. LE provided and supervised the neuropsychological testing procedures. BK-S and RV performed scans and processed and analyzed the neuroimaging data. BK-S wrote the manuscript with the help of all co-authors. KN and MM assisted in all aspects. All authors were involved in working on the manuscript.

FUNDING

This work was supported by grants R01MH097892 and K24AT009198 to Dr. HL.

ACKNOWLEDGMENTS

We thank the technicians at the UCLA Ahmanson & Lovelace Brain Mapping Center for their support.

SUPPLEMENTARY MATERIAL

The Supplementary Material for this article can be found online at: https://www.frontiersin.org/articles/10.3389/fpsyt.2020.548904/full#supplementary-material

Supplementary Figure 1 | Higher baseline FA was associated with larger clinical improvements with memantine but not placebo treatment on anxiety and apathy symptoms. Higher baseline FA in regions associated with geriatric depression was associated with greater improvement in anxiety symptoms in the left ALIC and SLF and bilateral CGC and IFO in ESC/MEM treated participants. In the right SFO, there was a similar effect for apathy (note that higher scores reflect weaker symptoms). There was no relationship between FA and clinical improvement in the placebo group. While partial Spearman correlation coefficients (controlling for age, sex, baseline HAMD score and scanner) were used, the plots depict (non-ranked) original values for better interpretability. HAMA = Hamilton Anxiety Scale; AES = Apathy Evaluation Scale.

REFERENCES

1. Charney DS, Reynolds CF III, Lewis L, Lebowitz BD, Sunderland T, Alexopoulos GS, et al. Depression and Bipolar Support Alliance consensus statement on the unmet needs in diagnosis and treatment of mood disorders in late life. *Arch Gen Psychiatry.* (2003) 60:664–72. doi: 10.1001/archpsyc.60.7.664
2. Li Y, Lu J. Childhood adversity and depression among older adults: results from a longitudinal survey in China. *Glob Clin Transl Res.* (2019) 1:53–7. doi: 10.36316/gcatr.01.0007
3. Unutzer J. Clinical practice. Late-life depression. *N Engl J Med.* (2007) 357:2269–76. doi: 10.1056/NEJMcp073754
4. Gonzalez HM, Haan MN, Hinton L. Acculturation and the prevalence of depression in older Mexican Americans: baseline results of the Sacramento area latino study on aging. *J Am Geriatr Soc.* (2001) 49:948–53. doi: 10.1046/j.1532-5415.2001.49186.x
5. Chen YM, Huang XM, Thompson R, Zhao YB. Clinical features and efficacy of escitalopram treatment for geriatric depression. *J Int Med Res.* (2011) 39:1946–53. doi: 10.1177/147323001103900540

6. Nelson JC, Delucchi K, Schneider LS. Efficacy of second generation antidepressants in late-life depression: a meta-analysis of the evidence. *Am J Geriatr Psychiatry.* (2008) 16:558–67. doi: 10.1097/01.JGP.0000308883.64832.ed
7. Diniz BS, Butters MA, Albert SM, Dew MA, Reynolds CFIII. Late-life depression and risk of vascular dementia and Alzheimer's disease: systematic review and meta-analysis of community-based cohort studies. *Br J Psychiatry.* (2013) 202:329–35. doi: 10.1192/bjp.bp.112.118307
8. Mitchell AJ, Subramaniam H. Prognosis of depression in old age compared to middle age: a systematic review of comparative studies. *Am J Psychiatry.* (2005) 162:1588–601. doi: 10.1176/appi.ajp.162.9.1588
9. Singh-Manoux A, Dugravot A, Fournier A, Abell J, Ebmeier K, Kivimaki M, et al. Trajectories of depressive symptoms before diagnosis of dementia: a 28-year follow-up study. *JAMA Psychiatry.* (2017) 74:712–8. doi: 10.1001/jamapsychiatry.2017.0660
10. Wilkins CH, Mathews J, Sheline YI. Late life depression with cognitive impairment: evaluation and treatment. *Clin Interv Aging.* (2009) 4:51–7. doi: 10.2147/CIA.S3154
11. Carpenter CR, Avidan MS, Wildes T, Stark S, Fowler SA, Lo AX. Predicting geriatric falls following an episode of emergency department care: a systematic review. *Acad Emerg Med.* (2014) 21:1069–82. doi: 10.1111/acem.12488
12. Mansbach WE, Mace RA. Predicting functional dependence in mild cognitive impairment: differential contributions of memory and executive functions. *Gerontologist.* (2019) 59:925–35. doi: 10.1093/geront/gny097
13. Tunvirachaisakul C, Gould RL, Coulson MC, Ward EV, Reynolds G, Gathercole RL, et al. Predictors of treatment outcome in depression in later life: a systematic review and meta-analysis. *J Affect Disord.* (2018) 227:164–82. doi: 10.1016/j.jad.2017.10.008
14. Saade YM, Nicol G, Lenze EJ, Miller JP, Yingling M, Wetherell JL, et al. Comorbid anxiety in late-life depression: relationship with remission and suicidal ideation on venlafaxine treatment. *Depress Anxiety.* (2019) 36:1125–34. doi: 10.1002/da.22964
15. Lavretsky H, Reinlieb M, St Cyr N, Siddarth P, Ercoli LM, Senturk D. Citalopram, methylphenidate, or their combination in geriatric depression: a randomized, double-blind, placebo-controlled trial. *Am J Psychiatry.* (2015) 172:561–9. doi: 10.1176/appi.ajp.2014.14070889
16. Binesh N, Kumar A, Hwang S, Mintz J, Thomas MA. Neurochemistry of late-life major depression: a pilot two-dimensional MR spectroscopic study. *J Magn Reson Imaging.* (2004) 20:1039–45. doi: 10.1002/jmri.20214
17. Hashimoto K. Emerging role of glutamate in the pathophysiology of major depressive disorder. *Brain Res Rev.* (2009) 61:105–23. doi: 10.1016/j.brainresrev.2009.05.005
18. Choi DW. Glutamate neurotoxicity and diseases of the nervous system. *Neuron.* (1988) 1:623–34. doi: 10.1016/0896-6273(88)90162-6
19. Amidfar M, Reus GZ, Quevedo J, Kim YK. The role of memantine in the treatment of major depressive disorder: clinical efficacy and mechanisms of action. *Eur J Pharmacol.* (2018) 827:103–11. doi: 10.1016/j.ejphar.2018.03.023
20. Kishi T, Matsunaga S, Iwata N. A meta-analysis of memantine for depression. *J Alzheimers Dis.* (2017) 57:113–21. doi: 10.3233/JAD-161251
21. McShane R, Areosa Sastre A, Minakaran N. Memantine for dementia. *Cochrane Database Syst Rev.* (2006) CD003154. doi: 10.1002/14651858.CD003154.pub5
22. Lavretsky H, Laird KT, Krause-Sorio B, Heimberg BF, Yeargin J, Grzenda A, et al. A randomized double-blind placebo-controlled trial of combined escitalopram and memantine for older adults with major depression and subjective memory complaints. *Am J Geriatr Psychiatry.* (2019) 28:178–90. doi: 10.1016/j.jagp.2019.08.011
23. Krause-Sorio B, Siddarth P, Laird K, Ercoli L, Narr K, Barrio J, et al. [^{18}F]FDDNP PET binding predicts change in executive function in a pilot clinical trial of geriatric depression. *Int Psychogeriatr.* (2020) 1–8. doi: 10.1017/S1041610219002047
24. Ballmaier M, Kumar A, Elderkin-Thompson V, Narr KL, Luders E, Thompson PM, et al. Mapping callosal morphology in early- and late-onset elderly depression: an index of distinct changes in cortical connectivity. *Neuropsychopharmacology.* (2008) 33:1528–36. doi: 10.1038/sj.npp.1301538
25. Ballmaier M, Kumar A, Thompson PM, Narr KL, Lavretsky H, Estanol L, et al. Localizing gray matter deficits in late-onset depression using computational cortical pattern matching methods. *Am J Psychiatry.* (2004) 161:2091–9. doi: 10.1176/appi.ajp.161.11.2091
26. Du M, Liu J, Chen Z, Huang X, Li J, Kuang W, et al. Brain grey matter volume alterations in late-life depression. *J Psychiatry Neurosci.* (2014) 39:397–406. doi: 10.1503/jpn.130275
27. Lavretsky H, Ballmaier M, Pham D, Toga A, Kumar A. Neuroanatomical characteristics of geriatric apathy and depression: a magnetic resonance imaging study. *Am J Geriatr Psychiatry.* (2007) 15:386–94. doi: 10.1097/JGP.0b013e3180325a16
28. Sexton CE, Mackay CE, Ebmeier KP. A systematic review and meta-analysis of magnetic resonance imaging studies in late-life depression. *Am J Geriatr Psychiatry.* (2013) 21:184–95. doi: 10.1016/j.jagp.2012.10.019
29. Reppermund S, Zhuang L, Wen W, Slavin MJ, Trollor JN, Brodaty H, et al. White matter integrity and late-life depression in community-dwelling individuals: diffusion tensor imaging study using tract-based spatial statistics. *Br J Psychiatry.* (2014) 205:315–20. doi: 10.1192/bjp.bp.113.142109
30. Guo W, Liu F, Xun G, Hu M, Guo X, Xiao C, et al. Disrupted white matter integrity in first-episode, drug-naive, late-onset depression. *J Affect Disord.* (2014) 163:70–5. doi: 10.1016/j.jad.2014.03.044
31. Wen MC, Steffens DC, Chen MK, Zainal NH. Diffusion tensor imaging studies in late-life depression: systematic review and meta-analysis. *Int J Geriatr Psychiatry.* (2014) 29:1173–84. doi: 10.1002/gps.4129
32. Alexopoulos GS, Murphy CF, Gunning-Dixon FM, Latoussakis V, Kanellopoulos D, Klimstra S, et al. Microstructural white matter abnormalities and remission of geriatric depression. *Am J Psychiatry.* (2008) 165:238–44. doi: 10.1176/appi.ajp.2007.07050744
33. American Psychiatric Association. *Diagnostic and Statistical Manual of Mental Disorders*. Washington, DC (2013).
34. Hamilton M. Development of a rating scale for primary depressive illness. *British J Soc Clin Psychol.* (1967) 6:278–96. doi: 10.1111/j.2044-8260.1967.tb00530.x
35. Folstein MF, Folstein SE, McHugh PR. "Mini-mental state". A practical method for grading the cognitive state of patients for the clinician. *J Psychiatr Res.* (1975) 12:189–98. doi: 10.1016/0022-3956(75)90026-6
36. Nierenberg AA, DeCecco LM. Definitions of antidepressant treatment response, remission, nonresponse, partial response, and other relevant outcomes: a focus on treatment-resistant depression. *J Clin Psychiatry.* (2001) 62 (Suppl. 16):5–9.
37. Hughes CP, Berg L, Danziger WL, Coben LA, Martin RL. A new clinical scale for the staging of dementia. *Br J Psychiatry.* (1982) 140:566–72. doi: 10.1192/bjp.140.6.566
38. Albert MS, DeKosky ST, Dickson D, Dubois B, Feldman HH, Fox NC, et al. The diagnosis of mild cognitive impairment due to Alzheimer's disease: recommendations from the National institute on aging-Alzheimer's association workgroups on diagnostic guidelines for Alzheimer's disease. *Alzheimers Dement.* (2011) 7:270–9. doi: 10.1016/j.jalz.2011.03.008
39. Wechsler D. *The Wechsler Adult Intelligence Scale, III Manual.* San Antonio: The Psychological Corporation (1997). doi: 10.1037/t49755-000
40. Brandt J. The hopkins verbal learning test: development of a new memory test with six equivalent forms. *Clin Neuropsychol.* (1991) 5:125–42. doi: 10.1080/13854049108403297
41. Jak AJ, Bondi MW, Delano-Wood L, Wierenga C, Corey-Bloom J, Salmon DP, et al. Quantification of five neuropsychological approaches to defining mild cognitive impairment. *Am J Geriatr Psychiatry.* (2009) 17:368–75. doi: 10.1097/JGP.0b013e31819431d5
42. Jak AJ, Preis SR, Beiser AS, Seshadri S, Wolf PA, Bondi MW, et al. Neuropsychological criteria for mild cognitive impairment and dementia risk in the framingham heart study. *J Int Neuropsychol Soc.* (2016) 22:937–43. doi: 10.1017/S1355617716000199
43. Hamilton M. The assessment of anxiety states by rating. *Br J Med Psychol.* (1959) 32:50–5. doi: 10.1111/j.2044-8341.1959.tb00467.x
44. Marin RS, Biedrzycki RC, Firinciogullari S. Reliability and validity of the apathy evaluation scale. *Psychiatry Res.* (1991) 38:143–62. doi: 10.1016/0165-1781(91)90040-V
45. Guy W. Clinical global impressions (CGI) scale, modified. In: Rush JA, editor. *Task Force for the Handbook of Psychiatric Measures. Handbook of Psychiatric Measures.* 1st ed. Washington, DC: American Psychiatric Association (2000).

46. Andersson JL, Skare S, Ashburner J. How to correct susceptibility distortions in spin-echo echo-planar images: application to diffusion tensor imaging. *Neuroimage.* (2003) 20:870–88. doi: 10.1016/S1053-8119(03)00336-7
47. Smith SM. Fast robust automated brain extraction. *Hum Brain Mapp.* (2002) 17:143–55. doi: 10.1002/hbm.10062
48. Smith SM, Jenkinson M, Johansen-Berg H, Rueckert D, Nichols TE, Mackay CE, et al. Tract-based spatial statistics: voxelwise analysis of multi-subject diffusion data. *Neuroimage.* (2006) 31:1487–505. doi: 10.1016/j.neuroimage.2006.02.024
49. Altman DG, Gore SM, Gardner MJ, Pocock SJ. Statistical guidelines for contributors to medical journals. *Br Med J.* (1983) 286:1489–93. doi: 10.1136/bmj.286.6376.1489
50. Conover WJ, Iman RL. Rank transformations as a bridge between parametric and nonparametric statistics. *Am Stat.* (1981) 35:124–9. doi: 10.1080/00031305.1981.10479327
51. Conover WJ. The rank transformation—an easy and intuitive way to connect many nonparametric methods to their parametric counterparts for seamless teaching introductory statistics courses. *WIREs Comput Stat.* (2012) 4:432–8. doi: 10.1002/wics.1216
52. Song S-K, Yoshino J, Le TQ, Lin S-J, Sun S-W, Cross AH, et al. Demyelination increases radial diffusivity in corpus callosum of mouse brain. *NeuroImage.* (2005) 26:132–40. doi: 10.1016/j.neuroimage.2005.01.028
53. Walter M, Lord A. How can we predict treatment outcome for depression? *EBioMedicine.* (2015) 2:9–10. doi: 10.1016/j.ebiom.2014.12.008
54. Alexopoulos GS, Glatt CE, Hoptman MJ, Kanellopoulos D, Murphy CF, Kelly RE Jr, et al. BDNF val66met polymorphism, white matter abnormalities and remission of geriatric depression. *J Affect Disord.* (2010) 125:262–8. doi: 10.1016/j.jad.2010.02.115
55. Yuen GS, Gunning FM, Woods E, Klimstra SA, Hoptman MJ, Alexopoulos GS. Neuroanatomical correlates of apathy in late-life depression and antidepressant treatment response. *J Affect Disord.* (2014) 166:179–86. doi: 10.1016/j.jad.2014.05.008
56. Alexander AL, Lee JE, Lazar M, Field AS. Diffusion tensor imaging of the brain. *Neurotherapeutics.* (2007) 4:316–29. doi: 10.1016/j.nurt.2007.05.011

Conflict of Interest: HL has received research grants from Allergan, NIMH, NCCIH, PCORI, and the Alzheimer's Research & Prevention Foundation.

The remaining authors declare that the research was conducted in the absence of any commercial or financial relationships that could be construed as a potential conflict of interest.

Advantages of publishing in Frontiers

OPEN ACCESS
Articles are free to read for greatest visibility and readership

FAST PUBLICATION
Around 90 days from submission to decision

HIGH QUALITY PEER-REVIEW
Rigorous, collaborative, and constructive peer-review

TRANSPARENT PEER-REVIEW
Editors and reviewers acknowledged by name on published articles

Frontiers
Avenue du Tribunal-Fédéral 34
1005 Lausanne | Switzerland

Visit us: www.frontiersin.org
Contact us: frontiersin.org/about/contact

REPRODUCIBILITY OF RESEARCH
Support open data and methods to enhance research reproducibility

DIGITAL PUBLISHING
Articles designed for optimal readership across devices

FOLLOW US
@frontiersin

IMPACT METRICS
Advanced article metrics track visibility across digital media

EXTENSIVE PROMOTION
Marketing and promotion of impactful research

LOOP RESEARCH NETWORK
Our network increases your article's readership